

Fatigue strength of repaired cracks in welded connections made of very high strength steels

Akyel, Abdulkadir

DOI

[10.4233/uuid:1d20cb03-ae0d-4ff7-9e41-7a8a9f5e6be4](https://doi.org/10.4233/uuid:1d20cb03-ae0d-4ff7-9e41-7a8a9f5e6be4)

Publication date

2017

Document Version

Final published version

Citation (APA)

Akyel, A. (2017). *Fatigue strength of repaired cracks in welded connections made of very high strength steels*. [Dissertation (TU Delft), Delft University of Technology]. <https://doi.org/10.4233/uuid:1d20cb03-ae0d-4ff7-9e41-7a8a9f5e6be4>

Important note

To cite this publication, please use the final published version (if applicable). Please check the document version above.

Copyright

Other than for strictly personal use, it is not permitted to download, forward or distribute the text or part of it, without the consent of the author(s) and/or copyright holder(s), unless the work is under an open content license such as Creative Commons.

Takedown policy

Please contact us and provide details if you believe this document breaches copyrights. We will remove access to the work immediately and investigate your claim.

Fatigue strength of repaired cracks in welded connections made of very high strength steels

A. Akyel

Fatigue strength of repaired cracks in welded connections made of very high strength steels

PROEFSCHRIFT

ter verkrijging van de graad van doctor
aan de Technische Universiteit Delft
op gezag van de Rector Magnificus prof. Ir. K.C.A.M. Luyben
voorzitter van het College voor Promoties
in het openbaar te verdediging
op woensdag 11 oktober 2017 om 12:30

door:

Abdulkadir AKYEL
Civiel ingenieur
geboren te Kulu, Turkije

Dit proefschrift is goedgekeurd door de
promotor: Prof. ir. F.S.K. Bijlaard
copromotor: Dr. M.H. Kolstein

Samenstelling promotiecommissie:

Rector Magnificus,	voorzitter
Prof. ir. F.S.K. Bijlaard,	Technische Universiteit Delft, promotor
Dr. M. H. Kolstein,	Technische Universiteit Delft, copromotor

Onafhankelijke leden:

Prof. dr. I.M. Richardson	Technische Universiteit Delft
Prof. dr. ir. J. Maljaars	Technische Universiteit Eindhoven
Prof. dr. M. Veljkovic	Technische Universiteit Delft
Prof. dr. ir. J. Wardenier	em. hgl. 2008 Technische Universiteit Delft, National University of Singapore, Singapore
Dr. ir. R.J.M. Pijpers	TNO



This research was carried out under project number M82.8.12460 in the framework of the Research Program of the Materials Innovation Institute (M2i) in The Netherlands (www.m2i.nl).

ISBN 978-94-91909-47-4

Printed by: Ridderprint B.V.

Keywords: Very High strength steels, Repaired welded connections, Cast steels, Fatigue

Copyright © 2017 Abdulkadir Akyel. All rights reserved. No part of this publication may be reproduced, stored in a retrieval system, or transmitted in any form or by any means, electronic, mechanical, photocopying, recording or otherwise, without the prior permission in writing from the proprietor.

Acknowledgements

After obtaining my Master's degree in Civil Engineering at Delft University of Technology, I was offered the opportunity of doing a PhD and I did not hesitate to take this opportunity. The involvement of an experimental programme in the project and the outstanding test facilities in the Stevin Laboratory were two main encouraging factors for taking this opportunity. I think it was fortunate decision.

First, I would like to thank my supervisors Prof. Frans Bijlaard and Dr. Henk Kolstein for guiding my progress, their dedicated support and valuable comments on my work. They were always available for answering my questions and for discussing all issues of the project. I learned the scientific approach, to establish an experimental programme, set up test facilities, conduct research and to communicate with industrial partners.

Furthermore, I would like to acknowledge the valuable discussions and input from Prof. I. Richardson and Dr. M. Janssen.

This thesis contains the results of an extensive experimental programme. There are hard workers behind these results: the laboratory technicians. Many thanks are extended to Arjen van Rhijn, John Hermsen, Louis den Breejen, Kees van Beek and Kevin Mouthaan who helped me during the experimental work. Without them it would have been impossible to finalise this enjoyable work.

I am grateful to all of my colleagues in the laboratory and in the Steel Structures group. With them by the way, we solved all world problems during coffee breaks. I would also like to express my gratitude for the very enjoyable collaboration with master students Dimitris, Maarten and Tom.

Further, I would like to thank the Material Innovation Institute (M2i), Allseas Engineering and the steel association "Bouwen met Staal" for their support of the research. The progress meetings with them were very inspiring and there were very fruitful discussions and valuable contributions from their experience point of view. I would also like to mention the members of Cluster 7, Advanced Joining and Disassembly of the M2i. There were always very productive discussions on material science and the welding process.

I would also like to acknowledge Prof. T. Ummenhofer and Ing. P. Weidner from the Karlsruhe Institute of Technology for providing HiFIT equipment and their assistance in the application of the equipment. Also thanks to Jan Sinke from Hillebrand B.V. for manufacturing the test specimens.

Finally, I would like to express my deepest gratitude to my family for supporting me to do PhD research. I would not have managed without them.

Summary

The Civil engineering industry demands the design of simple and highly loaded structures for economical fabrication. The fabrication cost can be minimized with optimisation of the assembly expenses by reduction of the amount of joints, reduction of the complexity of joints and slender structural members. Using very high strength steels may provide an economical solution for highly loaded slender members. Very high strength steels with yield strengths of up to 1300 MPa for structural purposes have been available since many years. However, the application of very high strength steels for civil engineering structures is still limited due to restricted available knowledge about the production, manufacturing process and structural response of very high strength steel structures. Research has been carried out to determine the structural behaviour of very high strength steels. With view of this, EN 1993-1-12 (2007) was introduced for designing structures with steels of up to 700 MPa yield strengths, but it does not cover steels with higher yield strengths.

Members with a slenderness frequently used in civil engineering structures show a high tendency towards elastic-plastic buckling. The use of high strength steels leads to slender members with thin wall thicknesses as result of which the self-weight of these structures is reduced and this reduction causes high variations in the stresses under fluctuated live loads. Hence, the fatigue strength of very high strength steel structures is one of the most important design criteria for fatigue loaded structures.

Pijpers (2011) performed a study on the effective application of very high strength steels for civil engineering structures from a fatigue strength point of view. Truss structures were recommended to limit deflection of the slender members and to improve buckling behaviour. In addition, recommendations were given for the improvement of welded connections of truss structures with a view to high nominal stress variation. A reduction of stress concentrations in welded connections may compensate the relatively low fatigue strength of welded connections. The possibility of selecting the shape of cast steels should result in joints with lower stress concentrations. Hence, truss structures with cast nodes can be one of the options for an effective application of very high strength steels in fatigue loaded structures. The research of Pijpers (2011) revealed that very high strength steels may have a positive influence on the fatigue strength of welded connections. However, fatigue damage is inevitable in fatigue loaded welded structures. Therefore, the repair of fatigue damaged welded connections made of very high strength steels is essential to prolong the fatigue life of the structures. Little is known about the repair procedure of fatigue damaged welded connections made of very high strength steels and the fatigue life extension after

repair. The main aim of the current research was to determine the fatigue strength of repaired welded connections made of very high strength steels. It was concentrated on the quenched and tempered cast and rolled steels with yield strengths of 690 MPa and 890 MPa. The research consisted of a literature survey, an experimental study and an analysis of the experimental results.

Fatigue cracks are usually initiated at the weld toes of welded connections. However, in the research of Pijpers (2011), unexpectedly, failures were observed in the base material of welded connections made of very high strength steels. The visual inspection on the fracture surfaces revealed that the crack initiation points contain some material imperfections. A literature study was performed on the possible defects in steels and the effects of these defects on the fatigue strength of material. The study revealed that the defects at surface and subsurface of the material lead to fatigue crack initiation in the material under very high cycle regime. The origin and reason of these imperfections are evaluated by electron microscopic examination. Using similar approach, a microscopic examination was applied on the fracture surface of the base material failures. In addition, chemical composition measurements were performed at the crack initiation locations of the rolled steels. The examination revealed that the fatigue crack initiation in the cast steels results of internal voids and pores. In rolled steels, a repair weld was discovered at the fatigue crack initiation locations. This means that the base material of the rolled steels was damaged during the manufacturing process and that the damages were (probably not so well) repaired by welding.

The main challenge of the current study was to establish a repair procedure for the fatigue crack repair in welded connections. An extensive literature study was conducted to evaluate the state of the art of the repair procedures. The main conclusion of the literature study is that procedures to repair fatigue damaged welded connections should be standardised yet. The emphasis was put on the most frequently used methods, such as the hole drilling method, grinding, peening, splice plate method, welding and combinations of these methods. The literature study showed that repair by welding and subsequently a high frequency mechanical impact treatment (HFMI) provides high fatigue strength for repaired welded connections. With HFMI, the fatigue crack initiation life and the initial stage of the fatigue crack propagation is improved. Pijpers (2011) concluded that the fatigue crack initiation stage of the welded connections made of very high strength steels is longer than the welded connections made of mild steels. Since very high strength steel has some positive influence on the fatigue crack initiation life, the repair by welding without HFMI was selected for the experimental study. Nevertheless, weld procedures for repair welds are not discussed in literature. Discussions with industry and The Welding Institute (TWI) revealed that in practice the welding procedures of the original weld connections -before fatigue damage- are used for the repair welds.

The effectiveness of the fatigue crack repair procedure can be evaluated based on a comparison between the fatigue strength of repaired welded connections and the fatigue

strength of original welded connections. The results from the study of Pijpers (2011) were available, where the emphasis was put on the fatigue strength of welded connections made of very high strength steels and these results were used for the comparison. Therefore, material and specimens for the experiments of the current research were selected based on the research of Pijpers (2011). Accordingly, the emphasis was put on the repair by welding of artificial cracks in base material and fatigue cracks in welded connections. Strain gauges were applied on the plate specimens to determine the crack initiation and after that, the crack propagation was visually monitored until failure, which was defined when the specimens broke into two pieces. With strain gauges and test rigs, average and range values of force, displacements and strain gauge measurements were stored during fatigue tests. An alarm system was used to detect the fatigue crack initiation life. The alarm system shuts down the loading when the measured strain deviates 50 μ strain from the original value, which made it possible to define the crack initiation life and location. Fatigue crack initiation life was specified as the number of cycles where the strain range measurement started to deviate from the regular shape. The nominal stresses were calculated by converting average values of the strain gauges with the uniaxial Hook's law.

The experimental programme of the research consisted of a repaired artificial crack in the base material and repaired fatigue damaged V-shape welded connections. For the specimens with an artificial crack, the test strips were cut from the base material plates of S690 and S890. A semi elliptical artificial crack was created at the middle of the specimens by electrical discharging machining. The length of the artificial crack was equal to half the width of the specimens and the depth of the artificial crack was half the thickness of the specimens. The V-shape welded strips were cut from the welded rolled plates to rolled plates, and rolled plates to cast plates. The specimens were manufactured from S690 and S890 rolled steels and from cast steels with the similar yield strengths G10MnMoV 6-3 and G18NiMoCr 3-6 respectively. The welding of the specimens was executed with ceramic backing to obtain smooth weld root geometry. The fatigue tests were executed with four point bending test setups. The V-shape welded specimens were exposed to fatigue loading to create fatigue cracks at the weld toe, where the crack growth was visually monitored. When the crack length reached half the width of the specimens, the experiment was terminated and the created cracks were repaired by welding. For V-shape welded specimens, this stage was called the crack creation phase.

The repair of the fatigue cracks was conducted in several steps. First, a magnetic particles inspection was performed on the welded connections to determine the dimension and the location of the fatigue cracks. The detected cracks were removed by a disk and a burr grinder. The crack removal process was executed gradually with regular magnetic particle inspections to ensure that the crack was completely removed and to avoid unnecessary material removal. In some specimens, fatigue cracks were initiated at the weld root of the specimens. The root cracks were repaired from the weld cap by removing material from the cap up to the weld root. Then, after the crack removal process, the prepared weld groove

was filled by welding, for which the welding procedure of the original welded connection was used. After that, the weld geometry was reshaped to create smooth transition between the weld and the base material. The repair of the artificial crack in the base material was done with a similar procedure and the only difference was that the magnetic particle at the initial stage was not performed because the location of the artificial crack was known and could be seen by the naked eye. In V-shape welded specimens, fatigue cracks initiated at the weld toe of welded connections and these cracks were repaired. Consequently, the repaired side of the weld had a new weld toe, while another side of the weld was still from the original weld that was exposed to a certain number of cycles during the crack creation stage. When the cumulative damage rule of Miner is taken into consideration, due to the fatigue damage on the original weld at the crack creation stage, there is a big chance that cracks initiate at the original weld toe after the repair. The aim of the study was to determine the fatigue strength of the repair weld. In accordance with this, it was required to avoid crack initiation at the weld toe of the original weld. Therefore, the weld toe of the original weld was treated with High Frequency Impact Treatment (HiFIT). After that, the repaired specimens were tested again with the same stress range as in the crack creation stage.

In addition, fatigue crack growth tests were performed on the base material of S690 and S890 rolled steels. Pre-notched specimens were cyclically loaded in a four point bending test rig, where the crack growth was monitored by a crack detection gauge. Fatigue crack growth parameters and the threshold stress intensity factor for very high strength steels were determined and these parameters were used for the fatigue crack propagation life estimation of the plate test specimens.

A literature study was conducted on analytical models for fatigue life predictions. The total fatigue life consists of two stages: fatigue crack initiation life and fatigue crack propagation life. For the fatigue crack initiation life, the notch stress approach was used. The application procedure of the approach is summarized by Hüeck et al., (1981) and in the FKM guideline (2012). In the current study, both sources are used for the prediction. The models are a function of various parameters, such as yield strength of the material, mean stress, plate thickness, loading mode, weld toe angle and notch radius. The effects of these parameters on the fatigue strength were studied. The fatigue crack propagation life was estimated by the fracture mechanics approach. The crack growth rate is a function of the stress intensity factor, which is determined by the crack size, crack geometry, plate thickness, plate width and weld width. The effects of these parameters on the fatigue crack propagation life were studied separately.

The experimental results were compared with the results of the fatigue prediction models. However, not all input values for the prediction models were measured during testing and the manufacturing process. The fatigue strength was predicted by using conservative values for the unknown parameters, which were defined from literature. In order to take the effects of unknown parameters and assumptions of the prediction models into account, the results

of the experiments were adjusted using influence factors and a reference stress range was determined. The fatigue strength curves of the prediction models were compared with adjusted data. The test results were adjusted with the mean stress factor and loading mode factor. The mean stress factors were calculated for residual stress $\sigma_r = \sigma_y$ and loading mode for tension. The prediction curves showed reasonable agreement with the test results. A statistical analysis was performed on the raw and adjusted test data for determination fatigue strength curves. In the statistical analysis, the regression coefficient was taken either with a variable or was fixed $m = -3$ or $m = -5$. The characteristic stress range $\Delta\sigma_c$ and the mean fatigue strength $\Delta\sigma_{\text{mean}}$ at $2 \cdot 10^6$ cycles were determined for all regression coefficients for the raw and adjusted stress ranges.

The fatigue strength curves from the statistical analysis were compared to the relevant detail categories of EN 1993-1-9 (2006). The fatigue strength curves of raw data and adjusted data satisfied the requirement of the detail categories. In addition, the fatigue strength curves of the base material failure of rolled and cast steels were also compared with the design curves of DNVGL C203 (2016) recommendation and the requirements were met. The fatigue strength curves of the repaired V-shape welded connections were compared with the fatigue strength curves of V-shape welded connections in the as-welded condition. It was revealed that with the established repair procedure, the fatigue strength of fatigue damaged welded connection can be regained. Moreover, there were additional run-outs data after the repair, which means that the fatigue strength of the repair weld can even be better than the original weld. The comparison between fatigue strength curves of the test data and the prediction models showed good agreement. Especially the prediction models according to the FKM guideline (2012) resulted in an accurate fatigue strength prediction.

Samenvatting

De civiele industrie eist het ontwerpen van eenvoudige en hoog belaste constructies om deze constructies economisch te kunnen produceren. De productiekosten kunnen worden geminimaliseerd door optimalisatie van montagekosten, door vermindering van het aantal verbindingen, vermindering van de complexiteit van verbindingen en het gebruik van slanke constructie-elementen. Het gebruik van zeer hoge sterkte staal biedt een oplossing voor hoog belaste slanke constructie-elementen. Zeer hoge sterkte staalsoorten met nominale sterktes tot 1300 MPa zijn al geruime tijd verkrijgbaar voor constructie toepassingen. Echter, de toepassing van zeer hoge sterkte staalsoorten in civiele constructies nog beperkt. De beperkte kennis over productie, fabricageproces en gedrag van deze staalsoorten onder hoge belastingen zijn de belangrijkste redenen van de beperkte toepassing. Om het gedrag van zeer hoge sterkte staalsoorten te bepalen, worden onderzoeken uitgevoerd en de resultaten hebben geleid tot het introduceren van EN 1993-1-12 (2007) waar de ontwerpregels voor staalsoorten met sterktes tot S700 zijn vastgesteld, maar voor hogere staalsoorten is dit niet geregeld in deze norm.

Elementen met een slankheid die in civiele constructies veel voorkomt hebben een sterke neiging tot elastisch-plastische knik. Het gebruik van hoge sterkte staalsoorten leidt tot slanke constructie-elementen met geringe wanddiktes, als gevolg waarvan het eigen gewicht van de constructies verminderd is. Het lage eigen gewicht van constructies veroorzaakt onder niet-permanente belastingen grote variatie van de spanningen en hoge nominale spanningen onder vermoeiingsbelasting. Daardoor, is de vermoeiingssterkte van zeer hoge sterkte staalconstructies één van het belangrijkste ontwerpcriteria voor o vermoeiingsbelaste constructies.

Pijpers (2011) heeft een studie gedaan naar de effectieve toepassingen van hoge sterkte staalsoorten voor civiele constructies vanuit het oogpunt van vermoeiingssterkte. Voor het beperken van doorbuiging en het verbeteren van stabiliteitsgedrag van constructies werden van vakwerkconstructies gebruik gemaakt. Daarnaast werd een aanbeveling gedaan voor de verbetering van gelaste verbindingen van vakwerkconstructies door de effecten van de hoog nominale spanningsvariatie te compenseren. Lage spanningsconcentraties kunnen de vermoeiingssterkte van lasverbindingen onder hoge nominale spanningsvariëaties compenseren. Gietstaal biedt mogelijkheden om knopen met verschillende vormen te ontwerpen en dit kan voor knopen met lage spanningsconcentraties zorgen. De vakwerkconstructie met gegoten knooppunten kan een mogelijkheid zijn voor een effectieve toepassing van zeer hoge sterkte staal in op vermoeiingsbelaste constructies. Uit

dat onderzoek bleek dat zeer hoge sterkte staalsoorten positieve effecten op de vermoeiingssterkte van gelaste verbindingen kan hebben. Aan de andere kant, het ontstaan van vermoeiingsscheuren in op vermoeiingsbelaste staalconstructies is onvermijdelijk. Om de vermoeiingslevensduur van deze constructies te kunnen verlengen, zijn methoden voor het repareren van vermoeiingsscheuren van groot belang. Er is weinig bekend over de reparatieprocedure van vermoeiingsscheuren in gelaste verbindingen gemaakt van zeer hoge sterkte staal soorten en daarmee de verlenging van de vermoeiingslevensduur na de reparatie. Het hoofddoel van dit promotieonderzoek is het vaststellen van de vermoeiingssterkte van gerepareerde gelaste verbindingen, gemaakt van zeer hoge sterkte staal. De nadruk is gelegd op gewalste staalsoorten en gietstaalsoorten met een vloeisterkte van 690 MPa en 890 MPa. Het onderzoek bestaat uit een literatuurstudie, een experimentele studie en een analyse waarin de experimentele resultaten zijn vergeleken met voorspellingsmodellen en literatuur.

Het ontstaan van vermoeiingsscheuren in gelaste verbindingen gebeurt meestal bij de lasteen. In het onderzoek van Pijper (2011), werd onverwacht scheurinitiatie en scheurgroei waargenomen in het moedermateriaal van gelaste verbindingen, gemaakt van zeer hoge sterkte staalsoorten. Visuele inspectie van de breukoppervlakken heeft aangetoond dat de scheurinitiatiepunten enkele onvolkomenheden bevatten. Er werd een literatuurstudie over de mogelijke onvolkomenheden in staal en de effecten ervan op de vermoeiingssterkte van het materiaal uitgevoerd. Uit de studie bleek dat de onvolkomenheden op het oppervlak en net onder het oppervlak kunnen leiden tot initiatie van vermoeiingsscheuren in het materiaal onder zeer hoge aantallen wisselingen. Bovendien bleek dat de oorsprong en de oorzaak van onvolkomenheden door een inspectie met een elektronenmicroscop werden bepaald. Daarom is een microscopisch onderzoek uitgevoerd op de breukoppervlakken van proefstukken van het moedermateriaal dat was bezwaken. Daarnaast werden metingen aangaande de chemische samenstelling gedaan bij de scheurinitiatiepunten van het moedermateriaal van gewalst staal. Uit microscopisch onderzoek blijkt dat de inwendige poriën het ontstaan van vermoeiingsscheuren in gietstaal veroorzaken. In het gewalst staal (moedermateriaal) werden de reparatielassen ontdekt bij de vermoeiingsscheurinitiatie punten. Dit betekent dat het moedermateriaal van het gewalste staal tijdens het fabricageproces werd beschadigd en dat de beschadigde staalplaten door toepassing van een of andere lasprocedure zijn gerepareerd.

De grootste uitdaging van het huidige onderzoek was het vaststellen van een reparatieprocedure voor de te repareren vermoeiingsscheuren in gelaste verbindingen. Er is een uitgebreide literatuurstudie gedaan om de bestaande beschikbare reparatie procedures te beoordelen. De belangrijkste uitkomst van de literatuurstudie is dat de reparatieprocedure voor de door vermoeiingsbeschadigde gelaste verbindingen nog niet is gestandaardiseerd. De nadruk werd gelegd op de meest gebruikte methoden, zoals de methode van het boren van een gat aan het begin en het einde van de scheur, slijpen, peening, het toepassen van de splice platen methode, lassen en combinaties van deze methoden. De literatuurstudie toont

aan dat reparatie door lassen met daarop volgend van een high frequency mechanical impact treatment (HFMI) wat resulteert in een hoge vermoeiingssterkte voor de gerepareerde gelaste verbindingen. Met HFMI is de scheurinitiatielevensduur en het beginstadium van de scheurgroeilevensduur verbeterd. Pijpers (2011) concludeerde dat de scheurinitiatielevensduur van de gelaste verbindingen gemaakt van zeer hoge sterkte staal, langer is dan verwacht. Aangezien het materiaal een positieve invloed op de scheurinitiatielevensduur heeft, is de reparatie met lassen zonder HFMI gekozen voor experimenten. In de literatuur worden de lasprocedures voor reparatielassen niet besproken. Overleg met de industrie en The Welding Institute (TWI) heeft ertoe geleid dat de lasprocedure waarmee oorspronkelijke lasverbinding is gelegd -voor het optreden van vermoeiingsschade- ook voor de reparatielassen kan worden gebruikt.

De effectiviteit van de reparatieprocedure kan door middel van een vergelijking tussen de vermoeiingssterkte van gerepareerde gelaste verbindingen en de vermoeiingssterkte van originele gelaste verbindingen worden beoordeeld. De resultaten van het onderzoek van Pijpers (2011) waren beschikbaar, waarbij de nadruk lag op de vermoeiingssterkte van gelaste verbindingen, gemaakt van zeer hoge sterkte staal, en deze resultaten zijn voor de vergelijking gebruikt. Daarom zijn materialen en maten van proefstukken voor de experimentele studie van het huidige onderzoek geselecteerd aan de hand van het onderzoek van Pijpers (2011). Derhalve lag de nadruk op de reparatie van kunstmatige scheuren in het moedermateriaal en vermoeiingsscheuren in gelaste verbindingen. De scheurinitiatie in proefstukken werd met behulp van rekstroken bepaald en daarna werd de scheurgroei tot het bezwijken visueel gemonitord. Het bezwijken is gedefinieerd als de proefstukken breken in twee stukken. Met behulp van rekstroken en een test opstelling werden gemiddelde en ranges van krachten, verplaatsingen, en rekstrook metingen tijdens testen digitaal opgeslagen. Om de scheurinitiatielevensduur te bepalen werd een alarmsysteem gebruikt. Indien een rekstrook zich dicht bij een scheur bevond en er werden afwijkende waarde range van 50 μ rek bereikt, schakelde het alarmsysteem de test opstelling uit. Met behulp van die rekstrook wordt de locatie van de vermoeiingsscheur gedefinieerd. Scheurinitiatie werd in de experimenten gedefinieerd als het aantal wisselingen tot de eerste afbuiging van de dichtst bij de scheur gelokaliseerde rekstrookmeting. De gemiddelde waarden van rekstrook metingen zijn met behulp van de uniaxiale wet van Hook omgezet om de nominale spanningen te berekenen.

Het experimentele programma van het onderzoek betrof de proefstukken van een gerepareerde kunstmatige scheur in het moedermateriaal en gerepareerde door vermoeiing beschadigde V-las verbindingen. De moedermateriaal strips werden uit platen van S690 en S890 gesneden. Met vonkverspanen werd een elliptische kunstmatige scheur in het midden van de proefstukken gecreëerd. De lengte van de kunstmatige scheur was gelijk aan de halve breedte van het proefstuk, en de diepte van de kunstmatige scheur bedroeg de helft van de dikte van het proefstuk. De V-las proefstukken werden gemaakt van gelaste verbindingen uit gewalst staal en gewalste staal platen en verbindingen uit gewalst staal en

uit gietstaal. De materialen voor de proefstukken waren de gewalste staalsoorten S690 en S890 en respectievelijk de gietstaalsoorten G10MnMoV 6-3 en G18NiMoCr 3-6. Om een vloeiende laswortel geometrie te creëren, werden de lassen met keramische backing uitgevoerd. De proefstukken werden getest met een vier punts buigproef opstelling. De V-las proefstukken werden zodanig beproefd dat er vermoeiingsscheuren bij de lasteen ontstonden. De scheurgroei werd visueel gemonitord. Indien de scheurlengte van de breedte van het proefstuk bereikte, werd het experiment beëindigd en de gecreëerde scheuren werden met lassen gerepareerd. Voor V-las proefstukken werd dit stadium de scheurvoorbereidings fase genoemd.

De reparatie van vermoeiingsscheuren is in een aantal stappen uitgevoerd. Ten eerste werd een magnetisch onderzoek op de gelaste verbindingen uitgevoerd om de vermoeiingsscheuren te detecteren. De gedetecteerde scheuren werden met behulp van een slijp- en freestol weggeslepen. Het slijpproces werd geleidelijk uitgevoerd met regelmatig magnetisch onderzoek. Op die manier werd ervoor gezorgd dat de scheuren volledig verwijderd werden en ook om onnodig diepe groeven te vermijden. In sommige proefstukken waren vermoeiingsscheuren in de laswortel van de verbinding ontstaan. De wortelscheuren werden ook via de laskap gerepareerd met het verwijderen van materiaal vanaf de laskap tot de laswortel. Na het scheur verwijderingsproces werd de voorbereide lasnaad door middel van lassen gevuld. De lasprocedure van de oorspronkelijke lasverbinding werd ook voor de reparatielas toegepast. Na het lassen werd de lasgeometrie van de gerepareerde lasverbinding door slijpen aangepast om een vloeiende overgang tussen het las- en het moedermateriaal te bewerkstelligen. De reparatie van de kustmatige scheuren in het moedermateriaal werd met het volgen van dezelfde procedure gedaan. Het enige verschil was dat magnetisch onderzoek in het beginstadium niet nodig was, want de locatie en de lengte van kunstmatige scheur waren bekend en konden met het blote oog worden waargenomen. In V-las proefstukken werden vermoeiingsscheuren bij de lasteen van de lasverbinding geïnitieerd en deze zijn gerepareerd. Daardoor heeft de gerepareerde kant van de lasverbinding een nieuwe lasteen, terwijl de andere kant van de lasverbinding nog steeds de oorspronkelijke lasteen heeft, die aan een aantal wisselingen tijdens de scheur voorbereidingsfase werd blootgesteld. Als de cumulatieve schaderegel van Miner wordt nageleefd, is er grote kans dat er vermoeiingsscheuren bij de oorspronkelijke lasteen na de reparatie ontstaan. Het doel van het onderzoek was om de vermoeiingssterkte van gerepareerde lassen te bepalen. Daarom was het noodzakelijk om scheurinitiatie bij de lasteen van de oorspronkelijke las na de reparatie te vermijden. Derhalve werd de lasteen van de originele las met High Frequency Impact Treatment (HiFIT) behandeld. Daarna werden de gerepareerde proefstukken opnieuw beproefd met hetzelfde spanningsniveau als in de scheurvoorbereidingsfase.

In aanvulling op de vermoeiingsproeven zijn er scheurgroeitests op het moedermateriaal van S690 en S890 gewalste staalsoorten gedaan. Initiële defecten zijn op de proefstukken aangebracht en werden cyclisch belast in een vier punts buigstestopstelling. De

scheurgroei in de proefstukken werd met scheurgroeiastroken gemonitord. De scheurgroeiparameters en drempelwaarde van spanningsintensiteitsfactor werden voor zeer hoge sterkte staal bepaald en de scheurgroeiparameters werden gebruikt voor schatting van de scheurgroei levensduur van gelaste proefstukken.

Een literatuurstudie werd uitgevoerd naar analytische modellen ten behoeve van de voorspelling van de vermoeiingslevensduur. De totale vermoeiingslevensduur bestaat uit twee fasen: scheurinitiatielevensduur en scheurgroei levensduur. De kerfspanningstheorie werd gebruikt voor de voorspelling van de scheurinitiatielevensduur. De toepassingsprocedure van de theorie wordt door Hück et al. (1981) en in de FKM-richtlijn samengevat. Beide bronnen zijn in de huidige studie gebruikt. De modellen zijn een functie van verschillende parameters zoals de vloeisterkte van het materiaal, gemiddelde spanning, plaatdiktes, belastingmodus, lashoek en lasradius. De effecten van deze parameters op vermoeiingssterkte werden bestudeerd. De scheurgroei levensduur werd berekend op basis van de breukmechanicatheorie. De scheurgroei snelheid is een functie van de spanningsintensiteitsfactor die wordt bepaald door scheurmaten, geometrie van een scheur, plaatdikte, plaatbreedte en lasbreedte. De effecten van deze parameters op de scheurgroei levensduur werden afzonderlijk bestudeerd.

De vermoeiingstestresultaten werden met de resultaten van de voorspellingsmodellen vergeleken. Niet alle waarden van de input parameters voor de voorspellingsmodellen werden tijdens het fabricageproces en het testen gemeten. De vermoeiingssterkte werd met conservatieve waarden voor de onbekende parameters voorspeld en deze conservatieve waarden voor de onbekende parameters werden aan de hand van de literatuur bepaald. Om met de effecten van de onbekende parameters en de aannames van voorspellingsmodellen rekening te houden, zijn de resultaten van de experimenten aangepast met invloedsfactoren en werd er een referentie spanningsrange bepaald. De vermoeiingssterktecurves van de voorspellingsmodellen werden met de aangepaste testresultaten vergeleken. De resultaten van het experimenten werden met de gemiddelde spanningsfactor en de belastingmodus factor aangepast. De gemiddelde spanningsfactoren werden berekend uitgaande van een restspanning gelijk aan de vloeigrens en een trekbelasting. De voorspellingscurves kwamen goed overeen met de testresultaten. Voor de statistische analyse werd de coëfficiënt voor de lineaire regressie gekozen als variabele of als $m = -3$ of $m = -5$. Voor alle coëfficiënten is de karakteristieke vermoeiingssterkte en de gemiddelde vermoeiingssterkte bepaald bij $2 \cdot 10^6$ wisselingen voor spanningsranges zoals die zijn gemeten en voor de aangepaste spanningsranges. De vermoeiingssterkte werd met de vermoeiingssterkte van de originele lasverbindingen (niet gerepareerd) vergeleken.

De vermoeiingssterktecurves uit de statistische analyse zijn met de relevante detail categorie van EN 1993-1-9 (2006) vergeleken. De vermoeiingssterktecurves, bepaald op basis van de ruwe data en de aangepaste data, voldeden aan de eisen van de detail categorieën. Bovendien zijn de vermoeiingssterktecurves van testresultaten van de moeder materiaal vergeleken met de vermoeiingscurves van DNGL C203 (2016) en de

curves van testresultaten toonden een goede overeenkomst met de curves van de norm. De vermoeiingscurves van de gerepareerde lasverbindingen zijn vergeleken met de vermoeiingscurves van de originele lasverbindingen en het bleek dat de vermoeiingssterkte van de door vermoeiing beschadigde lasverbindingen met de originele lasprocedure kunnen worden gerepareerd. Overigens, na de reparatie, waren er meer run-outs, hetgeen betekent dat de vermoeiingssterkte van de reparatielas zelfs beter kan zijn dan van de originele las. De curves van de voorspellingsmodellen kwamen goed overeen met de testresultaten. Vooral de voorspellingsmodellen volgens de FKM richtlijn leidden tot een nauwkeurige voorspelling van de vermoeiingssterkte.

Table of contents

SUMMARY	I
SAMENVATTING.....	VII
TABLE OF CONTENTS	XIII
LIST OF SYMBOLS.....	XIX
ABBREVIATIONS	XXIII
CHAPTER 1 INTRODUCTION	1
1.1 General	1
1.2 Very high strength steel.....	2
1.3 Problem definition	3
1.4 Research objectives.....	5
1.5 Outline.....	5
PART I: MATERIAL IMPERFECTIONS	7
CHAPTER 2 LITERATURE REVIEW.....	9
2.1 Introduction	9
2.2 Possible defects in steels	10
2.2.1 Defects in cast steels.....	10
2.2.2 Rolling defects	15
2.2.3 Acceptance criteria of defects	20
2.3 Fatigue strength of material containing small defects	30
2.4 Effect of surface roughness on fatigue strength	35
2.4.1 General	35
2.4.2 Theoretical approach of evaluation of surface roughness	37
2.5 Effect of inclusions on fatigue strength.....	40

2.6	Critical inclusion size for steel.....	41
2.6.1	The conventional method of extrapolating experimentally	42
2.6.2	Estimation critical inclusion size.....	43
2.7	Estimation of maximum inclusion size in material	47
2.7.1	Extreme value theory.....	47
2.7.2	The procedure for extreme value defect rating.....	48
2.8	Summary	52
CHAPTER 3 MICROSCOPIC EXAMINATION OF THE FRACTURE SURFACES		55
3.1	Introduction	55
3.2	Test material and test specimens.....	58
3.3	Preparation for microscopic examination	58
3.4	Microscopic examination on fracture surfaces.....	60
3.4.1	Fracture surfaces of rolled steels	60
3.4.2	Fracture surfaces of cast steels	72
3.5	Summary	76
PART II: REPAIR OF FATIGUE CRACKS IN WELDED CONNECTIONS.....		79
CHAPTER 4 LITERATURE REVIEW.....		81
4.1	Introduction	81
4.2	Repair methods for shallow fatigue cracks.....	82
4.2.1	Grinding.....	82
4.2.2	Peening	86
4.2.3	Gas tungsten arc (GTA) remelting	94
4.3	Repair methods for deep fatigue crack.....	95
4.3.1	Hole drilling.....	95
4.3.2	Splice plate.....	100
4.3.3	Repair by welding	103
4.4	Summary	109
CHAPTER 5 PLATE EXPERIMENTS.....		113
5.1	Introduction	113
5.2	Experimental programme	114

5.2.1	Fatigue test programme	114
5.2.2	Fatigue test rigs	115
5.2.3	Crack monitoring.....	117
5.2.4	Weld shape.....	119
5.3	Test specimen preparation.....	121
5.3.1	Specimens with an artificial crack in the base material	121
5.3.2	V-shape welded specimens made of rolled steels.....	123
5.3.3	V-shape welded specimens made of cast and rolled steels	125
5.4	Repair procedures	127
5.4.1	Repair of artificial crack in base material	127
5.4.2	Repair of fatigue cracks in V-shape welded plates.....	130
5.5	Fatigue test results.....	136
5.5.1	Repaired artificial crack in the base material	136
5.5.2	V-shape welded specimens made of rolled steels.....	138
5.5.3	V-shape welded specimens made of cast and rolled steels	141
5.6	Summary	143
CHAPTER 6 FATIGUE CRACK GROWTH EXPERIMENTS.....		145
6.1	Introduction	145
6.2	Experimental programme	146
6.2.1	Test programme	146
6.2.2	Preparation of specimens	146
6.2.3	Test setup.....	147
6.2.4	Crack propagation monitoring.....	148
6.2.5	Testing procedure.....	152
6.3	Test results.....	154
6.3.1	Crack growth in base material.....	154
6.3.2	Analysis of the test results	156
6.4	Summary	161
PART III: ANALYSIS OF THE TEST RESULTS.....		163
CHAPTER 7 LITERATURE REVIEW.....		165
7.1	Introduction	165

7.2	Notch stress approach	166
7.2.1	Background and principles.....	166
7.2.2	Critical distance approach.....	168
7.2.3	Fictitious notch rounding approach	169
7.2.4	Highly stressed volume approach.....	169
7.2.5	Calculation procedure.....	170
7.3	Fracture mechanic approach.....	171
7.3.1	Background and principles.....	171
7.3.2	Fracture mechanics approach for fatigue crack growth	173
7.3.3	Calculation procedure.....	174
7.4	Analytical prediction of fatigue limit	175
7.5	Fatigue assessment from the FKM guideline.....	177
7.5.1	Nominal stress approach.....	178
7.5.2	Local stress approach.....	187
7.6	Summary	190
CHAPTER 8 FATIGUE LIFE PREDICTION		193
8.1	Introduction	193
8.2	Prediction of fatigue crack initiation life	194
8.2.1	Analytical prediction of fatigue endurance limit	194
8.2.2	Fatigue endurance limit prediction according to the FKM guideline.....	208
8.3	Prediction of fatigue crack propagation life.....	216
8.3.1	Thickness factor	219
8.3.2	Initial crack size factor.....	220
8.3.3	Loading mode factor.....	221
8.3.4	Crack shape factor	222
8.3.5	Weld width factor.....	224
8.3.6	Plate width factor	225
8.4	Comparison of predictions and test results	226
8.4.1	Repaired artificial crack in the base materials.....	227
8.4.2	V-shape welded specimens made of rolled steels.....	230
8.4.3	V-shape welded specimens made of cast and rolled steels	233
8.4.4	Base material cracks	237

8.5	Summary	241
CHAPTER 9 ANALYSIS OF FATIGUE TEST RESULTS		243
9.1	Introduction	243
9.2	Approach of analysis	244
9.2.1	Adjustment factors for test data.....	244
9.2.2	Statistical analysis	246
9.3	Evaluation of fatigue tests data	247
9.3.1	Repaired artificial crack in the base material	248
9.3.2	V-shape welded connections made of rolled and cast steels	271
9.4	Summary	310
PART IV: CLOSURE.....		313
CHAPTER 10 CONCLUSIONS AND RECOMMENDATIONS		315
10.1	Evaluation of research project	315
10.2	Conclusions	317
10.2.1	Microscopic examinations on the fracture surfaces.....	317
10.2.2	Fatigue crack growth tests.....	318
10.2.3	Fatigue life prediction models.....	319
10.2.4	Fatigue tests on base material of very high strength steels with a repaired artificial crack.....	320
10.2.5	Fatigue tests on repaired V-shape welded connections made of high strength rolled and cast steels	322
10.3	Recommendations for further research.....	327
REFERENCES.....		331
APPENDICES		341
Appendix A. Material properties and manufacturing of specimens.....		343
Appendix B. Material specification.....		347
Appendix C. Manufacturing steps and geometry of the specimens.....		351
Appendix D. Repair of the specimens		355
Appendix E. Fatigue test results.....		445
Appendix F. Hardness measurements.....		453

List of symbols

a	Crack length in plate thickness direction	[mm]
a_f	Allowable crack length in plate thickness direction	[mm]
a_i	Initial crack length in plate thickness direction	[mm]
a_N	Intersection on log N axis	[-]
a_R	Depth of surface roughness	[μm]
a_s	Critical depth for surface roughness	[μm]
b	Regression coefficient	[-]
c	Crack length in plate width direction	[mm]
c_f	Allowable crack length in plate width direction	[mm]
c_i	Initial crack length in plate width direction	[mm]
d	Diameter or width of the specimen	[mm]
da/dN	Crack growth rate in plate depth direction	[mm/cycle]
$d_{0,9}$	Depth of the highly stressed volume	[mm]
$f_{ai,Np}$	Initial crack size factor	[-]
$f_{cs,Np}$	Crack shape factor	[-]
f_{FAT}	Fatigue class conversion factor	[-]
$f_{lm,Ni}$	Loading mode factor, crack initiation stage	[-]
$f_{lm,Np}$	Loading mode factor, crack propagation stage	[-]
$f_{lm,b,Nf}$	Loading mode factor for base material crack, total fatigue life	[-]
$f_{lm,w,Nf}$	Loading mode factor for weld toe crack, total fatigue life	[-]
$f_{L/t,Np}$	Weld width factor, crack propagation stage	[-]
f_m	Mean stress factor	[-]
f_{Ni}	Ration of N_i to N_f	[-]
f_{Np}	Ration of N_p to N_f	[-]
$f_{nr,Ni}$	Notch radius factor, crack initiation stage	[-]
f_{sr}	Surface roughness factor	[-]
$f_{sr,\sigma}$	Surface roughness factor for nominal stress	[-]
$f_{sr,\tau}$	Surface roughness factor for shear stress	[-]
$f_{t,Ni}$	Thickness factor, crack initiation stage	[-]

$f_{t,Np}$	Thickness factor, crack propagation stage	[-]
f_w	Net area correction factor	[-]
$f_{w,\sigma}$	Fatigue strength factor for normal stresses	[-]
$f_{w,\tau}$	Fatigue strength factor for shear stresses	[-]
$f_{w,Np}$	Plate width factor, crack propagation stage	[-]
$f_{\theta,Ni}$	Weld toe angle factor, crack initiation stage	[-]
k	Slope of fatigue strength curve	[-]
k_s	Thickness factor, EN 1993-1-9	[-]
m	Slope of the fatigue curve	[-]
n	Number of specimens	[-]
n	Exponent constant for thickness factor	[-]
$n_{\sigma}(\rho)$	$K_t - K_f$ ratio for local stress gradient	[-]
$n_{\sigma}(d)$	$K_t - K_f$ ratio for nominal stress gradient	[-]
s	Multi-axiality coefficient	[-]
s	Standard deviation	[-]
t	Thickness of specimens	[mm]
x_i	$\text{Log}\Delta\sigma$	[-]
y_i	$\text{Log}N$	[-]
C	Crack growth rate coefficient	[mm/cycle]
C_L	Location constants	[-]
F_Z	Cumulative probability function	[-]
G_{σ}	Stress gradient for normal stresses	[mm ⁻¹]
$G_{\sigma,d}$	Nominal stress gradient	[mm ⁻¹]
$G_{\sigma,\rho}$	Local stress gradient	[mm ⁻¹]
G_{τ}	Stress gradient for shear stresses	[mm ⁻¹]
K	Stress intensity factor	[N/mm ^{3/2}]
K_c	Critical stress intensity factor	[N/mm ^{3/2}]
$K_{E,\sigma}$	Residual stress factor for normal stresses	[-]
$K_{E,\tau}$	Residual stress factor for shear stresses	[-]
K_f	Fatigue notch factor	[-]
\check{K}_f	Approximated fatigue notch factor	[-]
K_I	Stress intensity factor for mode I	[N/mm ^{3/2}]

K_s	Coating factor	[-]
K_t	Stress concentration factor	[-]
$K_{T,D}$	Temperature factor	[-]
K_V	Surface treatment factor	[-]
$K_{WK,a}$	Design factor for axial loading case	[-]
$K_{WK,b}$	Design factor for bending loading case	[-]
$K_{WK,s}$	Design factor for shear loading case	[-]
$K_{WK,t}$	Design factor for torsion loading case	[-]
$K_{WK,\sigma}$	Design factor for normal stresses	[-]
$K_{WK,\tau}$	Design factor for shear stresses	[-]
L	Weld width	[mm]
M	Bulging correction factor	[-]
M_b	Crack depth shape factor, bending stress component	[-]
M_f	Mean stress sensitivity	[MPa]
M_{kb}	Stress concentration correction factor, bending stress	[-]
M_{km}	Stress concentration correction factor, membrane stress	[-]
M_m	Crack depth shape factor, membrane stress component	[-]
N	Number of cycles	[Cycles]
N_c	Number of cycles at characteristic stress range	[Cycles]
N_f	Total fatigue life	[Cycles]
N_i	Number of cycles at crack initiation	[Cycles]
N_{knee}	Number of cycles at knee point of fatigue strength curve	[Cycles]
R	Stress ratio	[-]
R_z	Average value of surface roughness	[μm]
S_0	Inspection area for inclusion	[mm^2]
$V_{0,9}$	Highly stressed volume	[mm^3]
W	Plate width	[mm]
α^*	Critical distance	[mm]
ε	Sum of unknown random errors	[-]
η	Notch sensitivity factor	[-]
θ	Weld toe angle	[$^\circ$]
ρ	Radius	[mm]

ρ_f	Fictitious notch radius	[mm]
ρ^*	Microstructural support length	[mm]
σ	Applied stress	[MPa]
σ_a	Stress amplitude	[MPa]
$\sigma_{Ea,0}$	Fatigue endurance limit for zero mean stress	[MPa]
σ_{Ea}	Endurance stress amplitude of material	[MPa]
σ_{kaE}	Endurance stress amplitude of notch	[MPa]
σ_m	Mean stress	[MPa]
σ_{na}	Nominal stress amplitude	[MPa]
σ_{nom}	Nominal stress	[MPa]
σ_{notch}	Stress at the notch	[MPa]
$\sigma_{notch,a}$	Actual stress at the notch	[MPa]
$\sigma_{notch,all}$	Allowable notch stress	[MPa]
σ_r	Residual stresses	[MPa]
σ_u	Tensile strength	[MPa]
σ_w	Fatigue limit for material with defects	[MPa]
$\sigma_{M,w}$	Fatigue limit for defect free material	[MPa]
σ_y	Yield strength	[MPa]
$\varphi_{M,c}$	Critical inclusion diameter for steel matrix	[μm]
$\varphi_{R,c}$	Critical inclusion diameter for surface roughness	[μm]
χ	Normalized stress gradient	[-]
$\sqrt{\text{area}}$	Area of imperfection perpendicular to applied stress	[μm]
$\sqrt{\text{area}_R}$	Equivalent imperfection area for surface roughness	[μm]
$\Delta\varepsilon$	Strain range	[-]
$\Delta\sigma$	Stress range	[MPa]
$\Delta\sigma_b$	Bending stress range component	[MPa]
$\Delta\sigma_c$	Characteristic fatigue strength	[MPa]
$\Delta\sigma_{n,Ni}$	Adjusted test data for crack initiation life	[MPa]
$\Delta\sigma_{n,Np}$	Adjusted test data for crack propagation life	[MPa]
$\Delta\sigma_m$	Membrane stress range component	[MPa]
$\Delta\sigma_{mean}$	Mean fatigue strength	[MPa]

$\Delta\sigma_n$	Nominal stress range	[MPa]
$\Delta\sigma_{nE}$	Endurance stress range	[MPa]
$\Delta\sigma_{test}$	Measured stress range during fatigue tests	[MPa]
$\Delta\sigma_{n,b,Nf}$	Adjusted test data for base material crack, total fatigue life	[MPa]
$\Delta\sigma_{n,w,Nf}$	Adjusted test data for weld toe crack, total fatigue life	[MPa]
Δa	Crack growth increment in depth direction	[mm]
ΔF	Force range	[N]
ΔK	Stress intensity range	[N/mm ^{3/2}]
ΔK_c	Critical stress intensity range	[N/mm ^{3/2}]
ΔK_{th}	Threshold stress intensity range	[N/mm ^{3/2}]
ΔN	Increment of number of cycles	[Cycles]

Abbreviations

4pb	Four point bending
EDM	Electrical discharging machining
EDS	Energy dispersive X-ray spectroscopy
FCAW	Flux core arc welding
HFMI	High frequency mechanical impact treatment
HiFIT	High frequency impact treatment
IIW	International Institute of Welding
Hv	Material hardness
NDT	Non-destructive testing
PIT	Pneumatic impact treatment
TWI	The Welding Institute
UP	Ultrasonic peening
UIP	Ultrasonic impact peening

Chapter 1

Introduction

1.1 General

The common demand in civil engineering industry is to design simple and highly loaded structures from an economical point of view. Optimisation of fabrication and assembly cost could be realised by minimizing the number of joints, complexity of joints and use of slender members. The use of very high strength steel provides slender members with reduced wall thicknesses. The decrease of wall thickness results in reduction of self-weight and volume of structures which lead to cost saving in production, transportation and erection. In addition, decrease of the wall thicknesses of members will allow for smaller size of weld volumes and consequently, the reduction in weld consumables and lower energy consumption for welded connections.

However, slender members show high tendency to buckling, which is mainly a function of the elastic modulus of the material and the elastic modulus of steel is independent of the yield strength. Therefore, copying steel structures made of mild strength steels to identical very high strength steel structures would not lead to benefitting from the advantages of very high strength steels. Accordingly, the design methodology needs to be modified for very high strength steels. Truss structures can provide a solution for limiting deflection in range of acceptance criteria for deflection governed steel members and to overcome the stability problem of the slender elements.

Moreover, low self-weight of very high strength structures causes high variation of the stresses under live loads, which results in a high nominal stress range in the structures. For fatigue loaded structures, it makes fatigue strength of the structures one of the important governing design criteria. With decreasing stress concentration in the connections, low fatigue life due to high nominal stress range can be compensated. The freedom of choosing the shape of cast steels should result in joints with a lower stress concentration. Hence, truss structures with cast joints can be one of the options for effective application of very high

strength steels in fatigue loaded structures [Pijpers, 2011]. However, fatigue damage is inevitable for fatigue loaded welded steel structures. Therefore, the repair of the fatigue cracks in welded connections is unavoidable to prolong the fatigue life. In case of repair of welded connections made of very high strength steels little is known for the repair procedure and fatigue life extension after the repair. A fatigue crack repair procedure is needed for the repair of fatigue damaged welded connections made of very high strength steels.

1.2 Very high strength steel

The technological development makes it possible to produce very high strength steels with desirable weldability, toughness and ductility properties. Especially, the automotive and crane industry have been making use of very high strength steels in the last few decades. However, the tendency of the use of very high strength steels in civil engineering structures is still not very common due to limited knowledge about the consequences of manufacturing process and experimentally determined structural behaviour of the material. Accordingly, design codes provide limited information for designing very high strength steel structures for steels with yield strengths above 700 MPa [Pijpers, 2011]. Nowadays, very high strength steels can be produced with yield strengths up to 1300 MPa for civil engineering application. In the current study, it was concentrated on the quenched tempered S690 and S890 rolled and cast steels. Table 1.1 shows a general description of different steel types and the application area of these steels in buildings and civil engineering structures.

Table 1.1 Different steel types and application areas [Pijpers, 2011].

Yield strength	General	Typical steel	Applications
<300	Regular structural	S235	Buildings
300	Conventional high strength steel		Bridges
400		S355	High rise buildings
500		S460	
600			
700	Very high strength steels	S690	Cranes
800		S890	Bridges
900		S960	High rise buildings
1000		S1100	
1300		S1300	
>1300			1570/1760/1860

Research has been conducted to get familiar with the response of the high strength steel to structural loads. According to the state of the art, fatigue strength is one of the governing design criteria for an effective application of very high strength steels for fatigue loaded structures. According to design code EN 1993-1-9 (2006); part of Eurocode 3, the fatigue strength of welded connections mainly depends on the applied detail, plate thickness and machining condition and not on the steel grades.

Furthermore, in a fatigue loaded very high strength steel structure, the absolute and relative stress variation will be higher compared to those in structures made of lower grade steels. Accordingly, design methodology should be modified for high strength steel based on this stress state. Designing welded connections with lower stress concentrations might compensate fatigue strength for the stress state with high variation. The freedom of choosing the shape of the cast steels should result in joints with low stress concentrations. Therefore, the combination of very high strength rolled steels with cast steels can provide improved fatigue resistant structures.

In the last decade, more cast steel parts have been used in bridge structures, offshore structures and building structures. The common steel casting material used in bridge structures has yield strength up to 355 MPa. However, current technology makes it possible to produce cast steels up to yield strength of 1100 MPa with good weldability which makes it possible to manufacture high strength hybrid steel structures [Pijpers, 2011].

Moreover, the ratio of the yield and tensile strength of very high strength steels is generally close to unity and therefore, very high strength steels are known as brittle material. The effects of cooling process and alloy elements on mechanical properties have been comprehended in detail. With the controllable cooling process and alloy elements, very high strength steels with suitable toughness and ductility can be produced nowadays. In addition to improvements in the production process of very high strength steels, the development in the welding technology is also in progress to provide suitable welded connections. Currently, the welding consumables with a yield strength of 900 MPa are available for use in steel structures. The aim is to produce weld consumables with yield strengths of up to 1100 MPa and to improve ductility of the available weld materials. Nevertheless, with current available knowledge, it is possible to manufacture welded connections with high strength steels where all requirements for welded joints are met.

1.3 Problem definition

Pijpers (2011) studied the applicability of very high strength steels for civil engineering structures. State of the art has shown that it is technically possible to use very high strength steels for structural purposes. However, it was found out that the beneficial effects of very high strength steels can be questionable for fatigue loaded structures, due to relatively high

stress variations. In that study, it was focused on the determination of fatigue strength of very high strength steels. The improvement was made in the design methodology to compensate the detrimental effects of high stress variation by placing the welded connections outside of the high stress concentration region. This was realised by using cast joints in truss specimens. Proceeding the experiments on the truss specimens, an extensive experimental programme was carried out on plate test specimens made of very high strength steels. Unexpectedly, in the welded plate test specimens, fatigue crack initiation and propagation was observed in the base material of rolled and cast steels.

Fatigue crack initiation in the base material of welded connections results in interesting debate. Because in welded steel structures, fatigue cracks will generally initiate at weld toe of the connections. Accordingly, fatigue cracks inspections are usually executed at the welded area. If fatigue crack initiation in the base material of the welded connections made of very high strength steels could be a regular issue, the entire structures need to be inspected during fatigue cracks inspections. In some cases, it is not possible and it is too expensive. Therefore, it is absolutely essential to identify the reason of fatigue crack initiation in the base material of the welded plate specimens of that study.

Furthermore, designing sustainable structures is becoming one of the important policies of countries. Reuse of materials, prolonging the service life of the existing structure and repairing the damaged structures is part of the design of sustainable structures. Pijpers (2011) showed that the use of very high strength steels provides some advantages in terms of fatigue strength. But, little is known about repair of fatigue cracks in welded connections made of very high strength steels. Moreover, very high strength steels are highly susceptible to thermal cycles during the welding process. The effects of repairing fatigue cracks by welding, which means re-welding the material, need to be determined and it is essential to evaluate the consequence of re-welding. The results of the current research may make it closer the effective application of very high strength steels in the civil engineering industry by providing a guideline for the fatigue cracks repair procedure and the expected fatigue life extension after the repair. Figure 1.1 shows two main subjects of this research.

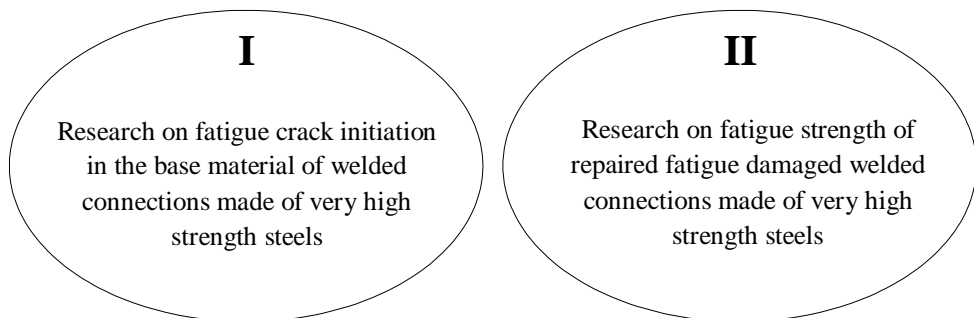


Figure 1.1 Two main parts of the research.

1.4 Research objectives

The main objective of this research is to determine the fatigue strength of repaired fatigue damaged welded connections made of very high strength cast and rolled steels. In addition, the reason of fatigue crack initiation and propagation in the base material of welded connections made of very high strength steels needs to be determined for reliable application of very high strength steels in the civil engineering industry. The objectives of the research can be summarised as follows;

- to evaluate fatigue crack initiation and propagation in the base material of welded connections made of very high strength steels;
- to determine fatigue strength of repaired fatigue damaged welded connections made of very high strength rolled and cast steels;
- to evaluate parameters which influence fatigue crack initiation life and fatigue crack propagation life;
- analytical determination of fatigue crack initiation life by notch stress approach and fatigue crack propagation life by fracture mechanics approach;
- to prepare recommendations for the fatigue strength evaluation of repaired welded connections made of very high strength steels.

Extensive literature review is performed to reveal the state of the art for the defined objectives. In the literature survey, it is concentrated on fatigue crack initiation in the base material of very high strength steels, effects of material imperfections on the fatigue strength of the base material of very high strength steels and available theories for evaluation of the material imperfections. In addition, the available fatigue crack repair procedures are evaluated and applicability conditions of the methods are examined. In order to analyse fatigue test results, a study has been carried out on the analytical prediction models for fatigue strength of welded connections.

1.5 Outline

The research consists of four parts; Part I: Material imperfections, Part II: Repair of fatigue cracks in welded connections, Part III: Analysis of the plate test results and Part IV: Closure.

Part I: Material imperfections, consists of Chapter 2 and Chapter 3. Chapter 2 gives a literature review on material imperfections and the effect of imperfections on fatigue strength of very high strength steels. Chapter 3 focuses on the results of the microscopic examination on the fracture surfaces of the base material failure of the welded connections made of very high strength steels.

Part II: Repair of fatigue cracks in the welded connections consists of Chapter 4, Chapter 5 and Chapter 6. Chapter 4 gives a literature review on fatigue crack repair methods for fatigue damaged welded connections. Chapter 5 presents an extensive experimental programme on the fatigue strength of repaired welded plate specimens made of very high strength rolled and cast steels. Chapter 6 describes fatigue crack growth tests on high strength rolled steels to determine the fatigue crack growth parameters for fracture mechanics analysis.

Part III: Analysis of the plate test results consists of Chapter 7, Chapter 8 and Chapter 9. Chapter 7 shows a literature review on the analytical models for fatigue life predictions. Chapter 8 shows fatigue crack initiation and propagation life prediction models for the repaired welded plate specimens and comparison between the prediction models and the test results. A statistical analysis of the experimental results is given in Chapter 9.

Part IV: Closure consists of Chapter 10 which presents the conclusions and recommendations of the research. Figure 1.2 schematises the thesis outlines.

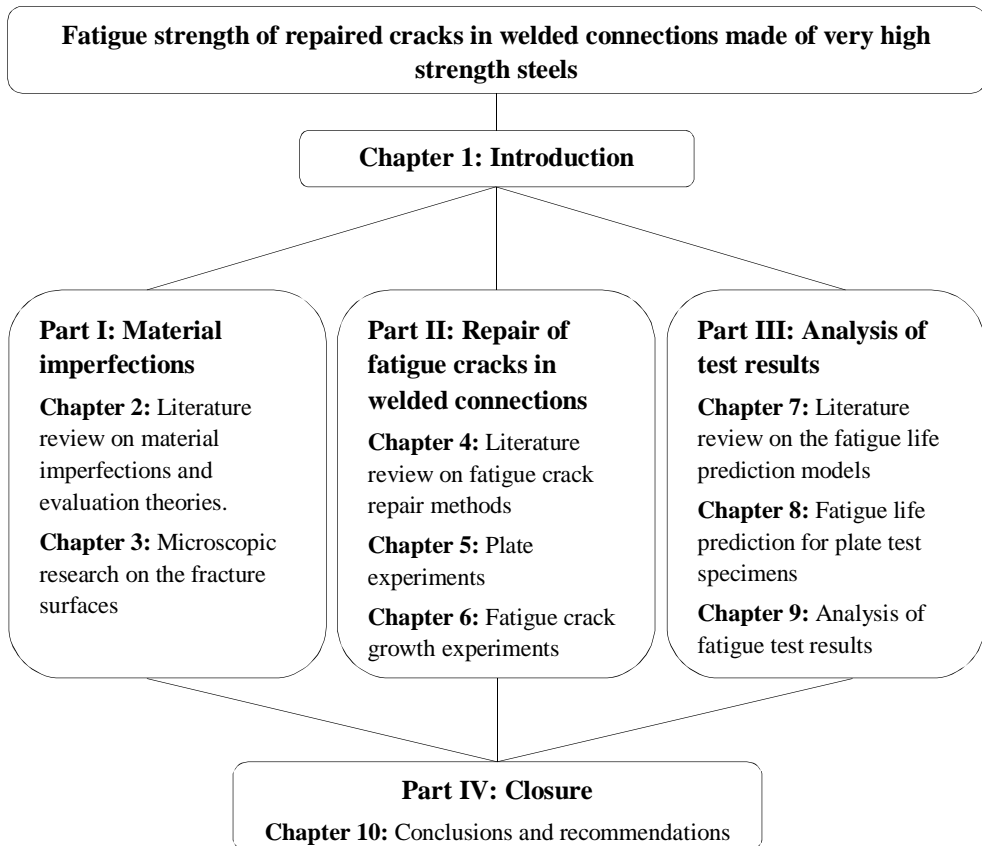


Figure 1.2 Schematic representation of the thesis outline.

Part I: Material imperfections

Part I: Material imperfections consist of Chapter 2 and Chapter 3, where the effects of the material imperfections on the fatigue strength of materials are evaluated.

Chapter 2 presents an extensive literature review on the effects of the internal material defects on the fatigue strength of very high strength steels for very high cycle fatigue life. The analytical evaluation of the internal defects for high cycle fatigue regions is dealt with. The acceptance criteria for structural steels are given based on the inspections standards.

Chapter 3 focuses on the visual and microscopic examination on the fracture surfaces of the base material failures in welded specimens from research programme of Pijpers (2011). The examination is performed on the fracture surfaces of the rolled and cast steels.

Chapter 2

Literature review

2.1 Introduction

Every metal contains defects. These can vary from an atomic scale that is located in the crystallographic structure to visibly detectable large defects that are introduced during the production process. The material defects introduced during the production process might be avoidable, or at least reduced to such a level that they require no additional treatment like heat treatment, surface cures, adding additional alloys etc. The complicated chemical and physical reactions that take place during the manufacturing process may result in inhomogeneity and defects (inclusions, pores etc.) in the material. It will cause non-uniform properties and can result in problems during processing, fabrication and service of metal structural components. An inappropriate manufacturing process or absence of a suitable control system at every stage of the production might introduce defects and residual stresses which can affect the capacity of the structure in service and make it susceptible to failure.

A finalized research programme revealed that the fatigue behaviour of welded connections made of very high strength cast and hot rolled steels are susceptible to internal material imperfections and material surface roughness [Pijpers, 2011]. In that research, extensive experimental work was executed for welded connections made of very high strength steels. Fatigue cracks initiation and propagation have been observed in the base material of some test specimens. In general, fatigue crack initiation and propagation is observed at the weld toe of the cap and root dependent on the loading situation. This provides practical solutions for the inspection of welded steel structures, where usually the weld areas are only inspected at the end of appropriate inspection intervals. The possibility of a fatigue crack in the base material of welded structures requires very detailed inspection of the entire structure which is practically impossible and would be very expensive.

The crack formation in the parent material of welded structures is not a commonly seen phenomenon and it is necessary to find out whether this also holds for structures made of

high strength steels. In this context, literature review is concentrated on possible defects in steel, and the effect of these imperfections on the fatigue strength of the structures.

Section 2.2, focuses on the identification of commonly seen imperfections in steels. Section 2.3 presents the fatigue strength of material containing small defects. Section 2.4 focuses on effects of surface roughness on the fatigue strength of materials. Section 2.5, concentrates on the effect of inclusions on the fatigue strength. Section 2.6 presents the critical inclusion size below which, fatigue cracks will not occur. Section 2.7 explains the methods to determine the maximum inclusion size in a volume of steel by using a statistical approach.

2.2 Possible defects in steels

2.2.1 Defects in cast steels

2.2.1.1 Porosity

Gas solubility in molten metal is higher than in solid metal. Consequently, some amount of the dissolved gas is extracted from the molten metal during solidification. This leads to a wide distribution of gas during the casting process. An amount of gas may also remain dissolved and results in problems during the manufacturing process or during service of the structure. The chemical reaction between some of the ingredients can also cause gas production during the melting process [Wilby et al. 2012].

Appropriate circumstances have to be created to give any air in the mould the opportunity to escape. During casting, the creation of air pockets can be avoided by completely filling the mould. In this regard, a sand mould is more suitable for extraction of air than using a permanent mould system. However, it must be taken into account that gas can also be produced by the walls of the mould due to disruption of resins at high temperature or high humidity content in the mould material. This can also cause porosity, which may be several millimetres in size, on the surface of the casting. Disturbance within the flow of the molten material can cause retention of in air such a way that the air may not have time to escape to the surface and disappear before solidification. In some casting cases, chemical additives are added just before casting, which can activate gas occurrence as a result of chemical reactions. In such circumstances, it is important to provide adequate time for finishing reactions before casting while supplying enough heat to prevent cooling of the material and keep the casting sufficiently hot to avoid solidification before the mould is filled completely [Wilby et al., 2012]. Figure 2.1 shows the pores which caused crack initiation under a fatigue load.

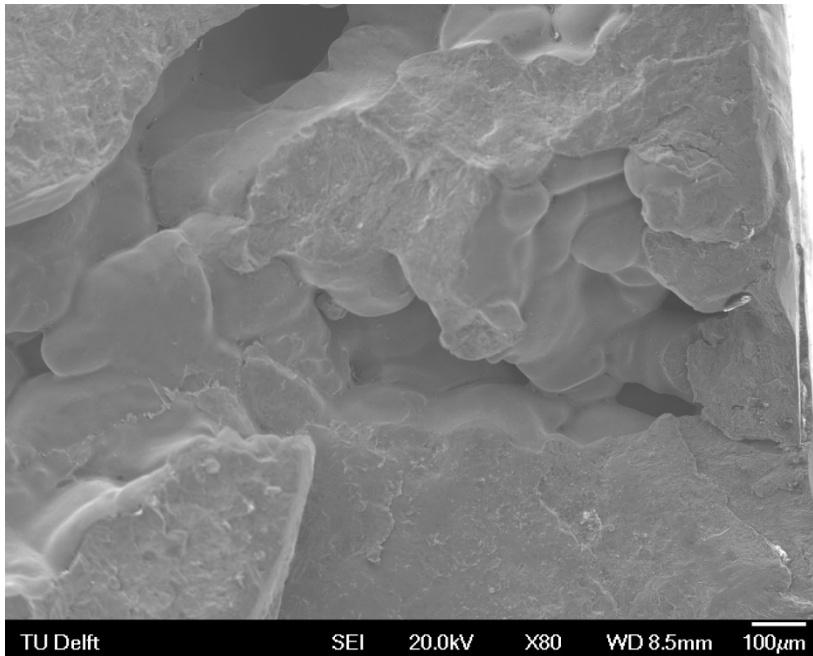


Figure 2.1 Pores on fracture surface of cast steel.

Throughout the air releasing process, pores can be connected to the surface, which can be detected by dye penetration techniques or they can fully remain in the material and radiographic techniques are needed to detect them. The detected pores are divided into two categories: macro porosity and micro porosity. Macro porosity is when the pores are large enough to be visible without magnification during radiographic inspection, while micro porosity indicates pores that are only detectable with magnification. Both macro porosity and micro porosity result from a combination of metal shrinkage and gas occurrence at the solidification phase. It has been found that the formation of pores decreases in layers containing fewer amounts of inclusions and grain finer alloys. Therefore, it has been concluded that inclusion free castings have less pores than castings which contain inclusions [Becker et al., 2002].

Usually, static properties of materials are not affected by micro porosity. However, the fatigue strength of cast alloys is negatively affected by the existence of porosity. The fatigue strength reduction is remarkable when the porosity propagates to the surface due to the resulting notch effect. There is little or no effect on the fatigue properties of material when the size of the micro pores is less than 0.2 mm. Besides the micro pore size, the shape of the pores is also important. The elongated pores have a greater effect than round pores [Becker et al., 2002].

2.2.1.2 Inclusions

The inclusions are categorised in two groups; indigenous and exogenous. Indigenous inclusions are small intermetallic particles, such as sulphides, oxides and silicates formed by chemical reactions between the various ingredient of the alloy and also with the atmosphere. They are usually very small and microscopic magnification is necessary for the identification of these indigenous inclusions (see Figure 2.2) However, when inclusions take place at grain boundaries, they particularly disturb the mechanical properties of the material. For example, sulphide films at the grain boundary are harmful to the ductility and toughness of cast steels [Becker et al., 2002]. According to Wilby et al., (2012), they will not cause a problem if they are distributed throughout an ingot or casting.

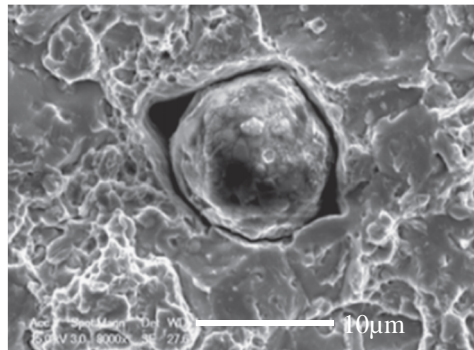


Figure 2.2 Inclusion on the fracture surface of high strength steel [Lei et al., 2012]

In contrast to indigenous inclusions, exogenous inclusions are larger and result from inadvertent unfamiliar matter, such as broken sections of refractory linings and their size can be several centimetres [Wilby et al., 2012]. After solidification of casted material, they might be located beneath the external casting surfaces, in case there is insufficient time to rise up or settle because of the density differences between the inclusions and molten metal. Exogenous inclusions are mostly oxides and mixtures of oxides and are primarily slag or dross particles, which are oxides, that result from the reaction between metal and oxygen in the air during melting. Exogenous inclusions can be removed from the melt before casting by filtration [Becker et al., 2002].

Inclusions can be found in any metal casting material and might have harmful effects. For example, a high content of inclusions can cause splitting of the bearings in service, resulting in inefficient performance of the bearings and expedite abrasion under service loading. Furthermore, under service conditions, inclusions can become stretched in the direction of the loading. Consequently, it may cause plastic deformations or fracture and fragmentation of the inclusions. Inclusions cause poor properties in transverse direction, generating local notch effects, which result in areas sensitive to fatigue cracking and several inclusions located in line can result in lamellar tearing [Wilby et al., 2012].

2.2.1.3 Segregation

The chemical element distribution in ingots may be non-uniform and some areas can become rich in certain elements of material phases while other regions still lack some amount of these elements [Wilby et al., 2012] (see Figure 2.3). The variation in chemical composition on a microscopic scale in a micro structure, such as dendrites and grains, is identified as micro segregation, while a variable distribution in the chemical composition on macroscopic scale is defined as macro segregation [Becker et al., 2002].

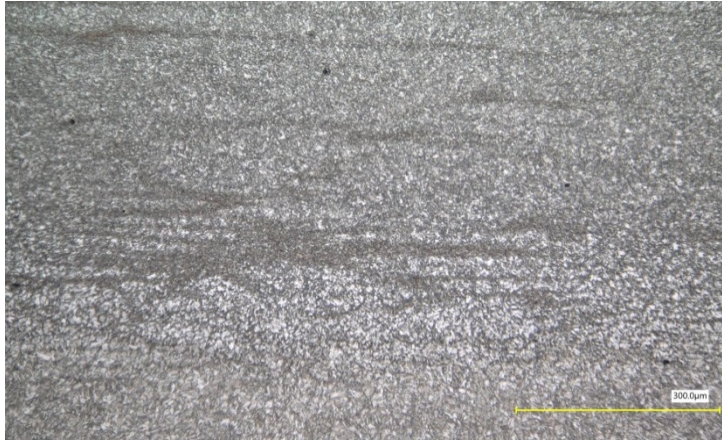


Figure 2.3 Segregation in high strength rolled steel.

Micro segregation describes the concentration of elements in inter-dendritic regions and can be a few to several microns in size. Micro segregation can be presented in a cast condition and can be removed by heat treatment. In case of macro segregation, the alloying elements show gradient variation from the surface to the centre of a casting [Becker et al., 2002]. In addition, macro segregation may form concentration gradients over a large distance. It can cause a variation in ductility of the material which might cause unprocessability of the material in the processing cycles and if it remains in the end product, it can result in non-uniform material properties. This kind of local composition difference may lead to corrosion problems, embrittlement and unacceptable end product according to material certification. [Wilby et al., 2012].

2.2.1.4 Oxide films

Similar to inclusions, oxide films are related to the pouring characteristic of the casting. Oxide films are formed on the surface of the material when it is poured into the mould. When these films are arrested in the casting instead of being released from it, it will form a linear discontinuity and will most probably be a location of crack initiation (see Figure 2.4). Elimination of oxide films results in an improvement in static properties and in the fatigue life of the material.

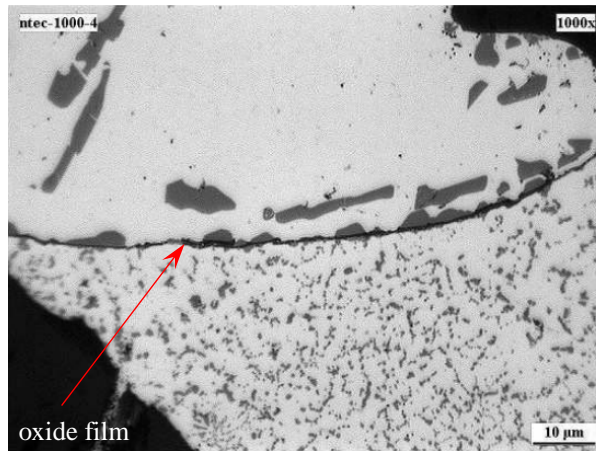


Figure 2.4 Separation in material due to an oxide film [Campbell, et al., 2006].

In nonferrous casting process, additional care needs to be taken for the formation of oxide film due to low carbon content. These films will have more detrimental defects in the material, when the films are covered by the material due to improper material flow or water falling, which may occur during falling of material from one level to another level for filling the mould. Oxide films occurrence can be eliminated by filling the casting from bottom with a controlled system, by pumping the metal into the mould using pneumatic or electromagnetic pumps [Becker et al., 2002].

2.2.1.5 Hot tear and hot cracking

Becker et al., (2002) gives quite a good description of these imperfections, which is summarised in this section. In the solidification stage, tearing or hot cracking can occur when a high amount of shrinkage occurs and when the casting has a low resistance to induced stresses by the geometrical constraints of the mould (see Figure 2.5). This type of cracking is also known as hot shortness, which usually occurs in grains of all casting alloys.

Hot cracking is identified as a crack or fracture which is caused by internal stresses that arise after solidification and during the cooling down stage. Hot tearing is a crack or fracture which occurs before completion of the solidification stage due to obstructed contraction. Hot tears occur near to the end of solidification when the shrinkage of the casting is hindered by the mould.

An appropriately selected casting process, alloy selection, part and mould design, controlled process of solidification and refinement of gains can reduce the possibility of hot crack occurrence. Resistance to cracking at the solidification temperature, which is known as hot strength, is dependent on the alloy used. The crack resistance capability of alloys shows a variation. Hence the cracking susceptibility of alloys becomes important in the final alloy selection in order to meet the crack free requirement of the final casting sections.

The use of grain refinement is necessary to ensure a fine, equated grain structure, which is important for hot-short alloys or in casting design in order to reduce cracking. The use of fine grains minimises the grain boundary effects and consequently provides a reduction in local stress concentrations.

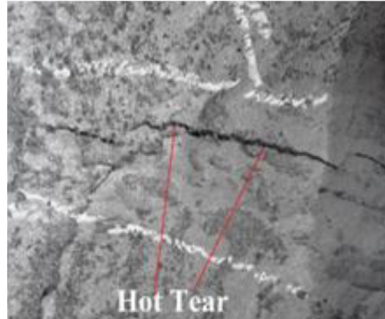


Figure 2.5 Hot tear in cast material [Juriani, 2015]

The design of the mould has an important influence on the formation of hot cracking. An inappropriate mould design usually causes hot cracking. Therefore, it is essential to prevent sudden shape changes in cross sectional areas and the use of inappropriate radii or filled corners or angles. These are important design requirements, that need to be followed to avoid stress concentration which can occur during and after solidification. Hot tear and hot cracks are usually detectable during inspection. Hot tears are quite large and usually repaired by welding. Their effects are not easily presumable in case that they are not repaired. They are usually harmful for the casting properties, but under some conditions the harmful effect is not observable. The formation of hot tears is caused by a combination of factors, such as alloy type, metal purity and mould hardness. However, improper casting design is the main cause of the hot tears. In the design stage, care should be taken that solidified sections are not exposed to tensile forces resulting from shrinkage during solidification, because the strength of alloys is not sufficient to resist the tensile forces before completion of solidification.

2.2.2 Rolling defects

Different problems in the rolling process can cause certain defects that depend on the interaction between the plastically deforming rolled piece and the elastically deforming rolling equipment: rolls and roll mill. Due to high rolling forces, the rolls straighten and bend and the entire mill is elastically deformed. Because sheet thickness is greater than the gap between unloaded tolls, this will deform the roll mill. Therefore, for getting exactly the required thickness, it is essential to know the elastic constant of the mill [Dieter et al., 1988].

Under un-loaded conditions, the rolls must be perfectly parallel to each other. Otherwise one edge of a rolled sheet will be thinner than the other edge and since volume and width are not changing, this edge of the sheet lengthens more than the other edge and causes formation of arch shape. There are two main outlooks regarding a sheet shape. The first one is related to the uniform thicknesses in transverse and longitudinal directions. Currently, this property of sheet can be measured accurately. Nowadays, it can be done by different automatically controlled systems. The second significant aspect of a rolled sheet is flatness. An accurate measurement of this property is difficult, especially during the rolling process. Measurement takes place while the sheet moves through the rolls. The rolling process has important effects on flatness of a sheet. The elongation difference between different regions of a sheet will cause waviness in a thin sheet [Dieter et al., 1988].

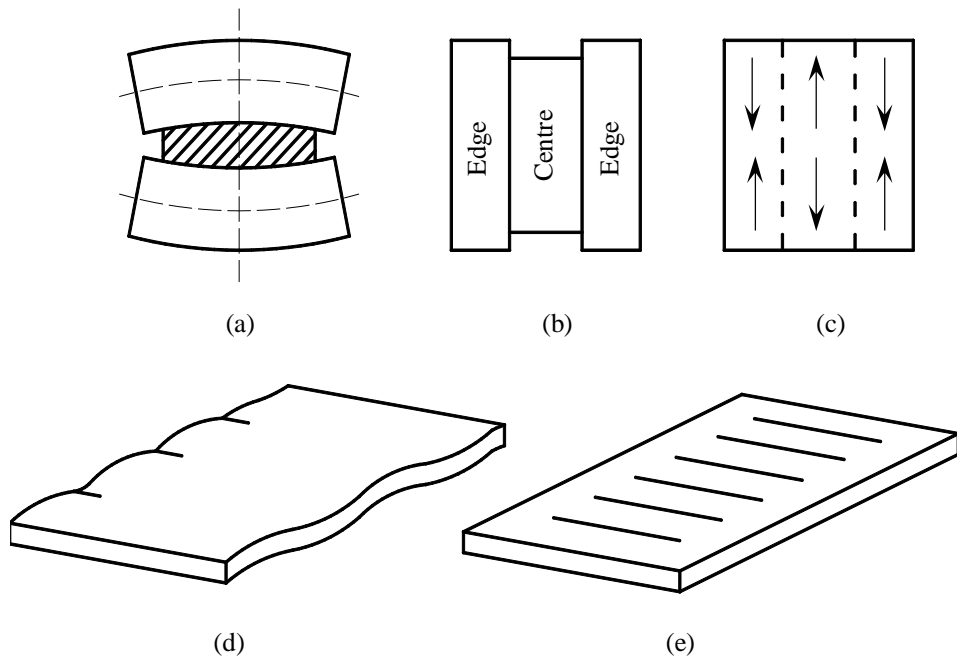


Figure 2.6 Production of long edge due to rolls deflections [Dieter et al., 1988].

When the rolls are bent as in Figure 2.6a, stretching of the edge of the sheet in longitudinal direction will be greater at the sides than in the middle of the sheet. In case of free edge, meaning that that edges are free to move relative to the centre, it will cause a shape that is indicated in Figure 2.6b. However, the sheet will sustain its body continuation and the strains due to rolling will redistribute. This will lead to tension in centre position of the sheet, while the edge of the sheet will be exposed to compression in the rolling direction as shown in Figure 2.6c. The compression stresses may result into edge buckle or a wavy edge

(see Figure 2.6d). The different condition of strain distribution at the long edge can also cause short “zipper breaks” or even crack in the centre of the sheet, depending on thickness and length of a sheet (see Figure 2.6e). This kind of discontinuities can obviously be solved by curving the roll parallel to its axis. The curving is kind of giving pre-deflection to the roll. In this way, they will provide a parallel gap to a sheet during deflection of rolls [Dieter et al., 1988].

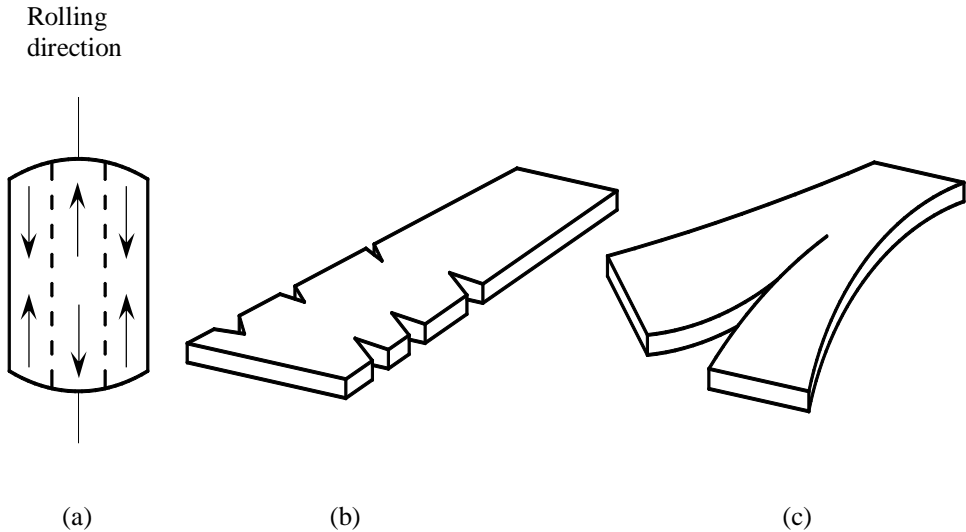


Figure 2.7 Defects due to lateral deployment [Dieter et al., 1988].

Inhomogeneity in deformation of a rolled sheet can cause problems with shape and flatness in the end product. Some kind of inhomogeneous deformation may cause cracking problems. When a work piece crosses through the rolls, all contained elements in width direction will tend to expand in lateral direction of its location. As can be expected, the transverse friction forces between rolls and the sheet are resisted to this expansion of tendency. Due to the friction hill, which is higher on the centre of the sheet, the elements at the centre area of the sheet will expand much less than the element at the outer side, near the edge. The thickness decreasing in the centre of the sheet will result in a length increase, although thickness reductions at the edge of the sheet go into lateral spread. This may result in a slight rounding at the end of the sheet (see Figure 2.7a). Since the continuity between the edge and centre exists the edges of the sheet are exposed to tension, which may cause edge cracking (see Figure 2.7b). The strain distribution indicated in Figure 2.7a may lead to a centre split to the sheet under certain circumstances (see Figure 2.7c) [Dieter et al., 1988].

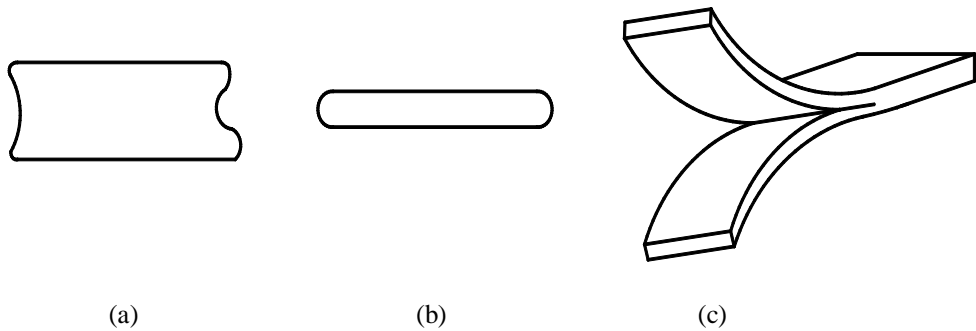


Figure 2.8 Edge shape of different rolling defects [Dieter et al, 1988].

Edge cracking can also be a result of inhomogeneous deformation in the thickness of a sheet. In some rolling conditions, only one surface of the work piece is deformed, which results into less deformations in thick slabs. The cross section of this kind of sheets is shown in Figure 2.8a. With further rolling the sheet, the overhanging material cannot be pressed directly and it will be forced to lengthen by material closer to the centre. This process establishes tensile stresses and the tensile stresses can be so high that they activate edge crack occurrence. This kind of cracking can initiate initial ingot failure in hot rolling. In case of heavy thickness reductions, in such a way that the deformation stretch in thickness direction of the sheet and centre of the sheet will show a tendency to expand laterally more than the surface, which results in barrelled edges (see Figure 2.8b). The tensile stresses due to barrelling of edges trigger to edge cracking. This kind of lateral deformation may result in greater spread occurrence near the centre, the surfaces are located in tension, while the centre is in compression. This stress distribution also occurs in the rolling direction and in case of any metallurgical weakness in the centre line of the sheet, this may cause fracture through the weak line (see Figure 2.8c). This kind of fracture is called alligatoring. This fracture type becomes important when the sheet is exposed to bending during the rolling process. The bending will occur when one roll is located higher or lower than the centreline of the roll gap [Dieter et al., 1988].

2.2.2.1 Scabs

Scabs are defined as material overlaps in different forms and degrees and they may be randomly spread over the surface of the rolled products. They are partially connected with the base metal. These defects can occur in rolling direction as tracks or lines (see Figure 2.9).

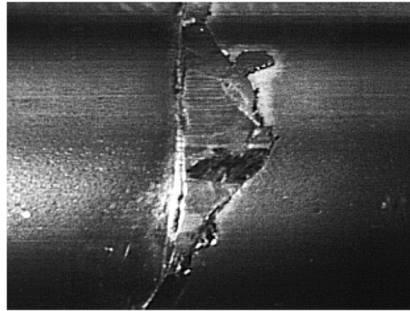


Figure 2.9 Scab on rolled steel surface [Kling et al., 2007].

Scabs disturbance may also occur during the transportation of the steel plates to the hot rolling mill and in the course of passing across the preheating furnace it will form scabs like defects during hot rolling. Additionally, any damaged or locked transport roller of the roller table causes a damaged hot strip and these damages will later become visible in the form of scabs [Becker et al., 2009].

2.2.2.2 Scale, scale tracks, scale pits

The oxygen in the atmosphere can form the iron oxide layer on the casting surface in the course of continuous slab casting. Afterwards, hot-rolling with this layer is called scale (see Figure 2.10). Scale tracks and scale pores also occur in the form of the scale.

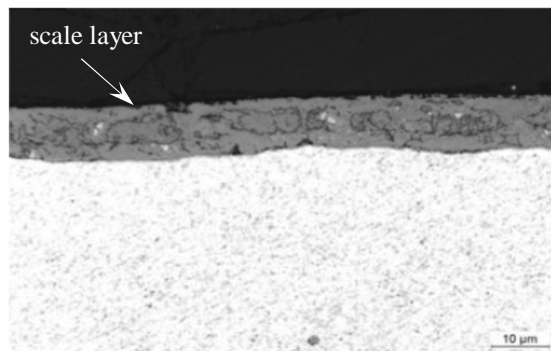


Figure 2.10 Morphology of scale layer [Yu et al., 2012].

The formation of scales depends on time and temperature and is a function of chemical composition, surface condition and temperature of located atmosphere. Charging and heating up in reheating furnace causes a rise in oxidizing atmosphere and this is removed by atomizing water on the surface with high pressures before roughing mill. The roughing mill will reduce thickness of the sheet. During the roughing mill, scales are created again and these scales are removed again before finishing mill by application of high pressure descaling. Another layer of scale can result in the course of finishing mill and with curling of the strip. The removal process of the scales must be performed with high attention to

prevent scales in the last product. On the possible causes of scales in the last product, is that they can remain in the last product due to blocked nozzles in high pressure descaling and this results in track like defects. Additionally, rolling conditions, friction on the roller gaps, wear and tear in the rollers and thermal and mechanical load on the rollers can also provide conditions for the formation of scale particles and these might be buried into the surface of the sheet [Becker et al., 2009].

2.2.2.3 Abrasion, grooves, scratches

Abrasion, grooves and scratches are formed due to mechanical damage with varying widths, depths and lengths on the surface of a rolled product (see Figure 2.11) They are mostly located longitudinally or transversely in the rolling direction. They may be lapped and may contain scales. The formation of this kind of damages occurs as a result of relative movements between the rolled sheet and parts of the rolling installation. Curling and uncurling of hot rolled sheets and impacts during transportation are mainly the reason of formation defects in longitudinal direction. Furthermore, the relative movement between loose bobbins will cause the grooves and scratches in rolled products. These imperfections can occur in hot condition of the sheet. In this case, the damaged spot will scale and may be lapped in consequent passes. This depends on the location of the damages [Becker et al., 2009].

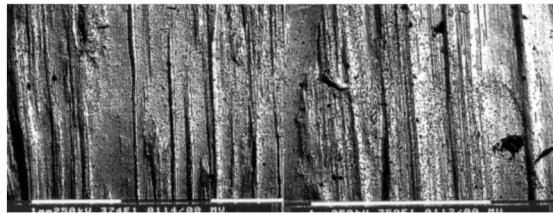


Figure 2.11 Grooves on rolled product [Gonzalez et al., 2007].

2.2.3 Acceptance criteria of defects

Technological developments provide methods to produce almost defect free materials. Consequently, this leads to more energy consumption which causes an increase of the production cost. The increase of production cost is an undesirable consequence for the material user. Therefore, it is permitted that materials may contain certain limited amounts of defects. Since materials inevitably contain defects, the defect size has to be limited in order to avoid their unfavourable effect on material properties. For this purpose, standards have been established to describe delivery conditions of the material.

Standards identify chemical composition, mechanical properties of material, allowable defects in material and its product dimensions, tolerances of dimensions and acceptance level of tolerance deviations. Defects in material can be detected by non-destructive

techniques (NDT). The acceptance levels of imperfections in materials are related to the non-destructive method used. The application of NDT is also standardised and tolerable defects in materials are mentioned in related standards. Nowadays, most of the cast steel material is examined by two NDT methods: ultrasonic examination and magnetic particle testing. The procedure and tolerable defects for cast steels is given in Section 2.2.3.1 for magnetic particles and in Section 2.2.3.2 for ultrasonic examination. The NDT examination of hot rolled steels is done for profile products and for flat products separately. Since current research is concentrated on rolled plate products, the ultrasonic examination for flat products is dealt with here. Section 2.2.3.3 gives the general procedure for ultrasonic examination of flat products with thicknesses of 6 mm or larger.

2.2.3.1 EN 1369 (2012) magnetic particle testing

The standard indicates rules for defects detection, inspection, and quality of material based on detected defects in cast steels by using magnetic particle examination. The inspection area and the percentage of casting to be inspected should be agreed between manufacturer and purchasers. The inspected area is specified by the type of discontinuity and severity level. The inspection surface of material has to be clean, free from rust, sand, scale, and moulding coating remnant, oil, grease or any other pollutant which may obstruct correct inspection. Surface of cast materials is cleaned with different methods. When sand blasting or shot blasting is used as a surface clean method, the applied pressure must be as light as possible, with which sufficient clean surface can be obtained, in order to prevent sealing or closing possible defects.

The detected discontinuity can vary in shape and size. The difference between the discontinuity evidences is made depending on the ratio the length L of evidence and its width W . If length L of detected findings is smaller than three times the width W , it is classified as a non-linear indication and it is indicated by SM. The detected indication is called linear when the length L is larger than or equal to three times the width W . The linear indications are represented by LM. This classification is done for one detected indication. But in some cases, aligned indications can be observed during the inspections. Aligned indications can be divided into two groups: linear and non-linear. An indication is defined as linear aligned indication when the distance between two indications is smaller than the length L of the longest discontinuity in the alignment. When the gap between indications is smaller than 2 mm and at least three indications are observed, these signs are defined as non-linear aligned indications. Aligned indication is represented by AM.

The qualification of the material is based on the scale of indications and their types. For this identification, the standard makes use of severity levels terminology. The severity levels are established as a reference scale for various types of detected signs. The severity levels of non-linear indication are given in Table 2.1. The severity levels are defined by the length (largest dimension of indication) of the smallest signs, L_1 , that can be taken into account for

evaluation and the maximum length, L_2 , of the indications. In case of aligned indications, L_2 is a cumulative dimension. For classification, the most unfavourable location, where the greatest severity of discontinuities has been observed, has to be selected and it must be a 105 mm x 148 mm frame.

Table 2.1 Severity levels for magnetic particle testing non-linear indications.

Characteristics		Severity levels						
		SM 001	SM 01	SM 1	SM 2	SM 3	SM 4	SM 5
Direct visual testing		Magnification glass or eyes		The naked eye				
Magnification for observation of magnetic particles signs		≤ 3		1				
Length L_1 of smallest signs to be considered in [mm]		No indication allowed	0.3	1.5	2	3	5	5
Non-linear indications (SM)	Maximum total surface area allowed in [mm ²]	-	-	10	35	70	200	500
	Maximum individual length L_1 allowed in [mm]	No indication allowed	1	2 ^a	4 ^a	6 ^a	10 ^a	16 ^a
See Annex C of the standard-Figure		-	-	C.1	C.2	C.3	C.5	C.5
^a A maximum number of two indications of the designated maximum individual lengths is permitted. Note: The evaluation should be performed according to the values of this table. The reference figures are given for information.								

The qualification of the cast material is done according to measured size of indication on the surface. In the standard, figures are given for identification of severity of the indication and accordingly to determine the quality of the material. Figure 2.12 shows an example of these figures, that are used for qualitative evaluations. All detected indications must be measured and indications with a greater length than L_1 need to be taken into account.

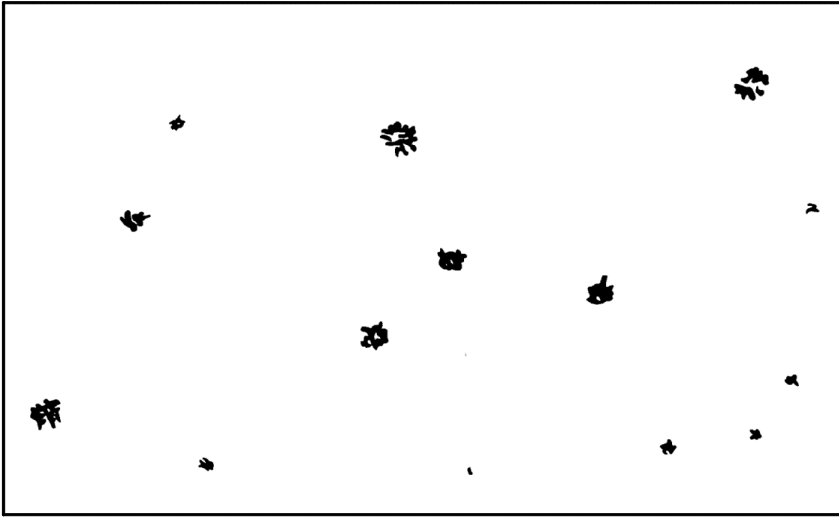


Figure 2.12 Reference figure of severity level SM3, scale of 1:1.



Figure 2.13 Reference figure of severity level LM 5-AM 5, scale 1:1.

The evaluation of aligned and linear indications is done in a similar way. The length of each indication needs to be established and the indications exceeding the minimum length, which need to be taken into account, should be determined for the qualification assessment. The threshold values for minimum indication need to be taken into account, depending on the required severity level of the material. The quality evaluation should be performed on the

surfaces where unfavourable indications are expected. The inspection area should not be smaller than 105 mm x 148 mm frame area. The evaluation criteria of severity levels are given in Table 2.2. The lengths of linear and aligned signs are summated in case of lengths exceeding the minimum length and the results are compared to cumulative values as given in Table 2.2. For qualitative evaluation of the material, the reference figures are given for the linear and aligned indications. Figure 2.13 shows an example of these figures. The quantitative evaluation needs to be made according to values in the tables.

Table 2.2 Severity levels for magnetic particle testing linear and aligned indications.

Characteristics	Severity levels																			
	LM 001	LM 01	LM 1	LM 2	LM 3	LM 4	LM 5	LM 6	LM 7	AM 001	AM 01	AM 1	AM 2	AM 3	AM 4	AM 5	AM 6	AM 7		
	Direct visual testing	Magnifying glass or the naked eye		The naked eye																
Magnification for observation of magnetic particles indications	≤ 3		1																	
Length L ₁ of smallest signs to be considered in [mm]	No indication allowed	0.3	1.5	2	3	5	5	5	5											
Agreement of indication ^a isolated (I) or cumulative (C)	I or C		I	C	I	C	I	C	I	C	I	C	I	C	I	C	I	C	I	C
Maximum length L ₂ of linear (LM) and aligned (AM) indications allowed [mm]	No indication allowed	1	2	4	4	6	6	10	10	18	18	25	25	45	45	70				
See Annex D of EN 1369 (2012) Figure	-		D.1	D.2	D.3	D.4	D.5	D.6	D.7											
^a The linear and aligned indications shall be taken into consideration for the calculation of the cumulative length. Note: The evaluation should be made according to the values of this table. The reference figures are given for information.																				

2.2.3.2 EN 12680-1 (2003) ultrasonic examination- steel casting for general purposes

This standard gives the requirements for ultrasonic examination to quantify cast steels for general purposes. The procedures are described to determine material discontinuities in material. This standard is applicable for material with wall thickness up to 600 mm.

The detected indications are classified by their dimensions. Discontinuities with dimensions that are smaller than or equal to the sound beam are called point discontinuity. Discontinuities with larger dimensions are identified as complex discontinuities. Discontinuities with two measurable dimensions are called planar discontinuity and the detected indications are called volumetric discontinuity if they have three measurable dimensions. The acceptance criteria for planar discontinuities are given in Figure 2.14 for different severity levels. The horizontal axis (b) of this figure shows the distance between surface and indications and vertical axis (a) is representing the largest acceptable individual indication area in square millimetres.

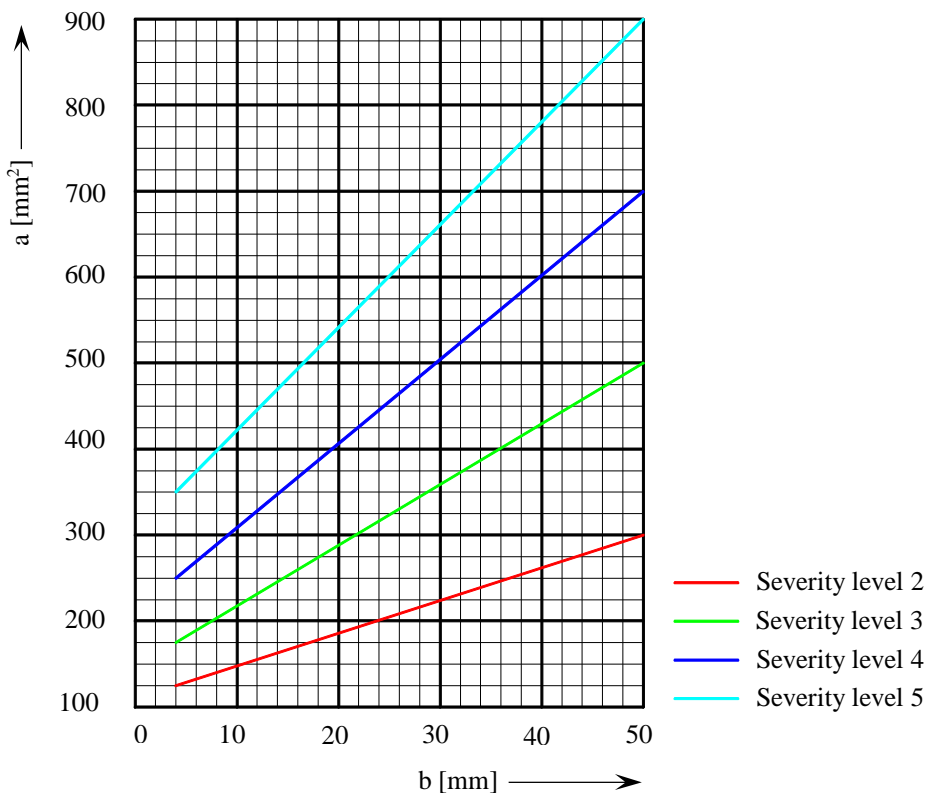


Figure 2.14 Acceptance limits for individual planar indications.

As can be concluded from Figure 2.14, indications with measurable dimensions are not allowed for Severity level 1. In addition to this figure, the following requirements are demanded. The largest dimension of indications in through wall direction may not exceed 10% of the wall thickness. This statement is not valid for indications with a measurable length smaller than 10 mm. Furthermore, the dimension through wall direction of such signs must be less than 25% of the wall thickness or 20 mm. In order to evaluate an indication as single indication, the greatest distance between indications must be 10 mm.

The acceptance criteria for volumetric discontinuities are given in Table 2.3. If any discontinuity exceeds these criteria, it is considered unacceptable. The wall thickness of a section is divided in two zones; rim zone and core zone (see Figure 2.15). Table 2.3 also shows the acceptance levels of discontinuities of these zones.

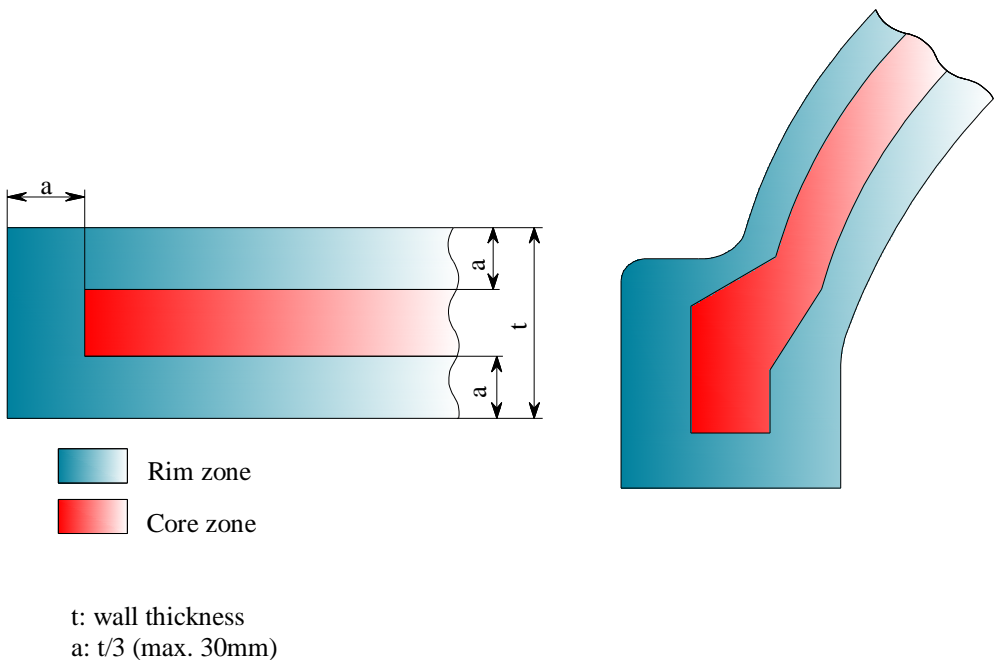


Figure 2.15 Division of wall thickness into zones.

Table 2.3 Acceptance limits for volumetric discontinuities.

Feature	Unit	Zone	Severity levels																	
			1	2		3	4		5											
Casting wall thickness at the examined area	mm		-	≤50	>50	>100	≤50	>50	>100	≤50	>50	≤50	>100	≤50	>100	≤50	>100	≤50	>100	
Reflectors without measurable dimension																				
Largest diameter of equivalent flat-bottomed hole	mm	Rim zone Core zone	3	a															Not use as criterion	
Number of discontinuities to be recorded in a frame 100 mm X 100 mm	-	Rim zone	3 ^b	5		6		6		Not use as criterion							Not use as criterion			
		Core Zone		Not use as criterion		Not use as criterion														
Reflectors with measurable dimension																				
Largest diameter of equivalent flat-bottomed hole	mm	Rim zone Core zone	3	a															Not use as criterion	
Maximum values of dimension in through wall direction of discontinuities	-	Rim zone	15% of zone thickness															20% of zone thickness		
		Core zone	15% of wall thickness															20% of wall thickness		
Maximum length without measurable width	mm	Rim zone	75	75	75	75	75	75	75	75	75	75	75	75	75	75	75	75	75	75
		Core zone	75	75	100	100	100	100	100	100	100	100	100	100	100	100	100	100	100	100
Largest individual area ^{c,d}	mm ²	Rim zone	Not permitted															3000	4000	
		Core zone	10000	10000	15000	15000	15000	15000	15000	15000	15000	15000	15000	15000	15000	15000	15000	15000	15000	15000
Largest total area for a reference area	mm ²	Rim zone	10000	10000	10000	10000	10000	10000	10000	10000	10000	10000	10000	10000	10000	10000	10000	10000	10000	10000
		Core zone	10000	15000	15000	15000	15000	15000	15000	15000	15000	15000	15000	15000	15000	15000	15000	15000	15000	15000
Reference area	mm ²		150000=(390 mm X 390 mm)															100000=(320 mm X 320 mm)		

^a For material wall thickness not greater than 50 mm, holes with diameter above 8 mm are unacceptable.

^b Collected in core zone and rim zone.

^c If indications are less than 25 mm, they must be considered as one imperfection.

^d When the indication is detected in core zone by an individual reflector and thickness of reflector is lesser than 10% of wall thickness, then 50% higher value of this table can be accepted for level 2 to level 4 and for level 5 no limit is specified.

2.2.3.3 EN 10160 (1999) ultrasonic testing of steel flat product of thickness equal to or greater than 6 mm

This standard explains the application procedure of ultrasonic testing to determine internal imperfections of flat rolled steel products without coating. The standard is suitable for flat steel products with thicknesses varying from 6 mm to 200 mm. The products are qualified for two locations; body and edge of the flat product. Four quality classes are defined for the flat product body and five quality classes for the edge of the product. The quality classes of product body are indicated by S₀, S₁, S₂ and S₃ and the quality classes for the product edges are indicated with E₀, E₁, E₂, E₃ and E₄.

The scanning of flat product body is executed by continuous examination along the line of a grid. The distance between grids is specified according to quality classes. For quality classes of S₀ and S₁, the grid of a 200 mm square parallel to the edge of the flat product is used. For the last two quality classes S₂, S₃, the grid is reduced to 100 mm square, which is parallel to the edge of the flat product. The acceptance criteria for the body of flat products depend on the type of probe that is used for the scanning. The acceptance values of these four quality classes are given in Table 2.4 and Table 2.5 for double transducer probes and normal transducer probes respectively.

Table 2.4 Acceptance criteria for testing with double transducer probes for the body of flat products for thicknesses < 60 mm.

Classes	Unacceptable individual discontinuity (mm ²)	Acceptable cluster of discontinuities	
		Area considered ^a (mm ²)	Maximum density not greater than
S ₀	S > 5000	1000 < S ≤ 5000	20 in the most populated 1 m X 1 m square
S ₁	S > 1000	100 < S ≤ 1000	15 in the most populated 1 m X 1 m square
S ₂	S > 100	50 < S ≤ 100	10 in the most populated 1 m X 1 m square
S ₃	S > 50	20 < S ≤ 50	10 in the most populated 1 m X 1 m square
^a Area of each discontinuity in the cluster.			

Table 2.5 Acceptance criteria for testing with normal transducer probes for the body of flat products for thicknesses <60 mm.

Classes	Unacceptable individual discontinuity	Acceptable cluster of discontinuities	
		Dimensions considered ^a	Maximum density not greater than
S ₀	S >5000 mm ²	1000<S≤5000 mm ²	20 in the most populated 1 m X 1 m square
S ₁	S >1000 mm ²	100<S≤1000 mm ²	15 in the most populated 1 m X 1 m square
S ₂	Defects for which the flaw echo has an amplitude greater than the characteristic curve Ø 11 mm	Between Ø 8 mm and Ø 11 mm	10 in the most populated 1 m X 1 m square
S ₃	Defects for which the flaw echo has an amplitude greater than the characteristic curve Ø 8 mm	Between Ø 5 mm and Ø 8 mm	10 in the most populated 1 m X 1 m square
^a Dimension of each discontinuity in the cluster.			

The inspection of the edges of the flat product is done by examining a zone over four edges of the product. The width of the inspection zone depends on the thickness of the material. Table 2.6 shows the inspection zone width according to the thickness of the product.

Table 2.6 Zone width for flat product edges.

Thickness of the flat product, t, (mm)	Zone width (mm)
6≤t<50	50
50≤t<100	75
100≤t<200	100

The edges of the flat products are qualified by five different quality classes. Table 2.7 shows the acceptance criteria for each quality class.

Table 2.7 Acceptance criteria for flat product edge zone.

Classes	Allowable individual discontinuity size		Minimum discontinuity dimension considered L_{\min} (mm)	Allowable number of discontinuities smaller than the maximum are S_{\max} and longer than L_{\min} per 1 m length
	Maximum dimension L_{\max} (mm)	Maximum area S_{\max} (mm^2)		
E ₀	100	2000	50	6
E ₁	50	1000	25	5
E ₂	40	500	20	4
E ₃	30	100	15	3
E ₄	20	50	10	2

2.3 Fatigue strength of material containing small defects

Fatigue loads cause slip band occurrence in the material in the very early stage of loading and some of these slip bands can become micro cracks. Some of these micro cracks can remain within a grain and some of these cracks propagate through the grain boundaries. Then they may not have sufficient energy to propagate through the next grain and it will stop propagating. It is generally assumed that the micro cracks initiate at the initial stage of loading and they become important from an engineering point of view when propagation takes place. Accordingly, fatigue limit of material is determined by a stress level below which micro crack is not propagating. Thus, fatigue limit is not related to the stress level of the fatigue crack initiation. As fatigue cracks already initiate at very early stage of loading, the threshold for crack propagation is represented by the threshold stress intensity factor. It has been experimentally investigated that the threshold stress intensity value of material containing small defects is a function of the Vickers hardness and the imperfection size. According to test results, the relation between threshold stress intensity value and Vickers hardness is [Murakami, 2002]:

$$\Delta K_{\text{th}} = 3.3 \cdot 10^{-3} (H_v + 120) \cdot (\sqrt{\text{area}})^{1/3} \quad (2.1)$$

where ΔK_{th} is $\text{MPa}/\text{m}^{1/2}$ and $\sqrt{\text{area}}$ is in μm . $\sqrt{\text{area}}$ is defined as the area of internal or surface imperfection projected area perpendicular to the applied stress axis (see Figure 2.16). In order to assess fatigue crack propagation of micro cracks, the stress intensity factor due to the applied load needs to be compared with the stress intensity threshold

value. The stress intensity factor for material containing small defects is determined by Murakami et al., (1989) as a function of $\sqrt{\text{area}}$.

For internal defects:

$$K_I = 0.5\sigma\sqrt{\pi\sqrt{\text{area}}} \quad (2.2)$$

For surface defects:

$$K_I = 0.65\sigma\sqrt{\pi\sqrt{\text{area}}} \quad (2.3)$$

and σ is the applied stress.

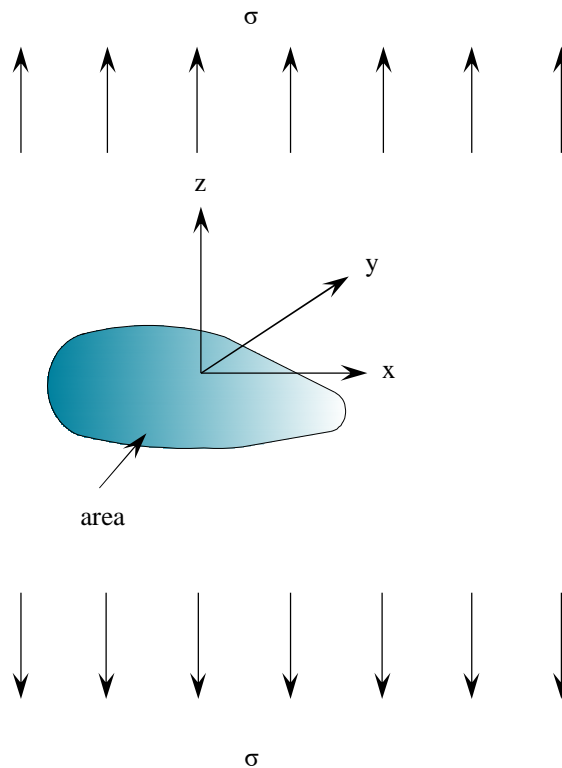


Figure 2.16 Representation of projected defect area [Murakami, 2002].

According to equations (2.1) and (2.2), fatigue crack propagation can be avoided by keeping the applied stress intensity factor, K_I , lower than the threshold stress intensity factor, ΔK_{th} , of material. As the material already contains a defect, the applied stress becomes the driving force for the crack propagation. In other words, when the applied stress is below a certain value, the crack will not propagate. This is known as fatigue limit or constant amplitude fatigue limit. Based on this assumption, the equations (2.1) and (2.2)

can be combined and the critical applied stress can be calculated. Thus, the fatigue limit of a material with an internal small defect can be expressed for $R = -1$ as:

$$\sigma_w = \frac{C_L \cdot (H_V + 120)}{(\sqrt{\text{area}})^{1/6}} \quad (2.4)$$

where σ_w is fatigue strength H_V is the Vickers hardness and C_L is the location constant and it is determined as 1.43, 1.41 and 1.56 for surface, subsurface and internal defects respectively. The location of the defect is described by the depth of it with respect to the material surface [Lei et al., (2012)]. Accordingly, subsurface defects locate in depths between 5-40 μm and internal defects are defined as defects locate in depths larger than 40 μm . Surface defects touch to the surface and locate in depths less than 5 μm .

Equation (2.4) is determined for a stress ratio, $R = -1$. Fatigue strength of material is influenced by mean stress. It was experimentally investigated that adjusting the prediction equations by using Goodman's diagram lead to non-conservative fatigue strength estimations. Based on experimental results, the equations for the fatigue strength of material containing small defects is written in general form including the effect of stress ratio as follows:

$$\Delta K_{th} = 3.3 \cdot 10^{-3} (H_V + 120) (\sqrt{\text{area}})^{1/3} \cdot \left[\frac{1-R}{2} \right]^\alpha \quad (2.5)$$

$$\sigma_w = \frac{C_L \cdot (H_V + 120)}{(\sqrt{\text{area}})^{1/6}} \cdot \left[\frac{1-R}{2} \right]^\alpha \quad (2.6)$$

where $\alpha = 0.226 + H_V \cdot 10^{-4}$

There is also a limitation for applicability of these equations. These equations are limited to defect size $\sqrt{\text{area}} = 1000 \mu\text{m}$. For defects or cracks larger than this value, the estimated fatigue strength by these equations is non-conservative. It has also been observed that the threshold stress intensity value for defects or cracks with $\sqrt{\text{area}} > 1000 \mu\text{m}$ tends to become constant for the material [Murakami, 2002].

Based on equations (2.4) and (2.6), the fatigue strength for material without defects goes to infinity. However, in general the crack will nucleate along the slip band or at grain boundary, thus infinite fatigue strength does not really exist. In this context, the fatigue limit of defect free material is approximately obtained by:

$$\sigma_{M,w} \cong 0.5 \cdot \sigma_u \cong 1.6 \cdot H_V \quad (2.7)$$

Konuma et al., (1986) executed rotary bending fatigue tests on quenched and tempered 0.35% C and 0.55% C steels. Fatigue strength was also predicted by equation (2.4) for a comparison with the test results. Microscopic examination was executed on the fracture surfaces of the specimens. The predicted fatigue limit and the results of the experiments are

given in Table 2.8. The size of inclusions was determined by microscope and it is used for fatigue limit predictions. When the applied stress at location of an inclusion is greater than the predicted fatigue limit, the inclusions are expected to be a location for fracture. The ratio of nominal stress at inclusion location to predicted fatigue limit, σ'/σ'_w is greater than 1.0 for each specimen, which means that the inclusions become a fracture origin. This was observed during the tests. Figure 2.17 shows the graphical representation of the test results for the nominal stress at the inclusion and the predicted fatigue limit versus the applied nominal stress. The curve of fatigue strength prediction shows the same trend with the curve of nominal stress at the inclusion which shows that the prediction model is accurate enough.

Ma et al., (2010) and Sun et al., (2013) also showed that fatigue strength prediction from equations (2.5) and (2.6) reasonably fits to the results of experiments.

Table 2.8 Size and location of inclusions and predicted fatigue limit [Konuma et al., 1986].

Material	Hardness Hv [kgf/mm ²]	Nominal stress at surface σ [MPa]	Cycles to failure $N_f \times 10^6$	Inclusion area [μm^2]	Distance from surface [μm]	Nominal stress at inclusion σ' [MPa]	Predicted fatigue limit σ'_w [MPa]	σ'/σ'_w
S35C	570	724	4.02	1134	42	716	599	1.20
	610	713	4.40	2204	200	681	600	1.14
	672	717	3.23	641	66	706	721	0.97
	655	735	2.19	1023	50	727	679	1.07
	638	724	1.08	1960	70	712	629	1.13
	657	686	1.48	1254	30	681	669	1.02
S55C	782	887	9.35	473	250	838	842	0.99
	775	918	2.37	769	290	858	802	1.07
	797	897	2.35	750	143	868	824	1.05
	801	896	4.40	491	110	874	857	1.02
	803	892	7.87	1257	375	817	803	1.02
	831	910	4.01	1257	175	874	819	1.05

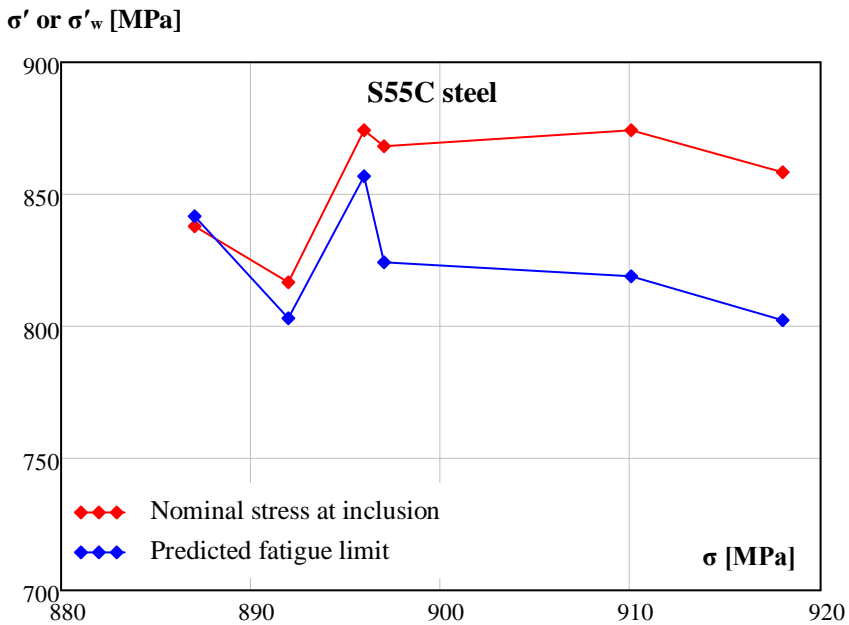
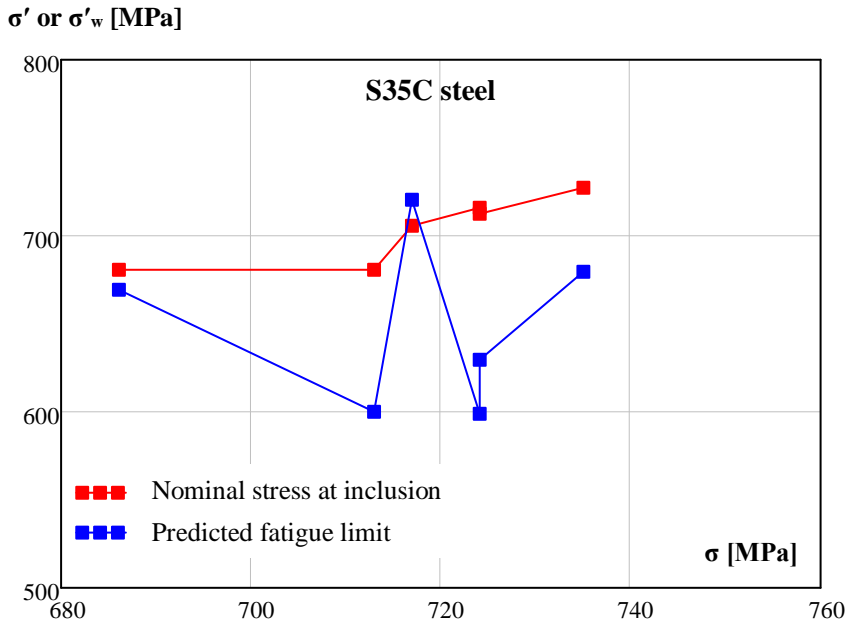


Figure 2.17 Graphical representation of the test results.

2.4 Effect of surface roughness on fatigue strength

2.4.1 General

As mentioned before, reverse slip band at the grain will cause fatigue crack initiation in defect free material. The slip bands will take place at the favourable locations where lower constraint exists. Accordingly, the material surface is one of the likely locations for the slip bands occurrence. Consequently, various surface effects can have an important influence on the fatigue life. The fatigue crack initiation is influenced by stress concentrations. Therefore, surface roughness and surface damage will result in probable crack initiation locations because of high stress concentration at surface discontinuities [Schijve, 2009].

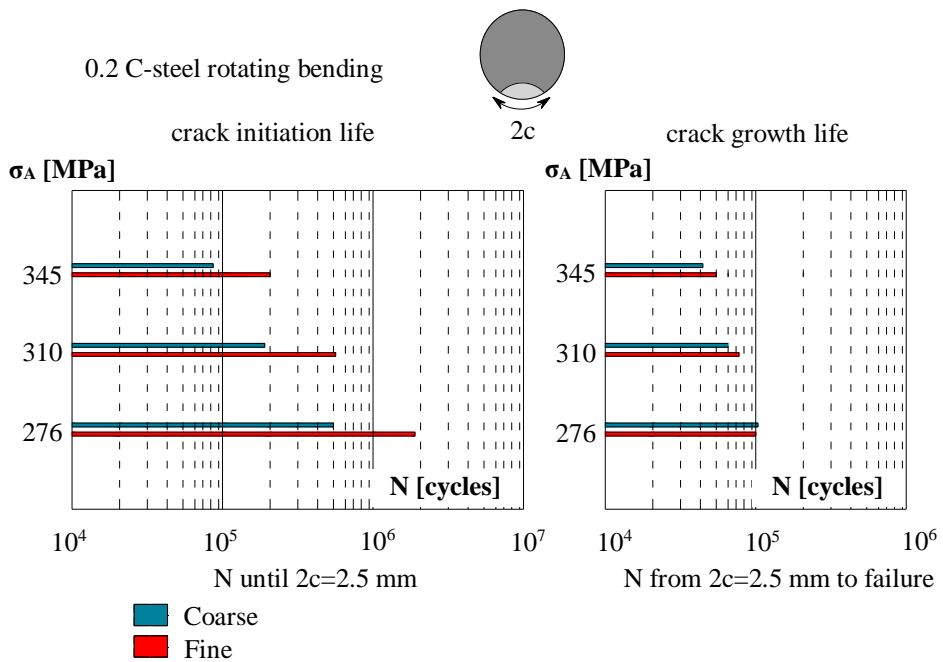


Figure 2.18 Effect of surface on the crack initiation and crack growth period [Schijve, 2009].

For example, results of tests on the effect of surface roughness on fatigue crack initiation and fatigue crack propagation are shown in Figure 2.18. A rotary bending fatigue test carried out on specimens with two different surface roughness values. A circumferential crack length of 2.5 mm has been defined as crack initiation life. The crack propagation life has been defined from the crack initiation life until the failure of specimens. The test results showed that the surface roughness influences the fatigue crack initiation life, while the

fatigue crack propagation is rarely affected by the surface roughness. As expected, the fatigue crack initiation life increases at a lower stress range. By further reducing stress range, the fatigue crack initiation life increases and at a certain stress range, the fatigue crack initiation life becomes infinite which confirms the threshold value for fatigue limit [Schijve, 2009].

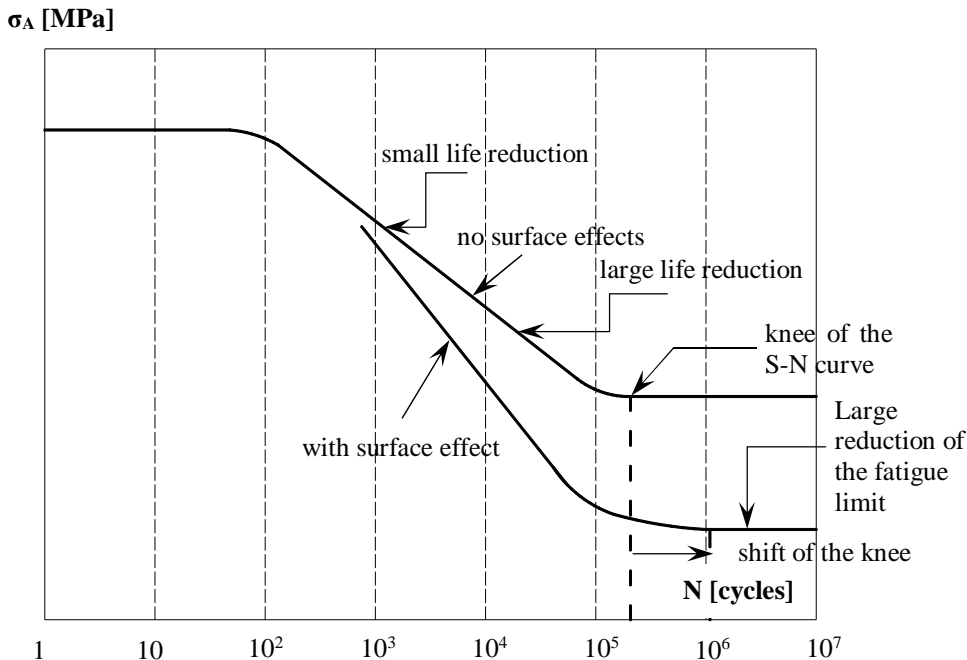


Figure 2.19 Surface effects on S-N curve [Schijve, 2009].

The relation between stress amplitude σ_A and the effect of surface roughness on the S-N curve is given in Figure 2.19. This curve is determined by extrapolation between the upper bound fatigue limit stress amplitude which causes failure in material in few numbers of cycles, and the lower bound fatigue limit stress amplitude, under which no fatigue failure occur. Further on in this chapter, this will be referred to as fatigue limit. The existence of surface discontinuities leads to fatigue crack initiation at stress amplitude lower than fatigue limit, which means that the surface discontinuities cause the fatigue limit reduction. The decline of the fatigue limit results in a lower slope of the curve. Consequently, fatigue strength will significantly decrease in the high cycle fatigue region. Furthermore, the fatigue crack growth life will be longer because of relatively lower stress amplitude. It consequently causes shifting in the knee point of the S-N curve (see Figure 2.19) [Schijve, 2009]

2.4.2 Theoretical approach of evaluation of surface roughness

In material without defects, fatigue cracks initiate at the surface of the material and consequently surface roughness affects fatigue strength of the material. Siebel et al., (1956) found that the depth of a surface groove influenced the fatigue strength of material. Takahashi et al., (1999) studied the effect of surface roughness on fatigue strength of material in order to identify these effects quantitatively. It was found that the pitch, interface effect between notches, is a critical feature for evaluating the effects of surface roughness on fatigue strength of material. The difficulty here is to implement surface roughness parameter, depth and pitch, for fatigue strength evaluation. There is no simple relation between fatigue strength and these parameters that can be used. To cope with this difficulty, a representative parameter, $\sqrt{\text{area}_R}$, is used and it contains the effect of both pitch $2b$ and depth a_R . The fatigue limit of specimens with surface roughness is determined by the threshold condition for non-propagating of a micro crack induced at the root of a notch. In this way, the notch problem is converted to a fatigue crack issue which has already been solved. The complexity is reduced to simple known phenomena [Murakami, 2002].

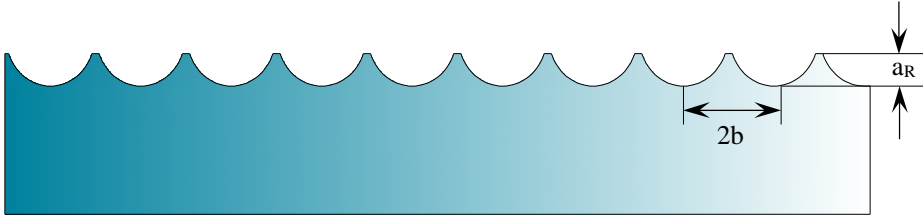


Figure 2.20 Definition of depth and pitch for periodic surface notches [Yang, et al., 2006].

Extensive numerical analysis has been performed by Murakami, (2002) to predict representative equivalent defect sizes. The analyses were performed for artificially created surface roughness with a depth of, a_R and a pitch $2b$ of periodic notches (see Figure 2.20). The equivalent defect size has been determined as follows:

$$\text{If } \frac{a_R}{2b} \leq 0.195 \quad \frac{\sqrt{\text{area}_R}}{2b} = 2.97 \cdot \left(\frac{a_R}{2b}\right) - 3.15 \cdot \left(\frac{a_R}{2b}\right)^2 - 9.74 \cdot \left(\frac{a_R}{2b}\right)^3 \quad (2.8)$$

$$\text{If } \frac{a_R}{2b} > 0.195 \quad \frac{\sqrt{\text{area}_R}}{2b} = 0.38 \quad (2.9)$$

Fatigue strength for surface notches can be rewritten as:

$$\sigma_{R,w} = \frac{C_L \cdot (H_V + 120)}{(\sqrt{\text{area}_R})^{1/6}} \cdot \left[\frac{1-R}{2} \right]^\alpha \quad (2.10)$$

Since the notches are located at the surface of the material, C_L is equal to 1.43 (see Section.2.3).

In actual production conditions, surface roughness has irregular notch shapes. The periodic surface notches can be artificially created for a certain condition. In case of unequal notches, the peak to peak distance can be considered as $2b$ where small peaks or valleys are ignored and for fatigue strength prediction; the average value of the measured $2b$ can be used (see Figure 2.21) [Itoga et al., 2003].

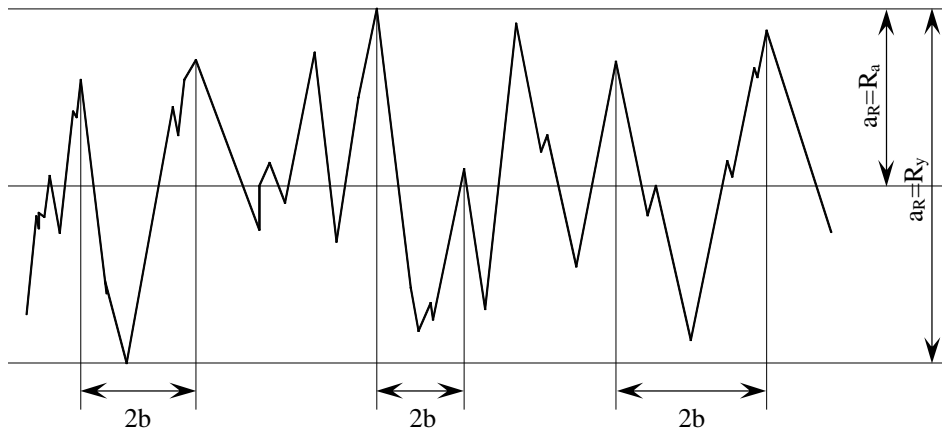


Figure 2.21 Definition of depth and pitch for irregular surface notches [Itoga et al., 2003].

Itoga et al., (2003) considered an experimental validation of this approach. The rotary bending tests were executed in a laboratory in air at ambient temperature on specimens with different surface roughness values made of Ni-Cr-Mo steel (JIS SNCM439). The chemical composition and mechanical properties of the material is given in Table 2.9 and Table 2.10 respectively.

Table 2.9 Chemical composition (wt.%) of material [Itoga et al., 2003].

Steel	C	Si	Mn	P	S	Cu	Ni	Cr	Mo
SNCM439	0.38	0.3	0.76	0.018	0.014	0.08	1.72	0.75	0.15

Table 2.10 Mechanical properties of steel [Itoga et al., 2003].

Steel	σ_y (MPa)	σ_u (MPa)	Elongation (%)	Reduction of area (%)
SNCM439	1490	1863	9	45

Material was oil quenched at 880 °C for 60 minutes and subsequently a temperature of 200 °C was maintained for 60 minutes. The surface of the material was polished and three different levels of surface roughness were prepared. Before preparation of surface roughness, hardness measurement was performed on the material surface and 700 H_v measured at the surface. Hardness of material gradually decreased within 20 μm from the surface and reached the constant value of 600 H_v. The specimen in polished condition is indicated by BF and the specimens with different surface roughness values are encoded by R10, R16 and R19. The results of the surface roughness measurements are given in Table 2.11, where R_y and R_a represent the maximum and average value of notch depth, respectively.

Table 2.11 Surface roughness values of the specimens [Itoga et al., 2003].

Roughness	BF	R10	R16	R19
R _y (μm)	0.659	10.24	16.47	19.26
R _a (μm)	0.092	1.386	2.142	3.154

Table 2.12 Experimentally and analytically determined fatigue limits [Itoga et al., 2003].

Specimen	Average pitch 2b (μm)	Height a _R (μm)		a _R /2b		Predicted fatigue limit σ _{R,w,p} (MPa)		Experimental fatigue limit σ _{R,w,e} (MPa)
		R _y	R _a	R _y	R _a	R _y	R _a	
R10	35.7	10.24	1.38	0.29	0.04	759	934	1000
R16	49.3	16.47	2.14	0.33	0.04	719	870	850
R19	55.5	19.26	3.15	0.35	0.06	705	819	850

In short fatigue life region below 10⁵ cycles, cracks initiated at the specimen surfaces and fatigue life declined with increase of surface roughness. In long fatigue life region, it is seen that the inclusions locations became critical for fatigue crack initiation instead of the surface roughness. Fatigue strength of the specimens was predicted with the explained theoretical approach and the test results were compared with the analytical prediction (see Table 2.12). The analytical calculation was performed for two different notch depths: maximum notch depth R_y and average value of notch depth R_a. The prediction with average depth shows a reasonable match with the test results.

2.5 Effect of inclusions on fatigue strength

Inclusions are chemical composites that exist in steel and alloys. They are the result of chemical reactions of the impurities. They occur during melting, pouring and deoxidation. They usually become the location of fatigue crack initiation for fatigue loaded elements. Due to inclusion susceptibility of very high strength steels, the inclusions have more detrimental effects on very high strength steels [Wang et al., 2002]. In addition, the inclusions affect the mechanical properties of ultra-high strength ($\sigma_{0.2} = 1848$ MPa and $\sigma_u = 1917$ MPa) steels, where reduction in tensile strength of the material is observed. Specially, the low cycle fatigue properties of high strength steel elements have been remarkably influenced by the presence of inclusions [Zeng, et al., 2007].

In Section 2.2.1.2, it is mentioned that they can also occur during deoxidation of steel. Therefore, inclusions usually contain oxides and deoxidation alloys like sulphide, nitride, and phosphide. These inclusions are also called natural inclusions. The inclusions are alien articles in steel and they consequently cause inhomogeneity of metal structures. The effects of inclusions on the material need to be considered for the application of steels.

The following parameters must be taken into account to analyse the effect of inclusions on fatigue strength:

- Inclusion shape and size
- Adhesion of inclusions to the steel matrix
- Elastic constant of inclusions and the steel matrix

All these parameters basically affect the stress distribution around an inclusion. Accordingly, these effects can be presented with a stress concentration factor.

Inclusion shape and inclusion size: The inclusion shape and inclusion size are important for determination of stress concentration effects. Much research has been carried out for determining stress concentration factors of an inclusion with the assumption of different shapes of inclusion. It has been found that this estimation lead to rough approximation of stress concentration factors. As the stress concentration highly depends on the geometry of an imperfection, a slight change of the estimated shape has a significant effect on the stress concentration value. This is the main cause lack of success for the determination of stress concentration factors for inclusions. Because the found inclusions in high strength steels have different shapes and mostly differ from the assumed shapes. This makes it difficult to determine a reliable fatigue strength of high strength steels based on stress concentration factors. In addition, inclusions are arbitrarily distributed in steel matrix and accordingly, this causes random stress concentrations in material which makes it rather complicated to assess the fatigue strength of the material based on the stress concentration. Furthermore, the bonding between steel material and inclusions is also not perfect and this often causes gaps between inclusions and the steel matrix. These gaps behave as a crack in the material. In this case, the theory of the stress concentration factor is invalid [Murakami, 2002].

However, the shape and size of imperfections need to be known for fatigue strength determination of material according to $\sqrt{\text{area}}$ method as described in Section 2.3.

Adhesion of inclusions to steel matrix: The steel matrix, inclusion types and interface properties between inclusion and material matrix are the most determinative parameters for crack initiation at inclusions. If the bonding between the inclusion and the matrix is not sufficiently strong, debonding occurs in the initial loading stage. This internal failure will not show any plastic deformation and the condition of the debonding is given by the applied interface stress. Under cyclic loading, this will lead to crack propagation from the interface into the matrix in a very early stage of loading. In case of a strong bonding between inclusion and matrix, the strength of the bonding resists the occurrence of breaking between inclusion and matrix. Plastic deformation will be assembled into a material matrix under cyclic loading. Inclusions will arrest the dislocation in the matrix. This blockage will lead to hitting between dislocation and inclusion, which finally results in debonding or a crack in the inclusion. For crack initiation at inclusion, it is not necessary to have debonding or cracking in the inclusion. In some cases, crack initiation takes place at interface of inclusion due to the stress concentration effect of inclusions [Tanak et al., 1981],[Kunio et al., 1981]. Fatigue crack propagation mechanism under low cycle fatigue loading will induce three different features of microstructure failure: initial debonding of the matrix and inclusion, short crack propagation and long crack propagation [Denda, et al., 1991].

Elastic constant of inclusion and steel matrix: Fatigue crack initiation is the origin of the stress concentration between inclusion and steel matrix. Stress concentration arises from the different thermal expansion coefficients during thermal cyclic loading and remote applied load due to the difference between elastic constants of inclusion and steel matrix. The deformation capability of inclusion and the material surrounding the inclusion can induce the crack initiation [Li., 2012].

In general, fatigue properties can be affected by inclusion in two ways. Firstly, the deformability of inclusion and matrix can show different properties. Low deformability of the inclusion can introduce microcracks which cause direct crack initiation and propagation at the initial stage of service. Secondly, inclusion may not cause microcracks, but they can still influence fatigue properties of material by introducing stress concentration between matrix and inclusion [Wang et al., 1996].

2.6 Critical inclusion size for steel

It is well known that for high strength steels non-metallic inclusions are potential locations for fatigue crack initiation under high cycle fatigue conditions. High cycle fatigue was defined by Li, (2012). He found that the number of cycles falls in a range between 10^7 and 10^{10} . In order to improve the high cycle fatigue behaviour of steel, the size and amount of

inclusions in steel need to be reduced. With the application of an advanced production process it is possible to decrease the content of inclusions and other detrimental defects. However, this will lead to high production cost and a high energy consumption. Both these consequences are undesirable, both for material user and the environment. Therefore, it is allowed that material may contain some amount of defects with limited size to avoid fatigue crack initiation as a result of inclusions. In this context, it is important to determine the critical inclusion size for fatigue limit of a material. Two methods are dealt with here: extrapolation from experimental results and estimation from theoretical approaches.

2.6.1 The conventional method of extrapolating experimentally

This method provides a procedure to determine critical inclusion size in a steel grade by examining fracture surfaces resulted from fatigue experiments where fatigue cracks initiated due to the inclusions. The method is a destructive examination and therefore the accuracy of the method highly depends on sufficient available test data. It requires extensive fracture surface examinations, where inclusions result in fracture of the specimens. The diameter of the inclusion is measured and the measurements are presented graphically, which shows the relation between the diameter and the location of the inclusion, as well as the distance of the inclusion to the surface. The vertical axis of the graph indicates the diameter of the inclusions and the distance of the inclusions to surface is placed at the horizontal axis. Then, a line is drawn by passing through the lowest two data points in such a way that below the line no other data point remains. The intersection point with distance at surface gives the value of the critical inclusion size. An example of execution of the procedure is given in Figure 2.22. In this figure, critical inclusion diameters are 8, 15.3 and 7.3 μm for ADFI-880, ADFI-920 and ADFI-940 steel respectively [Yang et al., 2006].

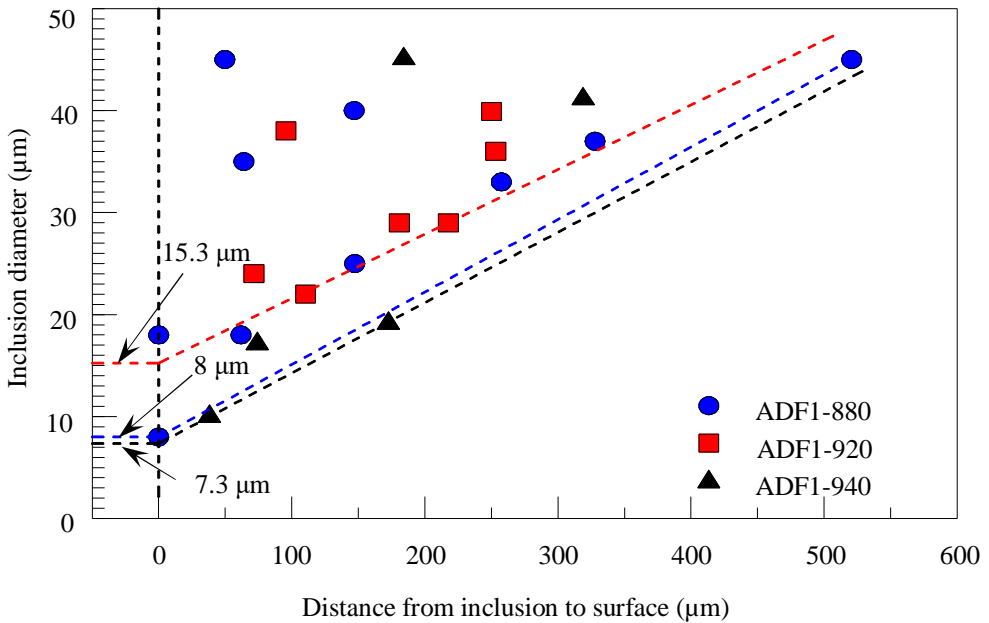


Figure 2.22 Determination of critical inclusion size by using the conventional extrapolation method [Yang et al., 2006].

2.6.2 Estimation critical inclusion size

Fatigue strength of material with internal or surface defects is a function of applied stress and defect size. Under a certain fluctuating stress amplitude, fatigue cracks will initiate at the location of inclusions when the inclusion size exceeds the critical value below which fatigue crack initiation may take place due to other phenomena, slip band at grain boundary, surface roughness etc.

The empirical expression for fatigue limit of defect free materials has been given in equation (2.7). It is assumed that the surface of the material is smooth enough not to cause fatigue crack initiation. In this case, the steel matrix and inclusion in material will become competitors in fatigue crack initiation locations. Fatigue strength of inclusion containing material is determined by the inclusion size and location and it is lower than fatigue strength of the defect free material. This is a dominant issue until a certain size of the inclusion, which is called the critical inclusion size. In other words, fatigue strength of material with inclusion will be equal to fatigue strength of defect free material at critical inclusion size. The empirical formulae for both cases are available: equations (2.4) and (2.7). The critical inclusion size can be determined from these equations for $\sigma_{M,w} = \sigma_w$

condition by assuming that subsurface and interior inclusions have spherical shape and the shapes of the inclusion at surface is hemispherical (see Figure 2.23) [Yang et al., 2006].

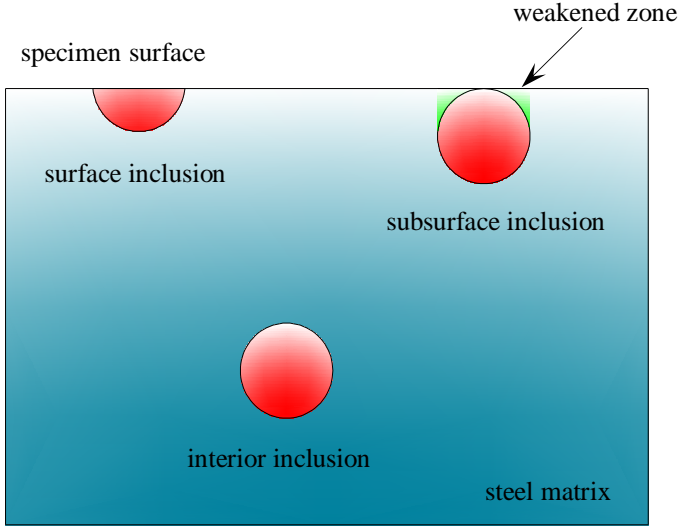


Figure 2.23 Inclusion types and locations in steel matrix [Yang et al., 2006].

Based on shape and theoretical assumption, diameter of inclusion can be determined by solving the equations (2.4) and (2.7). The results are given for surface, subsurface and interior respectively in expression (2.11) [Yang et al., 2006].

$$\varphi_{M,c} = 0.183 \cdot \left(1 + \frac{120}{H_v}\right)^6, 0.528 \cdot \left(1 + \frac{120}{H_v}\right)^6, 0.969 \cdot \left(1 + \frac{120}{H_v}\right)^6 \quad (2.11)$$

The critical inclusion diameters are determined for the condition smooth surface, for which it is assumed that the fatigue crack initiation due to surface roughness is not the case. However, in reality, rough material surface and inclusion in material may exist simultaneously. In this case, both of these imperfections become critical locations for fatigue crack initiation. For such conditions, the critical inclusion diameter is a function of representative equivalent surface defect size and it will be obtained for condition $\sigma_{R,w} = \sigma_w$. The critical inclusion diameter for the three locations; surface, subsurface and interior, is given in expression (2.12) [Yang et al., 2006].

$$\varphi_{R,c} = 1.6 \cdot \sqrt{\text{area}_R}, 1.06 \cdot \sqrt{\text{area}_R}, 1.91 \cdot \sqrt{\text{area}_R} \quad (2.12)$$

The critical inclusion diameter is determined for material with a smooth and a rough surface. Nevertheless, the boundary between rough and smooth surface needs to be determined to specify whether the inclusion or the surface roughness is determinant for the

fatigue strength of material. Surface roughness will be decisive for the fatigue strength in case of the material with deep surface notches. The decrease of surface notches leads to increased fatigue strength of material due to surface roughness. The increase of fatigue strength will take place until equivalent the surface defects have reached a critical value, below which surface notch defects have no influence on the fatigue strength. For such notches, the depth is very small with respect to pitches. Accordingly, equivalent surface defect, $\sqrt{\text{area}_R}$, is approximately equal to $2.97a_R$. The critical value of surface notches as can be determined by assuming $\sigma_{R,w} = \sigma_w$ and it is given by equation (2.13) [Yang et al., 2006].

$$a_s \cong 0.1716 \cdot \left(1 + \frac{120}{H_V}\right)^6 \quad (2.13)$$

In summary, when the surface is smooth ($a_R < a_s$), meaning that surface roughness is not critical for fatigue crack initiation, the critical inclusion size is determined by equation (2.11), $\varphi_c = \varphi_{M,c}$. In case of exceeding the critical notch depth ($a_R > a_s$), the critical inclusion size is obtained from equation (2.12), $\varphi_c = \varphi_{R,c}$ [Yang et al., 2006].

Yang et al., (2006) evaluated this approach by an experiment using three 42CrMo steels and two spring steels with different chemical compositions. One of the 42CrMo steels is also called “zero inclusion steel”, indicated by Z and contains inclusions less than $1\mu\text{m}$. The other two are represented by C1 and C2. Two spring steels are 50CrV4 and 54SiCrV6 and indicated as S1 and S2 respectively. The chemical composition, mechanical properties and value of surface roughness are given in Table 2.13 and Table 2.14 respectively.

Table 2.13 Chemical composition of steels [Yang et al., 2006].

Steel	C	Mn	Si	P	S	O	N	Cr	V	Mo
Z	0.43	0.02	0.32	0.002	0.0007	0.0004	0.003	0.90	-	0.26
C1	0.44	0.65	0.33	0.023	0.018	0.006	0.007	1.04	-	0.19
C2	0.4	0.58	0.26	0.014	0.009	-	-	0.99	-	0.18
S1	0.51	0.95	0.3	≤ 0.015	≤ 0.015	0.0029	-	1.1	0.13	-
S2	0.56	0.70	1.45	≤ 0.01	≤ 0.01	0.0022	-	0.65	0.15	-

Table 2.14 Mechanical properties of steels [Yang et al., 2006].

Specimen	E (GPa)	ρ (kg/cm ³)	σ_u MPa	H _{V0.5} (kgf/mm ²)	R _a (μ m)
Z-1	210	7850	1480	444	0.3
Z-2	210	7850	1197	400	0.3
C1-1	210	7850	1460	473	0.3
C1-2	210	7850	1014	387	0.3
C2-1	209.5	7850	1371	415	0.3
C2-2	209.5	7850	1215	369	0.3
S1	209	7850	1780	519	0.15
S2	209	7850	1729	515	0.31

Fatigue tests were executed with stress ratio $R = -1$ at room temperature. The tests were continued until 10^9 cycles in case no crack initiation was observed in the specimens. After testing, fracture surfaces of the specimens were examined by means of an electron microscope for determination of the inclusion size that causes crack initiation. The measured inclusion sizes were compared with analytically calculated inclusion size. The results are given in Table 2.15.

Table 2.15 Estimated critical and measured inclusion size [Yang et al., 2006].

Specimen	a [μ m]	a/2b	a _s [μ m]	Estimated critical size ϕ [μ m]			Experimental	
				Surface	Subsurface	Interior	ϕ [μ m]	Inclusion location
Z-1	0.3	≈ 0	0.72 > a	3.4	2.2	4.1	-	-
Z-2	0.3	≈ 0	0.83 > a	3.9	2.6	4.7	-	-
C1-1	0.3	≈ 0	0.67 > a	3.2	2.1	3.8	17	Surface
C1-2	0.3	≈ 0	0.87 > a	4.1	2.7	4.9	23.3	Interior
C2-1	0.3	≈ 0	0.79 > a	3.7	2.4	4.5	22.7	Surface
C2-2	0.3	≈ 0	0.93 > a	4.4	2.9	5.3	20	Surface
S1	0.14	≈ 0	0.60 > a	2.8	1.8	3.4	4.5	Interior
S2	0.14	≈ 0	0.60 > a	2.9	1.9	3.4	5.2 ^a /1.5 ^b	Interior

^a Maxima refer to inclusion cluster.

^b Diameter of the maximum inclusion in the cluster.

In the specimens from Z steels, fatigue cracks initiated on the surface matrix because of small inclusion size in steels. In the specimens from C1 and C2, fatigue crack initiation was observed at inclusion locations and measured inclusion sizes exceeded the estimated critical inclusion size. At fracture origin of S2 steel, a cluster of inclusions was detected and the maximum diameter of inclusion in the cluster was smaller than the estimated critical value. The maximum inclusion might not be able to nucleate fatigue crack, but when the cluster is considered its diameter exceeds the estimated critical value. This study has shown that the use of the established prediction models gives reasonable estimation for the critical inclusion size [Yang et al., 2006].

2.7 Estimation of maximum inclusion size in material

The current advanced production process of steels can provide more clear material. The inclusions in clean steel might consist of a few large ones and a cloud of small ones. In large volume of steel, it is difficult to inspect large inclusions which do not often occur. It is well known that the resistance and performance of steel is highly affected by the size of inclusions in steel volume. Much research has been carried out to predict the effect of inclusion and other defects on fatigue strength of steels. The results show that fatigue cracks mainly initiate at the location of inclusions and other defects in the material exposed to cyclic loading for very high cycles. The fracture very likely occurs at the largest inclusion in the material. Therefore, it is important to make an estimation for maximum inclusion size in a volume of material and to help material users estimate potential risk from inclusions [Zhang et al., 2005].

Currently, many inspection methods are available to detect inclusions in steel, such as materials surface analysis by optical microscopy, non-destructive testing and the fatigue fracture method. However, it is difficult to detect large inclusions by these methods. By optical microscopy, only a small volume of steel can be inspected. While the non-destructive testing method can inspect large volumes of steels, however, the detectable sizes of inclusion are limited; it is difficult to detect inclusions with small sizes. The fatigue fracture method is an effective method, but it is a time consuming process and expensive. In order to overcome these problems, the statistical extreme value method has been developed, based on the extreme value theory [Zhang et al., 2013].

2.7.1 Extreme value theory

Murakami, (1994) explained this theory and it is summarised in this section. This theory is applied for known cumulative probability of a certain population. If the cumulative probability, F_z , of a given population is known, the distribution of maximum values, Z_n ,

from sets of n individual has a cumulative function, F_{Z_n} , and it is related to the previous cumulative function, equation (2.14).

$$F_{Z_n} = (F_Z)^n \quad (2.14)$$

It can be shown that if the main distribution exponentially decreases, the distribution of extremes $X \equiv Z_n$ is asymptotically decreased by a largest extreme value distribution. It is also described by Gumbel distribution. It is described by the function:

$$F_x(x, \lambda, \delta) = \exp \left\{ -\exp \left[-\frac{(x - \lambda)}{\delta} \right] \right\} \quad (2.15)$$

λ and δ are respectively representing the location and scale parameter of this exponential distribution. The value of a certain location of distribution, P_{th} value of it is:

$$x(P) = F_x^{-1}(P) = \lambda + \delta \cdot y \quad (2.16)$$

where $y = \ln(-\ln(P))$. The distribution of defects in metal is presumed that it is nearly exponential or described by Weibull or log-normal distribution. These distributions are exponentially decreasing. Accordingly, it might be expected that the distribution of extreme defects can be described by the Gumbel distribution. The main aim of a statistic of extremes is to estimate extreme defects in a volume of material and it can be done by performing measurements on given set of control areas where maximum detected defects are recorded. It is assumed that x is the dimension of extreme defect and S_0 is the inspected area from a volume of material. Consequently, the return period of the characteristic largest defects in an area, S , will be determined by equation (2.17).

$$T = S/S_0 \quad (2.17)$$

The dimension of the defect with return period, T , can be calculated by:

$$x(T) = \lambda - \delta \cdot \ln \left[-\ln \left(1 - \frac{1}{T} \right) \right] \quad (2.18)$$

The location and scale parameters, λ and δ are calculated using the least square method.

2.7.2 The procedure for extreme value defect rating

A cross section perpendicular to the maximum principal stress, cut from an element. The surface of the cut specimen is polished and cleaned after the polishing. A standard fixed inspection area, S_0 , is determined from the polished surface. For the standard fixed inspection area, it is generally suggested that it can be equal to the area of a microscopic picture. In this area, the maximum size of defects is selected and subsequently the square

root of the projected area, $\sqrt{\text{area}_{\max}}$, of these defects is calculated. This procedure is repeated n times on S_0 area (see Figure 2.24).

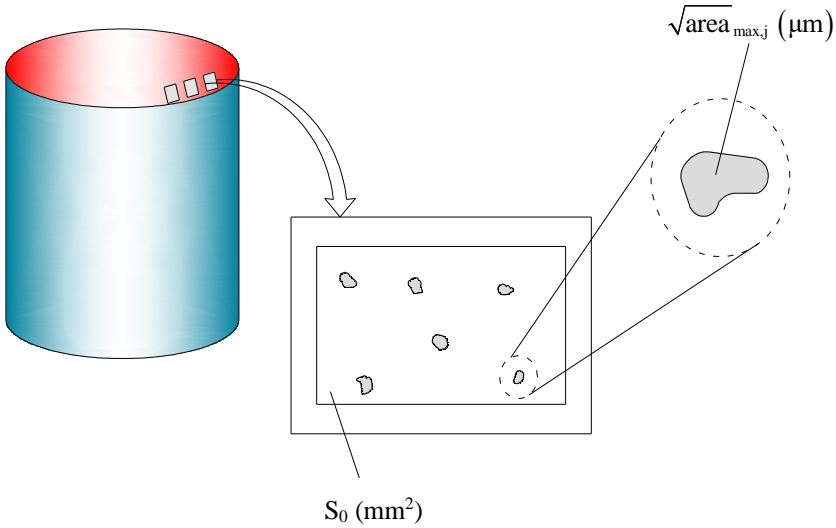


Figure 2.24 Example of defects inspection [Murakami 1994].

The calculated projected root area of the defects is classified from the smallest to the highest and indexed:

$$\sqrt{\text{area}_{\max,1}} \leq \sqrt{\text{area}_{\max,2}} \leq \dots \leq \sqrt{\text{area}_{\max,n}} \quad (2.19)$$

The cumulative distribution function, $F_j(\%)$, and reduced variants, y_j , are calculated from equation (2.20) and (2.21) respectively.

$$F_j = j \cdot \frac{100}{n+1} \quad (2.20)$$

$$y_j = -\ln \left[-\ln \left(\frac{j}{n+1} \right) \right] \quad (2.21)$$

The data are plotted in a probability paper for extreme value distribution. Figure 2.25 shows an example of this paper. Point j has an abscissa coordinate of $\sqrt{\text{area}_{\max,j}}$ while the ordinate axis present either F_j or y_j . It gives a straight line and the linear distribution of the maximum size of defects can be determined by equation (2.22).

$$\sqrt{\text{area}_{\max}} = a \cdot y + b \quad (2.22)$$

For:

$$y = -\ln \left[-\ln \left(\frac{T-1}{T} \right) \right]$$

$$T = \frac{S}{S_0}$$

S is the concentrated area.

a and b are determined by least square method by equation (2.23) and (2.24) respectively.

$$a = \frac{\left[n \cdot \sum (y_j \cdot \sqrt{\text{area}_{\max,j}}) - \sum y_j \cdot \sum \sqrt{\text{area}_{\max,j}} \right]}{\left[n \cdot \sum (y_j)^2 - (\sum y_j)^2 \right]} \quad (2.23)$$

$$b = \frac{\left[\sum \sqrt{\text{area}_{\max,j}} - a \cdot \sum y_j \right]}{n} \quad (2.24)$$

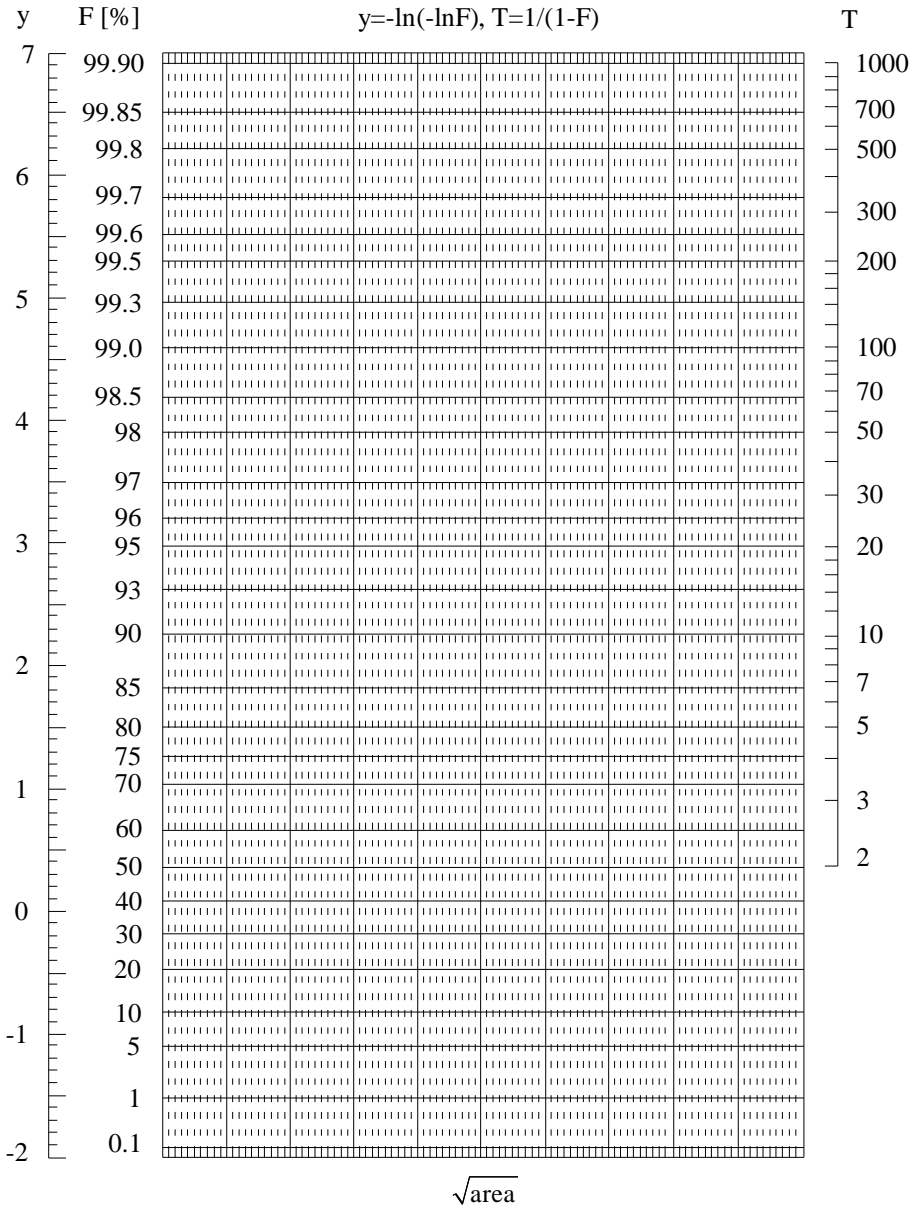


Figure 2.25 Probability paper for extreme value distribution [Murakami, 2002].

2.8 Summary

Defects can be found in all metals. They can vary from an atomic scale that is inherent to crystallographic structures, to large defects that are introduced during the process. The complicated chemical and physical reactions take place during manufacturing process. This may result in inhomogeneity and defects in material. These material imperfections will lead to various problems during processing, fabrication and service of metal elements. In order to avoid negative effects of the material defects, allowable defect size and inspection rules are standardised. These are given in the related documents.

Use of very high strength steel is common in automotive industry. In the last two decades, more research has been performed by this industry on fatigue strength of very high strength steels. Usually, a rotary bending test and tension-compression tests are performed for very high cycle fatigue. These reveal that the fatigue strength of very high strength steels is susceptible to material imperfections.

The main aim of these tests is that to find a relation between material properties and fatigue strength. This relation is established by using the hardness value of the material (equation (2.4)). The fatigue strength is increased by increasing the hardness of the material. The relation is established for the fatigue strength of defects free material and material containing defects. By using the equations of the fatigue strength for both cases, an equation for the critical defect size is determined (equation (2.11)). In the first instance, the relations are mainly determined for internal material defects. After defining the surface roughness problem as a surface defect, the equation for the critical inclusion size is reformulated for determination of critical surface roughness (equation (2.13)). These equations are validated using experimental results.

Ability of internal defects can be seen after fracture of sections. However, for a designer it is necessary to determine the size of an imperfection beforehand in order to take the effect of imperfection into account for fatigue strength estimation. For determination of imperfections in a volume of steel, the statistical extreme value theory is used. The results of this evaluation show a reasonable match with the experimental results.

The $\sqrt{\text{area}}$ theory is established for all kinds of steels with various thicknesses. However, the application of the theory is not common for structural steels. This might be due to applied high stresses at the structural steels. The structural elements expose high stress ranges which results in a lower number of cycles compared to the number of cycles in automotive applications. Therefore, fatigue cracks in structural steel usually initiate at the material surfaces, which is inductive to the crack initiation due to low strain conditions. In addition, the connections of steel structures have high stress concentrations, which are kept lower in automotive applications. Therefore, fatigue crack initiation due to internal material defects is rarely seen in structural steels. In case of crack initiation in structural steels, the internal defects are usually very large where the theory is invalid.

The common conclusion from relevant literature is that internal material imperfections can lead to fatigue crack initiation in high strength steel and these imperfections are detected by microscopic examination from the fracture surfaces. Pijpers, (2011) performed a study on fatigue strength of welded connections made of very high strength steels and in some test specimens, fatigue cracks initiation and propagation were observed in the base material of the specimens. At the crack initiation locations, some imperfections are detected by visual inspection. The evaluation of these imperfections is discussed in Chapter 3.

Chapter 3

Microscopic examination of the fracture surfaces

3.1 Introduction

Pijpers (2011) performed an experimental research on determination of the fatigue strength of welded connections made of very high strength steels. The experimental programme of the research was carried out for various loading configurations to get more insight in fatigue crack initiation and propagation in base material, weld toe and weld root of welded connections. Tests were executed under axial and four point bending loading conditions. With the use of four point bending test, a continuous bending moment was created on the weld area resulting in a compression and tension zone over the thickness.

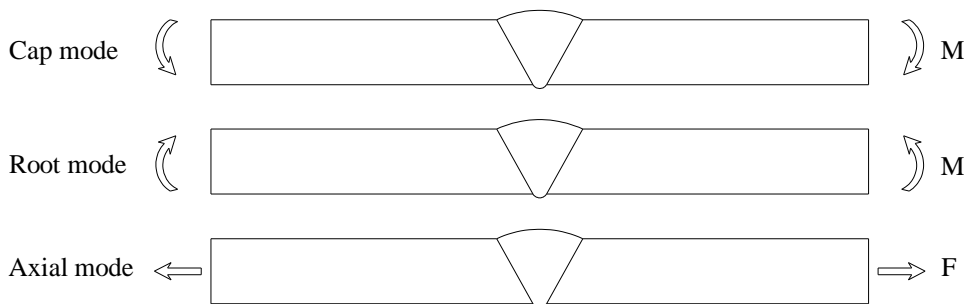


Figure 3.1 Loading mode configurations for test specimens [Pijpers, 2011].

Two bending modes were used: cap mode and root mode. A number of specimens were loaded with average tensile stress in the cap region: cap mode and some specimens were loaded with average tensile stress in the root region: root mode (see Figure 3.1). In axially

loaded specimens, fatigue crack initiation was expected to take place at the weld toe of the cap due to misalignment of the specimens as a result of welding. The misalignment will introduce secondary bending moment. Consequently, the average tensile stresses at the weld cap will be higher than the average tensile stresses at the weld root. All fatigue tests were executed under constant amplitude loading with a stress ratio, $R = 0.1$.

Table 3.1 Summary of experimental programme; Ax=axial loading, 4pb=four point bending [Pijpers, 2011].

Test series	Rolled steel	Cast steel	Thickness xWidth [mm]	Number of specimens	Loading	Weld shape	Backing
FAM	S690		12x33	7	Ax	Base material	-
FBM	S1100		10x33	7	Ax	Base material	
SA	S355		12x120	9	Ax	X-shape	
FA	S690		12x120	7	Ax	X-shape	
FB	S1100		10x100	7	Ax	X-shape	
V46x	S460		25x150	7/2	4pb/Ax	V-shape	
V69x	S690		25x150	7/2	4pb/Ax	V-shape	
V89x	S890		25x150	7/2	4pb/Ax	V-shape	
V11x	S1100		20x150	7/2	4pb/Ax	V-shape	
C46x	S460	G20Mn5	25x150	9	4pb	V-shape	
C69x	S690	G10MnMoV6-3	25x150	9	4pb	V-shape	
C89x	S890	G18NiMoCr3-6	25x150	9	4pb	V-shape	
C11x	S1100	G22NiMoCr5-6	20x150	9	4pb	V-shape	
CB46x	S460	G20Mn5	25x150	5	4pb	V-shape	Ceramic
CB69x	S690	G10MnMoV6-3	25x150	3/2	4pb/Ax	V-shape	Ceramic
CB89x	S890	G18NiMoCr3-6	25x150	5	4pb	V-shape	Ceramic
CB11x	S1100	G22NiMoCr5-6	20x150	5	4pb	V-shape	Ceramic

The experimental programme of the research work consisted of fatigue tests on base materials, X-shape welded connections and V-shape welded connections. The V-shape welded specimens were made of steel grades S460, S690, S890, and S1100 and cast steels with similar yield strength G20Mn5, G10MnMoV6-3, G18NiMoCr3-6 and G22NiMoCr5-6 respectively. The V-shape welded specimens were manufactured in three configurations: welded connections between rolled and rolled steels, welded connections between rolled steels and cast steels with and without ceramic backing. Surface of the base materials were in the as rolled condition and the welded parts in the as-welded condition. No any surface treatments or post weld treatments were applied. The overview of the experimental programme is given in Table 3.1. The results of the study have shown that application of very high strength steels in civil engineering structures is technically possible and high strength steels may have beneficial effects on the fatigue strength of base material and fatigue strength of welded connections.

The weld toe of welded connections is a critical location for fatigue loaded welded steel structures and fatigue cracks generally initiate at the weld toe of welded connections. This was also expected for the welded connections made of very high strength steels. However, unexpectedly, fatigue crack initiation and propagation was observed in the base material of some V-shape welded connections made of S460, S890 and S1100. According to the test results, not any base material failure was observed in the specimens made of S690 steel grade. The base material failures occurred in both: rolled and cast steel parts. Fatigue crack initiation and propagation in base material of welded connections is a not frequently seen phenomenon in steel structures.

However, as shown in Chapter 2, fatigue cracks can initiate in very high strength steels due to material imperfections. In the last two decades, more research studies have been performed by the automotive industry to determine the fatigue strength of very high strength steels. The materials are tested using rotary bending tests under tension-compression stress state for a very high cyclic fatigue regime. The results show that the fatigue strength of very high strength steel depends on the purity of the material. In other words, internal material defects may cause fatigue crack initiation in the material and trigger fatigue strength reduction of very high strength steels. In literature, it is also explained that the imperfection causing fatigue crack initiation in the material can be detected by examining fracture surfaces after failure. Since internal imperfections are very small, a microscopic examination becomes essential.

In the current research, visual inspection is performed on the fracture surfaces of the plate specimens with base material failures tested by Pijpers (2011). The visual examination revealed that the crack initiation locations contain some material imperfections. In order to identify origin and reasons of the imperfections, a microscopic examination is performed on these fracture surfaces.

3.2 Test material and test specimens

V-shape test specimens tested by Pijpers (2011) were manufactured from quenched and tempered steel plates with a thickness of 25 mm. Cast steel plates were produced with a thickness of 35 mm. After casting, the plates were quenched and tempered, and machined down to 25 mm thickness. Eventually, there was variation in thickness of the cast plates: between 25 and 28 mm. The quality of the cast steels was classified according to ASTM E 449-98 (1998) and it satisfied the NDT requirements of class I for weld edges and class II for other areas. Plates were inspected with two NDT methods; ultrasonic inspection according to EN 12680-1 (2003) and penetrant inspection according to EN 1371-1 (1997) [Pijpers, 2011]. The rolled steels were qualified according to EN 10225 (2001) for S460 and according to EN 10204 (2004) for S690, S890 and S1100. The chemical and mechanical properties of the plates are given in Appendix A.

After edge preparation, rolled plates and cast plates were welded by the flux-core arc welding (FCAW) process. Specimens made of S460, S690 and S890 were welded in overmatched condition, S1100 specimens in undermatched condition. Individual test strips were plasma cut from the welded plates, with a length of 1000 mm and a width of 160 mm. The width of the strips was reduced to 150 mm in the middle of the specimens by grinding from both sides. The welding data and the geometry of the specimens are also given in Appendix A.

3.3 Preparation for microscopic examination

The V-shape welded specimens with the base material failures were selected for the detailed inspections on the fracture surfaces. Fatigue crack initiation locations were visually specified on the fracture surfaces and the internal imperfections were observed at the fatigue crack initiation locations. The internal imperfections in the base material of the cast steels were easily detected on the fractures surfaces. The imperfections cause irregularity at the presented locations which makes them easily detectible. On the other hand, the fracture surfaces of the base material of the rolled steels generally show a very smooth plane and it is therefore difficult to detect any unusual imperfection on the fracture surfaces by visual inspection.

In four plate test specimens of the V-shape welded connections made of S460, S890 and S1100 steel grades, the crack initiation and propagation was observed in the base material of the rolled steel parts. Two base material failures were in S1100 rolled steel and the specimens were from the test series of the rolled steel to rolled steel welded connections. The other two specimens were made of S460 and S890 steel grades and they were from the test series for the rolled steels to cast steels connections. In addition to the base material

failure of the rolled steels, fatigue crack initiation and propagation were also observed in the base material of the cast steels. Similar to the rolled steels, not any visible crack initiation was monitored in the base material of G10MnMoV6-3 cast steel plates, which corresponds to the rolled steels grade of S690. In several test specimens, fatigue crack initiation and propagation was observed in the base material of cast steels. For each cast steel grade, the fracture surfaces of one specimen was selected for microscopic examination. More detailed information for selected specimens is given in Table 3.2.

Table 3.2 Material and weld conditions of the concentrated specimens.

Specimen	Material	Weld type	Crack location
CB461	S460-G20Mn5	V-shape weld	Rolled steel
CB892	S890-G18NiMoCr3-6	V-shape weld	Rolled steel
V113	S1100-S1100	V-shape weld	Rolled steel
V118	S1100-S1100	V-shape weld	Rolled steel
CB462	S460-G20Mn5	V-shape weld	Cast steel
C895	S890-G18NiMoCr3-6	V-shape weld	Cast steel
C112	S1100-G22NiMoCr5-9	V-shape weld	Cast steel
CB113	S1100-G22NiMoCr5-9	V-shape weld	Cast steel

Microscopic examination was performed using JEOL JSM 6500F scanning electron microscope. The fracture surfaces were cut from the specimens as thin as possible to be able to fit them into the chamber of the electron microscope. The width of the test plates was 150 mm and this is too long for the chamber of the electron microscope. The fracture surfaces are therefore cut into two pieces and accordingly, each fracture surface became two parts. (see Figure 3.2). This cutting process was done with caution, so that the crack initiation regions were not damaged. The specimens were sequentially cleaned with an ultrasonic cleaner by using acetone and ethanol. The duration of the cleaning process was two minutes for each cleaning step.

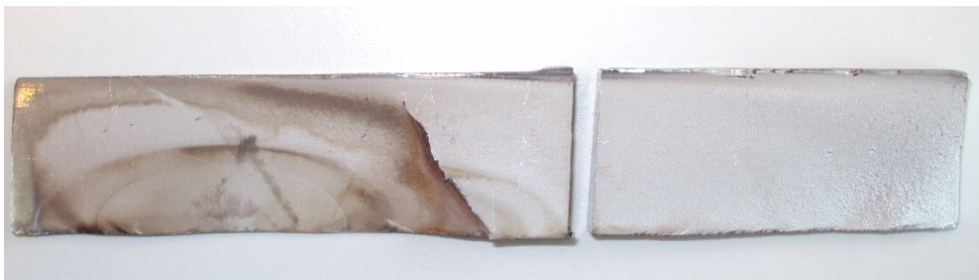


Figure 3.2 Prepared fracture surfaces for microscopic examination.

3.4 Microscopic examination on fracture surfaces

3.4.1 Fracture surfaces of rolled steels

The microscopic examination started with the specimen CB461 from the test series made for rolled to cast steel welded connection and the welding was executed with a ceramic backing plate. Fatigue crack initiation and propagation was observed in the base material of rolled steel part, 62 mm from the weld toe. The fracture surface and the crack initiation locations are shown in Figure 3.3. Visual inspection revealed that fatigue cracks initiated at two locations very near each other and they coalesced with each other after certain time and then propagated as one fatigue crack (see Figure 3.4).



a) Weld and crack initiation location.

b) Fracture surface of the specimen.

Figure 3.3 Overview of CB461 specimen.

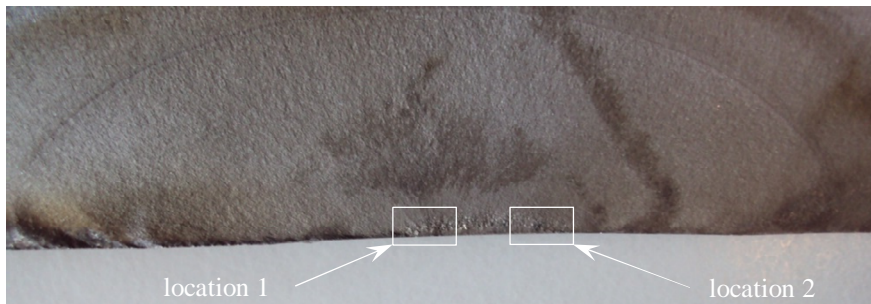
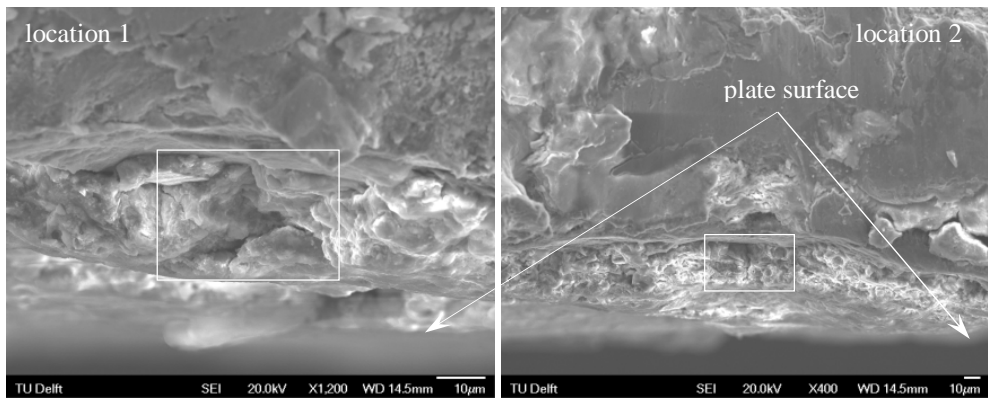
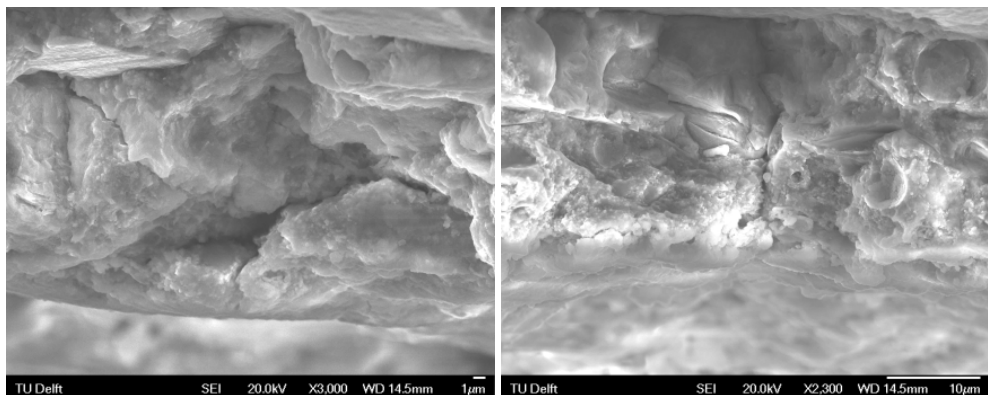


Figure 3.4 Fatigue crack initiation locations in CB461 specimen.

Figure 3.5a shows the microscopic images of the crack initiation points and it is clearly indicated that the structure of the crack initiation locations is different from the other part of the fracture surface. The detailed images for the crack initiation locations indicate a kind of dispersed inclusion (see Figure 3.5b). During steel production process to reduce the dissolved oxygen in steels, the de-oxidation process is carried out. In many cases, this is done by adding aluminium and magnesium. The chemical reaction between added alloys and oxygen can result in inclusions in steels. The inclusions are usually harder than the steel matrix and have a different deformation behaviour. Due to deformation behaviour difference between steel matrix and inclusions, the inclusions will be dispersed in the steels matrix during the steel rolling process. The dispersed inclusions contain several micro cracks and one micro crack can propagate under fatigue load instead of crack initiation in other locations. [Zhang et al., 2003].



a) Crack initiation locations.



b) Imperfection at the crack initiation points.

Figure 3.5 Microscopic images at the crack initiation locations.

The images only show the structure of the imperfection, which can also be a result of the rolling process. In order to identify the imperfection as an inclusion, the chemical

composition analyses need to be performed on the area of the imperfections. The analyses give the atom content of the imperfection which usually contains a high substance of de-oxidation alloys. Accordingly, energy-dispersive spectrometry (EDS) measurements were performed at the crack initiation locations. The measurements were carried out at three locations: both crack initiation locations and just above crack initiation region to specify the chemical composition difference between these regions. Figure 3.6 shows the areas of the measurements on the fracture surface.

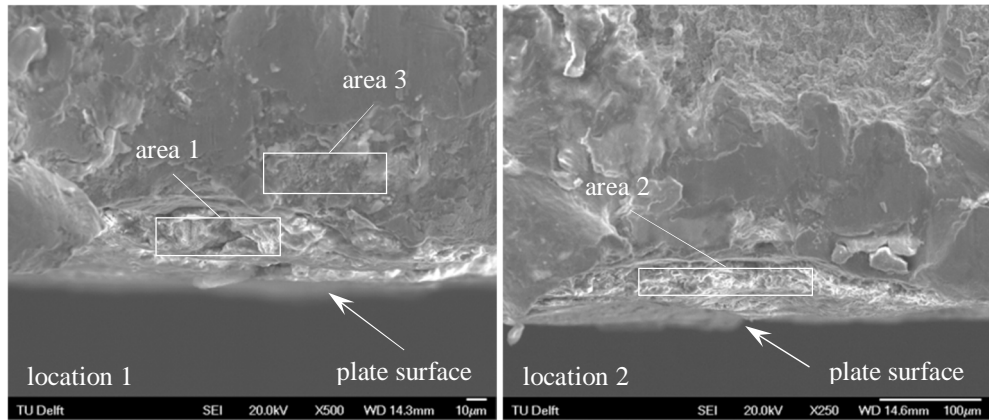


Figure 3.6 EDS measurement locations.

The EDS measurements on fatigue crack initiation locations are indicated by area 1 and area 2 and the measurement area just below the crack initiation location is shown by area 3. Table 3.3 shows the results of EDS measurements on the areas. The results revealed that the crack initiation locations contain a high amount of aluminium atoms which is the indication of an aluminium origin inclusion. The EDS measurement just below the crack initiation location 1 (area 3) shows that the iron atoms occupy the majority of the composition as it can be expected from the steel. According to these results, the crack initiation in the rolled steel of the specimen took place at the inclusion locations.

Table 3.3 Results of EDS measurements on fracture surface of CB461 specimen (Atom%).

	C-K	O-K	Al-K	S-K	Ti-K	Mn-K	Fe-K	Zn-K
Area 1	0.00	18.63	64.03	-	0.04	-	17.30	-
Area 2	0.00	15.25	67.31	-	0.39	-	12.00	5.09
Area 3	4.76	10.71	5.46	0.77	0.18	1.54	74.71	1.88

There was only one test specimen where fatigue crack initiation and propagation was observed in the base material of S460 rolled steels. Therefore, it was not possible to perform additional microscopic examination on the different specimens made of the same

steels grade. Therefore, it is also hard to conclude based on one result, that the crack initiation was due to the inclusions.

In this context, the examination was further continued with CB892 specimen. The welded specimen was manufactured for connection between S890 rolled steel and G18NiMnCr3-6 cast steel and the welding process was executed with a ceramic backing plate. During the fatigue test, fatigue crack initiation and propagation were observed in the base material of rolled steel 41 mm from the weld toe.



a) Weld and crack initiation location.

b) Fracture surface of the specimen.

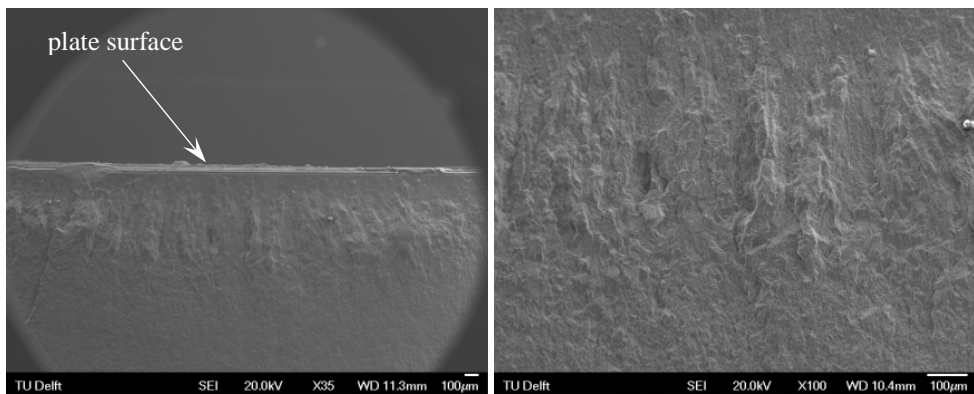
Figure 3.7 Overview of CB892 specimen.

Figure 3.7 shows an overview of the specimen where the welded connection and fracture surface of the specimen is indicated. In general, a very smooth fracture surface was observed, except at the fatigue crack initiation locations. The fatigue crack initiation locations show rough fracture surfaces. Figure 3.8 explicitly presents the rough fracture surfaces at the crack initiation locations. As can be seen from the figure, fatigue crack initiation took place at two locations near each other. In addition, the crack growth patterns can also be seen through the beach marks.



Figure 3.8 Fatigue crack initiation locations in CB892 specimen.

Figure 3.9 shows the microscopic images of the location 2 of the fatigue crack initiation. The rough surface at the fatigue crack initiation locations is more visible from the images and the fracture surface becomes smoother after a certain depth. This is completely reverse to usually known fatigue induced fracture surfaces. In general, micro cracks will grow very slowly after fatigue crack initiation, thus the fatigue crack growth rate is very small. The slow growth of cracks results in a smooth fracture surface, while a rough surface is induced due the fast fatigue crack propagation. Moreover, it is also commonly known that the fatigue crack growth in hard material is faster than in material with a lower hardness. Since the images present a transition from rough to smooth fracture surface, it can also be concluded that the material at the crack initiation points might be harder than the material just at the spot below.



a) *Fatigue crack initiation region.*

b) *Rough and smooth fracture surface.*

Figure 3.9 Feature of fatigue crack initiation locations.

From the images, it is difficult to specify the exact location of the first micro crack initiation point, while the feature of the fracture surface clearly indicated the crack initiation location on the specimen CB461. However, a semi elliptical rough fracture surface was detected and the EDS measurements were performed on different areas of the rough fracture surface. In addition, an EDS measurement was also carried out on the smooth fracture surface. Figure 3.10 shows the EDS measurement areas.

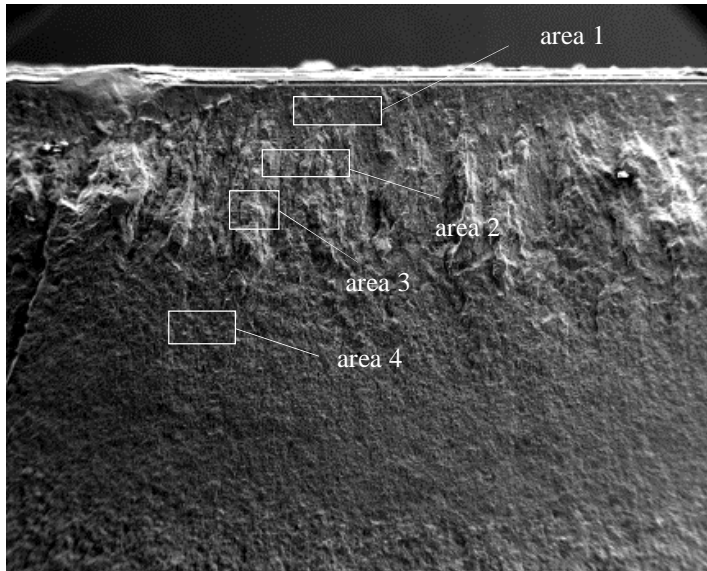


Figure 3.10 EDS measurement areas on the fracture surface.

Area 1, area 2 and area 3 refer to the fatigue crack initiation region and area 4 is located just below the crack initiation area to determine whether there are the chemical composition differences between the crack initiation region and another part of the fracture surface. Table 3.4 shows the results of the measurements and it is seen that there is no major chemical characteristic difference between the measured areas. The majority of the composition is occupied by iron atoms in all the measured areas.

Table 3.4 Results of EDS measurements on fracture surface of CB892 specimen (Atom%).

	B-K	C-K	Al-K	Si-K	Mn-K	Fe-K
Area 1	21.40	-	0.54	0.80	1.50	75.77
Area 2	18.99	-	0.53	0.56	1.16	78.76
Area 3	-	1.50	0.31	0.65	1.76	95.78
Area 4	-	2.86	-	0.89	1.53	94.72

The obtained results completely differ from the results of the specimen of CB461. It is therefore still hard to draw a conclusion as to the reason of the fatigue crack initiation and identification detected imperfections. However, regarding feature of the fracture surface, it is clearly visible that the fracture surface of the crack initiation region is different from the other parts of the fracture surface. The fracture surfaces were cut from the test plates for the microscopic examination. On the back side of the fracture surfaces, a large material discontinuity was discovered at a spot that was in line with the observed local rough

fracture surface (see Figure 3.11). It seems that the imperfection was located in the longitudinal direction of the plate. As mentioned before, the material at the crack initiation location might have a high hardness value, which was concluded from the rough fracture surface. The part with the hard material can show a different deformation behaviour under service load and it can cause stress concentrations. Consequently, this can lead to fatigue crack initiation in the material.



Figure 3.11 Material discontinuity at fatigue crack initiation location.

Since there was only one test specimen in which fatigue crack initiation and propagation were observed in the base material of S890 rolled steel, it was not possible to perform additional microscopic examination on the fracture surfaces of the same steel grade.

In two welded specimens made of S1100 rolled steel, fatigue crack initiation and propagation was observed in the base material. The specimens were manufactured for the welded connection rolled steel to rolled steel. The microscopic examination was continued with the V113 specimen, in which the base material failure was observed at the location 132 mm from the weld toe. The overview of the specimen is given in Figure 3.12.



a) Weld and crack initiation location.

b) Fracture surface of the specimen.

Figure 3.12 Overview of V113 specimen.

The fatigue crack development in this specimen looks rather complicated. It seems that the crack propagated from an existing small defect. The observed imperfection at the crack

initiation location differs from the detected imperfection in the previous specimens. Figure 3.13 presents the imperfection at the crack initiation region.



Figure 3.13 Fatigue crack initiation location in V113 specimen.

The fracture surface of the specimen was examined using an electron microscope and it was mainly focused on the fatigue crack initiation point which contains a large imperfection. The microscopic images show that the fracture surface of the fatigue crack initiation point is much rougher than the other part of the fracture surface (see Figure 3.14). The rough surface changes to the smoother fracture surface from the boundary of the imperfection. In the figure, the fracture surface of the imperfection and transition between the rough fracture surface to the smoother fracture surface are also indicated. A similar fracture surface feature was already discovered on the fracture surface of CB892 specimen.

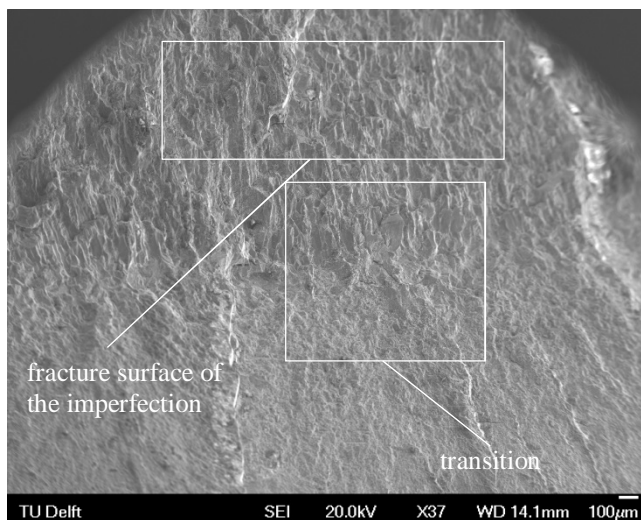


Figure 3.14 Fracture surface of the fatigue crack initiation location.

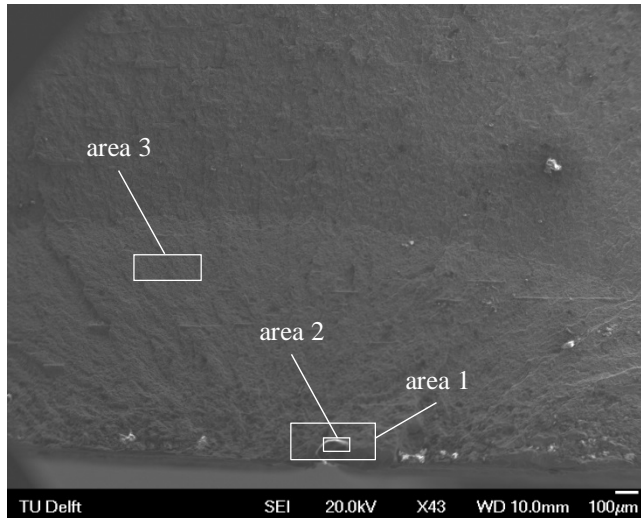


Figure 3.15 The areas for EDS measurements.

As specimens were broken into two pieces, one specimen has two fracture surfaces and both fracture surfaces can be inspected. The microscopic examination was performed on both fracture surfaces. The reason is that if the inclusions caused fatigue failure in the base material, the inclusion can remain in one of the fracture surfaces. Therefore, the EDS measurements are performed on the fracture surfaces where inclusions like imperfections are detected. On the fracture surface of V113 specimen, the EDS measurements were carried out on three areas: two areas on the fatigue crack initiation point and one area below the fatigue crack initiation point (see Figure 3.15)

Table 3.5 presents the results of EDS measurements. In area 1 and area 2 a higher carbon content was measured, while the carbon content decreased in area 3. Contrary to the decreasing carbon content, the content of iron atoms increased in area 3. The imperfection at the fatigue crack initiation region contained a high carbon content.

Table 3.5 Results of EDS measurements on fracture surface of V113 specimen (Atom%).

	C-K	Na-K	Al-K	Si-K	S-K	Ca-K	Cr-K	Mn-K	Fe-K	Ni-K
Area 1	56.99	0.55	0.62	0.79	0.14	0.16	0.13	0.27	26.68	0.42
Area 2	66.62	0.70	0.23	0.96	0.23	0.37	0.11	0.19	14.91	0.20
Area 3	24.77	-	0.31	0.86	-	0.13	0.30	0.50	57.58	0.99

Increase of carbon content causes a rise of material hardness and consequently reduces local deformability of the material and induces stress concentration at the location of hard material. The availability of the hard material at the fatigue crack initiation point was

confirmed by the microscopic images, that show a rough fracture surfaces. The microscopic examination was also performed on the fracture surface of V118 specimen and this specimen was also from the test series of welded connection between rolled and rolled steels. Fatigue crack initiation and propagation was observed in the base material 73 mm from the weld toe. The results of the examination are similar to the results of V113 specimen and therefore these results are not separately discussed.

The examinations on the fracture surfaces revealed that the fatigue cracks in the base material initiated at the location of an existing imperfection. The main conclusion as to the microscopic images is that the imperfections induced fatigue cracks and the crack initiation locations had a high hardness. From visual examination, it is seen that the imperfection is not only located at the fatigue crack initiation points and that they continue in longitudinal direction of the plates. However, the results of the EDS measurements remain insufficient to determine the origin and the reasons of the detected imperfections.

During the initial visual inspections, the focus was put on the fracture surfaces and the fatigue crack initiation locations. After the microscopic examination, an extensive visual inspection was performed on the fracture surfaces as well as on the plate surface of the specimens. Unexpectedly, some grinding marks were detected on the surface of the specimens with the base material failures in rolled steels. The plate surfaces were ground in longitudinal direction and the fatigue crack initiation took place in the ground areas. The grinding pitch may cause the stress concentration, which would lead to the fatigue crack initiation in the plates. On the plate surface of one specimen, it was clearly seen that the plate had been locally exposed to a heat treatment for some reason. In a more detailed examination, it was revealed that the treated locations contained a weld layer and the detected grinding marks were due to the removal process of the weld discontinuity. In other words, the plates were probably damaged during the manufacturing process. Then the damaged material was repaired by welding and the repair weld surfaces were ground to get smooth plate surfaces. Figure 3.16 shows the grinding marks and repair weld on the plate surface of a specimen.



Figure 3.16 Repair weld in the base material and grinding marks on the plate surface.

This detection clarifies the reason of observed the rough fracture surface at the fatigue crack initiation region and the imperfection behind of the fracture surfaces. In order to evaluate this repair weld, a piece of the material from the repaired area was cut and it was polished and etched. After this process, the weld layer and heat affected zone of the repair weld could easily be observed and it showed that the repair weld had been performed with one weld pass (see Figure 3.17). The plate surfaces and the back side cut of the fracture surfaces were visually inspected and the repair welds were detected in all specimens. Accordingly, fatigue crack initiation in the base material of the rolled steel is caused by the hidden repair weld in the base material. When the focus was put on the locations of the fatigue crack initiation, it was found that the crack initiations had taken place at the heat affected zone of the start stop points of the repair weld.

From the rough fracture surfaces at the fatigue crack initiation points, it is concluded that the material at those locations is harder than in the other region of the surface. For the verification, the hardness measurements were performed on the cross section of the repair weld, at 1 mm beneath the plate surface and on the heat affected zone of the repair weld 0.5 mm beneath the plate surface. The measurement results are given in Figure 3.18.

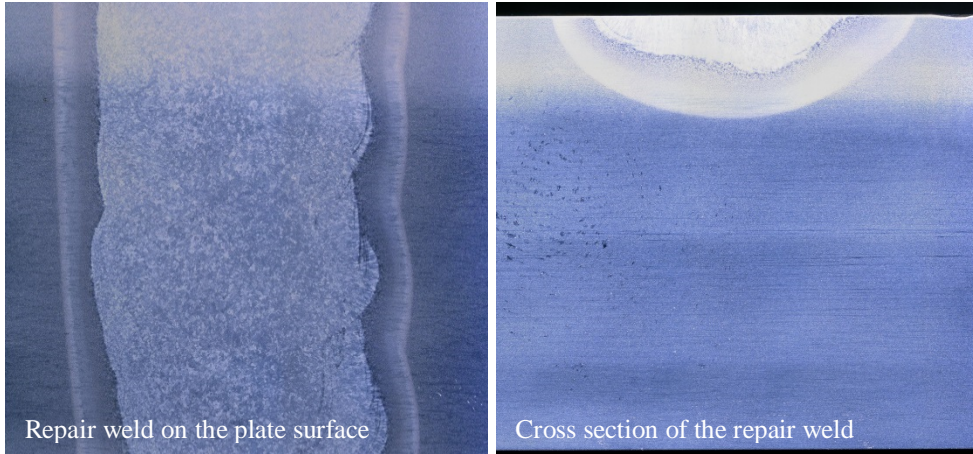
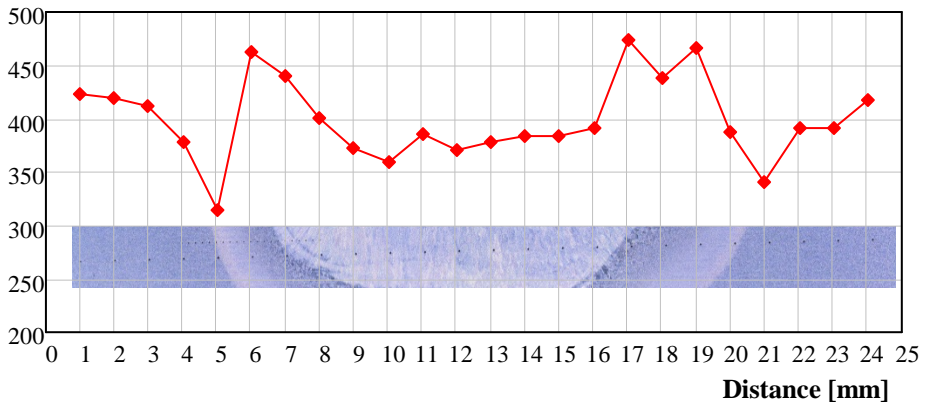


Figure 3.17 Macro graph of the repair weld on plate of S1100.

HV1 [kgf/mm²]



HV0.5 [kgf/mm²]

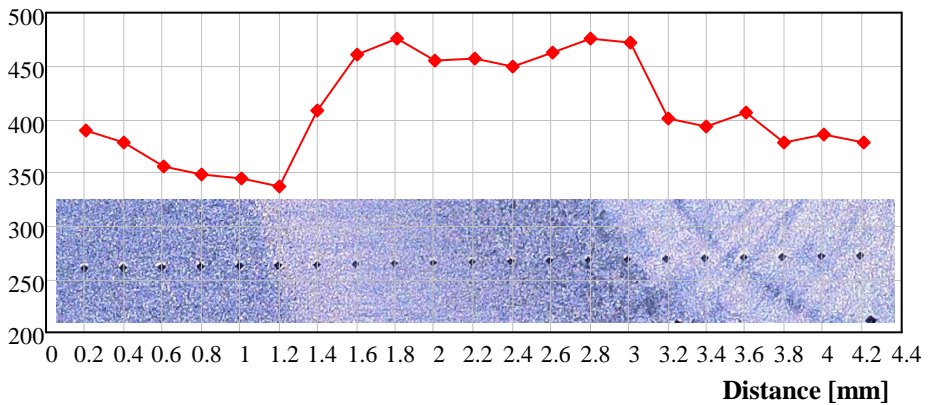


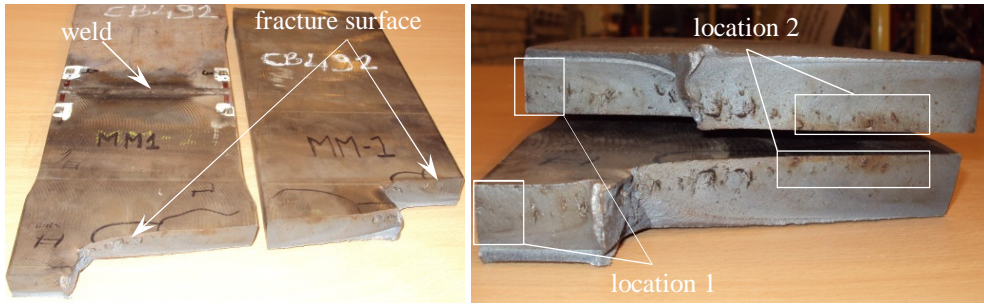
Figure 3.18 Hardness measurement on the repair weld.

Pijpers, (2011) measured the hardness of the V-shape welded specimens on the cross sections of the weld connections. Both hardness measurements were compared and the hardness value of the repair weld was approximately 20% higher than the hardness value of V-shape welded connections. The hardness values explain the reason of the observed rough fracture surfaces on the crack initiation regions. The comparison of the hardness values revealed that the repair weld may have performed in an improper way and accordingly it causes such a hardness increase. In addition, the cross section of the repair weld shows that the repair was executed with one pass weld. Without sufficient preheat temperature, one pass weld results into a very low temperature gradient during the cooling stage and consequently the material will cool down with a very high cooling rate, which induces very high hardness at the heat affected zone of the repair weld. The brittle behaviour of the hard material and high residual tensile stresses on the heat affected zone make the repair weld locations susceptible to fatigue crack initiation.

3.4.2 Fracture surfaces of cast steels

In addition to the base material failures in the rolled steels, there was also fatigue crack initiation and propagation in the base material of cast steels. The concentrated test specimens are given in Section 3.3. The fatigue crack initiation in the base material of the cast steels could be expected due to the production process of those steels. As mentioned in literature [Sigl et al., 2004], the cast steels may contain pores and inclusions which can cause fatigue crack initiation at the location of these imperfections.

The microscopic examination was performed on the fracture surface of the cast steel part of the test specimen CB462 in which fatigue crack initiation and propagation was observed at a location 131 mm from the weld toe. The specimen is from the test series of welded connection between S460 rolled and G20Mn5 cast steel with ceramic backing plate. Figure 3.19 shows the overview of the specimen. The fracture surface indicates that the fatigue crack initiation took place at two locations, which are also indicated in the figure. A fatigue crack was initiated at the edge of the plate: location 1 and at the plate surface; location 2. At location 1, the starting point of the fatigue crack initiation is easily detectable, while at location 2, it is difficult to find the exact point of the fatigue crack initiation. Several imperfections were observed on location 2 and those imperfections might have caused crack initiation simultaneously. Therefore, the exact fatigue crack initiation point could not be specified. The main aim of the microscopic examination is to identify the imperfections at the fatigue crack initiation points. Consequently, the examination was performed on the area of location 1 only, where the fatigue crack initiation point is clearly detectable.



a) Weld and crack initiation location.

b) Fracture surface of the specimen.

Figure 3.19 Overview of CB462 specimen.

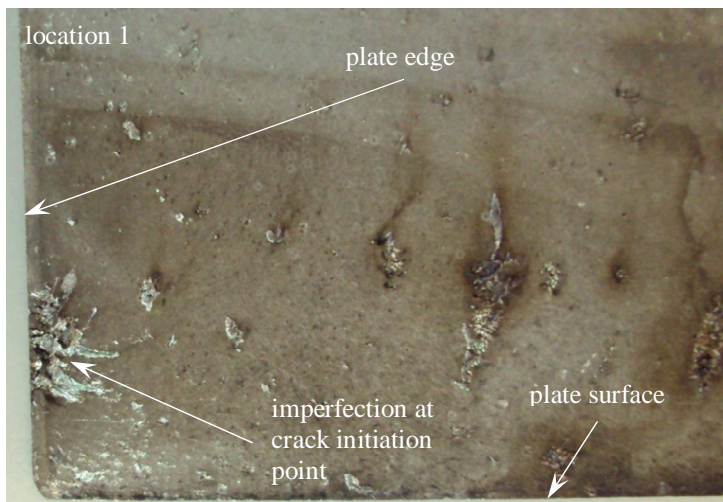


Figure 3.20 Imperfection at location 1 of CB462.

Figure 3.20 shows the imperfection at location 1. As can be seen, the imperfection at the crack initiation is easily detectable without any magnification device. Figure 3.21 presents the microscopic image of the imperfection at the crack initiation point of location 1. The image revealed that there are some non-fractured grains at the crack initiation point. It implies that there was no bonding between grains of both fracture surfaces. It can also be described as a hole in the material. If this imperfection is located on the plate surface, the specimen can be described as a pre-notched specimen. The radius at the boundary of the imperfections can be very small, even tends to zero. In both cases, it causes high stress concentration at the boundary of the imperfections. As a result, the boundaries become a highly likely location for the local plasticity and consequently for the fatigue crack initiation.

For fracture surface examination, one specimen was selected for cast steel grades G20Mn5, G18NiMoCr 3-6 and two specimens for steel grade G22NiMoCr 5-6. The fracture surfaces of these specimens were also examined by the electron microscope and similar imperfections were detected at the crack initiation point of the base material of cast steels. Figure 3.22, Figure 3.23 and Figure 3.24 show the fracture surfaces of those specimens with the microscopic images of detected imperfections at the fatigue crack initiation points.

Besides the fatigue crack initiation points, the imperfections were visually observed at a different location of the fracture surfaces. These locations were also examined by the electron microscope and similar imperfections were detected at those locations. The fatigue crack initiation took place from the imperfections at surface and subsurface of the plates. The reason of the fatigue crack initiation and propagation in the base material of cast steels was clearly determined and no additional EDS measurement was performed.

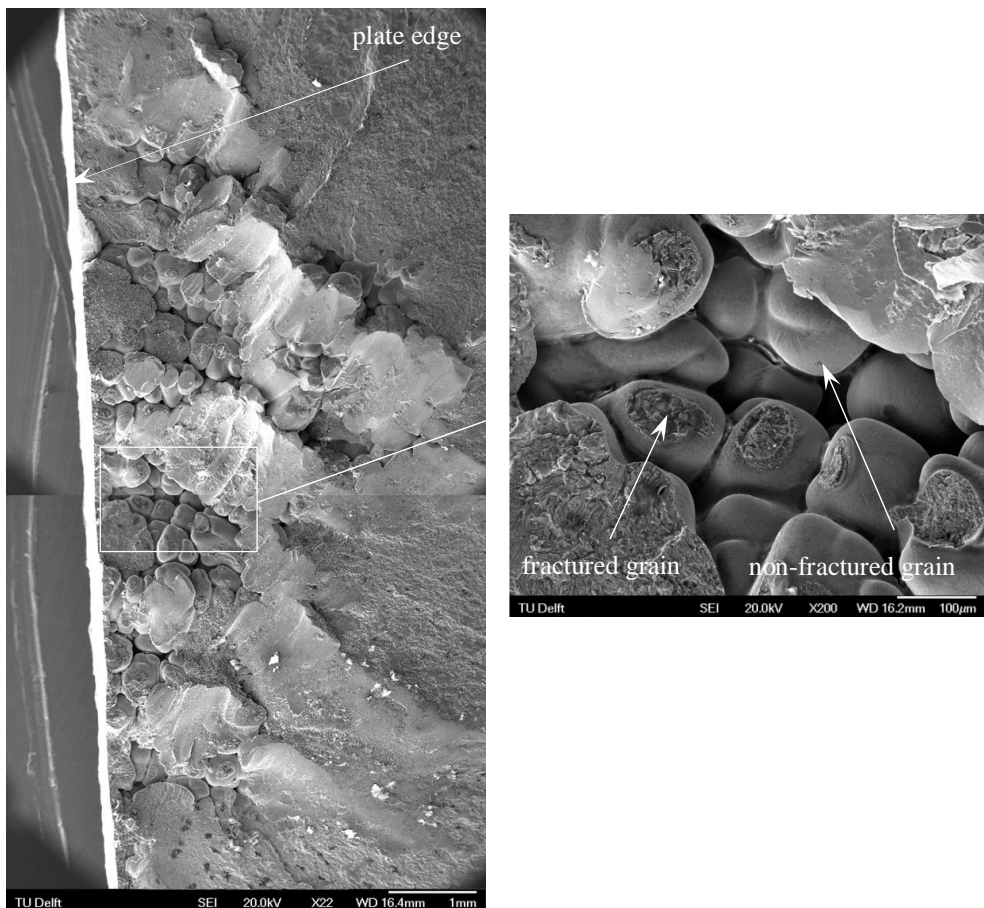


Figure 3.21 Imperfection at crack initiation point of location 1 of CB462.



Figure 3.22 Fracture surface of C895 and imperfection at the crack initiation point.

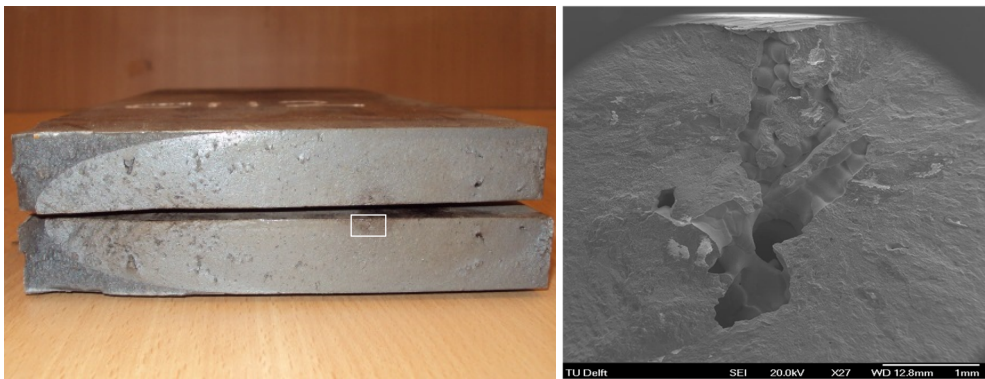


Figure 3.23 Fracture surface of C112 and imperfection at the crack initiation point.

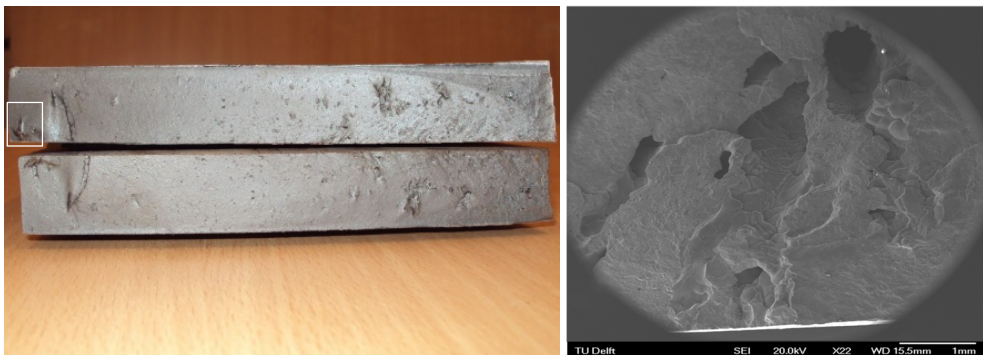


Figure 3.24 Fracture surface of CB113 and imperfection at the crack initiation point.

The results of the examination show that the pores at the surface and subsurface of the plate are the reason of the fatigue crack initiation in the base material of the cast steels. In general, cast steel is produced by casting liquid steel into the mould, followed by solidification. During this process, oxygen may become dissolved in the liquid metal. This

dissolved oxygen can combine with carbon to form carbon monoxide bubbled whereas liquid steels solidify. The formed gas bubbles will release during solidification, but in case of fast solidification, there will be insufficient time for the release and the gas will be arrested by solidified metal layer. In addition, shrinkage will occur throughout solidification and it will restrict bonding of grains which also results in pores with the consequence of a reduction of mechanical properties of the material. It is also seen that this kind of internal imperfections can influence fatigue strength of the material. In case of use cast steels, the fatigue strength reduction due to the internal imperfections should be taken into account for fatigue loaded structures.

3.5 Summary

This chapter presents the visual and microscopic examination on the fracture surfaces of the base material failure of the welded plate specimens made of the rolled and cast steels. The fatigue tests on these specimens were performed by Pijpers (2011). In order to discover the reason of fatigue crack initiation in the base material instead of welded connections, visual and microscopic examinations was performed on the fracture surfaces. In addition, EDS measurements were carried out on the fracture surfaces of the rolled steels. During the inspection, attention was mainly paid to the fatigue crack initiation region. From visual inspection of all the selected specimens, imperfections were detected on the fatigue crack initiation locations.

The microscopic images of crack initiation locations in the base material of rolled steels show that the fracture surfaces of the fatigue crack initiation regions are rougher than other parts of the fracture surface. These rough surfaces were observed up to a certain depth and then the fracture surface becomes smoother. It completely contrasts to usually known fatigue induced fracture surfaces. On the other hand, it indicates that the material at the fatigue crack initiation locations was harder than in another part, because fatigue crack propagation in a hard material will cause a rough fracture surface. The more detailed visual inspection revealed that the rolled steels contain some repair welds. Namely, fatigue cracks in the base material of rolled steels of V-shape welded connections took place at the locations of the repair weld. The reason of the repair weld was not found. It is assumed that the material was damaged during manufacturing and the damages were repaired by welding. The hardness measurement on the repair weld shows increase in hardness of the heat affected zone of the repair weld, which explains the observed rough fracture surfaces at the fatigue crack initiation locations. This kind of repair weld in the base material should be avoided as far as possible. If it is really necessary to repair by welding, the owner of the structure must be informed and the consequences should be discussed with relevant experts.

The microscopic examination on the fracture surface of the cast steels shows that the fatigue crack initiation in the base material of cast steels is the result of the pores at the

surface and subsurface of the plates. This kind of imperfections could be expected in cast steel due to its production process. In case of structural application of cast steels, the effects of the imperfections should be taken into account for fatigue loaded structures. According to ASTM E 446-98 (1998), the material used for the experiments has quality I for the weld area and quality II for other areas. It is seen that the specimens were failed away from the welded connection where probably the material has quality II. In order to verify this, it is recommended to perform fatigue tests on welded connections made of very high strength cast steels with quality I. It will also provide an opportunity to evaluate the reliability of the inspection documents, which allow some imperfections for the material with the quality I.

Part II: Repair of fatigue cracks in welded connections

Part II: Repair of fatigue cracks in welded connections consists of Chapter 4, Chapter 5 and Chapter 6 in which the experimental programme and the results of the experiments are dealt with.

Chapter 4 presents an extensive literature review on the fatigue repair methods for steel structures. The application procedure for each method is explained and experimental results or results from field application are given to evaluate the effectiveness of the method. The advantages, drawbacks and applicability conditions are specifically mentioned.

Chapter 5 shows the fatigue tests to determine the fatigue strength of repaired V-shape welded plate specimens. The test specimens were prepared from S690 and S890 rolled steels and from the cast steels with similar grades. The applied repair procedure is explained in detail.

Chapter 6 describes fatigue crack growth tests on the base material of S690 and S890 high strength rolled steels. Material parameters for the Paris fatigue crack growth law were established. In addition, the threshold stress intensity ranges for these steel grades were obtained from the experiments.

Chapter 4

Literature review

4.1 Introduction

Each structure is designed for a certain period of time, which is called the service life/economic life. In addition, besides their economic life, the structures under fluctuating loads have to be designed against fatigue. Fatigue is the formation of a crack due to the fluctuated design loading within elastic stresses. The service lives of structures stated at the beginning of the design and fatigue life are determined by following a calculation procedure based on acting loads and structural details. In some cases, the economic life of structures is longer than the fatigue life. Consequently, this makes it essential to concentrate on fatigue life extension. There is also a possibility that fatigue life extension is required for existing structures after reaching their service life. In both cases, fatigue life extension can be provided by repairing fatigue cracks and/or reinforcing critical locations of the structure. One of the objectives of the current study is to determine a suitable fatigue crack repair method and to evaluate the effectiveness of the method for welded connections made of very high strength steels. Various fatigue crack repair methods are available. These established methods are applied for fatigue crack repair in mild steels. Therefore, the available results and fatigue life extension by repair is meant for mild steels. The effectiveness of the methods on very high strength steel connections has not been established yet. During this literature study, available repair methods were examined. The application procedures and results of application on different steel grades have been studied. By comparing the various methods, an appropriate method will be selected and it will be used for the repair of fatigue damaged welded specimens made of very high strength steels.

Most emphasis was put on repair methods used like: grinding, hole drilling, splice plate, repair by welding, peening and gas tungsten arc remelting. These methods are suitable for the repair of fatigue cracks with certain depths. The methods are classified as repair methods for shallow and the deep cracks.

4.2 Repair methods for shallow fatigue cracks

4.2.1 Grinding

Grinding can be a useful tool to remove the part of a detail containing small cracks, especially the cracks at the edge of the plates or flanges. After the removal process, the created groove should be tapered with a slope of 2.5:1. The last stage of grinding, which is also called the finish grinding, should be performed parallel to the applied cyclic stresses. In this way, scratches created during the grinding process will be located parallel to the applied stresses. Consequently, occurrence of stress concentration at scratches can be avoided and the negative effect of grinding is eliminated. In addition, the effects of the possible cross sectional reduction need to be taken into account, where grinding can lead to strength reduction of the elements or connections [Dexter et al., 2013]. The grinding process is also utilised for fatigue strength improvement of welded connections. The execution of the grinding procedure for fatigue strength improvement of welded connections is given by Haagensen et al. (2001) in the IIW recommendations.

In welded connections, when the weld cools down to ambient temperature, some micro cracks can form due to shrinkage of the weld material in the cooling down phase. Under cyclic loads, these micro cracks will propagate and become small fatigue cracks. The removal of these micro cracks should improve the fatigue life of the welded connections. However, studies have shown that the fatigue strength improvement is not as high as expected. This might be due to created defects during grinding, which caused fatigue crack initiation in a very early stage of the service life [Fisher et al., 1979].

Grinding is also applied in other repair and retrofit techniques as a tool for finishing surfaces after hole drilling and repair welding. Two grinding tools are available: disc grinding and burr grinding. The application process as well as the effectiveness of the methods will be discussed in the following sections.

4.2.1.1 Disc grinding

Disc grinding is commonly used equipment in the metals removal process. The operator of the grinder has to perform the process very carefully in order to avoid too much material removal. In case of losing the control of the equipment, it will cause deep gouges in elements. For the repair of fatigue cracks, the aim of grinding is to remove material up to the crack depth and attention should be paid to avoid unnecessary material removal. When it is used as a fatigue strength improvement method, the objective of the grinding process is to remove a small amount of material. Dexter et al., (2013) specified the procedure for using a disc grinder as a repair method. Grinding should be performed at the weld toe and the depth of the grind should be a minimum of 0.8 mm and a maximum of 2 mm or 5% of

the plate thickness (see Figure 4.1). The process should be finalized with one pass. Kirkhope et al., (1999) showed that the fatigue strength improvement for a disc ground welded connection at 2 million cycles is in the range of 20-50%.

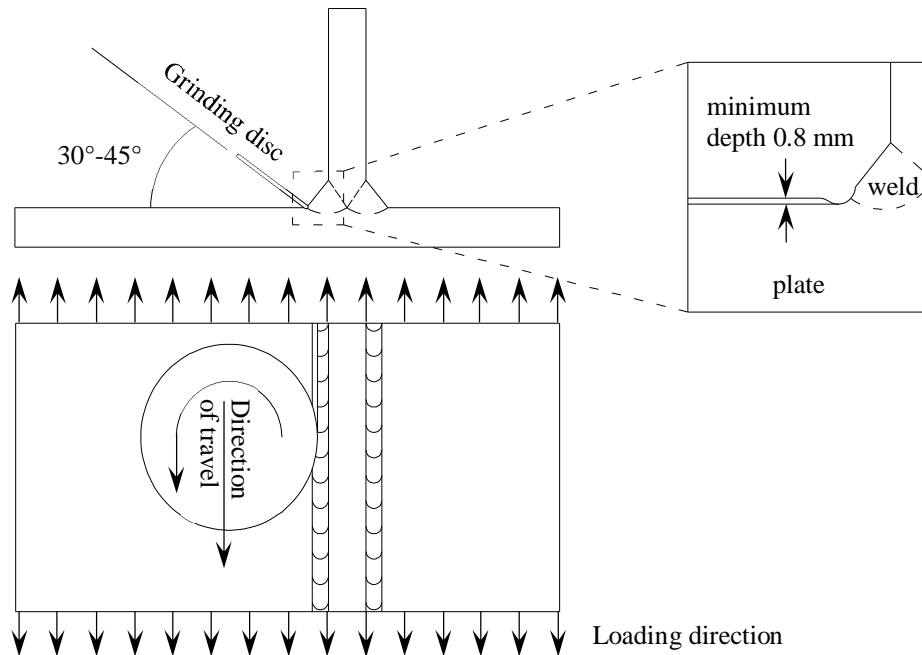


Figure 4.1 Schematisation of disc grinding process [Dexter et al., 2013].

The grinding wheels are in sizes from 101mm to 230 mm and made from aluminium oxide. Figure 4.2 shows a photo of a disc grinder with different wheel sizes.



Figure 4.2 Disc grinder with different wheel size [Dexter et al., 2013].

Fatigue life extension is actually a function of the repair depth attained after the total crack removal process has been achieved. It is experimentally shown that the original fatigue life can be regained when repaired crack depths are up to 30% of the plate thickness. Expected fatigue life extension is decreased for repaired depths exceeding this limit. The created groove geometries have an influence on the fatigue life extension. Groove geometries have to be designed in such a way that the cracks propagation is stopped and re-initiation of fatigue cracks is prevented. However, if crack re-initiation is inevitable, the groove geometry has to be capable to force crack initiation on the plate surface rather than in the bottom of the groove. By forcing crack initiation on the plate surface, the whole original plate thickness is re-established for crack propagation, which results in a longer fatigue crack propagation life. In addition, from an inspection point of view, inspection on the plate surface is easier and more reliable than inspection in a groove. For underwater applications, this is a very useful method, like for repair tubular joints of jacket platforms [Rodriguez-Sanchez et al., (2006)].

4.2.1.2 Burr grinder

Burr grinders are easier to utilize than disc grinders and provide the opportunity to be used in more complex regions where it is difficult to use disc grinders. Burr grinders are more suitable for last layer grinding or treatment of weld edges. It is also useful equipment for hole enlargement. On the other hand, the cutting rate of a burr grinder is lower than that of a disc grinder. Consequently, it is a slow process as compared to a disc grinder. The application of the process is similar to that of disc grinding. Since the equipment is different, it requires additional care and needs to be held differently (see Figure 4.3) [Dexter et al., 2013].

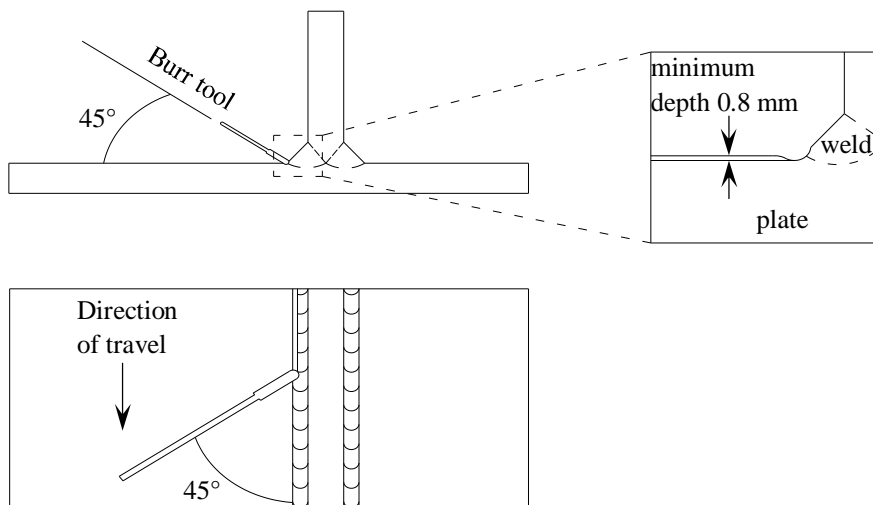


Figure 4.3 Execution burr grinding process [Dexter et al., 2013].

In practice, various rotary burr tips are available. For the crack removal process, tungsten carbide rotary butt tips with a radius of 4.7 to 8 mm are recommended. The burr grinder is also good equipment for finalizing ground surfaces with a stone attachment. This process will remove rough surfaces due to grinding at the surface.



Figure 4.4 Burr grinder with various carbide burr tips [Dexter et al., 2013].

The burr grinding treatment improves the fatigue strength of welded connections by the removal of surface defects and adjusting whole weld faces, which is also called full profile burr grinding. In this way, all weld faces are machined to remove surface defects, that existed during welding. In addition, grinding creates a smooth transition between base material and weld material. Consequently, a favourable weld shape with lower local stress concentration can be obtained. This post weld treatment can improve the fatigue strength in the range of 50 and 200% for fatigue strength at 2 million cycles. The improvement depends on the connection types [Kirkhope et al., 1999]. According to IIW recommendations, the fatigue strength improvement by grinding can increase the allowable stress range by a factor 1.5, which results in a fatigue life improvement by a factor 3.4 [Haagensen et al., 2001]. The improvement only affects at the applied location which means that the other locations of the improved connections might be critical for the fatigue crack initiation.

Fisher et al., (1979) applied this method on a fillet weld of cover plated beams. The cover plate was A36 steel with the yield strength of 295.8 MPa and the beam had a W14X30 profile. The tensile test on the beam material resulted in a yield strength of material of 251.7 MPa and 275.8 MPa for the flange and the web material respectively. Two fatigue test series were prepared in the as-welded condition and repaired fatigue damaged specimens. Fatigue tests were executed on the cover plate beams in the as-welded condition to determine the fatigue life of the connection. In a second test series, the fatigue tests were

executed on the specimens in the as-welded conditions to create fatigue cracks in the fillet weld of the cover plate. The specimens were exposed to a cyclic load until 75% of the lower confidence limit of the weld detail was achieved. Fatigue cracks were detected by ultrasonic inspection, magnetic particles examination and visual inspection with 10X magnification. When the defined number of cycles was reached, fatigue crack inspection took place and the detected cracks were removed by burr grinding. The grinding process was continued until the cracks became invisible. After the crack removal process, the test specimens were exposed to the cyclic loading again. The results of the second series were compared with the results of the first series. All data of the repaired specimens were located at the under confidence limit of the first series, which represented the fatigue strength of the fillet welded cover plated beam in the as-welded condition. Results showed that the removal of the small crack is not an effective repair method. After failure of the specimens, the fracture surfaces were examined and it appeared that the crack tip was not completely removed during the burr grinding process. This is a result of limiting the grinding depth to 2 mm. Consequently, an insufficient amount of material was removed.

4.2.2 Peening

Peening is a cold working process which creates plastic deformation at the surface of material by impacting with a tool or metal balls. It is mainly used as a fatigue strength improvement method for welded connections by introducing compressive stresses at the weld toe.

In welded steel structures, high residual tensile stresses can be introduced during welding. The thermal cycles due to welding lead to microstructural changes and volume expansion, which results in residual stresses. Furthermore, material shrinkage during cooling down stage also cause additional residual stress occurrence. As a result, the weld region of a welded connection contains high tensile residual stresses in the as-welded condition. Therefore, under service load, welded connections will be exposed to wholly tensile stresses even if the applied stresses are compressive. From a fatigue point of view, residual tensile stresses cause a decrease of the fatigue strength of welded connections. It can be improved by eliminating residual tensile stresses and introduce compressive stresses at the weld region. Peening is an option for introducing compressive stresses at the weld region. Peening can introduce compressive residual stresses up to a magnitude of material yield strength. Therefore, the method is more effective for high strength steels. In case of a repair weld, the combination with peening can lead to a long fatigue life extension.

In addition to this, plastically deformed material at the weld toe can also blunt sharp inclusions and it may create a smooth transition between the weld and the base material. As a result, the stress concentration at the weld toe will decrease. These are additional beneficial effects of peening [Kirkhope et al., 1999]. Moreover, since peening can blunt

small defects at the weld toe, it can also be used for repairing shallow fatigue cracks in the welded connections. The procedure and effectiveness on fatigue crack repair of hammer peening and ultrasonic peening is described in the following sections.

4.2.2.1 Hammer peening

Hammer peening is performed manually by means of a pneumatic or electrical hammer operation to create approximately 5000 blows/min. It is executed with hardened steel bits which have rounded hemispherical tips with varying diameters between 6 and 18 mm. The angle between weld face and hammer peening tools should be approximately 90 degrees and the angle between base material and hammer peening tools should be 45 degrees (see Figure 4.5). The movement at the weld toe should be at a rate of about 25 mm/s. IIW recommendations give extensive information about the application and quality control procedure of hammer peening [Haagensen et al., 2001]

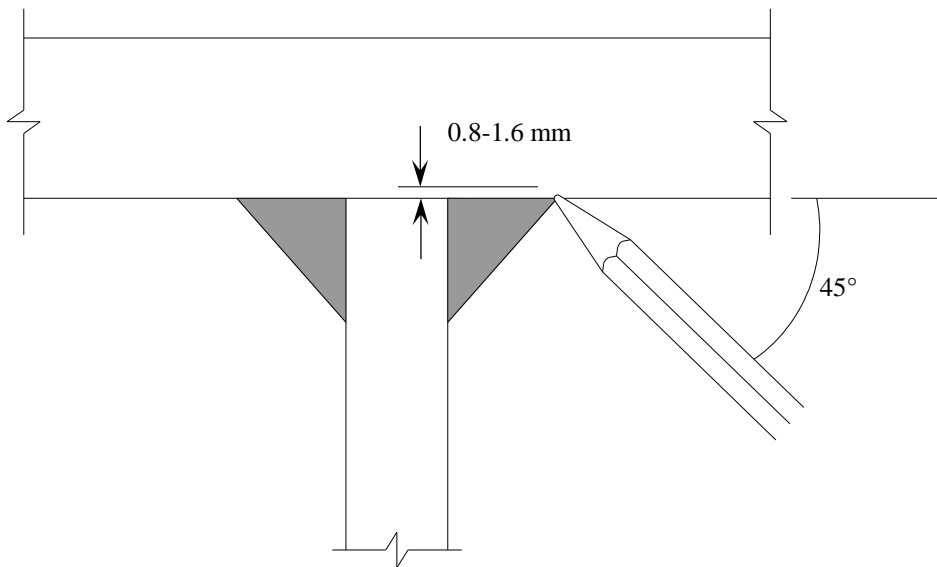


Figure 4.5 Illustration of application hammer peening [Dexter et al., 2013].

Various studies have been shown that applied pressure and the number of passes affect the created plastic deformation and induced residual stresses. These studies have shown that the best results can be obtained by applying lower pressure (280kPa) and a greater number of passes (up to 6). It is recommended that penetration should be between 0.8-1.6 mm. On the other hand, the penetration depth must be adjusted for different material thicknesses. The penetration depth of thin material should be lower and the peening must be carried out very carefully, so that the thickness of the element is not reduced too much. The generated compressive stresses are located in the depth of two to four times plastically deformed

grains. It is also shown that hammer peening is an effective method for surface crack repair up to 3 mm deep [Dexter et al., 2013].

In addition, hammer peening is a useful method to improve the fatigue strength of welded connections that are fatigue cracks free. Research studies have shown that hammer peening can increase fatigue resistance at least one detail category. It also has a beneficial effect on the fatigue strength of the repair weld and it was found that the fatigue strength of repair welds can be improved by 175% after hammer peening [Dexter et al., 2013].

Dexter et al., (2003) repaired the fatigue cracks in a girder with non-load bearing attachments by welding and with subsequent hammer peening treatment. The girder with non-load bearing attachment was exposed to cyclic load of 220 kN. The loading frequency varied from 2 to 2.5 Hz. The fatigue crack size in specimens versus to the number of cycles was regularly recorded and the crack length was measured. This procedure was followed until the established failure criterion was reached, which was defined as the development of a through thickness crack at least 50 mm in length along the weld toe. The cracked section was repaired by welding. After repair of the fatigue cracks, the fatigue test was continued. Some specimens were tested under as repaired conditions, while some of the repair welds were treated with hammer peening. Test results indicate that hammer peening significantly improves fatigue strength of the repair weld. The number of cycles determined that after repair weld with hammer peening is at least as same as the original detail.

Infante et al., (2004), used hammer peening as a repair method for welded fatigue test specimens. Fatigue tests were performed on fillet welded T joints (see Figure 4.6). The specimens were manufactured from medium strength structural steel with a yield strength of 400 MPa and an ultimate tensile strength of 555 MPa. The fillet weld was applied in an overmatched condition.

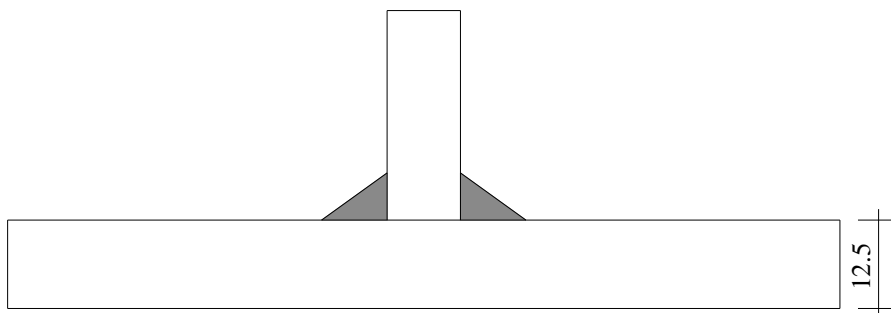


Figure 4.6 Fillet welded fatigue test specimen [Infante et al., 2004].

Specimens were tested with a three point bending test setup. An extensive experimental study was carried out during the research. Some specimens were tested until complete failure of the specimen or tested until 6 million cycles in case of runouts. Fatigue tests were performed on some specimens in the as-welded condition to determine the fatigue crack

growth behaviour in the specimens. Based on these test results, it was estimated that the crack with a 2.4 mm depth lead to 25% strain reduction in strain gauge measurements around the weld toe. The fatigue cracks in some specimens were repaired by hammer peening after observing this strain reduction. After the repair of the crack, fatigue test was continued until failure of the specimens. In same study, the welded connections were improved by grinding before testing. The test results show that the fatigue strength of a ground welded joint is the same as the fatigue strength of the welded joint repaired by hammer peening (see Figure 4.7). The study has also confirmed that hammer peening is effective until depths of 2.5-3 mm and that fatigue cracks with depths up to 3 mm can be repaired by hammer peening.

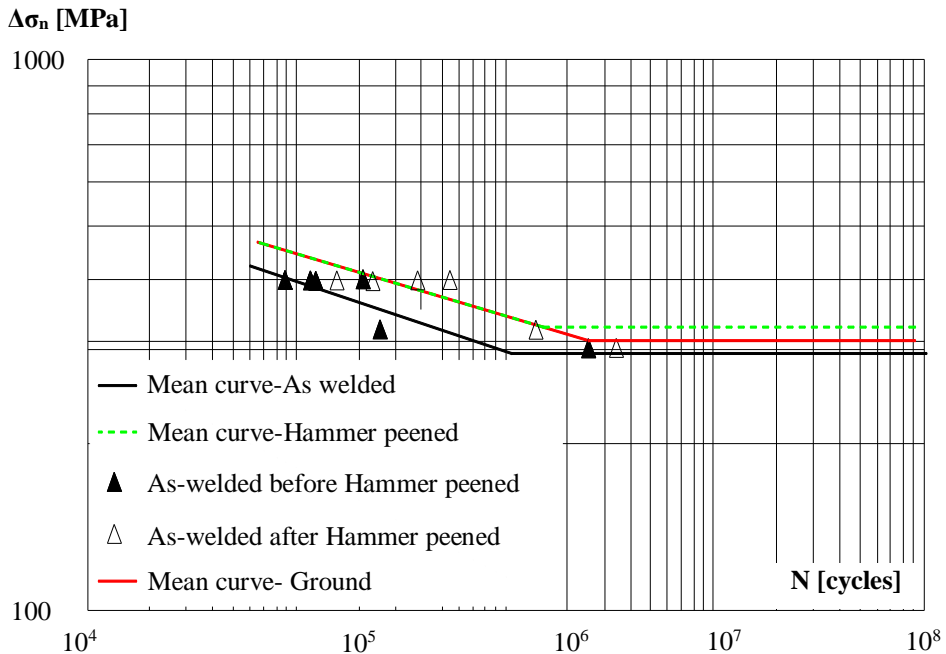


Figure 4.7 Comparison of S-N curves of repaired welded T joint [Infante et al., 2004].

Fisher et al., (1979) used hammer peening for repair of fatigue cracks in cover plated beam specimens. Test specimens were made of A36 and A58 steels, which have a yield strength of 295.8 MPa for A36 steel and 391.8 MPa for A58 steel and an ultimate tensile strength of 433 for A36 steel and 546.8 MPa for A58 steel. The beam test specimens were tested under constant amplitude cyclic load. Tests were performed until the crack length reached 19 mm at the weld toe and the crack depth was assumed to be between 1.6 mm and 4 mm. These cracks were repaired by hammer peening. The hammer peening was performed until the crack could not be detected by visual inspections. The fatigue tests on these specimens were resumed until failure. In some specimens, hammer peening was used as a fatigue strength

improvement technique for the original weld, before the repair. The results of the fatigue test revealed that use of hammer peening as an improvement method is more effective than using it as a fatigue crack repair method. The fracture surfaces of the specimens have shown that the crack tip of deep cracks with a depth above 3 mm, remained in the material and it propagated under fatigue load.

4.2.2.2 Ultrasonic peening

The ultrasonic peening (UP) is one of the modern newly developed and encouraging processes for the fatigue strength improvement method of welded connections. This process is also called ultrasonic impact treatment (UIT). The ultrasonic peening provides improvements on the fatigue strength of welded connections by eliminating detrimental residual tensile stresses and introducing compressive residual stresses at the surface of the material. It also improves the weld geometry and consequently reduces stress concentration at weld toe zones. The mechanical properties of the material surface layer are also improved. Fatigue test results have shown that the UP is the most effective improvement method as compared to traditional techniques such as: grinding, TIG dressing, heat treatment, hammer peening and shot peening [Dextra et al., 2008].

The UP technique combines the effect of the high frequency impacts of the special strikers and ultrasonic vibration in the treated material. During application of the ultrasonic treatment, the striker vibrates in the small gap between the end of the ultrasonic transducer and treated specimen, and impacts the treated area. The combination of high frequency movements and high frequency vibration induced in material is called the ultrasonic impact.

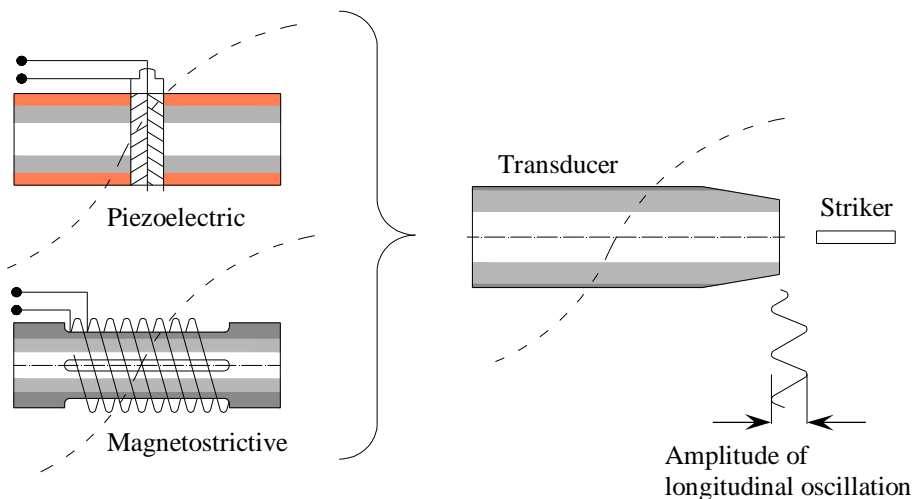


Figure 4.8 Schematic view of transducer for UP [Kudryavtsev et al., 2011].

In general, two types of ultrasonic transducers are used for UP: magnetostrictive and piezoelectric (see Figure 4.8). Both transducers conduct the same task of converting

alternation electrical energy to vibrating mechanical energy in a different manner. Magnetostrictive transducers first convert the alternating electrical energy from the ultrasonic generator to alternating the magnetic field. The created magnetic field is used to stimulate mechanical vibrations at an ultrasonic frequency resonant strip of magnetostrictive material. The magnetostrictive transducer converts the energy two times: electrical energy to magnetic energy and from magnetic energy to mechanical energy. This conversion causes some efficiency loss. Therefore, the effectiveness of the magnetostrictive transducer is lower than the effectiveness of piezoelectric transducers. In addition to this, a magnetostrictive transducer requires water cooling during application [Kudryavtsev et al., 2011].

Piezoelectric transducers convert the alternating electrical energy directly to mechanical energy. Nowadays, piezoelectric transducers are produced with more efficient and stable ceramic materials. It makes them suitable for use under different temperature and stress conditions, which make them more reliable. It reduces the energy cost by approximately 60% [Kudryavtsev et al., 2011].

The vibration frequency of ultrasonic transducers is typically between 20-30 kHz. As mentioned before, the transducer may be based on either piezoelectric or magnetostrictive technology. Regardless of what technology is used, the transducers will be vibrating with an amplitude of 20-40 μm . During this vibration, the striker will be impacted at varying stages by the transducer tip. These impacts actuate the striker and the striker impacts the treated surface. Repetition of these impacts vary from hundreds to thousands of times per second [Kudryavtsev et al., 2011].

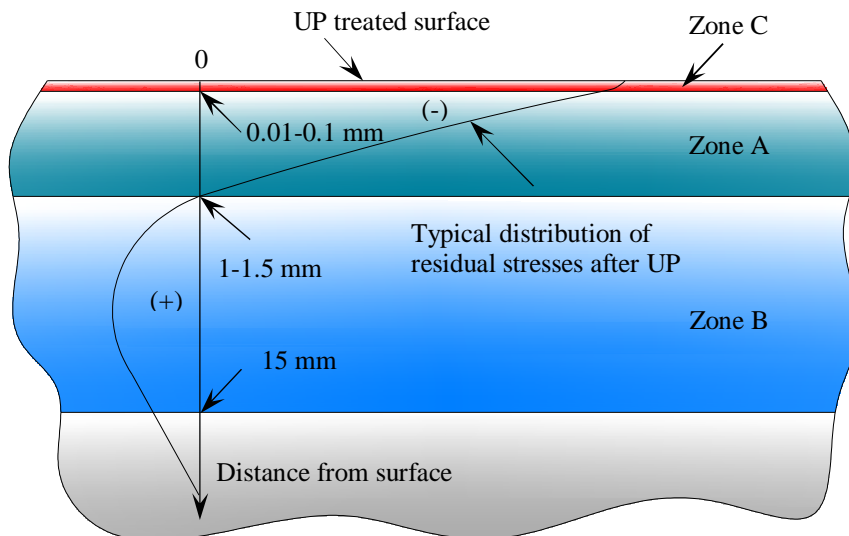


Figure 4.9 View of the cross section of UP treated material [Kudryavtsev et al., 2011].

Figure 4.9 gives a schematic view of the cross section an UP treated material. Zone A with a depth about 1-1.5 mm represents plastic deformation and compressive residual stresses after ultrasonic peening. Zone B presents the relaxation of residual stresses induced by welding. The depth of the layer is about 15 mm from the treatment surface. The zone of nanocrystallization at the surface is indicated by zone C and the depth is 0.01-0.1 mm from the surface [Kudryavtsev et al., 2011]. The application procedure and quality control assessment of UP are described in IIW recommendations [Marquis et al., 2016]

In same analogy with hammer peening, UP treatment removes the sharp inclusions and defects from the weld toe. It can therefore be an effective method for the repair of the shallow cracks where the crack depth remains in the area affected by UP. Kudryavtsev et al., (2005) concentrated on effectiveness of UP application to existing structures. The UP method was used for welded transverse non-load carrying test specimens which were exposed to a fatigue load. The data on mechanical properties and chemical composition of the base material are represented in Table 4.1. The geometry of the test specimens is shown in Figure 4.10.

Table 4.1 Chemical composition and mechanical properties of base material [Kudryavtsev et al., 2005].

% wt								σ_y	σ_u	δ
C	Si	Mn	S	P	Cr	Ni	Cu	(MPa)	(MPa)	(%)
0.21	0.205	0.52	0.019	0.007	0.04	0.04	<0.01	260	465	37.6

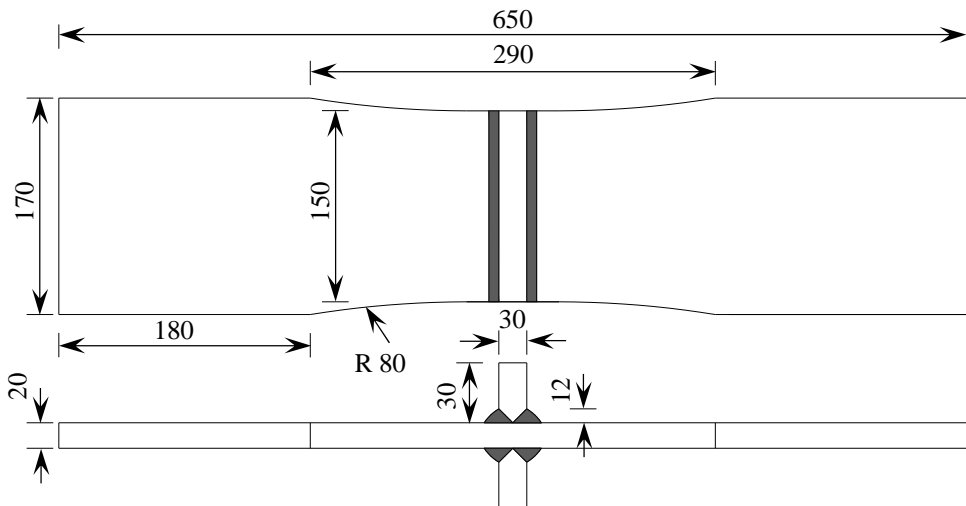


Figure 4.10 Specimen with welded non-load carrying transverse plate [Kudryavtsev et al., 2005].

The fatigue tests were performed under the following conditions: as-welded condition, UP treatment on weld toes before testing and UP treatment on weld toes after fatigue loading with the number of cycles corresponding to 50% of the expected fatigue life of samples in the as-welded condition.

The UP treatment provides a significant fatigue strength increase of welded specimens. Test results were compared based on limit stress with a corresponding stress range at 2 million cycles. As can be seen from Figure 4.11, the increase in limit stress range of UP treated welded specimens is 49 % (from 119 MPa to 177 MPa) compared to the as-welded condition. The improvement is 66% (119 MPa to 197 MPa) for specimens that were treated by UP after exposing to a fatigue load with the number of cycles corresponding to 50% of the expected fatigue life of specimens in the as-welded condition. The fatigue strength of welded specimens increased about 5-10 times by UP treatment. A higher increase of fatigue strength was observed in the specimens that treated by UP after exposing a fatigue load with the number of cycles corresponding to 50% of the expected fatigue life of specimens in the as-welded condition. This can be explained by a more beneficial redistribution of residual stresses and/or restoring fatigue damaged material by UP.

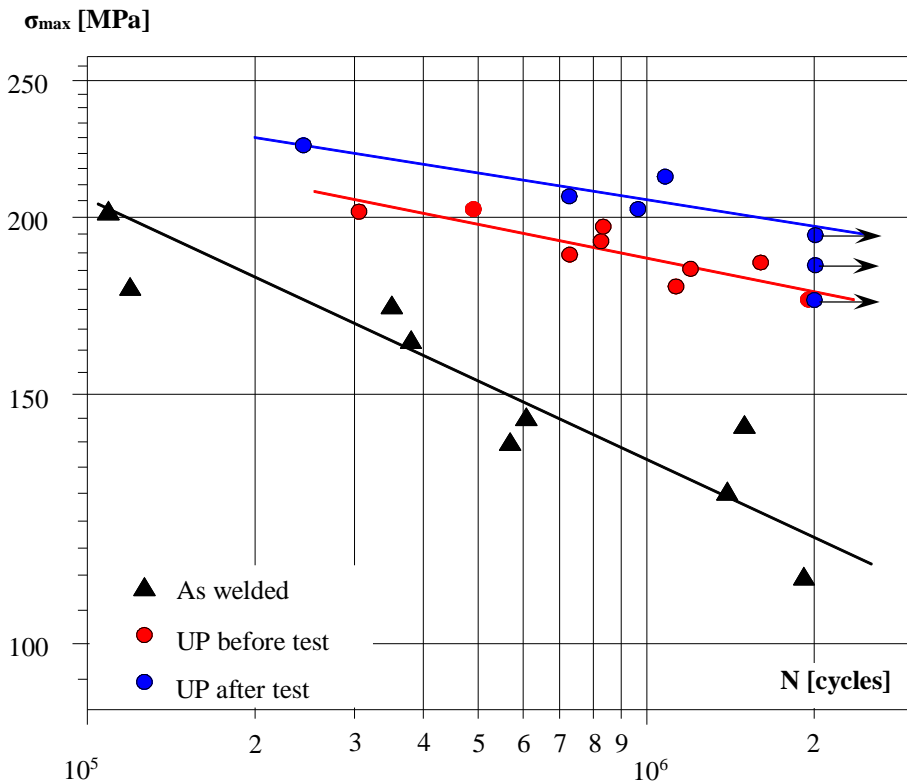


Figure 4.11 Fatigue strength curve of test results [Kudryavtsev et al., 2005].

The fatigue strength curve in the as-welded condition is indicated by a black line. The red line represents the fatigue strength curve of test specimens treated by UP before testing. The blue line is the fatigue strength curve of UP treated specimens that were tested until 50% of the number of cycles corresponding to expected fatigue life in the as-welded condition.

4.2.3 Gas tungsten arc (GTA) remelting

GTA process remelts a small amount of the weld toe and base material by a gas-shielded tungsten electrode. This is done by manually moving a gas shield tungsten electrode with a constant speed along the weld toe and just melting the metal without additional new filler material (see Figure 4.12). The method is generally effective for the repair of surface cracks with a depth of up to 5 mm. The GTA remelting method removes slag and inclusions at the weld toe and by reshaping the weld shape it can create a smooth transition between base and weld material. As a consequence, it reduces the stress concentration effects at the weld toe. Therefore, GTA remelting can also be used as a fatigue strength improvement technique for welded connections. However, it is not an easily performed process in the field and it requires highly skilled welders and good accessibility to the weld [Dexter et al., 2013].

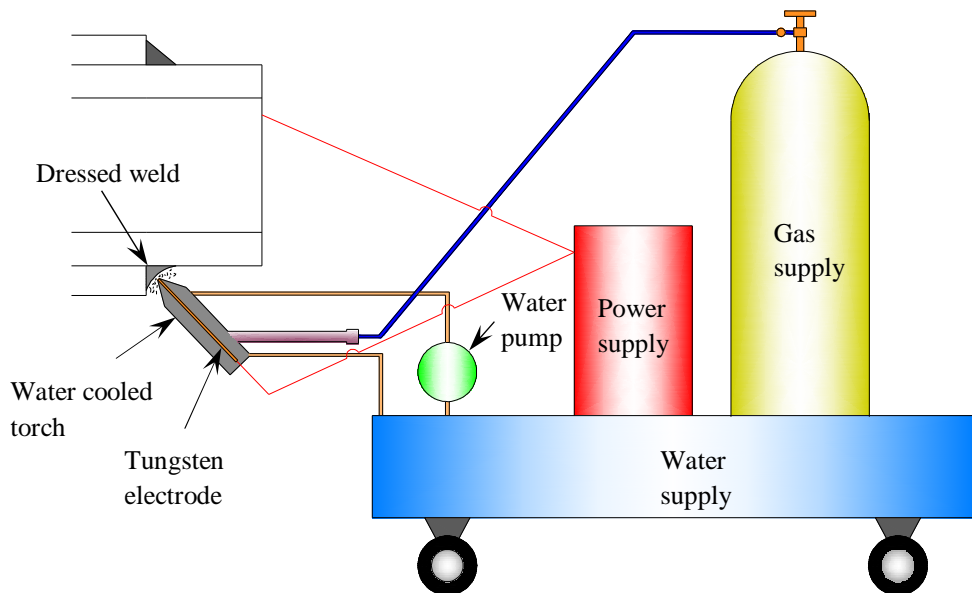


Figure 4.12 Schematisation GTA remelting process [Fisher et al., 1979].

In case of fatigue crack repair, a sufficient amount of material surrounding the crack will be melted in such a way that the crack can be eliminated after the solidification. The repair

process can be effective when the depth of the remelted zone reaches the crack tip. Insufficient penetration will cause leaving a crack buried below the surface. Such cracks will simply continue propagating under fatigue load and will lead to premature failure. The penetration depth of the remelted zone depends on the shielding gas used and the electrode cone angle. It was found that the application of the procedure with argon-helium shielding gas and a cone angle with 60° with respect to applied material results in the most effective penetration of the remelted zone [Fisher et. al, 1994].

Fisher et al., (1979) used the GTA remelting process for the repair of fatigue cracks at the cover plated beam. The test specimens were made from A36 and A58 steels. In a specimen, which had been successfully repaired, crack initiation and propagation was observed at the weld root. However, at 3 of 16 specimens, weld toe failure was observed. After evaluation of the fracture surfaces of these specimens, it appeared that weld toe failure of these specimens was the result of an inadequate remelting penetration. Due to lack of sufficient penetration depth of the GTA process, the remaining crack tip had propagated further after the repair of the crack. This result shows that the GTA remelting crack repair procedure is effective only if adequate penetration is achieved. In other words, the cracked section had to be completely remelted. This method was applied to other test series and it was expected that fatigue cracks in specimens of this series were deeper. In order to achieve suitable penetration depth, high heat input was used for the repair of the fatigue cracks in the specimens. After testing, fatigue cracks initiated at the root of the weld. From this it was concluded that higher heat input provides a sufficient penetration depth of the remelting zone. The results of fatigue tests showed that when adequate remelting is achieved, the fatigue strength of the damaged specimens can be regained. In other words, the fatigue strength of repaired specimens is the same as the fatigue strength of the specimens in the as-welded condition if the weld root is uncritical for the fatigue crack initiation.

4.3 Repair methods for deep fatigue crack

4.3.1 Hole drilling

Hole drilling is probably the most commonly used fatigue crack repair method. The method is performed by drilling a hole at the crack tip to remove the sharp notch at the crack tip. In this manner, further propagation of the fatigue cracks is inhibited. The effectiveness of this method depends on the hole diameter. The hole diameter must be large enough to be able to arrest crack propagation. As a rule of thumb, larger holes show a better performance, but this hole should not reduce the strength and stiffness of the structures. Based on experience, it is proven that a sufficient diameter of the hole is in the range of 50.8 mm to 101.6 mm for steel bridges according to Dexter et al., (2013). It depends on the application and in some

cases a smaller hole may also be sufficient. Large holes could not always be practical and the owners of structures feel uncomfortable with making such large holes in structures. For practical estimation of the hole diameter, the equation (4.1) can be used for steel bridges [Dexter et al., 2003], [Haagensen, 1994].

$$\frac{\Delta K}{\sqrt{\rho}} < 10.5\sqrt{\sigma_y} \quad (4.1)$$

where ΔK is the stress intensity factor range, σ_y is the yield strength of the material and ρ is the radius of the hole. If this relation is not satisfied, the crack will most likely reinitiate from the edge of the hole [Dexter et al., 2003].

Two types of drill bits are used for execution of the method: twist bits and annular cutter (see Figure 4.13). Twist bits can be used for holes with smaller diameters, up to 26 mm. For holes above this diameter, annular cutter will be more suitable. But, hole drilling with annular cutting is slower and the cut surfaces are not smooth. Therefore, the finishing layers need to be cleaned after the drilling process in order to create smooth surfaces. The use of flame cut must be avoided for hole drilling process. The flame cut can introduce a gouged surface and a heat affected zone, which may contribute to the new fatigue crack initiation points [Dexter et al., 2013].



Figure 4.13 Annular cutter and twist bits [Dexter et al., 2013].

The effectiveness of the repair methods depends on detection of the fatigue cracks, thus the reliability of non-destructive testing. Application of the hole drilling method starts with detection of the crack tips. In practice, magnetic particles and red dye penetration are the easiest methods to apply and the most frequently used non-destructive methods. The crack tip of the detected fatigue cracks needs to be determined. If the cracks have propagated

through the thickness of the element, fatigue crack tip inspections need to be performed on both sides of the element to ensure that the crack length is equal at the both sides. Therefore, it is recommended to drill a small reference hole to identify the crack tip at the other side of the element and in accordance with this, the coring machine will be placed in such a way that the bits of the machine are able to remove the crack tip at both sides of the structural element. The removal of the crack tip has to ensure that crack propagation will not occur after drilling. The diameter of the hole is determined by equation (4.1). The result of the calculation depends on the accuracy of the input data. Based on the input, the calculation may result in a hole diameter smaller than 26 mm. In practice, this diameter is not sufficient. For such cases, the minimum hole diameter should always be 26 mm. [Crear, 2001]

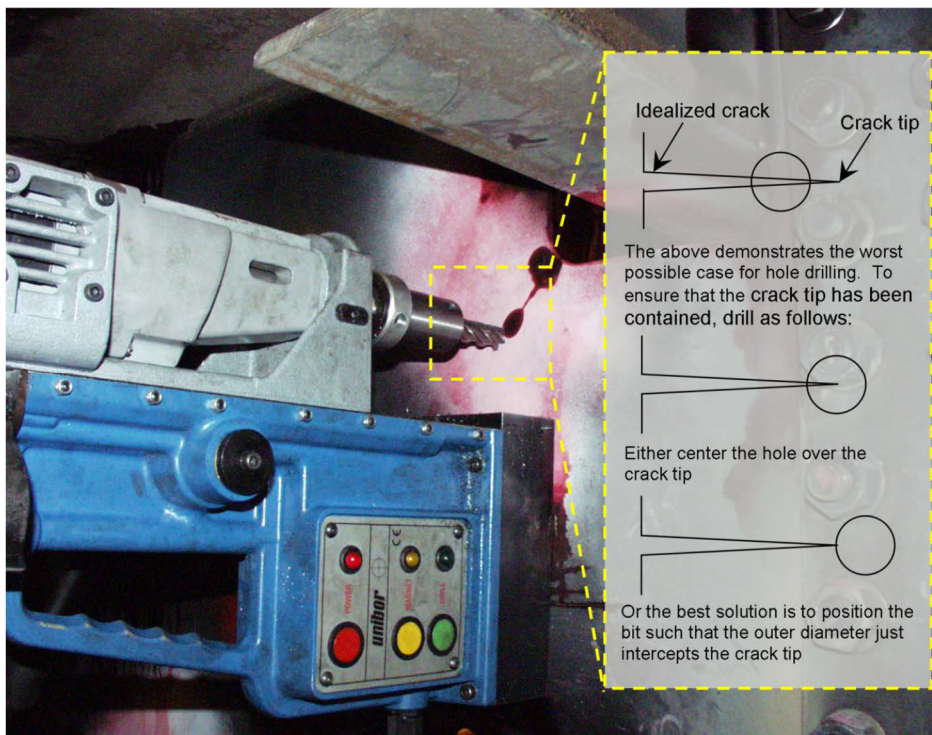


Figure 4.14 Application of hole drill method [Dexter et al., 2013].

Fisher et al., (1998) recommended to put an entire fully tensioned high strength bolt into hole. According to Dexter et al., (2013), the holes with diameters from 24.5 mm and 38.1 mm are more suitable for strengthening by high strength bolts. The bolt will introduce a favourable compressive stress around the hole, which will contribute to avoiding fatigue crack initiation and further fatigue crack propagation in case of a remaining crack tip in the material. Some engineers state, that the bolts may cause difficulties for the inspector for detecting cracks in case of re-initiation of fatigue cracks [Dexter et al., 2013]. Another

improvement for the hole drilling method is cold working. A mandrel is pulled through the hole and the hole is oversized, by which compressive stresses are introduced around the hole. The effectiveness of this improvement was found to be lower than that obtained by a using high strength bolt (see Figure 4.15) [Haagensen, 1994].

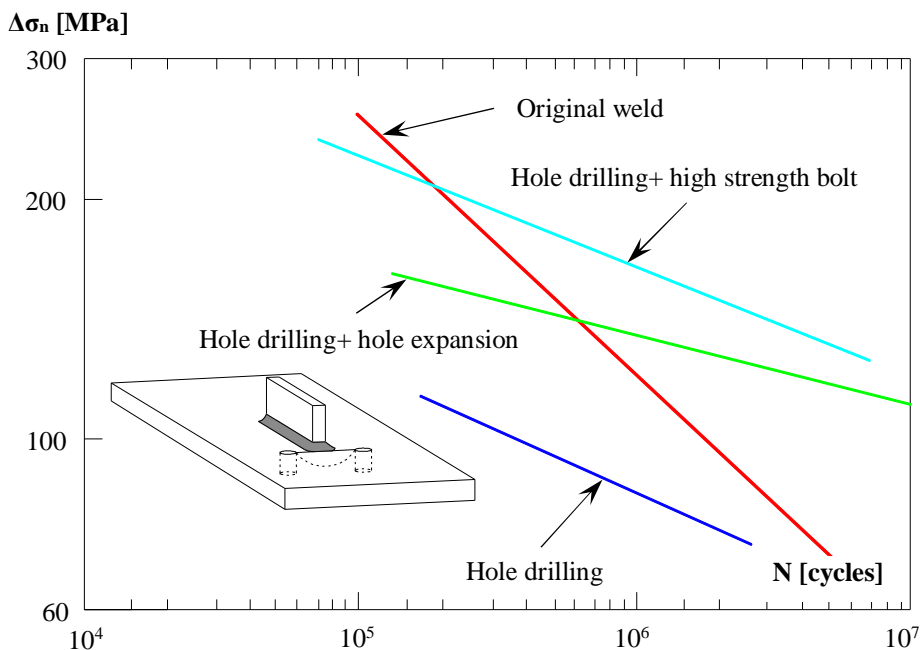


Figure 4.15 Fatigue strength of repaired fatigue damaged specimens by hole drilling method [Haagensen, 1994].

Dexter et al., 2003, used the hole drilling method for simplified models of transverse/longitudinal web frame connections test specimens (see Figure 4.16). The specimens were made from A36 and A572 grade 50 steels. The mechanical properties of the steels were obtained from material certificates. In accordance with this, A36 steel has an average yield strength of 347 MPa and an average ultimate strength of 485 MPa. The A572 grade 50 steel has an average yield strength of 446 MPa and an average ultimate strength of 515 MPa. Fatigue cracks in the web of the specimens were repaired by the hole drilling method. The stop hole was centred at a spot in front of the crack tip with a distance equal to the radius of the hole. This distance was chosen to be sure that the crack tip was removed. Different hole diameters are applied, varying from 14 mm to 76 mm. The aim was to determine the influence of the hole diameter on the effectiveness of the method. In one specimen, a high strength bolt was inserted in the stop hole and fully tensioned in order to evaluate fatigue strength improvement by a high strength bolt for the hole drilling method.

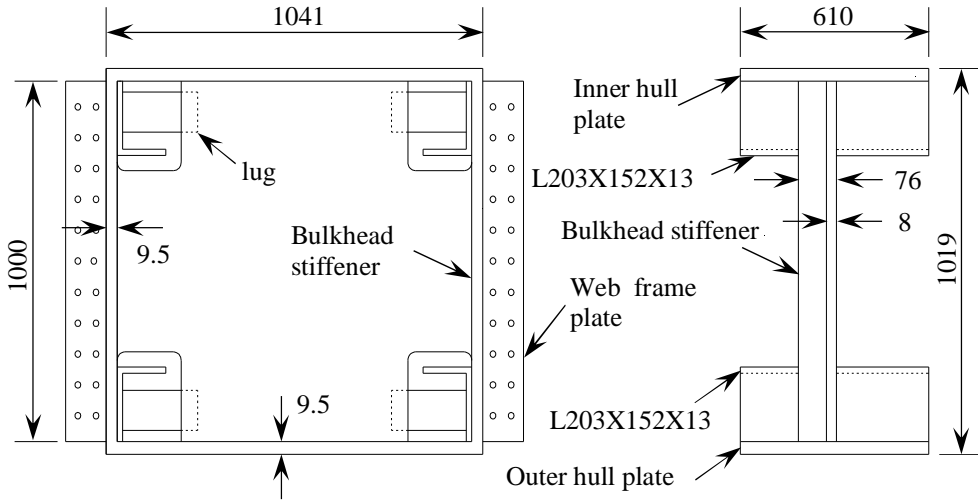


Figure 4.16 Simplified longitudinal/web frame connection specimen [Dexter et al., 2013].

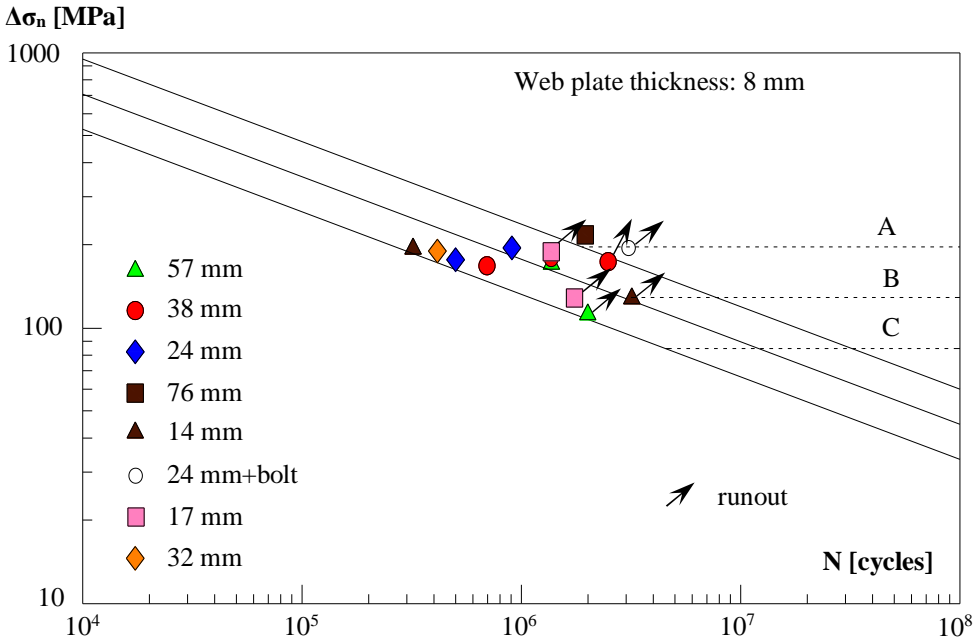


Figure 4.17 S-N curves for different hole size [Dexter et al., 2003].

Fatigue test results were compared with detail classes of the American Association of State High and Transportation Officials (AASHTO). The complete test results were located above detail class C of AASHTO, which is a representative detail category 90 of EN 1993-

1-9 (2006). AASHTO gives the detail class D, which is equal to detail category 71 of EN 1993-1-9 (2006), for hole drilled connections. As can be seen from Figure 4.17, the performance of the stop hole is improved by increasing the hole diameter. The best fatigue performance was obtained from a 24 mm stop hole with a fully tensioned 22 mm diameter high strength bolt.

4.3.2 Splice plate

With this method, crack containing sections are covered with plates on both sides. This method is also called doubler plate or doublers. The philosophy of this method for fatigue crack repair is to add extra cross sectional area at concentrated sections to reduce stress ranges at the crack locations. The reduction of stress ranges will form an obstacle to further crack propagation. This method is usually used for repair fatigue cracks in base material. Figure 4.18 shows an example of this method, which is applied for repairing the fatigue crack in the web of a girder.

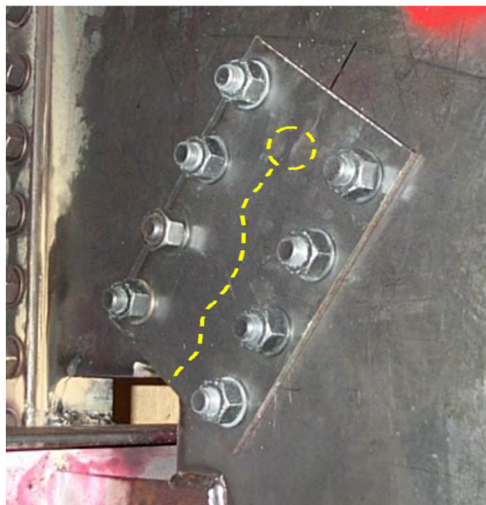


Figure 4.18 An example of splice plate repair. Dashed line represents crack path with a hole at crack tip [Dexter et al., 2013].

Additional plates can be attached either by welding or with high strength bolts. From a fatigue strength point of view, the use of high strength bolts is to be preferred, because in design standard and recommendations, higher detail categories are indicated for connections with high strength bolts. On the other hand, in order to install high strength bolts, it might require drilling a large number of holes and access to hole side of the cracked surface. For these reasons, this method could not always be cost effective or even possible. As it is true for all repair methods, care must be taken that any modification to a cracked area should not introduce new potential fatigue crack initiation points [Dexter et al., 2003].

The effectiveness of the repair method can be improved with the combination of the hole drilling method. A hole will be drilled at the crack tip. Subsequently, the splice plates will be installed at the cracked section. In this manner, further crack propagation is prevented and the stress range at the cracked section is reduced. The combination of the methods can provide a very effective repair method.

Yamasaki et al., (1984) also used this method for the repair of cracked base material. Deep notched wide plate specimens were prepared for monitoring fatigue crack propagation. All specimens were made of JIJ-SM50A steel plates with a yield strength 323 MPa and a tensile strength 490 MPa. First, fatigue cracks were created up to a length of 100 mm under fatigue stress range 98 MPa with stress ratio 0.09. The cracks in the specimens were repaired by means of the splice plate method. The splice plate method was applied with two configurations, with and without a stop hole at the crack tip. The test results showed that for the specimen with a stop hole, crack is stopped by means of a stop hole at a fluctuated loading of 2.5×10^5 cycles. The specimens without stop holes showed a slight crack growth after the repair. Very low fatigue crack propagation was observed compared to the fatigue crack propagation in the specimens without the splice plates. The results have shown that the bolted slice plate provides a sufficient increase in fatigue life and the method is more effective with a combination of hole drilling methods.

Dexter et al., (2003) used splice plate method for retrofitting cracked welded connections. Complex brackets attachment specimens were tested with sinusoidal load and with varying frequencies between 0.3 and 0.5 Hz. The test was executed with a maximum force range of 120 kN on both specimens (see Figure 4.19). The aim was to repair fatigue cracks by welding and reinforcing with splice plates. The fatigue strength of this kind of connections is represented with detail category E according to AASHTO S-N curve, which is comparable with the detail category 56 of EN 1993-1-9 (2006). The intention was to reach at least the fatigue strength of the original connection.



Figure 4.19 Test specimens with complex attachment brackets [Dexter et al., 2003].

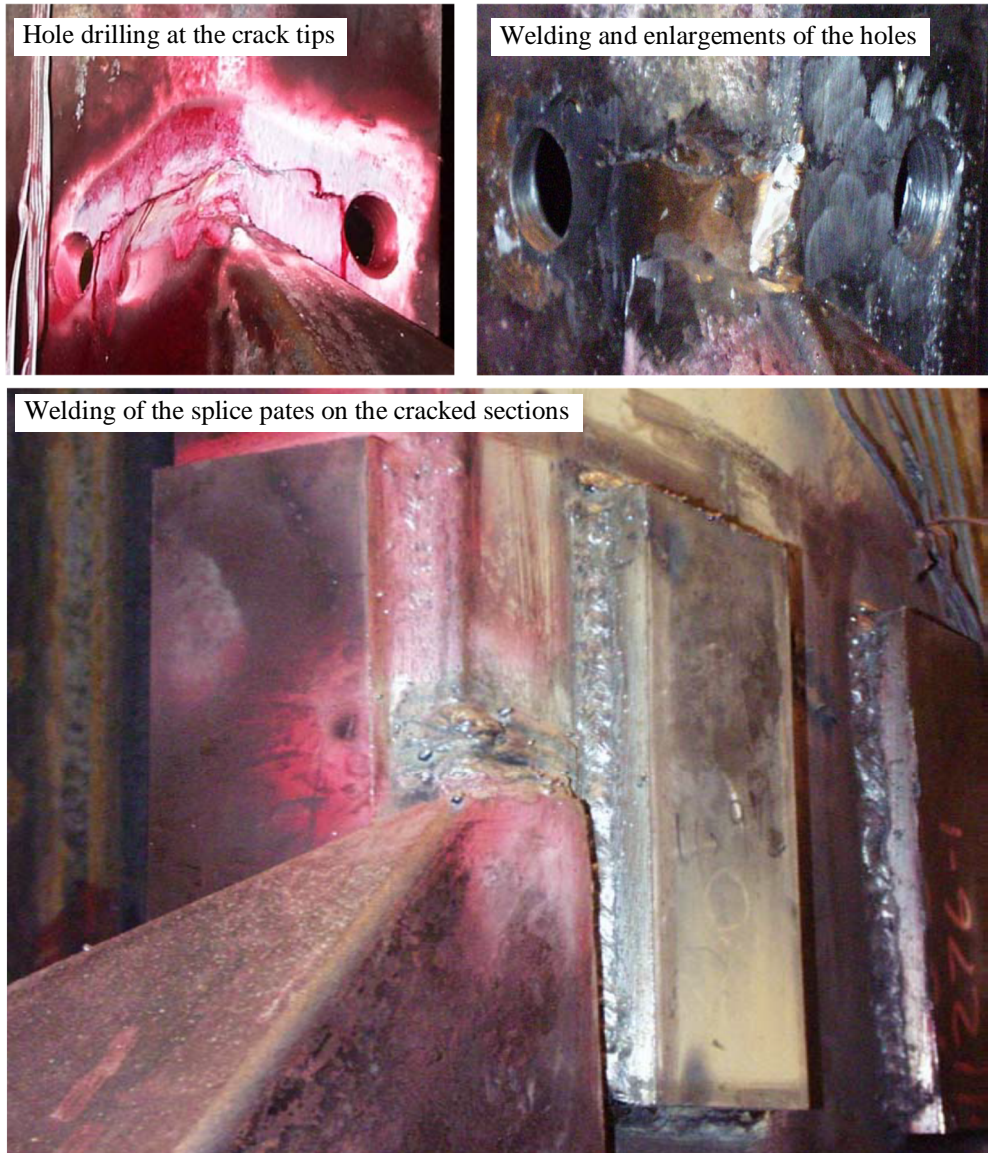


Figure 4.20 The steps of the crack repair [Dexter et al., 2003].

The cracks were repaired by two side weld repairs. The first step of repair was drilling a hole at the crack tips with diameters between 6 and 13 mm. After execution of welding in the cracked section, start and stop points of the welds were ground, and drilled hole diameters were enlarged 12 to 15 mm. In the next stage, the splice plates were welded to the flange and to the web of the rectangular hollow sections (see Figure 4.20). The results show that application of the splice plate improves the fatigue strength (see Figure 4.21)

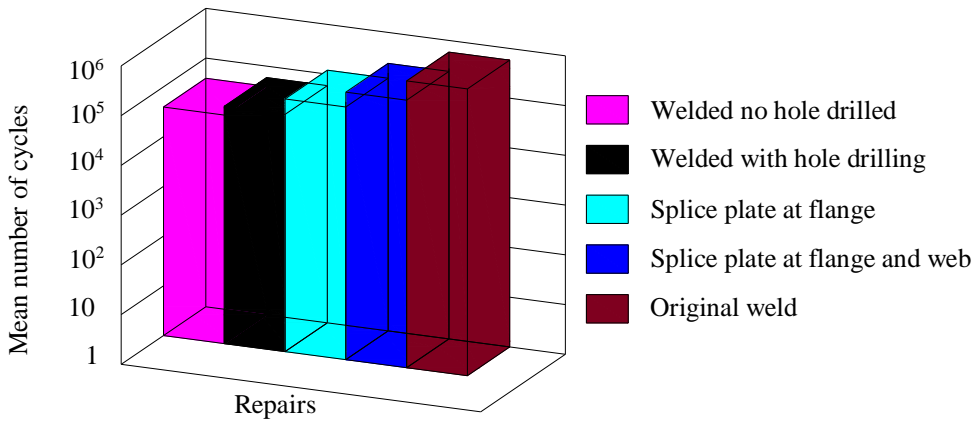


Figure 4.21 Comparison of different repair configurations [Dexter et al., 2003].

4.3.3 Repair by welding

Repair by welding is an effective method for the repair of long cracks. After detection of a crack, material is removed along the crack length up to the crack depth with preparing a V-shape groove. The prepared V groove is filled with weld metal. If both sides of the crack are accessible, the material removal process is executed through three quarter of the material thickness. After filling the weld groove, the same procedure is repeated for the other side of the section. In this manner, the entire crack will be replaced by the weld material. For the crack removal process, air arc gouging and grinding can be used although air arc gouging is the more preferred method. Figure 4.22 schematises the execution process of the air arc gouging. A disadvantage of using grinding is that the crack can become blurred or smeared in case of more material removal. This might create the possibility of hiding or masking the crack path and crack tip, or embedded flaws remaining in the repair weld. With the execution of air arc gouging, the crack tends to open as material is removed, which makes it easy to follow the crack path. In some cases, it is necessary to drill a hole in the structural elements in order to have access to the entire crack path. When this opening is created by means of a flam cut, the edge of the cutting should be ground smooth to avoid fatigue crack initiation at these discontinuities [Dexter et al., 2013].

This method is the most efficient when it is used for the repair of fatigue cracks in welded connections. [Borrego et al., 2009]. The repaired welded connections usually show the same fatigue life as the original weld detail. However, the application to repair fatigue cracks in base material is very rarely effective. In such applications, fatigue cracks will initiate in a period of time that is shorter than the time it took in the original non-welded detail to crack. If it is nevertheless essential to use this method for fatigue crack repair in base material, a combination with the splice plate method and hole drilling method can

increase efficiency of the repair weld in the base material. The splice plate will increase cross sectional area of the repaired the cross section and consequently it will decrease subjected stress ranges. [Dexter et al., 2013].

Depending on the detail, the cyclic load history before repair of welded connections has no influence on the fatigue life of the repaired welded connections. In addition, there is no harmful effect of multiple repair cycle determined on the fatigue strength.

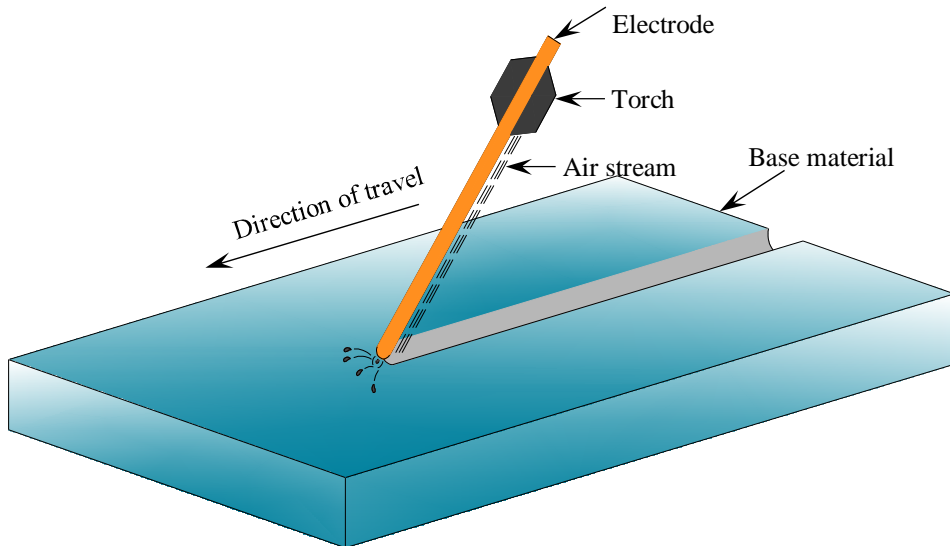


Figure 4.22 Air arc gouging process.

The application procedure of the method can be summarised by the following steps:

- Crack tips will be identified with dye penetrant or magnetic practices.
- Grind or air arc gouge the length of the crack and prepared groove should have a V or U shape.
- The prepared groove should be cleaned after crack removal and the groove shall be filled by means of the appropriate welding process.
- If it is possible to repair the cracks on both sides, first the crack shall be repaired on one side through three-quarters of the section thickness and the prepared weld groove shall be filled with weld material. After welding this side, the same procedure will be repeated on the opposite side. In this way, the crack will be filled with weld material.
- When the welding work is finalized, the weld shape is adjusted by grinding to eliminate irregularities due to the repair weld.

Yamasaki et al., (1984) used the repair by welding method for repairing fatigue cracks in a base material. The aim of the study was to evaluate the consequences of welding on the

fatigue crack propagation in the base material. Deep notched wide plate specimens were prepared for determining the fatigue crack propagation behaviour. The specimens were made from JIS-SM50A steel plates which have a yield strength of 323 MPa and a tensile strength of 490 MPa. The longitudinal direction of the specimens was coincident with the rolling direction of the plate. Fatigue crack propagation was observed with applying a stress range of 98 MPa and a stress ratio 0.09. Fatigue crack propagation was allowed until the crack length reached 100 mm. In this stage, the fatigue crack was repaired by welding. Fatigue crack propagation of the repaired specimens was measured. As could be expected, the fatigue crack growth rate of the repaired specimens was higher than the fatigue crack growth rate in the base material. This could be due to various negative influences from the welding. In order to determine only the effect of the weld induced residual stresses, some specimens were treated by a post weld treatment. The intention was to eliminate residual tensile stresses and to introduce compressive stresses at the welded area. The treatment showed the positive effect on the fatigue crack growth rate. The fatigue growth rate in the treated specimens was decreased. These results revealed that the effectiveness of repairing by welding will be enhanced by using a post weld impact treatment and this can be effective for the repair of base material cracks by welding.

A lot of research has been carried out on the repair of fatigue cracks by welding in laboratory conditions as well as in actual field conditions. Carrato, (1999) applied this method to repair fatigue damaged railway bridges. In 1990, the bridge was inspected and on the major line of the railroad line, fatigue cracks were detected in the welds of welded thru-plate girder spans and deck plate girder span at the bridge. These cracks were repaired by welding. The material was preheated and the detected cracks were removed from one side by air arc gouging. The crack removal process was executed at approximately half the thickness of the plate. After air arc gouging, the prepared groove was cleaned by rotary disc grinding. The cleaned groove was inspected visually as well as by means of the magnetic particles method after cooling at the ambient temperature. For the execution of the weld, the material was preheated again and the groove was filled with weld material. After each welding pass, the weld was visually inspected. The same procedure was applied on the other side of the cracked section. Then, the crack was filled by the weld material. These bridges have been subjected to over 20 million axle loads until 1999. Until that time, no new crack had been detected.

Effectiveness of repairing fatigue cracks by welding is an interesting topic since last decades. Kudryavtsev et al., (2011) concentrated on the effectiveness of repair weld in welded connections containing fatigue cracks at the weld toe. In addition, focus was also put on the effects of the multiple repair weld in the welded connections. For these purposes, specimens with non-load carrying longitudinal attachments were prepared (see Figure 4.23). The specimens were made of steel plates with a yield strength of 367 MPa and a tensile strength of 533 MPa. The weld was carried out manually by arc welding with full penetration.

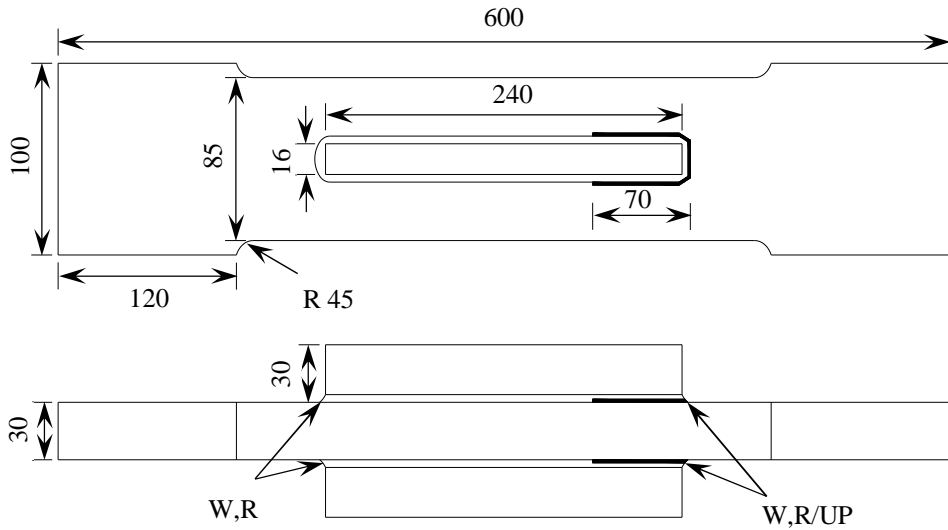


Figure 4.23 Welded specimens for fatigue test [Kudryavtsev et al., 2011].

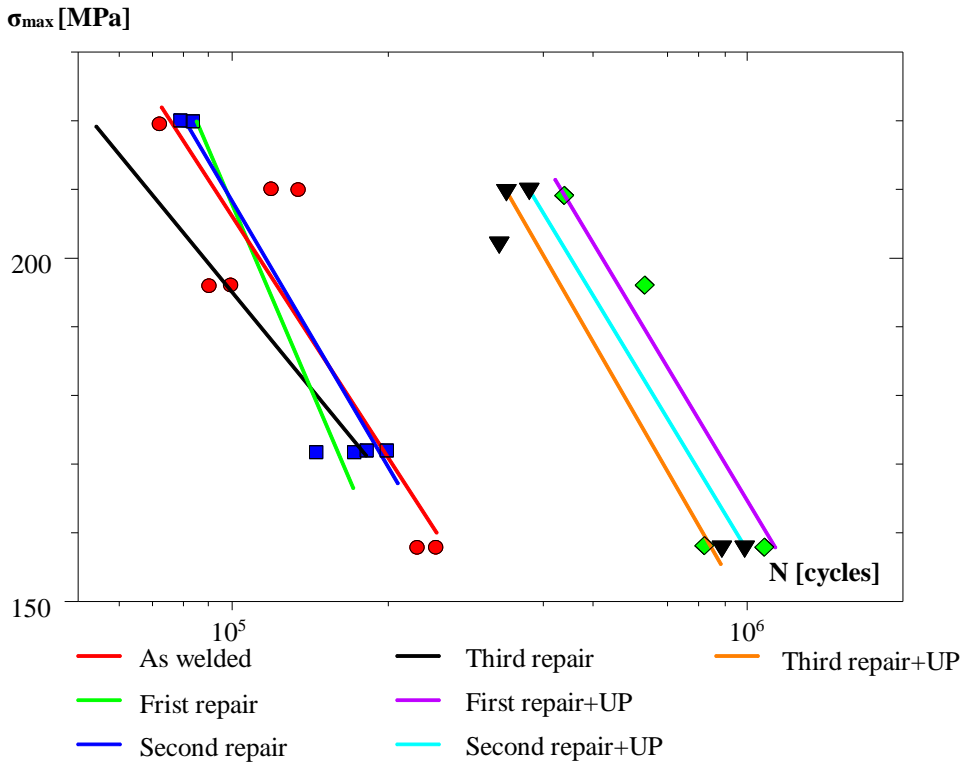


Figure 4.24 Fatigue test results [Kudryavtsev et al., 2011].

At the first instance, the specimens were tested in the as-welded conditions. The fatigue tests were executed with zero to tensile stress cycle ($R = 0$) and under different levels of the maximum stress. Fatigue tests were ended when the fatigue crack length at the surface reached 20 mm and the number of cycles until this crack size was recorded. The test results were determined for different conditions: as-welded (W), repair by gouging and welding (R) and repair by gouging and welding with subsequent ultrasonic peening (UP). The repaired specimens were tested under the same condition as the crack creation stage of the experiment. In some specimens, the multiple crack repair was carried out two or three times.

Fatigue test results showed that fatigue cracks repaired by welding recover the fatigue strength of welded specimens to the initial as-welded condition. It was also shown that multiple repair almost provided the fatigue strength of the initial as-welded condition. The influence of multiple repairs hardly affected the fatigue strength of the welded connection. The application UP as post weld treatment showed a significant increase in the fatigue strength of the repaired joint (see Figure 4.24).

Kudryavtsev et al., (2008) used the repair by welding method for the repair of fatigue cracks in base material. A hole was drilled in the middle of the fatigue test specimens and these specimens were exposed to a fatigue load (see Figure 4.25). Fatigue cracks were initiated at the edges of the hole and fatigue tests were carried out until the total crack length reached 76 mm. These fatigue cracks were repaired with different fatigue crack repair methods: overloading, drilling a hole at crack tips, drilling a hole at crack tips with installation of high strength bolts, local explosive treatment, local heat treatment and welding with and without ultrasonic peening of the weld toes.

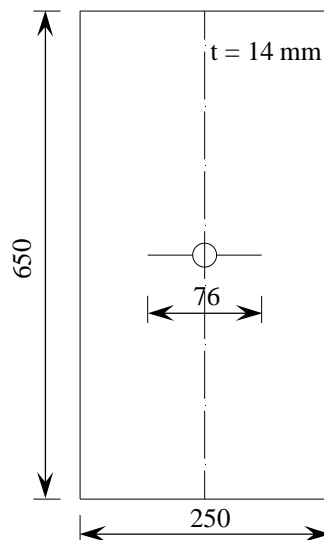


Figure 4.25 Specimen with fatigue crack [Kudryavtsev et al., 2008].

Chemical composition and mechanical properties of material used are given in Table 4.2.

Table 4.2 The chemical composition and mechanical properties of the material [Kudryavtsev et al., 2008].

Steel	C	Si	Mn	Cr	Ni	Cu	σ_y (Mpa)	σ_u (Mpa)	δ_5 (%)	KVC ⁻⁴⁰ (J/cm ²)
	%									
Low alloyed	0.096	0.57	0.71	0.25	0.27	0.3	367	533	28	64

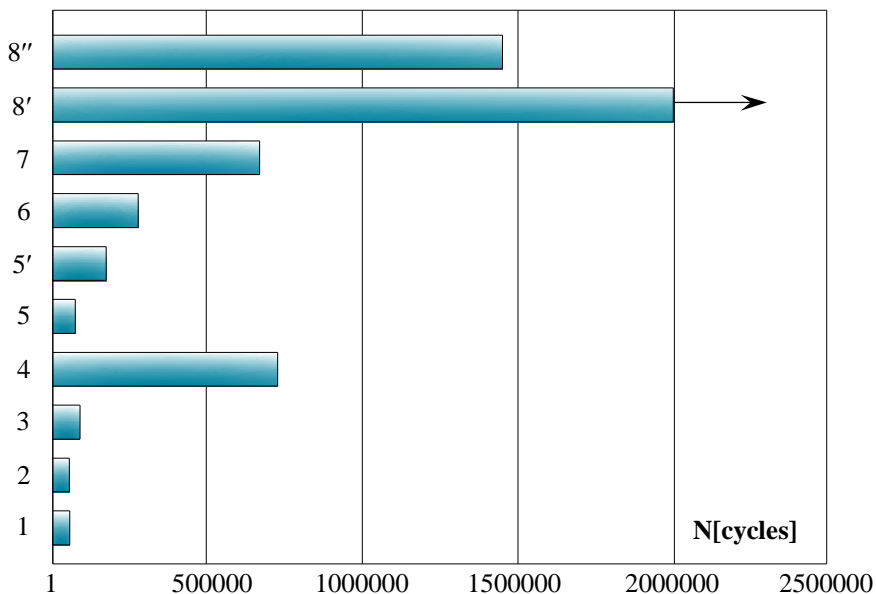


Figure 4.26 Comparison of different repair methods [Kudryavtsev et al., 2008].

In case of repair by welding, the created hole at the centre of the specimens was also filled by weld material. Fatigue tests were executed under zero to tension stress cycles ($R = 0$) with a maximum stress of 155 MPa. The results of fatigue tests for different repair methods are compared in Figure 4.26. In this figure, 1 represents the number of cycles at failure in as-welded condition. 2 and 3 show the results of drilling a hole at crack tip with and without cold working respectively, while 4 shows the result of hole drilling at the tip with installation of high strength bolts. 5 and 5' indicate the result of application of overloading up to yield and 70% of yield strength of the material respectively. Test results of local explosive treatment and local heat treatment are shown 6 and 7 respectively. Fatigue cracks were also repaired by welding with and without ultrasonic peening. These results are indicated with 8' for repair by welding with ultrasonic peening and 8'' repair by welding

without ultrasonic peening. As can be seen that repair by welding with subsequent ultrasonic treatment provided the longest fatigue life as compared to the other repair methods. This can be expected due to introduced compressive stresses by ultrasonic treatment. The application of the ultrasonic treatment can be too expensive or impossible in some cases. The fatigue strength of damaged welded connections can still be regained with repairing by welding without post weld treatment.

4.4 Summary

In practice, several fatigue cracks repair methods are available. The effectiveness of these methods depends on crack depth, crack location, joint configuration and accessibility to cracked sections. Surface cracks, meaning shallow cracks, which can be limited with crack depths up to 5 mm, can be repaired with grinding, hammer peening and gas tungsten arc re-melting. Through thickness crack and cracks deeper than 5 mm can be repaired by drilling a hole, applying slice plate and welding.

Grinding is an effective method to remove surface cracks at the fusion line of the welded connections. Grinding is also used as a post weld treatment method. It will reduce discontinuities at the weld toe by removing slag and inclusion at the weld toe. This process increases the crack initiation period and consequently increases the fatigue life. Grinding of crack must be performed very carefully to avoid unnecessary material removal, which would reduce cross section of the element. On the other hand, sufficient material has to be removed to prevent remaining crack tip in the section. A remaining crack tip would propagate further and lead to premature failure. After grinding, ground surfaces have to be checked for deep grinding marks, which need to be removed. Deep grinding marks cause stress concentration and they will lead to fatigue crack initiation in an early stage. Grinding must be performed in such way that grinding marks occur parallel to the applied stress. Due to notches after grinding and the limitation of grinding depth, this method is not very effective for fatigue crack repair.

Another repair method for surface fatigue cracks is hammer peening. This method is effective for cracks with depths up to 3 mm. Deeper cracks cannot be removed by hammer peening. In addition to removing fatigue cracks, this method also introduces compressive residual stresses at the treated region. These compressive residual stresses will reduce effective tensile stress ranges and have beneficial effects on the fatigue strength of the materials. Fatigue strength of damaged welded connections can be restored by hammer peening. Care should be taken with peened surfaces that after peening, pits should not be too deep to cause crack initiation in early stage of loading.

The GTA re-melting method is usually effective for repair of fatigue cracks with a depth up to 5 mm. GTA re-melting is a welding operation without additional filler material. It re-

melts amount of material at the weld toe and base material by means of the gas shielded tungsten electrode. It is also effective for improving the fatigue strength of welded connections. After re-melting of the weld toe, slag and inclusions can be eliminated and it reshapes the weld toe reducing stress concentrations at the weld toe. For fatigue crack repair, the effectiveness of this method depends on the depth of the re-melted zone. Insufficient penetration will leave the crack tip in the cross section and this crack tip will continue propagating under the fatigue load. After repair of fatigue cracks, the fatigue strength of the original non-cracked section can be regained. The disadvantage of this method is that it requires highly skilled welders and good accessibility of the crack region.

Hole drilling is the most widely used repair method for fatigue cracks in base material. In this method, a hole is drilled at the tip of the crack to remove the sharp notch at the crack tip. However, the holes need to have a sufficient diameter to become successful for the crack arrest. As a rule of thumb, larger holes are better as long as strength and stiffness of the structure or connection are not compromised. But larger holes are not always practical and they will give rise to inconvenience for the user. Therefore, an equation has been established for determination of the hole diameter. In some cases, a fully tensioned high strength bolt is placed into the hole. The bolt introduces a favourable compressive stress around the entire hole, which may contribute to preventing further crack growth. The results of this application have shown that this method gives better results than expected.

Another frequently used repair method is the splice plate method. The philosophy of splice plate for fatigue crack repair is to add across sectional area in order to reduce stress ranges. This method is usually used for repairing fatigue cracks in base material. Splice plates can either be attached by welding or with high strength bolts. From a fatigue resistance point of view, the bolted splice plates are always better than welded ones. However, a bolted connection may require drilling a large number of holes and requires access to the hole side of the cracked surface, and therefore may not always be cost effective or even possible. This method can also be combined with drilling a hole and welding. The combination of two methods gives better results than an individual application.

Repair by welding is a method for weld repair of long cracks. When a crack is detected, the material is removed along the crack length, through three-quarter the thickness of the section in the shape of a V. The V-shaped groove is then filled with weld metal and the process is repeated on the other side of the section, so that the entire crack is filled with weld material. This is to have the possibility of welding from both sides of the cracked section. If it is not possible to have access to both sides of the section, the crack will be repaired from one side. Air arc gouging is the preferred method of the crack removal process and for some cases grinding is also used. The disadvantage of using a grinder to remove cracked material is that the crack can become blurred or smeared as more material is removed and the crack root will remain in the material, which is not detectable. The repair by welding method is the most effective when used to repair a cracked weld detail, not a crack in non-welded base metal. The repair weld usually exhibits the same fatigue life

as the original non-cracked weld detail. Repair by welding can be combined with weld improvement techniques for higher fatigue strength. Especially the combination with a high frequency mechanical impact treatment gives a higher fatigue strength than in as-welded condition. In case of crack repair in base material, this combination might be used.

Finally, local heating and post tensioning are another method for retrofit of fatigue cracks. Both methods work based on the crack closure concept due to compressive stresses. Fatigue cracks can propagate when exposed to tensile stresses. Post tensioning force is applied to a cracked section and a plastic zone will occur at the crack tip. After relieving this post tensioning force, the crack tends to close and compressive stresses will be introduced at the crack tip. When the applied tensile stress range remains at a low level, an effective stress range will remain in the compression regime and it will hinder further crack propagation [Dexter et.al., 2013]. The idea of local heating is the same as post tensioning to introduce compressive residual stresses at crack tip. The crack tip is locally heated and this introduces a high magnitude of tensile stresses in the region of the heating position. After tapering off rapidly, these tensile stresses become compressive stresses surrounding the crack tip. The compressive stresses will retard fatigue crack propagation [Jang et al., 2002]. Only limited information is available about the effectiveness of these methods. Therefore, they are not dealt with separately.

Based on the literature review, several fatigue crack repair/retrofit methods are available for practise. It also appeared that each method has advantages, disadvantages and also applicability limitations. It appeared that the repair by welding method is a more suitable repair technique for the repair of the deep fatigue cracks in welded connections and in case of broken connections. The literature review also shows that currently available test results of this method are mainly meant for the mild steels. The re-welding process can influence the fatigue strength of welded connections made of very high strength steels. An experimental programme has been established to investigate the fatigue strength of repaired welded connections made of very high strength steels. The repair of the welded connections is conducted with the repair by welding method. Chapter 5 presents more detailed information on the experimental programme and the fatigue tests.

Chapter 5

Plate experiments

5.1 Introduction

Pijpers, (2011) presented that the use of very high strength steels in civil engineering structures is possible and that it may have beneficial effects on the fatigue strength of welded connections. His research was related to the fatigue design of new structures made of very high strength steels. However, the repair and fatigue life extension of existing high strength steel structures still need to be investigated by experiments, to provide more necessary knowledge for effective applications of the very high strength steels.

The literature review reveals that no standardised fatigue crack repair procedure is available. The selection of the repair methods depends on the loading conditions, fatigue crack location and direction of the crack propagations, accessibility of the crack location, and desired fatigue life extension. In case of fatigue crack repair in welded connections, repair by welding is the most effective repair method for mild steels. However, for welded connections made of very high strength steels, the effectiveness of this method needs to be determined. In the current research, an experimental work has been carried out to determine the fatigue strength of repaired base material and repaired welded connections made of very high strength steels. The results of the experimental programme give more insight for application of the repair procedure and the effects of the repair welds on the fatigue strength of the base material and welded connections made of very high strength steels.

Chapter 5 focuses on the fatigue experiments on plate specimens of repaired artificial crack in base materials and repaired V-shape welded connections made of very high strength steels. Section 5.2 presents the experimental programme and the execution of the tests. In Section 5.3, the preparation of the specimens is explained. Since the repair by welding is not standardised for very high strength steels, an existing repair procedure was followed with some modifications. A detailed description of the repair procedure is given in Section 5.4. Section 5.5 presents the fatigue test results of the repaired specimens.

5.2 Experimental programme

5.2.1 Fatigue test programme

Table 5.1 gives an overview of the experimental programme for the determination of repair weld effects on the fatigue strength of the base material and welded connections of very high strength steels. In Chapter 3, it is shown that an inappropriate repair weld in the base material can lead to fatigue crack initiation at the repair weld location. It can obviously reduce the fatigue strength of the base material. Therefore, the base material test strips with repair welds, made of S690 (BR69x series) and S890 (BR89x series) rolled steels, was tested to determine the effects of the repair welds on the fatigue strength of the base material. After that, fatigue tests were carried out on V-shape welded specimens, made of the rolled steel grades of S690, S890 and similar strength cast steels G10MnMoV6-3 and G18NiMoCr3-6. V-shape welded specimens were manufactured in two configurations: welded connections between rolled and rolled steels (VO series); specimens made of rolled and cast steels parts (CO series). The plates were welded with a ceramic backing strip for both configurations.

Table 5.1 Summary of plate test specimens; 4pb=four point bending.

Series	Roller steel grade	Cast steel grade	Thickness x width [mm]	Number of specimens	Loading	Weld type	Backing
BR69	S690	-	25x150	9	4pb	Base material	
BR89	S890	-	25x150	9	4pb	Base material	
VO69	S690	-	25x150	18	4pb	V-shape	Ceramic
VO89	S890	-	25x160	18	4pb	V-shape	Ceramic
CO69	S690	G10MnMoV6-3	25x160	18	4pb	V-shape	Ceramic
CO89	S890	G18NiMoCr3-6	25x160	18	4pb	V-shape	Ceramic

The chemical composition and the mechanical properties of the test plates are given in Appendix B. The mechanical properties and the chemical compositions were derived from the material certificates. The specimen geometries and the applied welding procedure are described in the sections on the preparation of the specimens. The surfaces of the steel plates were in as-rolled condition and the welded connections were in the as-welded condition. No any additional post weld treatment was applied. In repaired welded

connections, high frequency impact treatment (HiFIT) was applied at the weld toe of the original weld. This is described in the section of the repair procedures. Appendix C presents the manufacturing steps of V-shape welded specimens and the detailed geometry of the specimens.

The objective of the experiments is to establish a fatigue crack repair method for the repair of fatigue cracks in welded connections made of very high strength steels. It was planned to apply two different procedures for the repair by welding. According to the plan, each series of V-shape welded specimens will be divided into two samples and each sample will contain 9 test specimens. Therefore, 18 test specimens were manufactured for each test series. Hobbacher, (2016) recommends testing more than 10 specimens and for constant amplitude fatigue testing; at least 3 stress levels and 3 specimens for each stress level need to be tested for a proper statistical evaluation. Based on these recommendations, 9 test specimens were prepared for each sample of the series.

5.2.2 Fatigue test rigs

Fatigue tests on the plate specimens were carried out in the Stevin II Laboratory of the Delft University of Technology. Fatigue tests were carried out with a four point bending test setup. Two four point bending frames were set up for the fatigue tests. In one test rig, two specimens can be tested simultaneously (see Figure 5.1) and in another test frame, one specimen can be tested (see Figure 5.2). The experimental programme contained a large number of test specimens. The use of two test setups speeded up the execution of this large number of the test specimens.

Specimens were exposed to cyclic loading to initiate fatigue cracks and the propagation of these cracks was monitored until defined failure conditions. For the test series of repaired artificial crack in the base material, failure was defined in such a way that the specimens broke into two pieces. Fatigue tests on V-shape welded specimens were executed in two stages. In the first stage, the specimens were tested until the initiated fatigue crack length reached to half the width of the plate. In the second stage, the specimens were tested again after repair of the fatigue cracks. The fatigue test of the second stage was performed in the same conditions as the first stage. The failure of the second stage was defined such that the specimens were broken into two pieces. The fatigue tests were executed with a force controlled loading condition, which means that the force range was constant in all stages of the tests. All test series were tested under constant amplitude loading with the stress ratio $R = 0.1$.

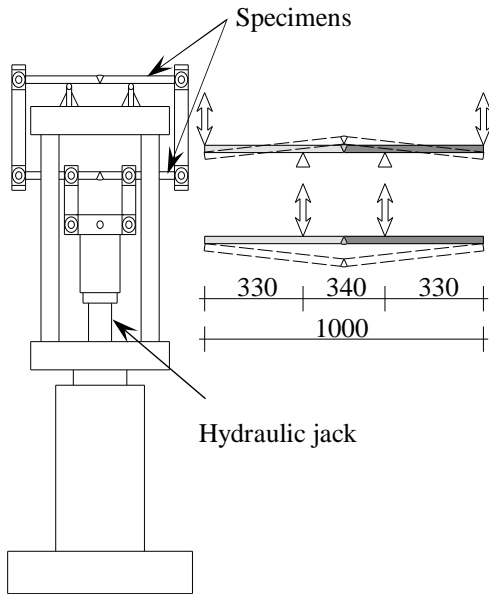


Figure 5.1 Four point bending test setup for double test specimens.

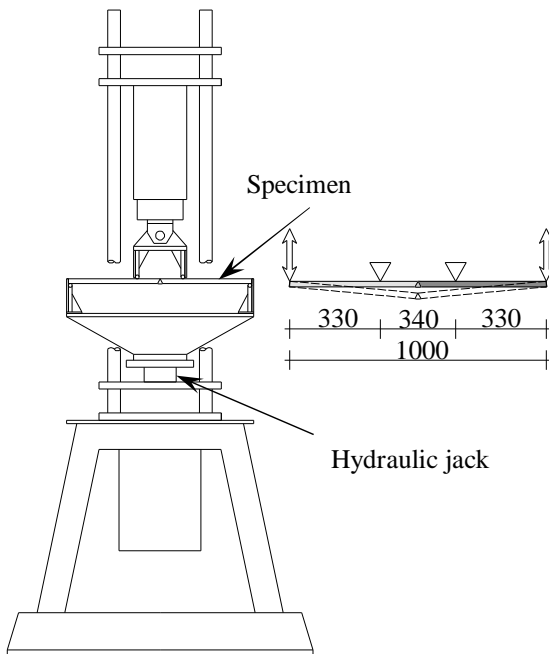


Figure 5.2 Four point bending test setup for single test specimen.

With four point bending loading, a constant bending moment was created in the weld area, resulting in a compression and a tension zone over the thickness of the specimens. Fatigue cracks usually initiate in the tension loaded part of the weld connections. The specimens of the repaired artificial crack in the base material contained a repair weld on one side of the specimens. The residual tensile stress due to the repair weld, stress concentration effect of the weld and the discontinuity of the repair weld makes the welded side of the specimens more susceptible to fatigue crack initiation. In order to investigate the effects of the repair weld on the fatigue strength, it is sensible to load these specimens in such a way that the welded side of the specimens is exposed to cyclic tensile stresses. For V-shape welded specimens, the specimens were loaded in such a way that the cyclic tensile stresses occurred at the weld cap.

5.2.3 Crack monitoring

Fatigue crack development in the test specimens was monitored by strain gauges. Each specimen contained 9 FLA-6-11 strain gauges to monitor the strain distribution at both sides of the weld. The strain gauges are able to measure the strain up to 3000 μ strain. The strain gauges were applied at 10 mm from the weld toe of the weld root and the weld cap. It was found that the strain concentration due to the weld geometry is negligible, which is shown by comparing the strain from measurements with the strain through the beam theory. Strain gauges were applied at the locations where relatively high fatigue crack initiation was expected. Three strain gauges were applied to each side of the weld toe at the weld cap and 3 strain gauges on one side of the weld toe at the weld root. During the fatigue tests, the average and range values of the force, the displacement and the strains were digitally recorded every 30 seconds and additional measurements were carried out by the system, for 20 μ strain changes in range values of a strain gauge measurement in meantime. The nominal stresses were calculated by converting average values of the strain gauges with the uniaxial Hook's law.

In the initial stage of the fatigue tests, the range values of the strain gauges were approximately constant; a straight line. The crack initiation was visible when the strain gauge data began to increase or decrease from the initial values. Increase or decrease of the strain gauges depends on the location of the strain gauges with respect to the crack and the crack could lead to increased tension, compression or discharge of the strain. Figure 5.3 shows an example of the saved strain range data versus to number of cycles of a fatigue test specimen. Although the distance between the strain gauges and the weld toe is constant, there was a scatter in the strain gauge measurements in the initial stage of the test. This can be explained by the deviation in distance of the strain gauges from the weld toe and variation in local thickness of the plate.

The fatigue crack initiation time is not known in advance and performing fatigue tests is a time consuming process. In order to determine the fatigue crack initiation location and the crack initiation life, an alarm system was used which shut down the loading when the deviation in the strain range measurement of a strain had exceeded 50 μ strain. It gave an indication for checking the location of the crack initiation on the specimens visually. Visual fatigue crack inspection was done by brushing some petroleum onto the surface of the inspected area. The petroleum penetrates into the crack and due to the fatigue load, the penetrated petroleum bubbles, which makes it possible to detect the crack visually.

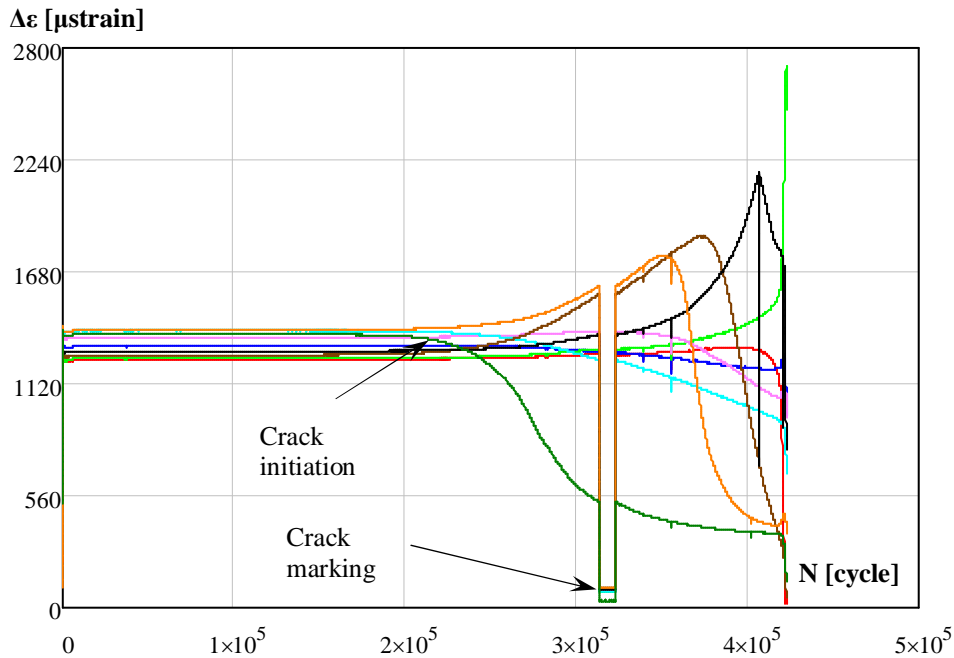


Figure 5.3 Strain range measurement of BR893 with crack marking procedure.

The number of cycles at which strain gauge values started to deviate from the regular shape, was defined as the fatigue crack initiation life, N_i , of the specimens. The total fatigue life, N_f , of the specimens was described as the number of cycles at failure, meaning that the specimens were broken into two pieces. The difference between number of cycles at the crack initiation and at the failure was called fatigue crack propagation life: N_p . When no fatigue cracks were observed in the specimens at 5 million cycles, the specimens were indicated as runouts.

When fatigue cracks initiated in the middle of the weld toe of the connections, it was not possible to monitor fatigue crack development through the thickness direction. In this case, the crack marking procedure was used to create beach marking at the boundary of the crack and these marks can be seen on the fracture surface after the fracture of the specimens. The

relation between the crack depth and the number of cycles was herewith established. In this procedure, the lower stress level in the specimen rose to 90% of the upper stress level in the specimens and the test was executed for 10000 cycles (see Figure 5.3). Due to change of the stress range, the crack boundaries became visible on the fracture surface. The stress range during the crack marking process was very low and the number of cycles made in this procedure will not contribute the fatigue damage of the specimens. This number of cycles is therefore excluded from the analysis.

Fatigue cracks may initiate at different locations of the welded connections: weld toe of the cap or the root or in the base material at a distance from the weld. The cracks initiate at the weld toe of the cap and grow through the heat affected zone (HAZ) into base material. The cracks at the weld toe of the root grow through the HAZ into the weld material. Figure 5.4 shows the locations of the crack initiations and the crack growth paths.

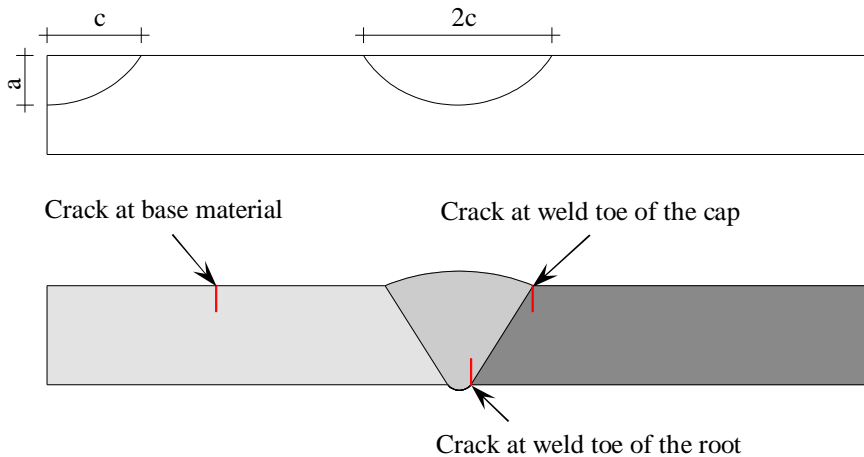


Figure 5.4 Fatigue crack initiation locations and crack growth path.

5.2.4 Weld shape

The use of very high strength steels provides an advantage in the design of high loaded slender structures. However, stability is a governing phenomenon for the slender structures and it is a function of the elastic modulus, which is constant for all structural steel grades. In accordance with this, applying very high strength steels to a structure designed with mild steels would not lead to benefit the advantage of using very high strength steels. It is therefore necessary to improve the structural design methodology in such a way that the structures met the stability requirements without loss of these advantages.

Pijpers, (2011) recommended a solution implying that truss structures could be a suitable option to prevent the stability problem in very high strength steel structures. With this kind of stiff structures, deflection of structure can be limited in allowed design requirements.

Moreover, cross sectional reduction of structural element results in a lower self-weight. Consequently, stress variation under live loads will be higher and higher stress ranges are to be expected for fatigue loaded structures. Additional design modifications are required to improve fatigue strength of these truss structures. It was proposed by Pijpers, (2011) to use cast steel nodes, in order to shift the weld areas outside the highly stress concentration regions. Furthermore, the stability property of circular hollow sections is the same for in plane and out of plane directions. This property makes circular hollow sections very efficient for high loaded structures. Consequently, this would be a useful solution for an effective application of very high strength steels in fatigue loaded structures.

According to EN 1993-1-9 (2006), X-shape welded connections, welded from both sides, have a higher fatigue class as compared to V-shape, welded from weld cap side, welded connections. Thus, from a fatigue strength point of view, X-shape welded connections are preferable. However, in the case of welding hollow sections, it is not possible to execute the welding from both sides and it inherently compels using V-shape weld connections for joints of circular hollow sections. Based on this reasoning, Pijpers, (2011) performed a research on the fatigue strength of V-shape welded plate specimens made of very high strength steels. That research comprised, a study carried out on extensive comparison of various V-shape weld grooves and advantages and disadvantages of the weld groove shape. Based on the comparison, the selected V-shape weld groove is given in Figure 5.5.

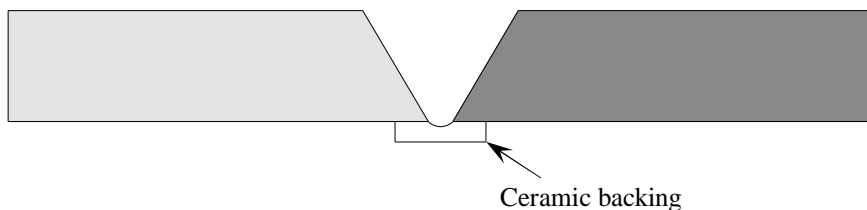


Figure 5.5 Selected V-shape weld groove.

The current study focused on the fatigue strength of the repaired welded connections made of very high strength steels. The efficiency of the repair weld on fatigue strength can be established by comparing the fatigue test results of repaired welded connections with the fatigue test results in the as-welded condition. Fatigue tests results from research of Pijpers (2011), in the as-welded condition, was used for the comparison of the fatigue test results of the current study. In order to prevent any influence from variation in the test results, the specimens of the current study were prepared with the same V-shape weld. A welding procedure was set up based on EN ISO 15614-1 (2004) and the welded connections were inspected using magnetic particles and ultrasonic inspection. The magnetic particles inspection was performed according to EN-ISO 17638 (2003) and the acceptance level of defects was level 2, based on EN-ISO 23278 (2009). The ultrasonic examination was executed according to ISO 17640 (2010) and the acceptance level was level 2 based on ISO 11666 (2010).

The weld specification of the repair weld was similar to the weld procedure of the original weld. The repair weld was also qualified with the same standards. The only difference was that, after repair of the weld, the connections were exposed to post weld treatments. The detailed explanation on the treatments is given in Section 5.4.

5.3 Test specimen preparation

5.3.1 Specimens with an artificial crack in the base material

For the determination of the repair weld effects on the fatigue strength of the base material, test specimens with an artificial crack were prepared from the base materials S690 and S890. Artificial cracks were created to reflect similar fatigue crack repair procedure that it is used for the repair of real fatigue cracks. In addition, material removal during the crack removal process can be kept under control and all specimens will have identical weld lengths, depths and geometries which enables prevention of the varieties due to the manufacturing process. By this, the test results can be immediately evaluated.

Repair of the fatigue cracks in structural elements is usually done when the concentrated cracks have reached a critical value. The repair and inspection interval of the structures is determined by performing a fitness of purpose analysis. The results of this analysis give the essential period of time for detected fatigue cracks to reach the critical, allowable crack size. The allowable crack size can be established by a failure assessment diagram (FAD) and the procedure of the assessment is given in BS 7910 (2013). However, the assessment requires certain material input parameters. If these parameters cannot be easily identified and no any other restrictions are predefined, half the thickness of the sections is assumed to be the allowable crack depth. With the same analogy, the depth of the artificial crack was chosen as half the thickness of the test specimen, which is 12.5 mm.

After crack initiation, the fatigue crack will usually form a semi elliptical shape. The artificial cracks were also created in a semi elliptical shape. The length of the artificial crack is determined based on considering the following aspects; the material removal process, feasibility of welding and workability for the welder. Accordingly, the artificial crack length was defined as half the width of the plate, 75 mm. To make the artificial cracks more like to a real fatigue crack, the crack width was maintained as narrow as possible and it was created with a width of approximately 0.6 mm. The artificial crack was created in the middle of the test specimens by a spark machining process which is also called electrical discharge machining (EDM).

The specifications of the materials are given in Appendix B. The test specimens were cut from S690 and S890 plates by water cutting with a length of 990 mm and a width of 160

mm. In the middle, the width of the specimens was reduced to 150 mm. Figure 5.6 shows the dimensions of the specimen, the artificial crack detail and its location in a specimen.

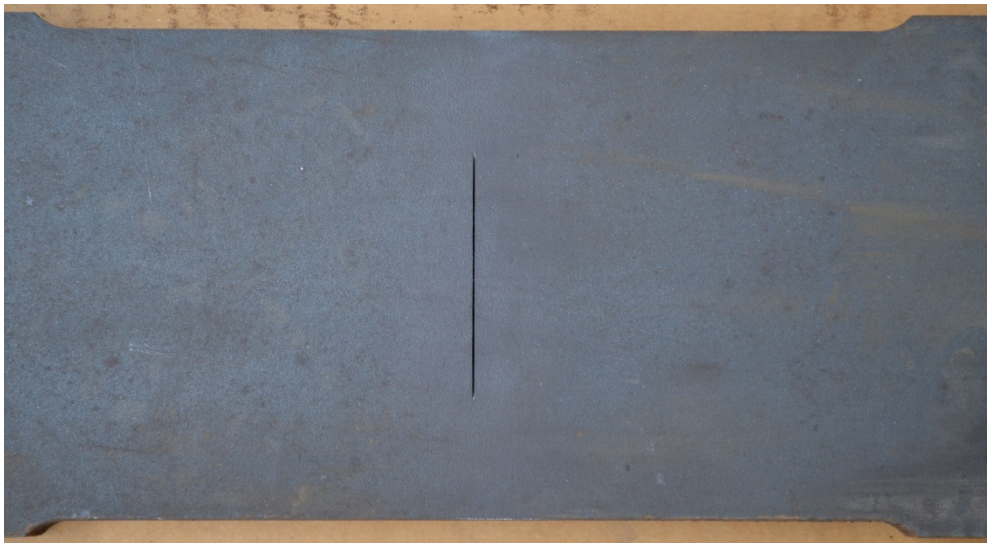
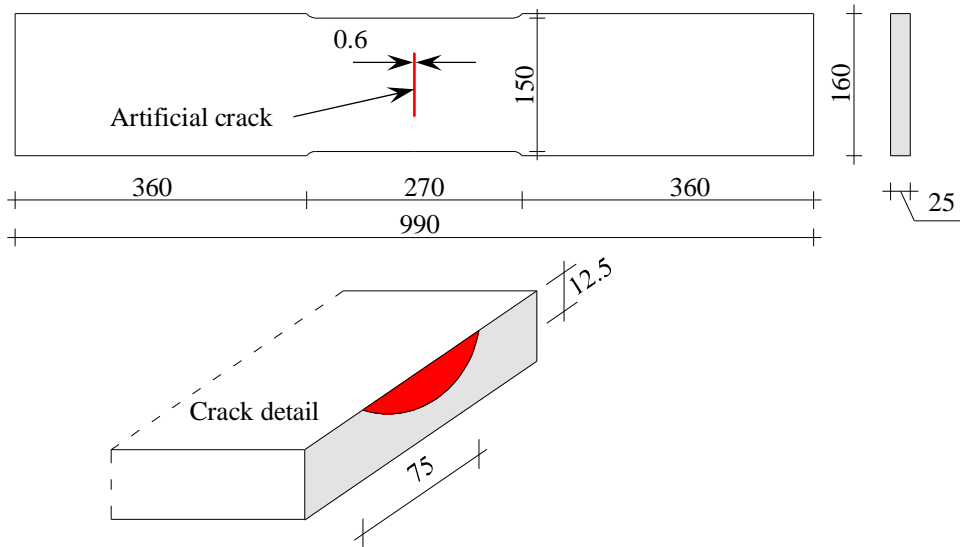


Figure 5.6 Geometry of specimens and detail of the artificial crack.

For each steel grade, 9 test specimens were prepared. They were encoded as BR69x for the specimens made of S690 and BR89x for the specimens made of S890. More detailed information about the geometry and the strain gauge configuration is given in Appendix C.

5.3.2 V-shape welded specimens made of rolled steels

For the determination of the fatigue strength repaired V-shape welded connections made of rolled steels, the specimens were prepared from steel grades of S690 and S890

The rolled plates were flame cut and the weld edges were machined to obtain 60° weld groove. The plates were welded by the flux-cored arc welding (FCAW), using a ceramic backing plate. The individual test plates were cut from the welded plated by plasma cut, with a width of 160 mm and a length of 1000 mm. The width of specimens from S690 plate was reduced to 150 mm at the middle of the plates. The mechanical properties and the chemical composition of the plates and weld material can be found in Appendix B. Figure 5.7 and Figure 5.8 show the geometry of the specimens made of S690 and S890 respectively and the strain gauge locations are also indicated. More detailed information about strain gauge locations is given in Appendix C.

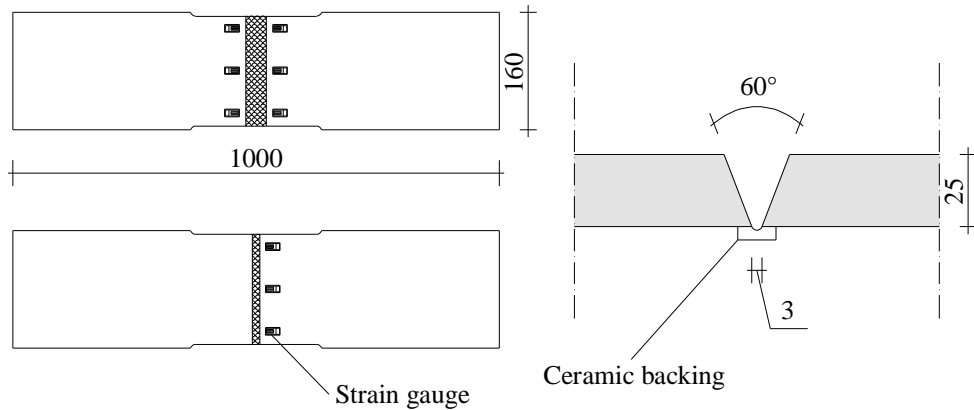


Figure 5.7 Geometry of VO69x specimens, rolled steel to rolled steel connection.

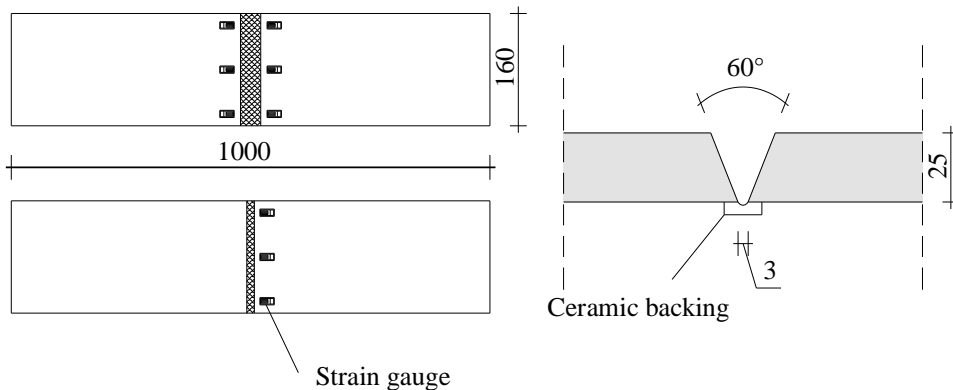


Figure 5.8 Geometry of VO89x specimens, rolled steel to rolled steel connection.

Table 5.2 gives the welding parameters and the geometry data of the V-shape welded connections between rolled steels and rolled steel plates made of S690 and S890 rolled steels. Figure 5.9 shows the macro graph of the welded connections of both series.

Table 5.2 Welding parameters and geometry data of V-series specimens.

Specimens	VO69x	VO89x
Rolled steel grade	S690	S890
Number of test specimens	18	18
Thickness [mm]	25	25
Length [mm]	1000	1000
Width [mm]	150	160
Preheat temperature °C (min)	100	125
Interpass temperature °C (max)	200	200
Weld metal cap	Megafill 742 M	Megafill 1100 M
Weld process	FCAW	FCAW
Heat input cap	0.8-1.4	0.8-1.4
Heat input fill	0.8-1.6	0.8-1.6
Weld metal root	Megafill 821R M	Megafill 821R M
Weld process	FCAW	FCAW
Heat input root	1.2-1.8	1.2-1.8
Backing	Ceramic	Ceramic
Gap [mm]	3	3

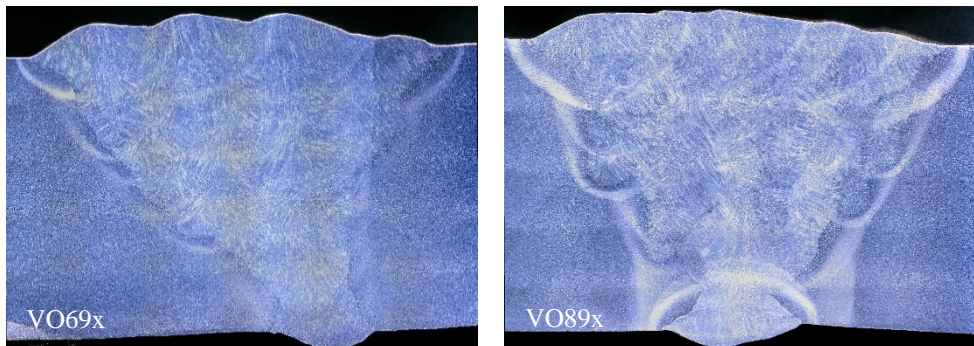


Figure 5.9 Macro graph of the weld connections.

5.3.3 V-shape welded specimens made of cast and rolled steels

For the determination of the fatigue strength V-shape repaired welded connections made between rolled and cast steels, specimens were prepared from steel grades of S690 and S890 and cast steels with similar yield strengths G10MnMoV6-3 and G18NiMoCr3-6 respectively. The detailed information about the cutting process of the specimens and the strain gauges configuration is given in Appendix C.

Appendix B gives the material specifications of the rolled and the cast steels. The cast steel plates were produced with a thickness of 40 mm. The cast steels were also quenched and tempered after casting and the thickness of the plates was reduced to 25 mm by machining from both sides of the plates. The measurements showed that the thickness of the cast plates varied from 24.5 mm to 26.5 mm. According to EN-ISO 8062-3 (2007), the cast plates satisfied CT11 for the linear dimensional casting tolerance. The surface of the plates was examined by magnetic particles and they satisfied severity levels of SM1, LM1 and AM1 according to EN 1369 (1996). To qualify the cast material according to internal imperfections, the plates were inspected by an ultrasonic examination based on EN 12680-1 (2003). The cast plates met the requirements of the quality I according to ultrasonic inspections.

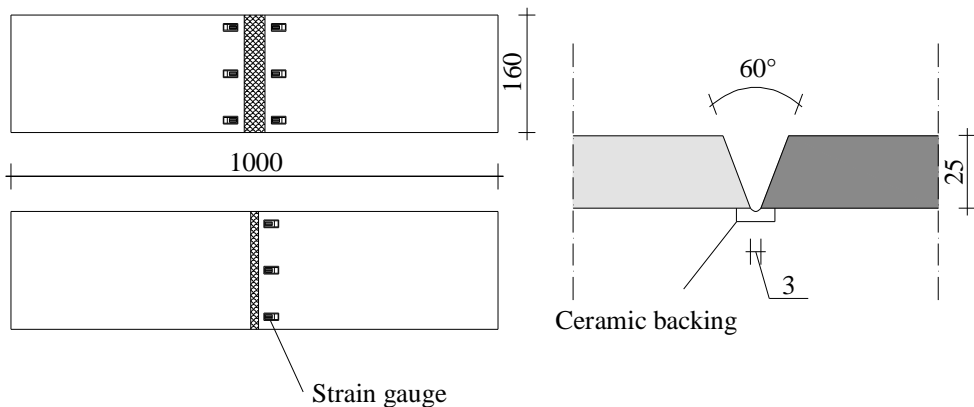


Figure 5.10 Geometry and weld shape of CO69x and CO89x test series.

The rolled plates were flame cut and the weld edges of the rolled plates and cast plates were machined to prepare a weld groove with 60° . After the weld groove preparation, the rolled plates were welded to the cast plates by the FCAW process with a ceramic backing plate. The individual test plates were plasma cut from the welded plates with a width of 160 mm and a length of 1000 mm (see Figure 5.10). Table 5.3 gives the welding parameters and the geometrical data of the specimens. Figure 5.11 shows the macro graph of the welded connections between the rolled and the cast steels.

Table 5.3 Welding parameters and geometry data for CO-series test specimens.

Specimens	CO69x	CO89x
Rolled steel grade	S690	S890
Cast steel grade	G10MnMoV6-3	G18NiMoCr3-6
Number of test specimens	18	18
Thickness [mm]	25	25
Length [mm]	1000	1000
Width [mm]	160	160
Preheat temperature °C (min)	100	125 and 165 for cast steel
Interpass temperature °C (max)	200	200
Weld metal cap	Megafill 742 M	Megafill 1100 M
Weld process	FCAW	FCAW
Heat input cap	0.8-1.4	0.8-1.4
Heat input fill	0.8-1.6	0.8-1.6
Weld metal root	Megafill 821R M	Megafill 821R M
Weld process	FCAW	FCAW
Heat input root	1.2-1.8	1.2-1.8
Backing	Ceramic	Ceramic
Gap [mm]	3	3

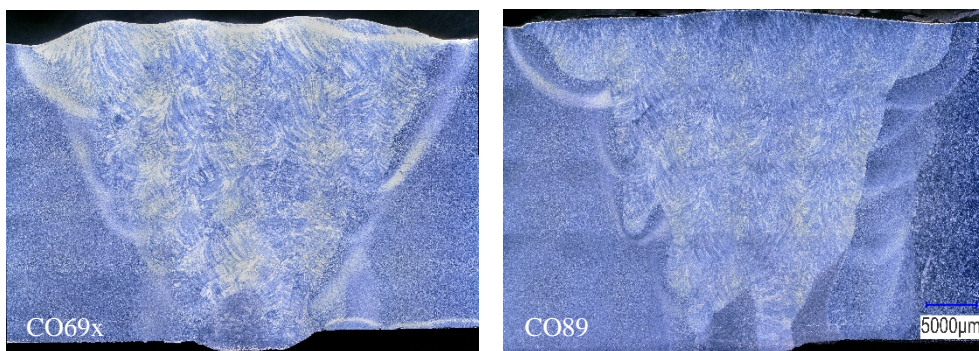


Figure 5.11 Macro graphs of the welded connections for rolled to cast steels.

5.4 Repair procedures

5.4.1 Repair of artificial crack in base material

The repair of the artificial cracks was performed by grinding the crack and welding. The length and the depth of the artificial cracks were measured. These were identical to those on the drawing, but there was some deviation in the shape of the cracks. The observed shape of some artificial cracks was not exactly in the semi elliptical form. The crack removal process was executed with a disc and a burr grinder. Initially, a small amount of material was removed by a disc grinder and further, the cracks were removed by a burr grinder.

The fatigue crack removal process may influence the fatigue strength of the repaired specimens. It is necessary to ensure that the cracks are completely removed and unnecessary material removal should be avoided. In order to fulfil this requirement, cracks are usually removed gradually and the area is regularly examined with an NDT method. In the current test specimens, the depth of the artificial cracks was known in advance. In accordance with this, the crack removal process was continued until it was assumed that the crack was completely removed. The weld grooves were prepared simultaneously. After that, the prepared weld grooves were inspected by the magnetic particle examination (see Figure 5.12).



Figure 5.12 The prepared weld groove with material removal process and NDT check on the weld groove.

When the examination revealed that there was not any indication of the crack tip, the prepared grooves were filled with the weld material. Table 5.4 presents the welding procedure and the weld material properties are given in Appendix B. The repair welds were inspected by magnetic particle and ultrasonic inspection. The repair weld satisfied the requirement of EN ISO 5817 (2007). Figure 5.13 shows the macro graphs of the repair weld in the base material.

Table 5.4 Welding parameters and geometry data of BR series specimens.

Specimens	BR69x	BR89x
Rolled steel grade	S690	S890
Number of test specimens	9	9
Thickness [mm]	25	25
Length [mm]	990	990
Width [mm]	150	150
Preheat temperature °C (min)	100	125
Interpass temperature °C (max)	165	165
Weld metal	Megafill 742 M	Megafill 1100 M
Weld process	FCAW	FCAW
Heat input	1.2-1.8	1.2-1.8

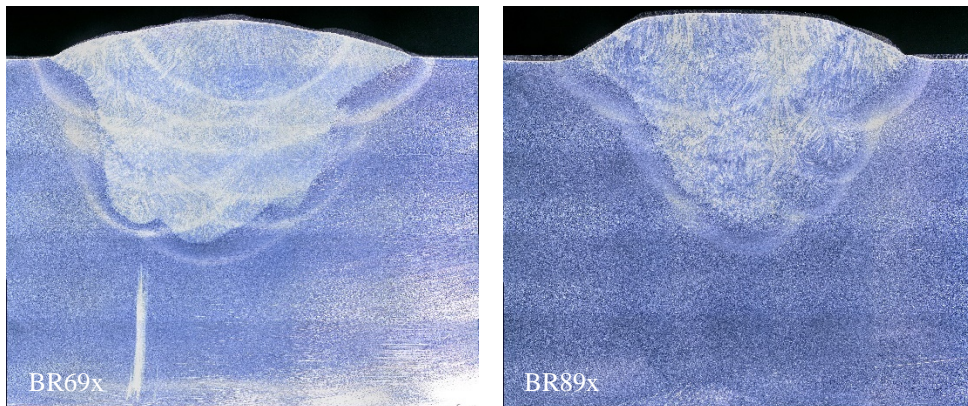


Figure 5.13 Macro graphs of repair weld in the base materials.

In general, start-stop points of weld layers show geometrical shapes that are different from other parts of the weld layer. In starting points of the weld, a bulge can be observed, while the stop points present cavities and these locations usually contain weld defects. In addition, start-stop points usually comprise high residual stresses (Zhang et al., 2012). The

discontinuities at the start-stop point can cause an additional stress concentration effect, which results in early fatigue crack initiation. The stress concentration effects of the start-stop points can be eliminated by reshaping these points. Therefore, the start-stop points of the specimens were ground after the repair of the artificial crack. Figure 5.14 shows the weld shape after grinding start-stop points. The geometry of the specimen, the weld geometry and the applied strain gauge configuration are shown in Figure 5.15. More detailed information for the strain gauge configuration is given in Appendix C.



Figure 5.14 The ground start-stop point of the repair weld.

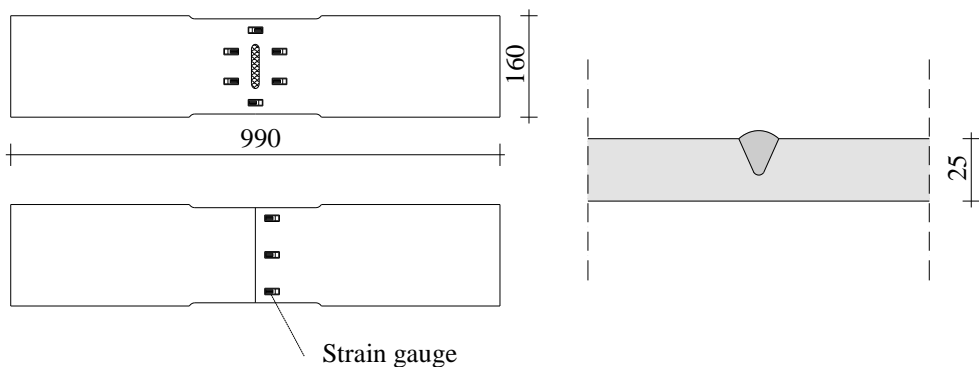


Figure 5.15 The geometry of the specimens with the applied strain gauge configuration.

Prior to the fatigue test, the edges of the specimens were slightly ground without defining a radius, to prevent fatigue crack initiation from the sharp edges of the specimens.

5.4.2 Repair of fatigue cracks in V-shape welded plates

V-shape welded specimens were tested under fatigue load until fatigue crack initiation and the propagation of the cracks was visually monitored. When the fatigue crack length reached half the width of the test specimens, the test was stopped and the specimens were removed from the test rigs for the fatigue crack repair. Fatigue cracks were initiated at the various locations of the weld joint: edge or middle of the weld toe at the weld cap and edge or middle of the weld toe at the weld root.

The accuracy of the crack length measurement depends on visibility of cracks, accessibility to crack locations and the person who performs the inspections. Basically, this aspect can lead to deviations of the measured fatigue crack length. The inaccuracy of the visual inspection may lead to inappropriate fatigue crack length detection. In addition, the visual inspections were mainly performed at the locations of the crack initiation that were indicated by the strain gauges. After a crack initiation, the strain distribution will vary on the welded connection and the strain gauges show increase/decrease or release in the strain measurements. This makes it difficult to detect additional crack initiations after the first crack appeared. In order to quantify the fatigue cracks, the application of a NDT method becomes essential. Due to easy application and simple equipment, magnetic particle inspection is a commonly used NDT method for the detection of surface cracks. The crack containing specimens were inspected by magnetic particle examination. The marking lines were drawn at the end of the crack length to indicate the fatigue crack locations and the boundary of the crack for the crack removal process (see Figure 5.16).

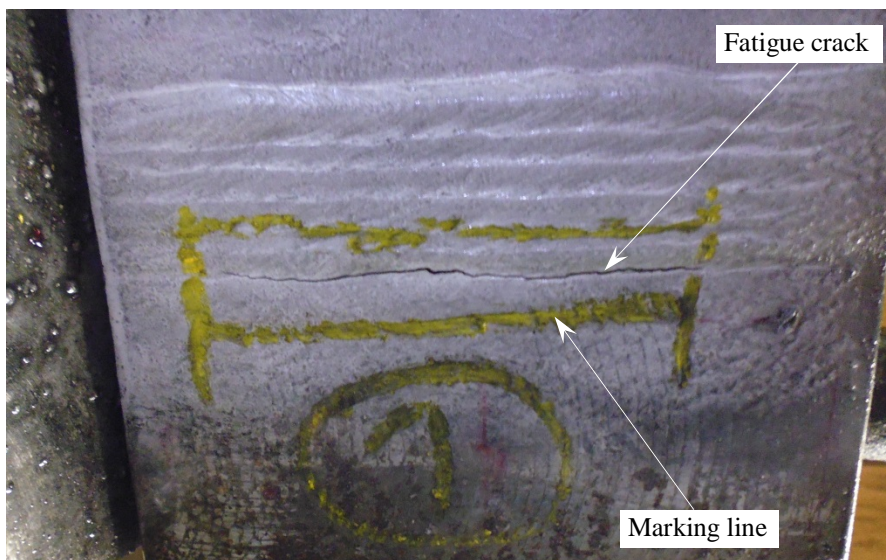


Figure 5.16 Detection of a crack in a specimen and marking line.

The crack removal process was executed with a disc and a burr grinder. Disc grinders were used only at the initial stage of the crack removal process. The disc size used must be suitable for the crack length such in order to prevent unnecessary material removal. Consequently, a small amount of material was removed by the disc grinder, and further, the crack removal process was continued with a burr grinder. By magnetic particle inspections, only the crack length can be determined and not the depth of the crack. Therefore, the crack removal process was performed gradually and the magnetic particle inspection took place regularly to avoid unessential material removal and too deep weld grooves. When it was assumed that the cracks were completely removed, the magnetic examination was performed again to ensure that the crack root had not remained in the material. During the crack removal process, the weld groove was prepared simultaneously (see Figure 5.17). In case of quite shallow cracks, the material removal process was continued up to at least $1/3$ of the material thickness, which was 8.5 mm for the test specimens of the current study. This minimum depth requirement is needed to obtain a suitable weld quality.



Figure 5.17 A weld groove after crack removal process.

After the crack removal process and magnetic particle inspections, the prepared weld grooves were filled with the weld material by using welding procedure of the original weld, which was used for manufacturing of the plate specimens. In case of a fatigue crack repair at the edge of the weld toe, a temporary plate was attached onto the edge of the specimens and the welding was started from the temporary plate to the weld groove (see Figure 5.18). This enables continuous welding and prevention of start-stop points at the edge of the test plates. After finalizing the repair process, these temporary plates were removed.



Figure 5.18 Temporary plates for the repair of the edge cracks.

As mentioned in Section 5.2.4, V-shape welds are preferred when welding from both sides is not possible. It also means that the root of the weld is inaccessible and fatigue cracks at the root of such welds might be visible when the cracks reach the weld cap. Consequently, the repair of these cracks is also performed from the weld cap. In the current study, fatigue cracks were observed at the weld toe of the weld root during the fatigue tests, although the root of the weld was exposed to the compression stresses. The cracks at the weld toe of the weld root were repaired from the weld cap. The material was removed from the weld cap through the thickness of the weld (see Figure 5.19). The prepared weld groove was filled with the weld material.

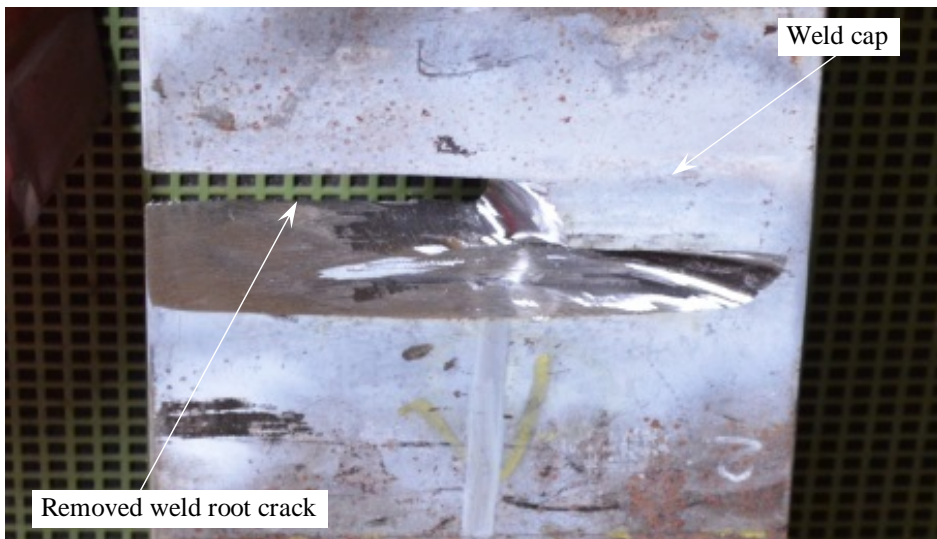


Figure 5.19. Removal of the crack at weld toe of weld root.

The fatigue crack length was determined by visual inspection and the procedure of the visual inspection is explained in the fatigue crack monitoring section. In some specimens, magnetic particle inspection revealed that the fatigue cracks at the weld toe of the weld root were longer than the length observed by the visual inspection. These cracks can be removed from the weld cap, but very little ligament remains after the crack removal process, which makes it difficult to satisfactorily fill the groove by welding. In some specimens, the crack was even as long as the weld length. These specimens were cut from the middle of the weld and the crack containing side of the weld was cut from specimens with 40° angle. In this way, half V-shape weld grooves were prepared and the plate pieces were welded together with attaching temporary plates at the edge of the plates (see Figure 5.20). The repair weld was executed without ceramic backing plates.



Figure 5.20 Half V-shape weld groove and temporary plates at the edges.

In general, fatigue crack repair in structures is executed in service conditions. This implies that the repaired connections are constrained by the elements that surround. In order to perform the fatigue crack repair process in a more realistic way, the specimens were constrained during the application of the repair weld. Figure 5.21 shows the constrain conditions of a specimen. The repair welds were examined by a magnetic particle inspection and an ultrasonic examination for the weld qualification. The repair process of each test specimen is listed in Appendix D with indication of the crack initiation locations and the strain gauge measurements.



Figure 5.21 Constrained specimen during the repair weld.

Furthermore, the applied repair method should not lead to fatigue strength reduction in a welded connection. The basic idea of the fatigue crack repair is to obtain the original fatigue strength of initial connections. When the fatigue cracks at the middle of the weld toe are repaired, the repair weld will cause changes on the weld toe geometry. This disturbs the stress distribution in the weld area. Especially, intersections between boundaries of the repair welds and the original weld cause sharp geometrical changes and they consequently cause high stress concentration at those points, which may result in very early fatigue crack initiation. Figure 5.22 shows the possible weld toe geometry after the fatigue crack repair.

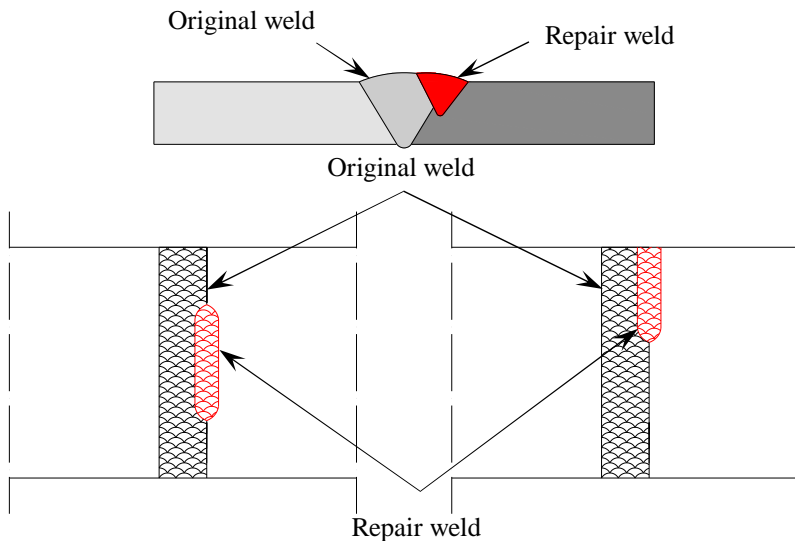


Figure 5.22 Discontinuity at the weld toe due to the repair weld.

The intersection points between the original weld and the repair weld contain the start-stop points of the repair weld cap. These could be locations of high residual stresses. Therefore, the combination high residual stresses and high stress concentration may easily promote the early fatigue crack initiation. In order to eliminate undesired effects of the stress concentration, discontinuities due to the repair weld were removed by grinding. Smooth transitions were created between the repair weld, the original weld and the base material (see Figure 5.23).

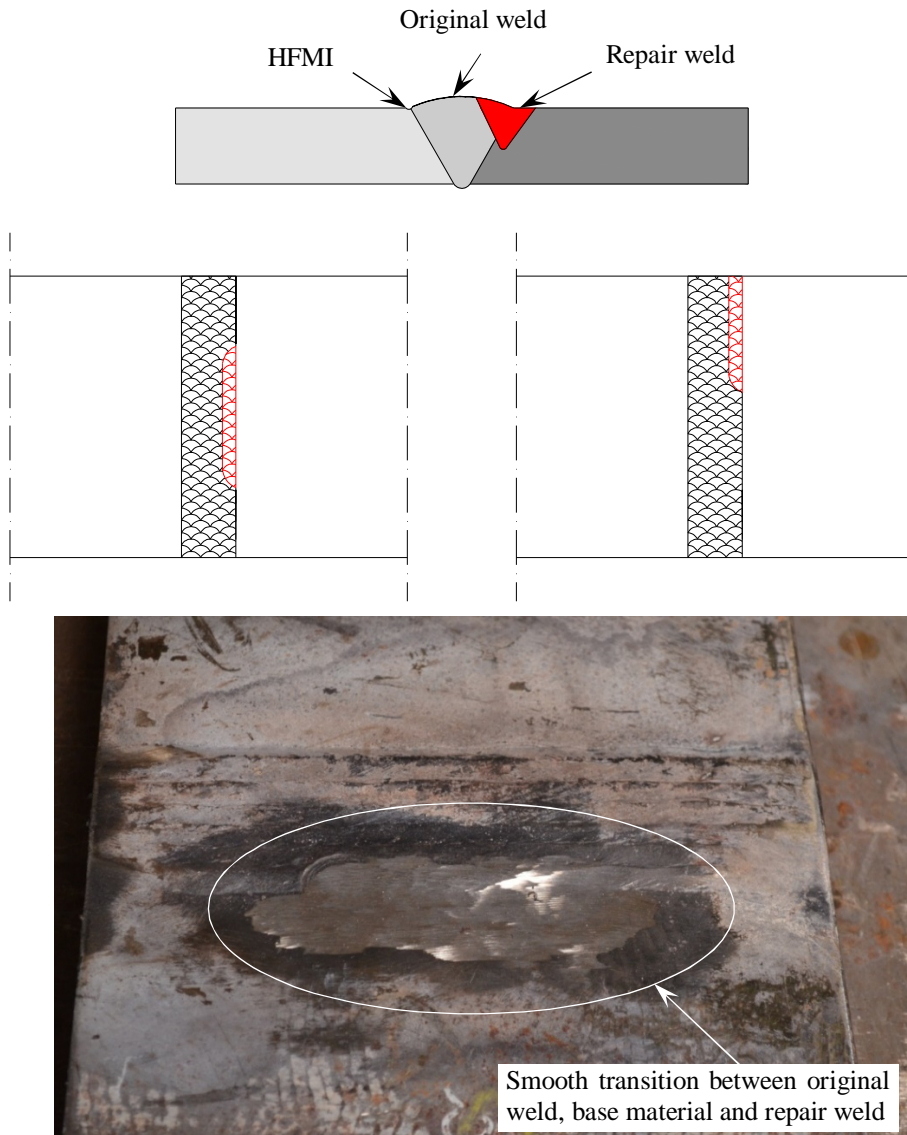


Figure 5.23 Weld geometry of repaired connection after the remove of discontinuities.

As can be seen in Figure 5.22, the repaired side of the welded connection has a new weld toe: the weld toe of the repair weld. However, the other side of the connection still contains the weld toe of the original weld which had the cyclic load history from the fatigue crack creation stage. When the cumulative damage rule of Miner is taken into account, fatigue crack initiation in the original weld toe is highly possible after the fatigue crack repair. In the current study, it was focused on the fatigue strength of the repaired welded connections made of very high strength steels. In order to reach this target, fatigue crack initiation in the weld toe of the original welds must be prevented. For this reason, the weld toes of the original welds were treated with a high frequency mechanical impact treatment (HFMI). For the VR69x series, pneumatic impact treatment (PIT) was used and the other series were treated with high frequency impact treatment (HiFIT).

5.5 Fatigue test results

5.5.1 Repaired artificial crack in the base material

For these specimens, it is difficult to make a comparison with a specific detail category of EN 1993-1-9 (2006). They could not be considered as a base material since they contain the repair welds. In order to specify them as welded connections, it is necessary that the weld was made along the whole width and through the thickness of the specimens. However, the weld was made through half the thickness of the specimens and the cap of the weld was exposed to the tensile load during the fatigue test. The weld shape can be compared with half the X-shape weld and the loading condition is the same as that for the loading of X-shape welded connections with bending, where one side of the weld cap is exposed to the tensile stresses. Therefore, the test results were compared with the detail category of X-shape welded connections and are represented with the detail category 80 in EN 1993-1-9 (2006). Figure 5.24 shows fatigue test results respect to the detail category 80 of EN 1993-1-9 (2006).

In the BR69x series, fatigue cracks initiated at the start-stop point of the repair weld. The fatigue crack initiation life of the specimens was almost equal to the fatigue crack propagation life. The fatigue test results are listed in Appendix E.

In the BR89x series, fatigue cracks initiated at start-stop points of the repair weld as well. After testing a few specimens, the start-stop points of the repair welds were ground further to create a smoother transition between the weld and the base material (see Figure 5.25). This additional treatment provided some shifting of the fatigue crack initiation from at the start-stop points to the middle of the weld toe and the movement was not at the desired level. In one of the specimens in these series, not any fatigue crack initiation was observed after 5 million cycles and the specimen is indicated as runout.

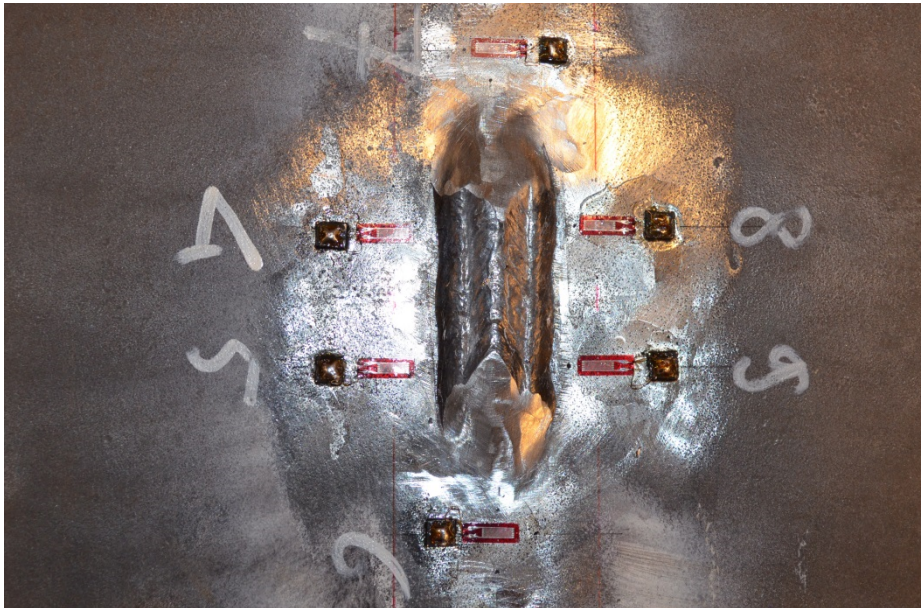


Figure 5.25. Additional grinding at start-stop points of the weld.

As appears from Figure 5.24, the test results of both series met the requirements of the detail category 80 of EN 1993-1-9 (2006) which represents the fatigue strength of the X-shape welded connections and it is conservative for this welding type.

5.5.2 V-shape welded specimens made of rolled steels

The specimens were tested under a constant amplitude fatigue loading to create fatigue cracks at the weld toe of the cap. This is called the cracks creation stage. In total, 18 specimens were prepared for each steel grade. In specimens of the VO69x series, fatigue cracks initiated at the weld toe of the cap and at the weld toe of the root, although the root of the weld was exposed to the compression stresses. In specimens of the VO89x series, fatigue cracks were observed at the weld toe of the cap as well as at the root. In addition, also fatigue crack initiation and propagation were observed in the base material of the specimens, far from the weld connections. The test results from the crack creation stage

were not further evaluated. The first samples, that consist of 9 test specimens of each series, were repaired and the fatigue tests were executed on these specimens. Those are dealt with in this section. The results of the fatigue tests on the repaired specimens are given in Appendix E.

Figure 5.26 shows the fatigue test results of the repaired specimens VR69x samples. No crack initiation was observed in two tests specimens, while in the crack creation stage, fatigue crack initiation and propagation were observed in the weld toes of these specimens. These are indicated as runouts. After the repair, fatigue cracks were initiated at the weld toe of the cap and mainly at the middle or near the middle of the specimens. They showed a relatively similar fatigue crack initiation and propagation life, about 50%. In one specimen, fatigue cracks initiated in the very early stage of the test. After failure of the specimen, an imperfection was observed on the fracture surface of the specimen, which was the reason for the early fatigue crack initiation. The fatigue strength of V-shape welded connections is indicated by detail category 71 of EN 1993-1-9 (2006). The test results met the requirements of the detail category 71 on EN 1993-1-9 (2006).

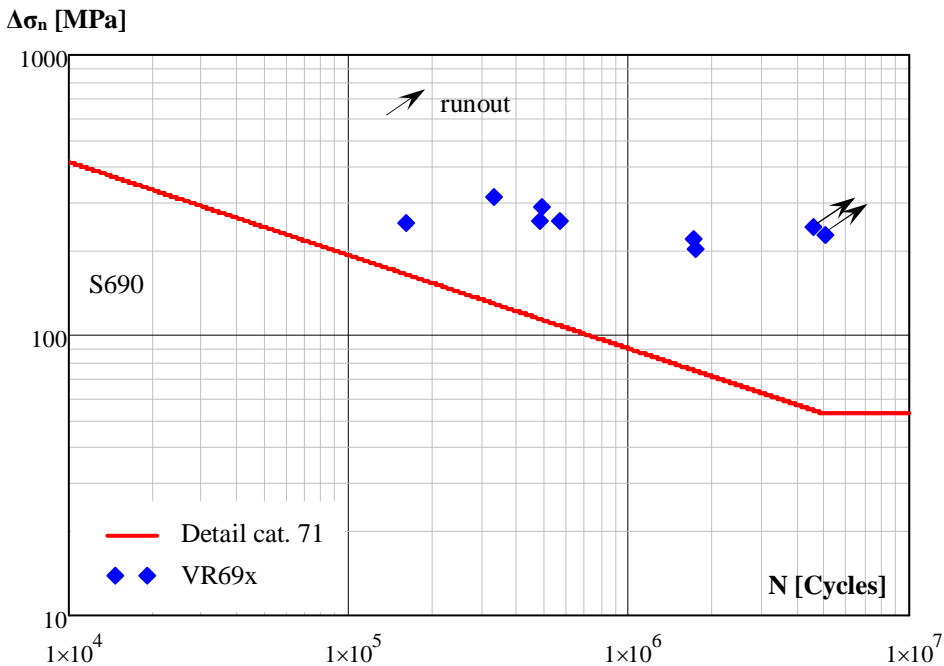


Figure 5.26 Fatigue test results of repaired VR69x series.

Figure 5.27 presents the fatigue test results of the VR89x series. Each sample of the test series consisted of 9 test specimens. However, 3 test specimens of this sample failed due to fatigue crack initiation and propagation in the base material, far from the welded connections in the crack creation stage. These specimens were not repaired and excluded

from second stage -fatigue tests on the repaired welded connections- of testing. Fatigue tests were therefore executed on the 6 repaired test specimens. In 2 test specimens, no fatigue cracks were observed and they were indicated as runouts. One of these specimens was already runout in the fatigue crack creation stage and this specimen was repaired, assuming that there was a fatigue crack with a length of 80 mm at the middle of the weld toe of the cap. In the remaining 4 repaired specimens, fatigue crack initiation and propagation was observed in the base material of the specimens. The fatigue crack initiations in the base material were far away (about 150-170 mm) from the weld toe and the strain gauges therefore reacted in the very late stage of the crack development. Therefore, the fatigue crack initiation life of these specimens was determined in a late stage of fatigue crack development. For the specimens with the base material failures, the number of cycles at the crack creation stage were included to the number of cycles at failure after the repair.

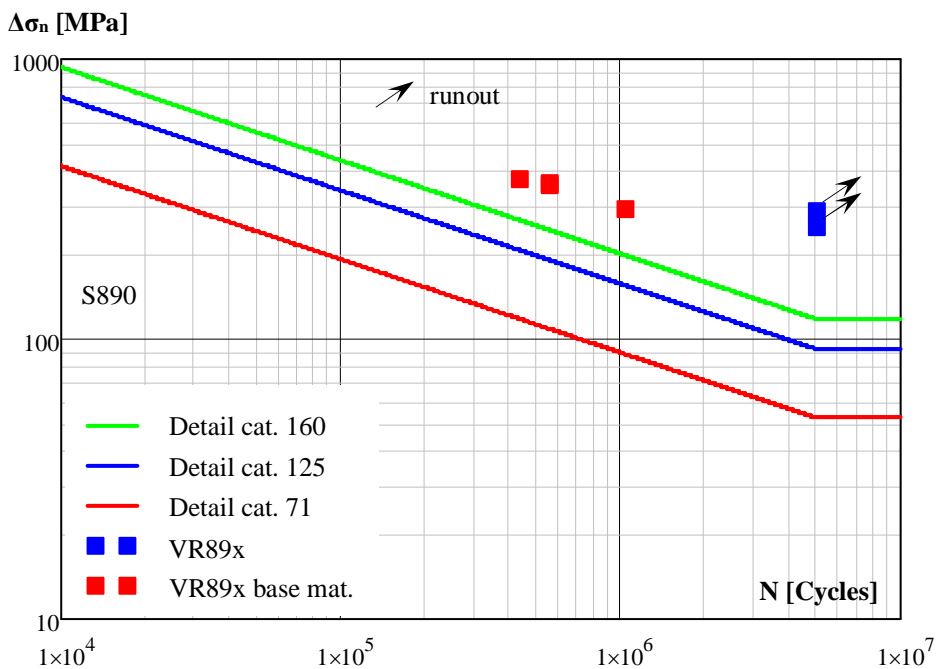


Figure 5.27 Fatigue test results of repaired VR89x series.

Consequently, the fatigue test results of these series are a combination of the results of repaired V-shape welded specimens and the results of the base material. The fatigue strength of base materials is represented by detail categories 160 and 125 in EN 1993-1-9 (2006) and these detail categories were added to Figure 5.27. It shows that the test results met the requirements of detail category 71 for repaired V-shape welded connections and detail categories of 160 and 125 for the base material.

remaining specimens, fatigue crack initiation and propagation was observed at the weld toe of the repair weld cap. The relation between the fatigue crack initiation life and the fatigue crack propagation life showed some inconsistencies. The fatigue crack initiation life varied between 17% and 68% of the total fatigue life. The test results of the weld toe cracks met the requirements of the detail category 71 of EN 1993-1-9 (2006). The test results of the base material failures satisfied the requirements of the detail categories 160 and 125 of EN 1993-1-9 (2006).

Figure 5.29 shows the fatigue test results of the CR89x series. In the majority of the specimens, the fatigue crack initiation and propagation was observed in the base material. Only in one specimen, the fatigue crack initiation and propagation was monitored at the weld toe of the cap, which was the repair weld toe at the cast steel part. Two specimens failed due to crack initiation and propagation in the base material of the cast steel. In 6 specimens, the failure was observed in the base material of the rolled steel. The result of the weld toe crack met the requirements of detail category 71 of EN 1993-1-9 (2006). The results of the base material failures satisfied the requirements of the detail categories 160 and 125 of EN 1993-1-9 (2006).

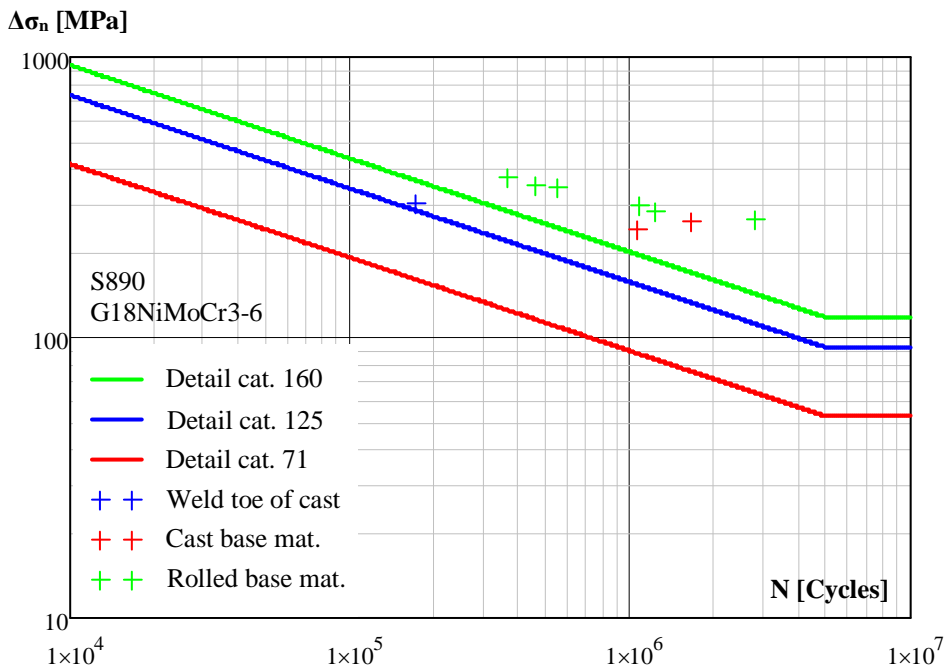


Figure 5.29 Fatigue test results of repaired CR89x series.

5.6 Summary

From relevant literature, it appears that little information is available about the fatigue crack repair procedure. Fatigue strength of repaired welded connections made of high strength steels is not acknowledged in literature. An experimental study was carried out to investigate fatigue strength of the repaired welded connections made of very high strength S690 and S890 steels.

Initially, fatigue tests were executed on the specimens of the repaired an artificial crack in the base material to investigate the response of the high strength steel base material to the repair weld. The fatigue cracks had initiated at the start-stop point of the weld cap. The specimens showed a similar fatigue crack initiation and propagation life. Comparison between the test results and the detail category of the design standard, EN 1993-1-9 (2006), showed that the test results satisfied the requirements of the detail category 80 of EN 1993-1-9 (2006).

The majority of the experimental programme consisted of the fatigue tests on the V-shape welded specimens. The specimens were made of S690 and S890 rolled steel and similar yield strength cast steels G10MnMoV6-3 and G18NiMoCr3-6. The welded connections were manufactured in two configurations: the welded connections rolled to rolled steels and the welded connections rolled to cast steels. The welding was executed with a ceramic backing. In the first stage, the specimens were tested at constant amplitude fatigue loading to create fatigue cracks at the weld toe of the cap. When the fatigue crack length reached half the width of the specimens, the experiments were terminated and the created fatigue cracks repaired. The test results of the crack creation stage were not dealt with in this study. In the second stage, fatigue tests were performed on the repaired V-shape welded specimens. The test results of the repaired welded connections satisfied the requirements of the detail category 71 of EN 1993-1-9 (2006). The specimens of VR69x series showed at similar fatigue crack initiation life and propagation life and this consistency was not seen in the test specimens of other series. In some specimens, fatigue crack initiation and propagation was observed in the base material of the cast steels and in the base material of S890 rolled steel. The major part of the specimens made of S890 rolled steel failed due to crack initiation and propagation in the base material of the rolled steel. In addition, the results with the base material failures met the requirements of the detail category 160 and 125 of EN 1993-1-9 (2006).

Chapter 6

Fatigue crack growth experiments

6.1 Introduction

In welded steel structures, fatigue crack initiation is inevitable under the fluctuated loading conditions. The use of very high strength steels significantly reduces the self-weight of the structures, which causes high stress variation due to the fluctuated live loads. In addition, the susceptibility of very high strength steels to notches or defects is higher than the lower steel grades. In welded connections, these kinds of defects are usually present, which might promote the fatigue crack initiation in welded connections of very high strength steels. The current study is focused on the fatigue strength of repaired fatigue damaged welded connections made of very high strength steels. In Chapter 5, the results of the experiments were shown and it was seen that the fatigue life of fatigue damaged connections could be regained with the explained repair procedure. However, immediately repair of each initiated fatigue crack may not always be possible. The fatigue cracks should be repaired when they reach the critical values. The critical value of the crack is determined by fitness for purpose assessment and it is extensively dealt with in BS 7910 (2013).

The fatigue propagation life from the initially detected crack to the critical crack can be calculated with the fracture mechanics approach. This approach utilizes the Paris law for the calculation of the fatigue crack propagation life. The Paris law contains material constants and these are determined by the fatigue crack growth tests.

Moreover, Pijpers (2011) studied the applicability of high strength steels for the civil engineering industry and at study revealed that it is technically possible. In the current study, a suitable fatigue crack repair procedure is provided for fatigue damaged V-shape welded connections made of very high strength steels. In order to determine fatigue crack propagation life in very high strength steels, the material constants are needed for the application of the Paris crack propagation law.

This chapter is focused on the fatigue crack growth experiments performed on the base material of S690 and S890 high strength rolled steels. In Section 6.2, the experimental programme is explained including preparation of the specimens and the execution of the tests. Section 6.3 presents the results of the experiments, the implementation of the results of the base material tests to V-shape welded connections and a comparison with the results from literature.

6.2 Experimental programme

6.2.1 Test programme

Table 6.1 shows the experimental programme for the fatigue crack growth tests on the base material of S690 and S890 specimens. The chemical and mechanical properties of the materials are given in Appendix B.

Table 6.1 Experimental programme for fatigue crack growth tests, 4pb = four point bending.

Series	Steel grade	Thickness x Width [mm]	Loading	Number of specimens
CG69x	S690	25x25	4pb	3
CG89x	S890	25x25	4pb	3

The procedures for the fatigue crack growth test are given in ASTM E 647 (2016) and EN-ISO 12108 (2012). In ASTM E 647 (2016), it is concentrated on the testing under tension loading conditions. The shape and standard size of the specimens are given in the documents. In EN-ISO 12108 (2012), the test procedure for both tension and bending loading conditions are dealt with and for the testing under bending load, different loading configurations are given i.e. three point bending, four point bending eight point bending etc. Since the fatigue crack growth tests are executed in four point bending loading condition, the testing procedure in EN-ISO 12108 (2012) is followed in this research.

6.2.2 Preparation of specimens

The dimensions of the standard test specimens are given in EN-ISO 12108 (2012). According to the document, the dimensions of the specimens are identified as a function of the specimen thickness. The plates for the fatigue tests have a thickness of 25 mm. The

dimensions of the specimens and the notch are calculated based on this thickness. Figure 6.1 shows the dimensions, the geometry and the notch detail of the specimens.

The specimens are cut from the plate with a width of 30 mm and a length with 150 mm by saw cutting. The saw cutting can introduce the residual stresses on the surface of the specimens and these residual stresses can influence the fatigue crack propagation behaviour. Therefore, the cut pieces are processed with an electric discharging machine (EDM) to reduce the width of the specimens to 25 mm and the length to 120 mm. In this way, the influenced surfaces by saw cutting are removed and the effects of residual stresses on the fatigue crack propagation are prevented. The notches in the specimens are also prepared with the EDM process.

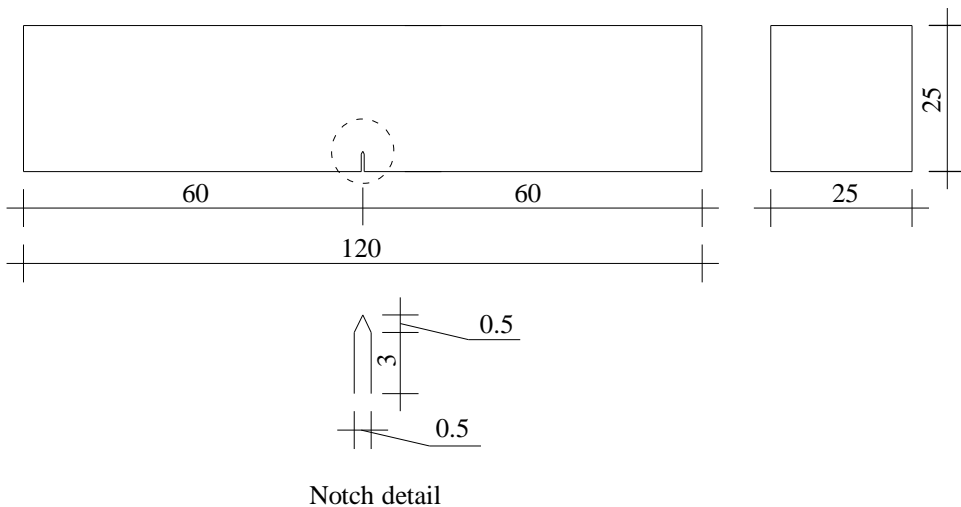


Figure 6.1 Geometry of the specimens with dimensions of the notch.

6.2.3 Test setup

Fatigue crack growth tests were carried out in the Stevin II laboratory of Delft University of Technology. Fatigue crack growth tests were executed with a four point bending test setup. Figure 6.2 shows the four point bending test setup and the loading configuration on a specimen.

The pre-notched specimens were loaded by using servo-hydraulic jack with a capacity of 100 kN. The specimens were loaded with stress ratio $R = 0.1$ which is also used for the fatigue test on the V-shape welded plate specimens and the results of the fatigue crack growth tests will be used for the prediction of the fatigue crack propagation life of repaired V-shape welded specimens. The pre-notched specimens were tested with a frequency of 15 Hz.

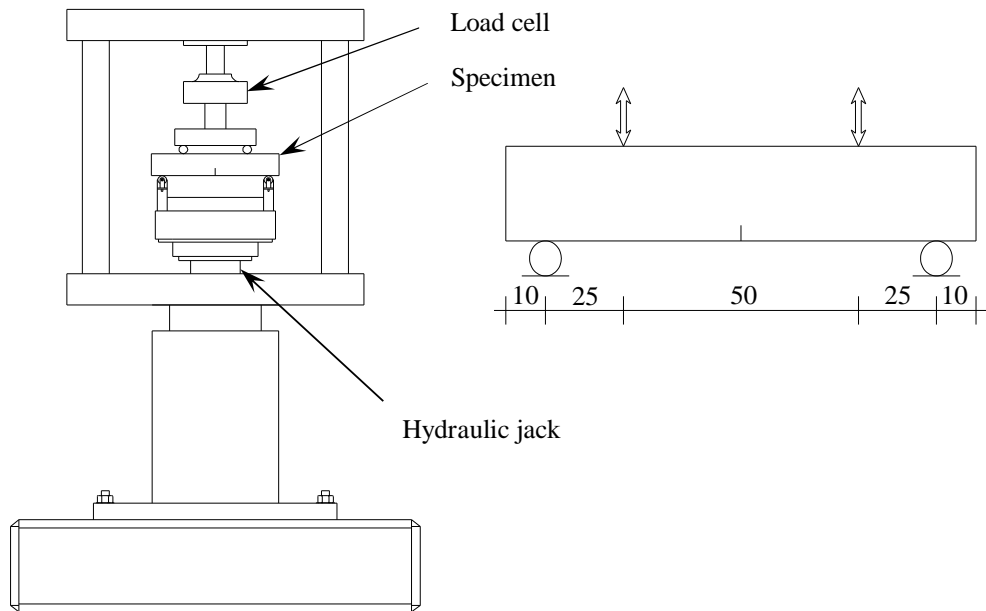


Figure 6.2 Four point bending setup for fatigue crack growth tests.

6.2.4 Crack propagation monitoring

Fatigue crack propagation in pre-notched specimens was monitored with crack detection gauges, a camera system and a clip gauge. On the crack growth path, a crack detection gauge, FAC-20, was applied to monitor crack propagation under cyclic loading. The crack detection gauges contain 41 grids, which are aligned with a distance of 0.5 mm (see Figure 6.3).



Figure 6.3 FAC-20 crack detection gauge with 41 grids.

The crack detection gauge was applied in such a way that the grids were located perpendicular to the crack growth path. During crack propagation, these grids were disconnected one by one and the disconnection of the grids changes the resistance of the gauge which provides information about the crack length and the number of cycles at the moment of the grids disconnection. Figure 6.4 shows an example of the measured resistance of crack detection gauge versus the number of cycles. As the distance between two grids is known, the number of cycles for disconnection of these two grids can be determined from the resistance measurements and according to this information the crack growth rate of the specimen can be calculated.

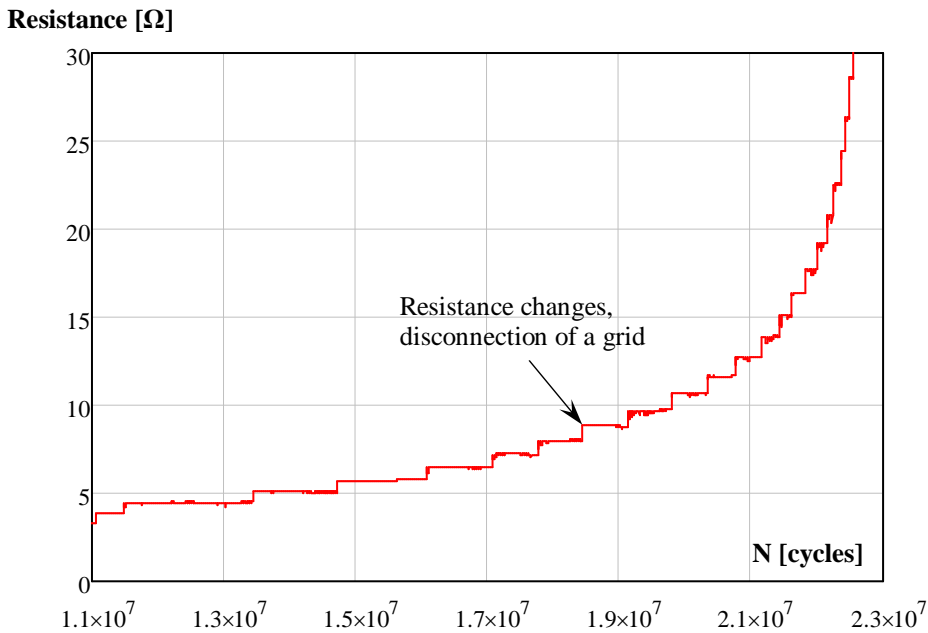


Figure 6.4 The measured resistance versus the number of cycles.

A camera system was placed at each side of the specimens to follow the crack propagation in the specimens. Figure 6.5 shows the camera system used and example images from the camera captures. The system was programmed in such a way that the cameras would take a picture of the crack path every 20 minutes. In addition, if the disconnection of a grid takes place in the meantime, the system makes an additional picture at the moment of disconnection of the grid. The moment a picture is taken, the system applies the maximum load to open the crack and the picture is taken at the crack open state, which makes the crack length and the crack tip more visible. By this, fatigue crack propagation can also be followed by means of the camera pictures. From one of the camera, the grid disconnection of crack detection gauge is monitored. The camera images can also be used for crack length measurement by a suitable image processing program.

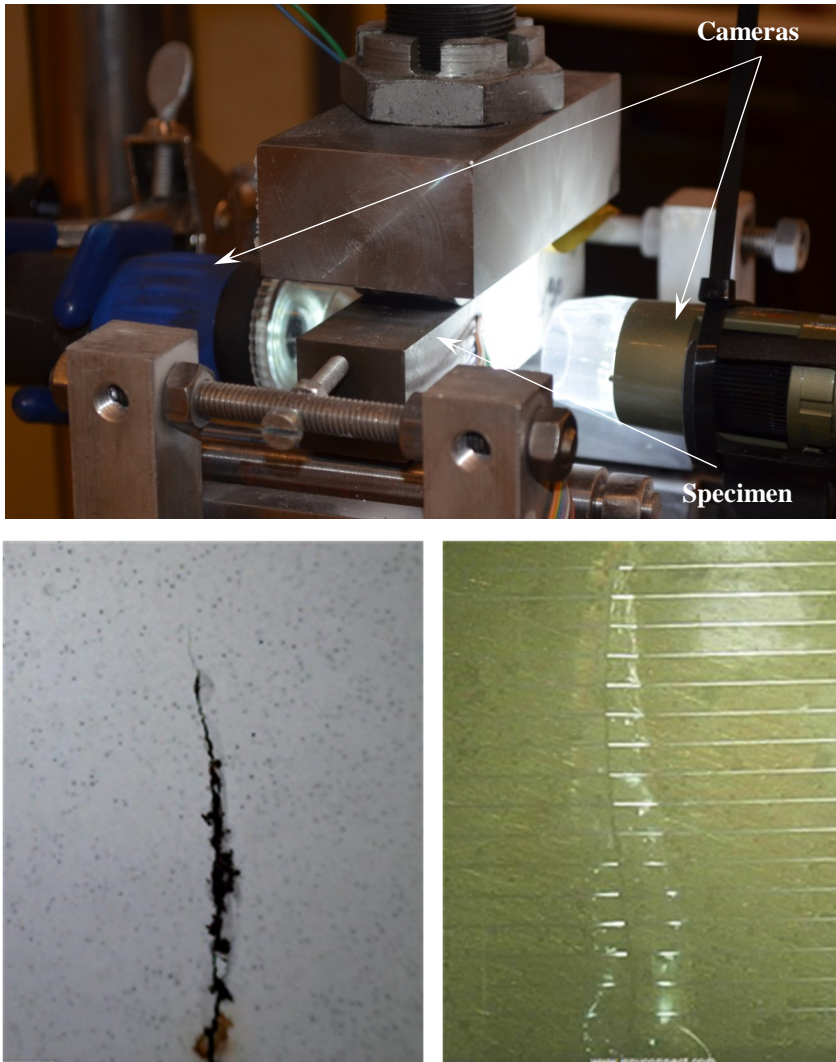


Figure 6.5 Camera system and images from the cameras.

Furthermore, a clip gauge was placed at the notched side of the specimens to measure the opening for the crack propagation (see Figure 6.6). The clip gauge measurements are plotted versus number of cycles and the graph is compared with the graph for the crack detection gauge resistance versus the number of cycles to evaluate crack propagation behaviour. Both graphs show the same trend line (see Figure 6.7). In addition, the clip gauge was used for monitoring the fatigue crack propagation at low stress range state.

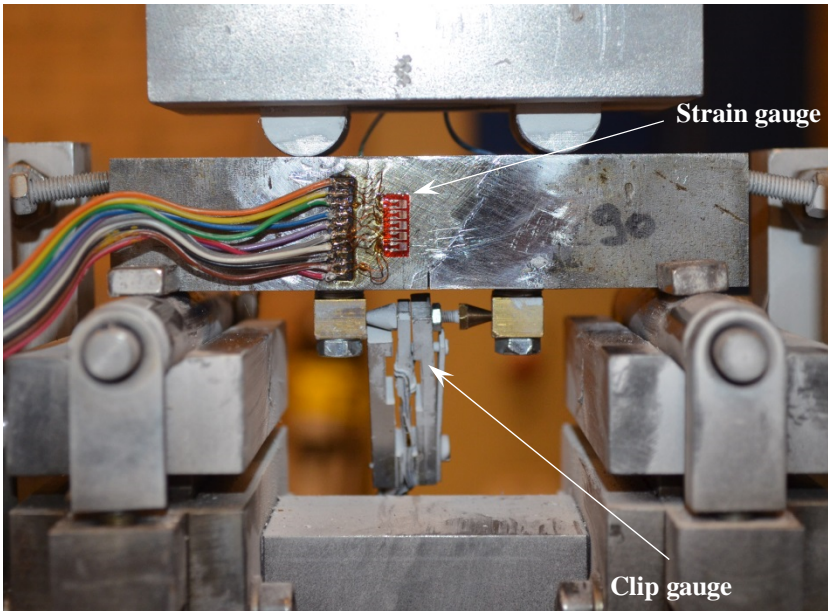


Figure 6.6 The configuration of the strain gauge and clip gauge.

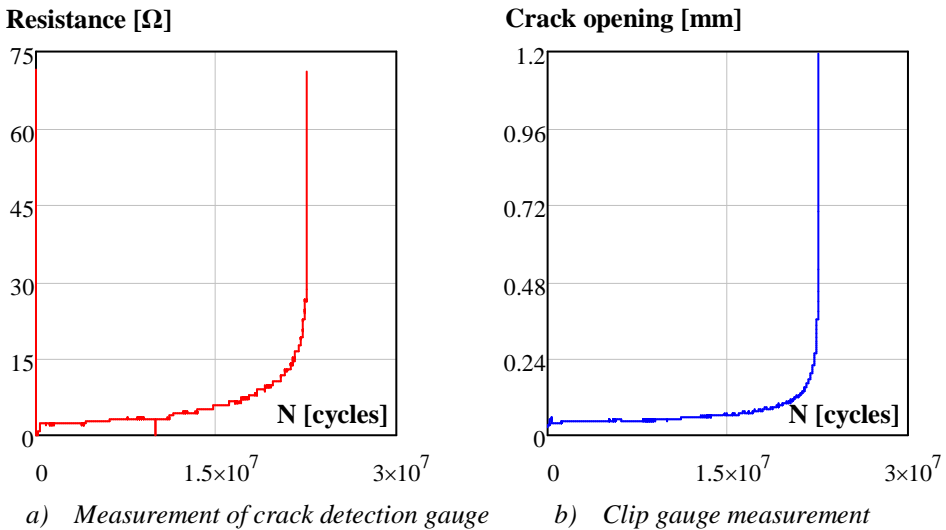


Figure 6.7 Clip gauge measurement and measurement of crack detection gauge.

Moreover, with fatigue crack growth tests, it was aimed to determine the material constants for Paris law and the threshold stress intensity factor, which represents the fatigue crack propagation resistance of the material. The stress intensity factors below the threshold value will not cause crack propagation. The threshold stress intensity factor is determined under a

very low stress range and consequently the fatigue crack growth rate is very low, with a magnitude of 10^{-8} mm/cycle. For such a very low crack growth rate, it is difficult to visually observe the crack propagation. In order to be sure for the growth of the crack, FYV-1-17 strain gauges are applied along the crack path to monitor strain distribution during crack propagation (see Figure 6.6). With crack propagation, the strain along the crack propagation path will increase or decrease, which depends on the position of the strain gauge with respect to the crack tip. These strain distribution changes give an indication for the crack propagation. Figure 6.8 shows strain measurements during a crack growth test.

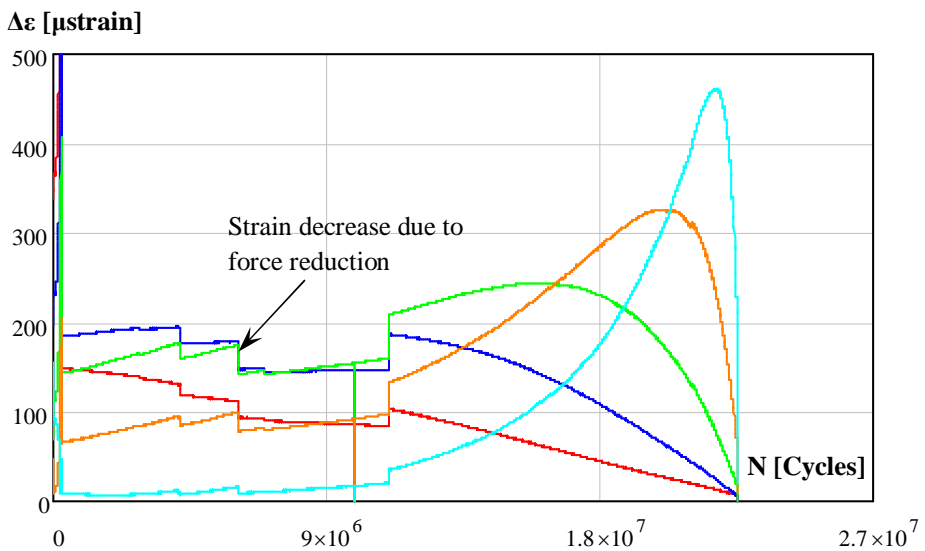


Figure 6.8 Strain gauge measurements of a crack growth test.

6.2.5 Testing procedure

The fatigue crack growth test procedure is given in ASTM E647 (2016) and ISO 12108 (2012) and the testing procedures of both standards are similar. In the documents, two testing procedures are described; stress intensity factor range, ΔK , increase and stress intensity factor range, ΔK , decrease.

The selection of the procedure depends on the crack growth rate region of interest. If it is aimed at determining a crack growth rate higher than 10^{-5} , the stress intensity factor range increase procedure is recommended and for the lower values of the crack growth rate, the stress intensity factor range decrease procedure is recommended. The stress intensity factor range increase procedure is usually used for the determination material constants for Paris

law. The stress intensity factor range decrease procedure is utilized for establishing the threshold stress intensity factor ΔK_{th} .

For the stress intensity factor range increasing method, the specimens are loaded with a constant load range. Due to the growth of the crack, the stress intensity factor range will increase and with each of the stress intensity factor ranges, the crack will grow at a high rate. Consequently, the crack growth rate can be determined versus the stress intensity factor range and it forms the linear part of the Paris crack growth curve. The material parameters for Paris law are determined from this linear part, where the material parameters are defined with the slope of the curve and the intersection point at the y-axis.

In the stress intensity factor range decreasing method, the applied stress range is gradually decreased after pre-cracking of the notched specimen. The decrease of the stress range is repeated until the desired crack growth rate is determined. The reduction of the stress range needs to be done in small steps to avoid retardation of the crack growth due to plasticity at the crack tip. The stress range reduction can be done in three different ways (see Figure 6.9). The minimum stress state can be kept constant, while the maximum stress level is reduced gradually. This load configuration can lead to occurrence of a plastic zone at the crack tip, which will influence the crack growth rate. Therefore, it is an unfavourable load sequence. Another way is to keep the maximum stress constant and to reduce minimum stress level. This load sequence is more favourable for preventing the crack retardation due to the plastic zone at the crack tip. However, this load sequence causes variation in the stress ratio values. Fatigue crack propagation behaviour is influenced by the stress ration, R value. In order to determine fatigue crack growth parameters for a constant R value, the maximum and minimum stress levels are reduced simultaneously.

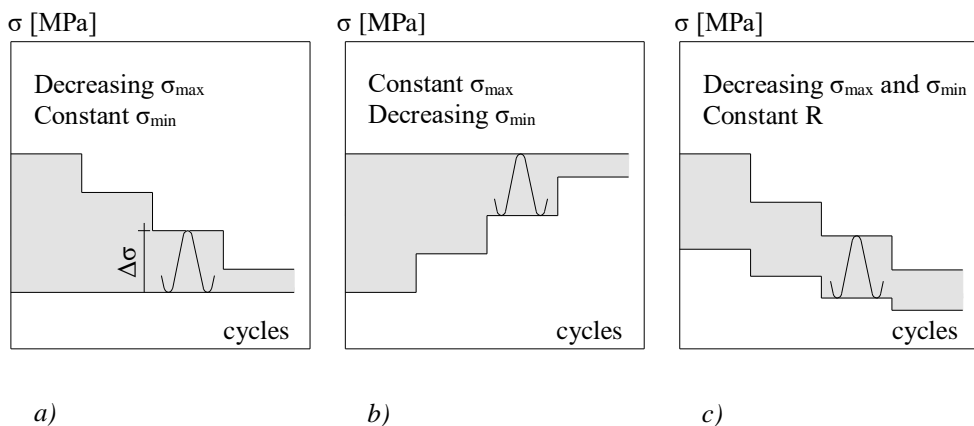


Figure 6.9 Various ways to decrease stress intensity factor.

In the current study, the threshold stress intensity values were determined with a constant R value of 0.1, which was also used for fatigue tests on the repaired V-shape welded specimens.

6.3 Test results

6.3.1 Crack growth in base material

The fatigue crack growth tests were performed on the base material of S690 and S890 rolled steels. The test results are graphically presented with the crack growth rate versus the stress intensity factor on a log-log scale. Figure 6.10 shows the results of fatigue crack growth tests on the specimens made of S690 rolled steels. The material parameters for Paris law are determined from the linear part of the curve. The parameter C is the intersection at the y-axis, the parameter m is the slope of the curve. The asymptote of the curve indicates the threshold stress intensity factor range of the material. Table 6.2 shows the parameters of the mean curve of the test results.

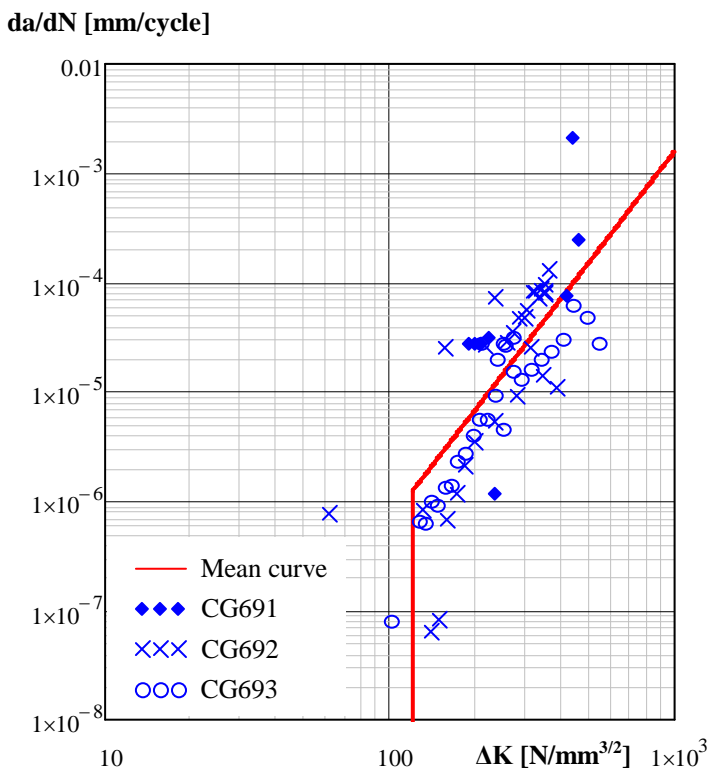


Figure 6.10 Results of fatigue crack growth tests on S690 rolled steel.

Table 6.2 Parameters of the mean curve for the specimens made of S690.

Series	m [-]	C [mm/cycle]	ΔK_{th} [N/mm ^{3/2}]
CG69x	3.377	$1.171 \cdot 10^{-13}$	120

Figure 6.11 shows the fatigue crack growth rate versus the stress intensity factor range for the base material of S890 rolled steel. The mean curve of the test results has been determined and accordingly fatigue crack growth parameters for Paris law are calculated. These parameters are given in Table 6.3.

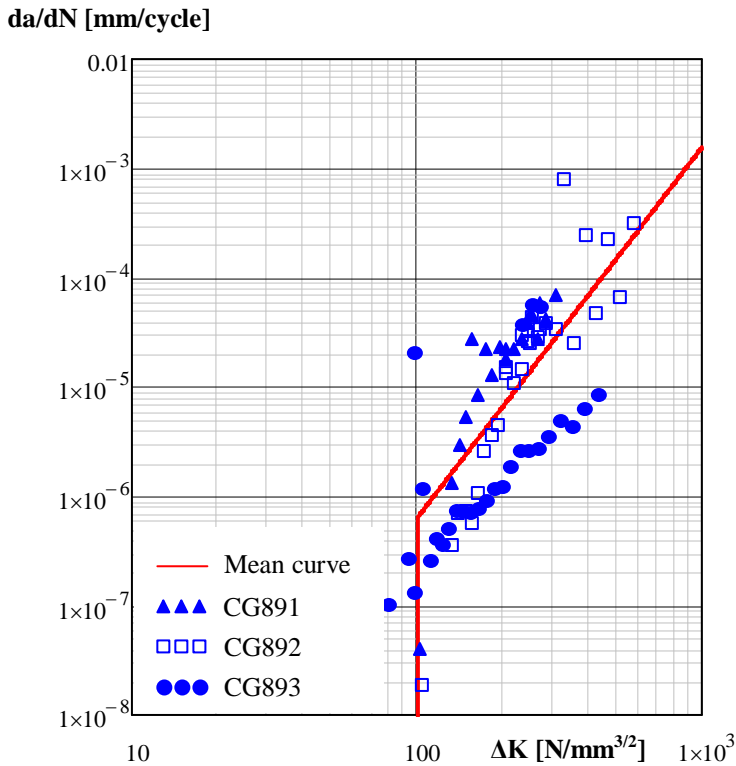


Figure 6.11 Results of fatigue crack growth tests on S890 rolled steel.

Table 6.3 Parameters of the mean curve for the specimens made of S890.

Series	m [-]	C [mm/cycle]	ΔK_{th} [N/mm ^{3/2}]
CG89x	3.394	$1.022 \cdot 10^{-13}$	100

6.3.2 Analysis of the test results

In welded connections, fatigue cracks initiate at the weld toe and propagate perpendicular to the loading direction. For V-shape welded connections, the crack propagation mainly takes place in the base material and the crack propagation in the heat affected zone is relatively small (see Figure 6.12). The crack propagation behaviour in the base material is affected by the induced residual stress due to the welding process.

BS 7910 (2013) provides material parameters for fatigue crack growth calculation and the parameters are valid for steels with yield strength up to 700 MPa. The parameters are given for the mean curve and the mean plus two standard deviations (mean + 2sd). It is explicitly mentioned that the values of the mean plus two standard deviations for $R \geq 0.5$ is recommended for the assessment of welded joints in order to take the effects of the residual stresses into account. In addition, this recommendation corresponds to the 97.7% probability of survival in fatigue life calculation and the S-N curves of BS 7608 (2014) are determined with the same probability of survival.

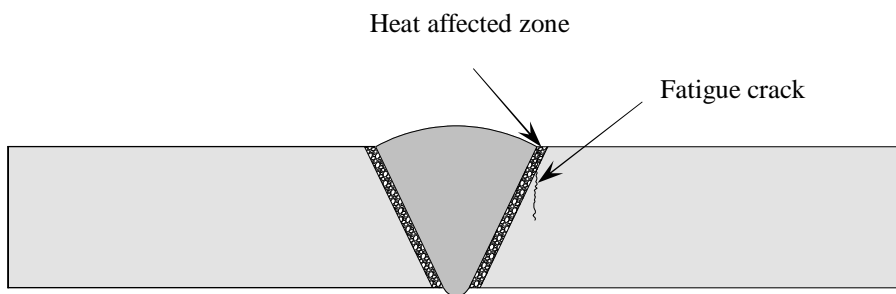


Figure 6.12 Fatigue crack propagation path in V-shape welded connections.

With the same analogy, the mean plus two standard deviation of the test data is determined for the test results for providing fatigue crack growth parameters of welded connection. Figure 6.13 shows the mean curve and the mean plus two standard deviation curve of the fatigue crack growth tests on S690 rolled steel. The parameters of the mean plus two standard deviations are given in Table 6.4.

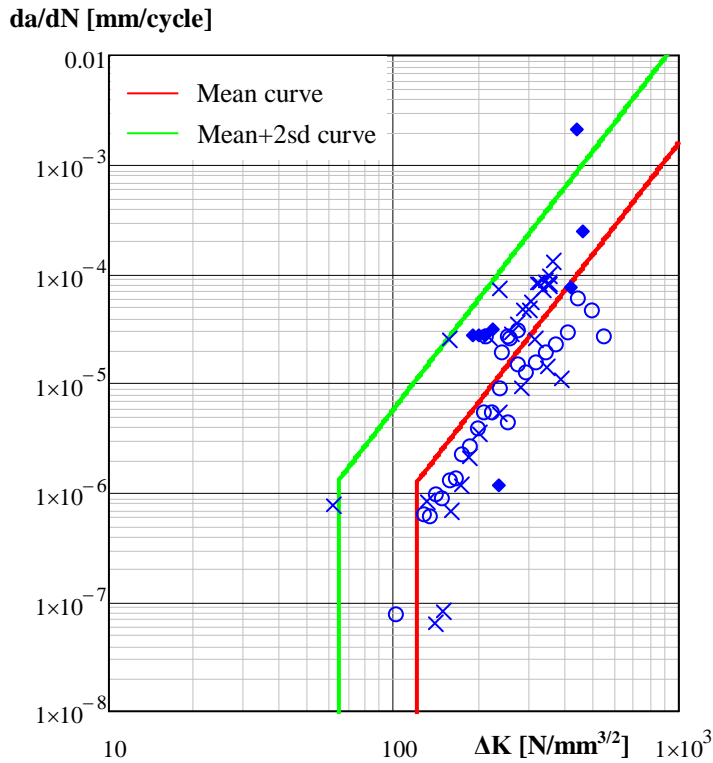


Figure 6.13 Mean and mean+2sd for the test results of S690 steels.

Table 6.4 Parameters of the mean +2sd curve for the specimens made of S690.

Series	m [-]	C [mm/cycle]	ΔK_{th} [N/mm ^{3/2}]
CG69x	3.377	$1.032 \cdot 10^{-12}$	64

Figure 6.14 shows the test results, the mean curve and the mean plus two standard deviations of the results of the fatigue crack growth tests on S890 rolled steels. The Paris law parameters of the mean plus two standard deviations are determined from the linear part of the curve and the threshold stress intensity factor is shown by the vertical asymptote of the curve in the figure. The determined values are summarised in Table 6.5.

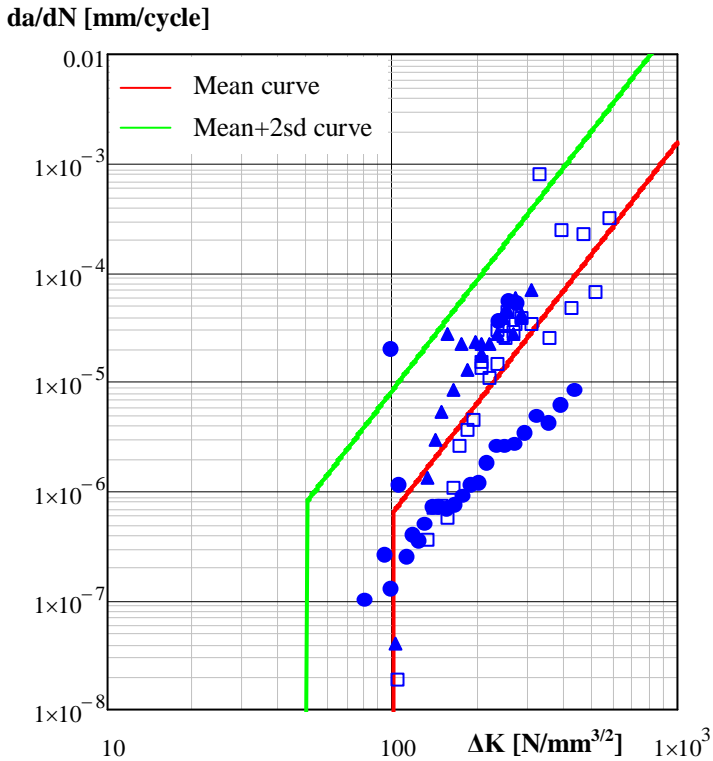


Figure 6.14 Mean and mean+2sd for the test results of S890 steels.

Table 6.5 Parameters of the mean +2sd curve for the specimens made of S890.

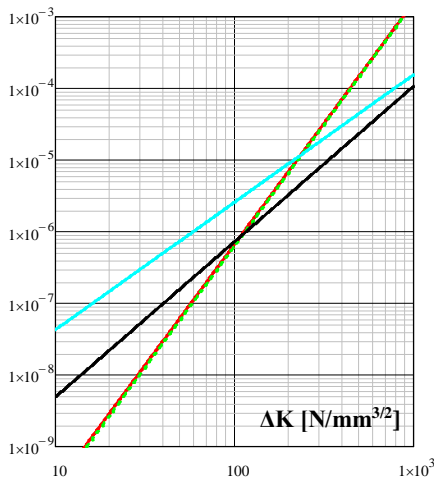
Series	m [-]	C [mm/cycle]	ΔK_{th} [N/mm ^{3/2}]
CG89x	3.394	$1.367 \cdot 10^{-12}$	50

A comparison was made with the test results of the current study and the results from literature. However, the results from literature presents for the linear part of the graph of the fatigue crack propagation rate versus stress intensity factor range. In other words, results for threshold stress intensity factor are not given in literature. Moreover, the provided fatigue crack growth parameters were determined according to the mean curve of the tests. Accordingly, the comparison was made for the values of the mean curves. Table 6.6 shows the fatigue crack growth parameters from literature. Figure 6.15 indicates the graphical presentation of the comparison.

Table 6.6 Fatigue crack growth parameters from literature for comparison.

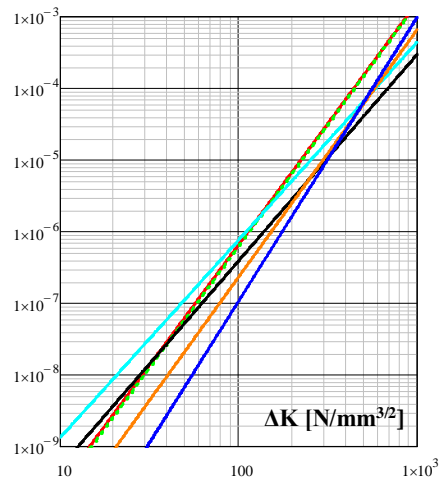
Grade	R	C [mm/cycle]	m [-]	Reference
S690	0.10	$3.31 \cdot 10^{-11}$	2.17	Demofonti et al. (2001)
S960	0.10	$7.09 \cdot 10^{-10}$	1.78	
S690	0.00	$6.83 \cdot 10^{-13}$	2.88	De Jesus et al. (2012)
	0.25	$2.32 \cdot 10^{-12}$	2.76	
	0.50	$2.95 \cdot 10^{-14}$	3.45	
	0.75	$1.30 \cdot 10^{-15}$	3.96	

da/dN [mm/cycle]



- Current study S690 R=0.1
- Current study S890 R=0.1
- S690 Demofonti et al. (2001) R=0.1
- S960 Demofonti et al. (2001) R=0.1

da/dN [mm/cycle]



- Current study S690 R=0.1
- Current study S890 R=0.1
- S690 De Jesus et al. (2012) R=0
- S690 De Jesus et al. (2012) R=0.25
- S690 De Jesus et al. (2012) R=0.50
- S690 De Jesus et al. (2012) R=0.75

Figure 6.15 Comparison of the fatigue crack growth results.

The specimens made of S690 and S890 show similar fatigue crack growth parameters. The comparison with the results from Demofonti et al., (2001) presents a substantial deviation. It reveals that the specimens of the current study show slower fatigue crack propagation at the low stress intensity range, while it is faster for the high stress intensity ranges. The results of the current study show more consistency with the result for De Jesus et al., (2012)

where similar fatigue crack propagation behaviour is observed. Due to the different stress ratio, R , values, the curves indicate a small variation, but the difference is not very large.

In general, the linear part of the fatigue crack propagation curve shows two slopes and accordingly two intersection points, C , to da/dN axis are specified. These curves are called two stage crack growth relation in BS 7910 (2013) and the parameters of both parts are given. There is also simplified curve where the linear part of the curve is presented with a constant slope. BS 7910 (2013) recommends the following values for the simplified curve; $C = 5.21 \cdot 10^{-13}$ and $m = 3$. The results of the current study are presented with a constant slope and accordingly these results are compared with the simplified curve of BS 7910 (2013) (see Figure 6.16). The comparison revealed that the fatigue crack growth rate of very high strength steels is similar to the simplified crack growth curve of BS 7910 (2013), which is given for steel with a yield strength up to 700 MPa. The observed small difference confirmed by literature [Barsom et al., 1999]. The main difference was observed at the high stress intensity values region where the fatigue crack propagation in very high strength steel is faster than in mild steels.

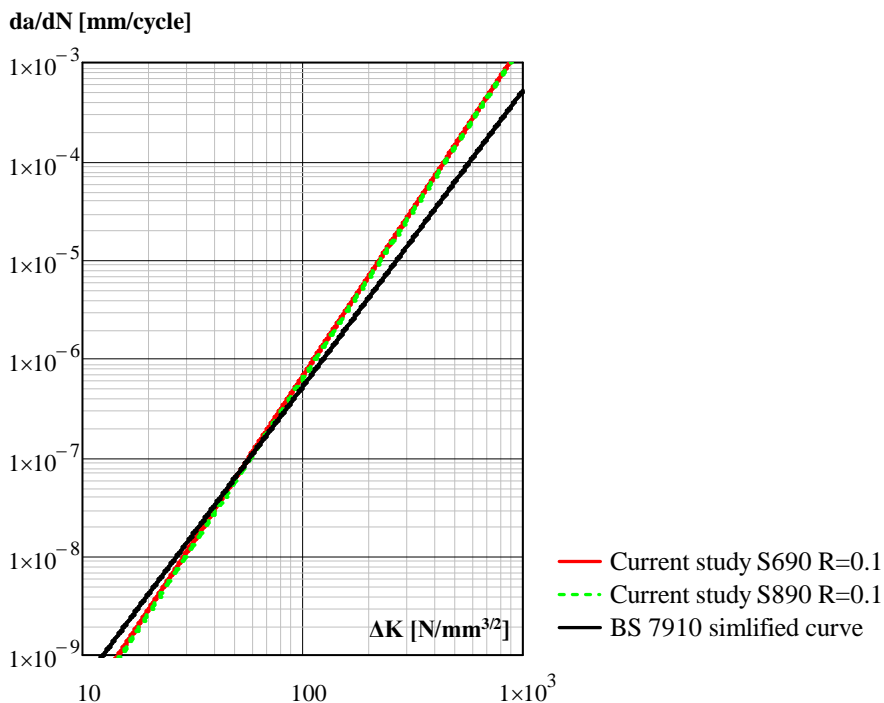


Figure 6.16 The comparison of the test results with simplified curve of BS 7910 (2013).

6.4 Summary

This chapter presents the results of the fatigue crack growth tests on the base material of S690 and S890 high strength rolled steels. The tests were performed to determine material parameters for the Paris fatigue crack growth law and, in addition, the threshold stress intensity factor range aimed to be determined. Fatigue crack growth tests were executed on pre-notched specimens with a four point bending test setup. The pre-notched specimens were prepared according to EN-ISO 12108 (2012). The tests were performed according to this standard with a constant amplitude loading and a constant stress range, R , of 0.1.

Fatigue crack propagation was monitored with a crack detection gauge, a clip gauge, a strain gauge and a camera system. The crack detection gauge was used for the quantitative crack propagation and other crack monitoring devices were used for the visual observation of the crack propagation. Fatigue crack growth rate of the material was calculated according to EN-ISO 12108 (2012) and the results were presented graphically. The material parameters for the Paris fatigue crack growth law were determined from the linear part of the curves and the threshold stress intensity values were specified as the stress intensity range corresponds to the fatigue crack growth rate 10^{-8} .

The test results were statistically analysed and the mean curves and the mean plus two standard deviation (mean +2sd) curves were determined. The mean curves of both steel grades were nearly similar. No significant difference found for the fatigue crack propagation rate. The curves were compared with the results from literature. The main conclusion was that the crack propagation behaviours of high strength steel grades are similar and there is very small difference can be expected.

The obtained material parameters will be used for prediction of the fatigue crack propagation life of repaired V-shape welded specimens. The mean plus two standard deviations was determined based on the recommendation of BS 7910 (2013). However, it is additionally mentioned that these curves satisfy 97.7% probability of survival which means that it already contains some safety range. Nevertheless, the predicted fatigue life will be compared with the test results of V-shape welded specimens which do not contain any safety range. The use of the mean curve plus two standard deviations will lead to very conservative prediction which will show large difference between the prediction life and the test results. Therefore, the material parameters for the mean curves will be used for the prediction fatigue crack propagation life of repaired V-shape welded specimens.

Part III: Analysis of the test results

Part III: Analysis of the test results consists of Chapter 7, Chapter 8 and Chapter 9, where fatigue strength prediction models, the comparison between the predicted fatigue strength and the test data and the results of a statistical analysis are discussed.

Chapter 7 presents a literature review on the fatigue strength prediction models. The notch stress theory is studied for the fatigue crack initiation life prediction. In this context, the fatigue assessment procedures of the FKM guideline and Huck et al. (1981) are used. The fracture mechanics approach is evaluated for the determination of the fatigue crack propagation.

Chapter 8 explains the implementation of the fatigue strength prediction models to the repaired V-shape welded specimens. By means of the prediction models, the effects of the main influence parameters have been studied. The fatigue test results are compared with the predicted fatigue strength according to the models.

Chapter 9 introduces a statistical analysis on the fatigue test data of repaired V-shape welded connections. S-N curves for the repaired specimens are determined and the curves are compared to the fatigue design curves of the standard and in addition, the fatigue strength of repaired V-shape welded connections is compared with the fatigue strength curves of V-shape welded connections in the as-welded condition.

Chapter 7

Literature review

7.1 Introduction

The fatigue strength of materials and connections is mainly determined by experiments. Structural elements and connections between structural elements are scaled down to be tested in laboratory conditions. The results of these scaled down tests are used to predict fatigue life of the structural elements in actual service size. In other words, the test results of scaled down specimens are extrapolated to estimate the fatigue strength of the elements or connections in actual size. The fatigue strength estimation is done with different approaches, nominal stress approach, structural stress approach and local approaches

With the development of computational and image technology, research on the local approaches appears and is focused on the investigation of local material properties and microstructural changes due to fatigue loading. Based on the investigations, it is aimed at obtaining more insight into fatigue crack initiation and propagation phenomena. It is also concentrated on the prediction of the relation between fatigue strength and mechanical properties of the material to reduce the necessity of expensive experimental fatigue strength investigations. Lawrence et al., (1978) developed an analytical model for the fatigue life prediction of the welded connections by using the notch stress approach. Currently, the fatigue strength assessment based on the local approach is included in the fatigue design recommendations of IIW, such as Hobbacher (2016), Fricke (2009), and the FKM guideline. The established analytical approaches are validated with experimental results.

This chapter presents the fatigue life estimation from prediction formulae. Namely, it is concentrated on the notch stress approach for fatigue crack initiation life and the fracture mechanics approach for fatigue crack propagation life. Section 7.2 presents the theory of the notch stress approach. The fracture mechanics approach is dealt with in Section 7.3. Section 7.4 describes an analytical approach for fatigue limit prediction. In Section 7.5, the fatigue assessments according to the FKM guideline are presented.

7.2 Notch stress approach

7.2.1 Background and principles

The notch stress approach was established based on the notch root approach. The notch root approach was utilized for assessing the fatigue strength life up to crack initiation induced by elastic-plastic strain amplitudes at the notch root. The determined fatigue strength properties of the notched specimens are comparable with the fatigue strength of the unnotched specimens. The assumption is that the mechanical material behaviour at the root of the notch is similar to the mechanical behaviour at the crack initiation location of unnotched specimens. In other words, the unnotched specimens are taken from the position of the notch and accordingly, both notched and unnotched specimens have the same microstructure, the same surface conditions, the same residual stress state and the same material volume at the crack initiation location. Figure 7.1 presents the analogy of the notch root approach for notched and unnotched specimens [Radaj, 1996]. The notch root approach was used in two routes: the notch strain approach and the notch stress approach. The notch strain approach focuses on the strain distribution at the notch root, while the notch stress approach is mainly concentrated on the stress state at the notch root.

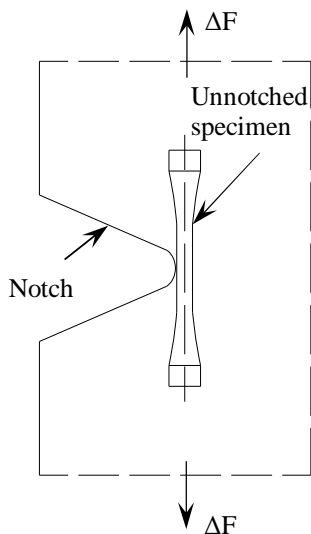


Figure 7.1 Crack initiation location of notched and unnotched specimen [Radaj, 1996].

The principle of the notch stress approach is to compare the stress at the root of the notch with the stress state that does not cause crack initiation in the unnotched specimens. At this stress level, the material is in the elastic stage, without large plastic deformation. Large

plastic deformation will eventually lead to cracks and failures. In this context, the notch stress approach only covers the fatigue crack initiation stage. The stress range to initiate a fatigue crack in a notched specimen should be the same as the fatigue crack initiation range of an unnotched specimen. The difference between these two specimens is the stress increase due to the notch. Thus, the stress range at the fatigue crack initiation of a notched specimen, also called fatigue limit, can be determined by reducing the fatigue limit of an unnotched specimen by the factor of stress concentration factor, K_t due to the notch [Schijve, 2012].

However, experiments have shown that the fatigue strength decrease due to the notch is smaller than by prediction based on a reduction using the elastic stress concentration factor, K_t . This is explained by the ‘microstructural support effect’. This means that the calculated stresses according to the elastic theory at the notch root are not determinant for the fatigue crack initiation. The governing stresses for the fatigue crack initiation are averaged over a small length or volume of the concentrated material. The microstructural support is valid for the sharp and milder notches, which are relatively small. Therefore, the microstructural effect also depends on the geometry of the specimens and especially the notch radius [Radaj et. al., 2006]. The microstructural effect is presented in various forms:

- The stress gradient approach
- The stress averaging approach
- The critical distance approach
- The highly stressed volume approach

The stress, which defines the fatigue behaviour, at the root of a notch, can be expressed as:

$$\sigma_{\text{notch}} = K_f \sigma_{\text{nom}} \quad (7.1)$$

where K_f is the fatigue notch factor and is determined by one of the above mentioned approaches. The relations between the fatigue notch factor, K_f , and stress concentration factor, K_t , shows the susceptibility of the material to notches and is expressed by:

$$\eta = \frac{K_f - 1}{K_t - 1} \quad (7.2)$$

The notch susceptibility, η , is larger for high strength steels than for the low strength steels, which is also experienced in practice. The notch sensitivity of the material increases when the fatigue notch factor, K_f , approaches 1.

For determination of the fatigue notch factor, K_f , various approaches are mentioned for the microstructural effect. The last three of these approaches are commonly used for the fatigue strength assessment of welded connections. The stress averaging approach is mainly used in the context of fictitious notch rounding.

7.2.2 Critical distance approach

Lawrence et al., (1981) have established a calculation procedure to estimate the fatigue strength of welded connections. The first step is to estimate the fatigue crack initiation locations. Subsequently, a stress analysis is performed to determine the elastic stress concentration factor K_t for these locations. The stress concentration factors can be determined by finite element analysis (FEM) or by using engineering formulae from literature for the considered connections. The fatigue notch factor K_f is calculated from the stress concentration factor K_t by using the critical distance approach, which was developed by Peterson (1950). According to this approach, the stress at critical depth α^* below the notch surface should be used for the fatigue effective notch stress and this critical depth is material dependent. Lawrence et al., (1981) approximated it for steels as follows:

$$\alpha^* = 0.025 \cdot \left(\frac{2068}{\sigma_u} \right)^{1.8} \quad (7.3)$$

Peterson (1950) used different values of α^* according to the hardness of the material or based on the ultimate tensile strength of the material. $\alpha^* = 0.254$ is used for soft annealed steel with 170 HB hardness and $\alpha^* = 0.0635$ for quenched and tempered steel with hardness 360 HB. Peterson (1950) determined the relationship between α^* and ultimate tensile strength of material for a notched steel bar under bending loading condition. Table 7.1 shows α^* values from tests of Peterson and compares them to the calculated values using the Lawrence approximation.

Table 7.1 Critical distance value, α^* , from Lawrence and Peterson [Radaj et al., 2006]

σ_u [N/mm ²]		345	518	690	863	1035	1380	1725
α^*	Peterson	0.38	0.25	0.18	0.13	0.089	0.051	0.033
	Lawrence	0.628	0.302	0.18	0.121	0.087	0.052	0.035

The relationship between K_f and K_t is given as:

$$K_f = 1 + \frac{K_t - 1}{1 + \frac{\alpha^*}{\rho}} \quad (7.4)$$

where ρ is the notch radius. The stress concentration factor K_t is mainly affected by the radius of the notch at the weld toe and scattering is shown along the weld toe. Lawrence et al., (1978) suggest using a maximum fatigue notch factor K_f for fatigue analysis. It is stated that the maximum fatigue notch factor K_f is obtained when the radius of the notch is equal

to the critical distance, $\rho = \alpha^*$. It is approximated that the fatigue notch factor K_f can be approximately equal to the stress concentration factor K_t in case of $\rho = \alpha^*$.

7.2.3 Fictitious notch rounding approach

This method was developed by Radaj (2006) and it is established based on the Neuber (1968) microstructural hypothesis. The hypothesis points out that the averaged notch stress in a small amount of material at the maximum stress is decisive for the fatigue crack initiation. In order to average the notch stress, the radius of the notch is fictitiously rounded and by that it reduces the elastic stress concentration factor K_t . The fictitious notch factor is given by:

$$\rho_f = \rho + s \cdot \rho^* \quad (7.5)$$

with the actual notch radius ρ the multiaxiality coefficient, s and the microstructural support length, ρ^* , which is a material constant. This method has mainly been used for low strength steels but it is not restricted to use for high strength steels. The fatigue notch factor K_f is calculated from the stress concentration factor K_t of a fictitiously rounded notch by the following expression:

$$K_f = 1 + \frac{K_t - 1}{\sqrt{1 + \frac{s \cdot \rho^*}{\rho}}} \quad (7.6)$$

The multiaxiality coefficient s depends on the stress state of the notch (plane stress, plane strain, in-plane and out of plane shear loading) and applies the multiaxial strength criterion. The worst case condition is reached when it is assumed that the radius of the real notch ρ is zero and the fictitious notch radius ρ_f become 1 where the fatigue notch factor K_f can be approximated as $K_f = K_t$ ($\rho_f = 1$). The static mean stress effects can be taken into account based on a Haigh diagram, but the Neuber hypothesis, which the approach is derived from, has not yet been verified for non-zero mean stress.

7.2.4 Highly stressed volume approach

Sonsino, (1993) has established this approach to contribute the statistical size effect at the notch and the effect of multiaxial local stress amplitude to the calculation of the notch stress concentration factor K_t . It combines the microstructural notch support effect with the statistical size effect. It is assumed that the fatigue crack initiation takes place at the location of the critical local stress amplitude which depends on the highly stressed volume of the material. Sonsino (1993) defines this volume of the material as the depth below the notch and a surface area where the maximum notch stress has decreased to 90 % of the

maximum stress at the notch. The fatigue notch stress factor can be determined from stress concentration factor, K_t , the endurable notch stress amplitude, σ_{kaE} , and material endurance limit, σ_{aE} .

$$K_f = \frac{\sigma_{aE}}{\sigma_{kaE}} \cdot K_t \quad (7.7)$$

The endurable notch stress amplitude is a function of the highly stressed volume of the material, $\sigma_{kaE} = f(V_{0.9})$.

The highly-stressed volume, $V_{0.9}$ is defined as the area where 90% of the maximum notch stress is exceeded. The depth of the region is determined by the normalized stress gradient, $d_{0.9}$.

$$V_{0.9} = d_{0.9} \cdot w \cdot \frac{\pi \cdot \rho}{8} \quad (7.8)$$

$$d_{0.8} = \frac{1}{\chi} \left(\chi = \frac{1}{\sigma_{notch}} \frac{d\sigma_{notch}}{dn} \right) \quad (7.9)$$

The notch stress gradient depends on the loading condition, the notch radius and the cross section dimensions. The relevant approximated formulae for the notch stress gradient can be found in literature or determined with the FEM analysis. For notches loaded in tension, $\chi = 2/\rho$ represents an appropriate notch stress gradient [Radaj et al., 2006].

7.2.5 Calculation procedure

First, the elastic stress concentration factor K_t for the notch is determined by using an empirical formula or performing a FEM analysis, which needs to be executed based on the elastic theory.

$$K_t = \frac{\sigma_{notch}}{\sigma_{nom}} \quad (7.10)$$

From the elastic stress concentration K_t , the fatigue notch factor K_f needs to be determined by using one of the explained approaches in Section 7.2.2 Section 7.2.3 and Section 7.2.4. When the notch stress, $\sigma_{notch,a}$, is calculated by taking the fatigue notch factor K_f into account, the calculated notch stress will be compared to the allowable notch stress, $\sigma_{notch,all}$. The calculated notch stress should not exceed the allowable notch stress.

$$\sigma_{notch,a} = K_f \cdot \sigma_{nom} \quad (7.11)$$

$$\sigma_{notch,a} \leq \sigma_{notch,all} \quad (7.12)$$

The allowable notch stress can be determined by fatigue tests or by the relationship between the fatigue strength and the static strength of materials.

7.3 Fracture mechanic approach

7.3.1 Background and principles

Fracture mechanics is a discipline that concentrates on the mechanical behaviour of cracks containing elements under loading conditions. Figure 7.2 shows the comparison between the conventional structural design and the fracture mechanics approach. In traditional structural design, the internal stress state, which results from the applied static load, is compared with the static material strength and the design is safe if the static material strength is higher than the applied stress. In case of the fracture mechanics approach, three parameters become important: flaw size, applied stress and fracture toughness of the material. Fracture mechanics assesses the crack containing material with combinations of these three variable parameters.

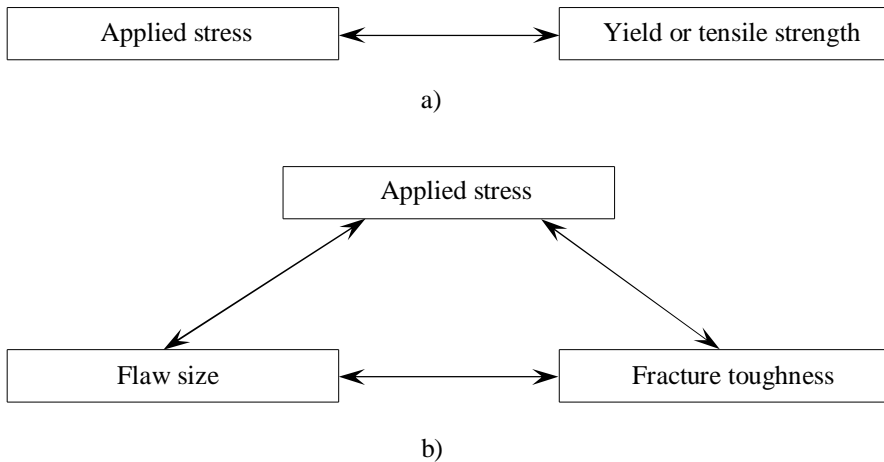


Figure 7.2 Comparison between a) Conventional structural design and b) Fracture mechanics approach [Anderson, 2005].

The fracture mechanics assessment can be performed with two alternative approaches: energy approach and stress intensity approach [Anderson, 2005].

Based on the energy approach, the crack extension occurs when the available energy is high enough to exceed the material resistance for the crack propagation. It is considered that an infinite plate is subjected to a uniform tensile stress. When a crack is created in the plate, the elastic energy in the plate will change, while the remaining ligament of the plate is still exposed to the same tensile stress. The elastic strain energy in the plate decreases by the amount of the stress free material times the elastic energy per unit. In case of crack growth due to loading, the released elastic energy is equal to the work that has been done by an

external force. When the material resistance to the crack propagation is known, the critical load for the crack propagation can be calculated and with the same analogy, vice versa is also possible. In all cases, it is assumed that the material behaviour is elastic. Therefore, this approach is suitable for brittle material. Griffith, (1920) developed this energy theory and it was modified by Irwin (1948) [Janssen et al., 2004].

Irwin suggested that the energy approach can be applied to ductile material as well. According to the modification, the material resistance to crack extension is the sum of the surface energy and the plastic work that occurs during crack extension.

Due to practical difficulties of the energy approach, defining the stress field at a crack tip was still a subject of interest to researchers. Therefore, the stress concentration factor K_t is defined to determine the stress state at the notch root of the notched specimens. The stress concentration concept is applicable to notches with a certain radius. When it is concentrated on the cracks, that have zero radius, the calculated stress according to the stress concentration factor K_t goes to infinity, which is not sensible for actual material. Irwin solved this problem in the 1950s by developing the stress intensity factor K . The stress intensity factor K characterizes the stress field ahead to a sharp crack [Barsom, et al., 2006]. The stress intensity K is calculated by the following general formula:

$$K = Y\sigma\sqrt{\pi a} \quad (7.13)$$

where σ is the applied stress, Y is a dimensionless factor depending on the geometry and a is the crack length. A crack will propagate when the stress intensity factor K at the crack tip exceeds the critical stress intensity value which is a material constant. The critical stress intensity factor K_c depends on the material toughness.

The crack may be exposed to one or more different loading types and these can lead to different crack opening types such as tensile load Mode I, in-plane shear Mode II and out of plane shear Mode III (see Figure 7.3).

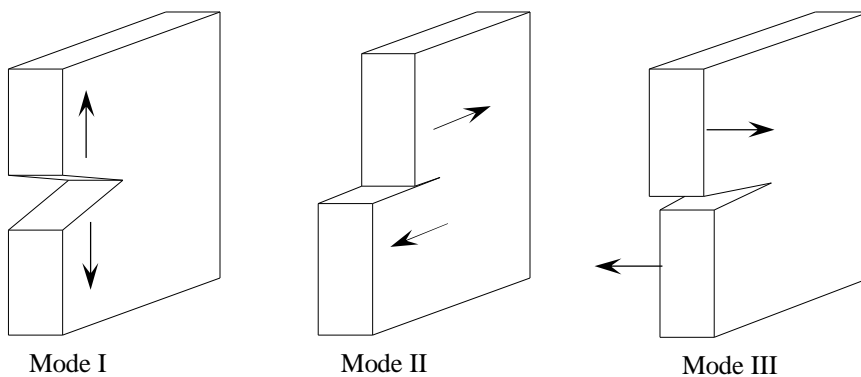


Figure 7.3 Different modes of a crack opening base on the loading conditions.

The crack can be exposed to a combination of different loading conditions. In that case, the stress intensity factor K will be determined for each loading condition separately and then the summation of the determined stress intensity factors represents the stress intensity factor for the combined loading conditions. The superposition of the stress intensity factor can be done for the same structural geometry, the same opening mode and the same crack geometry.

7.3.2 Fracture mechanics approach for fatigue crack growth

Paris et al., (1961) performed fatigue crack growth tests with the same stress ratio, but with different stress ranges. The results of the tests revealed that the crack growth rate is overlapping at certain crack lengths. Moreover, additional tests were executed with the same stress ratio and with different initial crack sizes and stress ranges. The results of these tests have also shown the overlapping of the crack growth rate at certain conditions. The fatigue crack rates versus the stress intensity factors were presented in the same graph and it was seen that the results of both tests are matching, which leads to the conclusion that fatigue crack growth rate is a function of the stress intensity factor range ΔK .

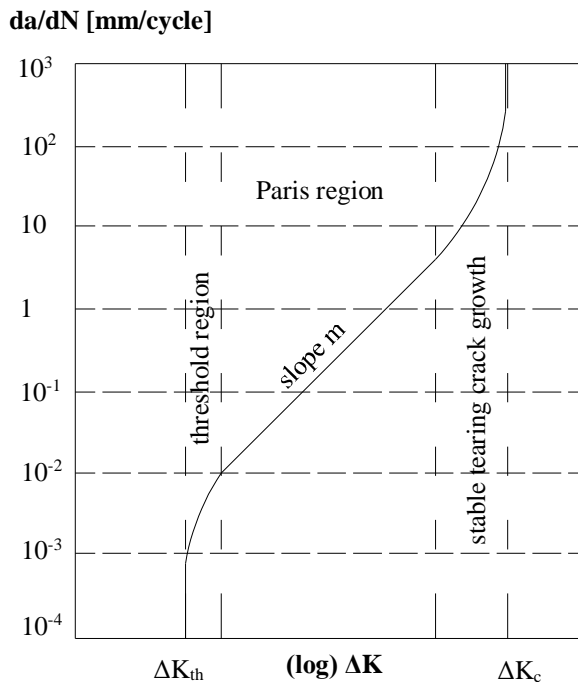


Figure 7.4. The regions of fatigue crack growth rate versus ΔK [Schijve, 2009].

Paris et al., (1963) determined a relationship between the fatigue crack growth rate and the stress intensity factor range of the crack (see equation (7.14))

$$\frac{da}{dN} = C\Delta K^m \quad (7.14)$$

where a is the crack length, N is the number of cycles, ΔK is the stress intensity factor range and C and m represents the material constants. The relation represents the linear part of the fatigue crack growth rate da/dN versus the stress intensity factor range ΔK curve. Extensive experiment results have shown that the $da/dN - \Delta K$ curve has two vertical lines (see Figure 7.4) [Schijve, 2009].

The vertical line on the left hand side represents the threshold stress intensity value. It is assumed that the crack with the stress intensity factor range below the threshold value ΔK_{th} will not grow under fatigue load. The vertical line on the right-hand side presents the critical stress intensity value which lead to a complete failure of the specimens. The remaining ligament of the cross section cannot resist the maximum applied load. In the Paris region, a linear fatigue crack growth was observed and determined with equation (7.14). The material constants in the equation are determined by fatigue crack growth tests. In literature, some values of these parameters are available for different material.

7.3.3 Calculation procedure

For fatigue loaded structures, the fracture mechanics approach is applicable after the crack initiation to determine the fatigue crack propagation life. It is performed by integration of the Paris law from initial (detected) crack a_i to final crack a_f (allowable) size. In this way, the fatigue crack propagation life is determined in terms of number of cycles.

$$N = \begin{cases} \int_{a_i}^{a_f} \frac{da}{C \cdot \Delta K^m} & \text{for } \Delta K > \Delta K_{th} \\ 0 & \text{for } \Delta K < \Delta K_{th} \end{cases} \quad (7.15)$$

The stress intensity values can be determined by FEM analysis or from some empirical formulae available in literature for various shapes of the crack and loading conditions. The empirical formulae are usually a function of the crack depth and the crack length. This makes it difficult to perform the integration analytically. This shortcoming can be solved in two ways. In the first method, the load spectrum (stress range versus number of cycles) is divided into the increments of the number of cycles, ΔN . The equation will be numerically integrated, which gives the crack growth increments in the thickness direction and along the crack direction. The procedure will be repeated for the next increment of number of cycles with adding the crack growth increment of the previous steps to the initial crack size.

In the second method, the thickness of the cross section between the initial crack and the allowable crack is divided into the increments Δa . This method is more suitable for constant amplitude fatigue load. For each increment of the crack, the number of cycles is determined ΔN and the crack length is adjusted based on the calculated number of cycles. The procedure is repeated for the next increment with increasing previously used crack depth with the selected increment and the crack length with the calculated crack length increment. For each step, the number of cycles ΔN will be determined and the fatigue crack propagation life is equal to the summation of each calculated ΔN .

7.4 Prediction of fatigue limit

In general, the fatigue strength of materials is determined with fatigue experiments. The time consuming process and required high costs for the performing experiments trigger researchers to find an analytical tool for the determination of the fatigue strength of the materials. Hence, the fatigue strength of materials is usually expressed either by the yield strength, the tensile strength or the hardness of the material. Radaj (2006) mentioned that the fatigue assessment by a local approach disregards the effects of the microstructure on the fatigue strength.

Murakami (2002) defined fatigue endurance limit amplitude of the material as a function of the hardness. The application of this theory and the expressions are given in Chapter 2. Hüeck et al., (1981) performed the similar work to predict the fatigue endurance limit of the material as a function of the yield strength or the tensile strength of the material. As a result, an analytical approach was developed by Hüeck et al., (1981) which is also summarised by Gudenhus et al., (1995).

According to Hüeck et al., (1981), the fatigue endurance limit amplitude of rolled steel can be expressed by equation (7.16). This expression is valid for fatigue loading with zero mean stress $\sigma_m = 0$ consequent with the stress ratio $R = -1$. This means that the elements are exposed to equal tensile and compression stress amplitudes.

$$\sigma_{aE,0} = 0.426 \cdot \sigma_y + 77 \quad (7.16)$$

Additional expressions are proposed for the determination of the fatigue endurance limit of the material. The effect of the manufacturing process, rolling and casting, is implemented in these expressions that are based on the tensile strength of the material. Equations (7.17) and (7.18) give a relation between the fatigue endurance limit amplitude and the tensile strength for rolled and cast steels respectively.

$$\sigma_{aE,0} = 0.45 \cdot \sigma_u \quad (7.17)$$

$$\sigma_{aE,0} = 0.27 \cdot \sigma_u + 110 \quad (7.18)$$

The fatigue endurance limit amplitude presents a stress value, below which fatigue crack initiation is not expected. The fatigue endurance limit can be extended to the finite fatigue life region. Therefore, it is necessary to determine the slope of the fatigue strength curve and the knee point of the fatigue strength curve. Hüeck et al., (1981) provided equations for these two characteristic parameters of the fatigue strength curve. According to Hüeck et al., (1981), the slope of the curve depends on the fatigue notch factor, K_f and the manufacturing process of the material, cast or rolled steels. The slope k , which is usually indicated by m , of the fatigue strength curve for rolled steels and cast steels is given with the expressions (7.19) and (7.20) respectively.

$$k = \frac{12}{K_f^2} + 3 \quad (7.19)$$

$$k = \frac{5.5}{K_f^2} + 6 \quad (7.20)$$

The knee point of the fatigue strength curves is defined as the number of cycles after which the fatigue strength of the material is constant. The knee point of the fatigue strength curve is expressed as a function of the slope, k . The knee point of the curve is determined by equation (7.21) for rolled steels and equation (7.22) for cast steels.

$$N_{\text{knee}} = 10^{6.4 - \frac{2.5}{k}} \quad (7.21)$$

$$N_{\text{knee}} = 10^{6.8 - \frac{3.6}{k}} \quad (7.22)$$

The equations of the fatigue endurance limit are expressed by either the yield strength or the tensile strength. In order to compare these equations, the relationship between the tensile strength and the yield strength is required. Fourneaux, et al., (2001) determined a relation between the tensile strength and yield strength for high strength steels (see equation (7.23)). The expression was determined based on the extensive tensile coupon tests on S355, S460, S690 and S890 rolled steel.

$$\sigma_u = \sigma \cdot \left(1 - 0.72 \cdot e^{-0.0027 \cdot \sigma_y}\right)^{-1} \quad (7.23)$$

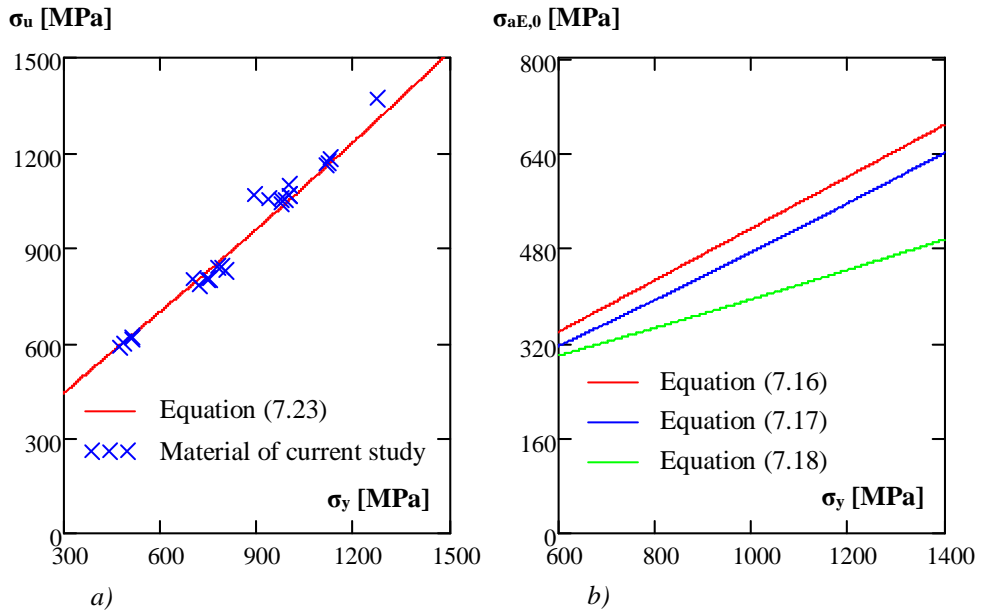


Figure 7.5 a) Comparison of material parameters to equation (7.23). b) Comparison of fatigue endurance limit equations.

Figure 7.5a shows the comparison between the values from equation (7.23) and the material parameters of the current study. The material parameters are given in Appendix A and Appendix B and the material properties are determined from the material certificates. The prediction by equation (7.23) shows good agreement with the material parameters of the current study. Equation (7.23) is substituted in equations (7.17) and (7.18) in order to express all fatigue endurance limit equations as functions of the yield strength. Figure 7.5b presents the comparison between the equations for the fatigue endurance limit predictions. Expressions (7.17) and (7.18) show conservative predictions of the fatigue endurance limit for rolled and cast steel respectively. The expressions provide the fatigue limit amplitude for 50% survival probability.

7.5 Fatigue assessment from the FKM guideline

The FKM guideline (2012) provides analytical procedures for the assessment machine components. Therefore, the guideline is valid for mechanical engineering and related fields. The assessment of the components is performed for static loading and for fatigue loading conditions. For each loading condition, the assessments are performed for the determined stress states such as the nominal stress and the local stress. Moreover, a distinction is made

between assessment of non-welded and welded components for each stress state. In addition, the FKM guideline provides some partial safety factors for the assessments. In this section, the fatigue assessment according to the FKM guideline is summarised for non-welded and welded components with the nominal and the local stress approach.

7.5.1 Nominal stress approach

The fatigue strength assessment is performed using nominal stresses for rod shaped components. The procedure can be extended for other types of components with the appropriate modifications.

7.5.1.1 Non-welded specimens

The fatigue endurance limit amplitude of the material is specified based on the tensile strength of the material for both tensile stresses, equation (7.24) and shear stresses, equation (7.25). The expression for the tensile stresses is used for the axial and the bending loading conditions. The expression for shear stresses is applied for the shear and the torsion loaded components.

$$\sigma_{aE,0} = f_{w,\sigma} \cdot \sigma_u \quad (7.24)$$

$$\tau_{aE,0} = f_{w,\tau} \cdot \sigma_{aE,0} \quad (7.25)$$

where $\sigma_{aE,0}$ is fatigue endurance limit amplitude for tensile stresses, $f_{w,\sigma}$ is the fatigue strength factor for tension loaded components, $\tau_{aE,0}$ is the fatigue endurance limit amplitude for shear stresses and $f_{w,\tau}$ is the fatigue strength factor for shear loaded components. Table 7.2 shows the values of the fatigue strength factors for various materials.

Table 7.2. Fatigue strength factors for the materials, Table 2.2.1 in the FKM guideline.

Material	$f_{w,\sigma}$	$f_{w,\tau}$
Hardening steel	0.40	0.57
Stainless steel	0.40	0.57
Forging steel	0.40	0.57
Steels other than these	0.45	0.57
Steel casting	0.34	0.57
Ductile irons	0.34	0.65
Malleable cast iron	0.30	0.75
Grey cast iron	0.34	1.00
Wrought aluminium alloys	0.30	0.57
Cast aluminium alloys	0.30	0.75

These expressions are valid for completely reversed loading configuration which means, zero mean stress and stress ratio $R = -1$. The number of cycles at the fatigue endurance limit, which is also called knee point, is defined as 10^6 . Furthermore, the used tensile strength value of the material should be valid for 97.5% probability of survival.

Equations (7.24) and (7.25) characterize the fatigue limit of a smooth specimen without taking into account any influences by the structures and environment. The effects of the environment and discontinuities are implemented with additional factors, such as: temperature factor, coating factor, surface treatment factor and surface roughness factor.

The temperature factor $K_{T,D}$ is set to 1 for normal temperatures which are specified for various materials as following:

- for fine grains structural steel from $-40\text{ }^{\circ}\text{C}$ to $+60\text{ }^{\circ}\text{C}$
- for other kinds of steel from $-40\text{ }^{\circ}\text{C}$ to $+100\text{ }^{\circ}\text{C}$
- for cast iron materials from $-25\text{ }^{\circ}\text{C}$ to $+100\text{ }^{\circ}\text{C}$
- for age hardening aluminium materials from $-25\text{ }^{\circ}\text{C}$ to $+50\text{ }^{\circ}\text{C}$
- for non-age hardening aluminium materials from $-40\text{ }^{\circ}\text{C}$ to $+100\text{ }^{\circ}\text{C}$.

For a lower temperature than the given values at above, the FKM guideline is not applicable. The FKM guideline provides the expression for higher temperature applications, where the fatigue endurance limit of the materials shows a reduction. The fatigue testing condition of the current study is therefore a normal temperature. The temperature factor $K_{T,D}$ calculation is not further discussed in this study.

The coating factor K_s takes the effects of the coating layer on the fatigue limit into account. It is applicable to the components made of aluminium. For the rolled and cast steels, it is equal to 1.

The surface treatment factor K_V considers the effects of the treated surface layer on the fatigue endurance limit of the components. The treatment process can change the properties of the surface and consequently, the fatigue endurance limit will be affected, which is taken into account by the surface treatment factor. In the FKM guideline, the surface treatment factors for steel are given for the various treatment methods. For example, for cold rolled steels, it is recommended to use 1.1-1.25 as surface treatment factor. For the material without surface treatment, $K_V = 1$ is used, which is the case for the test specimens of this study.

The roughness factor, $f_{sr,\sigma}$ or $f_{sr,\tau}$ takes the effects of the surface roughness on the fatigue endurance limit of the material into account. For a polished specimen, the surface roughness factor is $f_{sr,\sigma} = f_{sr,\tau} = 1$. The surface roughness factor is determined by equations (7.26) and (7.27) for tensile and shear stress condition respectively.

$$f_{sr,\sigma} = 1 - a_{r,\sigma} \cdot \log(R_z) \cdot \log\left(\frac{2 \cdot \sigma_u}{\sigma_{u,N,\min}}\right) \quad (7.26)$$

$$f_{sr,\tau} = 1 - f_{w,\tau} \cdot a_{r,\sigma} \cdot \log(R_z) \cdot \log\left(\frac{2 \cdot \sigma_u}{\sigma_{u,N,\min}}\right) \quad (7.27)$$

where R_z is the average roughness of the specimens in μm , σ_u is the tensile strength of the material, $f_{w,\tau}$ is the fatigue strength factor for cyclic shear stresses, $a_{r,\sigma}$ and $\sigma_{u,N,\min}$ are constants and given in Table 7.3. It has been found that $R_z = 200 \mu\text{m}$ can be used as average surface roughness for rolling skin, forging skin and casting skin.

Table 7.3 The constants of equations (7.26) or (7.27), Table 2.3.6 of the FKM guideline.

Material	$a_{r,\sigma}$	$\sigma_{u,N,\min}$ [MPa]
Steel	0.22	400
Steel casting	0.20	400
Ductile irons	0.16	400
Malleable cast iron	0.12	350
Grey cast iron	0.06	100
Wrought aluminium alloys	0.22	133
Cast aluminium alloys	0.20	133

The fatigue endurance limit, equation(7.24) or (7.25) of the material, needs to be adjusted with each influence factor. In order to simplify the application of the influence factors, a design factor is introduced with inclusion of each influence factor (see equation (7.28)). The fatigue endurance limit of the material is reduced by the design factor.

$$\begin{aligned} K_{WK,a} &= \left(K_{f,a} + \frac{1}{f_{sr,\sigma}} - 1 \right) \cdot \frac{1}{K_V \cdot K_s} && \text{for axial loading} \\ K_{WK,b} &= \left(K_{f,b} + \frac{1}{f_{sr,\sigma}} - 1 \right) \cdot \frac{1}{K_V \cdot K_s} && \text{for bending loading} \\ K_{WK,s} &= \left(K_{f,s} + \frac{1}{f_{sr,\tau}} - 1 \right) \cdot \frac{1}{K_V \cdot K_s} && \text{for shear loading} \\ K_{WK,t} &= \left(K_{f,t} + \frac{1}{f_{sr,\tau}} - 1 \right) \cdot \frac{1}{K_V \cdot K_s} && \text{for torsion loading} \end{aligned} \quad (7.28)$$

where;

$K_{f,a}$, $K_{f,b}$, $K_{f,s}$, $K_{f,t}$, fatigue notch factor for axial, bending, shear and torsion loading respectively

$f_{sr,\sigma}, f_{sr,\tau}$	surface roughness factor for tensile and shear stress conditions respectively
K_V	surface treatment factor
K_s	the coating factor.

The fatigue notch factor presents the influence of the shape and size of the component on the fatigue endurance limit of the material. The fatigue notch factor can be determined from the stress concentration factor K_t for axial, bending, shear and torsion loading condition. In case of unavailable analytical expression for the stress concentration factor K_t , the fatigue notch factor should be determined from experiments.

$$\begin{aligned}
 K_{f,a} &= \frac{K_{t,a}}{n_\sigma(\rho)} && \text{for axial loading} \\
 K_{f,b} &= \frac{K_{t,b}}{n_\sigma(\rho) \cdot n_\sigma(d)} && \text{for bending loading} \\
 K_{f,s} &= \frac{K_{t,s}}{n_\tau(\rho)} && \text{for shear loading} \\
 K_{f,t} &= \frac{K_{t,t}}{n_\tau(\rho) \cdot n_\tau(d)} && \text{for torsion loading}
 \end{aligned} \tag{7.29}$$

where;

$K_{t,a}, K_{t,b}, K_{t,s}, K_{t,t}$	stress concentration factor for axial, bending, shear and torsion loading respectively
$n_\sigma(\rho)$	$K_t - K_f$ ratio for local stress gradient
$n_\sigma(d)$	$K_t - K_f$ ratio for nominal stress gradient
ρ	notch radius
d	diameter or width of the specimen

The $K_t - K_f$ ratio presents the microstructural support effect and proposed by Siebel & Stieler (1955). The $K_t - K_f$ ratio for nominal stress is calculated according to equation (7.30) which depends on the stress gradient G_σ with mm^{-1} .

$$n_\sigma = \begin{cases} 1 + G_\sigma \cdot 10^{-\left(a_G - 0.5 + \frac{\sigma_u}{b_g}\right)} & \text{if } G_\sigma \leq 0.1 \\ 1 + \sqrt{G_\sigma} \cdot 10^{-\left(a_G + \frac{\sigma_u}{b_g}\right)} & \text{if } 0.1 < G_\sigma \leq 1 \\ 1 + \sqrt[4]{G_\sigma} \cdot 10^{-\left(a_G + \frac{\sigma_u}{b_g}\right)} & \text{if } 1 < G_\sigma \leq 10 \end{cases} \tag{7.30}$$

where G_σ is stress gradient, a_G and b_G are constants and given in Table 7.4 for different materials.

Table 7.4 The constants of equation (7.30) Table 2.3.1 of the FKM guideline.

Material	ag	bG [MPa]
Stainless steel	0.40	2400
Steel except for stainless steel	0.50	2700
Steel casting	0.25	2000
Ductile iron	0.05	3200
Malleable cast iron	-0.05	3200
Grey cast iron	-0.05	3200
Wrought aluminium alloys	0.05	850
Cast aluminium alloys	-0.05	3200

Furthermore, the analytical expression of the fatigue endurance limit amplitude of the material is determined for zero mean stress. For different mean stresses, the fatigue endurance limit amplitude needs to be adjusted by the mean stress factor f_m . The mean stress influences the fatigue crack initiation life. In general, tensile mean stresses reduce the fatigue life, whereas compressive mean stresses increase the fatigue life. In the FKM guideline, the effect of the mean stresses is taken into account by the mean stress factor. Four loading cases are handled: F1; the mean stress remains constant, F2; the stress ratio remains constant, F3; the minimum stress remains constant and F4 the maximum stress remains constant. The loading conditions F2, F3 and F4 are more applicable for specific cases, where the applied stresses are known, whereas F1 loading case can be used for more general cases. Thus, the mean stress factor for F1 loading is used in the current study (see equation (7.31))

$$f_m = \begin{cases} \frac{1}{1 - M_\sigma} & \text{if } \sigma_m < \frac{-1}{1 - M_\sigma} \\ 1 - M_\sigma \cdot \sigma_m & \text{if } \frac{-1}{1 - M_\sigma} \leq \sigma_m \leq \frac{1}{1 + M_\sigma} \\ \frac{1 + \frac{M_\sigma}{3} - \frac{M_\sigma}{3} \cdot \sigma_m}{1 + M_\sigma} & \text{if } \frac{1}{1 + M_\sigma} \leq \sigma_m \leq \frac{3 + M_\sigma}{(1 + M_\sigma)^2} \\ \frac{3 + M_\sigma}{3 \cdot (1 + M_\sigma)^2} & \text{if } \sigma_m \geq \frac{3 + M_\sigma}{(1 + M_\sigma)^2} \end{cases} \quad (7.31)$$

where σ_m is the mean stress and M_σ represents the mean stress susceptibility which is calculated by equation (7.32)

$$\begin{aligned}
 M_{\sigma} &= a_M \cdot 10^{-3} \cdot \sigma_u + b_M && \text{for normal stresses} \\
 M_{\tau} &= f_{w,\tau} \cdot M_{\sigma} && \text{for shear stresses}
 \end{aligned}
 \tag{7.32}$$

Where $f_{w,\tau}$ is the fatigue strength factor, a_M and b_M are constants and given in Table 7.5.

Table 7.5 Constants of equation (7.32), Table 2.4.1 of the FKM guideline.

Material	a_M	b_M
Steel	0.35	-0.10
Steel casting	0.35	0.05
Ductile irons	0.35	0.08
Malleable cast iron	0.35	0.13
Grey cast iron	0.00	0.50
Wrought aluminium alloys	1.00	-0.04
Cast aluminium alloys	1.00	0.20

With the inclusion of all influence factors, the fatigue endurance limit of the material can be calculated by equation (7.33) for axial loading condition. For bending, shear and torsion loading, the appropriate design factor should be implemented in the equation.

$$\sigma_{aE} = \frac{\sigma_{aE,0}}{K_{WK,a}} \cdot f_m
 \tag{7.33}$$

7.5.1.2 Welded specimens

In the FKM guideline, it is assumed that the characteristic fatigue endurance limit of welded specimens is independent of the material strength. The fatigue strength of welded specimens, which can already contain some weld imperfections with allowable sizes, depends on the structural detail, joint type and the weld geometry. Therefore, the material dependent fatigue endurance limit amplitude is not specified for welded specimens.

In the FKM guideline, the fatigue assessment of welded connections is performed with the fatigue design class of IIW recommendation (2016). The characteristic stress range values of the detail classes are utilized for the determination of the fatigue endurance limit amplitude. The characteristic stress range values of the fatigue classes are specified for the stress range at $2 \cdot 10^6$ cycles. However, the fatigue endurance limit for welded specimens is defined as the stress range at $5 \cdot 10^6$ cycles in case of constant amplitude loading. In accordance with this, the characteristic stress range value of the fatigue class need to be extended to $5 \cdot 10^6$ cycles and converted to a stress amplitude. This is done by fatigue class conversion factor f_{FAT} .(see equation (7.34))

$$f_{\text{FAT}} = 0.5 \cdot \left(\frac{N_c}{N_{\text{knee},\sigma}} \right)^{1/k_\sigma} \quad \text{for normal stresses}$$

$$f_{\text{FAT}} = 0.5 \cdot \left(\frac{N_c}{N_{\text{knee},\tau}} \right)^{1/k_\tau} \quad \text{for shear stresses}$$
(7.34)

Where

- N_c number of cycles at characteristic stress range, $2 \cdot 10^6$
- $N_{\text{knee},\sigma}, N_{\text{knee},\tau}$ number of cycles at knee point for normal and shear stresses
- k_σ, k_τ exponent of the S-N curve.

Table 7.6 Number of cycles at knee point and slope of the curve, Table 2.4.3 of the FKM guideline.

Steel and cast irons	Nominal stress		Shear stress	
	$N_{\text{knee},\sigma}$	k_σ	$N_{\text{knee},\tau}$	k_τ
Non-welded	10^6	5	10^6	8
Welded	$5 \cdot 10^6$	3	10^8	5

Table 7.6 shows the specified values of the knee point and the exponent of the S-N curves based on the applied stresses.

The fatigue endurance limit amplitude of the welded component is affected by the thickness of specimens and surface treatment, which is explained as surface treatment factor K_V in Section 7.5.1.1. The thickness effects on the fatigue endurance limit of welded specimens are taken into account by the thickness factor f_t . For the thickness factor f_t , the FKM guideline recommends two cases. In the first case, it refers to the IIW recommendation where the thickness factor is defined by equation (7.35).

$$f_t = \begin{cases} 1 & \text{if } t \leq 25 \\ \left(\frac{25}{t} \right)^n & \text{if } t > 25 \end{cases} \quad (7.35)$$

The second case is recommended for the experienced user or for the industry where extensive experience is available. For the second case, equation (7.36) is recommended.

$$f_t = \begin{cases} 1.1 & \text{if } t \leq 10 \\ \left(\frac{25}{t}\right)^{0.1} & \text{if } 10 < t \leq 25 \\ \left(\frac{25}{t}\right)^n & \text{if } t > 25 \end{cases} \quad (7.36)$$

where t is the thickness of the specimen and n is a constant, which is given in Table 7.7.

Table 7.7 Constant for the thickness factor, Table 2.3.7 of the FKM guideline.

Type of welded joint	n
Cruciform joints, transversely loaded T-joints, sheet with transverse stiffeners, ends of longitudinal stiffeners	
-as welded	0.3
-toe ground	0.2
Transversely loaded butt joints, as welded	0.2
Butt joints ground flush with the sheet, longitudinally loaded welds or gussets	0.1

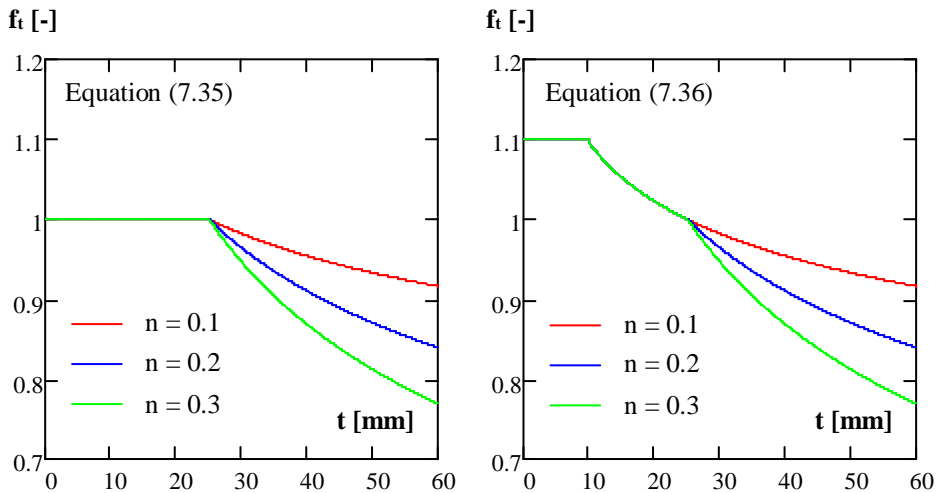


Figure 7.6 Comparison of the thickness factor equations for different exponent values.

Figure 7.6 shows the thickness factor variation for various thickness values according to both equation (7.35) and equation (7.36). The difference between the two cases can be seen for thicknesses up to 25 mm. For specimens thicker than 25 mm, the thickness factor values for both cases are the same. Equation (7.35) uses 25 mm as the reference thickness, while it

is 10 mm for equation (7.36). Moreover, according to equation (7.36), the fatigue endurance limit increases 10% for the specimens thinner than 10 mm.

The welding process introduces residual stresses at surround of the welded connections. The residual stresses influence the applied stress state on the welded connection. Residual tensile stresses increase the effective tensile stresses at the connection, while compressive residual stresses decrease the effective tensile stresses at the connection. Consequently, the residual tensile stresses cause a reduction in the fatigue endurance limit. The effects of the residual stresses are taken into account by the residual stress factor $K_{E,\sigma}$. Moreover, the existence of the residual stress alters the mean stress state in welded joints. The effects of the mean stress are described by the mean stress factor f_m , which is already given in Section 7.5.1. However, in the FKM guideline, a small difference is given for the mean stress calculation for welded connections. The mean stress susceptibility M_σ or M_τ is defined as a function of the intensity of the residual stresses. The residual stress factor $K_{E,\sigma}$ or $K_{E,\tau}$ and the corresponding mean stress sensitivity M_σ or M_τ are given for three residual stress intensity classes in Table 7.8.

Table 7.8 Residual stress factor $K_{E,\sigma}$ or $K_{E,\tau}$ and mean stress sensitivity M_σ and M_τ for welded specimens, Table 2.4.2 of the FKM guideline.

Intensity of residual stresses	$K_{E,\sigma}$	M_σ	$K_{E,\tau}$	M_τ
High	1.00	0.00	1.00	0.00
Medium	1.26	0.15	1.15	0.09
Low	1.54	0.30	1.30	0.17

The definition of the intensity classes is given as follows;

High residual stresses:

Complex thick walled components subject to strong multiaxial stresses
Design related global residual stresses.

Medium residual stresses:

Narrow girders with longitudinal welds and with transverse welds of less than 300 in length,

Transversely stressed welds on specimens with a sheet metal thickness of up to 10 mm,

Longitudinally stressed welds on elements with a sheet metal thickness of up to 16 mm, provided the transverse stress is lower than half the longitudinal stress.

All aluminium welded connections

Low residual stress:

Welding with subsequent stress relief heat treatment

If residual stresses can be ruled out

Not applicable for aluminium welded connections.

After determination of the influence factors, the fatigue endurance limit amplitude of the welded specimens is calculated by multiplying the characteristic stress range of the detail class by the influence factors (see equation (7.37)).

$$\sigma_{aE,w} = \Delta\sigma_c \cdot f_{FAT,\sigma} \cdot f_t \cdot K_v \cdot f_m \cdot K_{E,\sigma} \quad \text{for normal stresses} \quad (7.37)$$

where,

$\Delta\sigma_c$	characteristic stress range of the fatigue class
$f_{FAT,\sigma}$	fatigue class conversion factor or $f_{FAT,\tau}$ for shear stresses
f_t	thickness factor
K_v	surface treatment factor
f_m	mean stress factor
$K_{E,\sigma}$	residual stress factor or $K_{E,\tau}$ for shear stresses

7.5.2 Local stress approach

Fatigue assessment of components is performed by using local elastic stresses. The method is described for non-welded and welded components. There are several similarities between the local stress approach and the nominal stress approach. For similar aspects, reference is made to the sections on the nominal stress approach.

7.5.2.1 Non-welded specimens

The fatigue endurance limit amplitude of the material is specified based on the tensile strength of the material for both tensile stresses, equation (7.24) and shear stresses, equation (7.25). The expression for the tensile stresses is used for axial and bending loading conditions. The expression for shear stresses is applied for shear and torsion loaded components. The validity conditions of the equations are also specified for the local stress approach.

Equations (7.24) and (7.25) specify the fatigue endurance limit amplitude of the material for a smooth specimen. The effects of the shape, geometry, material surface condition and the environment are excluded from the prediction expressions. These effects are included in the prediction by additional adjustment factors, such as temperature factor, coating factor, surface treatment factor and surface roughness factor. The effects of these factors, implementation in the calculation procedure and the value or the expression of the factors are given in Section 7.5.1 for the nominal stress approach. According to the FKM guide, the same values or the expression of these factors should be used for the local stress approach.

Similar to the nominal stress approach, the fatigue endurance limit amplitude of the material needs to be adjusted with each influence factor. For practical application of the influence factors, a design factor is introduced, in which all influence factors are included (see equation (7.38))

$$\begin{aligned}
 K_{WK,\sigma} &= \frac{1}{n_\sigma} \cdot \left[1 + \frac{1}{\check{K}_f} \left(\frac{1}{f_{sr}} - 1 \right) \right] \cdot \frac{1}{K_V \cdot K_s} && \text{for normal stresses} \\
 K_{WK,\tau} &= \frac{1}{n_\tau} \cdot \left[1 + \frac{1}{\check{K}_f} \left(\frac{1}{f_{sr}} - 1 \right) \right] \cdot \frac{1}{K_V \cdot K_s} && \text{for shear stresses}
 \end{aligned}
 \tag{7.38}$$

where;

- n_σ and n_τ $K_t - K_f$ ratio, Section 7.5.1,
- \check{K}_f Estimated fatigue notch factor,
- f_{sr} Surface roughness factor, Section 7.5.1
- K_V Surface treatment factor, Section 7.5.1
- K_s Coating factor, Section 7.5.1.

The estimated fatigue notch factor \check{K}_f presents the influence of the shape and size of the component on the fatigue endurance limit amplitude of the material. The fatigue notch factor, \check{K}_f can be determined from the stress concentration factor K_t for normal and shear stresses. The fatigue notch factor determination based on the stress concentration and the stress gradient is described in Section 7.5.1. For local stress approach, the fatigue notch factor should not be smaller than 1 and the following expression is applicable;

$$\begin{aligned}
 \check{K}_f &= \max(K_{t,\sigma}/n_\sigma; 1) \\
 \check{K}_f &= \max(K_{t,\tau}/n_\tau; 1)
 \end{aligned}
 \tag{7.39}$$

Moreover, some constant values for \check{K}_f are given in the FKM guideline and can be used as approximate values (see Table 7.9).

Table 7.9 Approximate values for fatigue notch factor \check{K}_f , Table 4.3.1 of the FKM guideline.

Material	\check{K}_f
Steel	2.0
Steel casting	2.0
Ductile irons	1.5
Malleable cast iron	1.2
Grey cast iron	1.0
Wrought aluminium alloys	2.0
Cast aluminium alloys	1.2

For calculation of $K_t - K_f$, the stress gradient G_σ or G_τ needs to be determined. The stress amplitudes σ_a are calculated at the points nearby the location of the assessment. This extensive stress computation can be performed by the finite element method (FEM) analysis. From the stress changes, the stress gradient can be determined as follows:

$$G_\sigma = \frac{1}{\sigma_{1a}} \cdot \frac{\Delta\sigma_a}{\Delta s} = \frac{1}{\Delta s} \cdot \left(1 - \frac{\sigma_{2a}}{\sigma_{1a}} \right) \quad \text{for normal stresses}$$

$$G_\tau = \frac{1}{\tau_{1a}} \cdot \frac{\Delta\tau_a}{\Delta s} = \frac{1}{\Delta s} \cdot \left(1 - \frac{\tau_{2a}}{\tau_{1a}} \right) \quad \text{for shear stresses}$$
(7.40)

where,

- σ_{1a}, τ_{1a} stress amplitude at the surface
- σ_{2a}, τ_{2a} stress amplitude at Δs
- Δs distance between the points

Figure 7.7 shows the procedure for the determination of the stress amplitudes at the points to calculate the stress gradient.

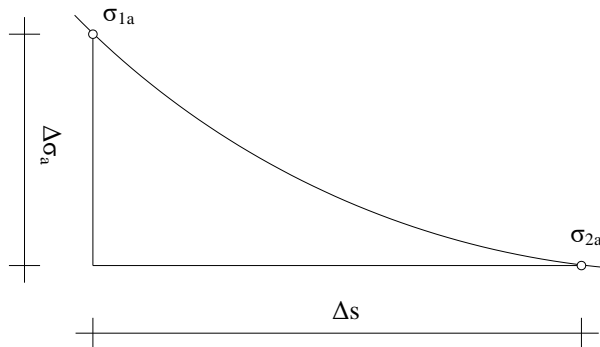


Figure 7.7 Stress amplitudes determined at point near by the assessment location.

When the stress distribution from a FEM analysis is unavailable, the stress gradient can be approximated by using the notch radius ρ and the dimension d of the components. The stress gradient for the normal stresses G_σ and for the shear stresses G_τ is calculated by equation (7.41).

$$G_\sigma = \frac{2}{\rho} + \frac{2}{d} \quad \text{for normal stresses}$$

$$G_\tau = \frac{1}{\rho} + \frac{2}{d} \quad \text{for shear stresses}$$
(7.41)

Furthermore, the analytical expression of the fatigue endurance limit of the material is determined for zero mean stress. For a different mean stress, the fatigue endurance limit

needs to be adjusted by the mean stress factor f_m . The mean stress factor f_m for local approach is the same as the nominal stress approach, which is already explained in Section 7.5.1. With inclusion of all influence factors, the fatigue endurance limit amplitude of the material is expressed by equation (7.42) for nominal stresses

$$\sigma_{aE} = \frac{\sigma_{aE,0}}{K_{WK,\sigma}} \cdot f_m \quad (7.42)$$

7.5.2.2 Welded specimens

The fatigue assessment of welded specimens according to the local stress approach is similar to the fatigue assessment procedure according to the nominal stress approach, which is described in Section 7.5.1.2. The only difference is that the fatigue classes of hot spot approaches are used for the assessment. The assessment is performed with the characteristic stress range values of the hot spot stress curves of IIW recommendation (2016). All adjustment factors are the same as the factors from the nominal stress approach and are applied with the same procedure as the nominal stress approach.

7.6 Summary

This chapter presents the literature review on the fatigue life prediction models. For fatigue crack initiation life, the notch stress approach is studied as well as the fracture mechanics approach for the fatigue crack propagation life.

Hück et al., (1981) defined the fatigue endurance limit amplitude of the material as a function of the yield strength. The expression of the fatigue endurance limit was specified for a smooth specimen under zero mean stress condition. The effects of the notch on the fatigue endurance limit amplitude are included with the fatigue notch factors. The fatigue notch factor presents the fatigue strength reduction due to the notch. The various methods for the fatigue notch factor determination were studied and the critical distance approach value will be used in the current study. The critical distance approach contains the effects of the yield strength on the fatigue strength of the material. The analytical approach of Hück et al., (1981) is specified for the fatigue assessment of non-welded components.

In addition, the FKM guideline also provides fatigue assessments on the non-welded and welded specimens. The FKM guideline presents two fatigue assessment methods: nominal stress approach and local stress approach. The assessment procedures of both approaches are similar and the main difference is that nominal stresses are taken into consideration for the nominal stress approach, while the hot spot stress/local stress state is used for the local stress approach. For non-welded specimens, analytical expressions are given and the expressions are determined for a smooth specimen under zero mean stress loading

condition. For various conditions, the influence factors are given and the fatigue strength according to the analytical expressions are adjusted with these factors. For welded specimens, the FKM guideline uses the characteristic stress range of the S-N curves. The characteristic value is given for $2 \cdot 10^6$ cycles and it is extended to the knee point, where the fatigue endurance limit is defined. Moreover, the effects of residual stresses, mean stress and notches are implemented in the assessment with the influence factors. The determination of the influence factors is explained in the FKM guideline.

In Chapter 8, these prediction models are used to predict the fatigue crack initiation life and the fatigue crack propagation life of the test specimens. The analytical expression will be modified for the implementation in welded connections. The preparation of the specimens and the results of the fatigue tests are already given in Chapter 5.

Chapter 8

Fatigue life prediction

8.1 Introduction

The connection between structural members is inevitable for manufacturing of steel structures. The connections are mainly made with bolts, welding and rivets. Manufacturing of connections introduces discontinuities, such as holes, notches and cross sectional changes which consequently affect the fatigue performance of the structure.

In the current study, it is concentrated on the fatigue strength of repaired fatigue damaged welded connections. Hence, an experimental programme was established and fatigue tests have been performed on the repaired V-shape repaired welded connections made of very high strength steels. The fatigue test results are given in Chapter 5. In addition, the analytical fatigue strength prediction models were studied and the applicability conditions of the models are described in Chapter 7. The comparison between the predicted fatigue strength from the models and the experiments will give more insight into the applicability of the models on welded connections. Moreover, the fatigue strength prediction models are a function of the material strength, loading condition, surface condition of the specimens and the geometry. Eventually, the models provide the opportunity to study the effects of these parameters on the fatigue strength of the material and to evaluate the influence of these parameters as a function of the material strength.

Furthermore, fatigue crack growth tests were performed on the base material of high strength rolled steels. The fatigue crack growth tests were performed on the small scale size specimens. The implementation of the small scaled test results on large scale specimens is also an important issue. Therefore, the results of the fatigue crack growth tests are used for the fatigue crack propagation life prediction of the repaired V-shape repaired welded specimens. In this way, the representativeness of the results from small scale specimens can be evaluated.

In this chapter, the fatigue strength of repaired V-shape welded specimens is predicted by analytical approaches. The fatigue life of the specimens consists of two parts, the fatigue crack initiation life and the fatigue crack propagation life. For the fatigue crack initiation life, the notch stress approach is used, while the fatigue crack propagation life is estimated with the fracture mechanics approach.

Section 8.2 presents the prediction of the fatigue crack initiation life. In Section 8.3, the prediction of the fatigue crack propagation life is described. Section 8.4 shows the comparison between the fatigue test results and the predicted fatigue strength curves.

8.2 Prediction of fatigue crack initiation life

According to the notch stress approach, the fatigue crack initiation life is influenced by the yield strength of material, surface roughness, mean stress level, residual stresses, loading condition, notch radius and weld toe angle in case of welded connections. The fatigue crack initiation life is basically represented by the endurance limit of the parent material or connections. The endurance limit is a stress amplitude, implying that, when the stress amplitude is below this limit, it will cause no fatigue damage. In the current study, two references have been used to determine the fatigue crack initiation life; the FKM, (2012) guideline and the analytical approach developed by Hück et al., (1981) which is summarised by Gudenhus et al., (1995).

8.2.1 Analytical prediction of fatigue endurance limit

The analytical determination of the fatigue endurance limit is described with details in Section 7.4. The fatigue endurance limit of the material is specified based on the yield strength of the material by Hück et al., (1981). As mentioned before, the fatigue endurance limit presents the stress amplitude below which the fatigue life is infinite. According to Hück et al., (1981), the fatigue endurance limit can be extended for the finite fatigue life region. Consequently, the knee point of the fatigue strength curve and the slope of the curve are also specified. These expressions are given for the base material.

However, in the current study, the focus was on effects of the repair weld on the fatigue strength of welded connections made of very high strength steels. It is therefore necessary to modify the model for welded connections. The differences between the base unnotched specimens and the welded specimens are as follows: stress concentration due to the weld geometry, residual stresses and a notch at the weld toe where the fatigue cracks usually initiate. Since the notch stress approach is used for the prediction, the fatigue notch factor K_f is the main parameter for identification of notch stress distribution at the notch. The fatigue notch factor K_f is a function of the stress concentration factor K_t . The determination

of the fatigue notch factor K_f was also described in Section 7.4. The critical distance approach takes the effects of the material strength into account. Hence, in the current study, this approach was used for the calculation of the fatigue notch factor K_f .

Athens et al., (1993) presents the notch stress concentration factors K_t for a butt welded connection as a function of the notch radius, plate thickness and loading conditions (see equation (8.1)) Figure 8.1 presents the definition of the weld toe angle and notch radius. Table 8.1 shows the values for the coefficients of the stress concentration factor.

$$K_t = \left(1 + b_1 \cdot \left(\frac{t}{\rho} \right)^{b_2} \right) \cdot \left(1 + \left[a_0 + a_1 \sin \theta + a_2 \sin^2 \theta + a_3 \sin^3 \theta \right] \cdot \left(\frac{t}{\rho} \right)^{l_1 + l_2 \cdot \sin \left(\frac{\theta + l_3 \cdot \pi}{180} \right)} \right) \quad (8.1)$$

Table 8.1 The parameters of stress concentration factor in equation (8.1).

Factor	a_0	a_1	a_2	a_3	b_1	b_2	l_1	l_2	l_3
Tension	0.169	1.503	-1.968	0.713	-0.138	0.2131	0.2491	0.3556	6.1937
Bending	0.181	1.207	-1.737	0.689	-0.156	0.2070	0.2919	0.3491	3.2830

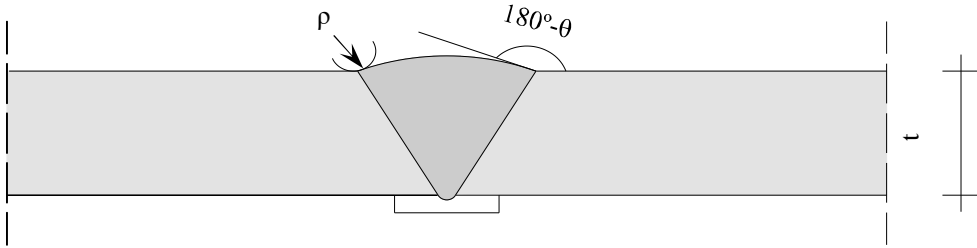


Figure 8.1 Definition of the weld radius and weld toe angel.

After calculation of the fatigue endurance limit amplitude, $\sigma_{aE,0}$, the knee point, N_{knee} , and the slope, k of the fatigue strength curve, the fatigue endurance limit amplitude can be extended to the medium and the high cycle region by equation (8.2)

$$\sigma_a = \begin{cases} \left(\frac{N_{knee} \cdot \sigma_{aE,0}^k}{N_i} \right)^{\frac{1}{k}} & \text{for } N_i < N_{knee} \\ \sigma_{aE,a} & \text{for } N_i > N_{knee} \end{cases} \quad (8.2)$$

The expressions are formulated based on the fatigue endurance limit stress amplitude. In order to compare these with the nominal stresses, the fatigue endurance limit amplitude needs to be converted to the fatigue endurance nominal stress range. Furthermore, in the nominal stress approach, the stress concentration effect of any discontinuity is not included in the calculation. The expressions for the fatigue strength prediction are defined based on

the local stress approach which includes stress due to the notches by the fatigue notch factor. In order to make an appropriate comparison with the test results, the determined fatigue endurance limit stress ranges need to be reduced by the fatigue notch factor. Equation (8.3) shows the expression for converting the calculated fatigue endurance limit amplitude σ_a to the fatigue endurance limit stress range $\Delta\sigma_{nE}$.

$$\Delta\sigma_{nE} = \frac{2 \cdot \sigma_a}{K_f} \tag{8.3}$$

The endurance limit is influenced by the surface roughness condition, the mean stress, the loading mode, the notch radius, the weld toe angle and the thickness of the specimen. The effects of the parameters are studied in the following sections. A similar parametric study on these parameters was also done by Pijpers (2011).

8.2.1.1 Effect of surface roughness

The surface roughness has an influence on the fatigue endurance limit of steel members. Hück et al., (1981) provided an expression for the calculation of the surface roughness factor as a function of the surface roughness value and the tensile strength of the material (see equation (8.4)). Figure 8.2 shows the surface roughness factor for various surface roughness values and the surface roughness factor variation versus to the yield strength of the material.

$$f_{sr, Ni} = 1 - 0.22 \cdot (\log R_z)^{0.64} \cdot \log \sigma_u + 0.45 \cdot (\log R_z)^{0.53} \tag{8.4}$$

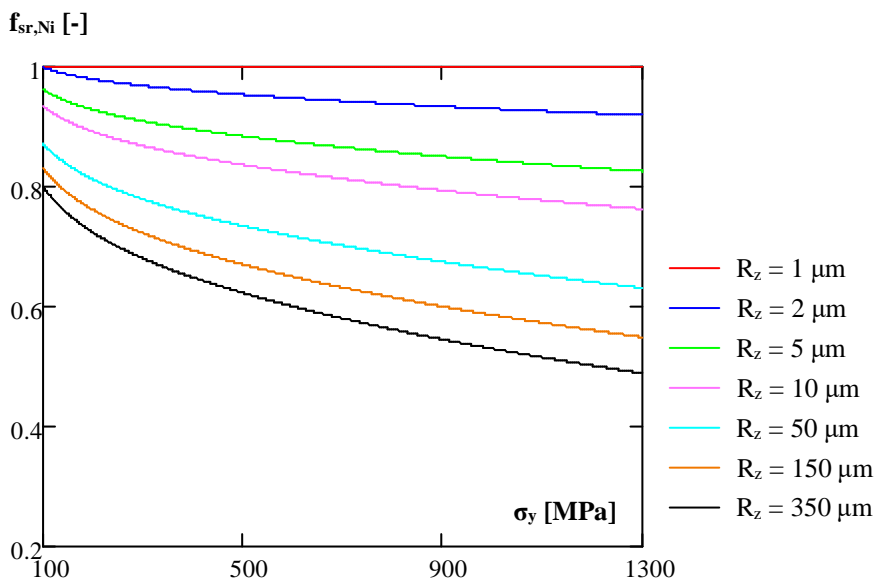


Figure 8.2 Surface roughness factor $f_{sr, Ni}$ for various values of roughness.

The effect of surface roughness on the fatigue endurance stress range is shown in Figure 8.3. The increase of the surface roughness causes a decrease in the fatigue endurance limit which is also mentioned by Schijve, (2009). In addition, the increase of the material yield strength causes a larger reduction in the fatigue endurance stress range with the increase of the surface roughness. This means that fatigue strength of very high strength steels is more susceptible to the surface roughness.

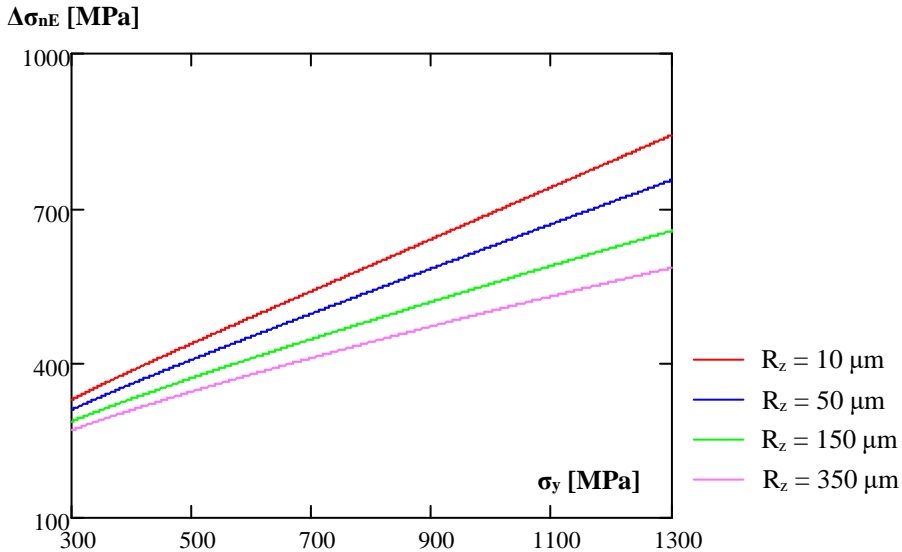


Figure 8.3 Effects of surface roughness on the fatigue endurance stress range.

The surface roughness R_z affects the fatigue crack initiation life of the base material. For welded connections, the effect of the surface roughness will be limited, compared to the notch effect of the weld toe. In accordance with this, the surface roughness factor $f_{sr, Ni}$ is taken as $f_{sr, Ni} = 1$ for the determination of the fatigue crack initiation life of welded connections. For the base material failures, it is calculated according to equation (8.4)

8.2.1.2 Mean stress effect

The increase of the mean stress by keeping the stress amplitude constant results in the larger maximum stresses σ_{max} for cyclic loading. Consequently, the crack will be exposed to a higher stress level which causes for the larger crack opening. It causes reduction in fatigue life and a lower fatigue endurance limit [Schijve, 2009]. Namely, the tensile mean stresses reduce the fatigue life, while the compressive mean stresses increase the fatigue life due to the crack closure effect.

In welded connections, the thermal cycles during the welding process introduce residual stresses in the surrounding of the welded connections. The mean stress is determined by the

stress ratio of the applied load and the induced residual stress during the manufacturing process. Haibach, (2006) proposed an expression for the effects of the mean stress on the fatigue endurance limit. The expression is a function of the mean stress, the residual stress and the endurance limit amplitude (see equation (8.5)).

$$f_m = \begin{cases} \frac{1}{1 + M_f} & \text{if } \frac{\sigma_m + \sigma_r}{\sigma_{aE,0}} < -1 \\ \frac{1}{1 + M_f \cdot \frac{\sigma_m + \sigma_r}{\sigma_{aE,0}}} & \text{if } -1 < \frac{\sigma_m + \sigma_r}{\sigma_{aE,0}} < -1 \\ \frac{1 + \frac{M_f}{3}}{(1 + M_f) \cdot \left(1 + \frac{M_f}{3} \cdot \frac{\sigma_m + \sigma_r}{\sigma_{aE,0}}\right)} & \text{if } 1 < \frac{\sigma_m + \sigma_r}{\sigma_{aE,0}} < 3 \\ \frac{1 + \frac{M_f}{3}}{(1 + M_f)^2} & \text{if } 3 < \frac{\sigma_m + \sigma_r}{\sigma_{aE,0}} \end{cases} \quad (8.5)$$

where,

$$M_f = 0.00035 \cdot \sigma_u - 0.1$$

M_f mean stress subfactor

σ_u tensile strength

σ_m mean stress

σ_r residual stress

$\sigma_{aE,0}$ fatigue endurance limit

Haibach, (2006) proposed the mean stress factor as ratio of the endurance limit amplitude with non-zero mean stress to the endurance limit with zero mean stress, see equation (8.6).

$$f_m = \frac{\sigma_{aE, \sigma_m \neq 0, \sigma_r \neq 0}}{\sigma_{aE, \sigma_m = 0, \sigma_r = 0}} \quad (8.6)$$

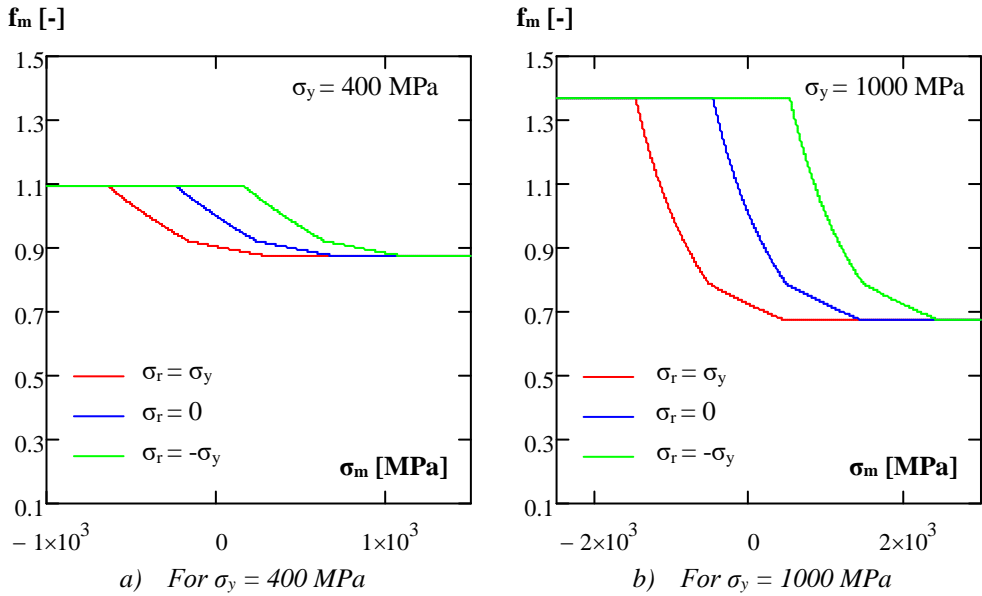


Figure 8.4 Mean stress factor f_m for residual stress level of $\sigma_r = 0$ and $\sigma_r = \pm\sigma_y$.

Figure 8.4 shows the mean stress factor f_m for the material as a function of the yield strength of $\sigma_y=400$ MPa and $\sigma_y=1000$ MPa with the inclusion of the residual stress for three levels $\sigma_r = 0$ and $\sigma_r = \pm\sigma_y$. The graphs clearly illustrate the mean stress susceptibility for high strength steels. When the absolute maximum stress level reaches the yield strength of the material, the mean stress factor f_m becomes the same for each case of the residual stress level. In that case, the cross section deforms plastically and redistribution of stresses will take place. The horizontal lines in Figure 8.4 are the result of this phenomenon.

8.2.1.3 Effect of notch radius

The notch stress concentration factor K_t for welded connection is given by equation (8.1). Anthes et al., (1993) defined this equation as a function of the notch radius ρ , loading mode, weld toe angle θ and the plate thickness t . Figure 8.5 shows the notch stress concentration factor K_t variation for the notch radius as a function of the plate thickness and with weld toe angle $\theta = 25^\circ$, under tension and bending loading conditions. It clearly shows that the lower notch radius causes the high stress concentration factor K_t . In addition, higher stress concentration factors K_t are obtained for the tension loading condition compared to the case of bending loading.

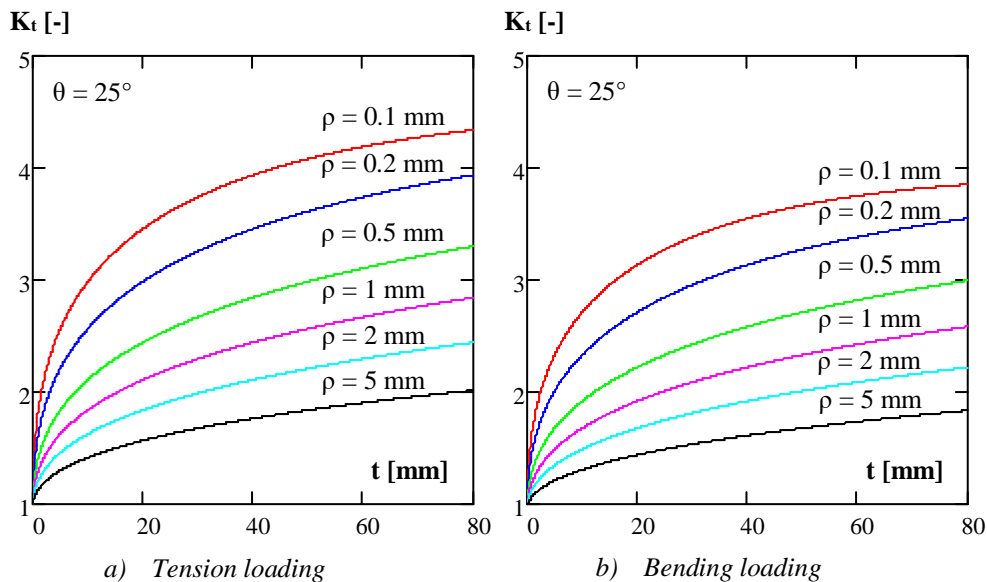


Figure 8.5 The notch stress concentration factor K_t for various notch radius and various plate thickness and for weld toe angle $\theta = 25^\circ$ under a) tension and b) bending loading.

Figure 8.6 presents a comparison between the notch stress concentration factor K_t and the fatigue notch factor K_f as a function of the notch radius ρ for two different yield strength levels $\sigma_y=500$ MPa and $\sigma_y=1000$ MPa and for weld toe angles $\theta = 25^\circ$ and $\theta = 45^\circ$ under the tension loading condition. The fatigue notch factor K_f was calculated according to the critical distance approach (Section 7.2.2). It appears that after notch radius $\rho = 2$ mm, the fatigue notch factor K_f is equal to the stress concentration factor K_t . At smaller notch radii, the stress concentration factor K_t becomes larger than the fatigue notch factor K_f . The increase of the weld toe angle has a significant influence on the stress concentration factor. The increase in the stress concentration factor K_t at near zero notch radius is approximately proportional to the increase of weld toe angle θ and it vanishes for larger notch radii.

As a result of the increase of the stress concentration factor K_t , the fatigue notch factor K_f is also influenced by the change of weld toe angle θ . The increase in the fatigue notch factor K_f is not proportional to the increase of the weld toe angle θ . It is also clearly seen that the fatigue notch factor K_f is higher for high strength steels at small notch radii. It explains the notch sensitivity of high strength steels. The difference in the fatigue notch factor for high strength steels disappears for larger notch radii.

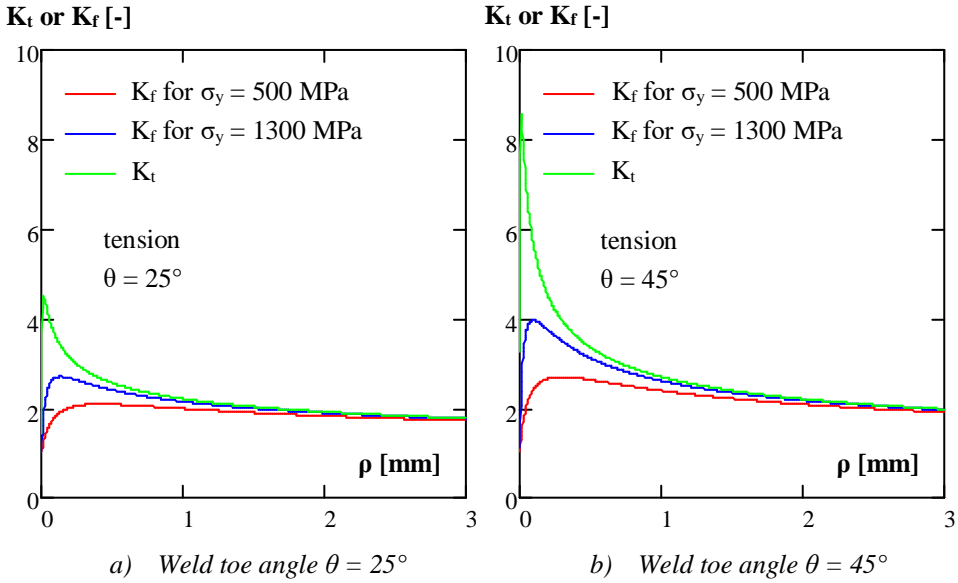


Figure 8.6 Fatigue notch factor K_f and stress concentration factor K_t as a function of notch radius ρ and for two different yield strength levels a) $\theta = 25^\circ$ and b) $\theta = 45^\circ$.

Fricke, (2009), suggests that a notch radius of $\rho = 1$ mm gives a good approximation for the notch stress calculation of the welded connections. This is valid for material thicker than 5 mm. For material thinner than 5 mm, $\rho = 0.005$ is recommended. The notch radius ρ has an effect on the fatigue strength of welded connections in case of $\rho \neq 1$ mm. Then, the notch radius effect on the fatigue endurance limit needs to be taken into account and this can be expressed by equation (8.7).

$$f_{nr, Ni} = \frac{\Delta\sigma_{n, Ni, \rho \neq 1}}{\Delta\sigma_{n, Ni, \rho = 1}} \quad (8.7)$$

Figure 8.7 shows the notch radius factor $f_{nr, Ni}$ for material with a yield strength of $\sigma_y = 300$ MPa, $\sigma_y = 500$ MPa and $\sigma_y = 1300$ MPa, for tension loading and respectively with a weld toe angle of $\theta = 25^\circ$ and $\theta = 45^\circ$.

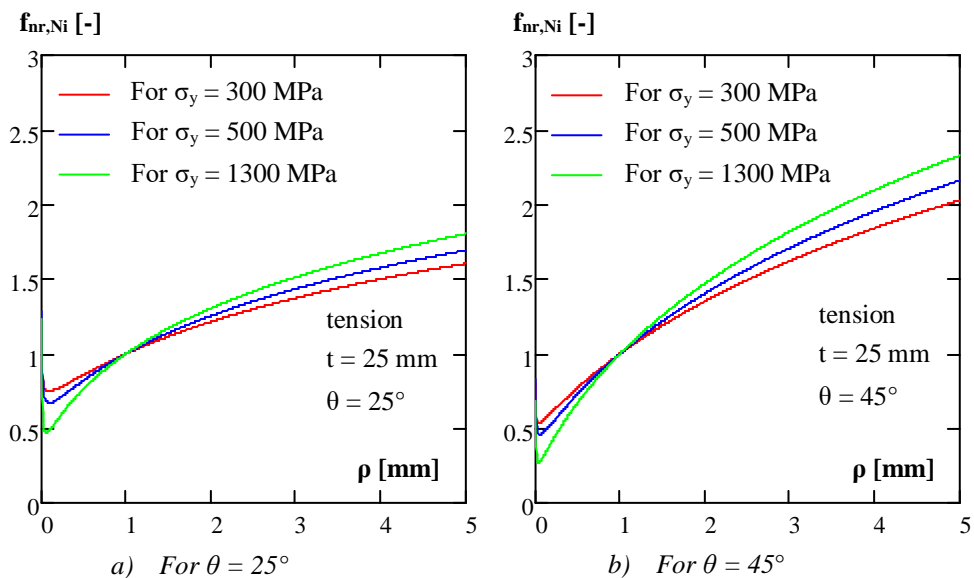


Figure 8.7. Notch radius factor $f_{nr, Ni}$ as function of notch the radius ρ in tension loading for yield strength $\sigma_y = 300$ MPa, $\sigma_y = 500$ MPa and $\sigma_y = 1300$ MPa.

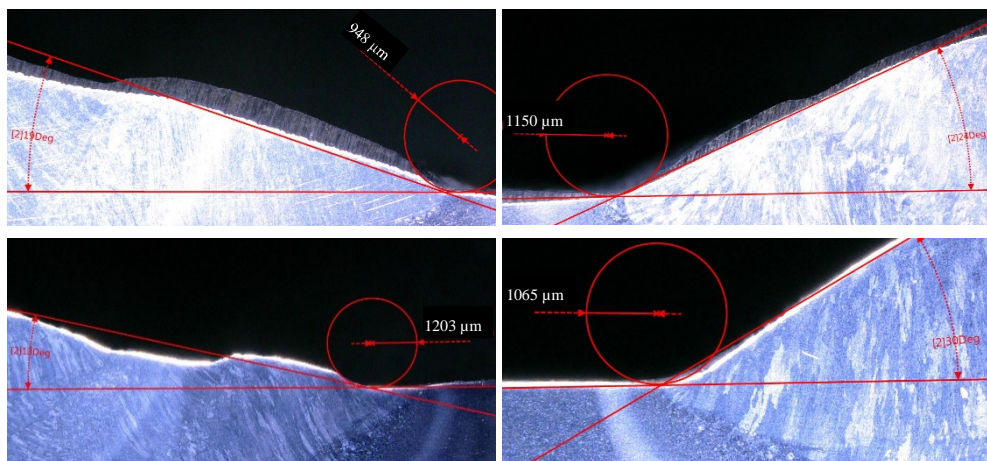


Figure 8.8 Measurements of notch radius and weld toe angle of V-shape welded specimens.

Figure 8.8 presents measurements of the notch radius and the weld toe angle of the V-shape welded specimens of the current study. The assumption for notch radius $\rho = 1$ mm is confirmed by measurements and the weld toe angle θ shows variations between 13° and 30° .

8.2.1.4 Loading mode

The stress concentration factor K_t of welded connections also depends on the loading mode, such as tension or bending. Consequently, the fatigue notch factor K_f is also a function of the loading mode. In case of bending, the stress gradient is larger compared with the tensile loading mode. The detrimental stress concentration effect on the fatigue strength decreases in large stress gradient situations. Consequently, the fatigue notch factor K_t for tension loading mode will be larger than for the bending loading mode. In order to evaluate the test results for the tension loading mode, the test results need to be adjusted with the loading mode factor $f_{lm,Ni}$. The loading mode factor $f_{lm,Ni}$ can be defined as the ratio between the fatigue endurance stress range in case of bending loading and the fatigue endurance stress range in case of tensile loading (see equation (8.8)).

$$f_{lm,Ni} = \frac{\Delta\sigma_{n,Ni,bending}}{\Delta\sigma_{n,Ni,tension}} \quad (8.8)$$

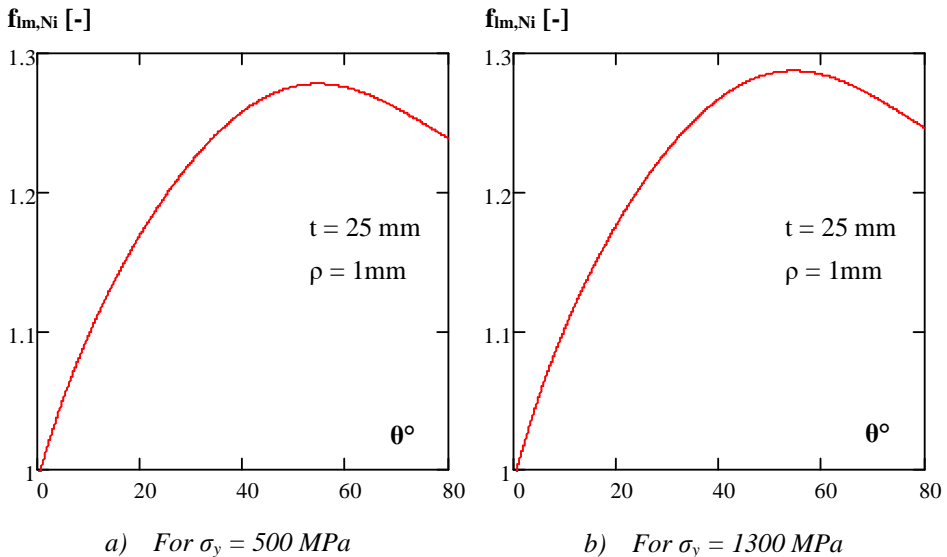


Figure 8.9 The loading mode factor $f_{lm,Ni}$ as a function of yield strength and weld toe angle.

Figure 8.9 presents the influence of weld toe angle θ on the loading mode factor $f_{lm,Ni}$ for two yield strength levels. It is shown that the effect of the material yield strength on the loading mode factor $f_{lm,Ni}$ is relatively small. Figure 8.10 compares the effect of the loading mode factor $f_{lm,Ni}$ of varying thicknesses with different weld toe angles and for two yield strength levels. The effect of the thickness on the loading mode factor $f_{lm,Ni}$ had almost disappeared for the specimens thicker than 20 mm.

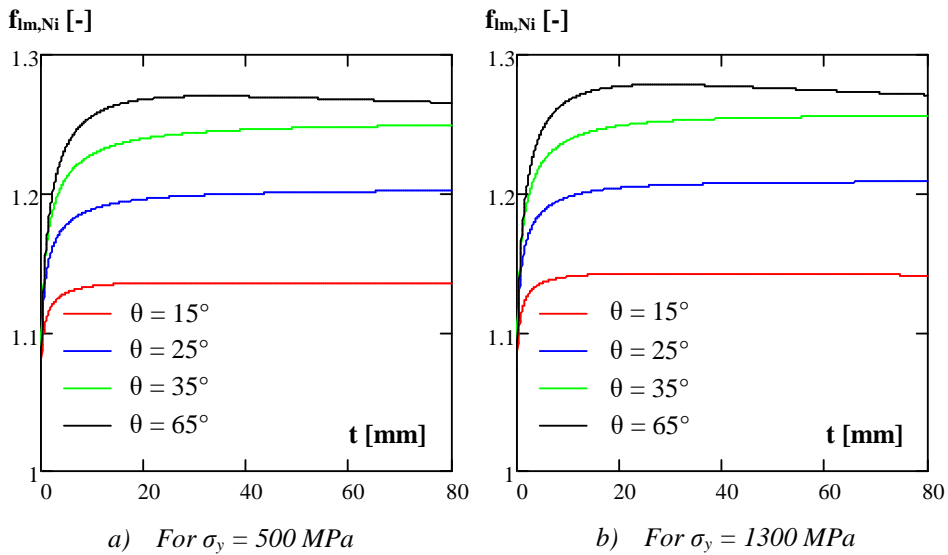


Figure 8.10 The loading mode factor $f_{lm,Ni}$ as function of plate thickness.

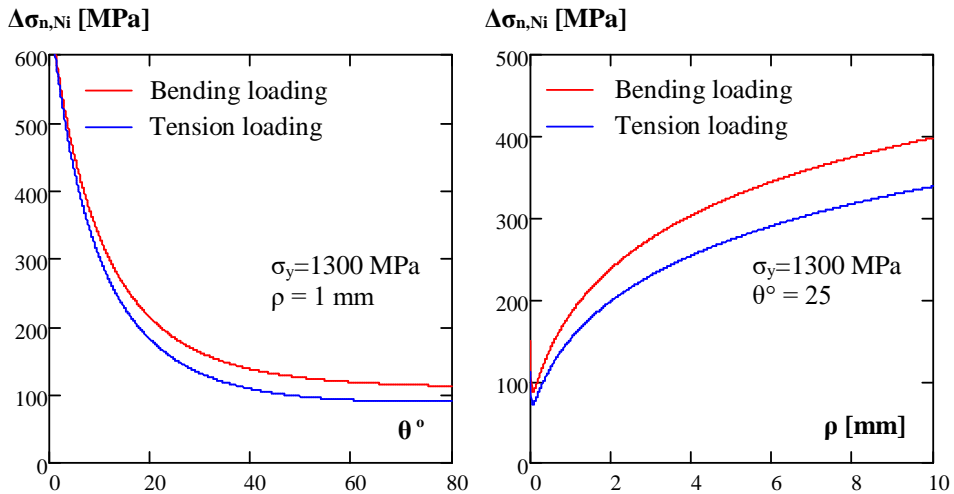


Figure 8.11 The effect of loading mode factor $f_{lm,Ni}$ on the fatigue endurance limit stress range $\Delta\sigma_{n,Ni}$.

Figure 8.11 shows the influence of the loading mode on the fatigue endurance stress range $\Delta\sigma_{n,Ni}$ for the various notch radii ρ and weld toe angles θ . The increase of the notch radii ρ improves the fatigue endurance stress range $\Delta\sigma_{n,Ni}$ and the notch radius ρ has more

detrimental effects on the fatigue endurance stress range $\Delta\sigma_{n,Ni}$ in case of tension loading. The increase of the weld toe angle θ decreases the fatigue endurance limit stress range $\Delta\sigma_{n,Ni}$.

8.2.1.5 Effect of weld toe angle

For the fatigue endurance stress range $\Delta\sigma_{n,Ni}$ prediction, the weld toe angle θ is taken into account for the calculation of the stress concentration factor K_t of the weld (see equation (8.1)). As can be seen from Figure 8.12, the effect of weld toe angle θ on the stress concentration factor K_t significantly decreases after $\theta^\circ = 25$. This weld toe angle is taken as reference and the weld toe angle factor $f_{\theta,Ni}$ is expressed in equation (8.9).

$$f_{\theta,Ni} = \frac{\Delta\sigma_{n,Ni,\theta \neq 25}}{\Delta\sigma_{n,Ni,\theta = 25}} \quad (8.9)$$

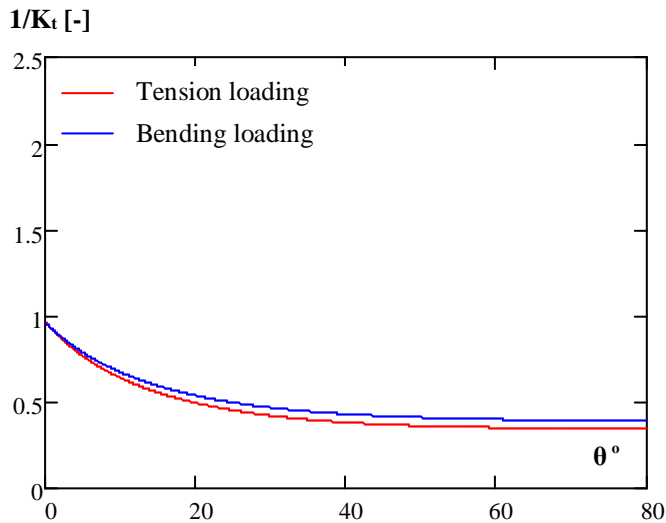


Figure 8.12. The effect of weld toe angle on stress concentration factor.

Figure 8.13 shows the weld toe angle factor $f_{\theta,Ni}$ with variation of the weld toe angle θ for two different yield strength levels. The weld toe angle factor $f_{\theta,Ni}$ is hardly influenced by the yield strength σ_y and loading mode.

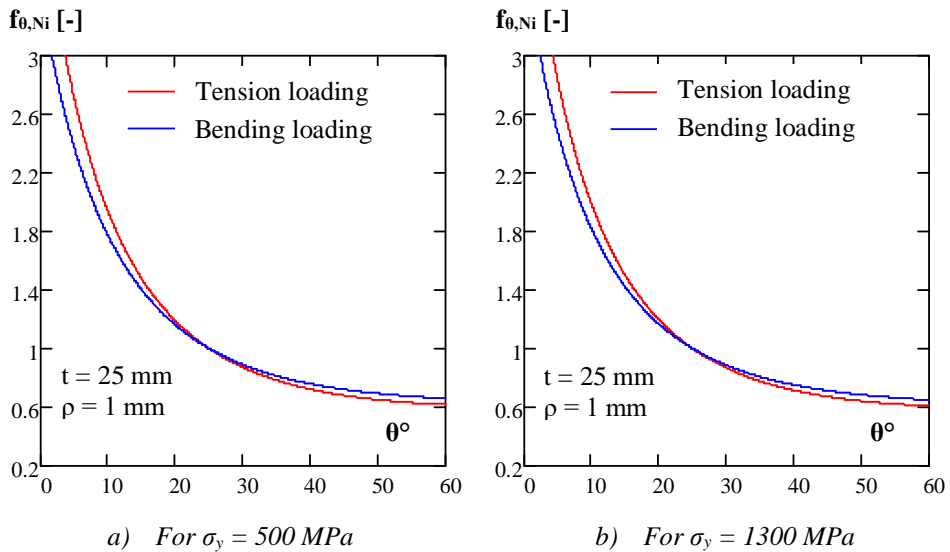


Figure 8.13 Weld toe angle factor $f_{\theta, Ni}$ for loading mode with two yield strength levels.

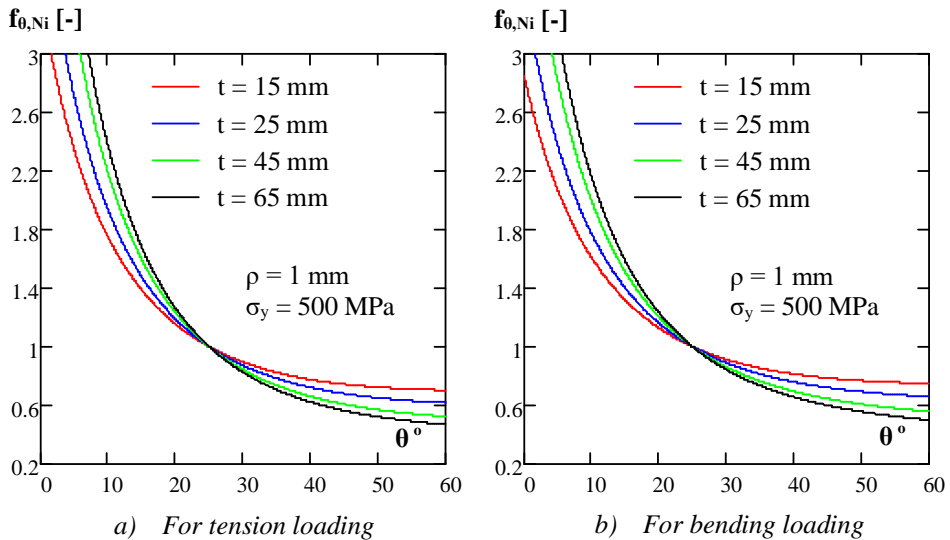


Figure 8.14 Effect of the thickness on the weld toe angle factor $f_{\theta, Ni}$ with loading mode.

Figure 8.14 presents the effect of the thickness on the weld toe angle factor $f_{\theta, Ni}$ for bending and tension loading modes. As also shown in from Figure 8.13, the effect of the loading mode is insignificant, while the weld toe angle factor $f_{\theta, Ni}$ slightly changes with varying thickness.

8.2.1.6 Thickness effect

The plate thickness of the specimens has an influence on the fatigue strength. Thicker plates show a lower fatigue resistance. In EN 1993-1-9 (2006), a reference thickness value is given below which the thickness of the specimens has no influence on the fatigue strength and the reference thickness value is 25 mm. According to EN 1993-1-9 (2006), the thickness factor k_s is calculated by equation (8.10).

$$k_s = \left(\frac{25}{t} \right)^{0.2} \tag{8.10}$$

With the same approach, the fatigue endurance stress ranges of the specimens are affected for the thicknesses above 25 mm. The thickness factor $f_{t,Ni}$ is accordingly defined by the ratio of the fatigue endurance stress range for the case $t \neq 25$ mm and $t = 25$ mm, which is expressed by equation (8.11).

$$f_{t,Ni} = \frac{\Delta\sigma_{n,Ni,t \neq 25}}{\Delta\sigma_{n,Ni,t = 25}} \tag{8.11}$$

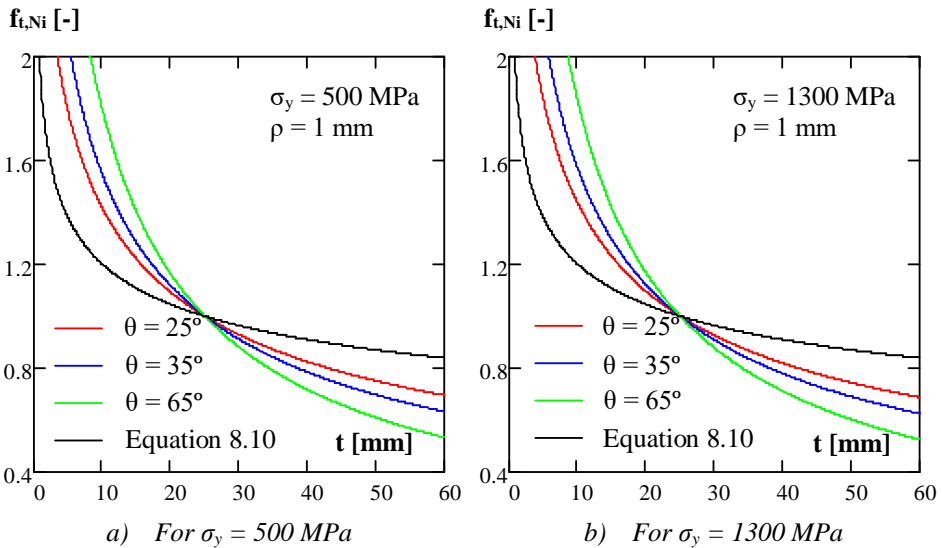


Figure 8.15 Thickness factor $f_{t,Ni}$ for various weld toe angles.

Figure 8.15 presents the thickness factor $f_{t,Ni}$ as a function of thickness for two different yield strength levels and various weld toe angles θ . It also shows that the thickness effect on the fatigue endurance limit is not influenced by the material yield strength. The thickness factor k_s from EN 1993-1-9 (2006) is compared with the established thickness factor $f_{t,Ni}$ according to the analytical prediction model. The comparison shows that the established

thickness factor $f_{t,Ni}$ leads to conservative fatigue strength reduction for the specimens with the thickness above 25 mm.

Figure 8.16 summarises the fatigue endurance stress range for welded structural member with a yield strength of $\sigma_y = 500$ MPa, $\sigma_y = 700$ MPa and $\sigma_y = 100$ MPa. The influence of the loading mode for the given the values of weld toe angle, notch radius, residual stresses and mean stresses can clearly be seen.

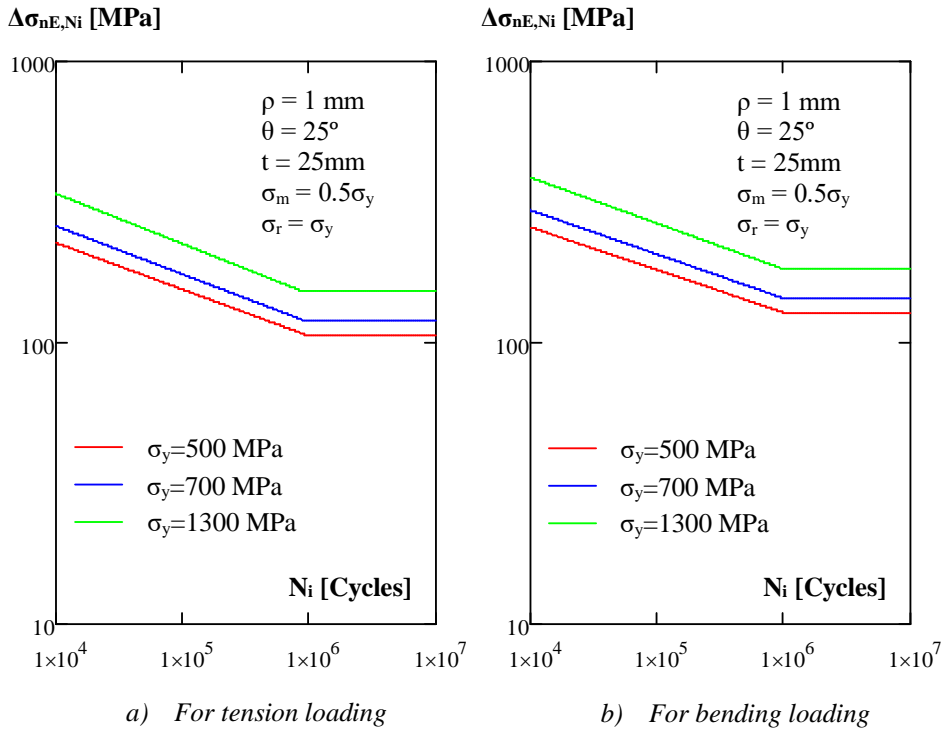


Figure 8.16 The endurable stress range for three yield strength levels.

8.2.2 Fatigue endurance limit prediction according to the FKM guideline

The fatigue assessment procedures according to the FKM guideline are explained in Section 7.5 with details. In this section, the fatigue assessment of the FKM guideline is implemented for the prediction of fatigue endurance limit for welded specimens.

The fatigue assessment according to the FKM guideline is grouped based on the available stress state, such as nominal stress and local stress. Both, the nominal stress and the local

stress approach are applicable for non-welded and welded components. For non-welded components, the fatigue endurance limit is specified as a function of the material tensile strength. The specified expression is valid for a smooth specimen under reverse loading, $R = -1$ condition. In case of variation in specimen surface and loading condition, the fatigue endurance limit of the material is modified with adjustment factors, which are also given in Section 7.5. The fatigue assessment of the welded component is performed by using the characteristic stress range values of the S-N curves from the IIW recommendation (2016). The characteristic stress range values of the S-N curves are given for certain conditions. For other conditions, the FKM guideline provides adjustment factors for the modification of the fatigue endurance limit.

However, the aim of this chapter is to predict fatigue strength of welded connections. The fatigue assessment of welded components according to the FKM guideline is executed with already known fatigue strength. In the current study, the fatigue endurance limit of the welded specimens was therefore determined by the analytical expression of non-welded specimens with some modifications. The difference between a non-welded specimen and a welded specimen is the stress concentration factor due to welding, the residual stress state and the microstructural changes in material due to welding. As mentioned by Radaj (2006), the microstructural effects on the fatigue strength are disregarded for the prediction of the fatigue crack initiation life.

The FKM guideline provides two approaches for fatigue assessment: the nominal stress approach and the local stress approach, which are already explained in Section 7.5.1 and Section 7.5.2 respectively. In the FKM guideline, the assessment procedure was established for the normal stress state and the shear stress state. The test specimens of the current study were exposed to the normal stress condition and therefore the assessment procedure of the normal stress condition is considered in this chapter. Section 8.2.2.1 presents the adaptation of the fatigue assessment of non-welded specimens to the welded component for the nominal stress approach while the modification in the local stress approach is dealt with in Section 8.2.2.2.

8.2.2.1 Nominal stress approach

For non-welded components, the fatigue endurance limit is defined as a function of the tensile strength of the material (see equation (7.24)). The fatigue endurance limit was adjusted with the surface roughness factor f_{sr} , surface treatment factor K_V , coating factor K_s , fatigue notch factor K_f and mean stress factor f_m . In order to implement this analytical approach to welded components, in addition to this, the fatigue endurance limit was modified with the fatigue class conversion factor f_{FAT} , the residual stress factor K_E and the thickness factor $f_{t,Ni}$.

The fatigue notch factor K_f is a function of the stress concentration factor K_t and the stress gradient. The stress concentration factor K_t for a butt weld connection is given by equation

(8.1). As can be seen from equation (7.29), the stress gradient needs to be determined for the nominal stress gradient $G_{\sigma,d}$ and local stress gradient $G_{\sigma,p}$. For the nominal stress gradient $G_{\sigma,d}$, the following expression is recommended in the FKM guideline:

$$G_{\sigma,d} = \frac{2}{t} \quad (8.12)$$

For the local stress gradient $G_{\sigma,p}$ calculation, the expressions are given in the FKM guideline for components with various shapes. The expression for the component in Figure 8.17 is used for the V-shape welded specimens of the current study (see equation(8.13)).

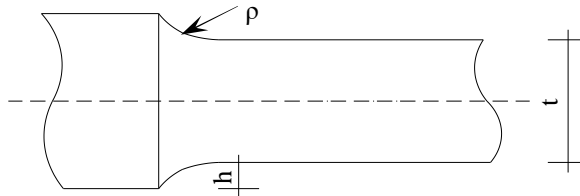


Figure 8.17 Component shape for local stress gradient equations.

$$G_{\sigma,p} = \frac{2.3}{\rho} \cdot (1 + \varphi) \quad (8.13)$$

where,

$$\varphi = \begin{cases} 0 & \text{if } \frac{h}{t} > 0.25 \\ \frac{1}{4 \cdot \sqrt{\frac{h}{\rho}} \cdot 2} & \text{if } \frac{h}{t} \leq 0.25 \end{cases}$$

Figure 8.18 shows the interpretation of the stress gradient expression for the V-shape welded specimens.

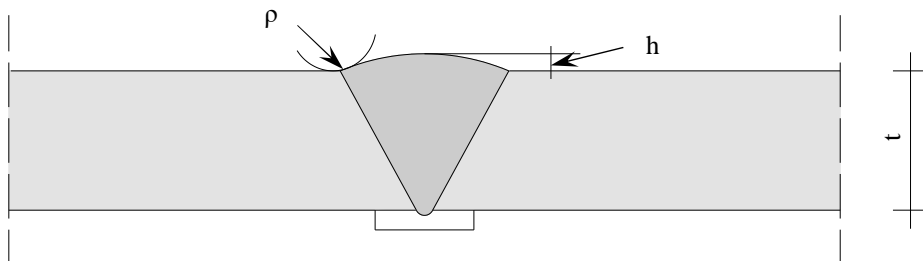


Figure 8.18 The parameters for stress gradient calculation on a V-shape welded specimen.

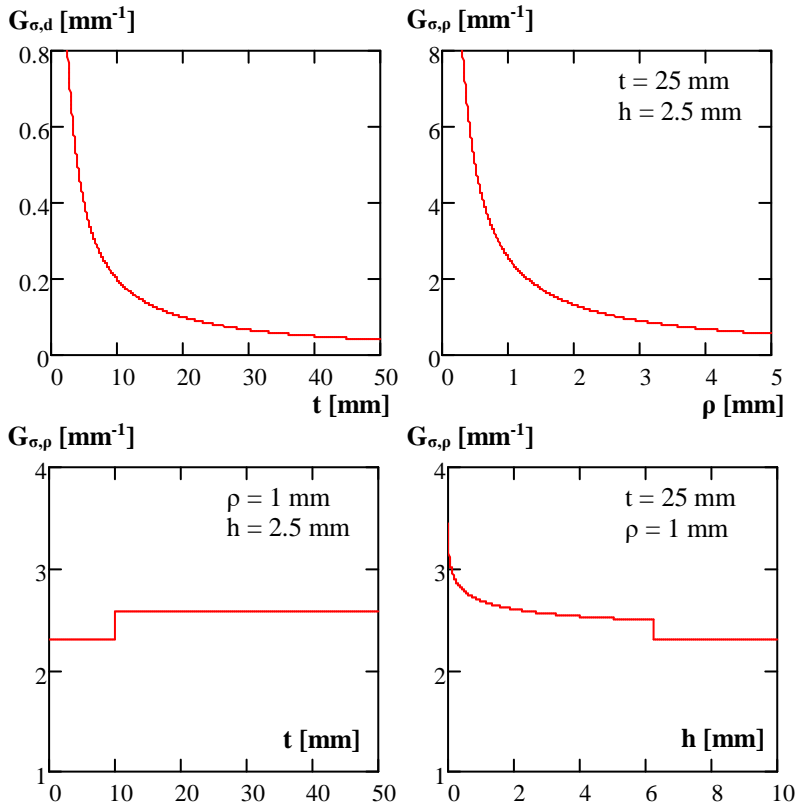


Figure 8.19 The nominal $G_{\sigma,d}$ and the local stress $G_{\sigma,\rho}$ gradient variation.

Figure 8.19 presents the nominal and the local stress gradient variation as a function of thickness, notch radius and the height of the weld cap.

Moreover, the characteristic stress ranges of the S-N curves are given for the stress range at $2 \cdot 10^6$ cycles. The knee point, where the fatigue endurance limit is defined, is specified for the stress range at $5 \cdot 10^6$ cycles. In order to extend the characteristic stress range values of the S-N curves, the fatigue class conversion factor f_{FAT} is used and for the normal stress condition (see equation (7.34), this is equal to 0.37. However, the fatigue endurance limit for non-welded components is identified for the number of cycles at $1 \cdot 10^6$ and it can be extended to the knee point $5 \cdot 10^6$ cycles with the same analogy. In this case, the fatigue class conversion factor is equal to 0.29.

The fatigue limit amplitude at the knee point can be extended to the finite fatigue life region (see equation (8.14)). In order to convert to nominal stress range, the amplitude value is multiplied by 2.

$$\sigma_{na} = \begin{cases} \left(\frac{N_{knee} \cdot \sigma_{aE}^k}{N_i} \right)^{\frac{1}{k}} & \text{for } N_i < N_{knee} \\ \sigma_{aE} & \text{for } N_i > N_{knee} \end{cases} \quad (8.14)$$

For welded specimens, $N_{knee} = 5 \cdot 10^6$ and $k = 3$ are recommended in the FKM guideline (see Table 7.6). Figure 8.20 summarises the fatigue endurance stress range for the welded structural members with a yield strength of $\sigma_y = 500$ MPa, $\sigma_y = 700$ MPa and $\sigma_y = 1300$ MPa according to the nominal stress approach of the FKM guideline.

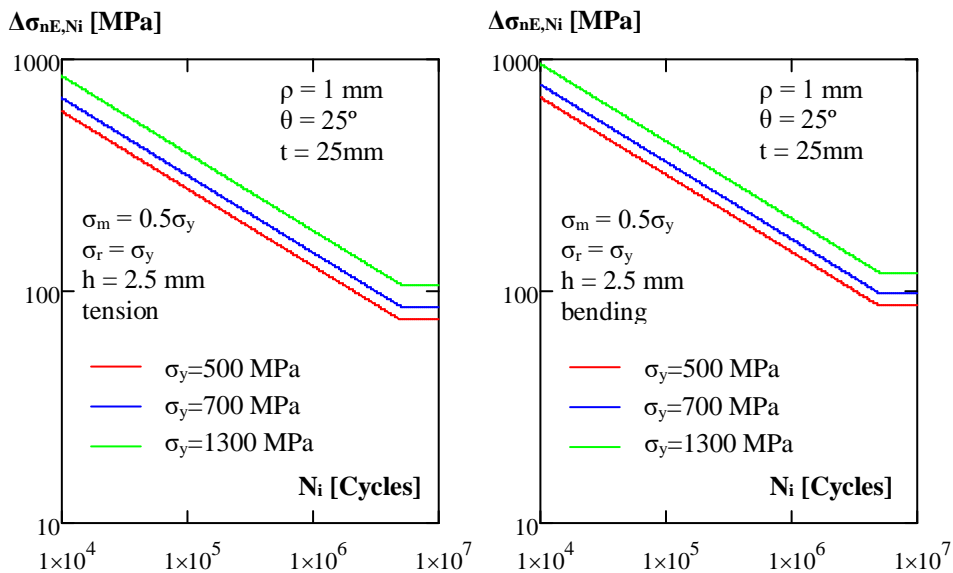


Figure 8.20 The fatigue endurance limit range for three yield strength levels.

8.2.2.2 Local stress approach

The procedure for the local stress approach is described in Section 7.5.2 for non-welded and welded components. For non-welded components, the fatigue endurance limit is specified as a function of the tensile strength of the material and the expressions for the nominal stress approach are valid for the local stress approach. After that the determined fatigue limit is multiplied by factors that affect the fatigue strength of the component. In case of welded components, the characteristic stress range of the S-N curves are used for the fatigue assessment. Since the local stress state is used for the assessment, the fatigue endurance limit is determined according to the characteristic stress range from the S-N curves of the hot spot stress approach.

In the current study, the endurance limit for non-welded specimens was modified to determine the fatigue endurance limit of repaired V-shape welded specimens. The fatigue

endurance limit of non-welded specimens was adjusted with the fatigue notch factor K_f , the surface roughness factor f_{sr} , surface treatment factor K_V , the surface coating factor K_s and the mean stress factor f_m . In addition, the fatigue endurance limit was modified with the fatigue class conversion factor f_{FAT} , the residual stress factor K_E and the thickness factor $f_{t,Ni}$ to take the effects of the welded connections into account.

The characteristic stress ranges of the S-N curves are given for the stress range at $2 \cdot 10^6$ cycles. The knee point, where the fatigue endurance limit is defined, is specified for the stress range at $5 \cdot 10^6$ cycles. In order to extend the characteristic stress range values of the S-N curves, the fatigue class conversion factor f_{FAT} is used and for the normal stress condition (see equation (7.34)). This is equal to 0.37. However, the fatigue endurance limit for non-welded components is identified for the number of cycles at $1 \cdot 10^6$ and it can be extended to the knee point $5 \cdot 10^6$ cycles with the same analogy. In this case, the fatigue class conversion factor is equal to 0.29.

The fatigue notch factor K_f is a function of the stress concentration factor K_t and the stress gradient G_σ . The expression for the stress concentration factor K_t of a V-shape welded connection is given by equation (8.1). In the FKM guideline, it is recommended to determine the stress gradient by FE analysis. If the results of a FE analysis are not available, equation (8.15) is recommended for the stress gradient of the normal stress state and it is used for the prediction model in the current study.

$$G_\sigma = \frac{2}{\rho} + \frac{2}{t} \quad (8.15)$$

Figure 8.21 shows the influence of the notch radius and the plate thickness on the stress gradient, G_σ . The notch radius has a significant effect on the stress gradient for thinner plates up to 10 mm.

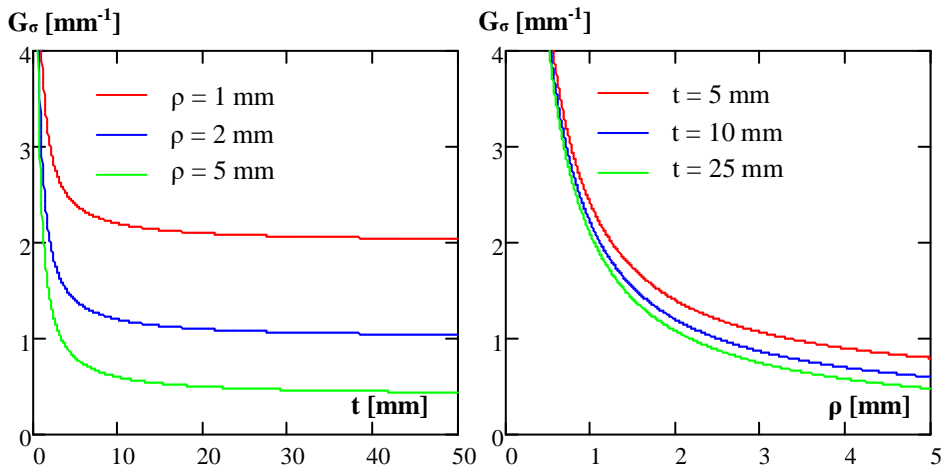


Figure 8.21 The stress gradient variation as a function of the thickness and notch radius.

The fatigue endurance limit amplitude value can be extended to the finite fatigue life region with expression (8.16).

$$\sigma_{na} = \begin{cases} \left(\frac{N_{knee} \cdot \sigma_{aE}^k}{N_i} \right)^{\frac{1}{k}} & \text{for } N_i < N_{knee} \\ \sigma_{aE} & \text{for } N_i > N_{knee} \end{cases} \quad (8.16)$$

The fatigue endurance limit amplitude σ_a was converted to the fatigue endurance stress range limit $\Delta\sigma_E$ by multiplying it by a factor of 2. During the fatigue test of the current study, the applied nominal stresses were measured. In the prediction model of the local approach, it was concentrated on the local stress at the notch root. In order to compare the test results with the results of the prediction, it is required to convert the local stress range to the nominal stress and this is done by dividing the local stress range by the stress concentration factor (see equation (8.17)).

$$\Delta\sigma_{naE} = \frac{2 \cdot \sigma_a}{K_t} \quad (8.17)$$

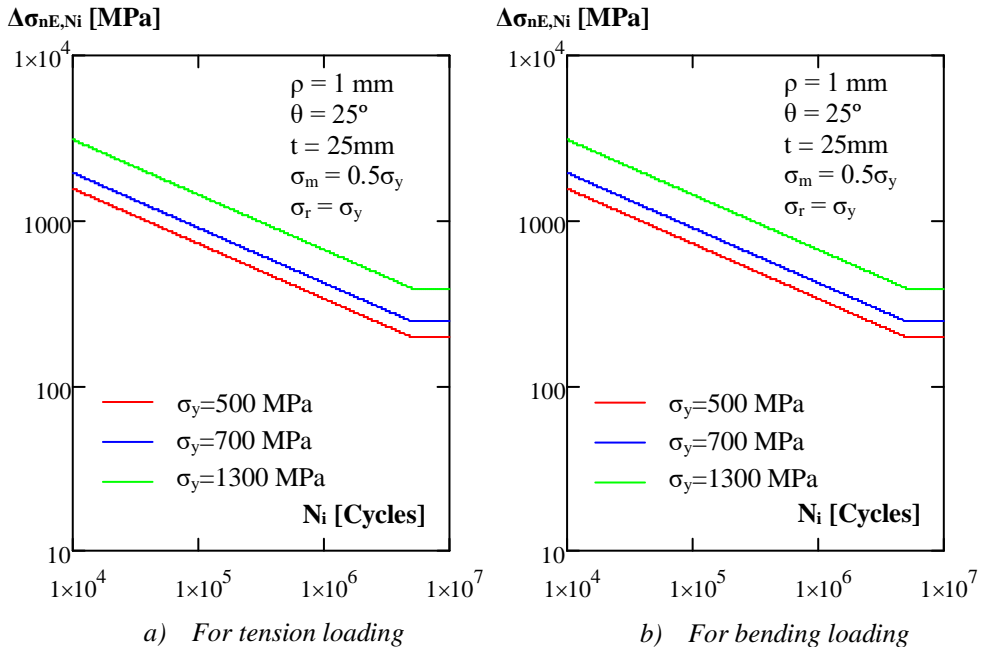


Figure 8.22 The fatigue endurance limit according to the local stress approach of the FKM guideline for three yield strength levels.

Figure 8.22 summarises the fatigue endurance stress range for the welded structural member with a yield strength of $\sigma_y = 500$ MPa, $\sigma_y = 700$ MPa and $\sigma_y = 1300$ MPa according to the local stress approach of the FKM guideline. In the local stress approach,

the stress gradient and consequently the fatigue notch factor is determining for the normal stress and shear stress state. The normal stress state contains tensile and bending stress conditions. Therefore, the loading mode has no influence on the fatigue endurance limit stress range for the local stress approach.

Figure 8.23 compares the fatigue endurance limit prediction models for material with a yield strength of $\sigma_y = 800$ MPa. The fatigue strength curves are determined for the analytical model of Hüeck et al., (1981), the nominal stress approach and local stress approach of the FKM guideline. The analytical approach of Hüeck et al., (1981) defines the knee point and the slope of the curve as a function of the fatigue notch factor. For the prediction models of the FKM guideline, these parameters are given as constant values (see Table 7.6). Therefore, the models show a very large deviation in the finite fatigue life region. As can be seen from the figure, the fatigue endurance limit stress range according to the analytical mode of Hüeck et al., (1981) and the nominal stress approach from the FKM guideline shows good agreement for both tension and bending loading modes. The prediction from the local stress approach of the FKM guideline shows a higher fatigue endurance limit which is in accordance with the local stress state. In other words, the fatigue endurance limit is not converted to the nominal stress state. For the conversion, the fatigue endurance limit for the local stress state needs to be divided by the stress concentration factor K_t .

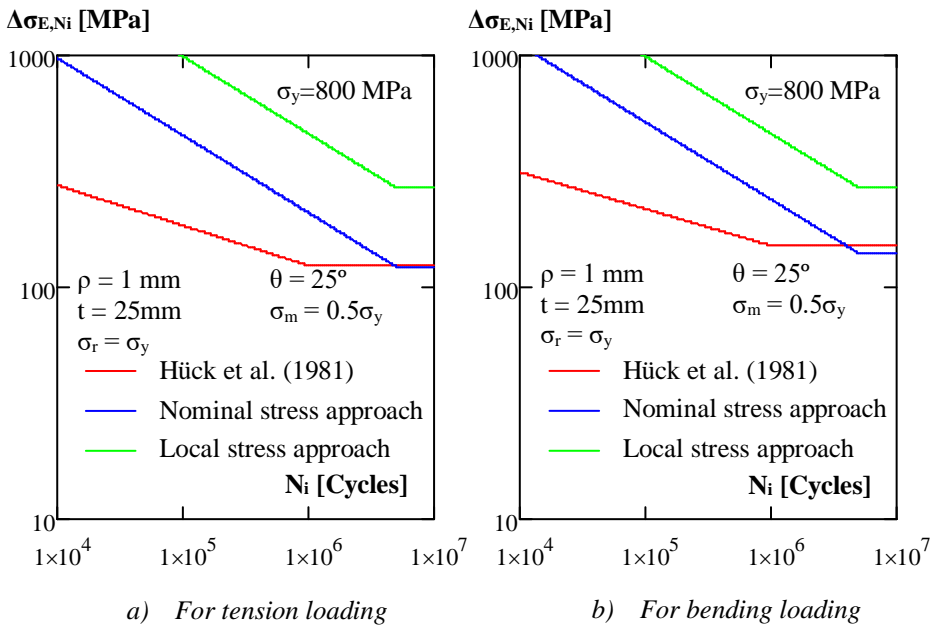


Figure 8.23 Comparison of the prediction models.

Figure 8.24 shows the comparison of the prediction models after the conversion and the fatigue endurance limit from the local stress approach of the FKM guideline converges with the fatigue endurance limit of the nominal stress approach of the FKM guideline as expected.

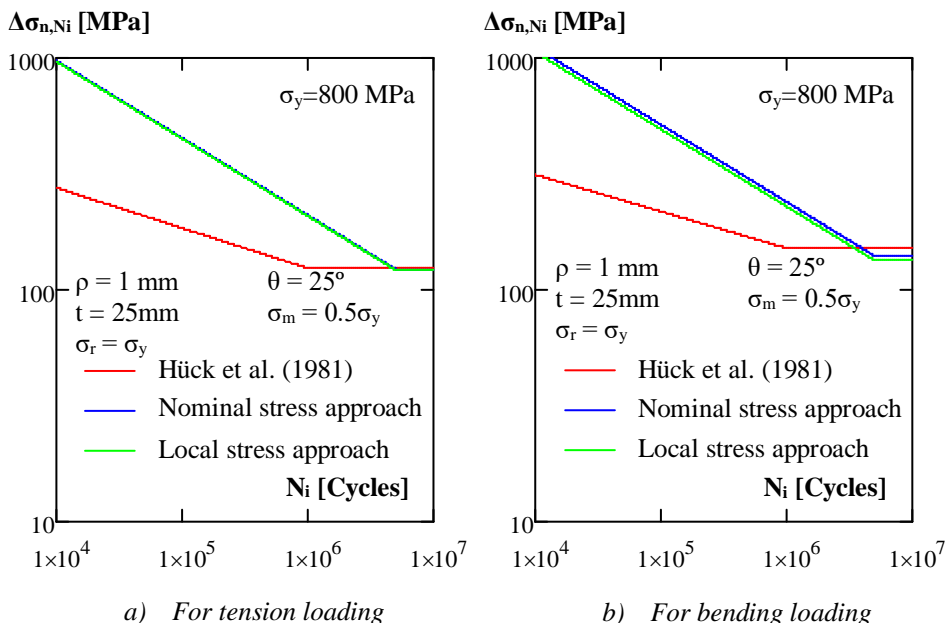


Figure 8.24 Comparison of the prediction models for nominal stress state.

8.3 Prediction of fatigue crack propagation life

Fatigue cracks originate from local defects or discontinuities. After fatigue crack initiation, the crack will propagate under fatigue loading. The fatigue crack growth life is predicted by using the fracture mechanics approach and is explained in Section 7.3.2. The fatigue crack propagation life is calculated by integration of the Paris equation (see equation (7.14)). The main parameter in the equation is the stress intensity factor range ΔK which is a function of the crack size, the applied stress range and the local geometry of the connection. Stress intensity factors can be determined from FEM analysis and in addition, extensive stress intensity factor solutions are available in literature. The procedure to calculate the fatigue propagation life is clearly explained in BS 7910 (2013). This standard also provides stress intensity factor solutions for various crack shapes. In the current study, the stress intensity values are calculated according to this standard.

When a crack is exposed to fatigue loading, it propagates in two directions: through thickness of the section and along the crack length. Figure 8.25 shows the shape of possible fatigue crack and size parameters; depth a , length $2c$. It is assumed that the material parameters in the Paris equation are the same for the crack propagation in both directions. The crack growth rate difference in the directions is implemented in the stress intensity factor solutions. The crack growth rate in depth and longitudinal directions is determined by equations (8.18) and (8.19) respectively.

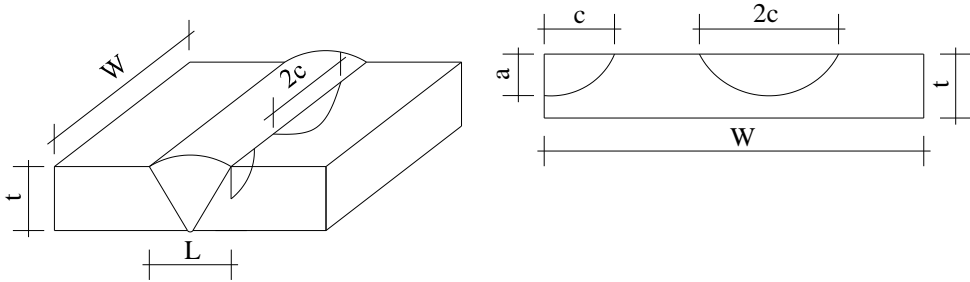


Figure 8.25 Crack shapes in a V-shape welded specimen.

$$\frac{da}{dN} = C\Delta K_a^m \quad (8.18)$$

$$\frac{dc}{dN} = C\Delta K_c^m \quad (8.19)$$

BS 7910 (2013) gives stress intensity factor solutions as function of the crack depth a , crack length $2c$, the thickness of specimen t and the width of the component W . For a crack in the stress concentration region, like in welded connections, an additional correction factor is used which is a function of weld width L , crack depth a , crack location and material thickness t . In accordance with this, the stress intensity factor range ΔK for welded connections is calculated by equation (8.20).

$$\Delta K = M \cdot f_w (M_{km} \cdot M_m \cdot \Delta\sigma_m + M_{kb} \cdot M_b \cdot \Delta\sigma_b) \quad (8.20)$$

M	bulging correction factor
f_w	net area correction factor
M_{km}	stress concentration correction factor of membrane stress component
M_m	crack depth shape factor for membrane stress component
M_{kb}	stress concentration correction factor of bending stress component
M_b	crack depth shape factor for bending stress component
$\Delta\sigma_m$	membrane stress range component
$\Delta\sigma_b$	bending stress range component

The stress intensity factor range ΔK was calculated for the crack growth through thickness and along the crack length. For both cases, the same stress intensity factor formula was used and the difference was implemented in correction factors.

The numerical integration of the Paris equation was programmed in a Mathcad routine and is used for the prediction of fatigue crack growth life. The Mathcad routine calculates the crack growth in depth and width directions and provides the number of cycles for crack growth from the initial crack size until the allowable crack size. If the initial crack is not known, BS 7910 (2013) recommends to use $a_i = c_i = 0.15$ mm as initial crack depth. The whole procedure was established according to linear elastic fracture mechanics. Therefore, the approach is invalid for plastic regions. In order to avoid plasticity problems, the allowable crack size is chosen to be $0.5 \cdot t$ for the depth and $0.5 \cdot W$ for the length.

In the prediction model, it is assumed that there is one crack initiated and one crack growth. In the test specimens, multiple cracks may initiate simultaneously, however, the coalesces of the multiple cracks are not taken into account for the model. The residual stress effects were neglected and it was assumed that the weld shape was constant, whereas in practice, it shows some variation. The correction factors for the stress concentration region of welded connections were calculated according to the given 2D model in BS 7910 (2013).

In Chapter 6, the results of the fatigue crack growth tests on the base material of S690 and S890 rolled steels were presented and the material parameters C and m for the Paris law were determined accordingly. For the fatigue crack propagation life prediction, these parameters were used. As can be seen from that chapter, a slight difference was observed between the parameters of both steel grades.

Fatigue crack propagation life is influenced by thickness of specimen, initial crack size, loading mode, crack shape, weld width and width of the specimen. In the following sections, the effects of these factors are evaluated. For the evaluation of the influence factors, the average value of the fatigue crack growth parameters of both steel grades is utilized and these are $C = 1.0965 \cdot 10^{-13}$ and $m = 3.385$. Table 8.2 summarises the input parameters for the evaluation of the influence factors.

Table 8.2. Parameters for the evaluation of the influence factors.

Parameters		Values
Initial crack depth, a	[mm]	0.15
Initial crack length, $2c$	[mm]	0.30
Plate width, W	[mm]	160
Loading mode		Tension or bending
Weld with-thickness ratio (L/t)	[-]	1.6
Crack type		Semi elliptical crack
Crack growth exponent, m		3.385
Crack growth coefficient, C	[mm/cycles]	$1.0965 \cdot 10^{-13}$

8.3.1 Thickness factor

In the design standards EN 1993-1-9 (2006) and the IIW recommendations (2016), the expressions for the thickness factor are given and for both design standards, 25 mm thickness is recommended as a reference thickness. Consequently, the fatigue strength of the specimens with a thickness above 25 mm is adjusted with the thickness factor. In the same approach, the thickness effect on fatigue crack growth can be expressed as ratio of the number of cycles for $t \neq 25$ mm and the number of cycles for $t = 25$ mm (see equation (8.21)).

$$f_{t,Np} = \left(\frac{N_{p,t \neq 25}}{N_{p,t=25}} \right)^{\frac{1}{m}} \quad (8.21)$$

where $m = 3.385$.

The weld width of the specimens is $L = 40$ mm for the specimen a thickness of $t = 25$ mm and the ratio, L/t , is 1.6. This ratio value is kept constant for the thickness factor $f_{t,Np}$ calculation. Figure 8.26 shows the thickness factor $f_{t,Np}$ for the tension and the bending loading as a function of various plate thicknesses.

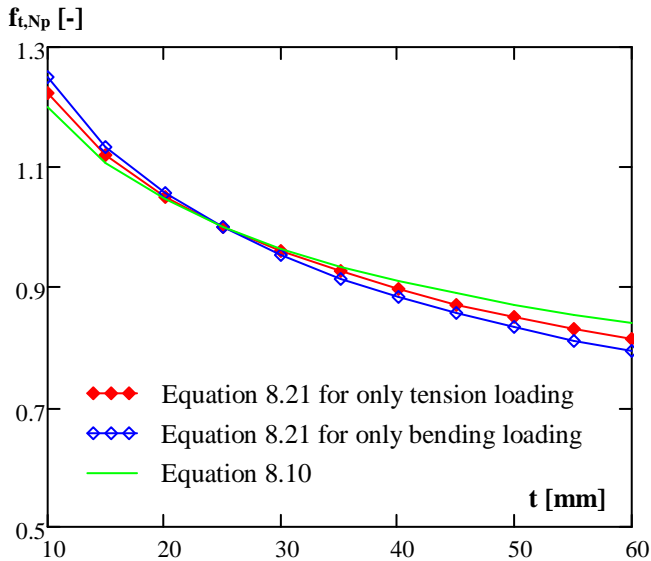


Figure 8.26 Thickness factor $f_{t,Np}$ for bending and tension loading.

The increase of thickness negatively influences the fatigue crack propagation life. In the figure, the thickness factors are compared with the thickness factor k_s equation of EN 1993-1-9 (2006). The comparison shows that the thickness factor $f_{t,Np}$ according to model leads to

conservative fatigue strength. The effect of loading on the thickness factor f_{t,N_p} is relatively small and the difference is approximately 2 %, which can be neglected.

8.3.2 Initial crack size factor

The stress intensity factor is a function of the crack size. Consequently, the crack size affects the fatigue crack propagation life. No clear definition is available for the transition between the fatigue crack initiation and the propagation stages. However, BS 7910 (2013) recommends 0.15 mm as initial crack depth for the cases where the initiation cracks size is not defined. The recommended initial crack depth is taken as reference value and the initial crack size factor f_{ai,N_p} can thus be defined as the ratio of number of cycles for $a_i \neq 0.15$ mm and $a_i = 0.15$ mm (see equation(8.22)).

$$f_{ai,N_p} = \left(\frac{N_{p,ai \neq 0.15}}{N_{p,ai = 0.15}} \right)^{\frac{1}{m}} \tag{8.22}$$

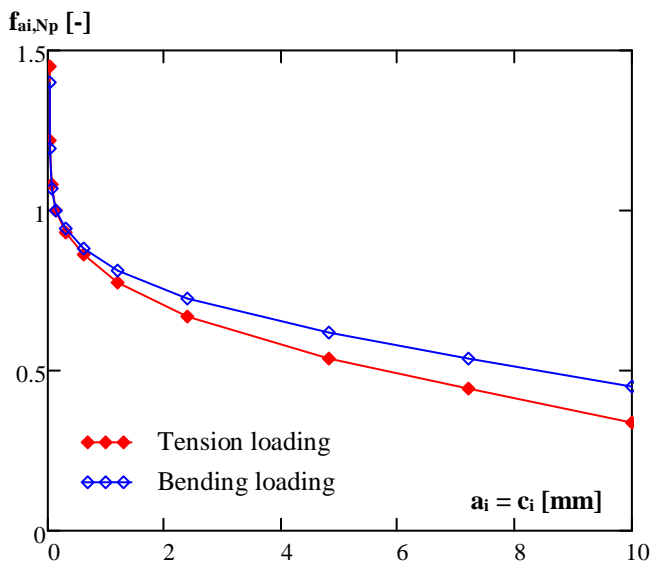


Figure 8.27 Effect of initial crack size factor f_{ai,N_p} on the fatigue crack propagation.

Figure 8.27 presents the effect of initial crack size on the fatigue crack propagation for the thickness $t = 25$ mm, the plate width $W = 160$ mm and the weld width $L = 40$ mm. The initial crack size factor f_{ai,N_p} is determined for a semi elliptical crack with 0.5 crack aspect ratio, $a/2c$. As expected, the increase of the initial crack size reduces the fatigue crack propagation life. The effect of the loading mode becomes remarkable with the increase of

the initial crack size. The tension loading mode causes faster fatigue crack propagation as compared to the bending loading mode.

8.3.3 Loading mode factor

The effect of the loading mode on the fatigue crack propagation is represented by the loading mode factor $f_{lm,Np}$. The loading mode factor $f_{lm,Np}$ is defined as the ratio between the number of cycles for bending loading and tension loading (see equation (8.23)).

$$f_{lm,Np} = \left(\frac{N_{p,lm=bending}}{N_{p,lm=tension}} \right)^{\frac{1}{m}} \quad (8.23)$$

Figure 8.28 shows the effects of the plate thickness and the initial crack size on the loading mode factor $f_{lm,Np}$. For the plate thickness variation, the ratio of the weld width and the plate thickness L/t are kept constant as 1.6. The increase of the plate thickness has limited effect on the loading mode factor $f_{lm,Np}$. The loading mode factor $f_{lm,Np}$ increases with the increase of the initial crack size. As expected a larger crack size has a detrimental effect on the fatigue crack propagation life for the tension loading mode as expected.

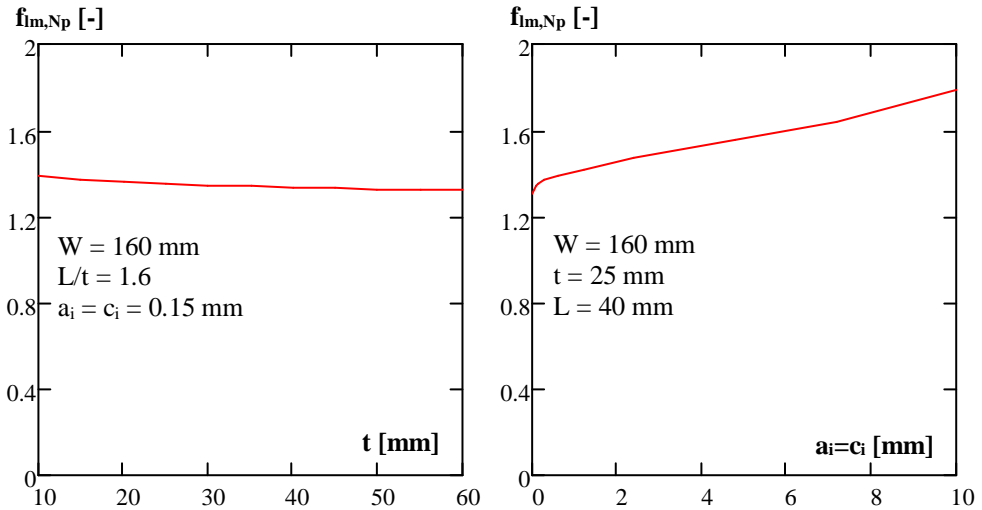


Figure 8.28 Loading mode factor $f_{lm,Np}$ for various thicknesses and initial crack size.

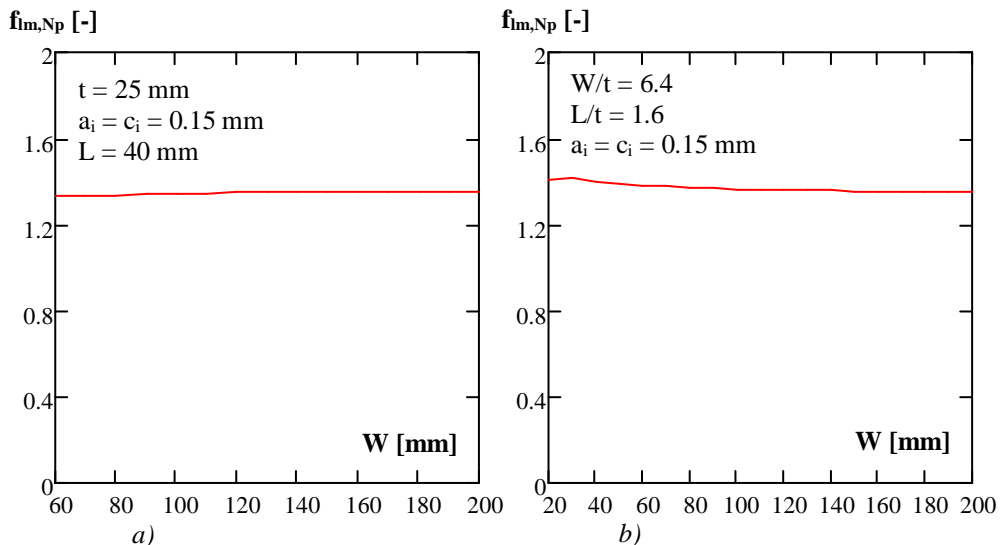


Figure 8.29 The effects of the plate width on the loading mode factor $f_{lm,Np}$.

Figure 8.29 presents the loading mode factor $f_{lm,Np}$ for various plate widths. The effect of the plate width is determined for two conditions. In the first condition (see Figure 8.29 a), the initial crack size, the weld width and the thickness are kept constant and it appears that there is no major influence of the plate width on the loading mode factor $f_{lm,Np}$. In the second condition (see Figure 8.29b), the initial crack size is maintained constant and the weld width and the plate thickness are specified as a function of the plate width. The following relationships are maintained for the specimen geometry: the ratio of the plate width and thickness $W/t = 6.4$ and the ratio of the weld width and the plate thickness $L/t = 1.6$. Figure 8.29b shows that the effect the plate width on the loading mode factor $f_{lm,Np}$ is insignificant.

8.3.4 Crack shape factor

Fatigue cracks can initiate in the middle of the plate and at the edge of the specimen. The cracks in the middle of the plate will propagate as semi elliptical cracks and the crack at the edge will propagate as half elliptical crack. The shape difference can also cause a distinction in the fatigue crack propagation behaviour. The crack shape factor $f_{cs,Np}$ can be defined as the ratio of the number of cycles for a half elliptical crack and the number of cycles for semi elliptical crack (see equation (8.24)).

$$f_{cs,Np} = \left(\frac{N_{p, \text{half elliptical}}}{N_{p, \text{semi elliptical}}} \right)^{\frac{1}{m}} \quad (8.24)$$

Figure 8.30 presents the effect of a half elliptical and a semi elliptical crack as a function of the plate thickness and the initial crack size. In case of a plate thickness variation, the required 60° weld bevel is met by keeping the L/t ratio constant as 1.6. The crack shape factor $f_{cs,Np}$ is determined for the tension and bending loading mode. Figure 8.30 shows that the loading mode has a very limited influence on the crack shape factor $f_{cs,Np}$. With increase of the plate thickness, the crack shape factor $f_{cs,Np}$ decreases for the tension loading mode, while it is constant for the bending loading mode. The crack shape factor $f_{cs,Np}$ decreases with the increase of the crack size under tension loading mode while it is almost constant for the bending loading mode.

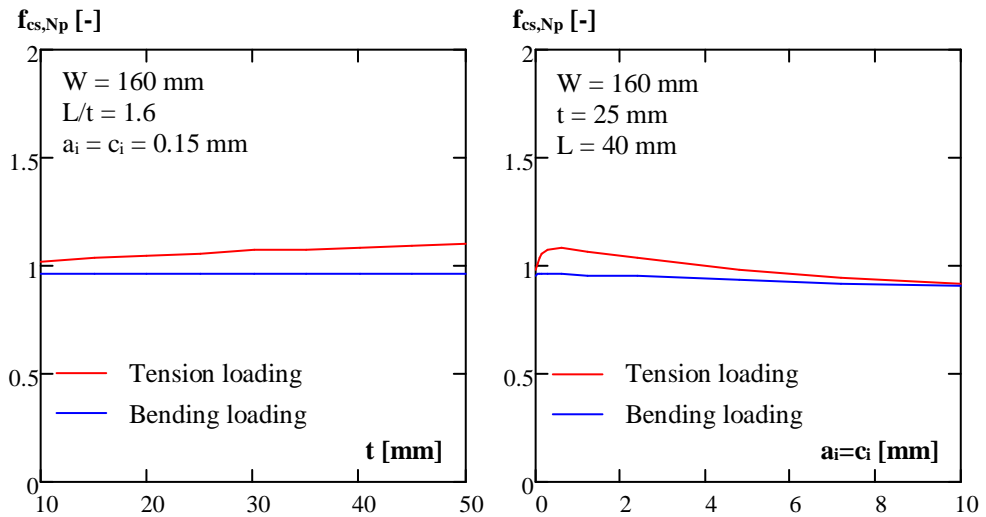


Figure 8.30 Crack shape factor $f_{cs,Np}$ for various plate thicknesses and initial crack size.

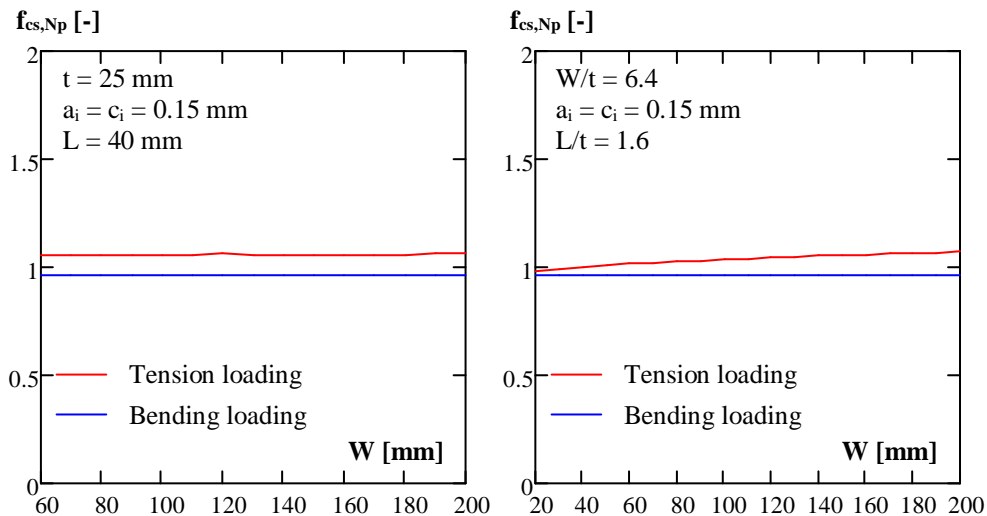


Figure 8.31 Effect of plate width on the crack shape factor $f_{cs,Np}$.

Figure 8.31 shows the effect of the plate width on the crack shape factor $f_{cs,Np}$. The crack shape factor $f_{cs,Np}$ is determined for a constant weld width L and a constant plate thickness t . For this condition, the crack shape factor was constant for both tension and bending loading mode and a small difference was indicated between loading modes. In addition, the crack shape factor $f_{cs,Np}$ was calculated for various weld widths L and thicknesses t with keeping the following ratios constant: $W/t = 6.4$ and $L/t = 1.6$. A comparison was made between the crack shape factors $f_{cs,Np}$ for tension loading and bending loading. The crack shape factor $f_{cs,Np}$ for the bending load remained constant with increase of the plate width while it showed a slight increase for the tension loading mode.

8.3.5 Weld width factor

The weld width depends on the plate thickness and the weld bevel angle. The weld bevel angle of the test specimens is 60° . The initial gap between the plates at the root was 3 mm and the plate thickness 25 mm. This geometry and additional enlargement due to the repair weld resulted in an average weld length $L = 40$ mm at the cap of the weld and the ratio of the weld width and the plate thickness, $L/t = 1.6$. For the evaluation of the effects of the weld width, $L/t = 1$ was chosen as reference value. Thus, the weld width factor $f_{L/t,Np}$ was formulated as the ratio of the number of cycles of the crack propagation for $L/t \neq 1$ and $L/t = 1$ (see equation (8.25))

$$f_{L/t,Np} = \left(\frac{N_{p,L/t \neq 1}}{N_{p,L/t=1}} \right)^{\frac{1}{m}} \quad (8.25)$$

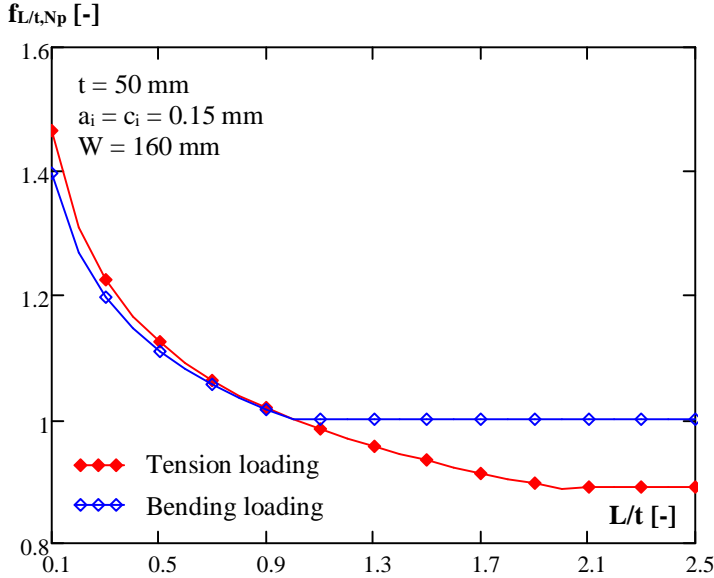


Figure 8.32 Weld width factor $f_{L/t,Np}$ for various L/t ratio.

Figure 8.32 shows the weld width factor $f_{L/t,Np}$ of variation in the L/t ratio with loading mode tension and bending. For $L/t < 1$, the loading mode effect on the weld width factor $f_{L/t,Np}$ is insignificant. When L/t is equal to 1, the weld width factor $f_{L/t,Np}$ becomes constant for the bending loading mode. The weld width factor $f_{L/t,Np}$ decreases to unity. In case of the tension loading, the weld width factor is constant for $L/t > 2$ and the weld width factor is smaller than 1.

8.3.6 Plate width factor

The ratio between the plate thickness and the plate width, W/t , is 6.4 and this value was used as reference. In this assumption, the width factor $f_{w,Np}$ is defined as the ratio of number of cycles of crack propagation for the case $W/t \neq 6.4$ and $W/t = 6.4$ (see equation (8.26))

$$f_{w,Np} = \left(\frac{N_{p,W/t \neq 6.4}}{N_{p,W/t=6.4}} \right)^{\frac{1}{m}} \quad (8.26)$$

Figure 8.33 presents the width factor $f_{w,Np}$ for various W/t ratios in case of tension and bending loading mode.

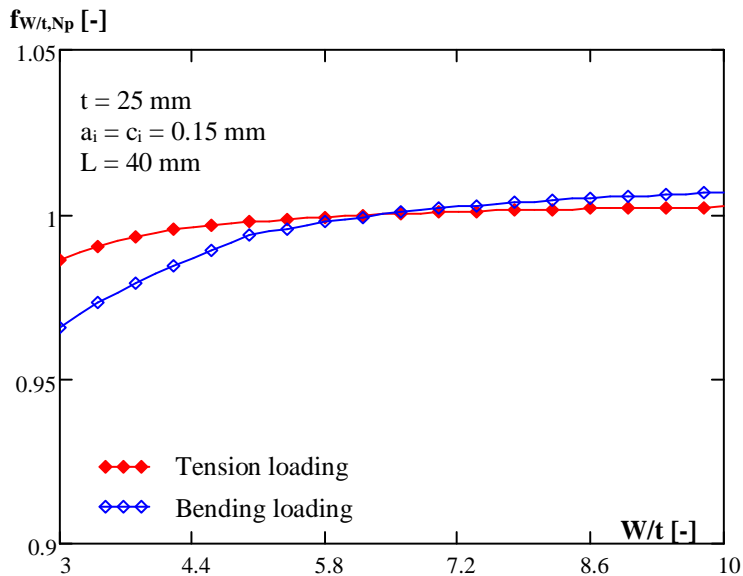


Figure 8.33 Plate with factor $f_{w,Np}$ for variation in W/t ratio.

For a low W/t ratio, the width factor $f_{w,Np}$ is influenced by the loading mode, but the effect is not very significant. From the reference value, $W/t = 6.4$, the width factor $f_{w,Np}$ becomes constant for the tension loading mode and it almost reaches unity. In case of the bending loading mode, a slight increase was observed after the reference value. However, this increase was very low and can be neglected.

8.4 Comparison of predictions and test results

The prediction models for the fatigue crack initiation life and for the fatigue crack propagation life were explained by considering the influence of geometrical and loading parameters. The influence of these parameters was determined separately. The fatigue test results are given in Chapter 5 and the results were compared with the results of the prediction models.

In the prediction models, various influence factors are dealt with and the results are discussed in the related sections. In order to study the various influence factors on the fatigue strength of the specimens, the measure a stress range of each specimen was adjusted to obtain the reference stress range for the fatigue crack initiation and propagation. The specimens were made from a plate with a thickness of 25 mm, for which the thickness

factor was equal to 1 and therefore, the adjustment factor for the thickness was disregarded. In case of the loading mode factor, the experiments were performed with four point bending setup. However, the fatigue limit in the models is given for the tension loading condition. In order to compare the test results with the results of the models, the test results need to be adjusted with the loading mode factor. In addition, the effect of the mean stress was also taken into account for the comparison. The fatigue crack initiation life was calculated for a thickness, $t = 25$ mm, for a high residual stress level $\sigma_r = \sigma_y$, notch radius $\rho = 1$ mm, mean stress $\sigma_m = 0.5\sigma_y$ and a weld toe angle $\theta = 25^\circ$.

$$\Delta\sigma_{n,Ni} = f_m \cdot f_{lm,Ni} \cdot \Delta\sigma_{test} \quad (8.27)$$

f_m Mean stress factor for crack initiation life
 $f_{lm,Ni}$ Loading mode factor for crack initiation life
 $\Delta\sigma_{test}$ Measured stress range during fatigue test life

$$\Delta\sigma_{n,Np} = f_m \cdot f_{lm,Np} \cdot \Delta\sigma_{test} \quad (8.28)$$

f_m Mean stress factor for crack propagation life
 $f_{lm,Np}$ Loading mode factor for crack propagation life
 $\Delta\sigma_{test}$ Measured stress range during fatigue test life

The fatigue crack initiation life of the test specimens was determined according to the strain gauge measurements. The strain gauge measurements close to the crack were used for the determination of the stress range and for the fatigue crack initiation life. The fatigue crack initiation life was specified as the number of cycles at which the strain gauge started to bend off from the regular shape. The accuracy of these measurements depends on the distance between the crack initiation location and the strain gauge. The number of cycles for the fatigue crack propagation life is determined with subtraction of the fatigue crack initiation life from the total fatigue life. In some test specimens, fatigue crack initiation and propagation was observed in the base material far from the welded connection. The strain gauges indicated the fatigue crack at a very late stage. For these specimens, the fatigue crack initiation life was determined either by the strain gauge reaction to the crack which occurred when the crack was already very large or by visual inspection before the strain gauge indications. In the prediction fatigue crack propagation life, the initial crack size was taken $a_i = c_i = 0.15$ mm which is recommended by BS 7910 (2013). The fatigue crack propagation life was determined for the initial crack growth up to the allowable crack size, which was defined when either the crack depth reached half the thickness of the plate $a_f = t/2$ or until the crack length became equal to half the width of the test specimens $2c_f = w/2$.

8.4.1 Repaired artificial crack in the base materials

The fatigue crack initiation life was predicted according to the analytical approach from Hück et al., (1981) (Section 7.4) and according to the nominal and local stress approach of

the FKM guideline. Figure 8.34 shows the comparison between the test results of the repaired artificial crack in the base material of S690 rolled steel and the predicted fatigue strength curve by the prediction models. The fatigue crack initiation life was determined according the analytical approach of Hück et al., (1981). The prediction model of the crack initiation life and propagation life were found to be conservative.

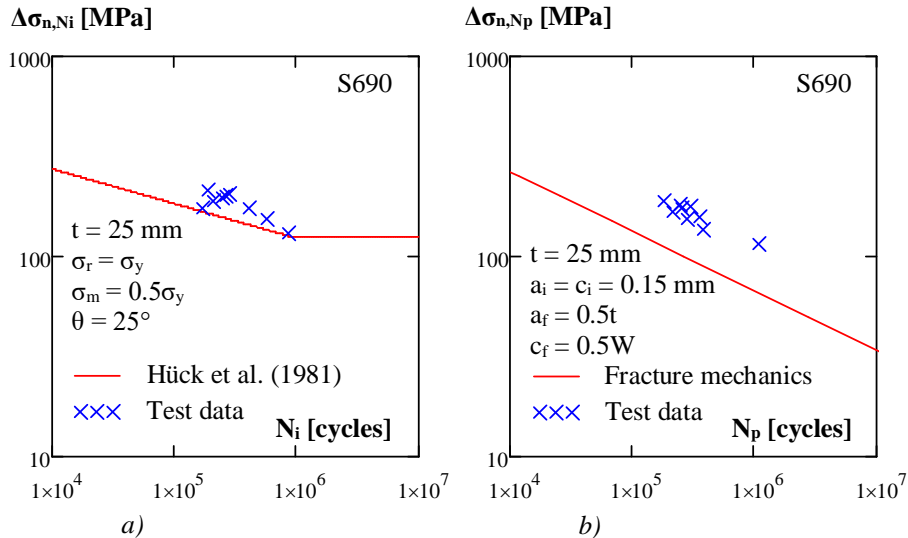


Figure 8.34 Comparison of test data with prediction models a) crack initiation life according to Hück et al., (1981), b) fatigue crack propagation life of BR69x series.

Figure 8.35 compares the fatigue crack initiation life of the repaired an artificial crack in the base material of S690 rolled steel with the prediction models according to the FKM guideline for the nominal and local stress approach. The fatigue crack initiation life prediction according to the nominal stress approach shows conservative results, while the result of the local approach slightly overestimated the fatigue crack initiation life prediction.

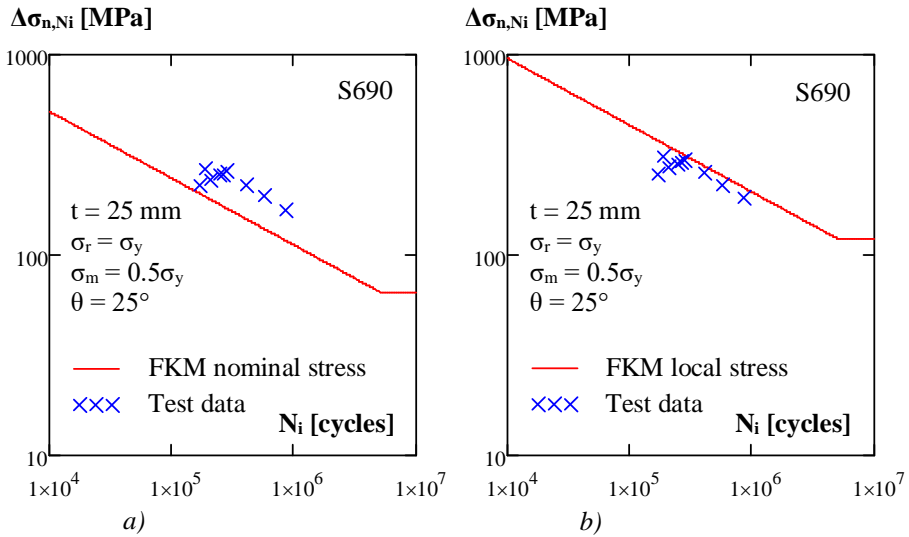


Figure 8.35 Comparison of test data with prediction models for crack initiation life according to the FKM guideline a) nominal stress approach b) local stress approach.

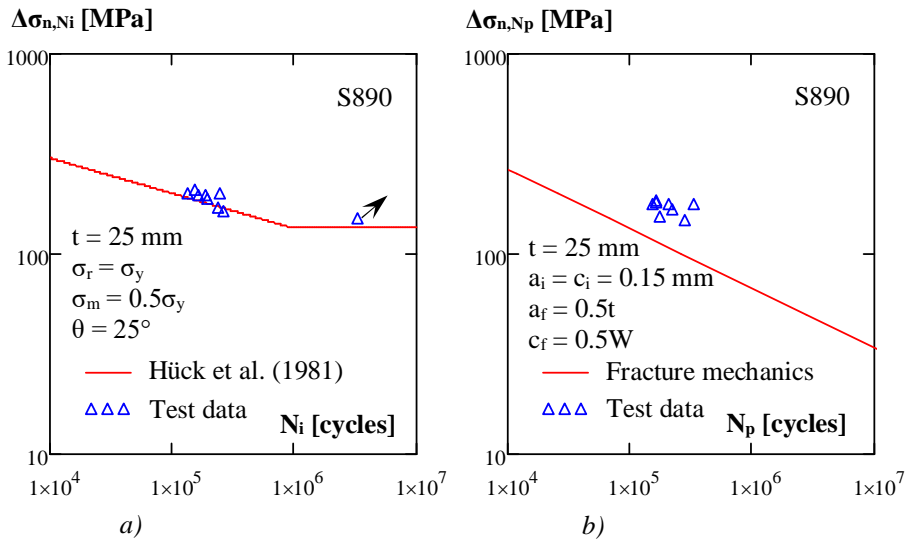


Figure 8.36 Comparison of test data with prediction models a) crack initiation life according to Hück et al., (1981), b) fatigue crack propagation life of BR89x series.

Figure 8.36 shows the comparison of the predicted fatigue crack initiation life and the crack propagation life with the test data of the tests specimens with the repaired artificial crack in the base material of S890. The fatigue crack initiation life was predicted according to the

approach of Hüek et al., (1981). The predicted fatigue crack initiation and propagation life reasonably matched with the test results. Figure 8.37 presents the fatigue crack initiation life prediction according to the FKM guideline by using nominal and local approach compared with the test results. The estimated fatigue crack initiation life according to the nominal stress approach is conservative, while the prediction by using the local stress approach overestimates.

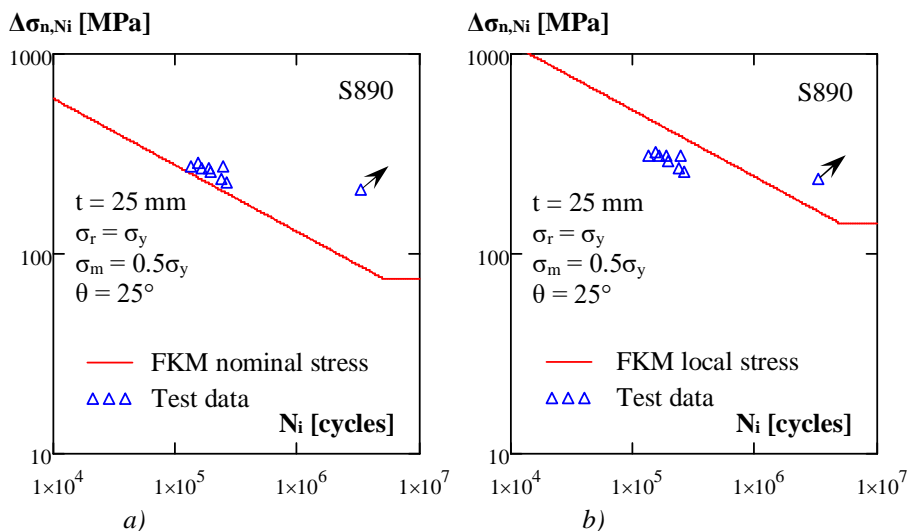


Figure 8.37 Comparison of test data with prediction models for crack initiation life according to the FKM guideline a) nominal stress approach b) local stress approach.

8.4.2 V-shape welded specimens made of rolled steels

Fatigue test specimens were made of S690 and S890. Figure 8.38 compares the predicted fatigue crack initiation life and the crack propagation life with the test data of the repaired V-shape welded specimens made of S690. The fatigue crack initiation life is determined by using the approach proposed by Hüek et al., (1981). The crack initiation life was reasonably estimated by the model. The prediction model of the crack propagation life seems to be conservative. The fatigue crack initiation life of one specimen remained below the predicted curve. In that specimen, premature failure was observed during testing. The fracture surface examination of this specimen revealed that the crack removal process was not properly performed and the crack root remained in the specimen, which caused premature failure.

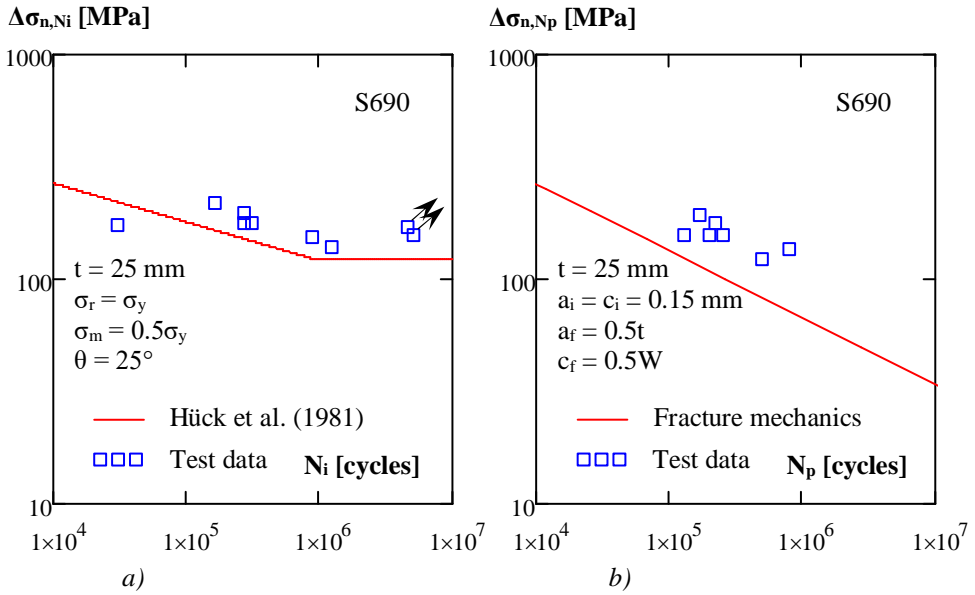


Figure 8.38 Comparison of test data with prediction models a) crack initiation life according to Hück et al., (1981), b) fatigue crack propagation life of VR69x series.

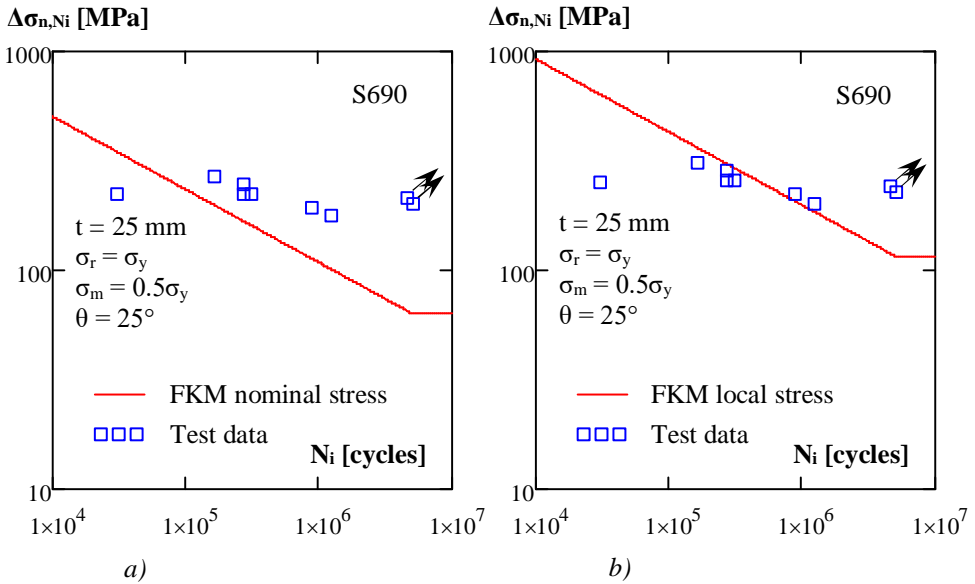


Figure 8.39 Comparison of test data with prediction models for crack imitation life according to the FKM guideline a) nominal stress approach b) local stress approach.

Figure 8.39 shows the comparison of the predicted fatigue crack initiation life according to the FKM guideline with the fatigue test data of the repaired V-shape welded specimens made of S890. The prediction according to the nominal stress approach was conservative, while the local stress approach showed a more accurate prediction.

In the majority of the repaired V-shape welded specimens made of S890 rolled steel, the fatigue crack initiation and propagation was observed in the base material. There were only two test data available to be evaluated for the fatigue strength of welded connections and those data were run-outs. The fatigue life prediction for the base material failure is given in Section 8.4.4.

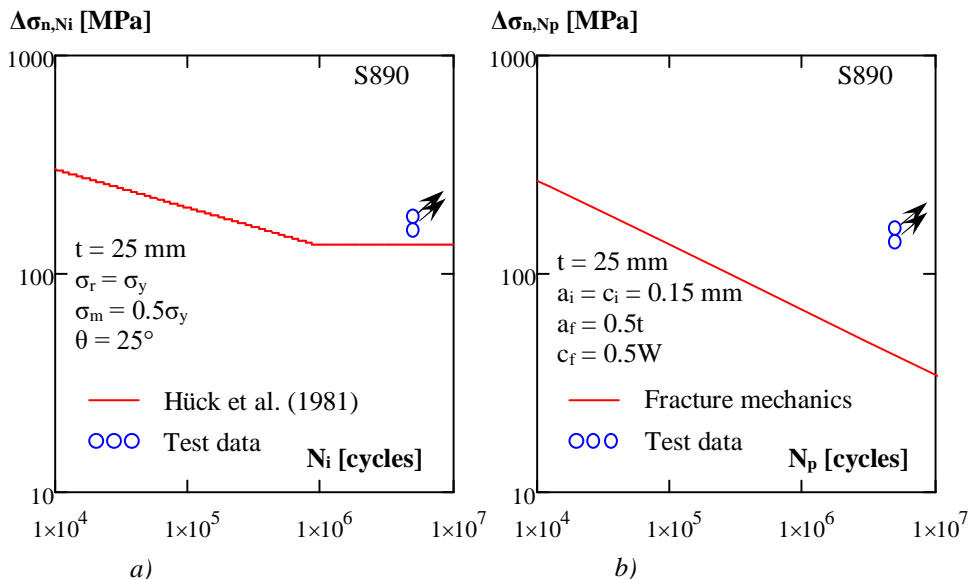


Figure 8.40 Comparison of test data with prediction models a) crack initiation life according to Hück et al., (1981), b) fatigue crack propagation life of VR89x series.

There was no any fatigue crack initiation at the weld toe of the welded connections. The comparison was made for runouts test data. Therefore, it is difficult to evaluate the accuracy of the prediction models. Figure 8.40 presents the comparison of the fatigue crack initiation life and the propagation life models with the test data of the repaired V-shape welded specimens made of S890. Figure 8.41 shows the fatigue crack initiation life prediction according to the FKM guideline. The test results were located on the fatigue limit line of the prediction model according to the local stress approach of the FKM guideline.

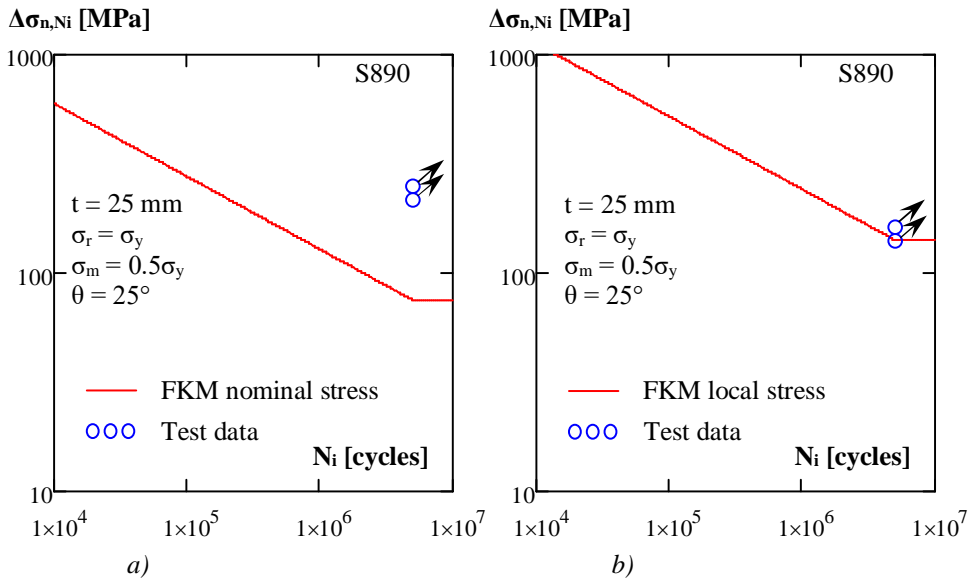


Figure 8.41 Comparison of test data with prediction models for crack initiation life according to the FKM guideline a) nominal stress approach b) local stress approach.

8.4.3 V-shape welded specimens made of cast and rolled steels

The specimens were made of S690, S890 and the cast steels with a similar yield strength, G10MnMoV 6-3 and G18NiMoCr 3-6 respectively. Fatigue crack initiation and propagation were observed at various locations of the specimens namely at the weld toe of the rolled steels side, at the weld toe of the cast steels side, in the base material of rolled and cast steels. The specimens with base material failure are evaluated in Section 8.4.4.

There are slight differences between the yield strength of the rolled and cast steels. In the prediction models of the fatigue crack initiation life, the yield strength of rolled steels is used for fatigue strength prediction of the fatigue cracks in the weld toe of the rolled steels and the yield strength of cast steels for fatigue strength prediction of the cracks in the weld toe of the cast steels side.

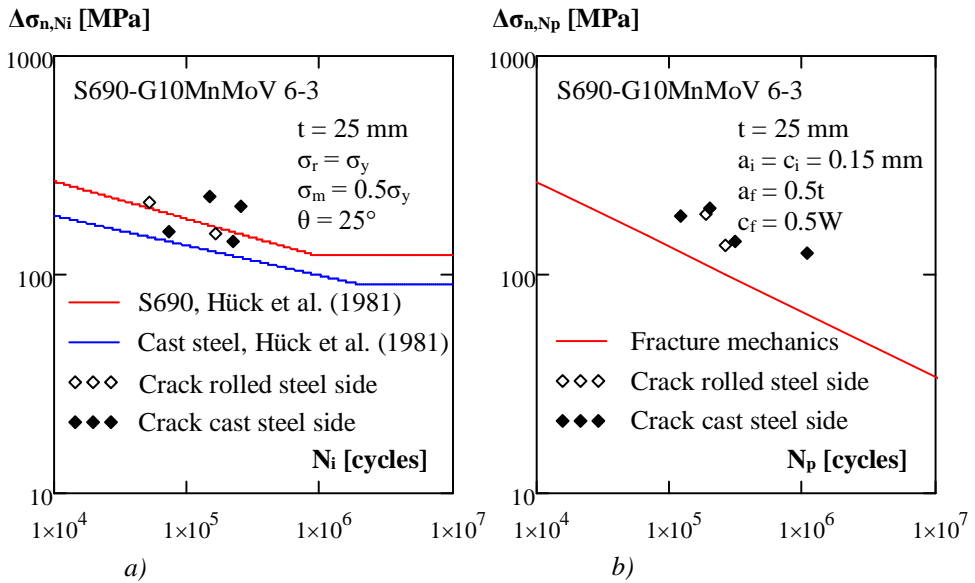


Figure 8.42 Comparison of test data with prediction models a) crack initiation life according to Hück et al., (1981), b) fatigue crack propagation life of CR69x series.

Figure 8.42 compares the fatigue test data of the repaired V-shape welded specimens made of S690 rolled and G10MnMoV 6-3 cast steel with the prediction models for the crack initiation life and the propagation life. The prediction models show reasonable agreement with the test data. Figure 8.43 presents the predicted fatigue crack initiation life according to the FKM guideline. The nominal stress approaches show reasonable agreement with the test data while the local stress approach slightly overestimates the fatigue crack initiation life as compared to the test data.

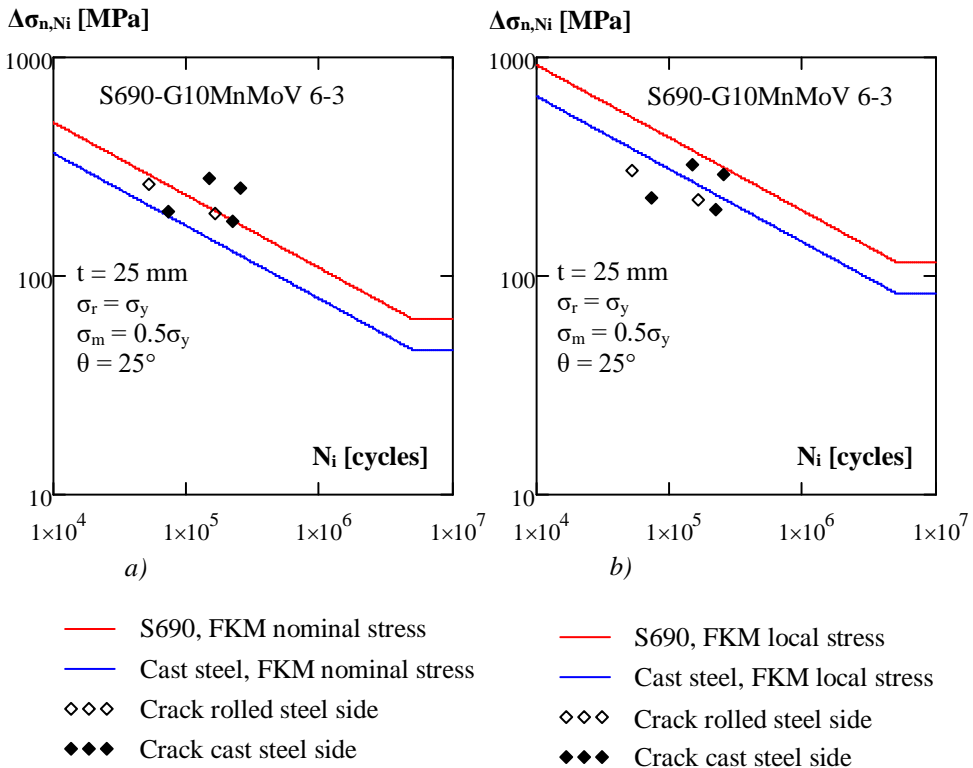


Figure 8.43 Comparison of test data with prediction model for crack initiation life according to the FKM guideline a) nominal stress approach b) local stress approach.

There was only one test specimen in the CR89x series where the crack initiation and the propagation was observed at the weld toe. The crack was at the weld toe of the cast steel side. The remaining specimens failed due to crack initiation and propagation in the base material of either in rolled steel or in cast steel parts. Figure 8.44 shows the comparison between the fatigue test data and the results of the prediction models. However, there is only one test result and it is difficult to evaluate the reliability of the prediction models. The fatigue crack initiation life prediction for cast steels is found to be conservative. In case of the crack propagation life, the prediction model shows good agreement with the test data.

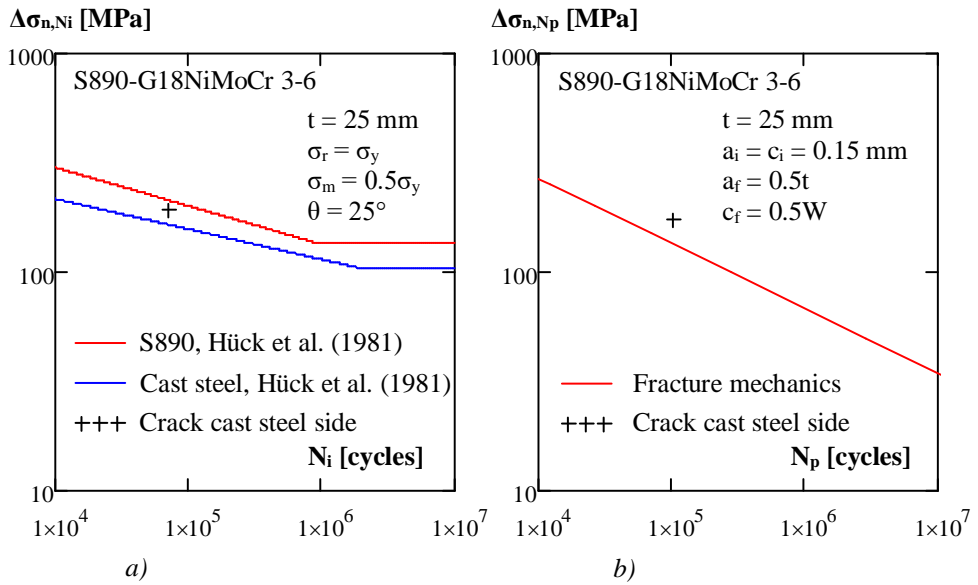


Figure 8.44 Comparison of test data with prediction models a) crack initiation life according to Hück et al., (1981), b) fatigue crack propagation life of CR89x series.

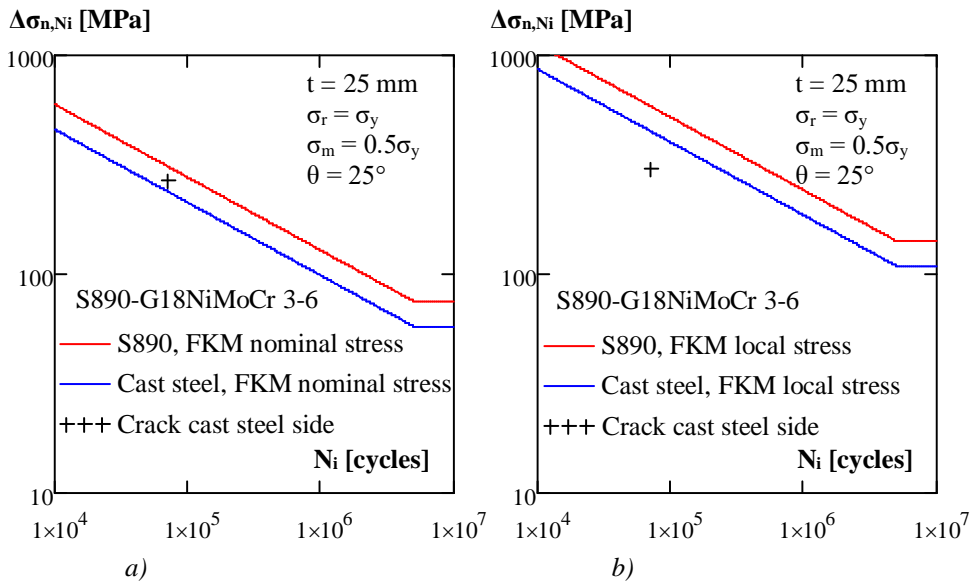


Figure 8.45 Comparison of test data with prediction models for crack initiation life according to the FKM guideline a) nominal stress approach b) local stress approach.

Figure 8.45 presents the fatigue crack initiation life prediction according to the FKM guideline. The crack initiation life prediction is made for rolled and cast steels separately. Using the nominal stress approach, the prediction for cast steel show good agreement with the test results. The prediction according to the local stress approach overestimates the crack initiation life for both the rolled and the cast steel.

8.4.4 Base material cracks

During fatigue tests on the repaired V-shape welded specimens, fatigue crack initiation and propagation was observed in the base material of the specimens. The base material failures were observed in S890 rolled steel and G10MnMoV 6-3, G18NiMoCr 3-6 cast steels.

The prediction models were adjusted for the fatigue life prediction of the base material failures. For the crack initiation life prediction, the surface roughness factor was taken into account. In the FKM guideline, surface roughness value $R_z = 200 \mu\text{m}$ is recommended for the rolling skin and the casting skin. For the prediction models from the FKM guideline, the slope $k = -5$ is recommended for the fatigue strength curve of base material and it is implemented in the models. The fatigue crack initiation life of the base material cracks is determined for stress concentration factor $K_t = 1$. For the crack propagation life, the stress intensity factor was adjusted to exclude the stress concentration effect due to the welding. Consequently, the stress concentration correction factors M_{km} and M_{kb} need to be equal to 1. The number of cycles at the crack creation stage were included to the number of cycles at the failure after the repair of weld toe cracks.

Figure 8.46 compares the prediction model of the fatigue crack initiation life according to the analytical approach of Hück et al., (1981) and fatigue crack propagation life with the fatigue test data of fatigue crack initiation in the base material of G10MnMoV 6-3. The fatigue crack initiation life according to the analytical model overestimates as compared to the test results. In case of fatigue crack propagation life, the model presents good agreement with the test data.

Figure 8.47 shows the fatigue crack initiation life prediction according to the FKM guideline for the nominal and the local stress approach. The fatigue crack initiation life from both approaches shows very accurate estimation with the test data. The fatigue strength curves for the crack initiation life of both approaches present the mean curve of the test data. On the fracture surfaces of the specimens, internal imperfections were detected at the crack initiation locations. These imperfections might significantly reduce the fatigue crack initiation life of the material. Consequently, the material without imperfection would show a higher fatigue resistance and in accordance with this, the prediction models might show a conservative fatigue crack initiation life.

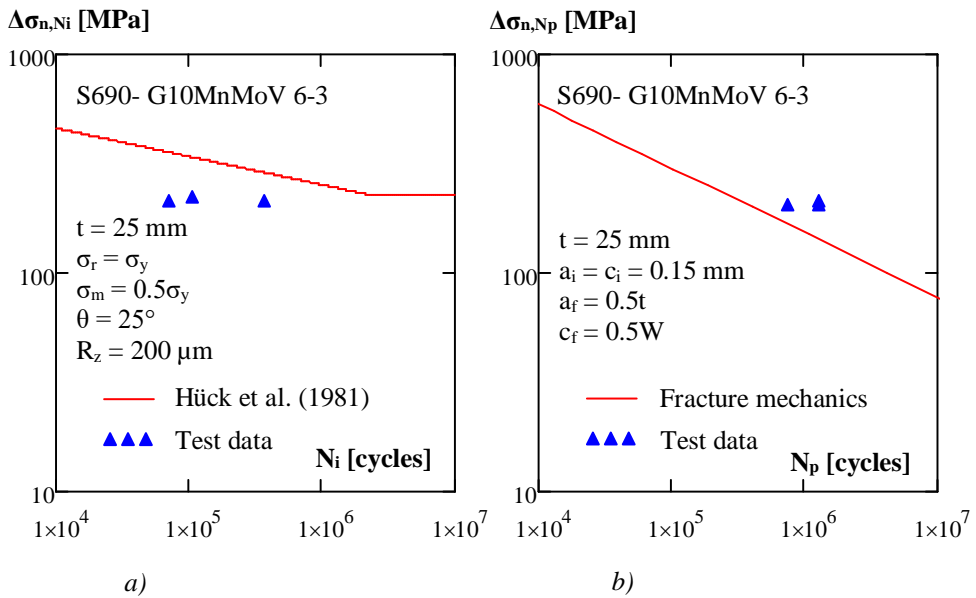


Figure 8.46 Comparison of test data with prediction models a) crack initiation life according to Hück et al., (1981), b) fatigue crack propagation life of base material G10MnMoV 6-3 cast steel.

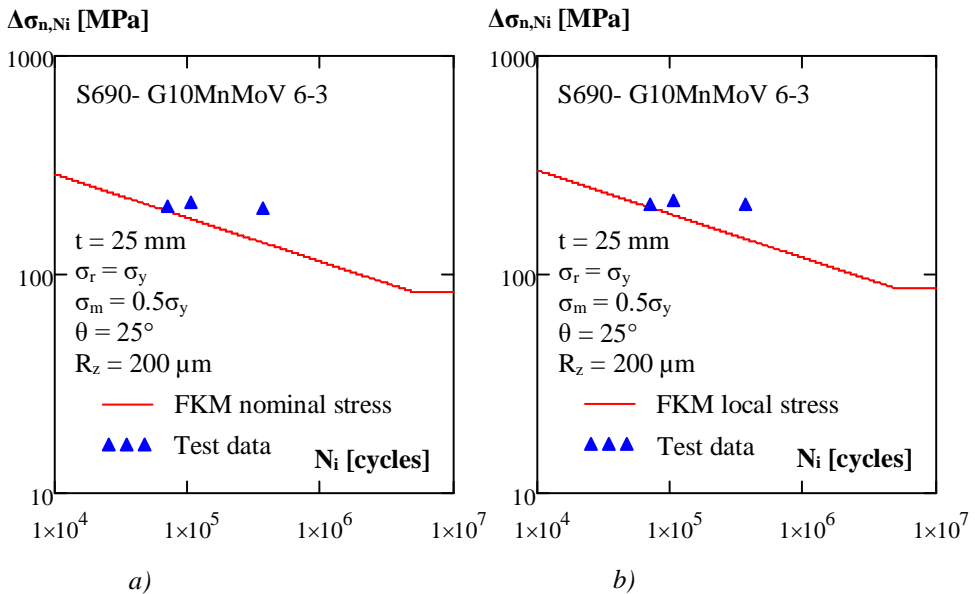


Figure 8.47 Comparison of test data with prediction models for crack initiation life according to the FKM guideline a) nominal stress approach b) local stress approach.

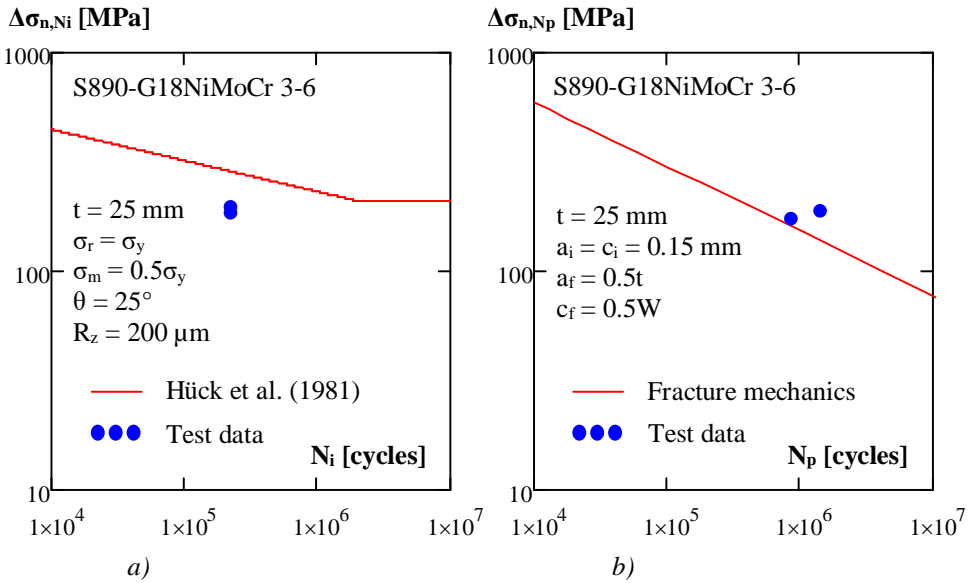


Figure 8.48 Comparison of test data with prediction model a) crack initiation life according to Hück et al., (1981), b) fatigue crack propagation life of base material G18NiMoCr 3-6 cast steel.

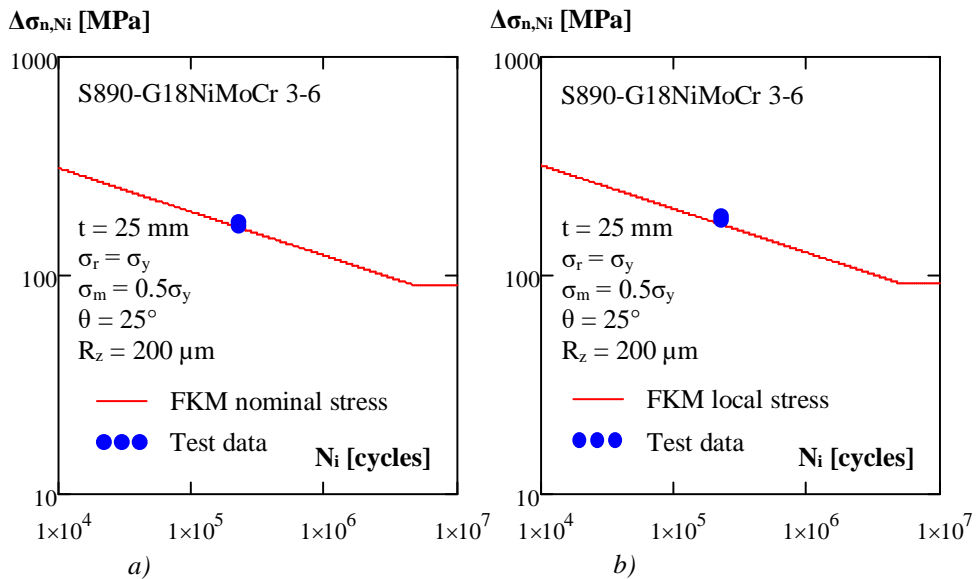


Figure 8.49 Comparison of test data with prediction models for crack initiation life according to the FKM guideline a) nominal stress approach b) local stress approach.

Figure 8.48 shows the comparison between the test data of the base material failure in G18NiMoCr 3-6 cast steel and the fatigue life prediction according to Hück et al., (1981) and the fatigue crack propagation life. The prediction of the fatigue crack initiation life is overestimated and this can be explained by the internal imperfections in the cast steels. The model of the fatigue crack propagation shows reasonable agreement with the test results. Figure 8.49 presents the fatigue crack initiation life prediction according to the FKM guideline and these prediction models show a very accurate fatigue strength estimation.

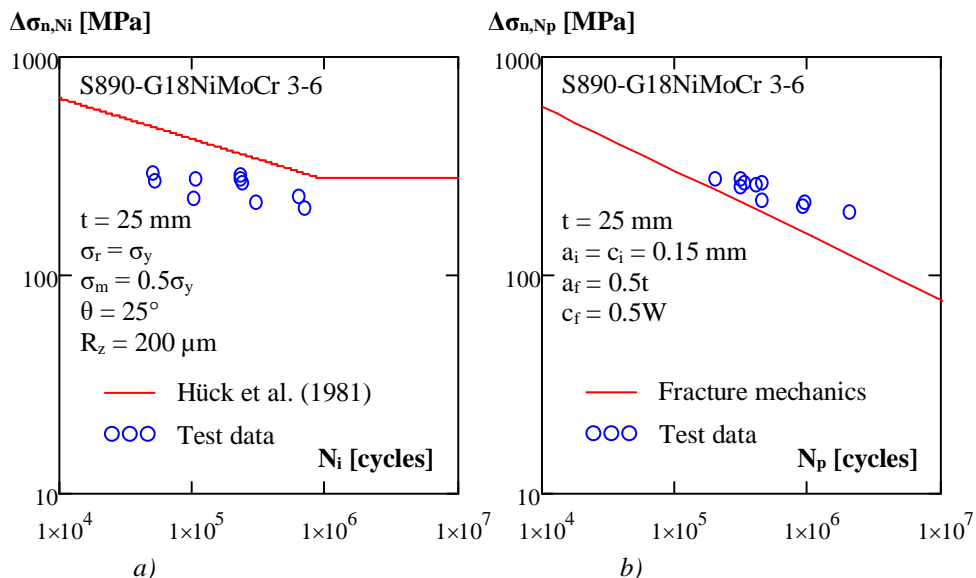


Figure 8.50 Comparison of test data with prediction models a) crack initiation life according to Hück et al., (1981), b) fatigue crack propagation life of base material S890 rolled steel.

Figure 8.50 presents the comparison of fatigue test data of the base material failure of S890 with the prediction model for the fatigue crack initiation life according to Hück et al., (1981) and the fatigue crack propagation life. The prediction model of the fatigue crack initiation life was found to be overestimated. The fracture surfaces of the specimens were examined and highly corroded locations were observed at the crack initiation locations. In other words, the corrosion pits on the surface might have caused the crack initiation in the base material of S890 steel. The corrosion pits induce local cross section reduction and the stress concentrations. The local stress increases as a result of these imperfections triggered the fatigue crack initiation in the base material and the fatigue strength reduction of the material. For the fatigue crack propagation life, the prediction model shows a reasonable estimation compared with the test results.

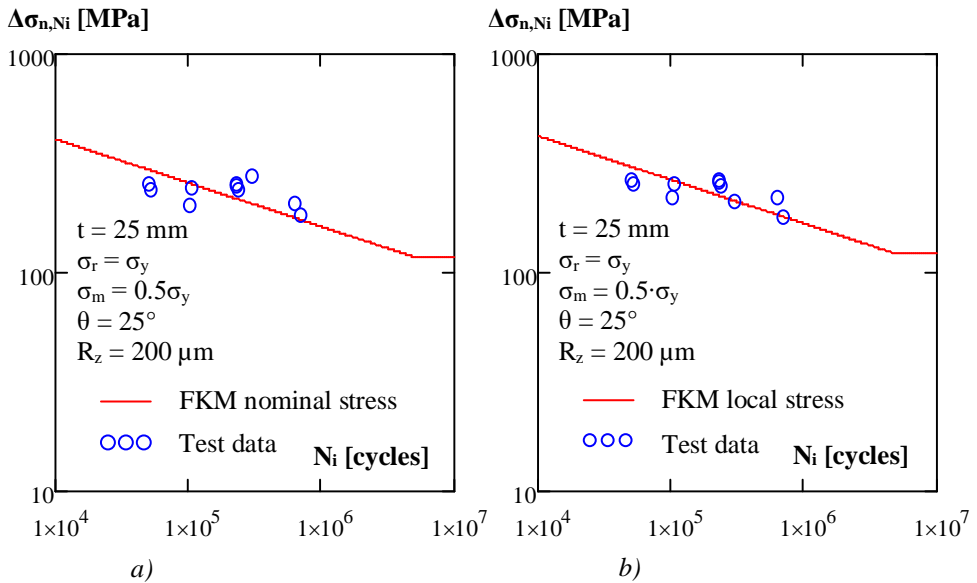


Figure 8.51 Comparison of test data with prediction models for crack initiation life according to the FKM guideline a) nominal stress approach b) local stress approach.

Figure 8.51 compares the fatigue test data of the base material failure in S890 rolled steel to the fatigue crack initiation life prediction according to the FKM guideline. The fatigue crack initiation life is determined with the nominal and the local stress approach. The prediction curves of the both approaches present very good agreement with the test data.

8.5 Summary

This chapter presents the prediction models for the fatigue crack initiation and propagation life of weld toe cracks and base material cracks. The theory and the application procedure of these prediction models are given in Chapter 7. In this chapter, the procedures of the models are modified for the prediction fatigue strength of repaired V-shape welded connections. The notch stress theory was used for the fatigue crack initiation life estimation and the linear elastic fracture mechanics approach was used for the fatigue crack propagation life prediction. The fatigue crack initiation life was calculated according the analytical model proposed by Hück et al., (1981) and the FKM guideline which proposes two approaches, the nominal and the local stress approach.

It was found that the fatigue crack initiation life of the unnotched components is affected by the surface roughness, yield strength and mean stress. The plate thickness of the

components and the loading mode will have an influence on the fatigue strength of notched specimens. In case of welded connections, the weld toe angle and notch radius at the weld toe was found to affect the fatigue strength of the connections. The stress at the weld toe arises with increase of the weld toe and decrease of the notch radius. It was found that high strength steels are more susceptible to the notch stress increase. The mean stress susceptibility increases with the increase of the yield strength of the material. Therefore, compressive mean stress can significantly improve the fatigue strength of high strength steels.

The fatigue crack propagation life is influenced by the loading mode, initial crack size, crack shape, weld width and the plate thickness of the specimens. The fatigue crack propagation life for the tension loading mode was found to be shorter than in case of the bending loading mode. As it is known, the increase of the initial crack size decreases the fatigue crack propagation life. The edge cracks and half elliptical cracks show a lower fatigue crack propagation life as compared to semi elliptical cracks.

The fatigue test results were compared with the prediction models. For the comparison, the fatigue test data were adjusted for the mean stress, thickness factor and the loading mode. The prediction models are given for the tension loading mode, while the test results were determined under bending loading condition. Hence, the test results were adjusted with the loading mode factor. For the residual stresses, it is assumed that the residual stress at the specimens is equal to the yield strength of the material.

The fatigue crack initiation life prediction model according to Hück et al., (1981) showed reasonable agreement with the test data of the welded connections. In case of a base material crack, it leads to an overestimated fatigue strength prediction. This can be explained by the internal imperfection in the base material of the cast steel and effect of the corrosion pits on the surface of the rolled steels. These material imperfections reduce the fatigue crack initiation life of the material.

As to the prediction models according to the FKM guideline, the nominal stress approach seems to be conservative for the fatigue crack initiation life prediction of weld toe cracks, while the local stress approach slightly overestimates the fatigue crack initiation life. Both nominal and local stress approach provide a very accurate fatigue crack initiation life prediction for the base material. The fatigue crack propagation life of weld toe cracks is conservatively predicted by the fracture mechanics approach. In case of the fatigue crack propagation life prediction for base material cracks, the fracture mechanics approach provides an accurate estimation.

Chapter 9

Analysis of fatigue test results

9.1 Introduction

A statistical analysis of the fatigue test data, which were presented in Chapter 5, is discussed in detail in this chapter. Chapter 5 contains background of the fatigue tests on the repaired artificial crack in the base material of S690, S890 and the repaired V-shape welded connections made of S690, S890 rolled steels and cast steels with similar yield strength. The procedure of testing and repairing fatigue cracks was extensively dealt with. Chapter 8, focused on the analytical prediction models for the fatigue crack initiation life and the propagation life. In addition, several influence factors were studied to evaluate the influence of these parameters on the fatigue strength of material and welded connections.

The aim of the statistical analysis is to determine the fatigue strength curves for the repaired fatigue damaged welded connections made of very high strength steels. The test results were adjusted by the influence factors and the adjusted test results were analysed separately. Furthermore, with the repair of the fatigue cracks, it is intended to regain the fatigue life of the connections. In other words, the fatigue life of repaired connections needs to be as long as the fatigue life of the original connections. Therefore, the fatigue strength of the repaired welded specimens was compared with the fatigue strength of the welded specimens in the as-welded condition (no repair).

The results of the prediction models were compared with the mean curves of the regression analysis of the test data. A comparison was made between the fatigue strength curves of the test data and the design curve of EN 1993-1-9 (2006). In that case, the lower bound curve of the scatter is used for the comparison.

Section 9.2 presents the analysis approach. In Section 9.3, statistical evolutions of the fatigue test data are given.

9.2 Approach of analysis

The specimens were made of steel plates with a thickness of 25 mm and therefore no adjustment was needed for the plate thickness. The fatigue tests were executed by using a four point bending test setup. However, the prediction models for the fatigue crack initiation life were established for the loading mode of tension. In order to compare the test results with the prediction models, the conversion of the loading mode was needed and the test data were adjusted with the loading mode factor. In Chapter 8, it was found that the fatigue life is affected by the residual stress state. The effects of the residual stresses were implemented in the mean stress factor, which is also used as an adjustment factor for the test results. In the fatigue tests, the fatigue cracks were initiated at various locations of the test specimens, e.g. in the base material, at the weld toe of the cap in the rolled and the cast steel side. In the statistical analysis, the test data with similar features were combined to increase the amount of data for an appropriate statistical evaluation.

9.2.1 Adjustment factors for test data

In Chapter 8, the influence factors were determined for the geometrical features of the specimens and for the loading mode. The influence factors were specified for the crack initiation and propagation life and it was revealed that there are slight differences in the influence factors between these two fatigue life stages. Additionally, the factors were defined for generalized conditions. However, the parameters for the determination of these factors may vary for each specimen. Therefore, adjusting each specimen with the same factors is not reasonable. In addition, the test results were already affected by the variation of the loading and the geometrical parameters for each specimen. This effect can be implemented in the adjustment factors with the ratio of the crack initiation life N_i to the total fatigue life N_f for the factors of crack initiation life and ratio of the crack propagation life N_p to the total life N_f for the factors of crack propagation life.

$$f_{N_i} = \frac{N_i}{N_f} \quad (9.1)$$

$$f_{N_p} = \frac{N_p}{N_f} \quad (9.2)$$

where N_i is the number of cycles at the crack initiation, N_p is the number of cycles for the crack propagation and N_f is the number of cycles at failure, which is defined such that the specimen is broken into two pieces.

The measured nominal stress range was modified with the adjustment factors to determine the reference stress ranges, which include the effect of loading mode and mean stress. The adjustment factors are determined for $\sigma_r = \sigma_y$, the mean stress $0.5\sigma_y$, the notch radius $\rho = 1$

mm and weld toe angle $\theta = 25^\circ$. The adjustment factors for the base material cracks were calculated for the stress concentration factor, $K_t = 1$. The adjusted stress range for the weld toe cracks and the base material cracks is given by equations (9.3) and (9.4) respectively.

$$\Delta\sigma_{n,w,Nf} = f_m \cdot f_{lm,w,Nf} \cdot \Delta\sigma_{test} \quad (9.3)$$

f_m Mean stress factor
 $f_{lm,w,Nf}$ Loading mode factor for fatigue life of weld toe crack
 $\Delta\sigma_{test}$ Measured nominal stress range during fatigue test

$$\Delta\sigma_{n,b,Nf} = f_m \cdot f_{lm,b,Nf} \cdot \Delta\sigma_{test} \quad (9.4)$$

f_m Mean stress factor
 $f_{lm,b,Nf}$ Loading mode factor for fatigue life of base material crack
 $\Delta\sigma_{test}$ Measured nominal stress range during fatigue test

As mentioned before, the adjustment factors for the crack initiation life and propagation life are different. The contribution of these parameters to the total fatigue life is proportional to the ratio of the crack initiation f_{Ni} and the crack propagation f_{Np} . Hence, the loading mode factor for weld toe crack is expressed by equation (9.5).

$$f_{lm,w,Nf} = f_{lm,w,Ni} \cdot f_{Ni} + f_{lm,w,Np} \cdot f_{Np} \quad (9.5)$$

$f_{lm,w,Ni}$ Loading mode factor for crack initiation life of weld toe cracks
 f_{Ni} Crack initiation life ratio of the specimen
 $f_{lm,w,Np}$ Loading mode factor for crack propagation life of weld toe cracks
 f_{Np} Crack propagation life ratio of the specimen

The loading mode factor for the base material cracks is given by equation (9.6).

$$f_{lm,b,Nf} = f_{lm,b,Ni} \cdot f_{Ni} + f_{lm,b,Np} \cdot f_{Np} \quad (9.6)$$

$f_{lm,b,Ni}$ Loading mode factor for crack initiation life of base material cracks
 f_{Ni} Crack initiation life ratio of specimen
 $f_{lm,b,Np}$ Loading mode factor for crack propagation life of base material cracks
 f_{Np} Crack propagation life ratio of specimen

Fatigue crack initiation life was predicted according to the analytical approach of Hück et al., (1981) and the FKM guideline where two approaches are described; nominal and local approach. Consequently, the influence factors for the crack initiation life were calculated based on these three models. Fatigue crack propagation life was calculated based on the fracture mechanics approach and the influence factors were determined accordingly. The predicted total fatigue life shows variation due three different models of the fatigue crack initiation life. In graphical representation of the fatigue strength curves, only models of the crack initiation life were mention since the propagation life is the same for all models. In other word, the test data were adjusted according to both the crack initiation models and propagation model. The models of the crack initiation life were only specified on the graph since these models cause variation in the total fatigue life prediction.

9.2.2 Statistical analysis

The statistical evaluation of the test results was performed according to Brozzetti et al., (1989), and this evaluation method is also used in EN 1993-1-9 (2006). The characteristic stress range at 2 million cycles, $\Delta\sigma_c$, was calculated for a 95% survival probability on a two sided confidence level of 75% of the mean, parallel to the mean. The fatigue strength curves are represented by a log-log linear relation between stress range $\Delta\sigma$, and the number of cycles up to failure N_f . The mean regression line was determined for a survival probability of 50% and is given by equation (9.7).

$$y_i = a_N + b \cdot x_i + \varepsilon \quad (9.7)$$

y_i	$\log N_f$
x_i	$\log \Delta\sigma$
a_N	Intersection on $\log \Delta\sigma$ axis
b	Regression coefficient
ε	Sum of unknown random errors

The constants in the equation a_N and b are determined by the least square method. The regression coefficient and the intersection on the $\log N$ axis were determined by equations (9.8) and (9.9) respectively.

$$b = \frac{n \cdot \sum (x_i \cdot y_i) - \sum x_i \cdot \sum y_i}{n \cdot \sum x_i^2 - (\sum x_i)^2} \quad (9.8)$$

$$a_N = \frac{1}{n} \cdot (\sum y_i - b \cdot \sum x_i) \quad (9.9)$$

where n is the number of specimens.

The stress range at 2 million cycles for a 50% survival probability $\Delta\sigma_{\text{mean}}$ was determined by equation (9.10). It represents the characteristic stress range of the mean strength curve of the data scatter.

$$\Delta\sigma_{\text{mean}} = 10^{x_{50\%}} \quad (9.10)$$

With

$$x_{50\%} = \frac{y_{50\%} - a_N}{b}$$

where

$$y_{50\%} = \log(2 \cdot 10^6)$$

The standard deviation defines the scatter between measured y_i and the calculated value by equation (9.7). The equation contains two random unknowns, which results in the degree of freedom of $n-2$ for a variable slope, b . In case of a constant slope b , only one unknown

remains in the regression line and the degree of freedom amounts to $n-1$. In accordance with this, the standard deviation is expressed in equation (9.11).

$$s^2 = \begin{cases} \frac{\sum [y_i - (a_N + b \cdot x_i)]^2}{n-2} & \text{if } b = \text{variable} \\ \frac{\sum [y_i - (a_N + b \cdot x_i)]^2}{n-1} & \text{if } b = \text{fixed} \end{cases} \quad (9.11)$$

Based on these values, the characteristic stress range $\Delta\sigma_c$ at 2 million cycles was calculated for a 75% confidence level of 95% probability of survival by the student t-distribution factor, $t_{0.95, n-x}$.

$$\Delta\sigma_c = 10^{x_{95\%}} \quad (9.12)$$

with

$$x_{95\%} = \frac{y_{50\%} - a_{95\%}}{b}$$

where $y_{95\%} = y_{50\%} - t_{0.95, n-x} \cdot s$ and $a_{95\%} = y_{95\%} - b \cdot x_{50\%}$.

For an appropriate statistical evaluation, according to Brozzetti et al. (1989), some requirements were defined. The results with $N_f > 5 \cdot 10^6$ cycles should be excluded from analysis and the regression coefficient, which represents the slope of the curve, need to be fixed to -3, the number of data points needs to be higher than 12 and the test results with runouts should not be included in the regression analysis. In the current study, not all test series contain more than 12 test results. For a small number of test data, conservative characteristic stress range $\Delta\sigma_c$ values of the fatigue strength are taken.

The analysis was performed for a fixed regression coefficient -3 and additionally for a fixed slope -5. It is assumed that the fatigue strength curves of very high strength steels tend to have a slope of -5. For the fixed slope analysis, the runouts were excluded. The regression coefficient was also determined by the least square method. The determination of the regression coefficient was conducted for two cases; with and without including the test data of runouts and the results with $N_f > 5 \cdot 10^6$, although the statistical analysis procedure recommends to exclude these results.

9.3 Evaluation of fatigue tests data

The fatigue test programme consisted of the repaired artificial crack in the base material and repaired V-shape welded connections made of very high strength steels. The results were evaluated for the test data from each steel grade separately if there were sufficient test data available for each of them.

The statistical analysis was performed on the raw data and the fatigue strength curves were determined from regression analysis. Fatigue strength curves were plotted for the mean, lower bound and upper bound of the data scatter. The test data are indicated on the curves. The lower bound curves of the data scatter were compared with the design curves of EN 1993-1-9 (2006).

In addition to this, the statistical analysis was performed on the test data, which was adjusted by the influence factors. Fatigue strength curves from the regression analysis were plotted for the mean, lower bound and upper bound of the data scatter, where the adjusted test data are indicated on the graphs. Furthermore, the mean curves of the analysis were compared with the curves of the prediction models. The models were separated for crack initiation and propagation life. In this section, the prediction curves are determined for the total fatigue life by the summation of the crack initiation and the propagation life with the constant fatigue endurance limit. Furthermore, the fatigue strength curves for the lower bound of data scatters of adjusted test data are compared with the fatigue design curves of EN 1993-1-9 (2006).

Moreover, the effectiveness of the repair procedure and the fatigue life extension after the repair can be examined by comparing the results of the repaired welded specimens with the results of the specimens in the as-welded condition. Pijpers (2011) studied the fatigue strength of welded connections made of very high strength steels. Focus was also put on the influence factors and the test data were adjusted accordingly. The results of that study are used for the comparison of the test results of the repaired specimens with the test results in the as-welded condition.

9.3.1 Repaired artificial crack in the base material

BR69x series

Table 9.1 shows the results of the statistical analysis on the raw and the adjusted fatigue test results of the repaired artificial crack in the base material made of S690.

Figure 9.1 presents the fatigue strength curves of the repaired artificial crack in the base material of S690 together with the results of the regression analysis, including mean, upper bound and lower bound of the data scatter. Figure 9.2 shows the fatigue strength curves of the adjusted test data and results of regression analysis with the mean, upper bound and lower bound of the data scatter. The influence factors for the crack initiation life were determined according to the prediction model developed by Hück et al., (1981). Figure 9.3 and Figure 9.4 indicate the fatigue strength curves for the mean, upper bound and lower bound of the adjusted data, where the influence factors of the crack initiation life were determined according to the FKM guideline for the nominal and the local stress approach respectively. Figure 9.5 compares the fatigue strength curves of the raw and the adjusted data with the lower bound of the data scatter for the fixed slope $m = -3$.

Table 9.1 Statistical analysis results on raw and adjusted data of BR69x series.

Series: BR69x series							
$\sigma_y = 790$ [MPa]							
	b = m	a_N	$\Delta\sigma_{\text{mean}}$	$\Delta\sigma_c$	s	$t_{0.95,n-x}$	n
Raw data	-3.05	12.97	179	154	0.11	1.90	9
	-3.00	12.87	178	154	0.10	1.86	9
	-5.00	17.58	208	181	0.16	1.86	9
Adjusted data	-2.86	11.95	113	95	0.11	1.90	9
Crack initiation life with Hück et al (1981).	-3.00	12.29	115	99	0.10	1.86	9
	-5.00	16.60	134	115	0.18	1.86	9
Adjusted data	-2.97	12.49	142	120	0.11	1.90	9
Crack initiation life with FKM nominal	-3.00	12.57	142	123	0.10	1.86	9
	-5.00	17.09	166	144	0.17	1.86	9
Adjusted data	-2.90	12.38	149	125	0.12	1.90	9
Crack initiation with FKM local	-3.00	12.63	151	129	0.11	1.86	9
	-5.00	17.20	176	151	0.18	1.86	9

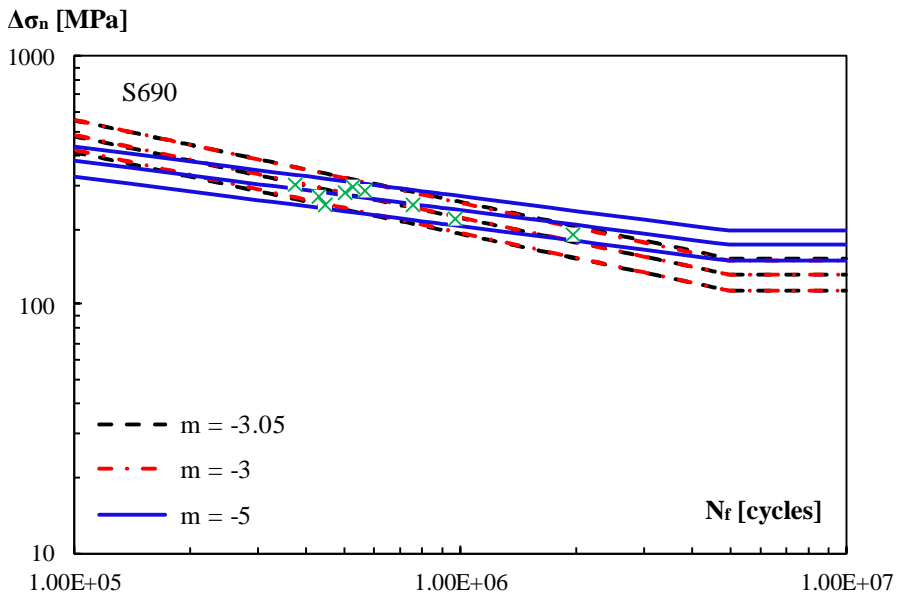


Figure 9.1 Raw fatigue results of BR69x series with mean, upper bound and lower bound of the data scatter.

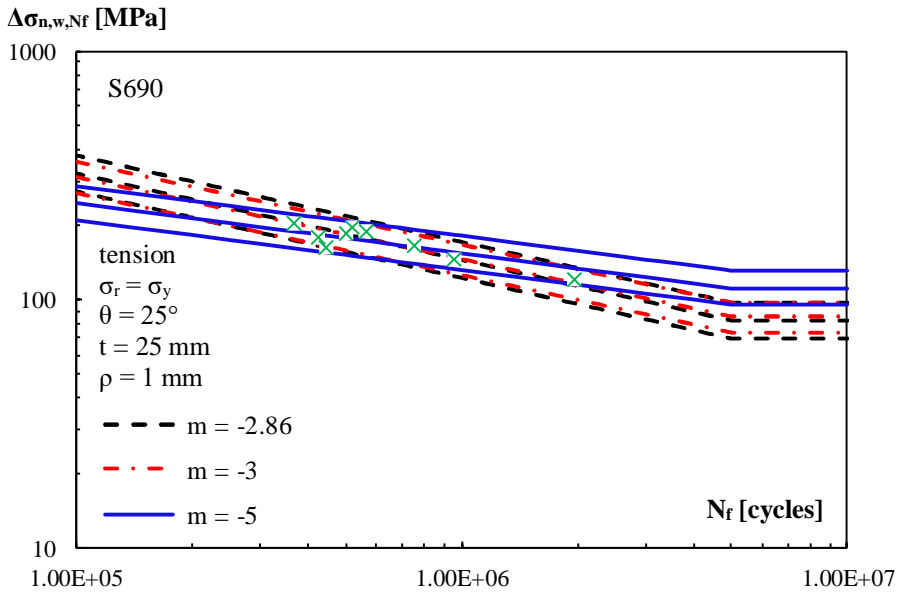


Figure 9.2 Adjusted fatigue results of BR69x series with mean, upper bound and lower bound of the data scatter; crack initiation life adjusted according to Hüeck et al., (1981).

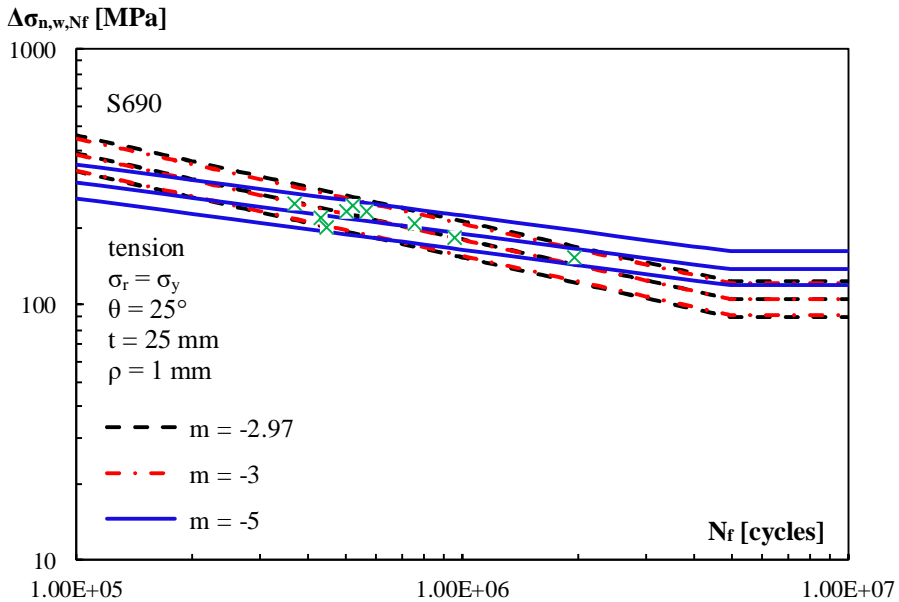


Figure 9.3 Adjusted fatigue results of BR69x series with mean, upper bound and lower bound of the data scatter; crack initiation life adjusted with the nominal stress approach of the FKM guideline.

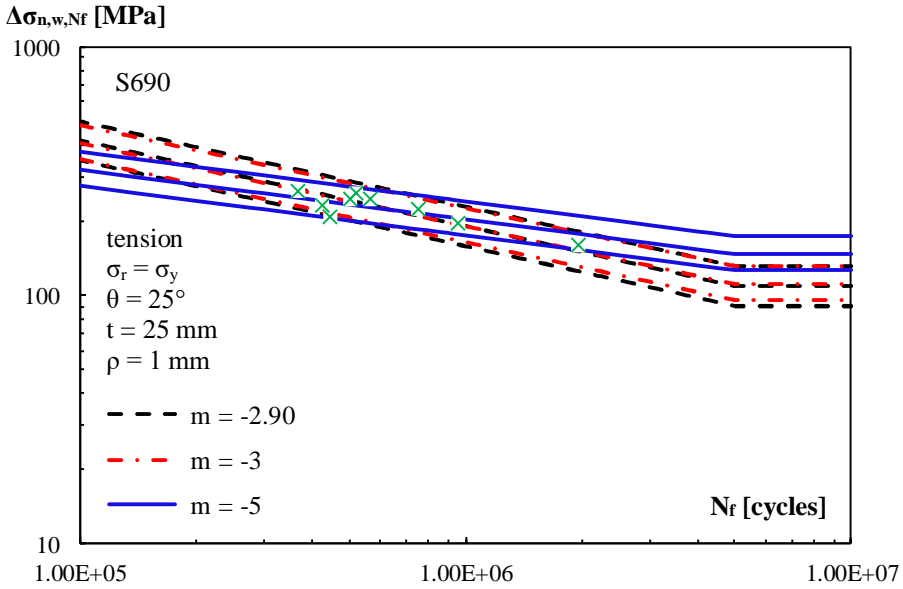


Figure 9.4 Adjusted fatigue results of BR69x series with mean, upper bound and lower bound of the data scatter; crack initiation life adjusted with the local stress approach of the FKM guideline.

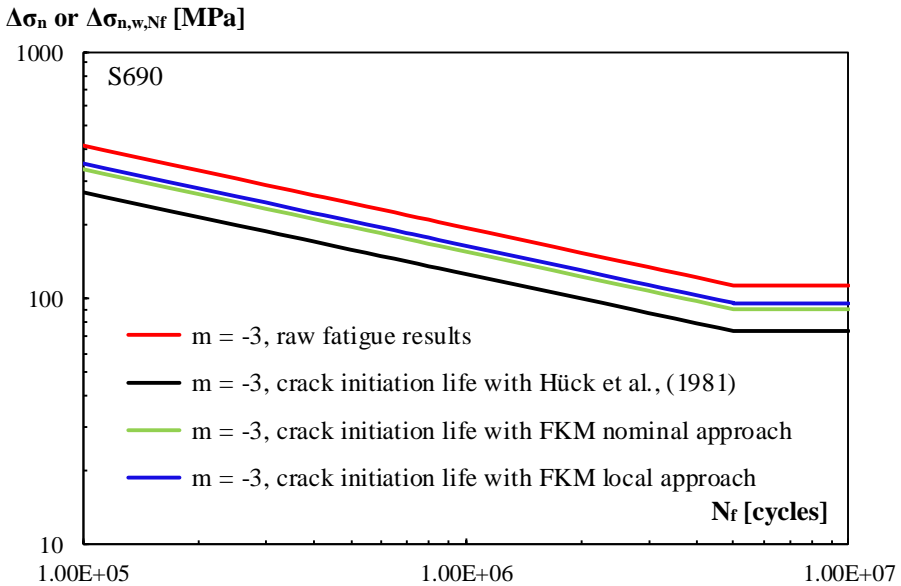


Figure 9.5 Comparison of the raw and the adjusted fatigue results with the lower bound of the data scatter for fixed slope $m = -3$.

Figure 9.6 shows the comparison between the mean curves of the statistical analysis on adjusted data and the prediction curve. The crack initiation life of the prediction curve was determined according to the analytical approach of Hück et al., (1981) and the fatigue test data adjusted with the influence factors of this model for crack initiation life. For $m = -5$, the prediction model is close to the mean curve of the adjusted test data. The fatigue limit of the prediction model is overestimated as compared to the mean curve for $m = -3$ and for $m = -2.85$. However, the slope of the prediction curve is much smaller than $m = -3$. Figure 9.7 compares the mean curves from the statistical analysis of the adjusted test data with the prediction model, where the nominal stress approach of the FKM guideline was used for the fatigue crack initiation life prediction. The prediction curve is conservative in comparison with the mean curves of the statistical analysis. The prediction curve is located at below the mean curves for $m = -3$ and for $m = -2.85$. Figure 9.8 presents the mean curves of the statistical analysis on the adjusted data compared with the prediction model where the crack initiation life is determined according to the local approach of the FKM guideline. The prediction model overestimates the fatigue strength of the specimens and the fatigue limit of the prediction model is very close to the mean curves for $m = -2.90$ and $m = -3$.

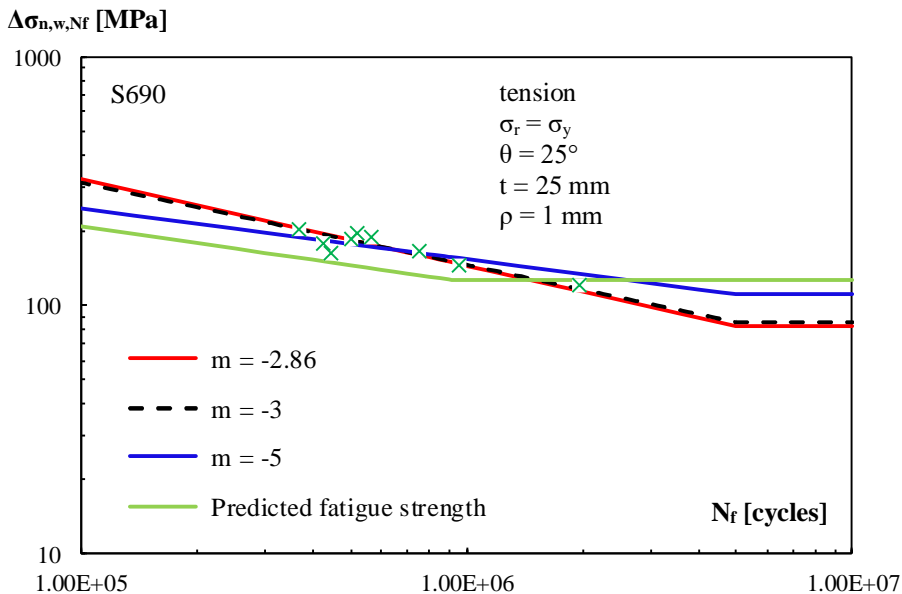


Figure 9.6 Adjusted test data of BR69x series with mean curves compared with the prediction model, crack initiation life determined according to Hück et al., (1981).

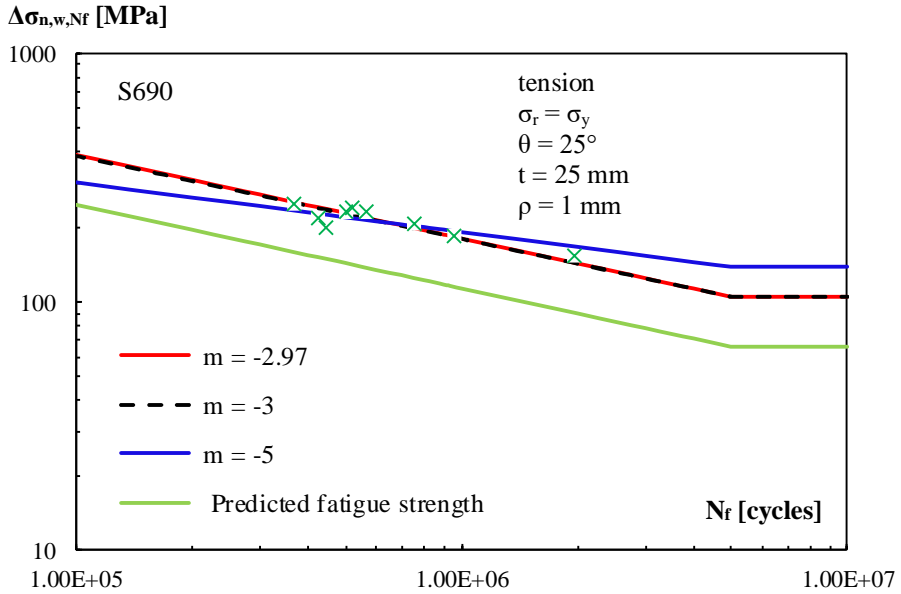


Figure 9.7 Adjusted test data of BR69x series with mean curves compared with prediction model, crack initiation life according to the nominal stress approach of the FKM guideline.

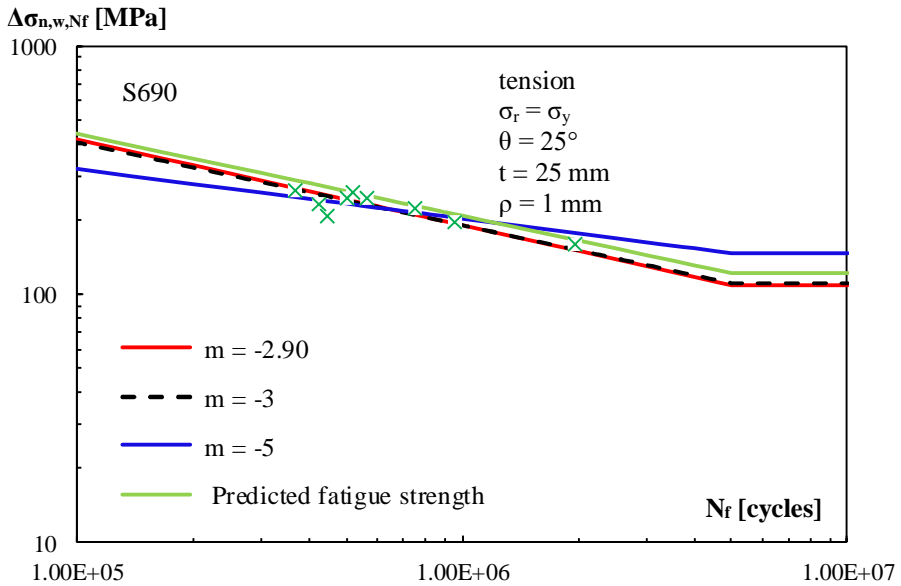


Figure 9.8 Adjusted test data of BR69x series with mean curves compared with prediction model, crack initiation life according the local stress approach of the FKM guideline.

Figure 9.9 compares the lower bound curves of the statistical analysis on the raw data of the BR69x series to the detail category 80 of EN 1993-1-9 (2006). The design curve of EN 1993-1-9 (2006) is found to be conservative. With $m = -3.05$, $\Delta\sigma_{\text{mean}} = 179$ MPa, $\Delta\sigma_c = 154$ MPa, with $m = -3$, $\Delta\sigma_{\text{mean}} = 178$ MPa, $\Delta\sigma_c = 154$ MPa.

Figure 9.10 shows the lower bound curves of the data scatter of the adjusted test data as compared to the detail category 80 of EN 1993-1-9 (2006). The test data were adjusted with the influence factors of the analytical approach of Hück et al., (1981) for fatigue crack initiation life. The fatigue strength curves of the test data are close to the design curve of EN 1993-1-9 (2006). With $m = -2.86$, $\Delta\sigma_{\text{mean}} = 113$ MPa, $\Delta\sigma_c = 95$ MPa, with $m = -3$, $\Delta\sigma_{\text{mean}} = 115$ MPa, $\Delta\sigma_c = 99$ MPa.

Figure 9.11 presents the lower bound curves of the data scatter of the adjusted test data compared with the detail category 80 of EN 1993-1-9 (2006). The influence factors for crack initiation life were determined according to the nominal stress approach of the FKM guideline. With $m = -2.97$, $\Delta\sigma_{\text{mean}} = 142$ MPa, $\Delta\sigma_c = 120$ MPa, with $m = -3$, $\Delta\sigma_{\text{mean}} = 142$ MPa, $\Delta\sigma_c = 123$ MPa. Figure 9.12 indicates the comparison between the lower bound curves of the adjusted data scatter and the detail category 80 of EN 1993-1-9 (2006). The crack initiation life was adjusted according to the local stress approach of the FKM guideline. With $m = -2.90$, $\Delta\sigma_{\text{mean}} = 149$ MPa, $\Delta\sigma_c = 125$ MPa, with $m = -3$, $\Delta\sigma_{\text{mean}} = 151$ MPa, $\Delta\sigma_c = 129$ MPa. The fatigue strength curves of the adjusted data for the nominal and the local stress approach are located above of the detail category 80 of EN 1993-1-9 (2006).

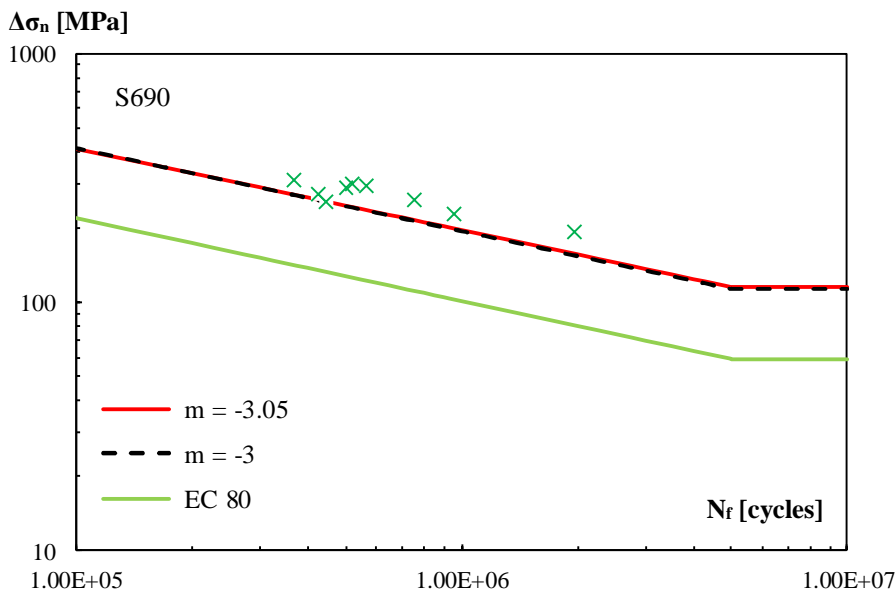


Figure 9.9 Raw fatigue test results of BR69x series with lower bound of the data scatter compared with the detail category 80 of EN 1993-1-9 (2006).

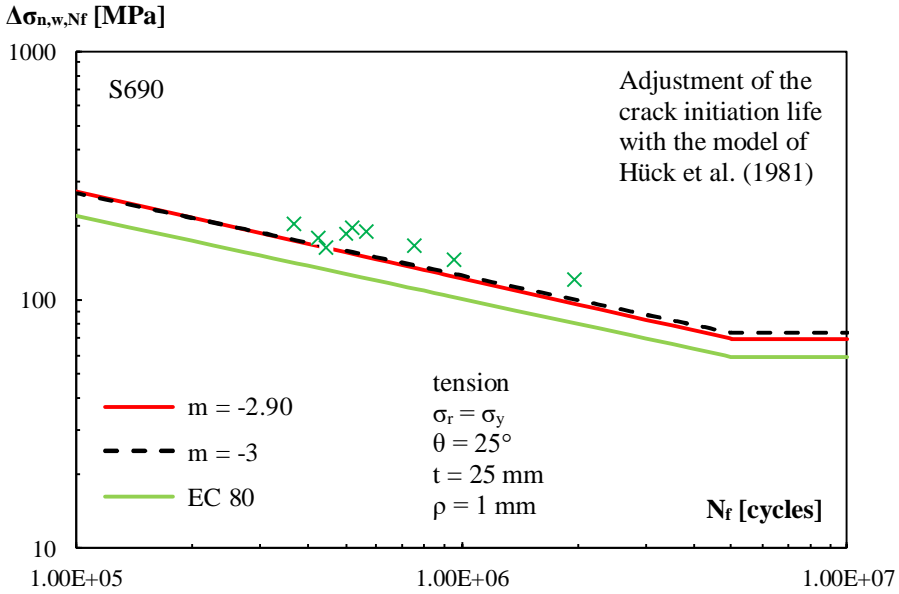


Figure 9.10 Adjusted fatigue test results of BR69x series with lower bound of the data scatter compared with the detail category 80 of EN 1993-1-9 (2006).

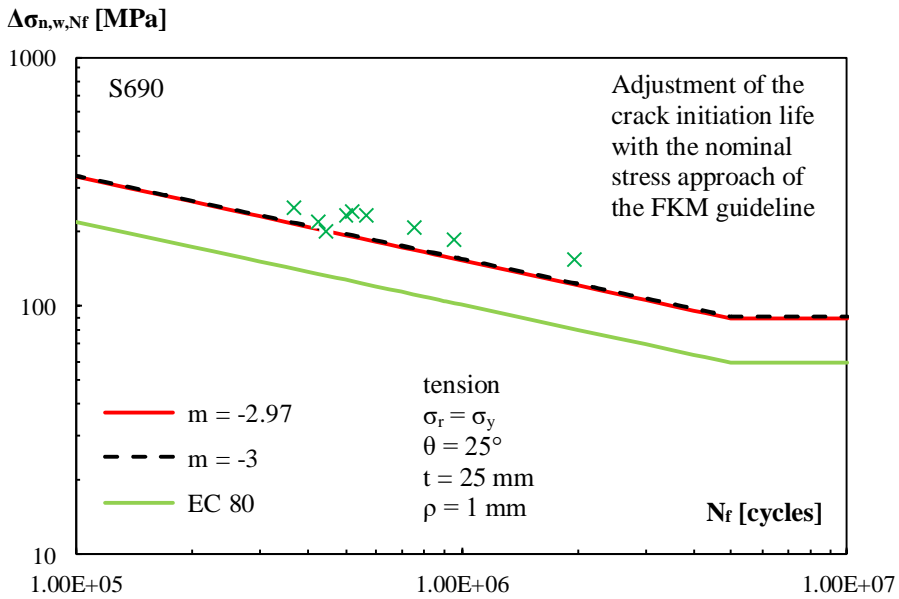


Figure 9.11 Adjusted fatigue test results of BR69x series with lower bound of the data scatter compared with the detail category 80 of EN 1993-1-9 (2006).

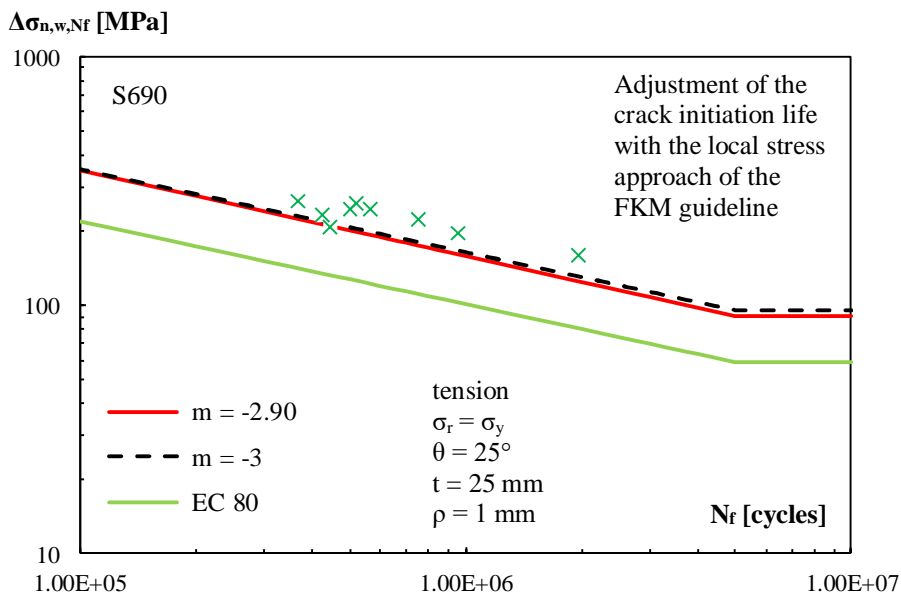


Figure 9.12 Adjusted fatigue test results of BR69x series with lower bound of the data scatter compared with the detail category 80 of EN 1993-1-9 (2006).

BR89x series

Table 9.2 shows the results of the statistical analysis on the raw and the adjusted fatigue test data of the repaired artificial crack in the base material of S890. Figure 9.13 presents the fatigue strength curves for the raw test data of the repaired artificial crack in the base material of S890 and the results of the regression analysis with the mean, upper bound and lower bound curves of the data scatter. Figure 9.14 shows the fatigue strength curves of the adjusted test data and the results of regression analysis with the mean, upper bound and lower bound curves of the data scatter. The crack initiation life of the fatigue test data was adjusted with the determined influence factors according to the analytical approach of Hück et al., (1981). In addition, the crack initiation life of the test results was adjusted with the influence factors determined according to the nominal and the local stress approach of the FKM guideline. The fatigue strength curves of the adjusted data according to these approaches are indicated by Figure 9.15 and Figure 9.16 respectively. In both figures, the fatigue strength curves are given for the mean, upper bound and lower bounds of the data scatter. The free slope of the fatigue strength curves was determined for both with and without inclusion of the runout data. The fatigue strength curves for the fixed slopes were determined without the runout data. Figure 9.17 shows the lower bound curves of the data scatter data with fixed slope $m = -3$ for the raw and adjusted data.

Table 9.2 Statistical analysis results on raw and adjusted data of BR89x series.

Series: BR89x series							
$\sigma_y = 985$ [MPa]							
	b = m	a_N	$\Delta\sigma_{\text{mean}}$	$\Delta\sigma_c$	s	$t_{0.95,n-x}$	n
Raw data	-5.46	18.76	225	191	0.20	1.90	9
	-1.67	9.57	113	90	0.09	1.94	8
	-3.00	12.84	173	151	0.09	1.90	8
	-5.00	17.69	215	190	0.14	1.90	8
Adjusted data	-5.40	17.38	137	113	0.23	1.90	9
Crack initiation life with Hück et al (1981).	-1.71	9.29	70	56	0.09	1.94	8
	-3.00	12.20	105	92	0.09	1.90	8
	-5.00	16.61	131	115	0.14	1.90	8
Adjusted data	-5.64	18.57	183	150	0.26	1.90	9
Crack initiation life with FKM nominal	-1.88	9.91	101	83	0.08	1.94	8
	-3.00	12.57	139	123	0.09	1.90	8
	-5.00	17.23	172	154	0.13	1.90	8
Adjusted data	-4.34	15.53	181	134	0.30	1.90	9
Crack initiation life with FKM local	-1.99	10.23	112	93	0.08	1.94	8
	-3.00	12.64	147	130	0.08	1.90	8
	-5.00	17.36	182	163	0.12	1.90	8

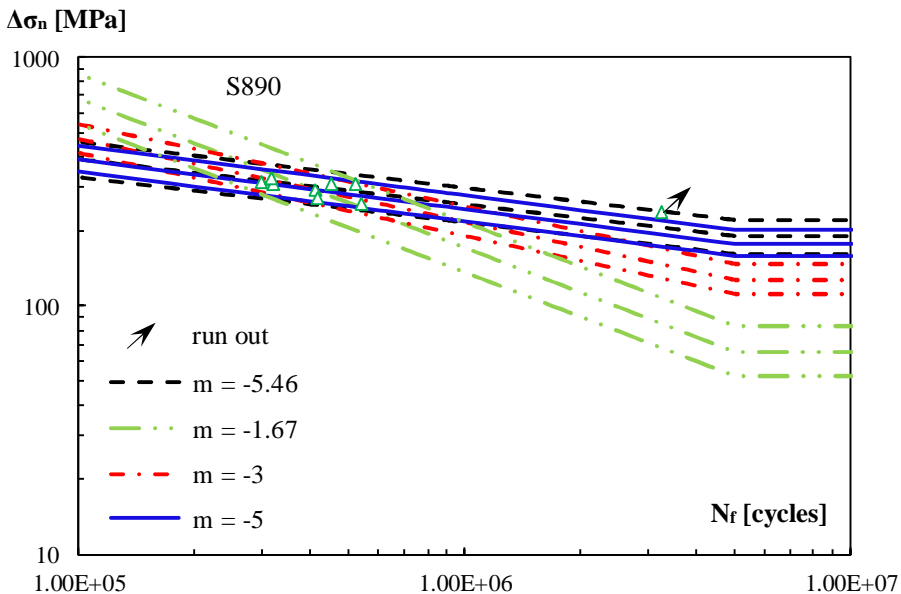


Figure 9.13 Raw fatigue results of BR89x series with mean, upper bound and lower bound of the data scatter.

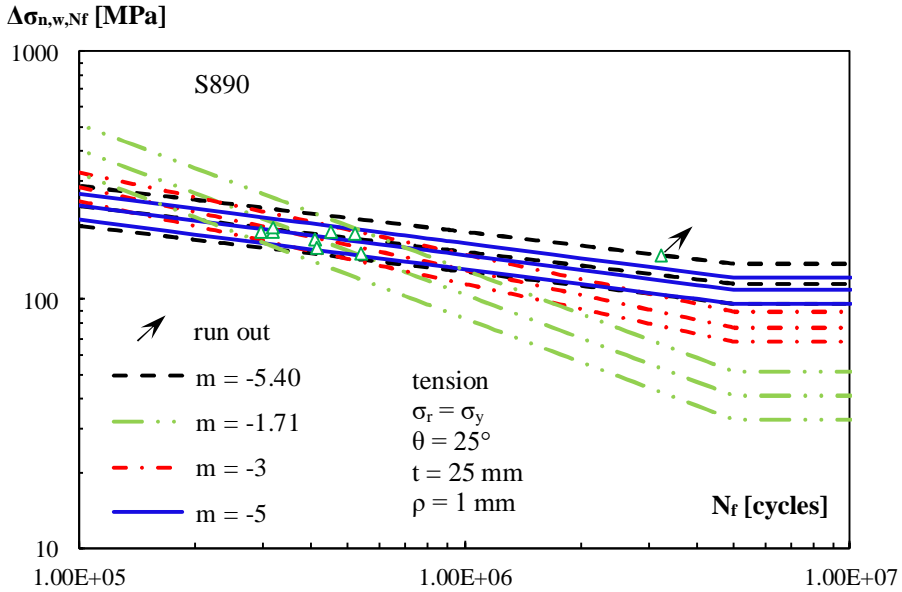


Figure 9.14 Adjusted fatigue results of BR89x series with mean, upper bound and lower bound of the data scatter; crack initiation life adjusted according to Hück et al., (1981).

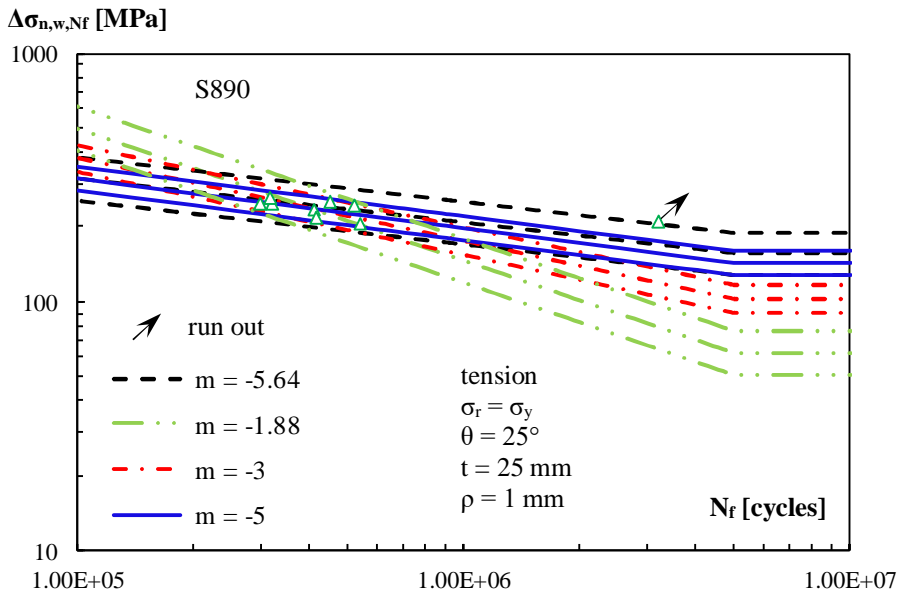


Figure 9.15 Adjusted fatigue results of BR89x series with mean, upper bound and lower bound of the data scatter; crack initiation life adjusted with the nominal stress approach of the FKM guideline.

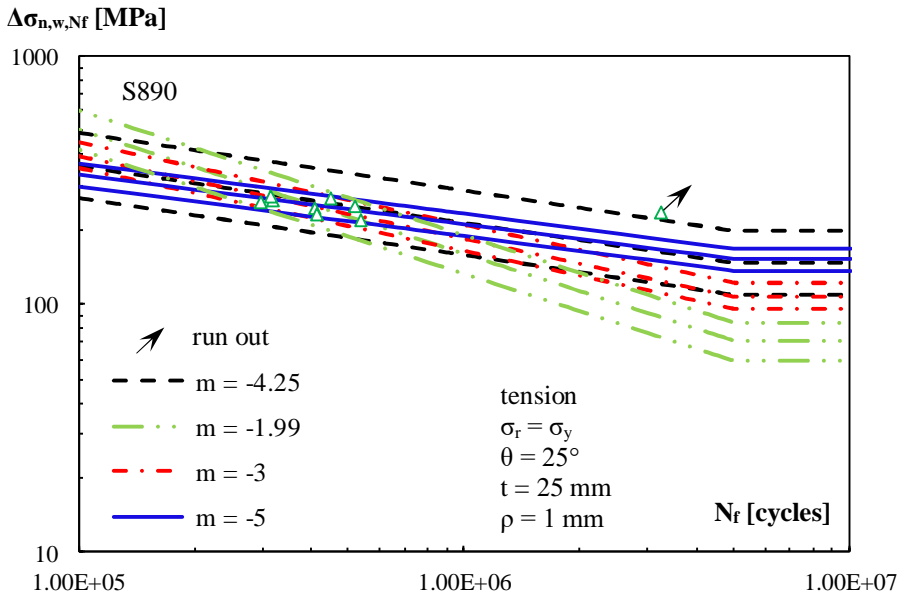


Figure 9.16 Adjusted fatigue results of BR89x series with mean, upper bound and lower bound of the data scatter; crack initiation life adjusted with the local stress approach of the FKM guideline.

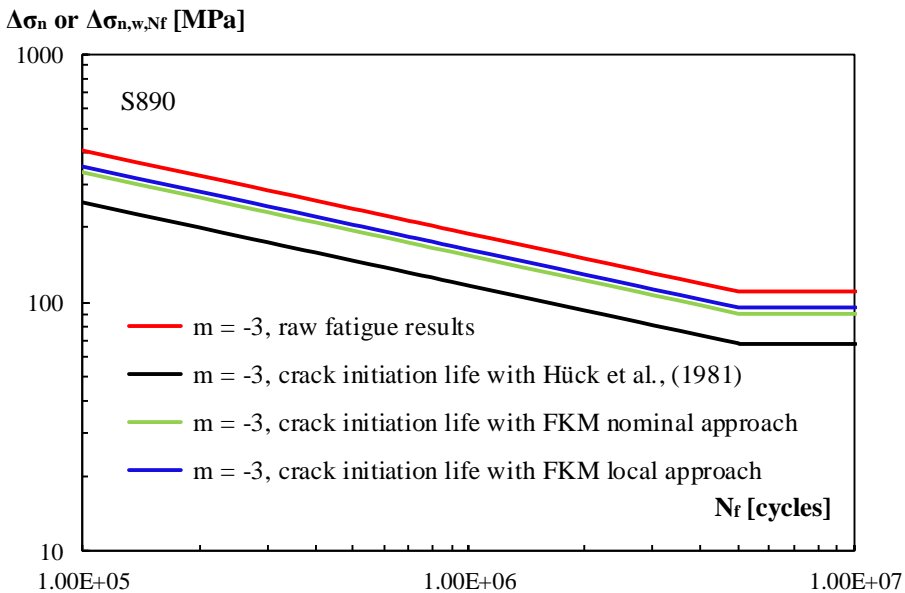


Figure 9.17 Comparison of the raw and the adjusted fatigue results with the lower bound of the data scatter for fixed slope $m = -3$.

Figure 9.18 compares the prediction model with the mean fatigue strength curves of the statistical analysis on the adjusted test data of the BR89x series. In the prediction model, fatigue crack initiation life is estimated with the analytical approach of Hück et al., (1981). The fatigue crack initiation life of the test data was adjusted with the influence factors determined by this approach. The fatigue limit of the prediction model was very close to the fatigue limit of the mean curve for $m = -5$. However, the cut-off limit of the mean curves is different than the cut-off limit of the prediction model. In the low cycle regime, the prediction model indicates a reasonable match with the mean curves for $m = -5$ and for $m = -5.40$. Figure 9.19 shows the comparison between the mean curves from the statistical analysis on the adjusted test data and the prediction model, where the crack initiation life is determined by using the nominal stress approach of the FKM guideline. The prediction model is conservative compared with the mean fatigue strength curve for $m = -3$. For the mean curves of $m = -5$ and $m = -5.62$, the prediction model was conservative for the high cycle fatigue region. However, the slope of the prediction curve, $m = -3$, was much larger than the slope of these mean curves. Figure 9.20 presents the mean curves from the statistical analysis on the adjusted test data and the prediction model, where the fatigue crack initiation life was determined with the local approach of the FKM guideline. The prediction model overestimates the fatigue strength of the specimens for the low cycles region.

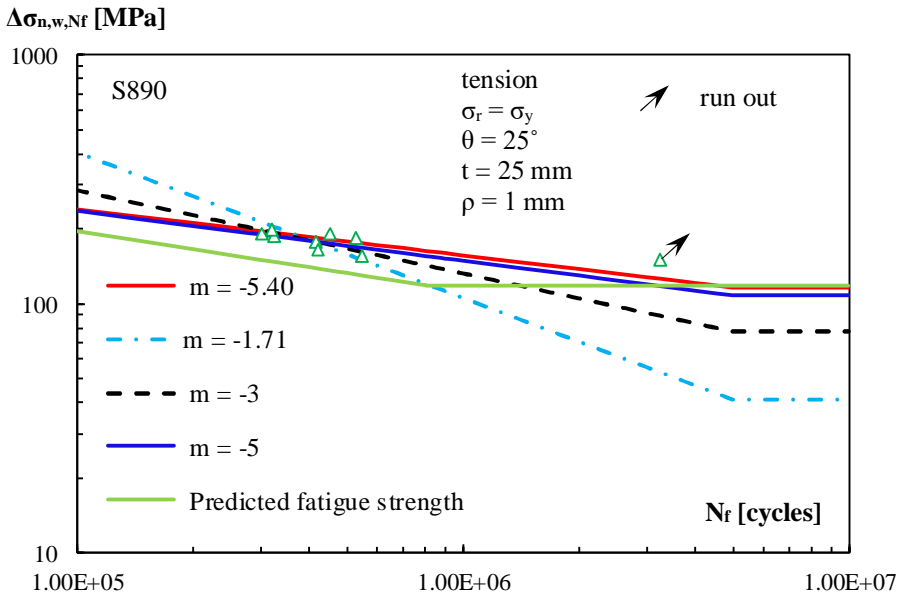


Figure 9.18 Adjusted test data of BR89x series with mean curves compared with the prediction model, crack initiation life determined according to Hück et al., (1981).

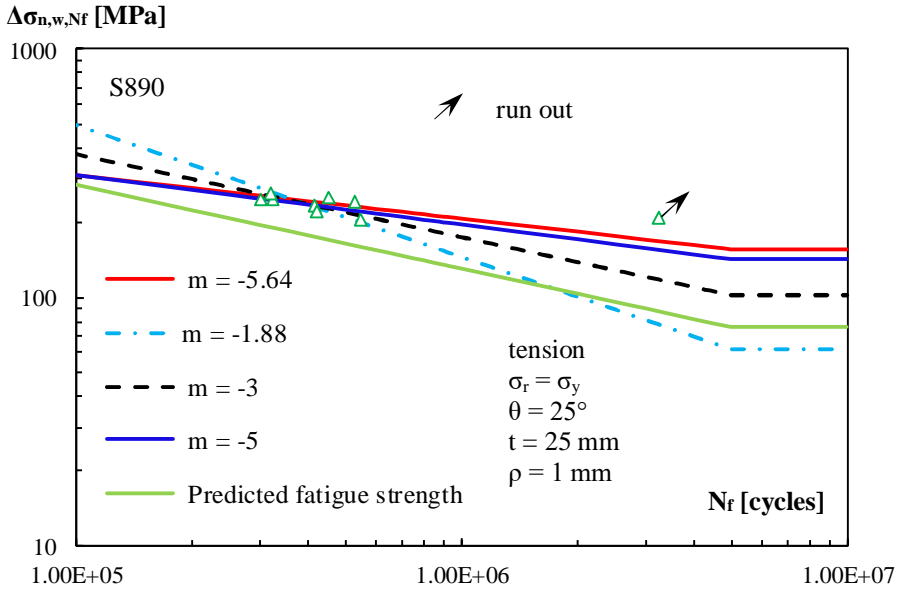


Figure 9.19 Adjusted test data of BR89x series with mean curves compared with prediction model, crack initiation life according to the nominal stress approach of the FKM guideline.

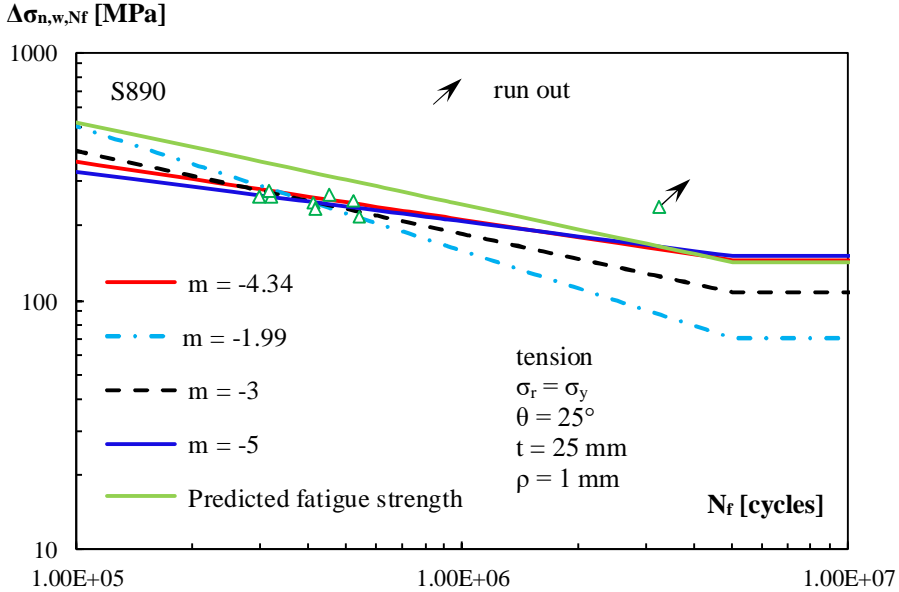


Figure 9.20 Adjusted test data of BR89x series with the mean curves compared with the prediction model, crack initiation life with the local stress approach of the FKM guideline.

Figure 9.21 presents the lower bound curves of the statistical analysis on the raw data of BR89x series compared with the detail category 80 of EN 1993-1-9 (2006). The design curve of EN 1993-1-9 (2006) is very conservative for all lower bound curves with different slopes. With $m = -5.46$, $\Delta\sigma_{\text{mean}} = 225$ MPa, $\Delta\sigma_c = 191$ MPa, with, $m = -3$, $\Delta\sigma_{\text{mean}} = 173$ MPa, $\Delta\sigma_c = 151$ MPa.

Figure 9.22 compares the lower bound curves of the adjusted test data of BR89x series with the detail category 80 of EN 1993-1-9 (2006). The crack initiation life of the test data was adjusted with the determined influence factors according to Hück et al., (1981). The design curve of EN 1993-1-9 (2006) is located underneath the lower bound curves of the data scatter. With $m = -5.40$, $\Delta\sigma_{\text{mean}} = 137$ MPa, $\Delta\sigma_c = 113$ MPa, with, $m = -3$, $\Delta\sigma_{\text{mean}} = 105$ MPa, $\Delta\sigma_c = 92$ MPa.

Figure 9.23 shows the lower bound curves of the data scatter of the adjusted test data compared with the detail category 80 of EN 1993-1-9 (2006). The crack initiation life of the test data was adjusted with the influence factors determined according to the nominal stress approach of the FKM guideline. With $m = -5.64$, $\Delta\sigma_{\text{mean}} = 183$ MPa, $\Delta\sigma_c = 150$ MPa, with, $m = -3$, $\Delta\sigma_{\text{mean}} = 139$ MPa, $\Delta\sigma_c = 123$ MPa.

Figure 9.24 indicates the comparison between the lower bound curves of the data scatter of the adjusted test data and the detail category 80 of EN 1993-1-9 (2006). The crack initiation life of the test data was adjusted according to the local stress approach of the FKM guideline. With $m = -4.34$, $\Delta\sigma_{\text{mean}} = 181$ MPa, $\Delta\sigma_c = 134$ MPa, with, $m = -3$, $\Delta\sigma_{\text{mean}} = 147$ MPa, $\Delta\sigma_c = 130$ MPa. The lower bound curves of the adjusted data according to both approaches of the FKM guideline are located at above of the design curve of EN 1993-1-9 (2006).

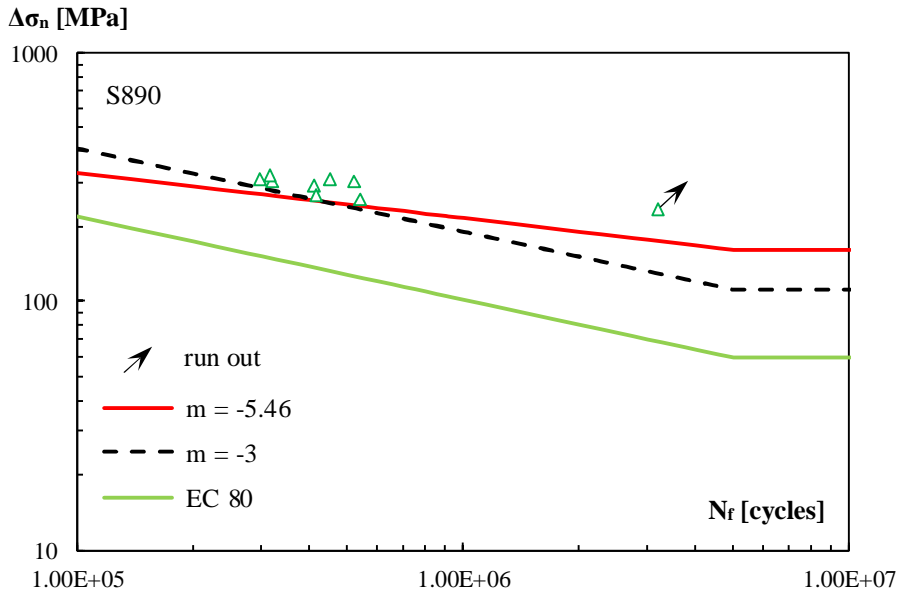


Figure 9.21 Raw fatigue test results of BR89x series with the lower bound of the data scatter compared with the detail category 80 of EN 1993-1-9 (2006).

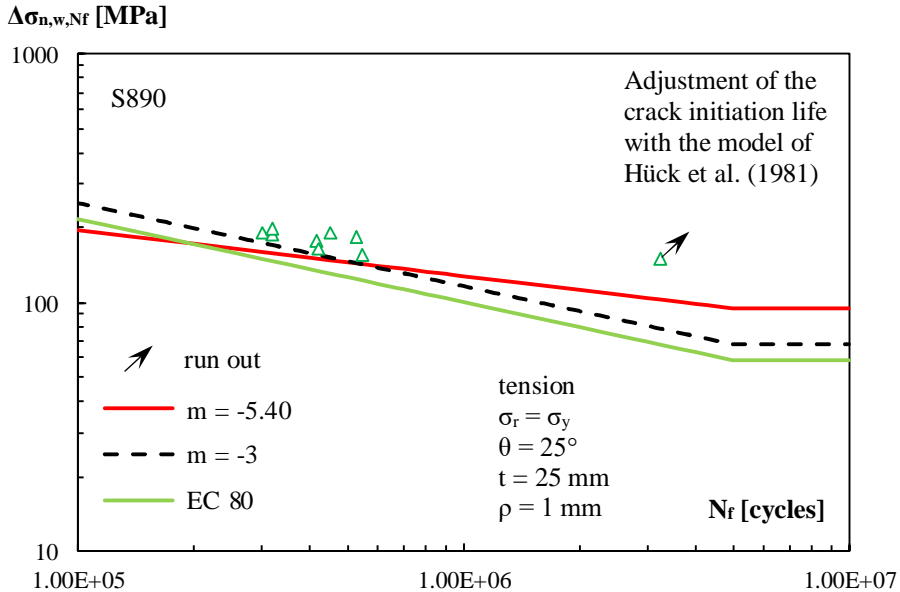


Figure 9.22 Adjusted fatigue test results of BR89x series with the lower bound of the data scatter compared with the detail category 80 of EN 1993-1-9 (2006).

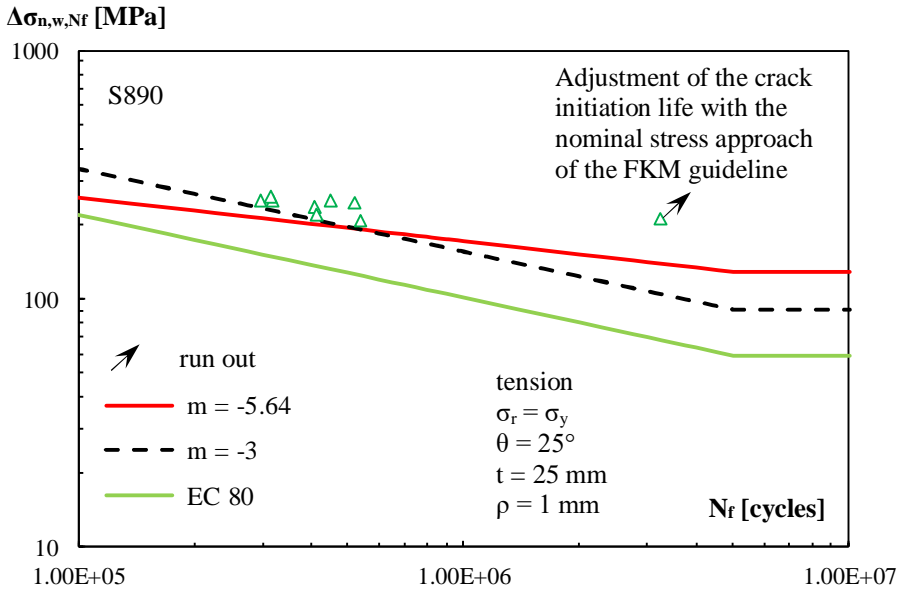


Figure 9.23 Adjusted fatigue test results of BR89x series with the lower bound of the data scatter compared with the detail category 80 of EN 1993-1-9 (2006).

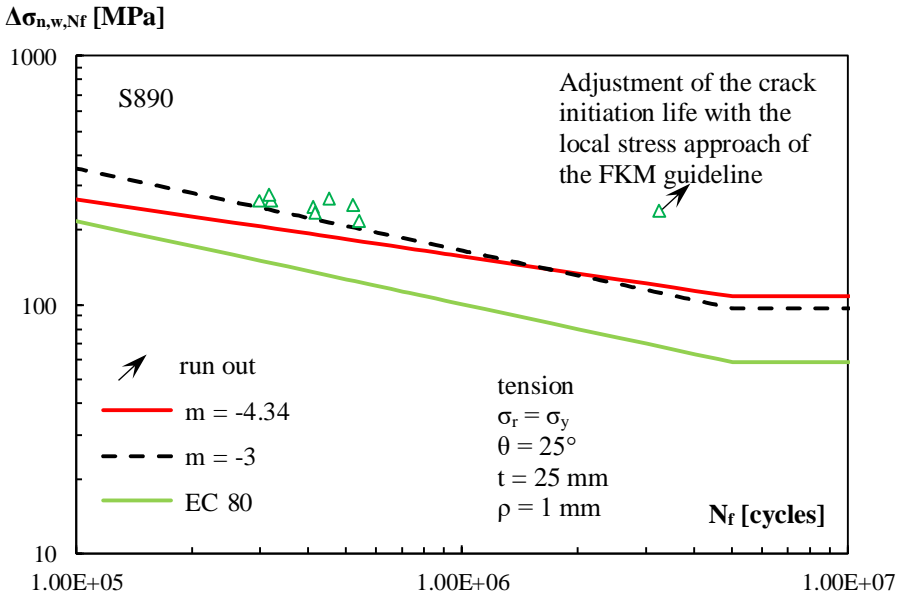


Figure 9.24 Adjusted fatigue test results of BR89x series with the lowed bound of the data scatter compared with the detail category 80 of EN 1993-1-9 (2006).

In the current study, the design curves of EN 1993-1-9 (2006) are used as reference curves for the comparison of the fatigue strength curves of the test. However, the design curves of EN 1993-1-9 (2006) are not dependent on the yield strength of the material and only specified for the connection types. Since the connection type of the BR69x and BR89x test series are similar, the test data of both series were combined and the statistical analyses were performed on the entire test data of both series. Table 9.3 shows the results of the statistical analysis on the combined raw and adjusted test data of the repaired artificial crack in the base material of S690 and S890. Figure 9.25 shows the fatigue strength curves of the repaired artificial crack in the base material, the results of regression analysis with the mean, the upper bound and lower bound curves of the data scatter. Figure 9.26 presents the fatigue results of the adjusted test data with the mean, upper bound and lower bound of the data scatter. The adjustment of the crack initiation life was made with the influence factors determined according to the analytical model of Hück et al., (1981). Figure 9.27 and Figure 9.28 indicate the fatigue strength curves of the adjusted data where the crack initiation life was adjusted with the influence factors of the nominal and local stress approach of the FKM guideline respectively. The fatigue strength curves are indicated with the mean, upper bound and lower bound curves of the data scatter. Figure 9.29 presents the lower bound curves of the data scatter data with fixed slope $m = -3$ for the raw and adjusted data.

Table 9.3 Statistical analysis results on the combined test data of BR test series.

Series: BRseries							
$\sigma_y = 790$ [MPa], $\sigma_y = 985$ [MPa]							
	m	a_N	$\Delta\sigma_{\text{mean}}$	$\Delta\sigma_c$	s	$t_{0.95,n-x}$	n
Raw data	-3.62	14.28	194	161	0.17	1.75	18
	-2.96	12.77	175	153	0.10	1.75	17
	-3.00	12.87	176	155	0.09	1.746	17
	-5.00	17.65	211	186	0.15	1.746	17
Adjusted data	-3.58	13.44	121	99	0.18	1.75	18
Crack initiation life with Hück et al (1981).	-2.91	12.03	109	93	0.11	1.75	17
	-3.00	12.23	110	95	0.11	1.75	17
	-5.00	16.63	132	116	0.16	1.75	17
Adjusted data	-3.31	13.16	151	119	0.20	1.75	18
Crack initiation life with FKM nominal	-2.96	12.48	140	122	0.10	1.75	17
	-3.00	12.58	141	124	0.10	1.75	17
	-5.00	17.17	169	149	0.15	1.75	17
Adjusted data	-2.92	12.28	152	113	0.22	1.75	18
Crack initiation life with FKM local	-2.94	12.51	148	129	0.10	1.75	17
	-3.00	12.65	149	131	0.10	1.75	17
	-5.00	17.29	179	158	0.16	1.75	17

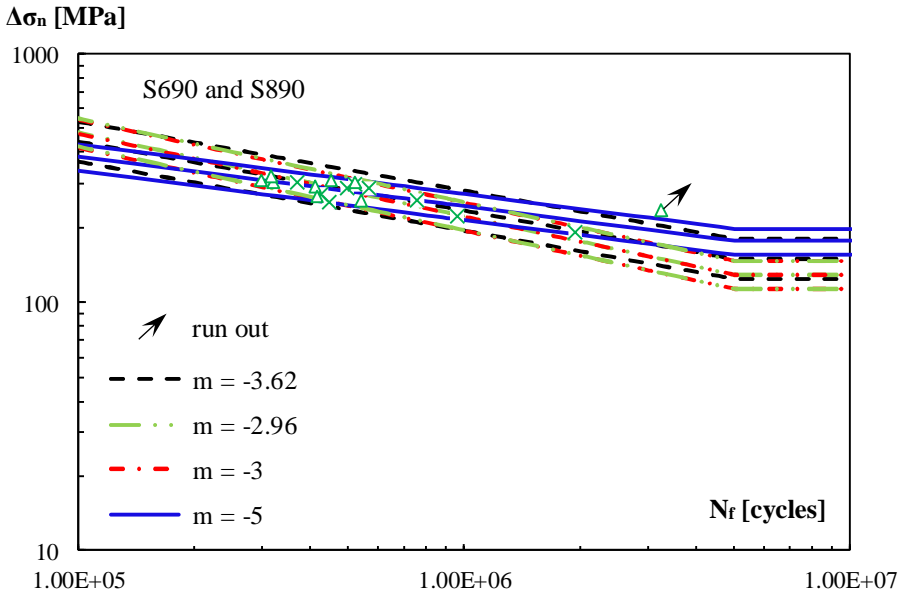


Figure 9.25 Raw fatigue results of BR series with mean, upper bound and lower bound of the data scatter.

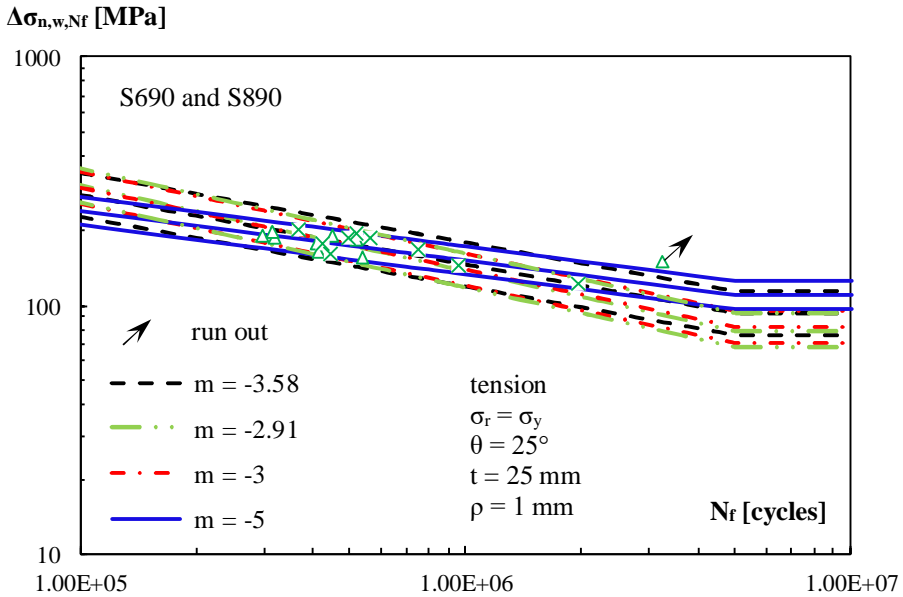


Figure 9.26 Adjusted fatigue results of BR series with mean, upper bound and lower bound of the data scatter; crack initiation life adjusted according to Hüeck et al., (1981).

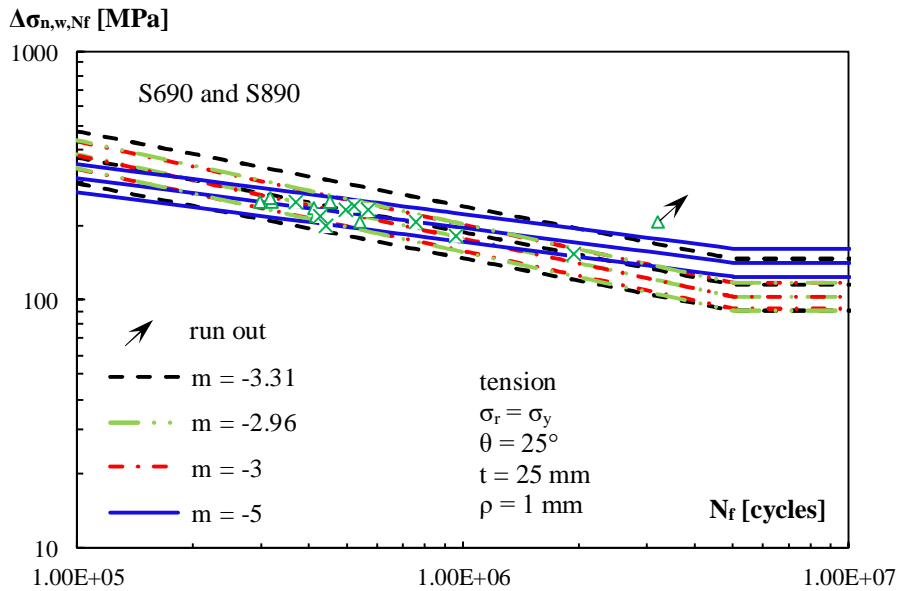


Figure 9.27 Adjusted fatigue results of BR series with mean, upper bound and lower bound of the data scatter; crack initiation life adjusted with the nominal stress approach of the FKM guideline

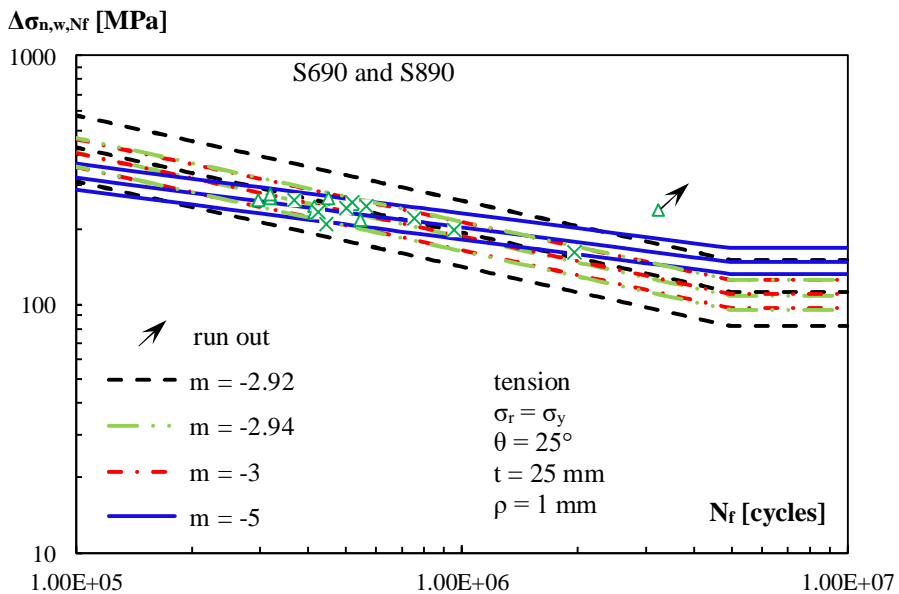


Figure 9.28 Adjusted fatigue results of BR series with mean, upper bound and lower bound of the data scatter; crack initiation life adjusted with the local stress approach of the FKM guideline.

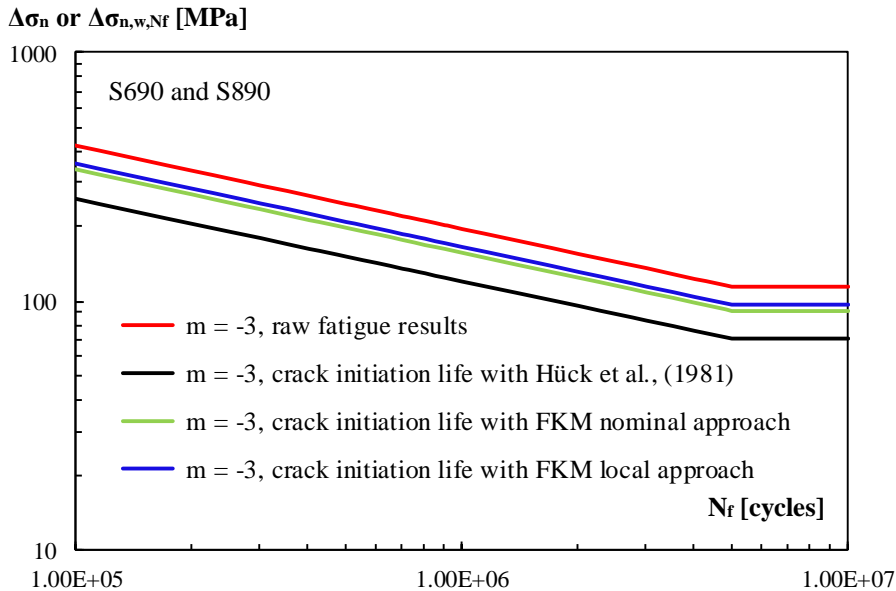


Figure 9.29 Comparison of the raw and the adjusted fatigue results with the lower bound of the data scatter for fixed slope $m = -3$.

Figure 9.30 shows the lower bound curves of the statistical analysis on the raw data of combined test results of the repaired artificial crack in the base material of S690 and S890 compared with the detail category 80 of EN 1993-1-9 (2006). The design curve of EN 1993-1-9 (2006) is very conservative, compared to the test results. With $m = -3.62$, $\Delta\sigma_{\text{mean}} = 194$ MPa, $\Delta\sigma_c = 161$ MPa, with, $m = -3$, $\Delta\sigma_{\text{mean}} = 176$ MPa, $\Delta\sigma_c = 155$ MPa.

Figure 9.31 compares the lower bound curves of the adjusted data with the detail category 80 of EN 1993-1-9 (2006). The fatigue crack initiation life of the test data was adjusted according to the model of Hück et al., (1981). The lower bound curve with $m = -3$ is close to the design curve 80 of EN 1993-1-9 (2006). With $m = -3.58$, $\Delta\sigma_{\text{mean}} = 121$ MPa, $\Delta\sigma_c = 99$ MPa, with, $m = -3$, $\Delta\sigma_{\text{mean}} = 110$ MPa, $\Delta\sigma_c = 95$ MPa.

Figure 9.32 presents the comparison between the lower bound curves from the statistical analysis on the adjusted data of BR series and the detail category 80 of EN 1993-1-9 (2006). The adjustment of the crack initiation life of the data was made with the determined influence factors by using the nominal approach of the FKM guideline. The test data show high fatigue strength compared to the design curve of EN 1993-1-9 (2006). With $m = -3.31$, $\Delta\sigma_{\text{mean}} = 151$ MPa, $\Delta\sigma_c = 119$ MPa, with, $m = -3$, $\Delta\sigma_{\text{mean}} = 141$ MPa, $\Delta\sigma_c = 124$ MPa. Figure 9.33 indicates a comparison of the detail category 80 of EN 1993-1-9 (2006) with the lower bound curves of the adjusted data, where the crack initiation life was adjusted according to the local stress approach of the FKM guideline. With $m = -2.92$, $\Delta\sigma_{\text{mean}} = 152$ MPa, $\Delta\sigma_c = 113$ MPa, with $m = -3$, $\Delta\sigma_{\text{mean}} = 149$ MPa, $\Delta\sigma_c = 131$ MPa.

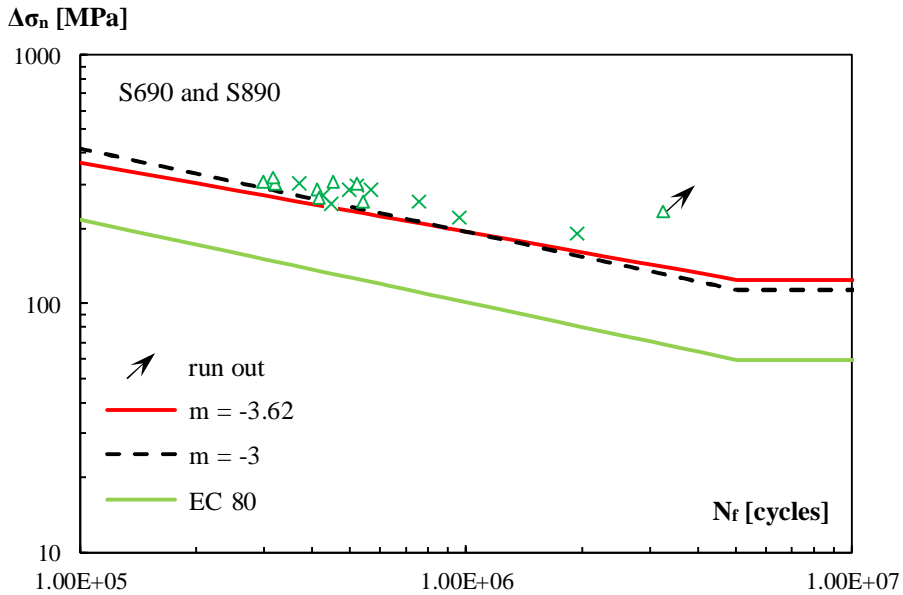


Figure 9.30 Raw fatigue test results of BR series with the lower bound of the data scatter compared with the detail category 80 of EN 1993-1-9 (2006).

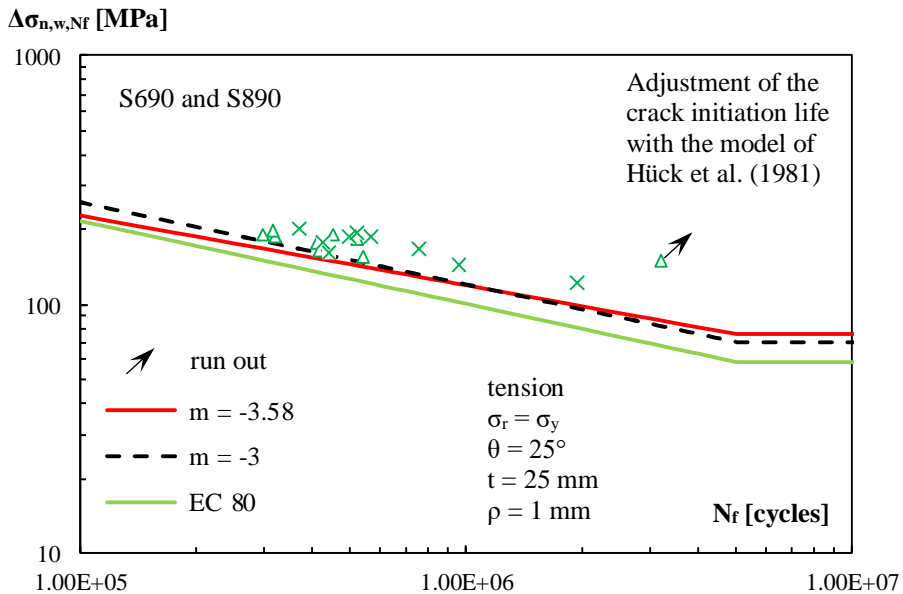


Figure 9.31 Adjusted fatigue test results of BR series with the lower bound of the data scatter compared with the detail category 80 of EN 1993-1-9 (2006).

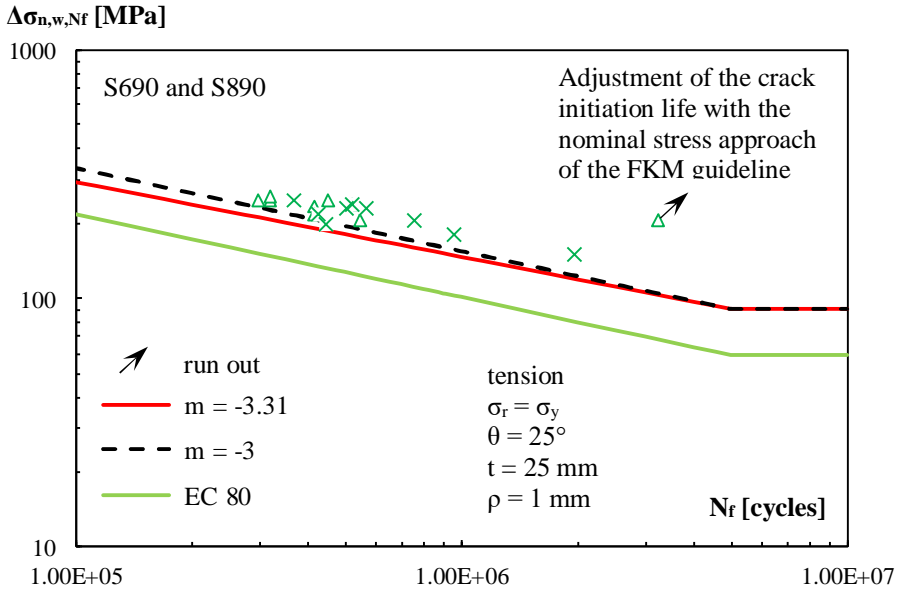


Figure 9.32 Adjusted fatigue test results of BR series with the lower bound of the data scatter compared with the detail category 80 of EN 1993-1-9 (2006).

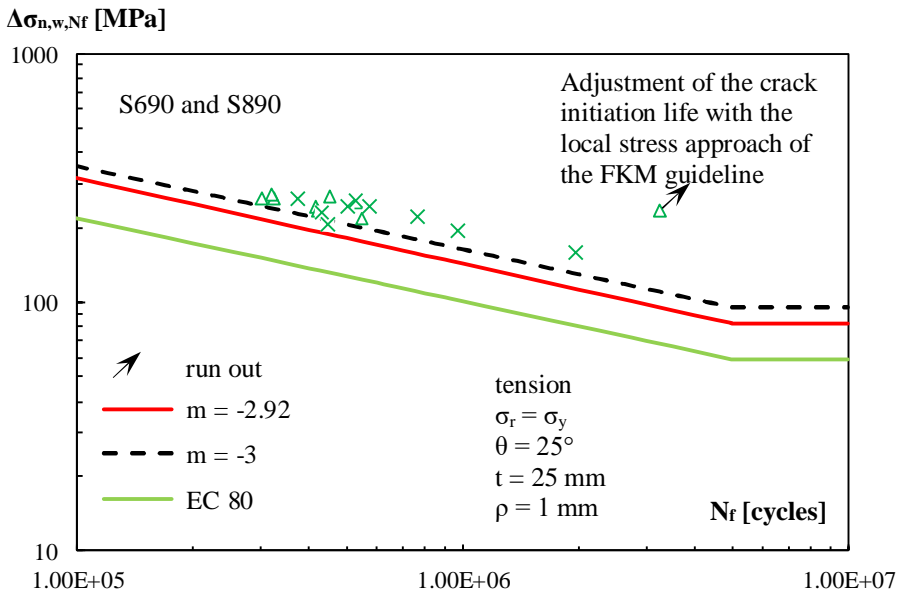


Figure 9.33 Adjusted fatigue test results of BR series with the lower bound of the data scatter compared with the detail category 80 of EN 1993-1-9 (2006).

9.3.2 V-shape welded connections made of rolled and cast steels

The main objective of the current study was to determine the fatigue strength curve of the repaired welded connections made of very high strength steels. For this purpose, V-shape welded specimens were prepared from S690 and S890 rolled steel grades and cast steels with similar yield strengths. The specimens were prepared for rolled steel to rolled steels connections and rolled steel to cast steel connections. In order to determine the effect of the yield strength on the fatigue strength, the test results from the specimens of each steel grade needed to be analysed separately. However, the crack initiation in the specimens took place at different locations, which has an influence on the fatigue strength. When the results were grouped based on the crack initiation locations for each steel grade, the amount of test data was significantly reduced and this made it impossible to perform a reliable statistical analysis on the test data of each steel grade. In addition, it was found that the test results of the repaired V-shape welded specimens were in the same scatter range. Therefore, the test results were combined based on the crack initiation locations.

In the repaired specimens, the fatigue cracks were initiated and propagated at the weld toe of the cap in the rolled steels part, at the weld toe of the cap in the cast steels part, in the base material of the rolled steels and in the base material of the cast steels. The fatigue strength of the repaired welded connections was compared with the fatigue strength of the connections in the as-welded condition. The fatigue strength curves for as-welded condition are determined from the study of Pijpers (2011).

9.3.2.1 Weld toe cracks in cap of rolled steels

Table 9.4 presents the statistical analysis results of the raw and the adjusted test data of the weld toe cracks at the cap in the rolled steels part. The adjusted data were located at the same stress range scatter and the inclusion of the run-out data makes the scatter even larger, which causes high susceptibility the determination of the slope of the curve. In order to avoid the fatigue strength curves with unreliable slopes, the run-out data were excluded from the regression analysis of the adjusted data. Figure 9.34 shows the raw fatigue test results of the weld toe cracks at the cap in the rolled steels part with the results of the regression analysis, the mean, upper bound and lower bound curve of the data scatter. Figure 9.35 presents the fatigue strength curves of the adjusted test data for the weld toe cracks at the cap in the rolled steels part as a result of the regression analysis with the mean, upper bound and lower bound of the data scatter. The adjustment of the crack initiation life of the data was made with the determined influence factors according to the analytical approach of Hüeck et al., (1981). Figure 9.36 and Figure 9.37 indicate the fatigue strength curves of the adjusted test data of the weld toe cracks at the cap in the rolled steels where the adjustment of the crack initiation life was done according to the nominal and local stress

approach of the FKM guideline respectively. In the figures, the results of the regression analysis are shown with the mean, upper bound and lower bound curves of the data scatter. Figure 9.38 presents the lower bound curves of the data scatter data with fixed slope $m = -3$ for the raw and adjusted data.

Table 9.4 Statistical analysis results on raw and adjusted data of the weld toe cracks at the cap in rolled steels parts of repaired V-shape welded specimens.

Grades: S690 and S890							
$\sigma_y = 749$ [MPa], $\sigma_y = 982$ [MPa]							
	m	a_N	$\Delta\sigma_{\text{mean}}$	$\Delta\sigma_c$	s	$t_{0.95,n-x}$	n
Raw data	-3.62	13.75	210	114	0.54	1.80	13
	-3.71	14.12	175	127	0.27	1.90	9
	-3.00	12.44	161	111	0.26	1.86	9
	-5.00	17.23	193	154	0.27	1.86	9
Adjusted data	-3.26	12.39	109	73	0.30	1.90	9
Crack initiation life with Hück et al. (1981)	-3.00	11.84	105	70	0.28	1.86	9
	-5.00	16.25	126	97	0.30	1.86	9
Adjusted data	-3.22	12.55	132	87	0.31	1.90	9
Crack initiation life with FKM nominal	-3.00	12.09	128	85	0.29	1.86	9
	-5.00	16.66	154	118	0.31	1.86	9
Adjusted data	-2.59	11.10	126	72	0.33	1.90	9
Crack initiation life with FKM local	-3.00	12.11	135	87	0.31	1.86	9
	-5.00	16.72	163	121	0.34	1.86	9

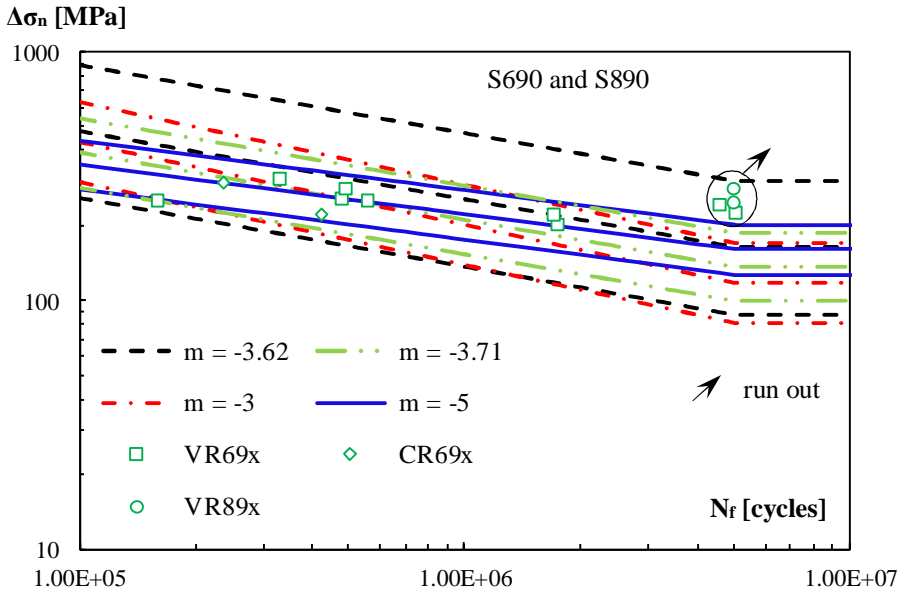


Figure 9.34 Raw fatigue results of weld toe cracks at the cap in rolled steel part with mean, upper bound and lower bound of the data scatter.

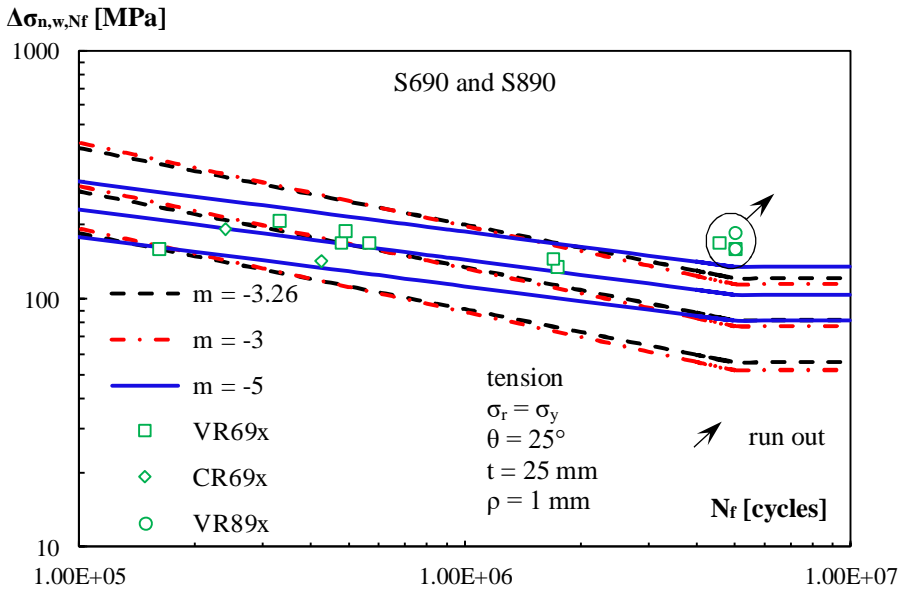


Figure 9.35 Adjusted fatigue results with mean, upper bound and lower bound of the data scatter; crack initiation life adjusted according to Hüek et al., (1981).

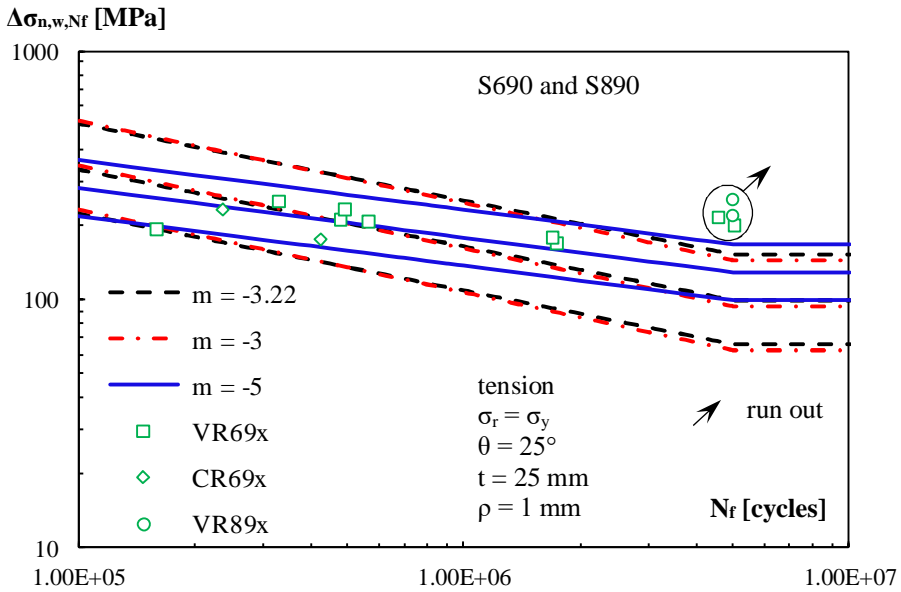


Figure 9.36 Adjusted fatigue test results with mean, upper bound and lower bound of the data scatter; crack initiation life adjusted with the nominal stress approach of the FKM guideline.

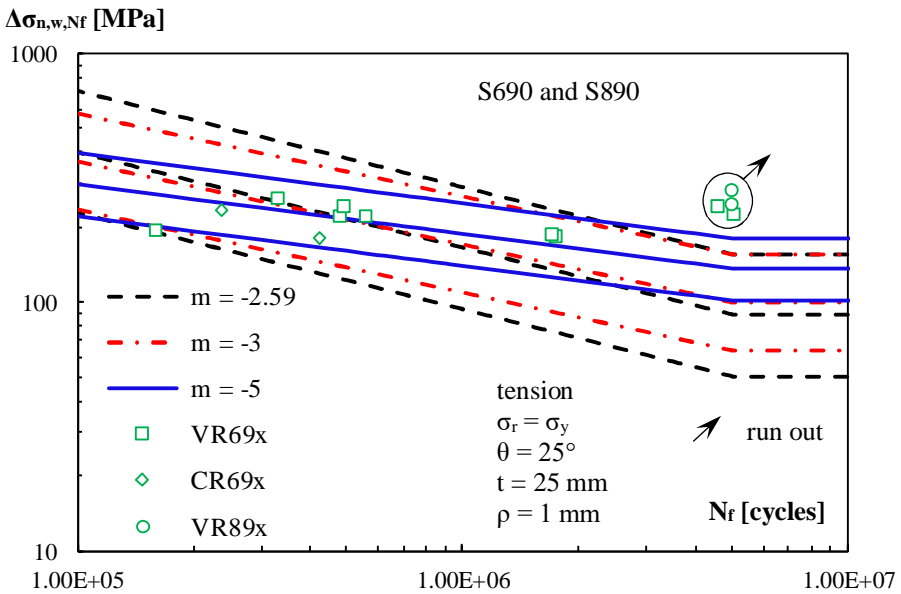


Figure 9.37 Adjusted fatigue test results with mean, upper bound and lower bound of the data scatter; crack initiation life adjusted with the local stress approach of the FKM guideline.

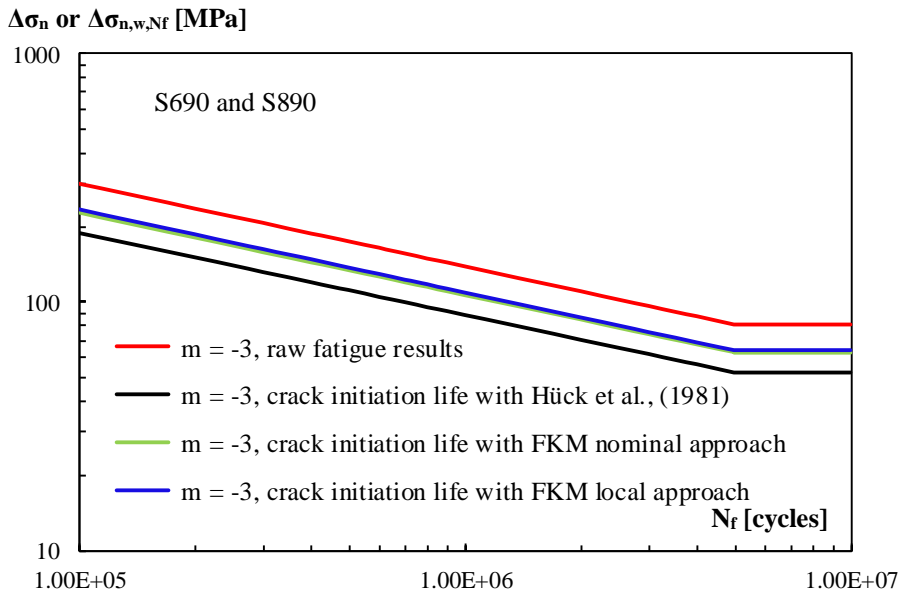


Figure 9.38 Comparison of the raw and the adjusted fatigue results with the lower bound of the data scatter for fixed slope $m = -3$.

In the statistical analysis, the fatigue test data of the specimens made of S690 and S890 is combined and accordingly, the fatigue strength was predicted for both steel grades. Figure 9.39 compares the prediction model with the mean strength curve of the statistical analysis on the adjusted test data of the weld toe cracks at the cap in the rolled steels part. The crack initiation life of the prediction model was determined with the analytical approach of Hüeck et al., (1981). The fatigue limit of the prediction model is close to the fatigue limit of the mean curve for $m = -5$. The cut-off limit of the prediction curve and the mean curves of the data scatter are different. The extrapolation of the cut-off limit of the prediction model makes the fatigue limit of the prediction model close to the fatigue limit of the mean curve for $m = -3$. Figure 9.40 shows the comparison between the mean curves from the statistical analysis of the adjusted data and the prediction model, where the fatigue crack initiation life is calculated with the nominal stress approach of the FKM guideline. The prediction model for S890 rolled steels is closer to the mean curve for $m = -3$. Figure 9.41 presents the mean curves from the statistical analysis on the adjusted test data and the curves of the prediction model, where the fatigue crack initiation life was determined according to the stress approach of the FKM guideline. The prediction model overestimates the fatigue strength compared with the mean curves from the regression analysis of the adjusted test data. The fatigue limit of the prediction curve for S690 is very close to the fatigue limit of the mean curve for $m = -5$.

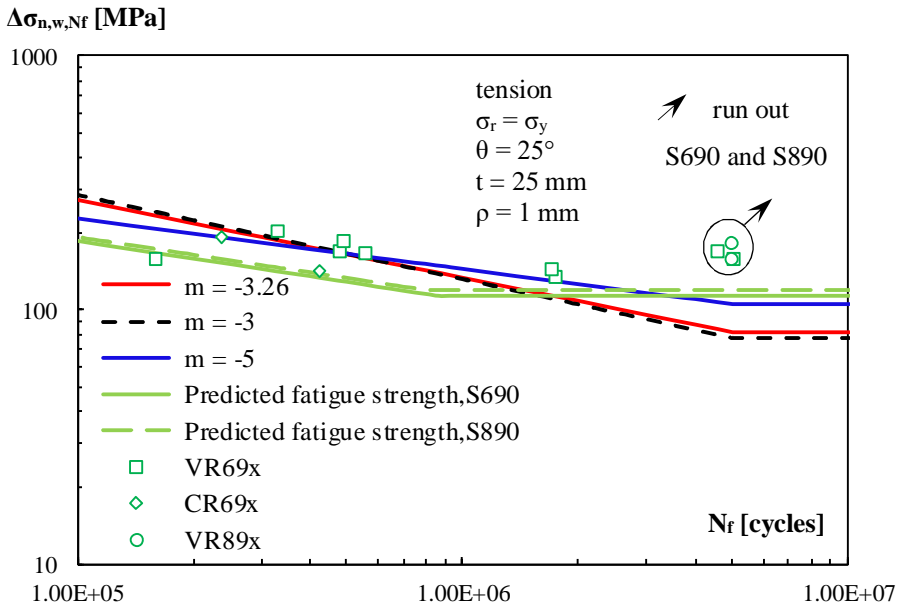


Figure 9.39 Adjusted test data of weld toe cracks with mean curves compared with the prediction model, crack initiation life determined according to Hück et al., (1981).

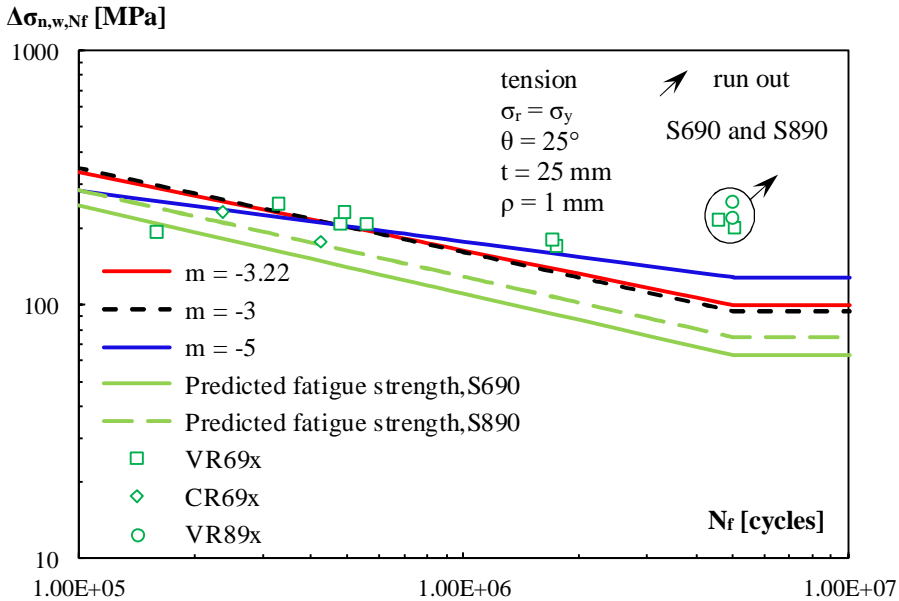


Figure 9.40 Adjusted test data of weld toe cracks with mean curves compared with prediction model, crack initiation life according to the nominal stress approach of the FKM guideline.

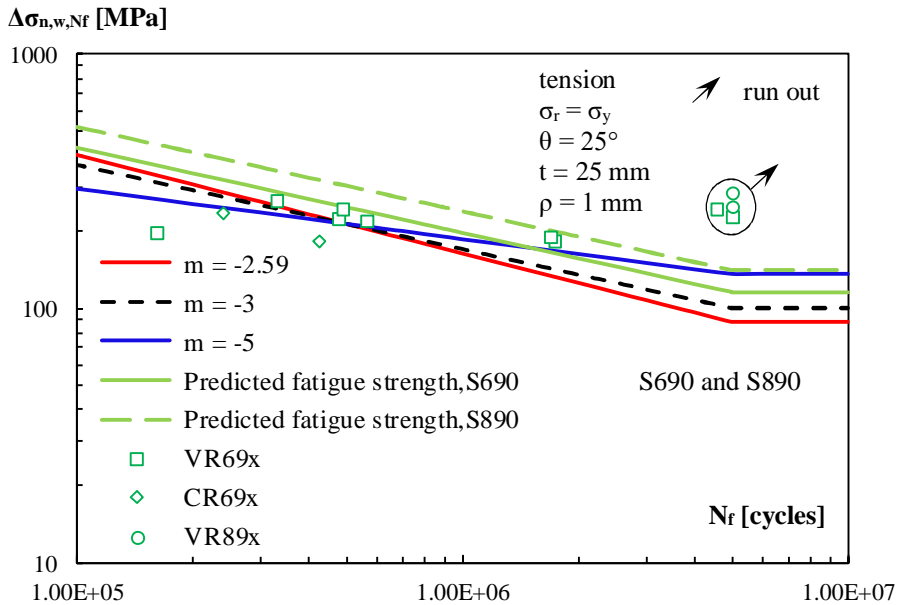


Figure 9.41 Adjusted test data of weld toe cracks with mean curves compared with prediction model, crack initiation life according to local stress approach of FKM guideline.

Figure 9.42 shows the lower bound curves of the statistical analysis on the raw data of the weld toe cracks at the cap in the rolled steels part compared to the detail category 71 of EN 1993-1-9 (2006). The design curve of EN 1993-1-9 (2006) is conservative as compared to the lower bound curves of the test data. With $m = -3.62$, $\Delta\sigma_{\text{mean}} = 210$ MPa, $\Delta\sigma_c = 114$ MPa, with $m = -3$, $\Delta\sigma_{\text{mean}} = 161$ MPa, $\Delta\sigma_c = 111$ MPa.

Figure 9.43 compares the lower bound curves from the statistical analysis on the adjusted test data with the detail category 71 of EN 1993-1-9 (2006). The adjustment of the crack initiation life of the test data was made with the determined influence factors according to the analytical approach of Hüek et al., (1981). The detail category 71 of EN 1993-1-9 (2006) matches with the lower bound curve for $m = -3$. With $m = -3.26$, $\Delta\sigma_{\text{mean}} = 109$ MPa, $\Delta\sigma_c = 73$ MPa, with $m = -3$, $\Delta\sigma_{\text{mean}} = 105$ MPa, $\Delta\sigma_c = 70$ MPa.

For the adjustment of the test data, the influence factors of the crack initiation life were determined by the nominal and local approach of the FKM guideline. Figure 9.44 and Figure 9.45 present the lower bound curves of the adjusted test data according to these approaches respectively. With $m = -3.22$, $\Delta\sigma_{\text{mean}} = 132$ MPa, $\Delta\sigma_c = 87$ MPa, with $m = -3$, $\Delta\sigma_{\text{mean}} = 128$ MPa, $\Delta\sigma_c = 85$ MPa for the nominal stress approach. With $m = -2.59$, $\Delta\sigma_{\text{mean}} = 126$ MPa, $\Delta\sigma_c = 72$ MPa, with $m = -3$, $\Delta\sigma_{\text{mean}} = 135$ MPa, $\Delta\sigma_c = 87$ MPa for the local stress approach. The lower bound curves for $m = -3$ are very close to the detail category 71 of EN 1993-1-9 (2006) for both approaches.

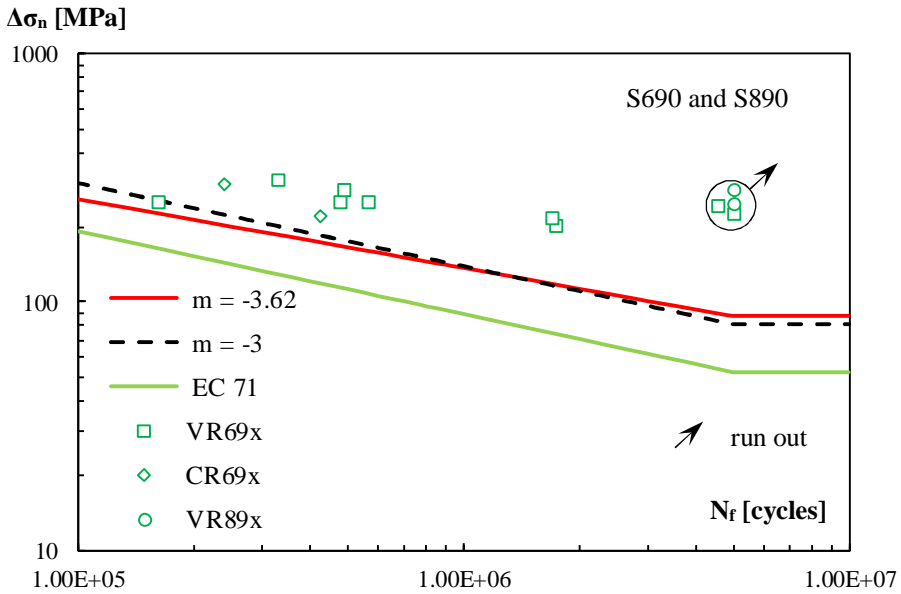


Figure 9.42 Raw fatigue test results of weld toe cracks in rolled steel parts with lower bound of the data scatter compared with the detail category 71 of EN 1993-1-9 (2006).

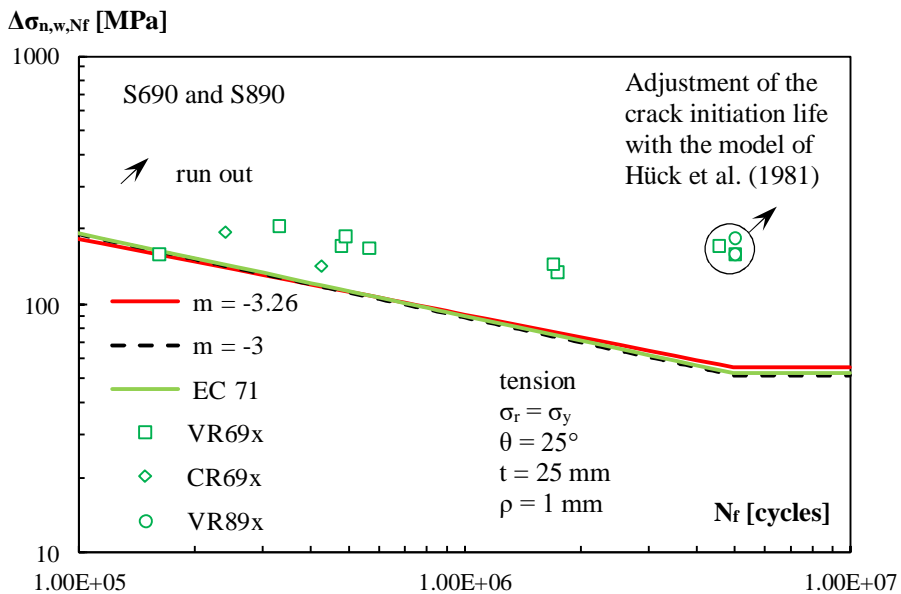


Figure 9.43 Adjusted fatigue test results of weld toe cracks in rolled steel parts with lower bound of the data scatter compared with the detail category 71 of EN 1993-1-9 (2006).

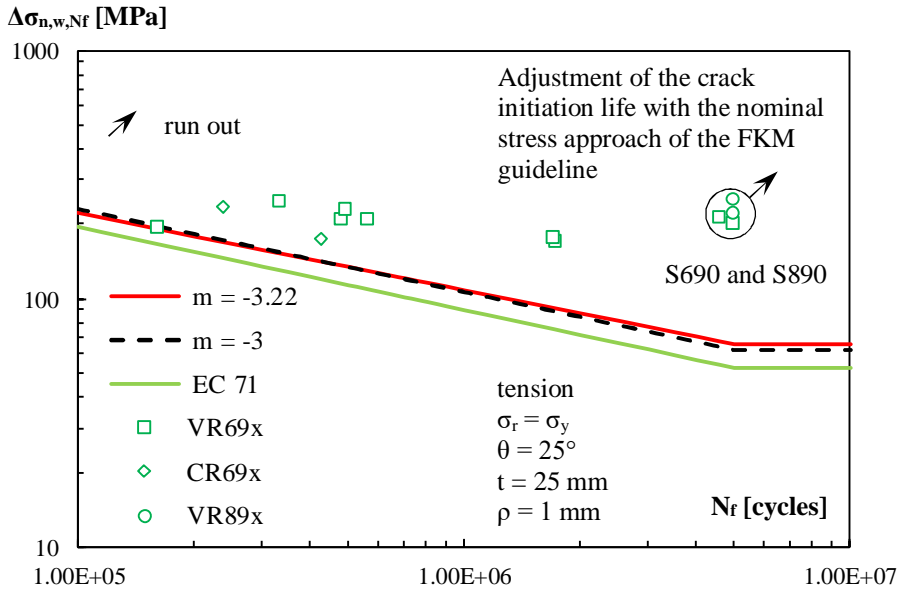


Figure 9.44 Adjusted fatigue test results of weld toe cracks in rolled steel parts with lower bound of the data scatter compared with the detail category 71 of EN 1993-1-9 (2006).

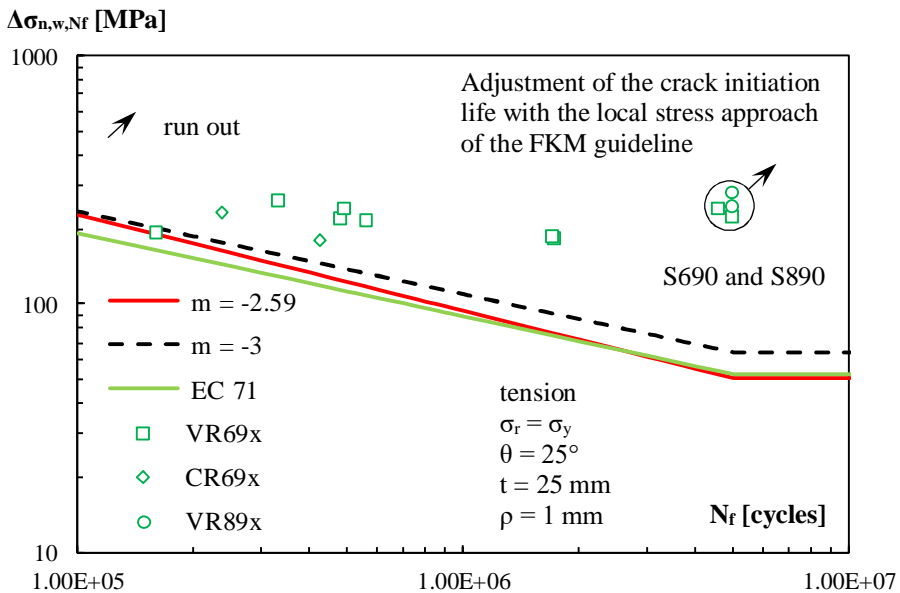


Figure 9.45 Adjusted fatigue test results of weld toe cracks in rolled steel parts with lower bound of the data scatter compared with detail category 71 of EN 1993-1-9 (2006).

The fatigue test results of the repaired V-shape welded connections were compared with the detail category 71 of EN 1993-1-9 (2006). However, EN 1993-1-9 (2006) makes no distinction between the mild and high strength steels. In order to evaluate the effectiveness of the repair method, it is necessary to compare the fatigue strength of the repaired welded connections made of high strength steels with the fatigue strength of the welded connections made of high strength steels in the as-welded condition. Pijpers (2011) performed a study on the fatigue strength of V-shape welded connections made of very high strength steels. The test results of the weld toe cracks at the cap in the rolled steels part are selected from that study and the statistical analysis was performed on the test results for the comparison. Figure 9.46 shows the comparison between the lower bound curves of the scatter for the repaired welded connections and the lower bound curves of the data scatter in the as-welded condition. The analysis was performed on the raw test data. With $m = -4.44$, $\Delta\sigma_{\text{mean}} = 217$ MPa, $\Delta\sigma_c = 141$ MPa, with $m = -3$, $\Delta\sigma_{\text{mean}} = 172$ MPa, $\Delta\sigma_c = 102$ MPa, with $m = -5$, $\Delta\sigma_{\text{mean}} = 207$ MPa, $\Delta\sigma_c = 145$ MPa for the test data in the as-welded condition. The curves of the repaired welded connections show good agreement with the curves from the test data of the as-welded condition. Pijpers (2011) adjusted the fatigue crack initiation life of the test data according to the analytical approach of Hück et al., (1981) and the propagation life with the influence factors from the fracture mechanics approach. These adjusted test data were compared with the adjusted test data of the repaired welded connections and the lower bound curves of the data scatter for both test series are given in Figure 9.47. With $m = -5.61$, $\Delta\sigma_{\text{mean}} = 160$ MPa, $\Delta\sigma_c = 114$ MPa, with $m = -3$, $\Delta\sigma_{\text{mean}} = 121$ MPa, $\Delta\sigma_c = 72$ MPa, with $m = -5$, $\Delta\sigma_{\text{mean}} = 146$ MPa, $\Delta\sigma_c = 105$ MPa for the adjusted test data in the as-welded condition. The fatigue strength curve of the repaired welded connection matches with the fatigue strength curve of the welded connection as-welded condition for $m = -3$. From both figures, it can be concluded that the fatigue strength of repaired fatigue damaged V-shape welded connections made of very high strength steels can be regained by applying the repair procedure, which was explained in Section 5.4.

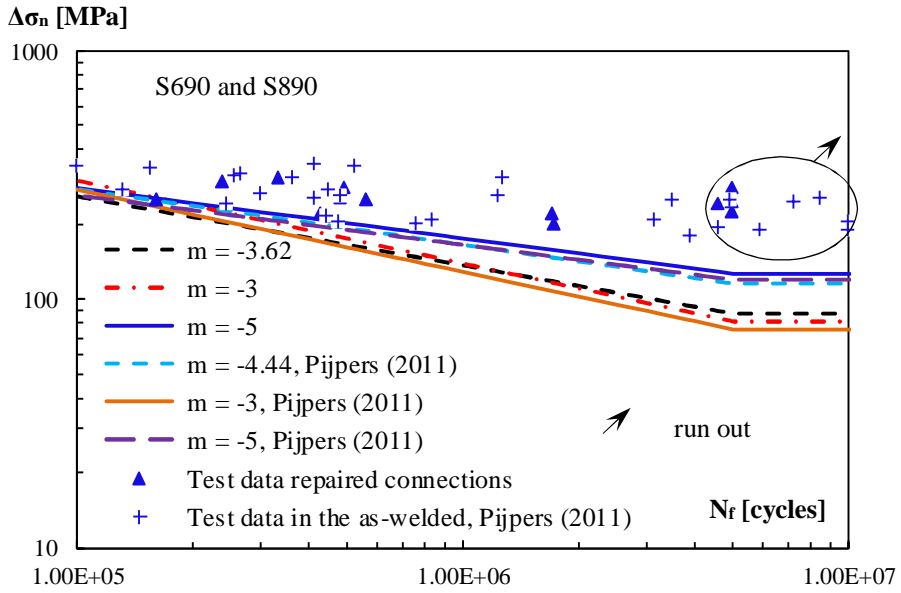


Figure 9.46 Comparison of the lower bound curves of the data scatter of repaired welded connections with the welded connections in the as-welded condition, raw data.

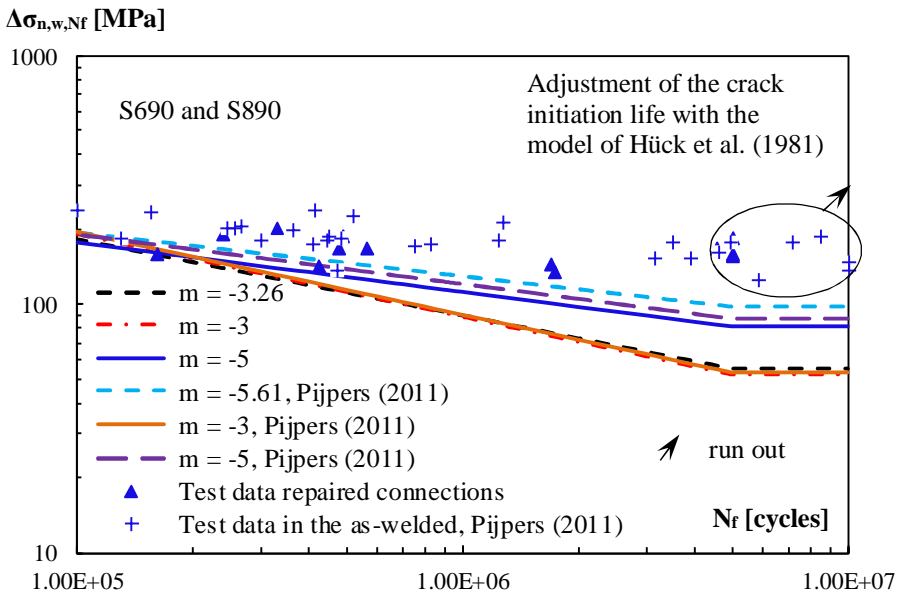


Figure 9.47 Comparison of the lower bound curves of the data scatter of repaired welded connections with the welded connections in the as-welded condition, adjusted data.

9.3.2.2 Weld toe cracks in cap of cast steels

Table 9.5 shows the results of the statistical analysis on the test data of the weld toe cracks at the cap in the cast steels part. The statistical analysis was performed on very limited test data. Therefore, the evaluation of the fatigue strength curves according to a free slope may result in unrealistic conclusions. The comparison between the strength curves with a fixed slope especially for $m = -3$, which is also the slope of the design curve of EN 1993-1-9 (2006), will be more appropriate.

Figure 9.48 presents the fatigue strength curves for the raw test data of the weld toe cracks at the cap in the cast steels part with the regression analysis, the mean, upper bound and lower bound of the data scatter. Figure 9.49 shows the fatigue strength curves of the adjusted test data of the weld toe crack at the cap in the cast steels part, results of regression analysis with the mean, upper bound and lower bound of the data scatter. The crack initiation life of the test data was adjusted with the influence factors which are determined according to the analytical approach developed by Hüeck et al. (1981). Figure 9.50 and Figure 9.51 indicate the fatigue strength curves of the adjusted test data weld toe cracks at the cap in the cast steels. The crack initiation life of the test data was adjusted according to the nominal and local stress approach of the FKM guideline respectively. In the figures, the results of the regression analysis are shown with the mean, upper bound and lower bound of the data scatter. Figure 9.52 presents the lower bound curves of the data scatter data with fixed slope $m = -3$ for the raw and adjusted data.

Table 9.5 Statistical analysis results on raw and adjusted data of weld toe cracks at the cap in cast steel parts

Grades: G10MnMoV 6-3 and G18NiMoCr 3-6							
$\sigma_y = 697$ [MPa], $\sigma_y = 1006$ [MPa]							
	m	a_N	$\Delta\sigma_{\text{mean}}$	$\Delta\sigma_c$	s	$t_{0.95,n-x}$	n
Raw data	-2.91	12.12	153	100	0.23	2.35	5
	-3.00	12.45	156	112	0.20	2.13	5
	-5.00	17.15	192	148	0.27	2.13	5
Adjusted data	-2.24	9.95	83	43	0.27	2.35	5
Crack initiation life with Hüeck et al. (1981)	-3.00	11.77	100	67	0.25	2.13	5
	-5.00	16.00	123	87	0.35	2.13	5
Adjusted data	-2.48	10.79	109	65	0.24	2.35	5
Crack initiation life with FKM nominal	-3.00	12.11	122	86	0.21	2.13	5
	-5.00	16.51	151	110	0.32	2.13	5
Adjusted data	-2.20	10.18	105	57	0.25	2.35	5
Crack initiation life with FKM local	-3.00	12.13	128	88	0.23	2.13	5
	-5.00	16.51	158	110	0.37	2.13	5

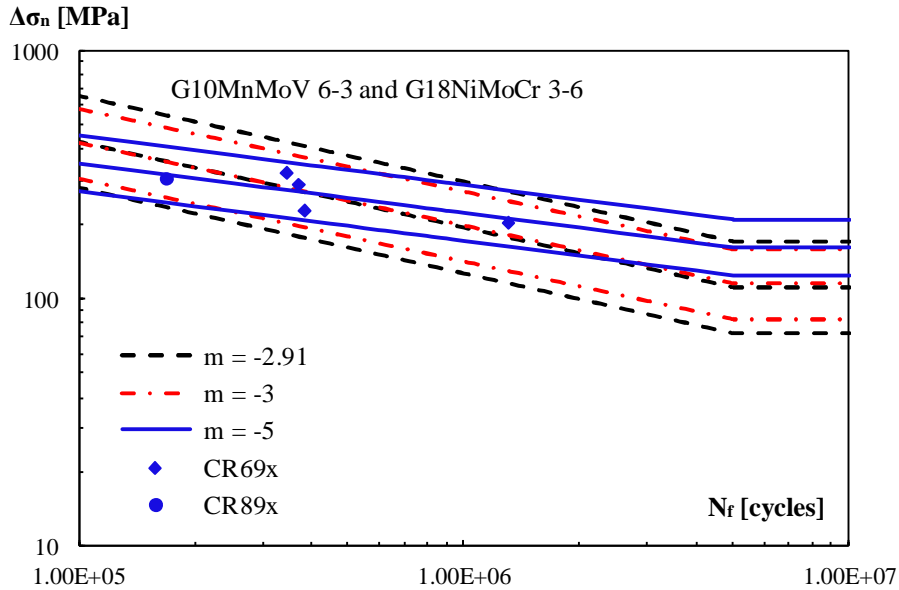


Figure 9.48 Raw fatigue results of weld toe cracks at the cap in cast steels part with the mean, upper bound and lower bound of the data scatter.

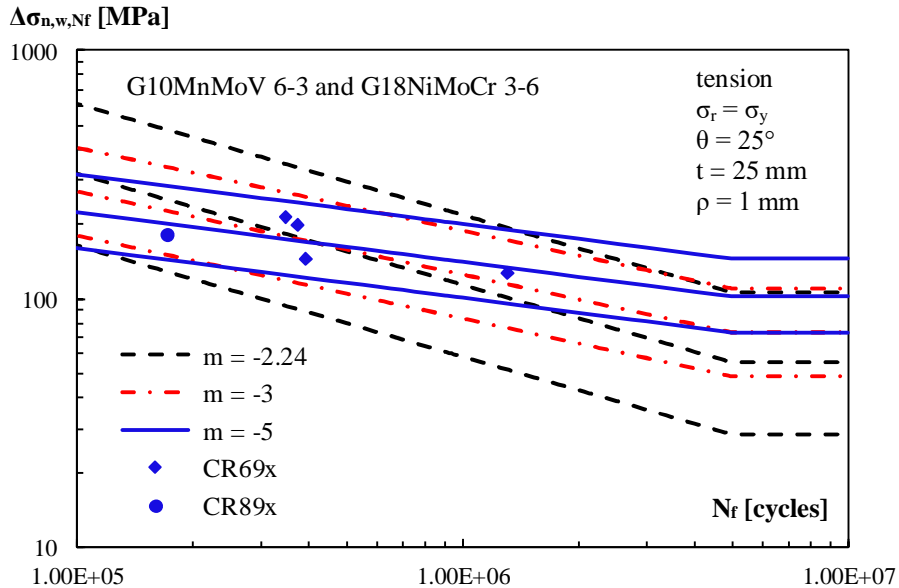


Figure 9.49 Adjusted fatigue results with mean, upper bound and lower bound of the data scatter; crack initiation life adjusted according to Hück et al., (1981).

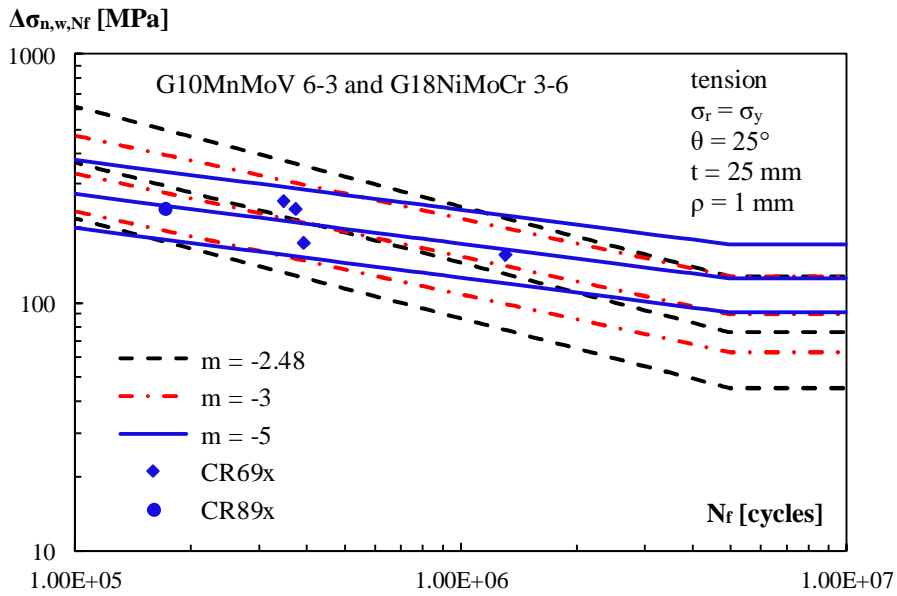


Figure 9.50 Adjusted fatigue results with mean, upper bound and lower bound of the data scatter; crack initiation life adjusted with the nominal stress approach of the FKM guideline.

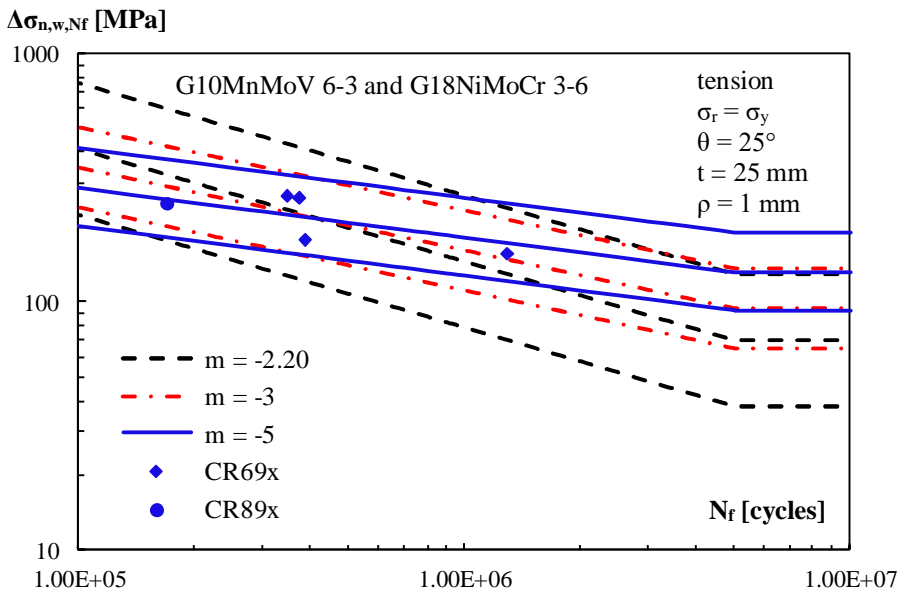


Figure 9.51 Adjusted fatigue results with mean, upper bound and lower bound of the data scatter; crack initiation life adjusted with the local stress approach of the FKM guideline.

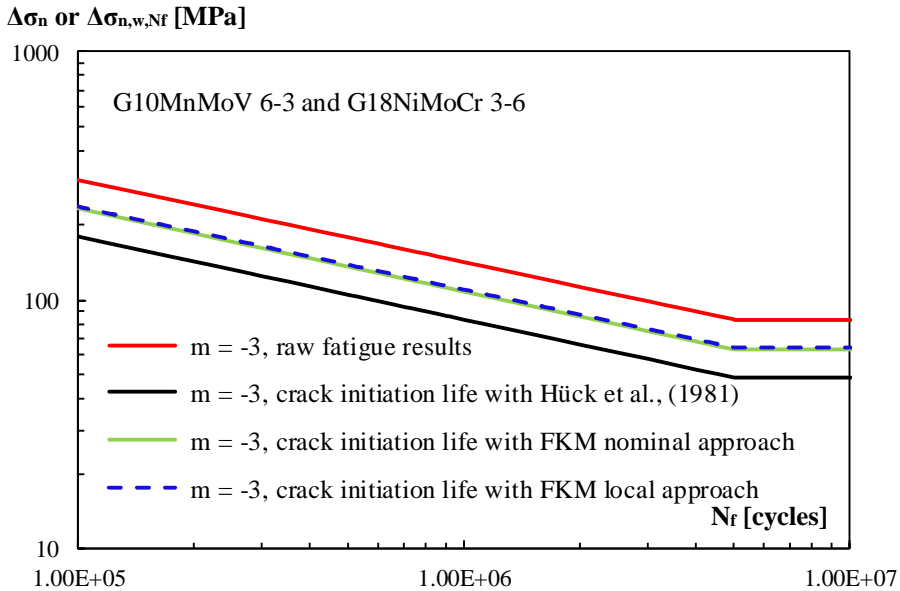


Figure 9.52 Comparison of the raw and the adjusted fatigue results with the lower bound of the data scatter for fixed slope $m = -3$.

The statistical analysis was performed on the test data of the weld toe crack at the cap in the cast steel parts. The difference between the steel grades was disregarded and the fatigue strength curves were determined for the combined test data from both steel grades. Since the prediction models are a function of the yield strength of the material, the prediction curves are calculated for both steel grades. Figure 9.53 presents the comparison between the mean strength curves from the statistical analysis on the adjusted data and the prediction curves for the cast steel grades G10MnMoV 6-3 and G18NiMoCr 3-6. In the prediction model, the crack initiation life is determined by the analytical approach of Hück et al., (1981) and hence the influence factors for the adjustment of the crack initiation life were also determined with the same approach. The fatigue limit of the prediction models is very close to the fatigue limit of the mean curve for $m = -5$. Figure 9.54 compares the mean curves from the statistical analysis on the adjusted data with the prediction curves, where the fatigue crack initiation life was calculated according to the nominal stress approach of the FKM guideline. The prediction curve for G18NiMoCr 3-6 is closer to the mean curve for $m = -3$ and the prediction curve for G10MnMoV 6-3 is conservative. Figure 9.55 shows the mean curves of the statistical analysis on the adjusted data compared with the prediction curves, where the fatigue crack initiation life was determined according to the local stress approach of the FKM guideline. The prediction curves are very close to the mean curve for $m = -3$ and the prediction curve of G10MnMoV 6-3 is located just at below the mean curve for $m = -3$, while the prediction curve of G18NiMoCr 3-6 is positioned at above of it.

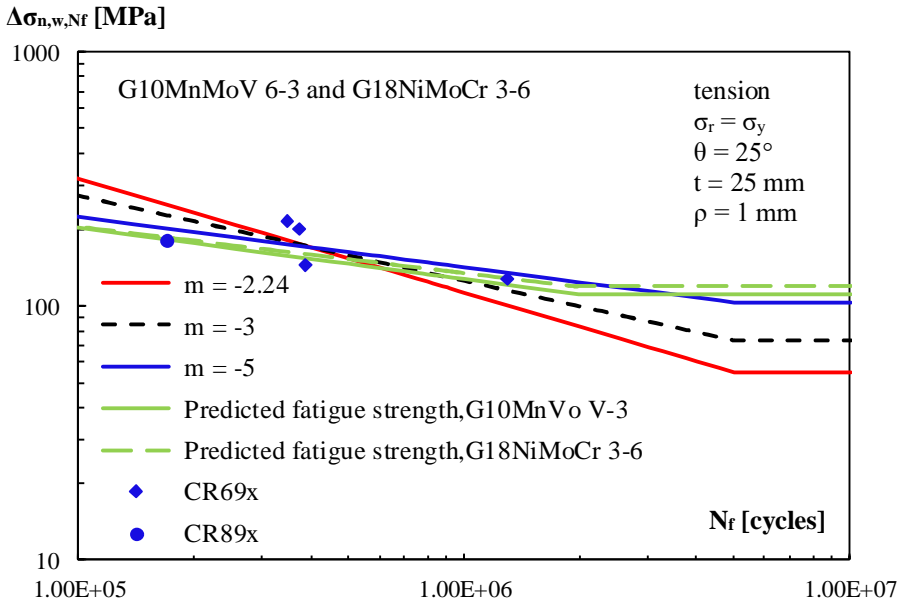


Figure 9.53 Adjusted test data of weld toe cracks in cast steels with mean curves compared with prediction model, crack initiation life determined according to Hück et al., (1981).

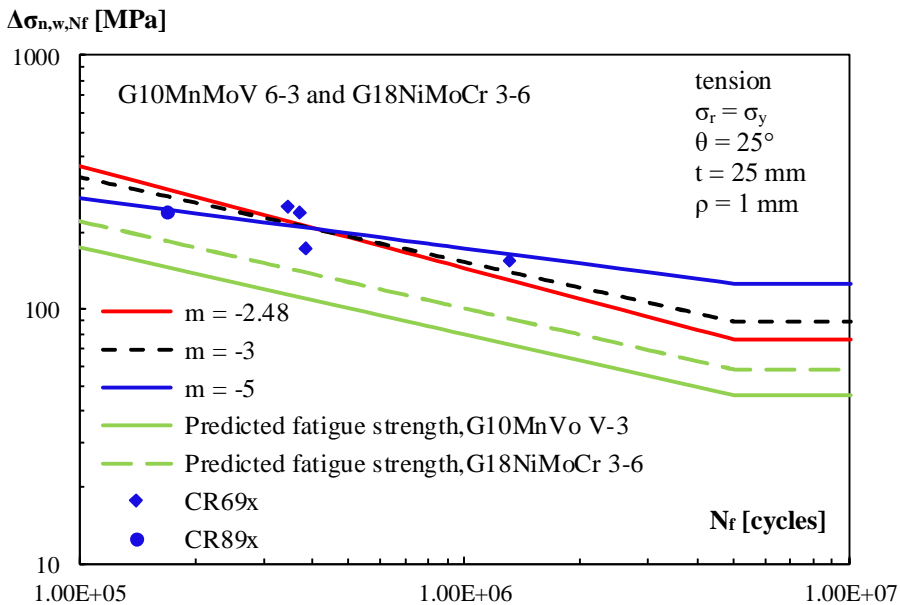


Figure 9.54 Adjusted test data of weld toe cracks in cast steels mean curves compared with prediction model, crack initiation life with nominal stress approach of the FKM guideline.

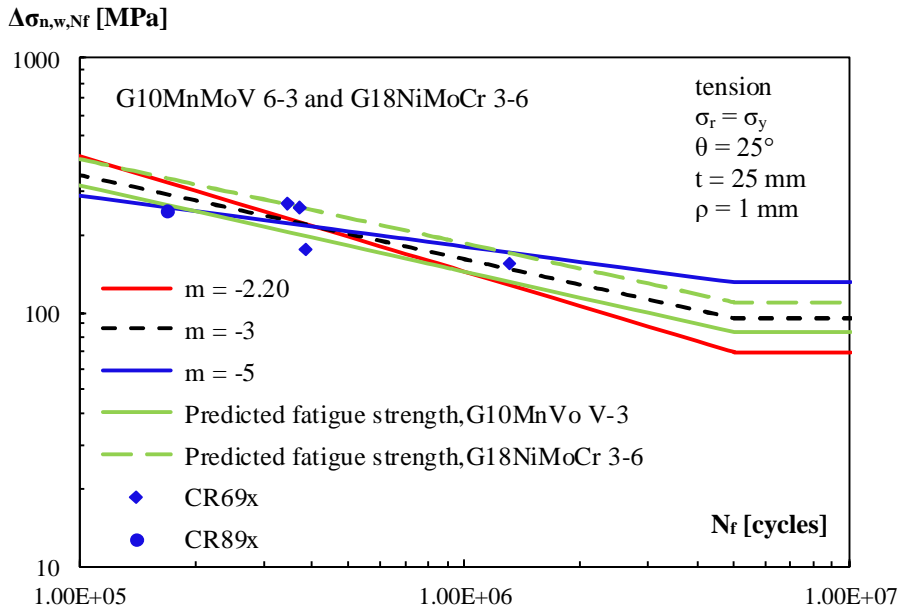


Figure 9.55 Adjusted test data of weld toe cracks in cast steels mean curves compared with prediction model, crack initiation life with the local stress approach of the FKM guideline.

Figure 9.56 compares the lower bound curves from the statistical analysis on the raw data of the weld toe crack at the cap in the cast steel parts to the detail category 71 of EN 1993-1-9 (2006). The lower bound curves of the data scatter are located at above of the design curve and it means that the design curve lead to the conservative fatigue strength. With $m = -2.91$, $\Delta\sigma_{\text{mean}} = 153$ MPa, $\Delta\sigma_c = 100$ MPa, with $m = -3$, $\Delta\sigma_{\text{mean}} = 156$ MPa, $\Delta\sigma_c = 112$ MPa.

Figure 9.57 shows the comparison between the lower bound curves from the statistical analysis on the adjusted data and the detail category 71 of EN 1993-1-9 (2006). The influence factors for the crack initiation life were determined with the approach of Hück et al., (1981) and the adjustment of data was made accordingly. The lower bound curve for $m = -3$ shows a reasonable match with the detail category 71 of EN 1993-1-9 (2006). With $m = -2.24$, $\Delta\sigma_{\text{mean}} = 83$ MPa, $\Delta\sigma_c = 43$ MPa, with $m = -3$, $\Delta\sigma_{\text{mean}} = 100$ MPa, $\Delta\sigma_c = 67$ MPa. Figure 9.58 and Figure 9.59 present the comparison between the detail category 71 of EN 1993-1-9 (2006) and the lower bound curves of the adjusted data of which the crack initiation life was adjusted with the influence factors of the nominal and local stress approach of the FKM guideline respectively. The lower bound curves of both approaches for $m = -3$ are reasonably close to the detail category 71 of EN 1993-1-9 (2006). With $m = -2.48$, $\Delta\sigma_{\text{mean}} = 109$ MPa, $\Delta\sigma_c = 65$ MPa, with $m = -3$, $\Delta\sigma_{\text{mean}} = 122$ MPa, $\Delta\sigma_c = 86$ MPa for the nominal stress approach. With $m = -2.20$, $\Delta\sigma_{\text{mean}} = 105$ MPa, $\Delta\sigma_c = 57$ MPa, with $m = -3$, $\Delta\sigma_{\text{mean}} = 128$ MPa, $\Delta\sigma_c = 88$ MPa for the local stress approach.

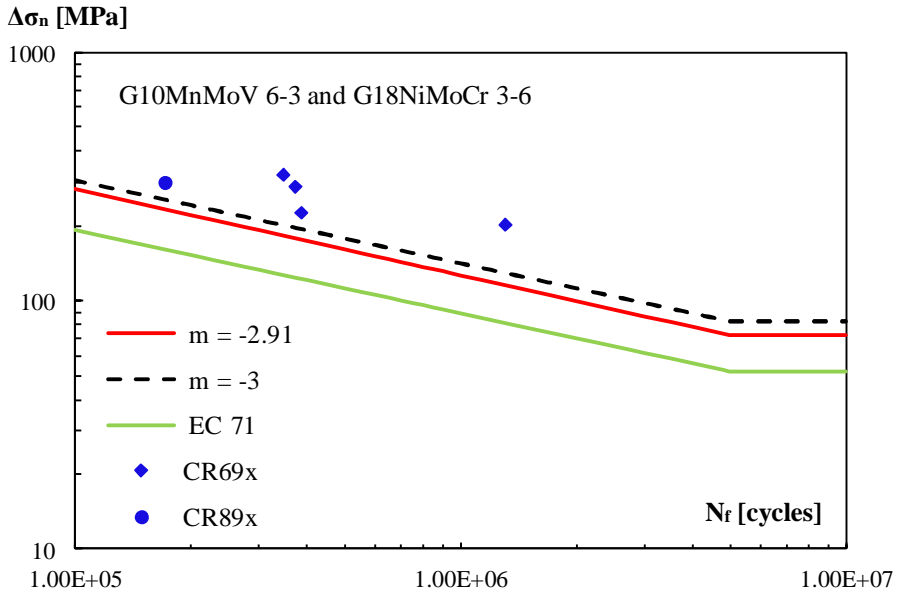


Figure 9.56 Raw fatigue test results of weld toe cracks in cast steel parts with lower bound of the data scatter compared with the detail category 71 of EN 1993-1-9 (2006).

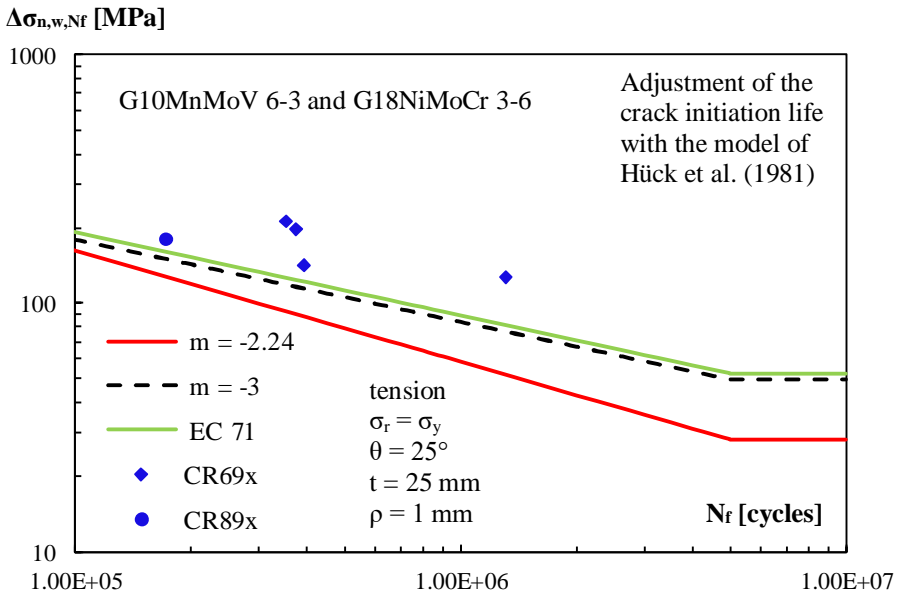


Figure 9.57 Adjusted fatigue test results of weld toe cracks in cast steel parts with lower bound of the data scatter compared with the detail category 71 of EN 1993-1-9 (2006).

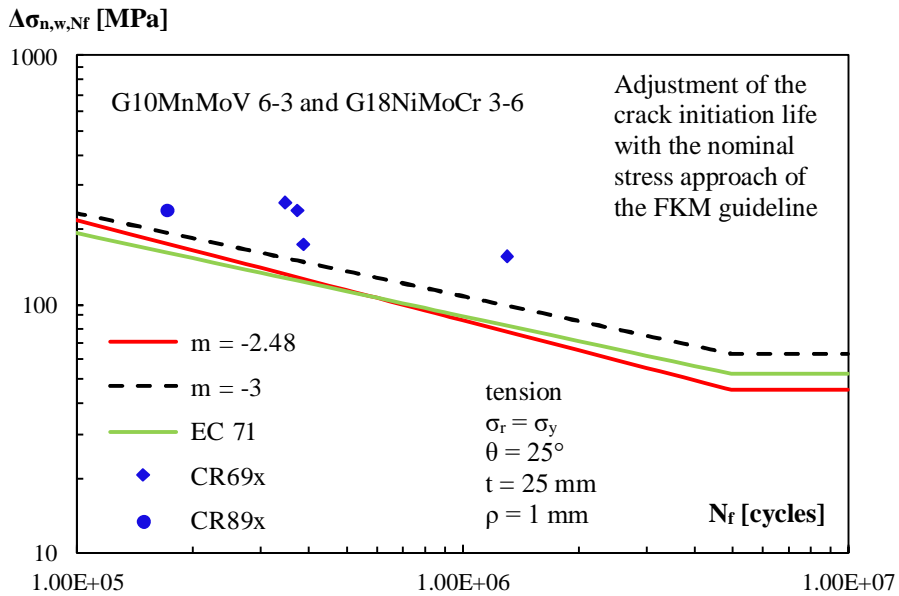


Figure 9.58 Adjusted fatigue test results of weld toe cracks in cast steel parts with lower bound of the data scatter compared with the detail category 71 of EN 1993-1-9 (2006).

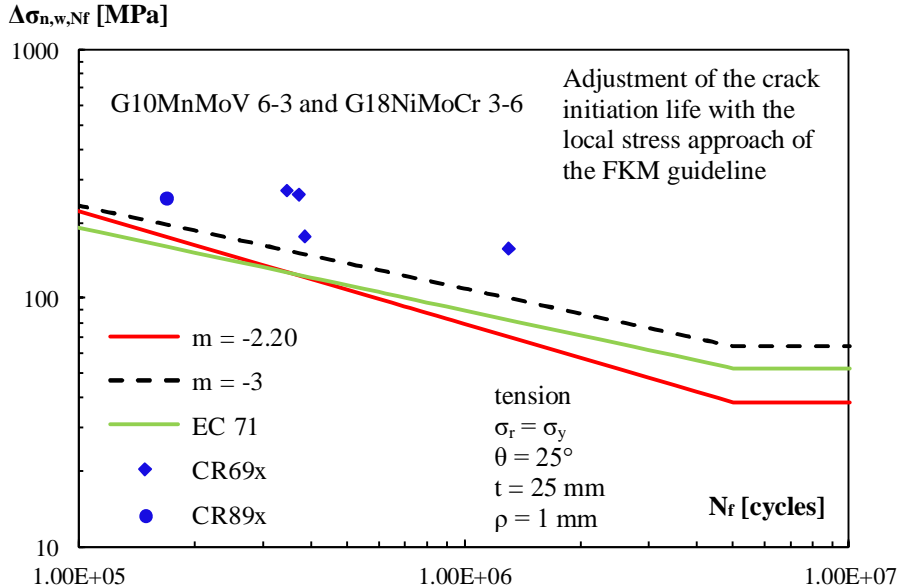


Figure 9.59 Adjusted fatigue test results of weld toe cracks in cast steels parts with lower bound of the data scatter compared with the detail category 71 of EN 1993-1-9 (2006).

The test data for the repaired V-shape welded connections were evaluated, where the cracks were initiated in the weld toe of the cast steels side. The fatigue strength curves from the statistical analysis were compared with the design curve of EN 1993-1-9 (2006) although EN 1993-1-9 (2006) does not makes no distinction between the fatigue design of rolled and cast steels. For the fatigue design of the welded connections made of cast steels, the recommendations are given in DNVGL-RP-C203 (2016). The detail classes for rolled steels are recommended for the fatigue design of the welded cast steel joints. The recommended design curve for V-shape welded connections is the same as the detail category 71 of EN 1993-1-9 (2006). Therefore, it is inessential to compare the test results with the recommended design curve of DNVGL-RP-C203 (2016) separately.

Furthermore, the objective of the fatigue crack repair is to prolong the fatigue life of the connections as long as the fatigue life of the original connection. This means that the effective repair method should completely regain the fatigue life of the damaged connections. In order to evaluate the method used for repair of the fatigue crack in the weld toe of cast steels, the fatigue strength curves were compared with the fatigue strength of the weld toe crack in cast steel in the as-welded condition. In the study of Pijpers (2011), it was also concentrated on the fatigue strength of the V-shape welded connections between rolled and cast steels. The statistical analysis was performed on the test data of the weld toe cracks in the cast steel parts of that study. Figure 9.60 shows the comparison between the lower bound curves of the data scatter of the repaired welded connections and the lower bound curve of the data scatter of the welded connections in the as-welded condition. The fatigue strength curves were determined with a statistical analysis on the raw data of in the as-welded condition. With $m = -2.65$, $\Delta\sigma_{\text{mean}} = 165$ MPa, $\Delta\sigma_c = 86$ MPa, with $m = -3$, $\Delta\sigma_{\text{mean}} = 174$ MPa, $\Delta\sigma_c = 105$ MPa, with $m = -5$, $\Delta\sigma_{\text{mean}} = 204$ MPa, $\Delta\sigma_c = 145$ MPa for the test data in the as-welded condition. The results of the statistical analysis on the data of repaired welded connections were already given in Table 9.5. Also, limited data were available for the weld toe cracks in cast steels in the as-welded condition. This makes it difficult for the determination of an appropriate free slope. The fatigue strength comparison for fixed slopes is more reasonable. The fatigue strength curves of the repaired welded connections for the fixed slopes show a good match with the fatigue strength of the connections in the as-welded condition. Pijpers (2011) adjusted the crack initiation life of the test data according to the analytical approach of Hück et al., (1981) and propagation life with the fracture mechanics approach. This adjusted test data is compared with the adjusted test data of the repaired welded connections and the lower bound curves of the data scatter for both test series is given in Figure 9.61. With $m = -1.96$, $\Delta\sigma_{\text{mean}} = 94$ MPa, $\Delta\sigma_c = 36$ MPa, with $m = -3$, $\Delta\sigma_{\text{mean}} = 117$ MPa, $\Delta\sigma_c = 67$ MPa, with $m = -5$, $\Delta\sigma_{\text{mean}} = 138$ MPa, $\Delta\sigma_c = 93$ MPa for the adjusted test data in the as-welded condition. The fatigue strength curves of the repaired welded connections match with the fatigue strength curves of the welded connections in the as-welded condition for the fixed slopes. This reveals that the fatigue life of damaged connections made of cast steels can be completely regained with the used repair procedure.

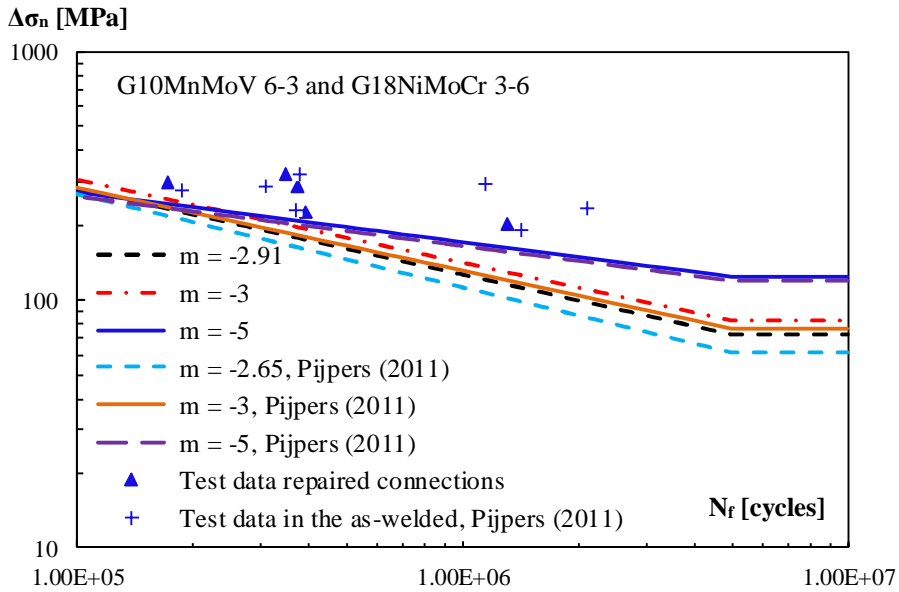


Figure 9.60 Comparison of the lower bound curves of the data scatter of repaired welded connections with the welded connections in the as-welded condition, raw data.

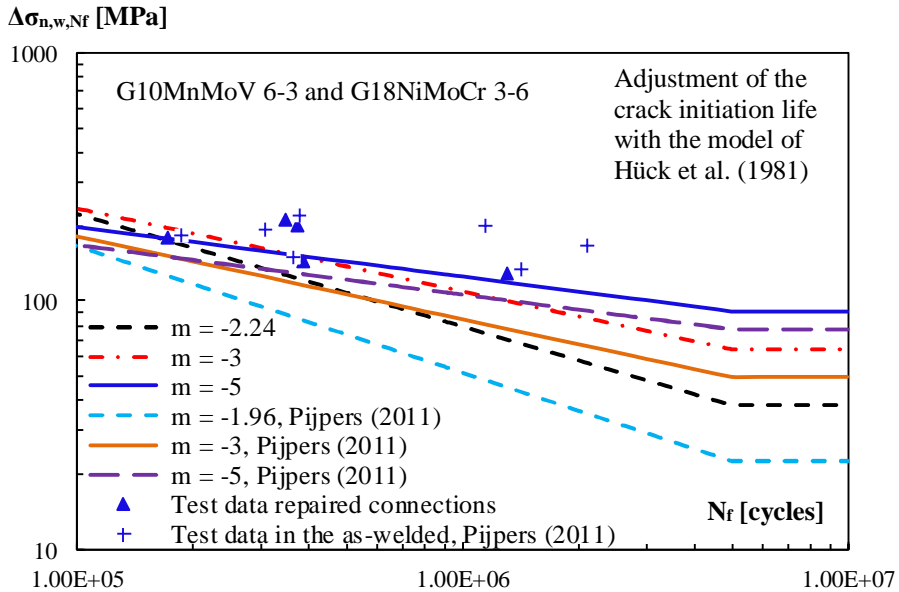


Figure 9.61 Comparison of the lower bound curves of the data scatter of repaired welded connections with the welded connections in the as-welded condition, adjusted data.

9.3.2.3 Cracks in base material of rolled steel

In the repaired V-shape welded test specimens made of S890 rolled steel, the crack initiation and propagation were observed in the base material of the rolled steel. For the statistical analysis of these data, the number of cycles at the crack creation stage is also included in the number of cycles after the repair of the weld toe cracks. Table 9.6 shows the results of the statistical analysis on the raw and adjusted fatigue test results of the base material cracks in S890 rolled steel.

Figure 9.62 presents the fatigue strength curves of the base material crack in S890 rolled steel the results of the regression analysis with the mean, upper bound and lower bound of the data scatter. Figure 9.63 shows the fatigue strength curves of the adjusted test data and the results of regression analysis inclusion of the mean, upper bound and lower bound of the data scatter. The adjustment of the crack initiation life was made with the determined influence factors according to the crack initiation life prediction model of Hück et al., (1981). The crack initiation life of the test data was also adjusted with the influence factors determined according to the nominal and local stress approach of the FKM guideline. The fatigue strength curves are indicated in Figure 9.64 and Figure 9.65 respectively, with the mean, upper bound and lower bound of the data scatter. Figure 9.66 shows the lower bound curves of data scatter data with fixed slope $m = -3$ for raw and adjusted data.

Table 9.6 Statistical analysis results on the raw and adjusted data of the base material cracks in S890 rolled steel.

Grades: S890							
$\sigma_y = 985$ [MPa]							
	m	a_N	$\Delta\sigma_{\text{mean}}$	$\Delta\sigma_c$	s	$t_{0.95,n-x}$	n
Raw data	-4.77	17.70	265	246	0.08	1.86	10
	-3.00	13.18	234	197	0.12	1.83	10
	-5.00	18.29	267	250	0.08	1.83	10
Adjusted data	-4.40	16.23	197	181	0.09	1.86	10
Crack initiation life with Hück et al. (1981)	-3.00	12.84	178	151	0.12	1.83	10
	-5.00	17.67	203	188	0.09	1.83	10
Adjusted data	-3.38	13.46	170	131	0.21	1.86	10
Crack initiation life with FKM nominal	-3.00	12.59	164	124	0.20	1.83	10
	-5.00	17.27	187	156	0.21	1.83	10
Adjusted data	-4.79	17.08	188	179	0.06	1.86	10
Crack initiation life with FKM local	-3.00	12.75	166	142	0.11	1.83	10
	-5.00	17.59	190	181	0.06	1.83	10

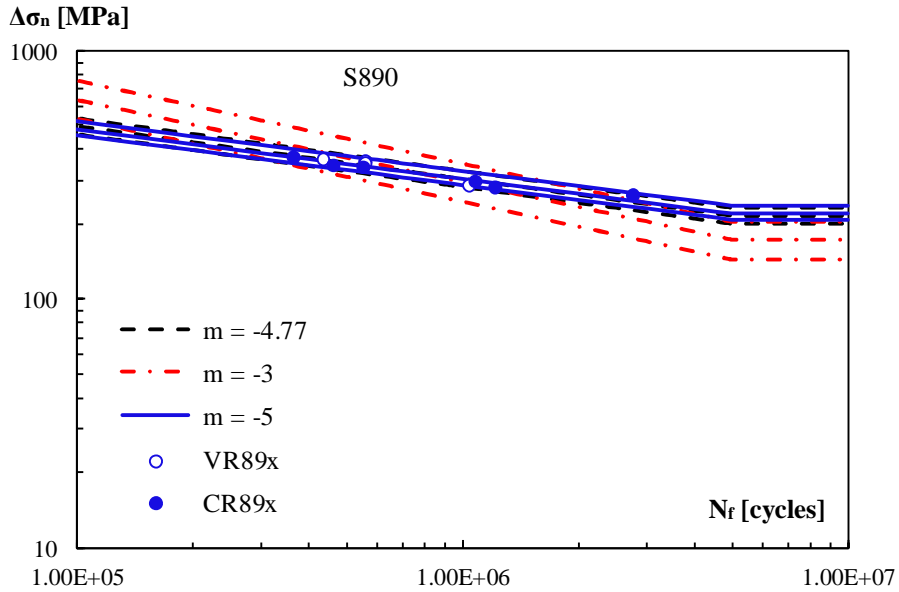


Figure 9.62 Raw fatigue results of the base material cracks in rolled steel part with the mean, upper bound and lower bound of the data scatter.

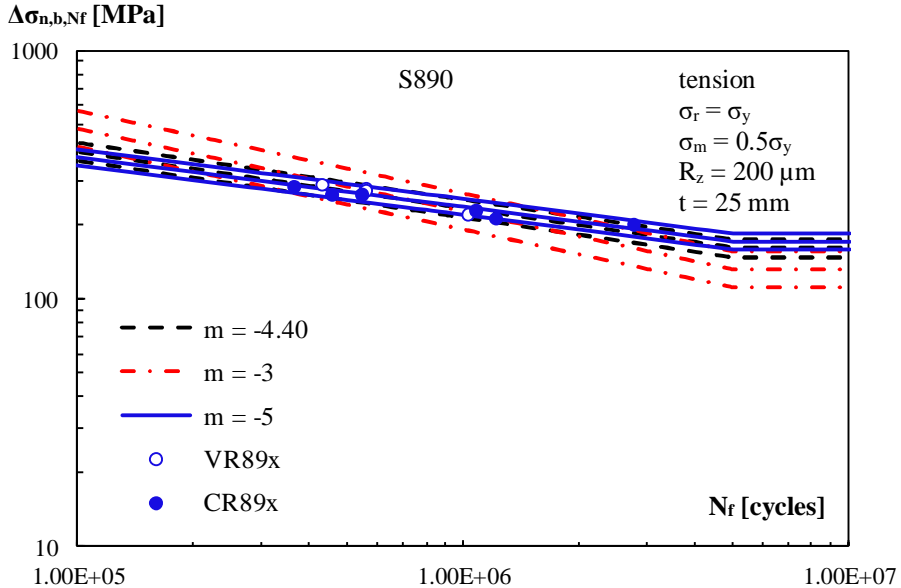


Figure 9.63 Adjusted fatigue results with mean, upper bound and lower bound of the data scatter; crack initiation life adjusted according to Hück et al., (1981).

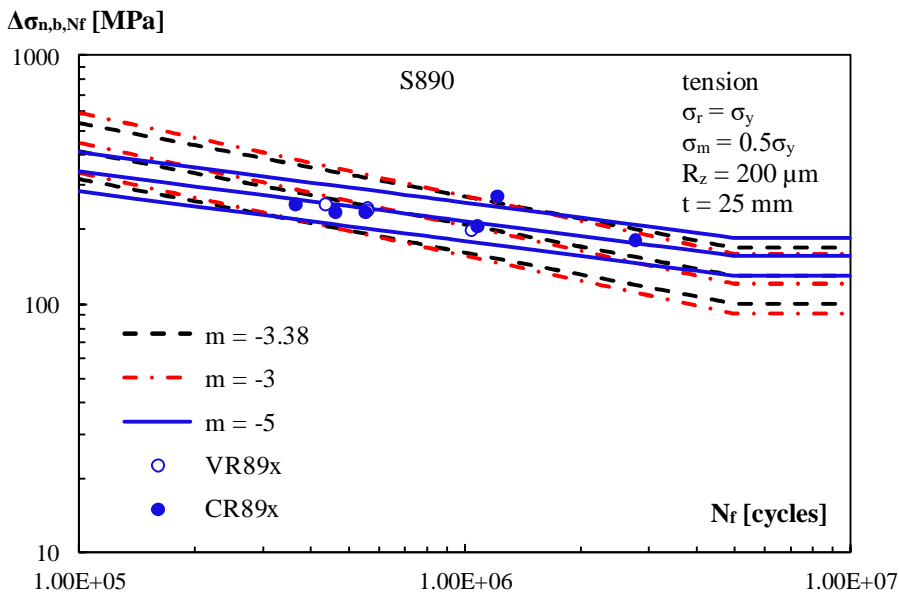


Figure 9.64 Adjusted fatigue results with mean, upper bound and lower bound of the data scatter; crack initiation life adjusted with the nominal stress approach of the FKM guideline.

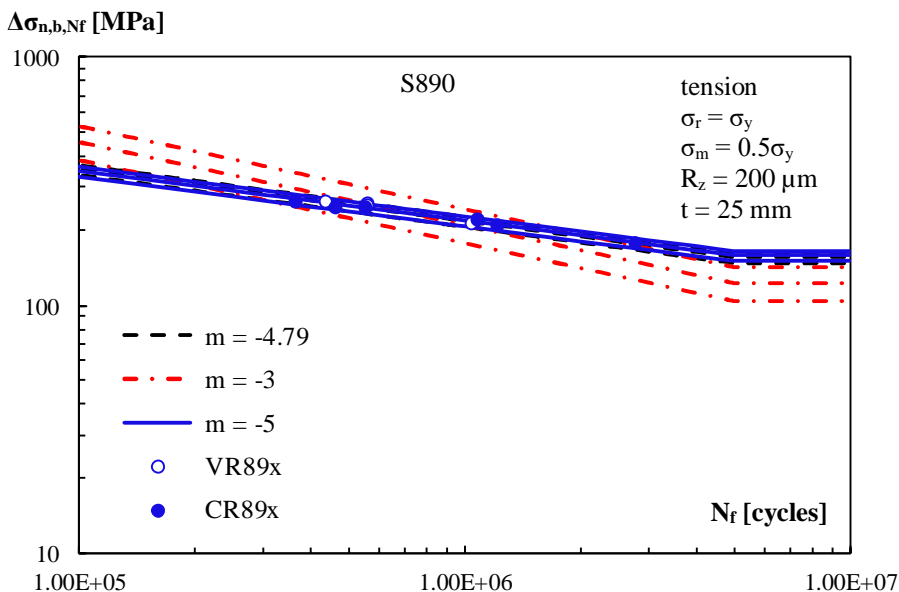


Figure 9.65 Adjusted fatigue results with mean, upper bound and lower bound of the data scatter; crack initiation life adjusted with the local stress approach of the FKM guideline.

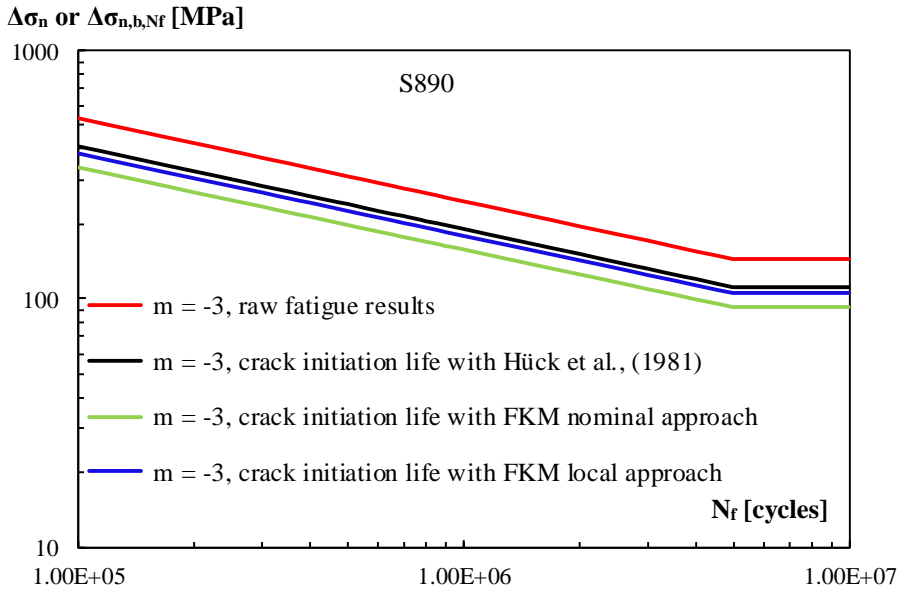


Figure 9.66 Comparison of the raw and the adjusted fatigue results with the lower bound of the data scatter for fixed slope $m = -3$.

The fatigue strength of the base material was determined with the stress concentration factor $K_t = 1$. Figure 9.67 presents the mean curves from the statistical analysis on the adjusted data of the base material cracks in S890 rolled steel compared with the prediction model, where the crack initiation life is determined with the analytical approach of Hüeck et al., (1981) and the adjustment factors for the crack initiation life are also calculated according to this approach. The prediction model shows the overestimated fatigue strength. Figure 9.68 shows the comparison between the prediction model and the mean strength curves from the statistical analysis on the adjusted test data of the base material cracks. The crack initiation life was determined according to the nominal stress approach of the FKM guideline. The fatigue limit of the prediction model matches with the fatigue limit of the mean curve for $m = -3$. Figure 9.69 compares the mean strength curves of the adjusted data with the prediction model where the crack initiation life was determined according to the local stress approach of the FKM guideline. The adjustment factors for the crack initiation life were determined by using the local stress approach procedure of the FKM guideline. The predicted fatigue strength shows good agreement with the mean curve of the adjusted test data for $m = -3$. The fatigue crack initiation life prediction according to the approaches of the FKM guideline was determined with a slope of -5 and with inclusion means stress effect.

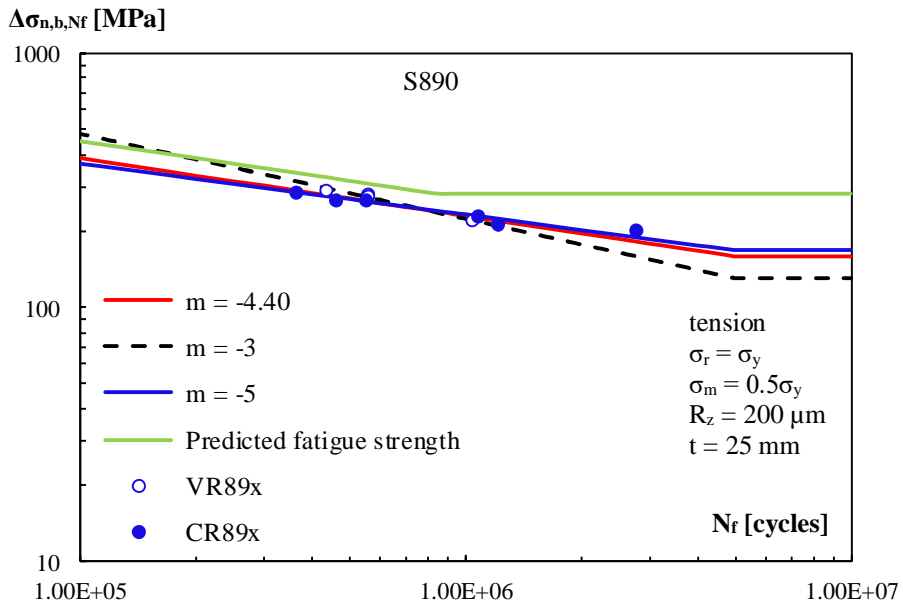


Figure 9.67 Adjusted test data of cracks in rolled steel with the mean curves compared with the prediction model, crack initiation life determined according to Hüeck et al., (1981).

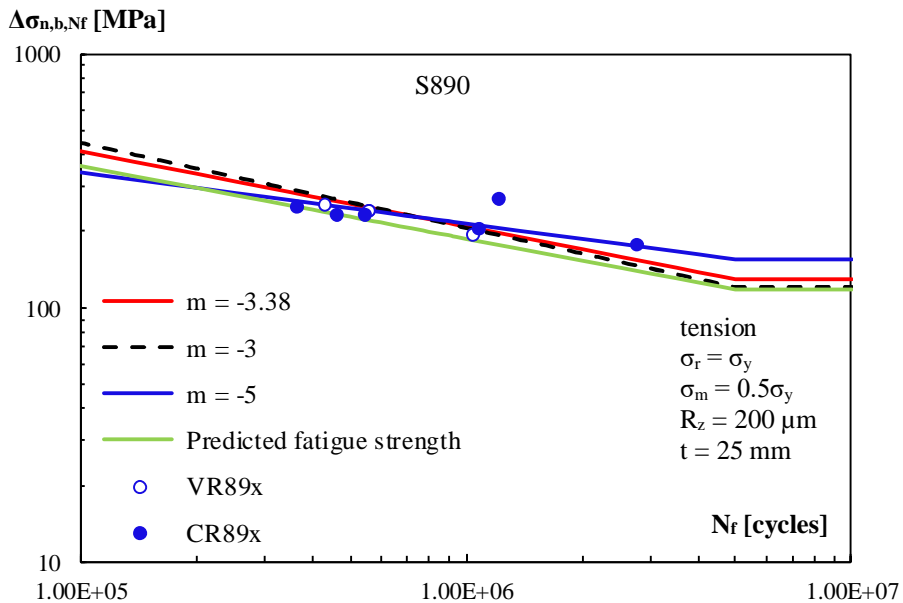


Figure 9.68 Adjusted test data of rolled steel cracks with mean curves compared with prediction model, crack initiation life with nominal stress approach of the FKM guideline.

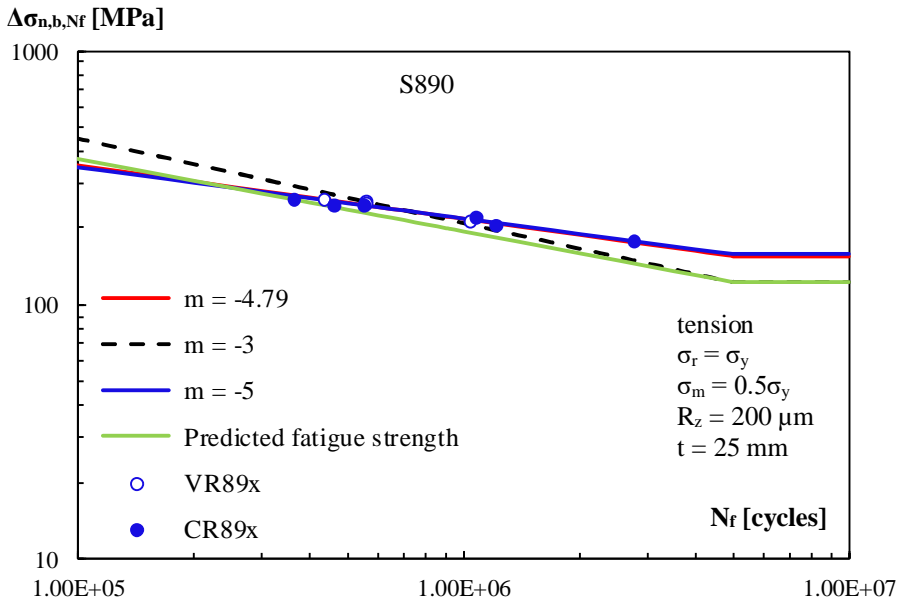


Figure 9.69 Adjusted test data of rolled steel cracks with mean curves compared with prediction model, crack initiation life with the local stress approach of the FKM guide.

Figure 9.70 compares the lower bound curves of the statistical analysis on the raw data of the base material cracks in the rolled steel with the detail category 125 of EN 1993-1-9 (2006). The design curve of EN 1993-1-9 (2006) is found to be conservative. With $m = -4.77$, $\Delta\sigma_{\text{mean}} = 265$ MPa, $\Delta\sigma_c = 246$ MPa, with $m = -3$, $\Delta\sigma_{\text{mean}} = 234$ MPa, $\Delta\sigma_c = 197$ MPa.

Figure 9.71 shows the lower bound curves of the statistical analysis on the adjusted data compared with the detail category 125 of EN 1993-1-9 (2006). The influence factors for the crack initiation life were determined with the analytical approach of Hück et al. (1981). The design curve of EN 1993-1-9 (2006) is very close to the lower bound curve for $m = -3$. With $m = -4.40$, $\Delta\sigma_{\text{mean}} = 197$ MPa, $\Delta\sigma_c = 181$ MPa, with $m = -3$, $\Delta\sigma_{\text{mean}} = 178$ MPa, $\Delta\sigma_c = 151$ MPa. Figure 9.72 presents the lower bound curves of the adjusted test data and the detail category 125 of EN 1993-1-9 (2006). The influence factors of the crack initiation life were determined with the nominal stress approach of the FKM guideline. The lower bound curve for $m = -3$ matches with the design curve 125 of EN 1993-1-9 (2006). With $m = -3.38$, $\Delta\sigma_{\text{mean}} = 170$ MPa, $\Delta\sigma_c = 131$ MPa, with $m = -3$, $\Delta\sigma_{\text{mean}} = 164$ MPa, $\Delta\sigma_c = 124$ MPa. The comparison between the lower bound curves of the adjusted data and the detail category 125 of EN 1993-1-9 (2006) is given in Figure 9.73. The crack initiation life of the test data was adjusted with the local stress approach of the FKM guideline. The lower bound curve for $m = -3$ is very close to the design curve 125 of EN 1993-1-9 (2006). With $m = -4.79$, $\Delta\sigma_{\text{mean}} = 188$ MPa, $\Delta\sigma_c = 179$ MPa, with $m = -3$, $\Delta\sigma_{\text{mean}} = 166$ MPa, $\Delta\sigma_c = 142$ MPa.

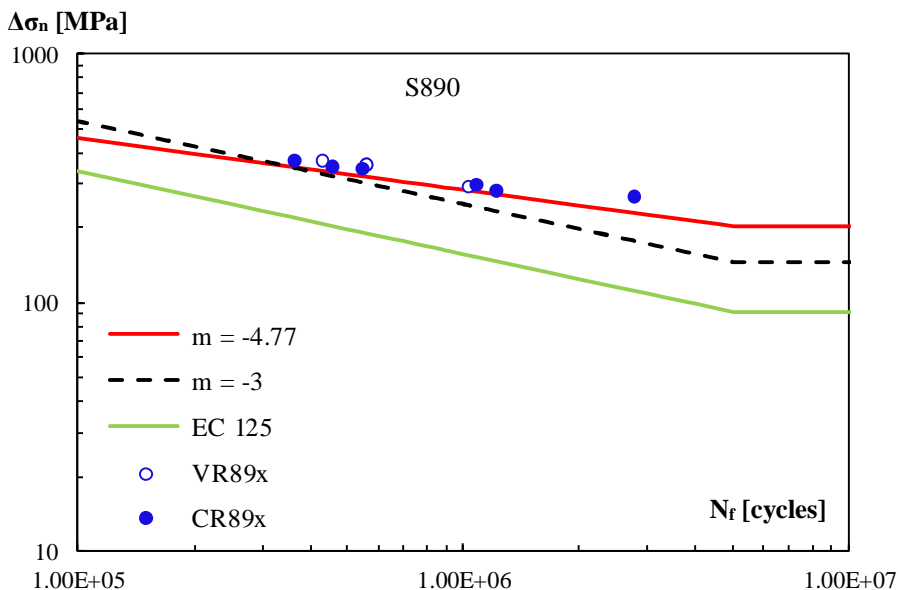


Figure 9.70 Raw fatigue test results of cracks in base material of rolled steel with the lower bound of the data scatter compared with the detail category 125 of EN 1993-1-9 (2006).

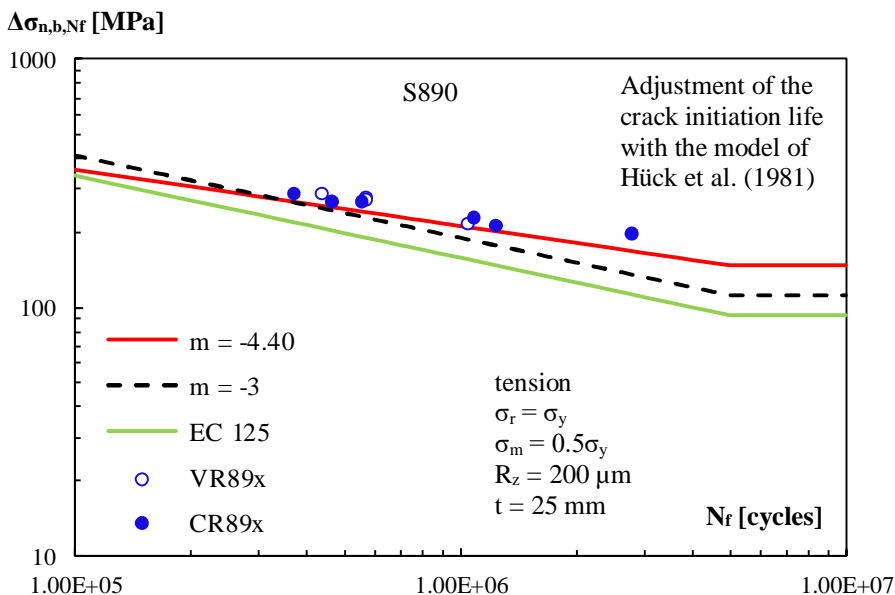


Figure 9.71 Adjusted fatigue test results of cracks in base material of rolled steel with the lower bound of the data scatter compared with detail category 125 of EN 1993-1-9 (2006).

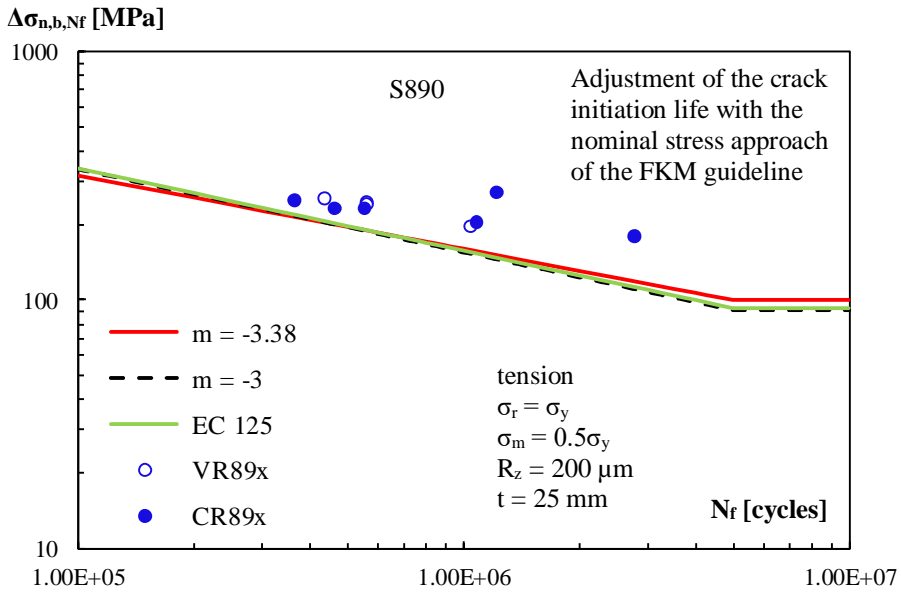


Figure 9.72 Adjusted fatigue test results of cracks in base material of rolled steel with lower bound of the data scatter compared with detail category 125 of EN 1993-1-9 (2006).

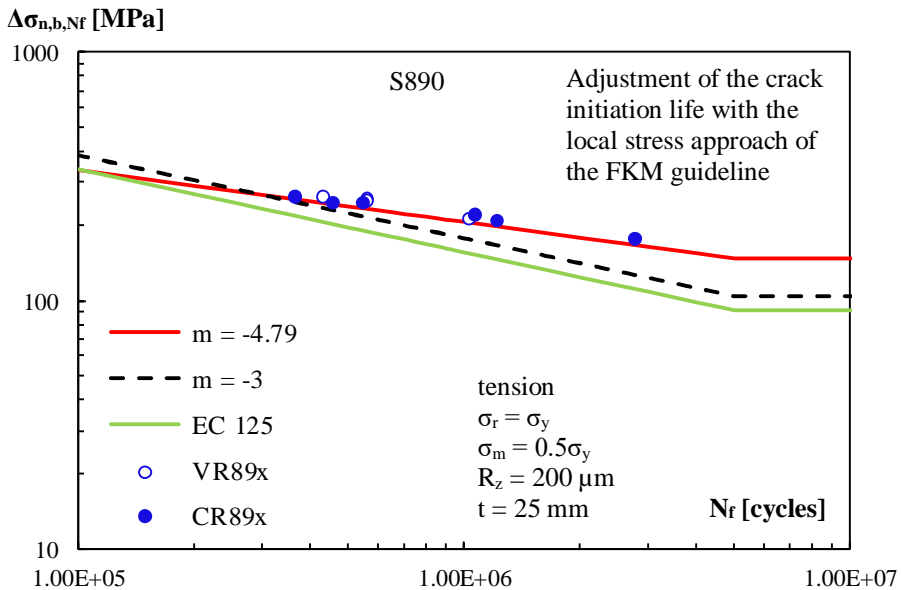


Figure 9.73 Adjusted fatigue test results of cracks in base material of rolled steel with lower bound of the data scatter compared with detail category 125 of EN 1993-1-9 (2006).

In EN 1993-1-9 (2006), no distinction is made between the fatigue strengths of various steel grades. The design curves in EN 1993-1-9 (2006) are also utilized for the fatigue design of high strength steel structures. Therefore, the lower bound curves of the data scatter are compared with the design curves of EN 1993-1-9 (2006). DNVGL-RP-C203 (2016) recommends a design curve for the fatigue design of base material of high strength steels. According to the document, the fatigue strength of a base material with yield strength above 500 MPa can be calculated with the design curve expressed with equation (9.13). In addition, the surface roughness of the material should not exceed $R_z = 3.2 \mu\text{m}$.

$$\log N = 17.446 - 4.70 \log \Delta\sigma \tag{9.13}$$

The design curve has a slope $m = -4.7$ and the characteristic stress range value at 2 million cycles $\Delta\sigma_c = 235 \text{ MPa}$. Figure 9.74 shows the lower bound of the statistical analysis on the raw data of base material cracks in S890 rolled steel compared with the design curve according to equation (9.13). The lower bound curves for a free slope and $m = -5$ are located at above the design curve. The lower bound curves of the adjusted data were also compared with the design curve of DNVGL-RP-C203 (2016). Figure 9.75, Figure 9.76 and Figure 9.77 present the comparison between the fatigue curves of the adjusted data and the design curve of DNVGL-RP-C203 (2016). The lower bound curves of the adjusted data are located at below the design curve.

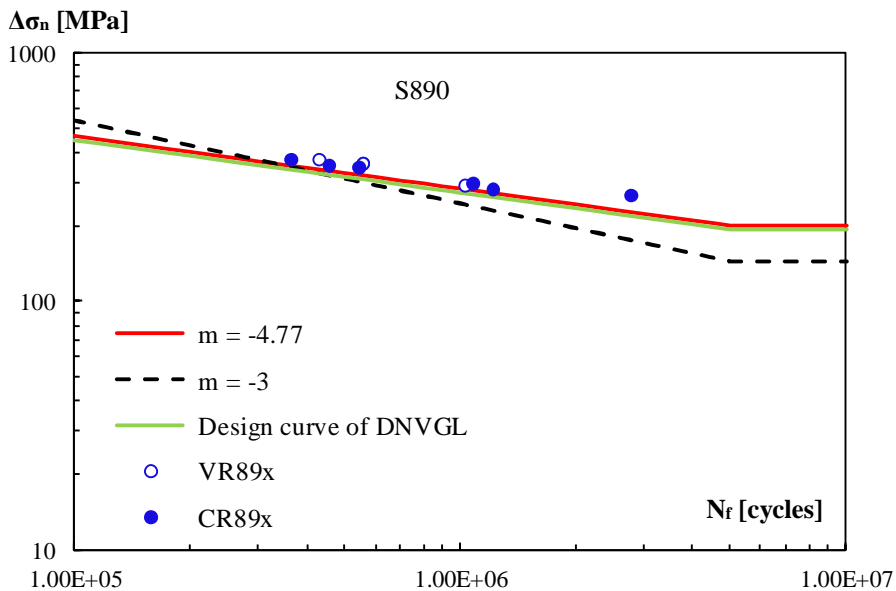


Figure 9.74 Raw fatigue test results of cracks in base material of S890 with lower bound of the data scatter compared with the design curve of DNVGL-RP-C203 (2016).

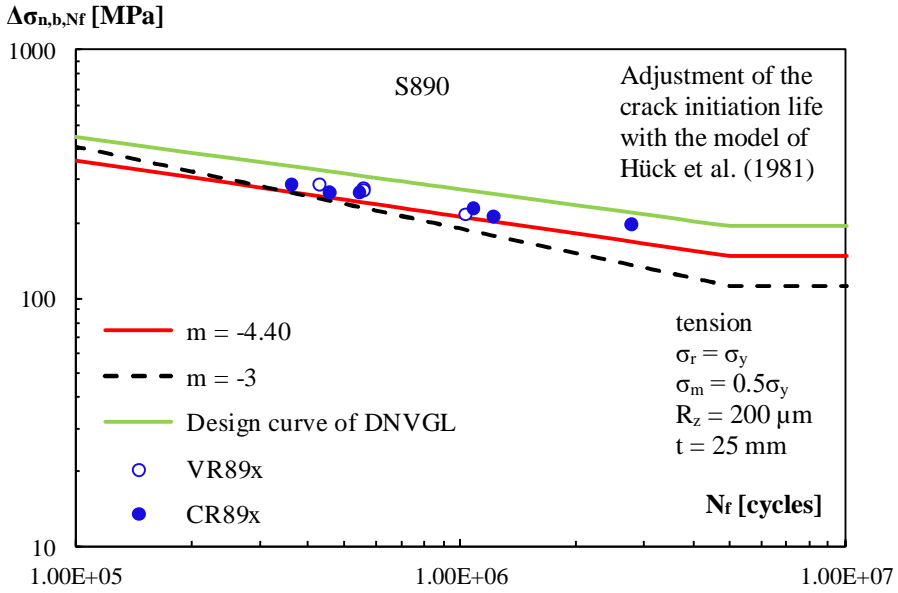


Figure 9.75 Adjusted fatigue test results of cracks in base material of S890 with lower bound of the data scatter compared with the design curve of DNVGL-RP-C203 (2016).

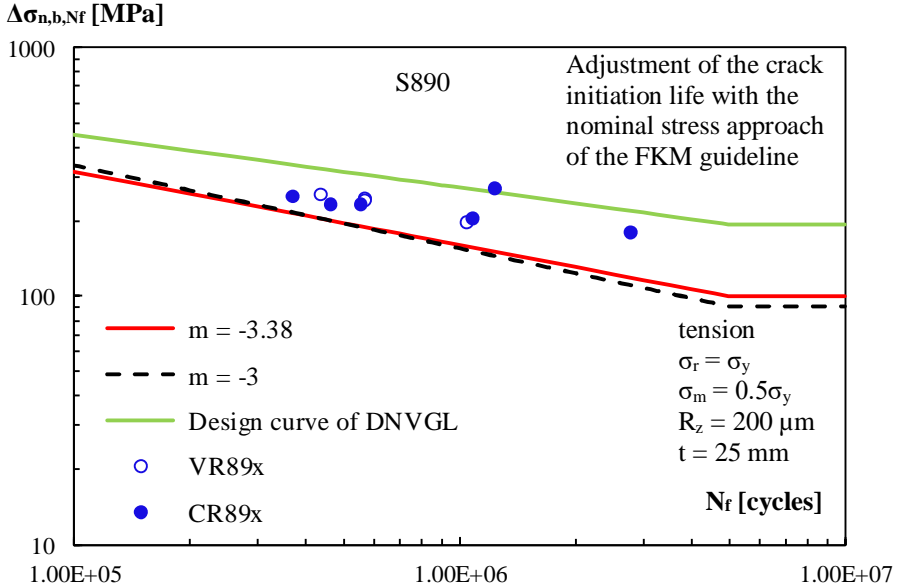


Figure 9.76 Adjusted fatigue test results of cracks in base material of S890 with lower bound of the data scatter compared with the design curve of DNVGL-RP-C203 (2016).

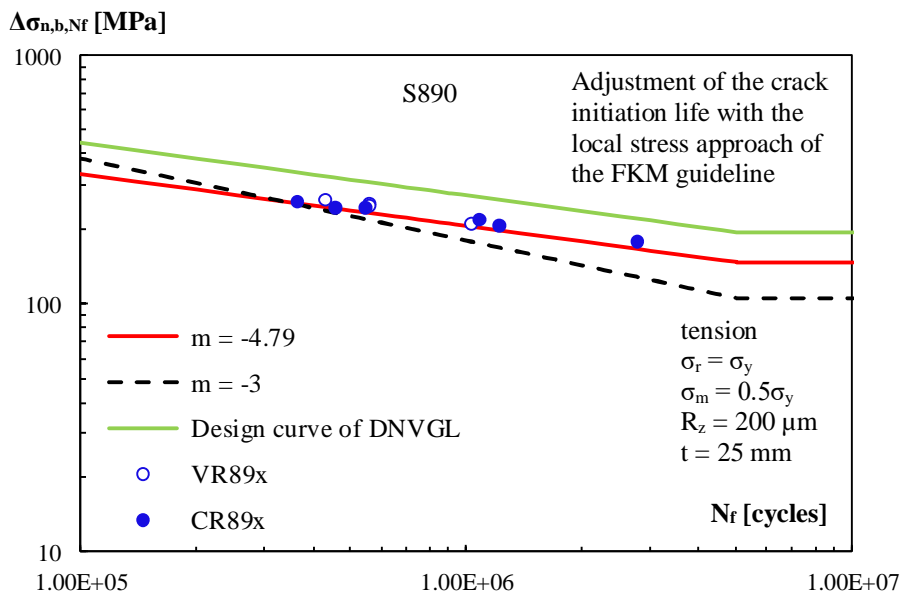


Figure 9.77 Adjusted fatigue test results of cracks in base material of S890 with lower bound of the data scatter compared with the design curve of DNVGL-RP-C203 (2016).

9.3.2.4 Cracks in base material of cast steels

In some specimens of repaired V-shape welded specimens made of rolled and cast steels, the fatigue cracks were observed in the base material of the cast steels. The statistical analysis was performed on the test data of the base material failure in cast steels and the test data of both cast steel grades were combined. From the collected data, it is seen that the base material failure of the specimens took place almost at a similar stress range and the number of cycles at failure are also similar, which makes it difficult to determine a free slope for the data scatter. Therefore, it was only concentrated on the results for the fixed slopes $m = -3$ and $m = -5$. Table 9.7 shows the results of the statistical analysis on the raw and adjusted test data of the base material cracks in the cast steels.

Figure 9.78 presents the fatigue strength curves of the base material cracks in the cast steels with the mean, upper bound and lower bound of the raw data scatter for the fixed slopes. Figure 9.79 shows the fatigue strength curves of the adjusted data with the mean, upper bound and lower bound of the data scatter. The adjustment factors for the crack initiation life were determined according to the approach of Hück et al., (1981). Figure 9.80 and Figure 9.81 also indicate the fatigue strength curves of the adjusted data with the mean, upper bound and lower bound of the data scatter. The crack initiation life adjustment was done with the nominal and the local approach of the FKM guideline respectively. Figure

9.82 shows the lower bound curves of data scatter data with fixed slope $m = -3$ for raw and adjusted data.

Table 9.7 Statistical analysis results on the raw and adjusted data of the base material cracks in the cast steel grades G10MnMoV 6-3 and G18NiMoCr 3-6.

Grades: G10MnMoV 6-3 and G18NiMoCr 3-6							
$\sigma_y = 697$ [MPa], $\sigma_y = 1006$ [MPa]							
	m	a_N	$\Delta\sigma_{\text{mean}}$	$\Delta\sigma_c$	s	$t_{0.95,n-x}$	n
Raw data	-	-	-	-	-	-	-
	-3	13.10	220	185	0.11	2.132	5
	-5	17.86	234	205	0.13	2.132	5
Adjusted data	-	-	-	-	-	-	-
Crack initiation life with Hück et al. (1981)	-3.00	12.70	171	136	0.14	2.13	5
	-5.00	17.17	182	149	0.20	2.13	5
Adjusted data	-	-	-	-	-	-	-
Crack initiation life with FKM nominal	-3.00	12.59	160	125	0.15	2.13	5
	-5.00	16.96	170	135	0.23	2.13	5
Adjusted data	-	-	-	-	-	-	-
Crack initiation life with FKM local	-3.00	12.68	167	134	0.13	2.13	5
	-5.00	17.12	177	146	0.20	2.13	5

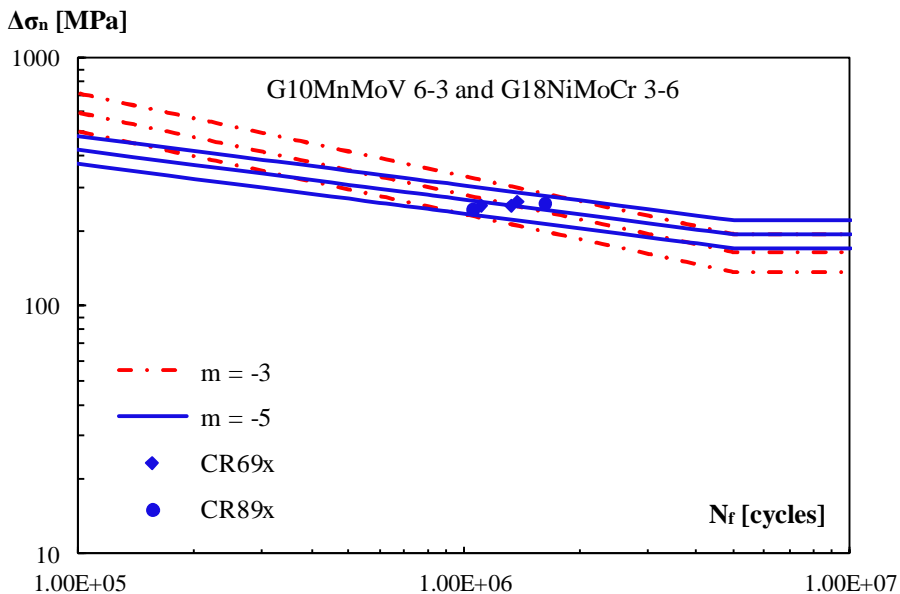


Figure 9.78 Raw fatigue results of the base material cracks in cast steels part with mean, upper bound and lower bound of the data scatter.

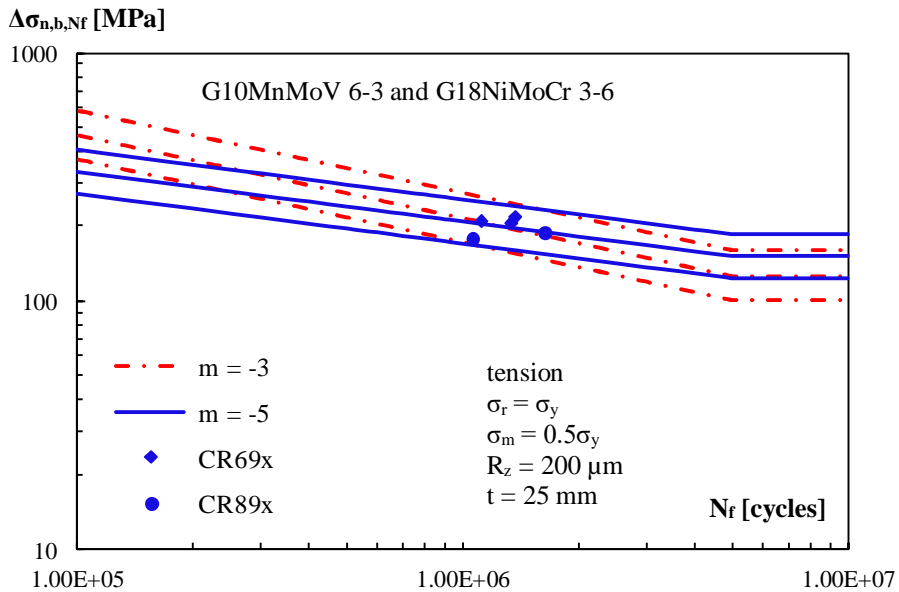


Figure 9.79 Adjusted fatigue results with mean, upper bound and lower bound of the data scatter; crack initiation life adjusted according to Hück et al., (1981).

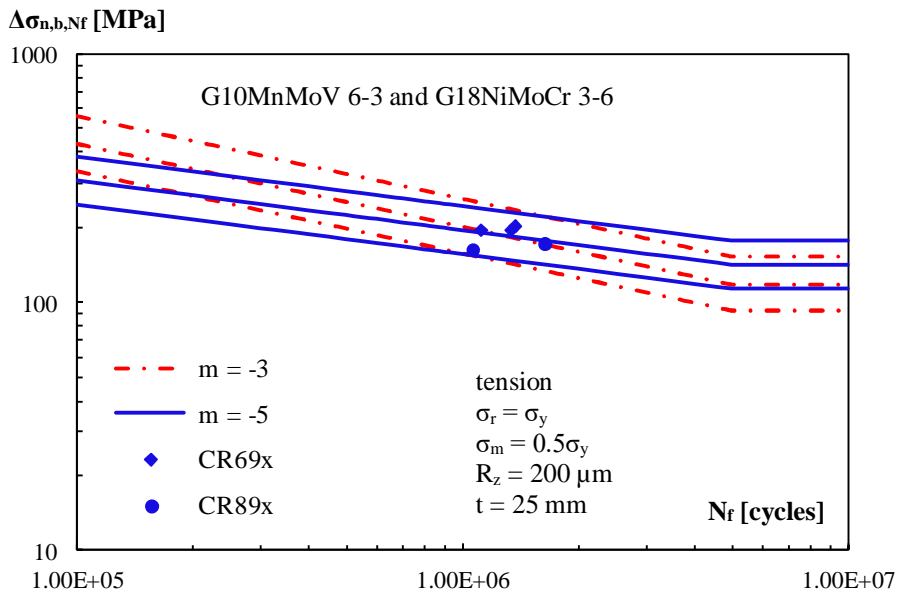


Figure 9.80 Adjusted fatigue results with mean, upper bound and lower bound of the data scatter; crack initiation life adjusted with the nominal stress approach of the FKM guideline.

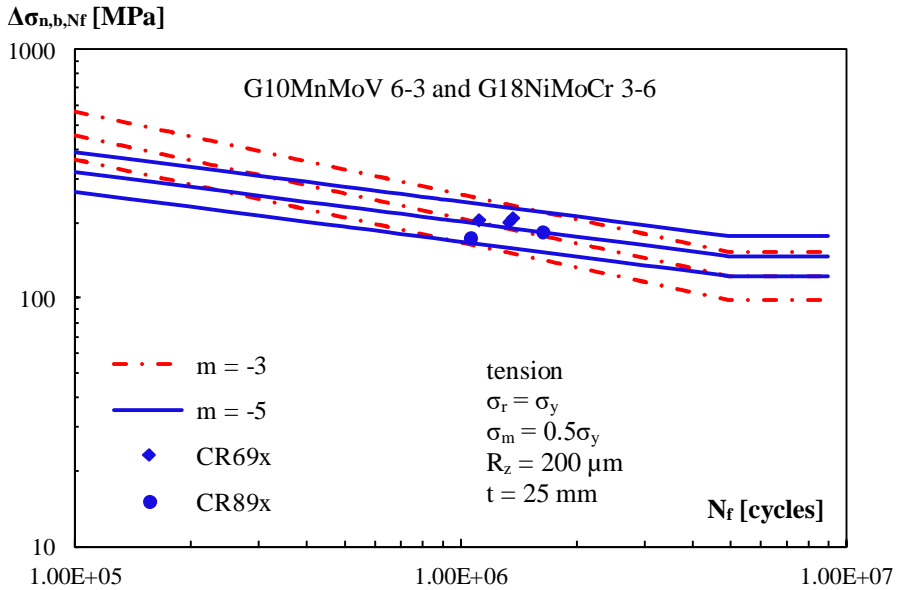


Figure 9.81 Adjusted fatigue results with mean, upper bound and lower bound of the data scatter; crack initiation life adjusted with the local stress approach of the FKM guideline.

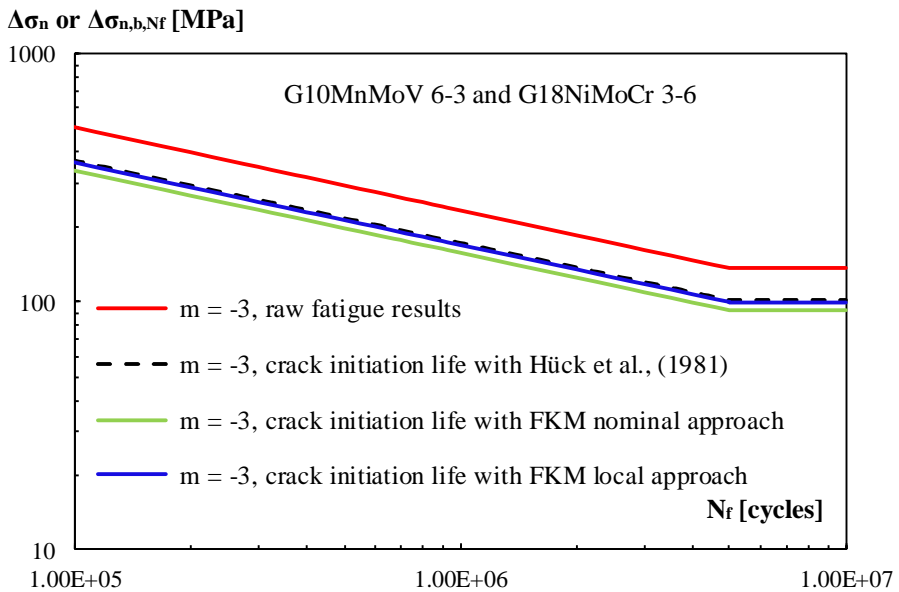


Figure 9.82 Comparison of the raw and the adjusted fatigue results with the lower bound of the data scatter for fixed slope $m = -3$.

Fatigue crack initiation and propagation was observed in the base material of G10MnMoV 6-3 and G18NiMoCr 3-6 cast steels and the test data of both steel grades were combined for the statistical analysis. Since the yield strengths of both materials are different, the prediction was made for both steel grades. Figure 9.83 shows the mean curves from the statistical analysis on the adjusted data of the base material crack in the cast steels compared with the prediction curves. The crack initiation life prediction was made with the analytical approach of Hüeck et al., (1981) and the adjustment factors were also determined based on this approach. The prediction model overestimates the fatigue strength of the material. The extrapolation of the cut-off limit of the prediction curves to 5 million cycles makes the fatigue limit close to the fatigue limit of the mean curve for $m = -5$. Figure 9.84 presents the predicted fatigue strength curves with comparison to the mean curve of the adjusted data scatter. The fatigue crack initiation life was determined according to the nominal stress approach of the FKM guideline. The prediction models show conservative fatigue strengths. Figure 9.85 compares the predicted fatigue strength curves with the mean curves of the adjusted test data. The local stress approach of the FKM guideline was used for the prediction of the crack initiation life. The predicted fatigue strength curves seem to be conservative. The fatigue limit of the prediction curve for G18NiMoCr 6-3 is closer to the fatigue limit of the mean curve for $m = -3$.

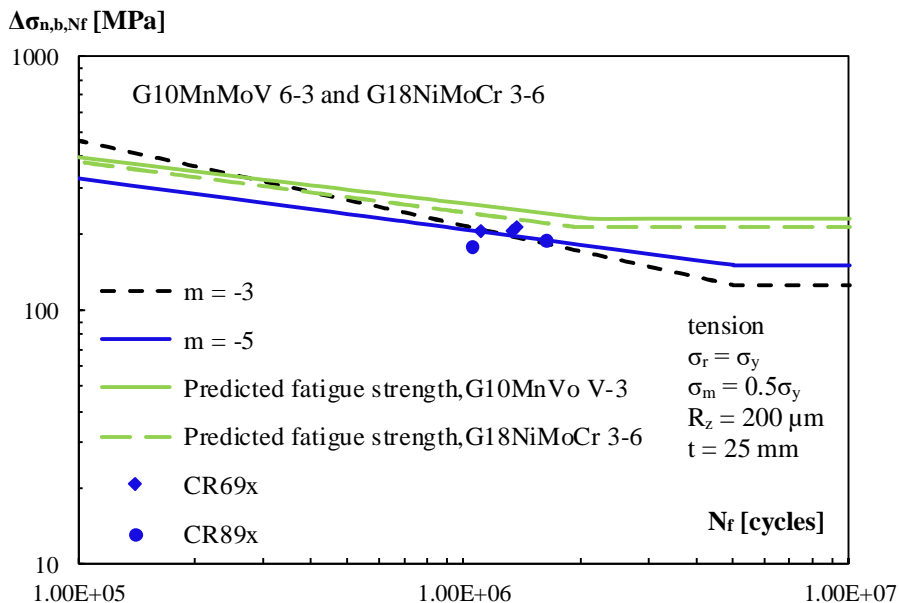


Figure 9.83 Adjusted test data of cracks in cast steels with the mean curves compared with the prediction model, crack initiation life determined according to Hüeck et al., (1981).

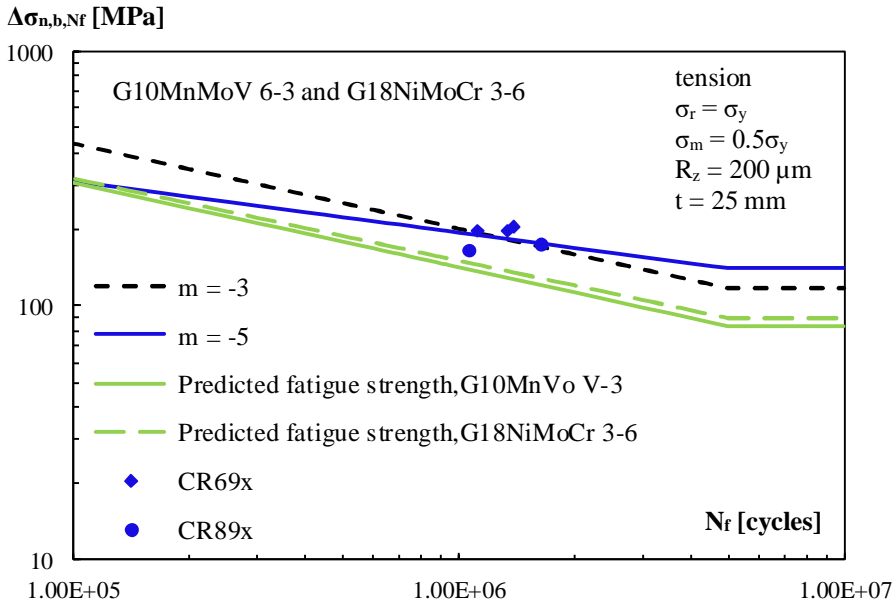


Figure 9.84 Adjusted test data of cracks in cast steels with the mean curves compared with prediction model, crack initiation life with nominal stress approach of the FKM guideline.

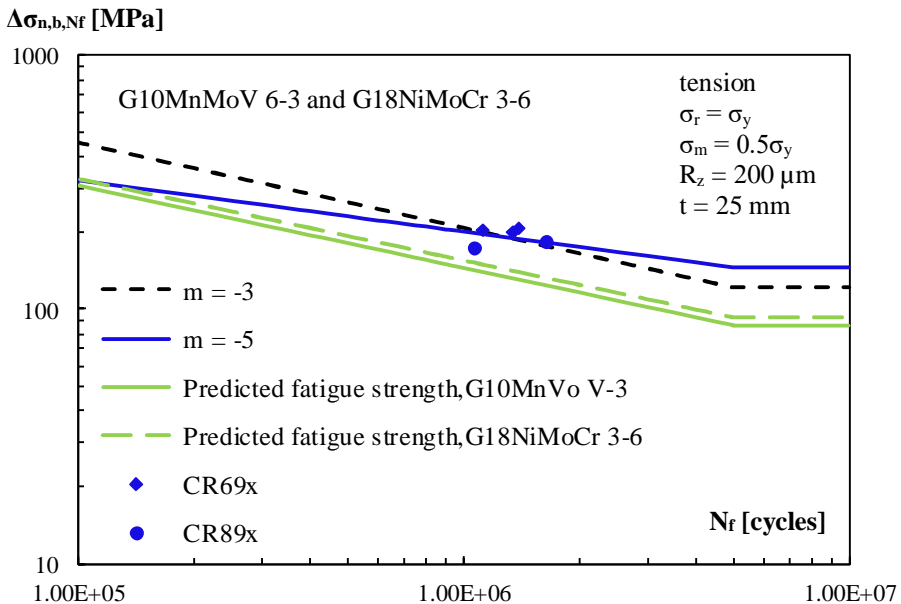


Figure 9.85 Adjusted test data of cracks in cast steels with mean curves compared with prediction model, crack initiation life according to local stress approach of FKM guideline.

Figure 9.86 shows the lower bound curves of the statistical analysis on the raw data of the base material cracks in the cast steels compared with the detail category 125 of EN 1993-1-9 (2006). The fatigue strength curves of the test results are located at the above of the design curve of EN 1993-1-9 (2006), which means that the detail category 125 of EN 1993-1-9 (2006) is conservative. With $m = -3$, $\Delta\sigma_{\text{mean}} = 220$ MPa, $\Delta\sigma_c = 185$ MPa.

Figure 9.87 presents the lower bound curves of the statistical analysis on the adjusted data compared with the detail category 125 of EN 1993-1-9 (2006). The adjustment factors for the crack initiation life were determined according to the approach of Hück et al., (1981). The design curve of EN 1993-1-9 (2006) is very close to the lower bound curve of the scatter for $m = -3$. With $m = -3$, $\Delta\sigma_{\text{mean}} = 168$ MPa, $\Delta\sigma_c = 134$ MPa.

Figure 9.88 indicates the lower bound curves of the statistical analysis on the adjusted data compared with the detail category 125 of EN 1993-1-9 (2006). The crack initiation life of the test data was adjusted with the determined influence factors according to the nominal stress approach of the FKM guideline. The lower bound curve for $m = -3$ reasonably matches with the detail category 125 of EN 1993-1-3 (2006). With $m = -3$, $\Delta\sigma_{\text{mean}} = 157$ MPa, $\Delta\sigma_c = 122$ MPa. Figure 9.89 compares the lower bound curves of the statistical analysis on the adjusted data compared with the detail category 125 of EN 1993-1-9 (2006). The crack initiation life adjustment was done by the local stress approach of the FKM guideline. The lower bound curve for $m = -3$ is very close the design curve of EN 1993-1-9 (2006). With $m = -3$, $\Delta\sigma_{\text{mean}} = 163$ MPa, $\Delta\sigma_c = 131$ MPa.

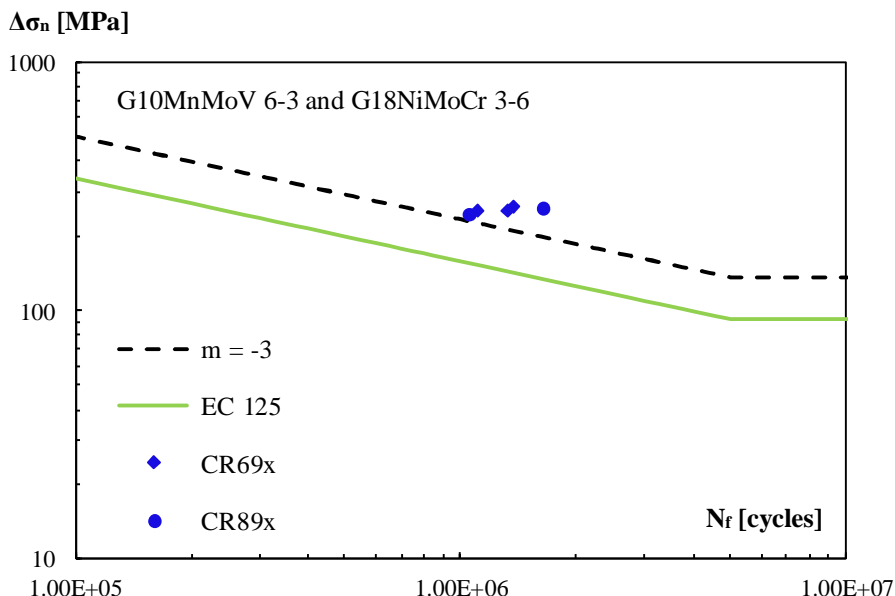


Figure 9.86 Raw fatigue test results of cracks in base material of cast steels with the lower bound of the data scatter compared with the detail category 125 of EN 1993-1-9 (2006).

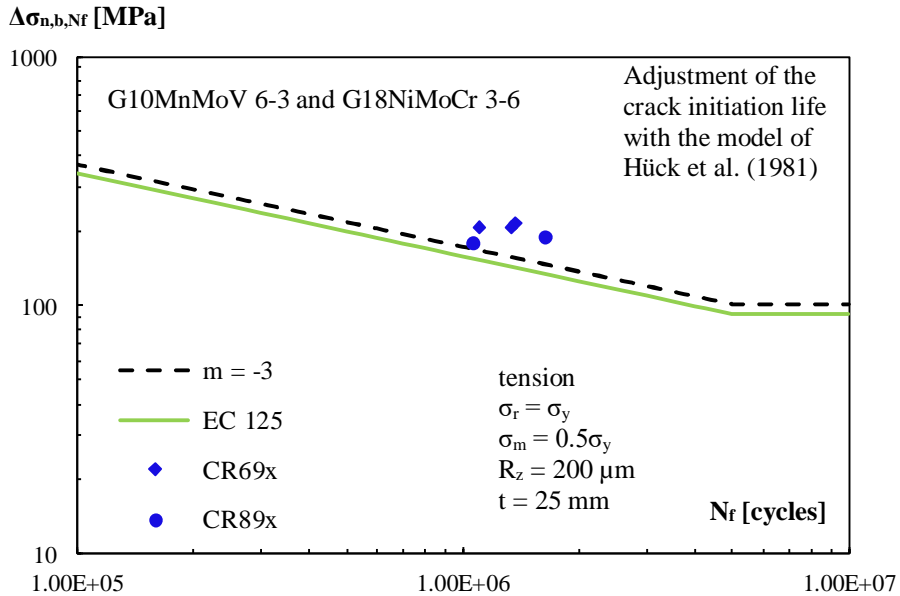


Figure 9.87 Adjusted fatigue test results of cracks in base material of cast steels with lower bound of the data scatter compared with the detail category 125 of EN 1993-1-9 (2006).

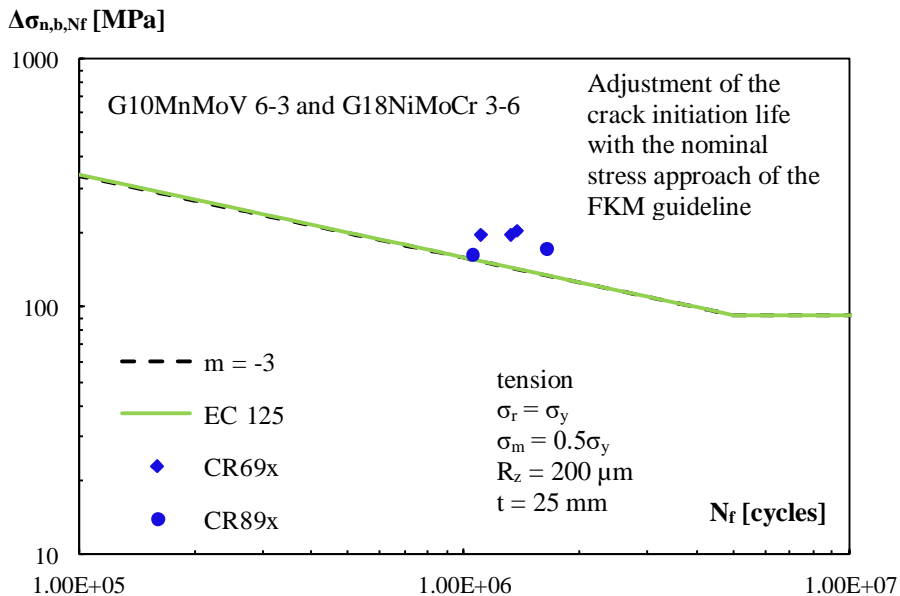


Figure 9.88 Adjusted fatigue test results of cracks in base material of cast steels with lower bound of the data scatter compared with the detail category 125 of EN 1993-1-9 (2006).

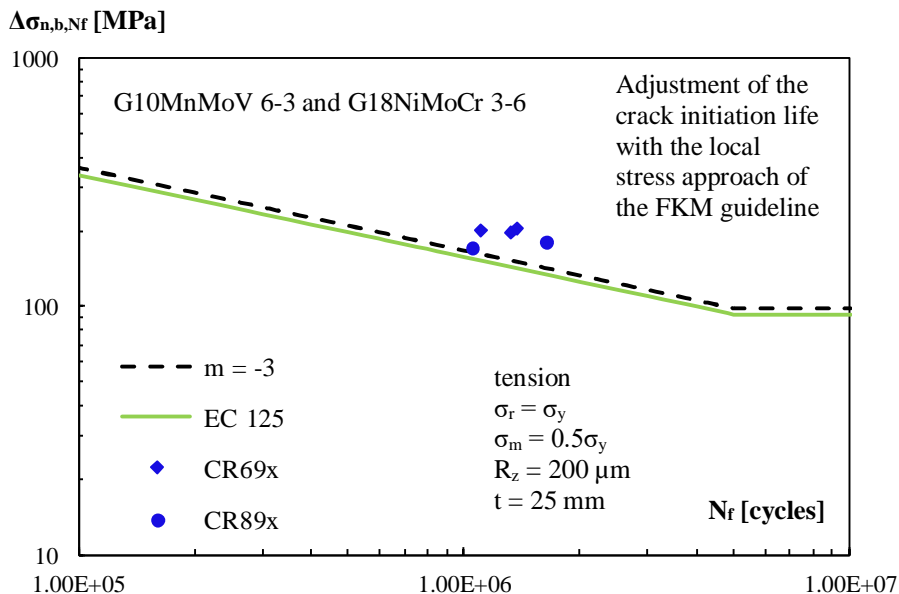


Figure 9.89 Adjusted fatigue test results of cracks in base material of cast steels with lower bound of the data scatter compared with the detail category 125 of EN 1993-1-9 (2006).

The fatigue strength curves of the test data were compared with the design curves of EN 1993-1-9 (2006). In EN 1993-1-9 (2006), it is stated that the standard is applicable for structural steels and no distinction is made between rolled and cast steels. However, DNVGL-RP C203 (2016) gives a recommendation for the fatigue design of cast nodes. In DNVGL-RP C203 (2016), the design curve C is recommended for the fatigue design of the base material of cast nodes. This curve is identical with the detail category 125 of EN 1993-1-9 (2006). Therefore, no additional comparison was made for the design curve C of DNVGL-RP-C203 (2016).

9.4 Summary

This chapter presents the results of the statistical analysis on the fatigue test data of repaired an artificial crack in the base material of S690 and S890 and repaired V-shape welded connections made of very high strength rolled and cast steels. The specimens of V-shape welded connections were manufactured from S690 and S890 rolled steels and from G10MnMoV 6-3 and G18NiMoCr 3-6 cast steels. The test results were adjusted for the loading mode tension, for residual stresses, $\sigma_r = \sigma_y$ and for the mean stress, $\sigma_m = 0.5\sigma_y$. The adjustment factors for the crack initiation life were determined for three different theories. The analysis was made on the raw and the adjusted data. The results of the analysis were

compared with the detail categories of EN 1993-1-9 (2006). In addition to that the fatigue strength results of base material failures were compared with the detail categories of DNVGL-RP-C203 (2016).

In the statistical analysis, the fatigue strength curves of the test data were determined for a free slope and fixed slopes, $m = -3$ and $m = -5$. The free slope was determined from the regression analysis with the least square method. The characteristic value of the fatigue strength curve at 2 million cycles, $\Delta\sigma_c$ and the mean fatigue strength, $\Delta\sigma_{\text{mean}}$ was determined for three slopes of the raw and the adjusted test data. The fatigue strength curves of the welded connections made of very high strength steels tend to have a slope of -3 while the fatigue strength curves of the base material show a tendency for a slope -5. This means that when the fatigue strength of the specimens is dominated by the crack propagation life, the slope of the fatigue curves becomes close to -3 and that, if the crack initiation life is determinant for the fatigue strength, the slopes of the curves approach -5.

The fatigue strength curves of the repaired artificial crack in the base material were compared with the detail category 80 of EN 1993-1-9 (2006) which represents the fatigue strength for X-shape welded connections. The fatigue strength of the raw data is approximately equal to the detail category 160 of EN 1993-1-9, which represents the fatigue strength curve of base material, For the adjusted test data, it approximately decreases to the detail category 100 of EN 1993-1-9 (2006).

The fatigue strength of the repaired V-shape welded connections satisfies the requirements of the detail category 71 of EN 1993-1-9 (2006). Based on the comparison between the fatigue strength curves of the raw data and the design curve 71 of EN 1993-1-9 (2006), it is seen that the design curve is conservative. For the adjusted data, the fatigue strength decreases significantly but it still satisfies the requirements of the detail category 71 of EN 1993-1-9 (2006).

Fatigue crack initiation and propagation was observed in the base material of rolled and cast steels of repaired V-shape welded specimens after the repair of the fatigue cracks in the welded connections. The statistical analysis was performed on these test data and the fatigue strength curves were compared with the detail category 125 of EN 1993-1-9 (2006). The fatigue strength curves of the raw data show higher fatigue strengths as compared to the detail category 125 of EN 1993-1-9 (2006). In the case of the adjusted data, the fatigue strength was reduced but it still meets the requirements of the detail category 125 of EN 1993-1-9 (2006).

The fatigue strength curves of the specimens were compared with the prediction models. Three prediction models were used for prediction of the crack initiation life: the analytical model by Hück et al., (1981) and the nominal and local stress approach of the FKM guideline. The analytical model of Hück et al., (1981) estimates the fatigue limit, the slope and the cut-off limit of the fatigue strength curves based on the yield strength of the material, which causes variations in the fatigue strength curves of the different steel grades.

In general, this approach gives good approximation to determine the fatigue limit for the welded connections, when the cut-off limit is extended to 5 million cycles. It overestimates the fatigue strength for the base materials. The nominal stress approach and the local stress approach of the FKM guideline estimates the fatigue strength limit of the welded connections as well as the fatigue strength limit of the base material with reasonable accuracy.

Part IV: Closure

Part IV: closure is contained in Chapter 10, in which the conclusions and recommendations of the research are highlighted.

Chapter 10

Conclusions and Recommendations

10.1 Evaluation of research project

The main aim of this research was to determine the fatigue strength of repaired fatigue damaged welded connections made of very high strength steels. For this purpose, the focus was put on the quenched and tempered rolled and cast steels with nominal yield strengths 690 MPa and 890 MPa. In addition, it was concentrated on the evaluation of the unexpected test results from the research programme of Pijpers (2011), referred to earlier. The research was carried out with a literature review, an extensive experimental programme and an analysis on the experiment results.

The effectiveness of a fatigue crack repair method can be evaluated by comparing the fatigue strength of the repaired connections with the fatigue strength of original/not repaired connections. The results of the previous research on the fatigue strength of welded connections made of very high strength steels were available for the comparison. In addition, the truss test specimens from that research were also available with the fatigue cracks in the welded connections. The specimens were made from S690 and S890 steel grades. These specimens can be repaired and the effectiveness of the fatigue crack repair method can be evaluated for large scale test specimens. This available knowledge was taken as basis for the preparation of the experimental programme.

In order to determine the effects of the repair weld on the base material, fatigue tests were performed on specimens of the repaired artificial crack in the base material of S690 and S890 steels. The artificial crack was created to avoid the fatigue crack creation stage which might take quite some time. The majority of the experimental work consisted of testing the V-shape welded plate specimens. The V-shape welded plates were manufactured in two configurations: welded rolled to rolled steel plates and welded rolled to cast steel plates. The welding application was executed with a ceramic backing. The V-shape welded specimens were made of S690, S890 rolled steel and with similar strength cast steels

G10MnMoV6-3 and G18NiMoCr3-6 respectively. The V-shape welded specimens were tested under fatigue load to create a fatigue crack in the welded connections. When the crack length reached half the width of the plate specimen, the cracks were repaired by welding and the repaired specimens were tested again until failure, which was defined such that the specimens broke into two pieces. All tests were executed with the four point bending test setups.

Additionally, fatigue crack growth tests were performed on the base material of S690 and S890 steels. A four point bending test setup was used for these tests. The testing procedures, geometry and size of specimens are given in ISO 12108 (2012). The fatigue crack growth tests were executed according to this standard. The fatigue crack initiation location was predefined by creating a notch in the specimens and the crack growth from the notch was monitored. The results of the experiments provided the material parameters and the threshold stress intensity factor range for very high strength steels to calculate fatigue crack propagation life based on the fracture mechanics approach.

A literature review was carried out on the analytical prediction models of fatigue life estimation. The notch stress theory was used for the prediction of the fatigue crack initiation life and the linear fracture mechanics approach for the fatigue crack propagation life. The fatigue crack initiation life was predicted by three methods: the analytical approach proposed by Hüick et al., (1981) and the nominal and local stress approach of the FKM guideline. The fatigue life predictions from the models were compared with the experimental results of the weld toe cracks and the base material cracks. A study was carried out to assess the effects of loading mode, thickness effects, effects of residual stress state, notch radius and weld toe angle on the fatigue strength. A statistical analysis was performed on the test results to compare them with the corresponding detail categories of EN 1993-1-9 (2006) and DNVGL-RP-C203 (2016). In the statistical analysis, the regression coefficient was either taken as a variable or fixed to $m = -3$ or $m = -5$. The characteristic fatigue strength at $2 \cdot 10^6$ cycles was determined for the mean curve and the lower bound curve of the data scatter. The lower bound curves of the data scatter were compared with the relevant design curves of EN 1993-1-9 (2006) and the mean curves with the prediction curves. In addition, the curves of the repaired welded specimens were compared with the fatigue strength from the test results of original/not repaired connections.

Furthermore, Pijpers (2011) observed fatigue crack initiation and propagation in the base material of the welded specimens. These specimens were examined and a literature review was carried out to identify the reason of the base material failure. Based on the literature review, a microscopic examination was performed on the fracture surfaces of these specimens. This microscopic examination was carried out on the fracture surfaces of S460, S890 and S1100 rolled steels and on the fracture surfaces of the cast steels with similar strengths G20Mn5, G18NiMoCr3-6 and G22NiMoCr5-6 respectively.

Section 10.2 presents the conclusions of this research programme and Section 10.3 gives an overview of the recommendations for further research.

10.2 Conclusions

The fatigue life of structural members is divided in the fatigue crack initiation life and fatigue crack propagation life. For welded connections, it is assumed that the fatigue crack initiation life is very short due to residuals stresses, imperfections at the weld toe and the notch at the fusion zone. Accordingly, the fatigue crack initiation life of the welded connections is usually neglected and the fatigue crack propagation stage is determinant of the fatigue life. From research results it was found that the fatigue crack initiation life of welded connections made of very high strength steels is longer than expected. The second general conclusion is that the fatigue strength of fatigue damaged welded connections made of very high strength steel can be regained with a procedure of repair by welding. The repair of the fatigue cracks needs to be executed in the similar conditions as the original manufacturing process.

The conclusions are presented in the following sections.

10.2.1 Microscopic examinations on the fracture surfaces

The microscopic research was carried out on the fracture surfaces of the base material failures that were observed during the research programme of Pijpers (2011). For the results of the microscopic research on the fracture surfaces of the base material, the following can be concluded:

- It was revealed that the base material of rolled steels was repaired by welding which caused fatigue crack initiation in the base material. The cracks initiated at the weld toe of the repair weld, which means that the weld toe conditions of the repair welds were more critical for the crack initiation compared to the weld toe conditions of the connections.
- The cross section of the repaired locations showed that the repair welds had been executed with one welding pass. This kind of repair welds needs to be performed with several weld passes, in order to provide a sufficient temperature gradient for the formation of suitable microstructures and to avoid high residual stress occurrence.
- High hardness values were obtained at the repaired weld location. It was concluded that the cooling time of the repair welds was very short. This means that the preheat temperature of the material was very low or it was not preheated at all. The repair welds were executed in an improper way.

- In practice, this kind of repair weld should be avoided in the base material as far as possible. If it is really necessary to repair the base material, the manufacturer must inform the owner of the structure, and the consequence of the repair needs to be discussed with experts. Since very high strength steels are susceptible to the thermal cycles of the welding process, additional attention needs to be paid to repairing base material of very high strength steels by welding.
- The microscopic images have shown that crack initiation in the base material of cast steels took place from the pores at the surface and at subsurface of the specimens. It is also mentioned in literature that the material imperfections at surface and subsurface are more critical for fatigue crack initiation.
- Due to the production process of cast steels, pores in the material are inevitable and it should be kept in mind that these imperfections may cause fatigue crack initiation in the base material of fatigue loaded elements.
- Very high strength steels are more susceptible to the notch as compared to steels with lower strengths. The pores at the surface of the very high strength cast steels cause small notches, which promote fatigue crack initiation. The occurrence of pores at the surface therefore needs to be prevented.
- The inspection standards for cast steels specify the quality of the cast steels based on the detected imperfection in the material. Fatigue loaded structures, cast steels with quality I, which should not contain detectable imperfections, should be used. However, according to inspection documents, the material is not examined 100% and the uninspected areas still may contain imperfections. Care should be taken with these imperfections.

10.2.2 Fatigue crack growth tests

Fatigue crack growth tests were carried out on the base material of S690 and S890 steels and the results lead the following conclusions:

- Fatigue crack growth behaviour of the steels depends on the stress intensity range, which is a function of the crack shape, thickness and width. The yield strength of the material has no effect on the fatigue crack growth rate of the steels.
- In experimental work, the threshold stress intensity factor range for high strength steels was determined and the results show that the yield strength of the material has negligible influence on the threshold stress intensity factor range.
- Very high strength steels are known to be brittle and hard material. Consequently, it is expected that the fatigue crack propagation in very high strength steels will be fast, which is responsible for the negative reputation of very high strength steels. The results of fatigue crack growth tests have shown that there is no different

fatigue crack growth behaviour between very high strength and lower strength steels.

- The results of the experiments show good agreement with the recommended values from BS 7910 (2013), which are given for steels with yield strengths lower than 600 MPa. This confirms that the fatigue crack growth is hardly affected by the yield strength of the material.

10.2.3 Fatigue life prediction models

Fatigue test results of the repaired fatigue cracks in the welded connections made of very high strength were compared with the prediction models. Fatigue crack initiation life and the fatigue crack propagation life were determined separately. For the prediction models the following conclusions can be made;

- Yield strength, surface roughness and mean stress affect the fatigue crack initiation life of the base material. In addition, thickness, loading mode, weld shape and notch radius at the weld toe have an influence on the fatigue strength of welded connections.
- The notch stress approach was used for the prediction of the fatigue crack initiation life. The notch sensitivity of the material was expressed by the fatigue notch factor and various approaches were studied for the determination of the fatigue notch factor. For assessing effect of very high strength steels, the microstructural notch support proposed by Lawrence et al., (1981) is the appropriate approach for the calculation of the fatigue notch factor. Hence, an increased notch radius or a decreased weld toe angle results in a higher fatigue strength with an increase of material yield strength.
- The study on the mean stress effect showed that susceptibility to mean stress increases with higher yield strengths. Consequently, compressive mean stresses have beneficial effects on the fatigue strength. Therefore, literature states that high frequency mechanical impact treatments, which introduce compressive stresses at weld toe, are more effective for fatigue strength improvement of welded connections made of very high strength steels.
- The fatigue crack initiation life was determined with three different approaches: the analytical approach proposed by Hück et al., (1981) and the nominal and local stress approach of the FKM guideline. The prediction model according to Hück et al., (1981) expresses the slope, knee point and fatigue limit of the material as a function of the material tensile strength. Therefore, it shows large deviations at the low and high cycle regions for the comparison with the test results. In general, it gives a good approximation for the fatigue limit determination of welded connections and overestimates for fatigue limit prediction of the base material.

- The nominal stress approach of the FKM guideline shows accurate fatigue crack initiation life predictions. For the weld toe cracks, it results in a conservative fatigue life prediction, while the prediction is more accurate for the base material.
- The local stress approach of the FKM guideline slightly overestimates the fatigue crack initiation life for weld toe cracks and for base material cracks, the estimation is more accurate.
- For comparison of fatigue test data with the prediction curve, the fatigue test data were adjusted with the mean stress factor in order to take the effect of the residual stresses into account as well as the loading mode factor to determine the fatigue strength for the tension loading mode. In the analytical approach of Hüeck et al., (1981), no distinction is made between the mean stress factor of welded and non-welded components and it is only given for non-welded specimens. In the current study, the mean stress factor was determined with the procedure for non-welded specimens and it causes a large stress range reduction in the test data. Therefore, the model overestimates the fatigue strength of the welded connections compared to the test results. In the FKM guideline, the mean stress factor is separately specified for non-welded and welded components and consequently, it provides a more accurate fatigue crack initiation life estimation.
- The fatigue assessment for non-welded components in the FKM guideline can be used for fatigue life estimation with the modifications given in Chapter 8.
- Fatigue crack propagation is a function of the crack growth rate and stress intensity factor range. Since the fatigue crack growth parameter of the steels is not affected by yield strength, the fatigue crack propagation life depends on the stress intensity factor range, which is a function of crack shape, stress range, width and thickness.
- The fatigue crack propagation life is determined by a fracture mechanics approach, and the material parameters from the fatigue crack growth tests were used for the prediction. The results from the prediction of fatigue crack propagation show reasonable agreement with the test results. Consequently, the results of the fatigue crack growth tests were verified by the experimental results.

10.2.4 Fatigue tests on base material of very high strength steels with a repaired artificial crack

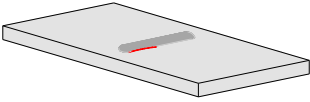
Fatigue tests were carried out on plate test specimens of repaired an artificial crack in the base material of S690 and S890 rolled steels. The results of the experiments lead to the following conclusions:

- Fatigue cracks initiated at the start-stop points of the repair weld. The start-stop points of the welding cause a high stress concentration effect and high residual

stresses. The start-stop points were ground after the welding to eliminate the effect of stress concentration, which means that high residual stresses promoted fatigue crack initiation at those locations.

- The fatigue crack initiation and propagation life of the specimens were approximately equal. About 45% of the fatigue life was occupied by the fatigue crack initiation life which is quite high as compared to welded connections.
- The fatigue strength of the repaired artificial crack in the base material tends to increase with yield strength according to results for the free slopes. The specimens made of S890 rolled steels show a higher fatigue strength when compared to the specimens made of S690 rolled steel.
- The fatigue strength of the specimens made of both steel grades satisfies the requirement of the detail category 125 of EN 1993-1-9 (2006) for analysis on raw data (see Table 10.1).

Table 10.1 Summary of fatigue strength results of repaired artificial crack in the base material.

Detail	Slope, m	$\Delta\sigma_c$ [MPa]	Steel grade	Description
Number of specimens; n = 9 for S690 n = 9 for S890 	-3.05/ -3/ -5	154/154/181	S690	Raw data, t = 25 mm, Bending
	-5.46/ -3/ -5	191/151/190	S890	
	-2.86/ -3/ -5	95/99/115	S690	Adjusted ¹ , t = 25 mm, Tension, $\sigma_r = \sigma_y$
	-5.40/ -3/ -5	113/92/115	S890	
	-2.97/ -3/ -5	120/123/144	S690	Adjusted ² , t = 25 mm, Tension, $\sigma_r = \sigma_y$
	-5.64/ -3/ -5	150/123/154	S890	
	-2.90/ -3/ -5	125/129/151	S690	Adjusted ³ , t = 25 mm, Tension, $\sigma_r = \sigma_y$
	-4.34/ -3/ -5	134/130/163	S890	

¹ Adjustment of crack initiation life was made according the prediction model of Hück et al., (1981).

² Adjustment of crack initiation life was made according the nominal stress approach of the FKM guideline.

³ Adjustment of crack initiation life was made according the local stress approach of the FKM guideline.

- The results have shown that the repair weld has limited detrimental effects on the fatigue strength of the base materials, based on the comparison with the design curve of EN 1993-1-9 (2006). This means that, with a proper repair procedure the fatigue strength reduction due to the repair weld can be limited.

10.2.5 Fatigue tests on repaired V-shape welded connections made of high strength rolled and cast steels

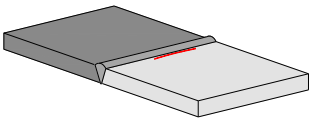
Fatigue tests were carried out on repaired fatigue damaged V-shape welded specimens made of high strength rolled and cast steels. During these fatigue tests, fatigue crack initiation and propagation were observed at various locations of the specimens: weld toe of the cap at the rolled steel side, weld toe of the cap at the cast steel side, in the base material of the rolled steel and in the base material of the cast steels. Due to limited available data, it was not possible to analyse the results based on the steel grades. The results were analysed according to the crack initiation and propagation locations and therefore the conclusions are also specified with the same analogy.

Weld toe crack in the cap of rolled steels

The analysis of the test data of the weld toe cracks at the cap of the rolled steel parts leads to the following conclusions:

- With the established repair procedure, the fatigue strength of the fatigue damaged V-shape welded connections made of very high strength steels can be regained and the comparison has shown that the fatigue strength of repaired connections is the same as the fatigue strength of the original weld. The effects of stress history are eliminated.
- It reveals that the repair by welding has no negative consequences on the fatigue strength of V-shape welded connections. The fatigue strength of the V-shape welded connections is not influenced by additional thermal cycles of the repair weld.
- After the repair weld, the welded connections were reshaped by grinding. It was aimed at avoiding the stress concentration effects at the intersection locations of the repair weld to the original weld. Further grinding up to the start-stop point may result in higher fatigue strength, as a result of the weld toe angle reduction. It was quantitatively determined from the weld toe angle factor.
- The fatigue strength results of the repaired V-shape welded connections satisfy the requirements of the detail category 71 of EN 1993-1-9 (2006) (see Table 10.2).
- The fatigue cracks initiated at the weld toe of the repair weld, which was achieved with treating the weld toe of the original weld by high frequency impact treatment (HiFIT). Therefore, the treatment is an effective method to eliminate the influences of the loading history before the repair.
- In general, it is assumed that the quality of repair welds is lower than the quality of the original weld. However, in the current study, there was one run-out specimen during the fatigue crack creation stage. But after the repair, there were three additional run-outs. This means that a repaired weld can even be better than the original weld.

Table 10.2 Summary of fatigue strength results of the weld toe crack at the cap in the rolled steel parts of the repaired V-shape welded connections.

Detail	Slope, m	$\Delta\sigma_c$ [MPa]	Steel grade	Description
Number of specimens; n = 13 with runouts n = 9 without runouts 	-3.62/ -3/ -5	114/111/154	S690 S890	Raw data, t = 25 mm, Bending
	-3.26/ -3/ -5	73/70/97	S690 S890	Adjusted ¹ , t = 25 mm, Tension, $\sigma_r = \sigma_y$
	-3.22/ -3/ -5	87/85/118	S690 S890	Adjusted ² , t = 25 mm, Tension, $\sigma_r = \sigma_y$
	-2.59/ -3/ -5	72/87/121	S690 S890	Adjusted ³ , t = 25 mm, Tension, $\sigma_r = \sigma_y$

¹ Adjustment of crack initiation life was made according the prediction model of Hück et al., (1981).

² Adjustment of crack initiation life was made according the nominal stress approach of the FKM guideline.

³ Adjustment of crack initiation life was made according the local stress approach of the FKM guideline.

- In the majority of the test specimens, fatigue cracks initiated at the root of the weld, during the fatigue crack creation stage. After repair of the cracks, no weld root cracks have been observed. The difference between two welding processes is the original weld executed, with a ceramic backing and without constraining the specimens, while the repair weld was performed without a ceramic backing and with constraining the specimens, which provide lower residual tensile stresses at the weld root. The results make the effectiveness of the backing plate questionable considering the residual stress state in the connections.

Weld toe crack in the cap of cast steels

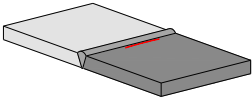
For the results of the weld toe cracks in the cap of the cast steel the following conclusions were made:

- The fatigue strength of the repaired weld toe cracks in the cast steel parts is the same as the fatigue strength of the original weld.
- Fatigue cracks initiated at the weld toe of the repair weld, which was achieved by treating the original weld toe with HiFIT.
- Since the fatigue strength of the connections was regained by the weld repair, the repair by welding has no negative influence on the fatigue strength of the welded connections made of cast steels.
- The fatigue strength of the weld toe cracks at the cap of the cast steels part satisfies the requirement of detail category 71 of EN 1993-1-9 (2006) according to

analysis of the raw data (see Table 10.3). The analysis of the adjusted data for the fixed slope $m = -3$ also tends to satisfy the requirements of the detail category 71 of EN 1993-1-9 (2006).

- The statistical analysis of the adjusted test data resulted that the characteristic stress range at 2 million cycles was lower than the characteristic stress range of detail category 71 of EN 1993-1-9 (2006). There were very limited data and the data showed a very narrow data scatter. Additional data were required for more reliable conclusions with regard to the adjusted data.

Table 10.3 Summary of fatigue strength results of the weld toe cracks at the cap in cast steel parts of the repaired V-shape welded connections.

Detail	Slope, m	$\Delta\sigma_c$ [MPa]	Steel grade	Description
Number of specimens; $n = 5$ 	-2.91/ -3/ -5	100/112/148	G10MnMoV 6-3 G18NiMoCr 3-6	Raw data, t = 25 mm, Bending
	-2.24/ -3/ -5	43/67/87	G10MnMoV 6-3 G18NiMoCr 3-6	Adjusted ¹ , t = 25 mm, Tension, $\sigma_r = \sigma_y$
	-2.48/ -3/ -5	65/86/110	G10MnMoV 6-3 G18NiMoCr 3-6	Adjusted ² , t = 25 mm, Tension, $\sigma_r = \sigma_y$
	-2.20/ -3/ -5	57/88/110	G10MnMoV 6-3 G18NiMoCr 3-6	Adjusted ³ , t = 25 mm, Tension, $\sigma_r = \sigma_y$

¹ Adjustment of crack initiation life was made according the prediction model of Hück et al., (1981).

² Adjustment of crack initiation life was made according the nominal stress approach of the FKM guideline.

³ Adjustment of crack initiation life was made according the local stress approach of the FKM guideline.

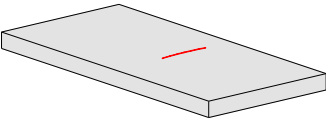
- EN 1993-1-9 (2006) makes no distinction between the fatigue strength of rolled steels and cast steel connections. DNVGL-RP-C203 (2016) recommends using the fatigue strength curve of rolled steels for cast steel connections. According to the recommendation, the curve F can be used for the assessment of V-shape welded connections and this curve is identical to the detail category 71 of EN 1993-1-9 (2006). In accordance with this, the results of the raw data satisfy the requirements of the curve F of DNVGL-RP-C203 (2016).

Fatigue cracks in the base material of S890 rolled steel

In the specimens containing S890 rolled steel, fatigue crack initiation and propagation was observed in the base material of S890 rolled steel, both during the crack creation stage and during testing of the repaired welded specimens. The base material failures after the repair were analysed and this lead the following conclusions;

- Visual examination on the fracture surface of the specimens revealed that there were some imperfections at the crack initiation location. They looked like corrosion pits. In some specimens, plate surfaces were cleaned with sand paper before testing and the crack initiations in the base material was observed in these specimens as well. Similar imperfections were detected on the fracture surfaces of these specimens. Cleaning with sand paper was not effective to avoid the crack initiation in the base material of the specimens. Consequently, the corrosion pits on the plate surface can be critical locations for the fatigue crack initiation.
- The fatigue strength of the base material meets the requirements of the detail category 125 of EN 1993-1-9 (2006), where this detail category represents fatigue strength of the base material (see Table 10.4). Accordingly, the imperfections have no major influence on the fatigue strength of the base material.

Table 10.4 Summary of fatigue strength results of base material cracks in the rolled steel.

Detail	Slope, m	$\Delta\sigma_c$ [MPa]	Steel grade	Description
Number of specimens; n = 10 	-4.77/ -3/ -5	246/197/250	S890	Raw data, t = 25 mm, Bending
	-4.40/ -3/ -5	181/151/188	S890	Adjusted ¹ , t = 25 mm, Tension, $\sigma_r = \sigma_y$
	-3.38/ -3/ -5	131/124/156	S890	Adjusted ² , t = 25 mm, Tension, $\sigma_r = \sigma_y$
	-4.79/ -3/ -5	179/142/181	S890	Adjusted ³ , t = 25 mm, Tension, $\sigma_r = \sigma_y$

¹ Adjustment of crack initiation life was made according the prediction model of Hüeck et al., (1981).

² Adjustment of crack initiation life was made according the nominal stress approach of the FKM guideline.

³ Adjustment of crack initiation life was made according the local stress approach of the FKM guideline.

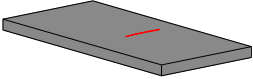
- The slope of the fatigue strength curve tends to decrease -5, which is expected for the fatigue strength curves of very high strength steels.
- In EN 1993-1-9 (2006), no additional fatigue design curves are provided for the fatigue assessment of very high strength steels. However, DNVGL-RP-C203 (2016) recommends an additional fatigue design curve for the base material of very high strength steels. The fatigue strength of raw data exactly matches with the recommended curve in DNVGL-RP-C203 (2016).

Fatigue cracks in the base material of cast steels

In the specimens containing cast steels, fatigue crack initiation and propagation were observed in the base material of the cast steels. The analysis of the test results of these specimens lead to the following conclusions:

- Fatigue crack initiation and propagation was observed in the base material of both G10MnMoV 6-3 and G18NiMoCr 3-6 cast steels.
- There were not any run-out specimens from the test series containing cast steels.
- The fracture surfaces of the specimens with the base material failure were visually inspected and some internal imperfections were detected at the crack initiation locations. The imperfections were at the surface and subsurface of the plate. This kind of imperfections was already examined during the microscopic examination on the fracture surfaces of the specimens from the previous research programme.

Table 10.5 Summary of fatigue strength results of base material cracks in the cast steels.

Detail	Slope, m	$\Delta\sigma_c$ [MPa]	Steel grade	Description
Number of specimens; n = 5 	-/ -3/ -5	-/185/205	G10MnMoV 6-3 G18NiMoCr 3-6	Raw data, t = 25 mm, Bending
	-/ -3/ -5	-/136/149	G10MnMoV 6-3 G18NiMoCr 3-6	Adjusted ¹ , t = 25 mm, Tension, $\sigma_r = \sigma_y$
	-/ -3/ -5	-/125/135	G10MnMoV 6-3 G18NiMoCr 3-6	Adjusted ² , t = 25 mm, Tension, $\sigma_r = \sigma_y$
	-/ -3/ -5	-/134/177	G10MnMoV 6-3 G18NiMoCr 3-6	Adjusted ³ , t = 25 mm, Tension, $\sigma_r = \sigma_y$

¹ Adjustment of crack initiation life was made according the prediction model of Hück et al., (1981).

² Adjustment of crack initiation life was made according the nominal stress approach of the FKM guideline.

³ Adjustment of crack initiation life was made according the local stress approach of the FKM guideline.

- According to the material certificate, the cast steels satisfy the requirements of quality I of the inspection documents, which allow very limited and small imperfections for the quality I materials. In addition, the inspection was not carried out on 100% of the plate surfaces. The crack initiation took place either due to very small allowable imperfections in the inspected area or due to larger imperfections in an uninspected area.
- The fatigue strength of the base material of cast steels satisfies the requirements of the detail category 125 of EN 1993-1-9 (2006). There were very limited data available for the analysis and the available data fell in the same scatter range.

Therefore, the fatigue strength for a free slope was not determined (see Table 10.5). In EN 1993-1-9 (2006), no differences are mentioned for the fatigue design of cast and rolled steels. DNVGL-RP-C203 (2016) recommends curve C for fatigue assessment of the base material of the cast joints. This curve is identical to the detail category 125 of EN 1993-1-9 (2006). The requirements of this recommendation document are also satisfied. Accordingly, the base material of cast steels meets the expected fatigue strength. In other words, the base material without imperfections might provide a higher fatigue strength.

10.3 Recommendations for further research

Based on the literature survey and the results of the current study, the following recommendations for further research are founded as follow:

- The literature review has shown that quite an extensive amount of research has been carried out to determine the fatigue strength of very high strength steels for structural applications. These data need to be systematically evaluated and a fatigue design rule for the materials with yield strengths above 690 MPa must be established. For the establishment of the design rule, welded connections should be classified, based on the welding procedure, weld shape, weld quality, possible residual stress state, the plate thickness and loading condition.
- More fatigue test data on repaired welded connections should be gathered. An increased amount of data provides opportunities for a reliable statistical analysis and evaluations.
- Repairing fatigue cracks in welded connections made of very high strength steels with various preheat temperatures that are lower than the preheat temperature of the original welds, or local preheating, need to be studied.
- The established repair procedure was applied to V-shape welded plate test specimens. The consequences of repairing fatigue cracks in large scale test specimens should be determined. The truss specimens in the Stevin II laboratory can be used for this purpose.
- In the majority of the V-shape welded plate specimens, fatigue crack initiation was observed at the weld root, during the crack creation stage. Therefore, it is expected that the improvement of the weld root quality will increase the fatigue strength of the connections. An additional research needs to be carried out on specimens welded with and without ceramic backing. The welding should be executed with and without constrain conditions. In this manner, the effect of the weld root geometry and the welding conditions on the fatigue strength on the welded connections can be studied. The results of the research can lead to optimum solution for manufacturing weld roots of the V-shape weld with a high quality.

- Hybrid laser arc welding application provides a narrow heat affected zone, limited hardness increase, good root penetration and low residual stress state. Since very high strength steels are susceptible to heat input for microstructural changes and mean stress, which can be either the result of applied stress or residual stress, hybrid laser arc welding may increase the fatigue strength of welded connections.
- The crack propagation life of V-shape welded connections is occupied by the crack propagation through the base material. In case of a half V-shape or K-shape welded connections, the crack will propagate in the heat affected zone of the connections. The microstructure of the heat affected zone is different with respect to the microstructure of the base material. As to the fatigue crack propagation life estimation for these cracks, the fatigue crack propagation behaviour in a heat affected zone of welded connections made of very high strength steels should be determined.
- The reliability of crack containing structures are determined by a fitness for purpose assessments. In fatigue loaded structures, crack contained elements are additionally exposed to static loads. The failure of these elements can take place either due to plasticity of the remaining ligament or due to reaching the critical stress intensity value of the materials. The critical stress intensity value can be determined by tests. BS7910:2013 provides some empirical relation between the Charpy-V value and the critical stress intensity value. But these relations are valid only for the material with a yield strength up to 480 MPa. Since the Charpy-V value of the materials is provided in the material certificate, these relations make assessment easier. This kind of relations should be established for very high strength steels as well.
- On the fracture surface of the base material in cast steels, some imperfections were observed at the crack initiation locations. The tested material, according to the material certificate, satisfied the quality I based on the inspections standards. For quality I material, the amount of allowed imperfections is very limited and with very small sizes. According to the inspection procedure, the plates are not inspected 100%. Therefore, additional research is needed to assess the allowable imperfection sizes and the inspection procedure is to be carried out from a fatigue strength point of view of the cast steels.
- Nowadays, advanced additive manufacturing techniques are developed for manufacturing steel elements. Due to the fast manufacturing process and freedom in shape of the sections, it can be used for manufacturing fatigue critical joints instead of casting. The fatigue strength of these components should be determined and the residual stresses and internal imperfections in wire based additive manufacturing of high strength steels may have considerable effects on the fatigue strength.

- Very high strength steels are usually used for highly loaded structures. Consequently, the material will be exposed to high stress ranges, which may result failures at low cyclic region; the number of cycles lower than 10^5 . The fatigue behaviour at low cyclic region should be determined for very high strength steels.
- Further research is needed for the fatigue behaviour of welded connections made of very high strength steels under variable amplitude loading. In reality, structures experience loading spectrum with a variable amplitude. Designing structures with constant amplitude loading might be either conservative or non-conservative. The crack closure effect due to overloading might not be beneficial for high strength steels.
- The residual stress state in very high strength steels needs to be studied. Very high strengths show high susceptibility to mean stress as compared to mild stress. Therefore, the magnitude of the residual stresses will have relatively large effects on the fatigue strength.
- Further study is needed on the fatigue strength of very high strength steels in corrosive environments. The corrosion process will not occur uniformly, which causes rough surfaces on the elements. The effect of the surface roughness was discussed in Chapter 8. It showed that high strength steels are more susceptible to surface roughness than mild strength steels.
- A study needs to be performed on the effects of blasting on fatigue strength of the very high strength steels. Blasting may improve the surface roughness and introduce compressive stresses on the surface. Especially the effect of the surface roughness after blasting may have a significant influence on the fatigue strength of the material.

References

- Anderson, T.L (2005). “Fracture mechanics, fundamentals and applications”. Taylor and Francis group. Boca Raton, Florida.
- ASTM E 446-98 (1998). “Standard reference radiographs for steel castings up to 2 in. (51mm) in thickness”. American Society for Testing Materials, West Conshohocken.
- ASTM E 647 (2016). “Standard test method for measurement of fatigue crack growth rate”. American Society for Testing Materials, West Conshohocken
- Athens, R.J., Volker, B.K., Seeger, T. (1993). “Kerbformzahlen von stumpfstößen und doppel T stößen”. Schweißen und schneiden, Vol: 45, No: 12, 685-688.
- Barsom, J.M., Rolfe, S.T. (1999). “Fracture and fatigue control in structures: Application of fracture mechanics”. Third edition, ASTM, Philadelphia, PA.
- Becker, D., Bierwith, J., Brachthäuser, N., Dopfer, R., Thulig, T. (2009). “Zero strategy in the cold rolling industry”. Comité international D'Étude Du Laminage Á froid du Feuillard D'Acier Cielffa, Fachvereinigung Kaltwalzwerke e.V.
- Becker, W. T., Shipley, R.J. (2002). “Failures related to casting”. ASM Handbook, Volume 11: Failure analysis and prevention.
- Borrego, L. P., Pires, J.T.B., Costa, J.M., Ferreira, J.M. (2009). “Mould steels repaired by laser welding”. Engineering failure analysis 16, 596-607.
- Branco, C.M., Infante, V., Baptista, R. (2004). “Fatigue behaviour of welded joints with cracks, repaired by hammer peening”. Fatigue fracture engineering material structures, 27, 785-798.
- Brozzetti, J., Hirt, M. A., Ryan, L., Sedlacek, G., Smith, I. F. C. (1989). Background information on fatigue design rules-Statistical evaluation-Chapter 9-Document 9.01. Eurocode 3 editorial Group.
- BS 7910 (2013). “Guide to methods for assessing the acceptability of flaws in metallic structures”. British Standards

- Institute, London.
- Campbell, T., Tiryakioğlu. (2006). “Modelling microstructure and properties: The contributions of grain size, DAS and biofilms”. Material Science Forum, Vols. 519-521, pp: 1453-1460.
- Carrato, J. L. (1999). “Should welding be used to repair structural steel.” Arema 1999 annual conference, Trucks and Structures, Chicago, IL.
- Crear, R. (2001) “EM 1110-2-6054, Engineering manual. Inspection, evaluation and repair of hydraulic structures.” U.S. Army corps of engineers, Washington.
- Demofonti, G., Riscifuli, S., Sonsion, C.M., Kaufmann, H., Sedlacek, G., Muller, C., Hanus, F., Wegmann, H.G. (2001). “High strength steels in welded state for lightweight constructions under high and variable stress peaks.” Final report EUR 19989, Luxemburg.
- Denda, T., Bretz, P.L., Tien, J.K. (1991) “Inclusion size effect on the fatigue crack propagation mechanism and fracture mechanics of a super alloy.” Metallurgical Transactions A, 23A, 519-526.
- Dexter, R. J., Ocel, J.M. (2013) “Manual for retrofit of fatigue cracks in steel bridges.” U.S. Department of transportation federal highway administration, FHWA-IF-12-020.
- Dexter, R.J., Fitzpatrick, R.J., Peter, D.L.St. (2003) “Fatigue strength and adequacy of weld repairs.” Ship structure committee, Washington D.C.
- Diete, E.,G., Bacon, D. (1988) “Mechanical Metallurgy.” McGraw-Holl Book Company, UK.
- DNV-GL (2016) “Fatigue design of offshore steel structures, Recommended practice DNVGL-RP-C203”, Norway.
- EN 1369, (2012) “Founding- Magnetic particle testing.” European committee for standardization, Brussels.
- EN 1371-1 (1997). “Founding- Liquid penetrant inspection- Part 1: Sand, gravity die and low pressure die castings.” European committee for standardization, Brussels.
- EN 10160, (1999) “Ultrasonic testing of steel flat product of thickness equal or greater than 6mm (reflection method).” European committee for standardization, Brussels.
- EN 12680-1, (2003) “Founding- Ultrasonic examination- Part 1: Steel

-
- casting for general purposes.” European committee for standardization, Brussels.
- EN 1993-1-9 (2006). “Design of steel structures-General- Part 1.9: Fatigue” European committee for standardization, Brussels.
- EN-ISO 5817 (2007) “Welding- Fusion welded joints in steel, nickel, titanium and their alloys beam welding executed- Quality levels for imperfections.” Geneva, ISO copyright office.
- EN-ISO 8062-3 (2007) “Geometrical product specifications-Dimensional and geometrical tolerance for moulded part-Part 3 : General dimensional and geometrical tolerance and machining allowance for casting.” European committee for standardization, Brussels
- EN-ISO 12108 (2012) “Metallic materials – Fatigue testing – Fatigue testing – Fatigue crack growth method.” Geneva, ISO copyright office
- EN-ISO 15614-1 (2004) “Specification and qualification of welding procedures for metallic materials – Welding procedure test Part 1: Arc and gas welding of steels and arc welding of nickel and nickel alloys.” Geneva, ISO copyright office.
- EN-ISO 17638 (2003). “Non-destructive testing of welds-Magnetic particles testing.” Geneva, ISO copyright office.
- EN-ISO 2378 (2009). “Non-destructive testing of welds-Magnetic particles testing-Acceptance levels.” Geneva, ISO copyright office.
- Fisher, J. W., Hausammann, H., Sullivan, M., Pense, A. (1979). “Detection and repair of fatigue damage in welded highway bridges. National cooperative highway research program (NCHRP) 206.” Transportation research board. Washington, D.C.
- Fisher, J.W., Kulak, G.L., Smith, I.F.C. (1998). “A fatigue primer for structural engineers.” National steel bridge alliance, Chicago.
- Fisher, J. W., Dexter, J.R. (1994). “Field experience with repair of fatigue cracks.” International conference of fatigue, Toronto, 45-52.
- Fisher, J. W., Dexter, R.J. (1994). “Weld improvement for fatigue life extension.” International conference on fatigue, Toronto, 82-87.
- FKM Guideline (2012) “Analytical strength assessment of components made of steel, cast iron and aluminium materials in
-

- mechanical engineering.” 6th Edition, Forschungskuratorium Maschinenbau, Frankfurt/Main, Germany.
- Fourneaux, P., Defourny, J., Bannister, A.C., Brownlow, P.J., Fattorini, F., Demofonti, G., et al. (2001) “Development of high strength steels with optimised Y/T ratio for high loaded applications.” Final report EUR 19987, Luxembourg.
- Gonzalez, J., Llano, J., Garcia, J. (2007). “Metallurgical application to work and back up rolls for hot and cold rolling of flat products.” International workshop on “Rolls for flat rolling of steel”, Bellary, India.
- Griffith, A.A. (1920). “The phenomena for rupture and flow in solids.” Philosophical Transactions, Series A, Vol. 221, pp: 163-198.
- Gudehus, H., Zenner, H. (1995). “Leitfaden für eine Betriebsfestigkeitsrechnung.” Verlag Stahleisen mbH, Düsseldorf.
- Haagensen, P.J., Maddox, S.J. (2001). “IIW Recommendations on post-weld improvement of steel and aluminium structures.” International institute of welding, IIW documents XIII-1815-00.
- Haagensen, P.J. (1994). “Methods for fatigue strength improvement and repair of welded offshore structures.” OMAE-Volume III, Material engineering, ASME, 419-427
- Haagensen, P.J., Statnikov, E.S., Lopez-Martinez, L. (1998). “Introductory fatigue tests on welded joints in high strength steel and aluminium by various methods including ultrasonic treatment.” International institute of welding, IIW document XIII-1748-98.
- Hobbacher, A.F. (2016). “Recommendations for fatigue design of welded joints and components.” IIW document IIW-2259-15, International institute of welding.
- Hück, M., Thrainer, L., Schütz, W. (1981). “Berechnung von Wöhlerlinien für Bauteile aus Stahl, Stahlguß und Grauguß synthetische Wöhlerlinien.” Bericht Nr. ABF 11 (zweite überarbeitete Fassung) VDEh, Düsseldorf.
- Infante, V., Branco, C.M. (2004) “A study on the fatigue behaviour of damaged welded joints repaired by hammer peening.” Lisbon university of technology, Portugal.
- Irwin, G.R. (1948) “Fracture dynamics. Fracture of metals.” American society for metals, Cleveland, OH, pp: 147-166.
- Itoga, H., Tokaji, K., Nakajima, “Effect of surface roughness on step-wise S-N

-
- M., Ko, H.-N. (2003). characteristic in high strength steel.” *International journal of fatigue*, 25, 379-385.
- ISO 11666 (2010). “Non-destructive testing of welds-Ultrasonic testing of welded joints-Acceptance levels.” Geneva, ISO copyright office.
- ISO 17640 (2010). “Non-destructive testing of welds-Ultrasonic testing of welded joints.” Geneva, ISO copyright office.
- Jang, C.D., Song, H.C., Lee, C.H. (2002). “Fatigue life extension of a through thickness crack using local heating.” *Proceedings of the twelfth international offshore and polar engineering conference*. Kitakyushu, Japan, 224-229.
- Janssen, M., Zuidema, J., Wanhill, R.J.H. (2004). “Fracture Mechanics.” VSSD, Delft
- Jesus de, A.M.P., Matos, R., Fontouro, B.F.C., Rebelo, C., Silvia da, L.S., Veljkovic, M. (2012) “A comparison of the fatigue behaviour between S355 and S690 steel grades.” *Journal of constructional steel research*, 79, pp: 140-150.
- Juriani, A. (2015) “Casting defects analysis in foundry and their remedial measures with industrial case study.” *Journal of mechanical and civil engineering*, Vol. 12, pp: 43-54.
- Kirkhope, K.J., Bell, R., Caron, L., Basu, R.I., Ma, K.-T., (1999). “Weld detail fatigue life improvement techniques Part I: Review.” *Marine structures*, 12, 447-474.
- Kling, S., Witte, M. (2007) “Advanced process and quality control in hot rolling mills using eddy current inspection.” *IV Conferencia panamericana de END Buenos aires*.
- Konuma, S., Furukawa, T. “Correlation between fatigue strength and hardness of hard steels having martensite structure.” 18th Fatigue symposium, Soc. Mater. Sci. Japan, 1986, pp: 5-9.
- Kunio, T., Shimizu, M., Yamada, K., Sakura, K., Yamamoto, T. (1981). “The early stage of fatigue crack growth in martensitic steel.” *International journal of fracture*, 17, 111-119.
- Kudryavtsev, Y., Kleiman, J., Lugovskoy, A., Lobanov, L., Knysh, V., Voitenko, O., Prokopenko, G. (2005). “Rehabilitation and repair of welded elements and structures by ultrasonic peening.” *International institute of welding, IIW document XIII-2076-05*.
- Kudryavtsev, Y., Kleiman, J., “Fatigue strength of structural elements with crack
-

- Knysh, V. (2008). repaired by welding.” International institute of welding, IIW Document XIII-2236-08.
- Kudryavtsev, Y., Kleiman, J., Iwamura, Y. (2011). “Fatigue improvement of high strength steel welded elements by ultrasonic peening.” 30th International conference on ocean, offshore and arctic engineering, Vol. 3, 629-637.
- Lawrence, F.V., Mattos, R.J., Higashida, Y., Burk, J.D. (1978). “Estimating the fatigue crack initiation life of welds.” Fatigue testing of weldments, ASTM STP, 648, pp.134-158.
- Lawrence, F.V., Ho, N., J., Mazumdar, P.K. (1981). “Predicting the fatigue strength of welds.” Annual reviews of material science, Volume: 11,401-425
- Lei, Z., Hong, Y., Xie, J., Sun, C., Zhao, A. (2012). “Effects of inclusion size and location on very high cycle fatigue behaviour for high strength steels.” Material science and engineering A, 558, 234-241.
- Li, S.X. (2012). “Effects of inclusions on very high cycle fatigue properties of high strength steels.” International material reviews, Vol. 57, 94-114.
- Ma, J., Zhang, B., Xu, D., Han, E.H., Ke, W. (2010). “Effects of inclusions and loading direction on the fatigue behaviour of hot rolled low carbon steel.” International journal of fatigue, 32, 1116-1125.
- Marquis, G.B., Barsoum, Z. (2016). “IIW recommendations for the HFMI treatment.” International institute for welding, IIW collections, Springer.
- Murakami, Y. (1994). “Inclusion rating by statistics of extreme values and its application to fatigue strength prediction and quality control materials.” Journal of research of the national institute of standards and technology, 99, 345-351.
- Murakami, Y. (2002). “Metal fatigue: Effects of small defects and non-metallic inclusions.” Amsterdam and Boston Elsevier.
- Murakami, Y., Usuki, H. (1989). “Quantitative evaluation of effects of non-metallic inclusion on fatigue strength of high strength steels I: Basic fatigue mechanism and evaluation of correlation between fatigue fracture stress and the size and location of non-metallic inclusions.” International journal of fatigue, 11, 219-298.
- Murakami, Y., Usuki, H. (1989). “Quantitative evaluation of effects of non-metallic inclusion on fatigue strength of high strength steels I:

-
- Fatigue limit evaluation based on statistics for extreme values of inclusion size." *International journal of fatigue*, 5, 299-307.
- Neuber, H. (1968). "Über die Berücksichtigung der Spannungskonzentration bei Sestigkeitsberechnungen." *Konstruktion*, 20, 245-251.
- Paris, P.C., Gomez, M.P., Anderson, W.E. (1961). "A rational analytical theory of fatigue." *The trend of engineering* Vol: 13, pp:9-14.
- Paris P.C., Erdogan, F. (1963). "A critical analysis of crack propagation law." *Transaction of ASME Series D* Vol: 85, 528-533
- Peterson, R.E., (1950). "Relation between stress analysis and fatigue of metals." *Proc. SESA*, 11, 199-206.
- Pijpers, R. (2011). "Fatigue strength of welded connections made of very high strength cast and rolled steels." *Doctoral dissertation*. Delft University of Technology, The Netherlands.
- Radaj, D. (1996). "Review of fatigue strength assessment of nonwelded and welded structures based on local parameters." *International journal of fatigue*, Vol. 3, No:3, pp: 153-170.
- Radaj, D., Sonsino, C.M., Fricke, W. (2006). "Fatigue assessment of welded joints by local approaches." *Woodhead publishing limited*, Cambridge, UK.
- Rodriguez-Sanchez, J. E., Rodriguez-Castellanos, A., Nunez-Farfan, J. (2006). "Fatigue crack repair profiles based on surface defect shapes." *Cientfica* Vol. 10 Num. 1, 9-14.
- Saberifar, S., Mashreghi, A.R., Mosalaeepur, M., Ghasemi, S.S. (2012). "The interaction between non-metallic inclusions and surface roughness in fatigue failure and their influence on fatigue strength." *Material and design*, 35, 720-724.
- Schijve, J. (2009) "Fatigue of structures and material." *Second edition*. Delft, The Netherlands, Springer.
- Schijve, J. (2012). "Fatigue prediction of welded joints and the effective notch stress concept." *International journal of fatigue*, 45, 31-38.
- Siebel, E., Stieler, M. (1955). "Significance of dissimilar stress distributions for cycling loading." *VDI-Zeitschrift*, 97(5), 121-126.
-

- Siebel, E., Gaier, M. (1956). "Influence of surface roughness on fatigue strength of steels and non-ferrous alloys." VDI-Z 99 1715-1723.
- Sigl, K.M., Hardin, R.A., Stephens, R.I., Beckermann, C. (2004). "Fatigue of 8630 cast steel in the presence of porosity." International journal of cast metals research Vol. 17 No.3, pp: 130-146.
- Sonsino, C.M. (1993). "Zur Bewertung des Schwingfestigkeitsverhaltens von Bauteilen mit Hilfe ortlicher Beanspruchungen." Konstruktion, Vol 45, pp:25-33.
- Sun, C., Lei, Z., Xie, J., Hong, Y. (2013). "Effects of inclusion size and stress ratio on fatigue strength for high strength steels with fish-eye mode failure." International journal of fatigue, 48, 19-27.
- Takahashi, K., Murakami, Y. (1999). "Quantitative evaluation of effect of surface roughness on fatigue strength." Engineering against fatigue, 693-703, A.A. Balkema, Ed., Sheffield U.K.
- Tanaka, K., Mura, T. (1981) "A theory of fatigue crack initiation on inclusion." Metallurgical Transactions, 13A, 117-123.
- Yamasaki, T., Kawai, Y., Maeda, Y. (1984). "Fatigue life of welded and bolted repair parts." Journal of structural engineering, 110, 2499-2512.
- Yang, Z.G., Zhang, J.M., Li, S.X., Li, G.Y., Wang, Q.Y., Hui, W.J., Weng, Y.Q. (2006) "On the critical inclusion size of high strength steels under ultra-high cycle fatigue." Material science and Engineering A, 427, 167-174.
- Yildirim, H.C., Marquis, G.B. (2012). "Fatigue strength improvement factors for high strength steel welded joints treated by high frequency mechanical impact." International journal of fatigue, 44, 168-176.
- Yu, X., Jiang, Z., Wang, X., Wei, D., Yang, Q. (2012). "Effect of coiling temperature on oxide scale of hot rolled strip." Advanced material research, 415-417, 853-858.
- Wang, P., Li, W., Wang, D. (2012). "Evaluation of maximum inclusion size and fatigue limit for high strength steel in rotating bending." Advanced materials research, 482-484, 1622-1627.
- Wang, Q.Y., Bathias, C., Kawagoishi, N., Chen, Q. (2002). "Effect of inclusion on surface crack initiation and gigacycle fatigue strength." International journal of fatigue, 24, 1269-1274.
- Wang, Y., Akid, R. (1996) "Role of non-metallic inclusions in fatigue, pitting and corrosion fatigue." NACE international, 62(2), 92-102.

-
- Wilby,A.J., Neale, D.P. (2012) “Defects introduced into materials during fabrication and service.” Material science and engineering Vol. III.
- Zeng, Y., Hogmei, F., Wang, X., Xie, X. (2007). “Study on micro-mechanism of crack initiation and propagation induced by inclusion in ultra-high strength steel.” Key engineering materials, 353-358, 1185-1190.
- Zhang, J.W., Lu, L.T., Wu, P.B., Ma, J.J., Wang, G.G., Zhang, W.H. (2013) “Inclusion size evaluation and fatigue strength analysis of 35CrMo alloy railway axle steel.” Material science and engineering A, 562, 211-217.
- Zhang, Y.H., Smith, S., Wei. L., Johnston, C. (2012). “Residual stress measurements and modelling.” Health and Safety Executive, RP938. Cambridge, UK.
- Zhang, J.M., Zhang, J.F., Yang, Z.G., Li, G.Y., Yao, G., Li, S.X., Hui, W.J., Weng, Y.,Q. (2005) “Estimation of maximum inclusion size and fatigue strength in high strength ADF1 steel.” Material science and engineering A, 394, 126-131.
- Zhang, L., Thomas, B.G. (2003). “Inclusions in continuous casting of steel.” XXIV steelmaking symposium, 138-183. Mexico.

Appendices

Appendix A. Material properties and manufacturing of specimens*

Table A.1 gives the chemical composition and Table A.2 the mechanical properties of the test materials. These values were taken from the material certificates. Figure A.1 shows the geometry of V-shape welded specimens [Pijpers, 2011]. The welding parameters of V-shape welded specimens are given in Table A.3.

Table A.1 Chemical composition of the test materials (%wt).

Material	C%	Si%	Mn%	P%	S%	Cr%	Mo%	Ni%		
S460	0.075	0.2	1.57	0.011	0.001	0.032	0.004	0.317		
S690	0.16	0.282	1.28	0.011	0.0007	0.025	0.39	0.032		
S890	0.168	0.281	0.98	0.012	0.0008	0.494	0.511	0.98		
S1100	0.158	0.271	0.87	0.012	0.004	0.47	0.46	1.95		
G20Mn5	0.21	0.56	1.45	0.013	0.002	0.15	0.13	0.2		
G10MnMoV6-3	0.11	0.45	1.7	0.011	0.003	0.11	0.39	0.46		
G18NiMoCr3-6	0.22	0.4	1.16	0.012	0.003	0.89	0.61	0.8		
G22NiMoCr5-6	0.23	0.47	0.96	0.011	0.002	0.8	0.57	0.2		
	V%	N%	Cu%	B%	Ti%	Al-T%	Nb	Al	Zr%	
S460	-	0.0037	0.16	0.0001	0.002	0.038	0.19	-	-	
S690	-	0.042	0.024	0.0019	0.003	0.08	0.024	-	0.0002	
S890	0.014	-	0.024	0.0022	-	-	0.011	0.074	-	
S1100	0.22	-	-	0.0016	-	-	0.013	0.061	-	
G20Mn5	-	-	-	-	-	-	-	-	-	
G10MnMoV6-3	0.1	-	-	-	-	-	-	-	-	
G18NiMoCr3-6	-	-	-	-	-	-	-	-	-	
G22NiMoCr5-6	-	-	-	-	-	-	-	-	-	

* From the research of Pijpers, (2011)

Table A.2 Mechanical properties of the test material.

Material	R _{p;0.2} [MPa]	R _m [MPa]	A %	Z %	RT [J]	-40 °C [J]	HB
G20Mn5	510	622	25.6	64	172-181	98	185
	485	599	27	64	172-181	100	180
	512	611	26.6	67.5	172-181	100	180
G10MnMoV6-3	743	799	18.6	64	98-135	37	245
	718	785	21.2	70.8	98-135	45	243
	775	841	18	67.5	98-135	40	257
G18NiMoCr3-6	976	1042	15.8	57.7	67-80	43	321
	972	1052	13.8	46.7	67-80	46	331
	1001	1070	12	36	67-80	36	333
G22NiMoCr5-6	1126	1185	12.6	40.7	86-75	33	366
	1113	1163	12.8	42.4	86-75	39	363
	1118	1171	12.6	42.2	86-75	32	363
S460	469	590	21			222	
S690	792	843	17.9			101	
S890	1000	1065	16.1			36	
	985	1065	14.3			36	
S1100	1273	1373	10			29	

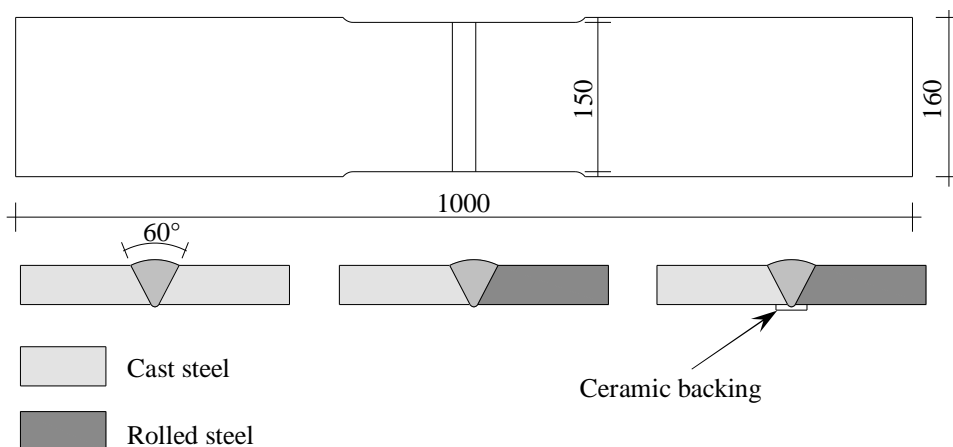


Figure A.1 Geometry of V-shape welded specimens and manufacturing configurations [Pijpers, 2011].

Table A.3 Welding parameters for the V-shape welded specimens [Pijpers, 2011].

Specimen code	V46x	V69x	V89x	V11x
Rolled steel	S460	S690	S890	S1100
Preheat temp.	-	100	125	125
Welding position	1G	1G	1G	1G
Numbers of weld layers	23	23	24	17
Weld metal cap	E81T1K2M	E111T1K	E120T1G	E120T1G
Weld process cap	FCAW	FCAW	FCAW	FCAW
Heat input cap [kJ/mm]	0.6-12	1.0-1.8	0.92-1.32	0.92-1.32
Weld metal root	E80CG	ER100SG	E120T1G	E120T1G
Gap [mm]	4.5±1.5	4.5±1.5	3	3
Weld process root	FCAW	FCAW	FCAW	FCAW
Heat input root [kJ/mm]	1.1-2.4	1.1-2.4	0.92-1.32	0.92-1.32
Specimen code	C46x	C69x	C89x	C11x
Rolled steel	S460	S690	S890	S1100
Cast steel	G20Mn5	G10MnMoV6-3	G18NiMoCr3-6	G22NiMoCr5-6
Preheat temp.	-	100	125	125
Welding position	1G	1G	1G	1G
Numbers of weld layers	23	23	24	17
Weld metal cap	E81T1K2M	E111T1K	E120T1G	E120T1G
Weld process cap	FCAW	FCAW	FCAW	FCAW
Heat input cap [kJ/mm]	0.6-12	1.0-1.8	0.92-1.32	0.92-1.32
Weld metal root	E80CG	ER100SG	E120T1G	E120T1G
Gap [mm]	4.5±1.5	4.5±1.5	3	3
Weld process root	FCAW	FCAW	FCAW	FCAW
Heat input root [kJ/mm]	1.1-2.4	1.1-2.4	0.98-1.36	0.98-1.36

Appendix B. Material specification

Appendix B presents the material properties of the current research. The values are taken from the material certifications.

Repaired base material

Table B.1 shows the chemical composition and Table B.2 mechanical properties of the steel plates.

Table B.1 Chemical composition of the steel plates (%wt).

Materials	C %	Si %	Mn %	P %	S %	Cr %	Mo %	Ni %
S690	0.16	0.20	0.92	0.009	0.003	0.33	0.41	-
S890	0.168	0.281	0.98	0.012	0.0008	0.494	0.511	0.98

Materials	V %	Nb %	Al %	Cu %	N %	B %
S690		-	-		-	-
S890	0.041	0.011	0.074	0.024		0.0022

Table B.2 Mechanical properties of the steel plates.

Material	R _{p,0.2} [MPa]	R _m [MPa]	A %	KVC	
				-40 °C [J]	-20 °C [J]
				S690	790
S890	985	1051	14.3	36	-

Weld material

Table B.3 shows the chemical composition and Table B.4 the mechanical properties of the weld material.

Table B.3 Chemical composition of the weld material (%wt).

Materials	C %	Si %	Mn %	P %	S %	Cr %	Ni %	Mo %
Megafil 742 M	0.047	0.422	1.736	0.015	0.012	0.455	2.26	0.382
Megafil 821 M	0.04	0.422	1.4	0.005	0.01	0.025	0.81	0.004
Megafil 1100 M	0.098	0.37	1.58	0.012	0.015	0.49	2.5	0.54
Materials	Cu %	Al %	V %	Ti %	Nb %			
Megafil 742 M	0.11	0.006	0.008	0.04	0.002			
Megafil 821 M	0.074	0.004	0.016	0.051	0.03			
Megafil 1100 M	0.128	0.09	0.011	0.08	0.006			

Table B.4 Mechanical properties of the weld material.

Materials	R_m	R_{p,0.2}	A	KVC		
				-20 °C	-40 °C	-60 °C
				[MPa]	[MPa]	[J]
Megafil 742 M	854	837	19		84	69
Megafil 821 M	645	588	28		121	89
Megafil 1100 M	1075	984	15	50	47	

V-shape welded specimens

Table B.5 presents the chemical composition and Table B.6 the mechanical properties of the steel plates.

Table B.5 Chemical composition of the steel plates (%wt).

Materials	C %	Si %	Mn %	P %	S %	N %	Al %	Cu %
S690	0.17	0.24	1.19	0.011	0.002	0.004	0.094	0.02
S890	0.18	0.29	1	0.014	0.001	0.005	0.038	0.03
G10MnMoV6-3	0.11	0.44	1.65	0.011	0.002	-	-	-
G18NiMoCr3-6	0.2	0.45	1.07	0.012	0.002	-	0.025	0.11
	Cr %	Ni %	Nb %	Mo %	V %	Ti %	B %	Zr %
S690	0.31	0.03	0.03	0.2	0.003	0.002	0.0026	0.001
S890	0.58	0.96	0.02	0.33	0.05	0.004	0.0005	0.001
G10MnMoV6-3	-	0.35	-	0.26	-	-	-	-
G18NiMoCr3-6	0.9	0.8	-	0.57	0.003	-	-	-

Table B.6 Mechanical properties of the steel plates.

Materials	R_{p,0.2} [MPa]	R_m [MPa]	A %	KVC -40 °C [J]				KVC -60 °C [J]				HB
				1	2	3	AVG	1	2	3	AVG	
S690	749	802	18					155	145	181	160	
S890	982	1069	12	46	53	47	49					
G10MnMoV6-3	697	802	19.6									252
G18NiMoCr3-6	1006	1101	13.4									316

Appendix C. Manufacturing steps and geometry of the specimens

Manufacturing steps

The rolled steel plates were delivered with the dimension of 2000x1500 mm (lengthxwidth) and the cast steel plates were produced with 1000x500 mm dimensions. The rolled plates were flame cut and the weld edges of the rolled steel plates and cast steel plates were machined to prepare the weld groove. After welding, strips were plasma cut to obtain the test specimens. Figure C.1 shows the manufacturing steps of V-shape welded specimens.

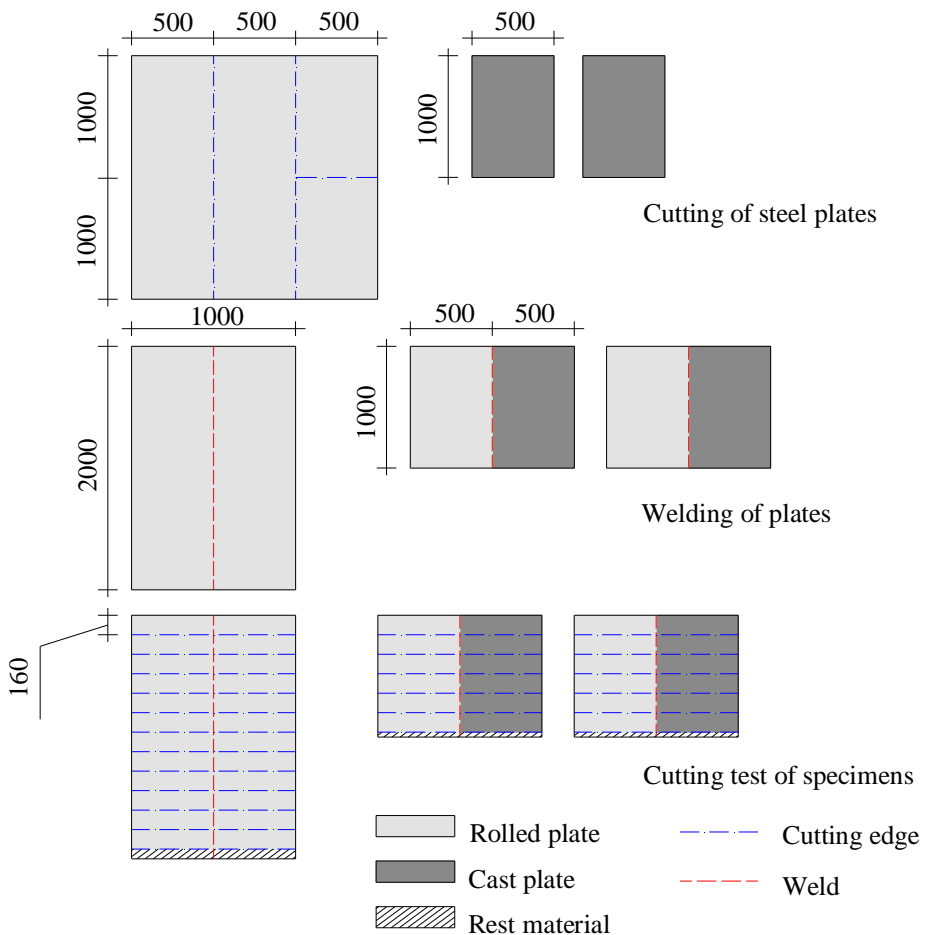


Figure C.1 Manufacturing steps of the V-shape welded specimens.

Geometry of specimens

Figure C.2 presents the position of the strain gauges and specimens geometry of BR69x and BR89x series. Figure C.3 shows the geometry detail of the specimens VR69x, Figure C.4 the specimens VR89x, CR69x and CR89x.

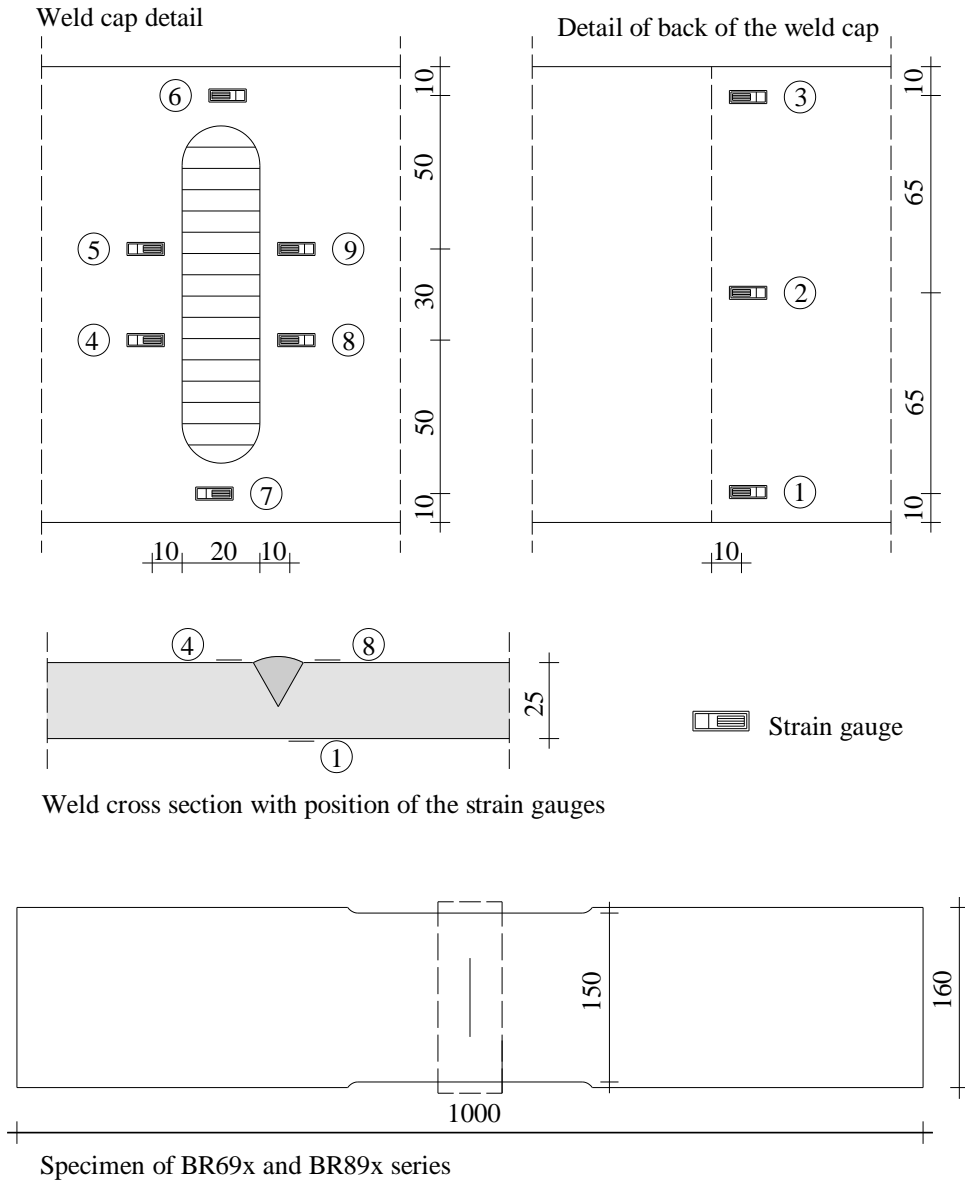


Figure C.2 Test specimens of BR69x and BR89x series.

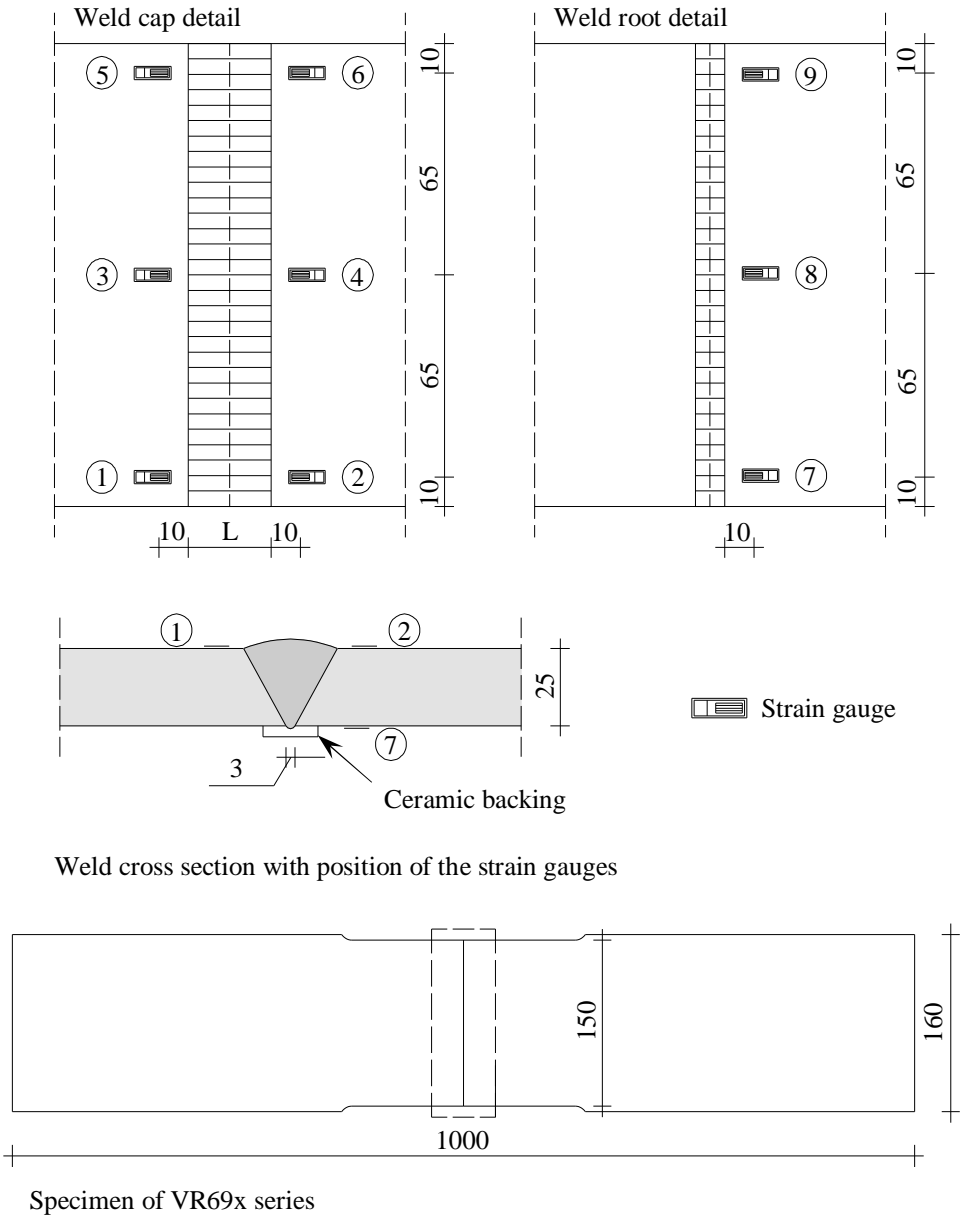
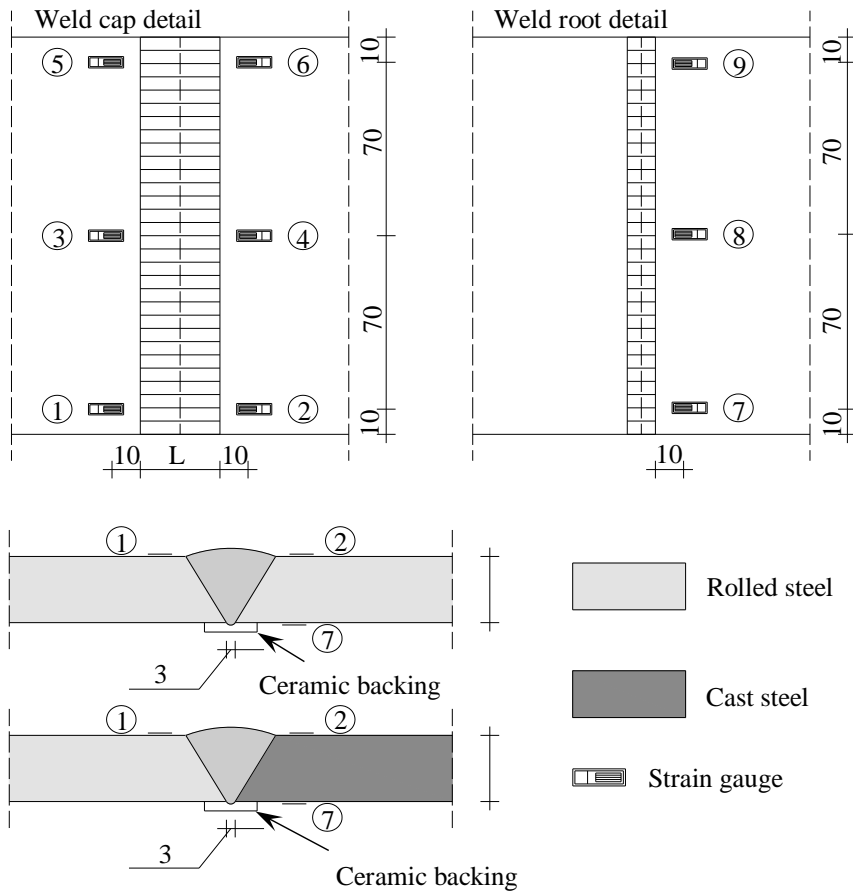


Figure C.3 Test specimens of VR69x series



Weld cross section with position of the strain gauges

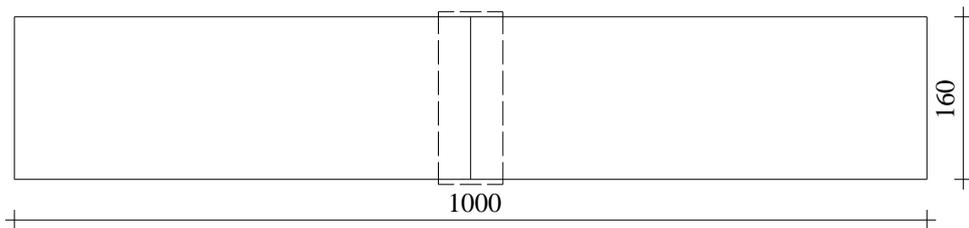


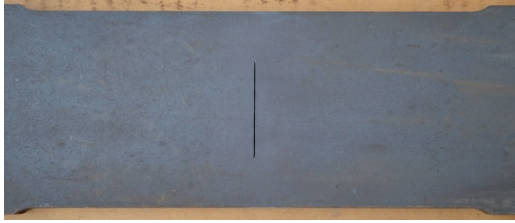
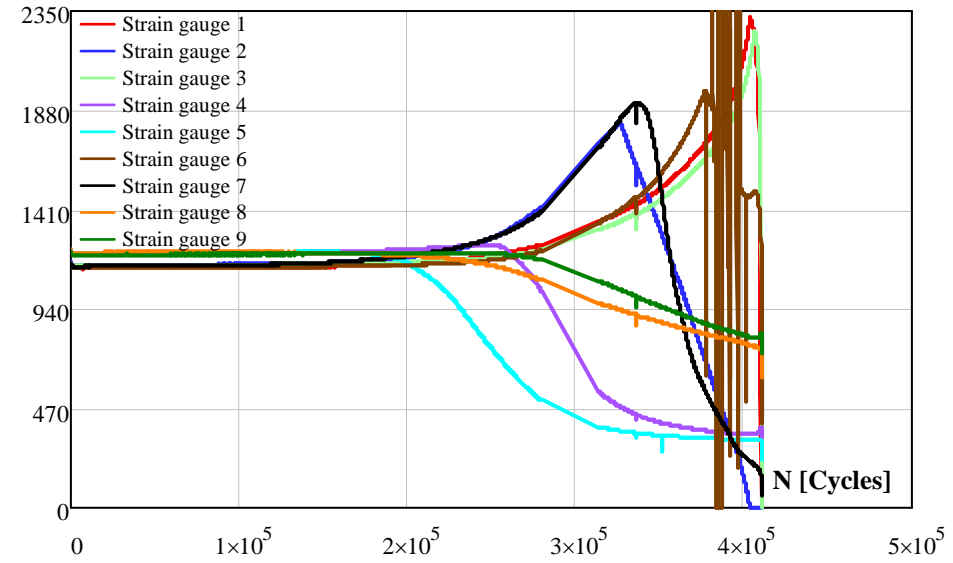
Figure C.4 Test specimens of VR89x, CR69x and CR89x series.

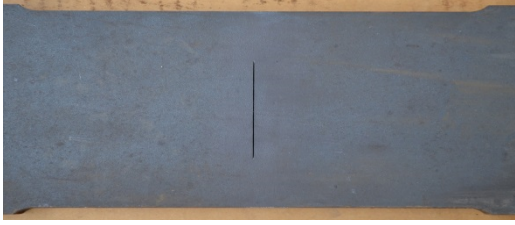
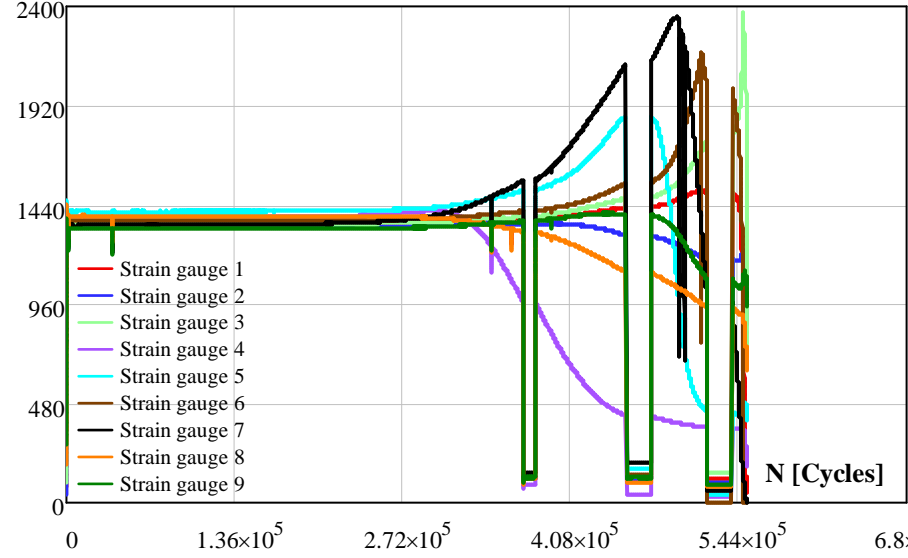
Appendix D. Repair of the specimens

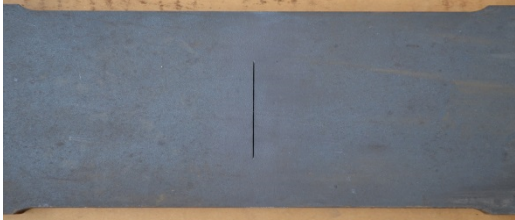
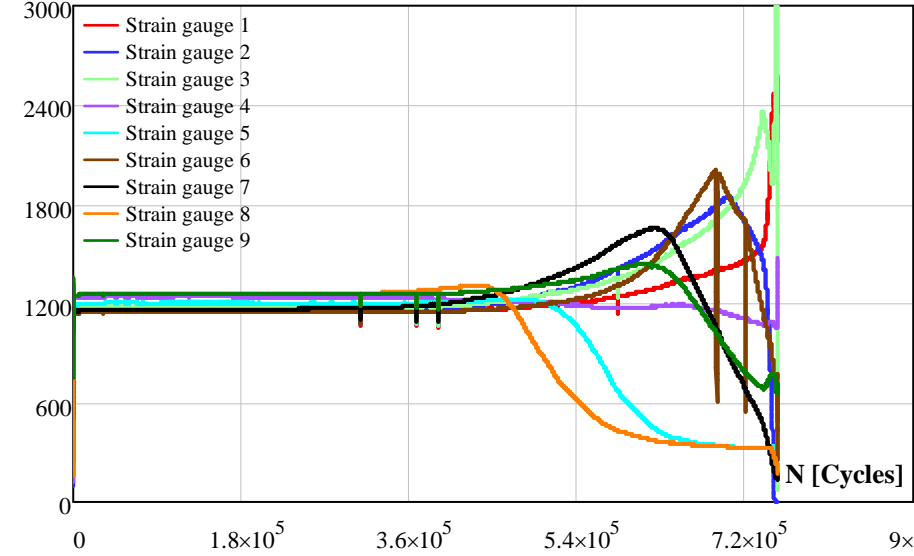
This appendix presents the overview of the repair of the fatigue plate specimens. The repair process of the specimens with an artificial crack in the base material is the same for all specimens. As an example, the repair procedure of one specimen is given. Since the applied stress range is different for each specimen, an overview of each specimen is dealt with separately. For each specimen, the following information is given: number of cycles at crack initiation, N_i , and the number of cycles at failure, N_f , where the test specimen is broken into two pieces. In addition, the strain gauge measurement of each specimen is graphically presented.

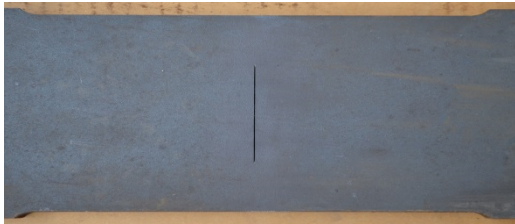
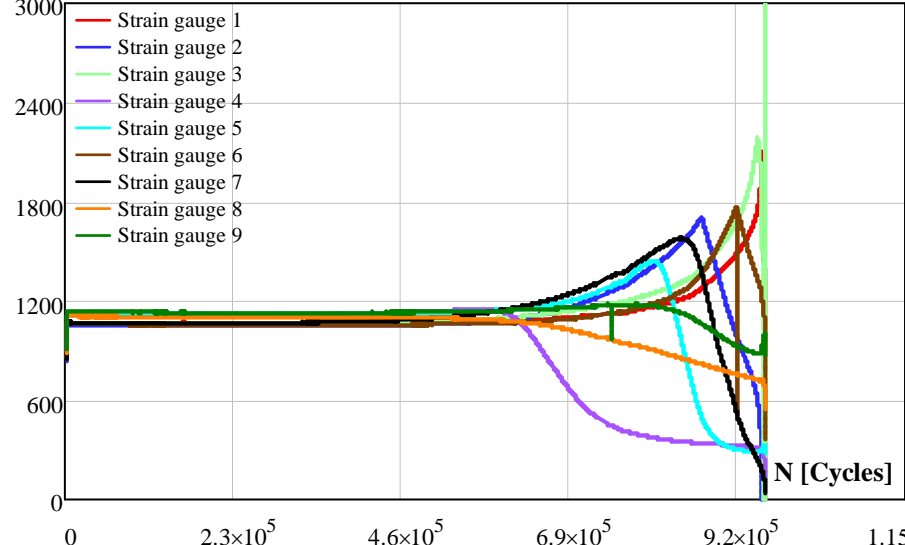
In case of V-shape welded specimens, each specific specimen is dealt with and for each specimen the following information is given: number of cycles at crack initiation, N_i and number of cycles at end of test, N_s during crack creation stage (fatigue tests on original weld), location of the fatigue crack observed during the test, location of detected cracks by magnetic particles, repair process of the detected cracks, location of crack initiation after the repair process, number of cycles at the crack initiation of the repaired specimen, N_i and number of cycles at failure of the repaired specimen, N_f where the specimens broke into two pieces. The number of cycles at crack initiation of runouts is indicated as 0. The strain gauge measurements of each specimen are graphically presented for both stage: the crack creation stage and after the repair of the fatigue cracks. The specimen with the base material failure and the number of cycles at the crack initiation are determined according to the reaction of the strain gauges. However, since the crack initiation location in the base material was far away from the weld toe, the strain gauges were reacted at a very late stage of the crack development. Therefore, the fatigue crack initiation life could be shorter than the determined value. In some cases, the fatigue cracks in the base material were detected by visual inspection before the strain gauge reactions and in that case the number of cycles at that moment is taken as the number of cycles at the crack initiation.

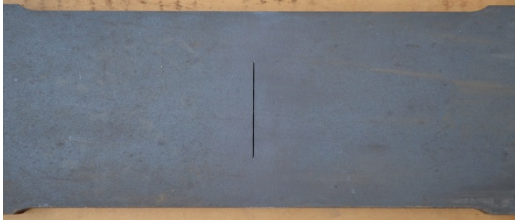
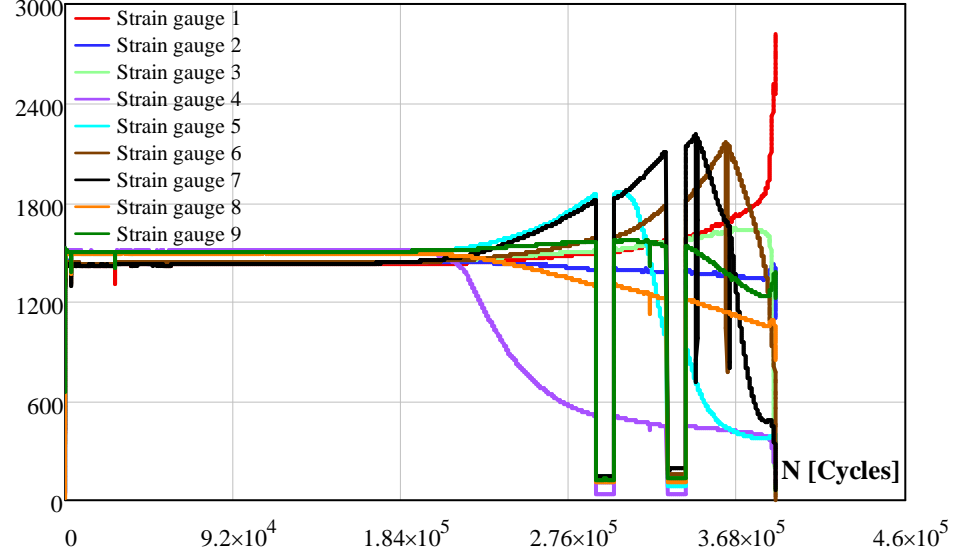
The V-shape welded specimens were encoded as VO69x, VO89x, CO69x and CO89x which were used during the crack creation stage. In order to distinguish between the test results of the crack creation stage and the test results after the repair of the cracks, the repaired specimens were encoded as VR69x, VR89x, CR69x and CR89x.

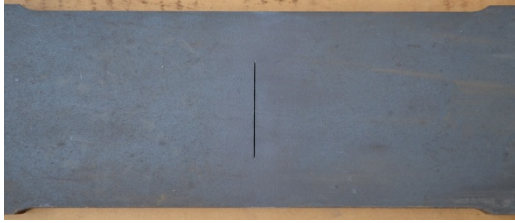
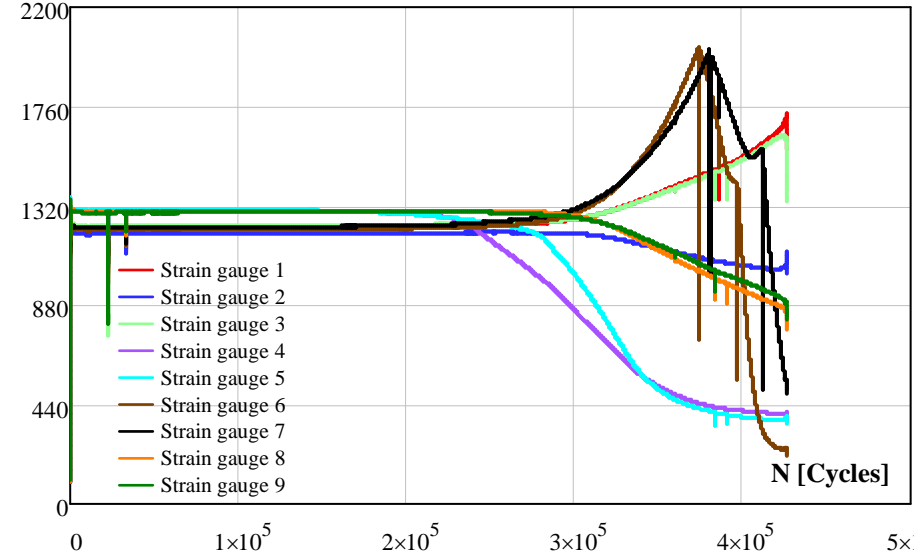
Specimen: BR691	Thickness [mm]	Rolled	24.9
<i>Artificial crack</i>			
			
<p><i>Repair of the crack:</i> The artificial crack is removed by the grinding process and the prepared groove is filled by welding.</p>			
			
<i>Test results of repaired specimen</i>			
N _i : 169423		N _r : 446022	
<p><i>Crack initiation location:</i> At the end of the weld, start-stop points. Strain measurements;</p>			
<p>Δε [μstrain]</p>  <p>N [Cycles]</p>			

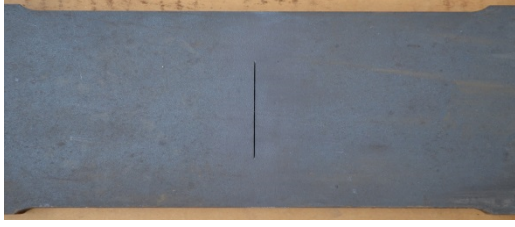
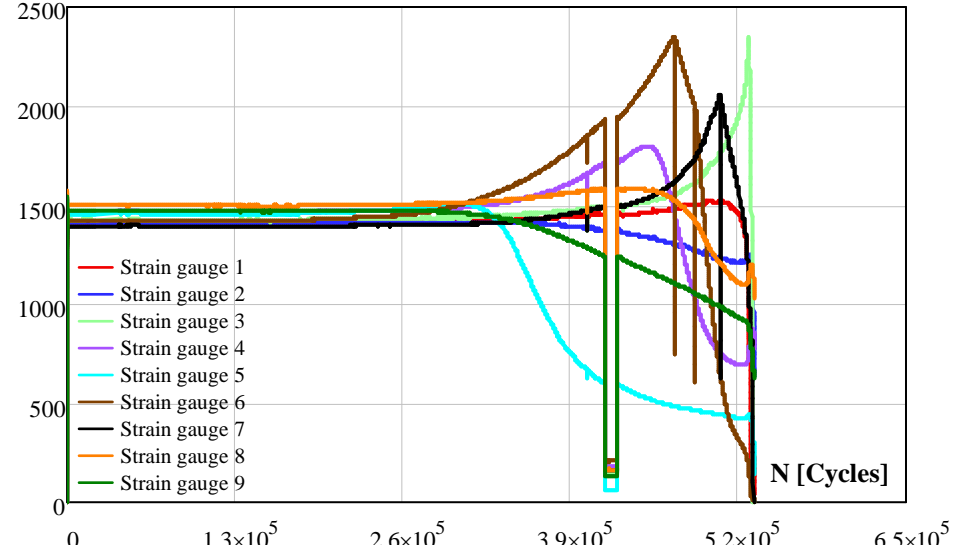
Specimen: BR692	Thickness [mm]	Rolled	24.8
<i>Artificial crack</i>			
			
<i>Repair of the crack:</i> The artificial crack is removed by the grinding process and the prepared groove is filled by welding.			
			
<i>Test results of repaired specimen</i>			
N_i : 248143		N_f : 500396	
<i>Crack initiation location:</i> At the end of the weld, start-stop points. Strain measurements;			
$\Delta\epsilon$ [μstrain]			
			

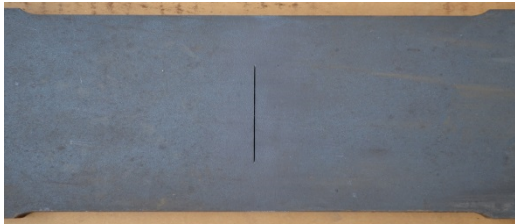
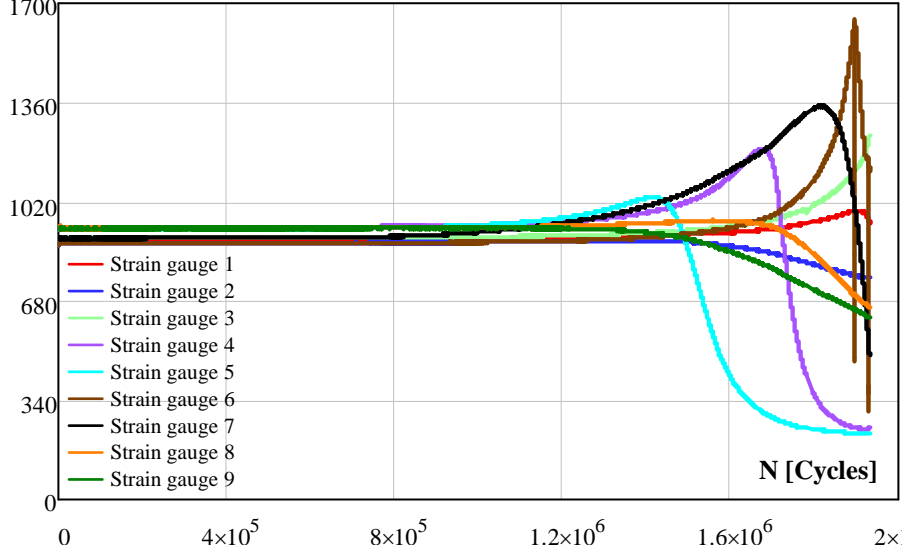
Specimen: BR693	Thickness [mm]	Rolled	25.2
<i>Artificial crack</i>			
			
<p><i>Repair of the crack:</i> The artificial crack is removed by the grinding process and the prepared groove is filled by welding.</p>			
			
<i>Test results of repaired specimen</i>			
N_i : 400383		N_f : 754808	
<p><i>Crack initiation location:</i> At the end of the weld, start-stop points. Strain measurements;</p>			
<p>$\Delta\varepsilon$ [μstrain]</p>  <p>N [Cycles]</p> <ul style="list-style-type: none"> — Strain gauge 1 — Strain gauge 2 — Strain gauge 3 — Strain gauge 4 — Strain gauge 5 — Strain gauge 6 — Strain gauge 7 — Strain gauge 8 — Strain gauge 9 			

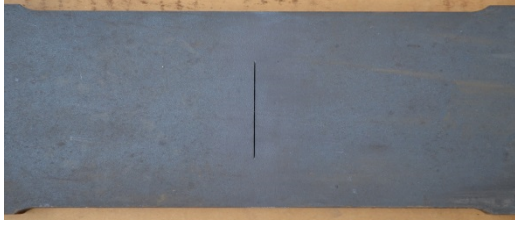
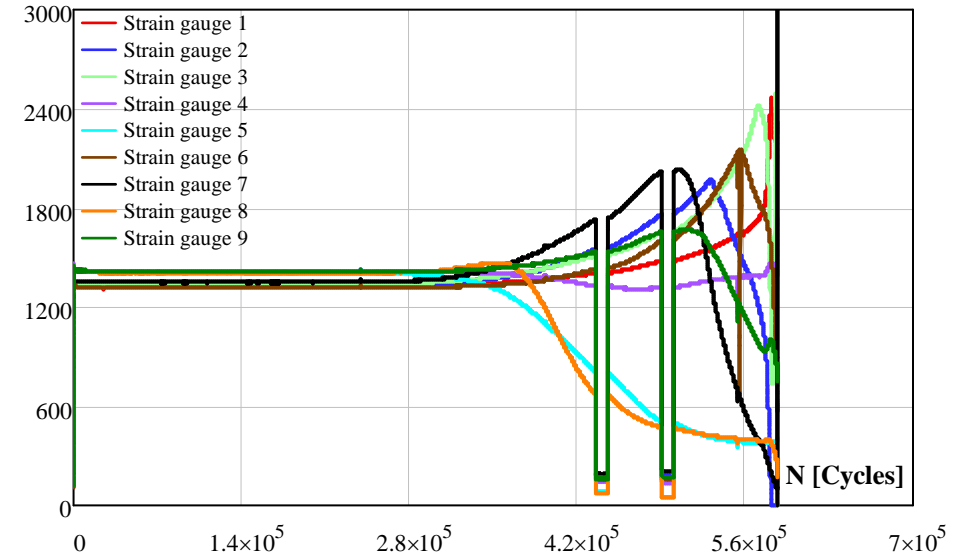
Specimen: BR694	Thickness [mm]	Rolled	24.7
<i>Artificial crack</i>			
			
<i>Repair of the crack:</i> The artificial crack is removed by the grinding process and the prepared groove is filled by welding.			
			
<i>Test results of repaired specimen</i>			
N_i : 578058		N_f : 959827	
<i>Crack initiation location:</i> At the end of the weld, start-stop points. Strain measurements;			
$\Delta\epsilon$ [μstrain]			
			

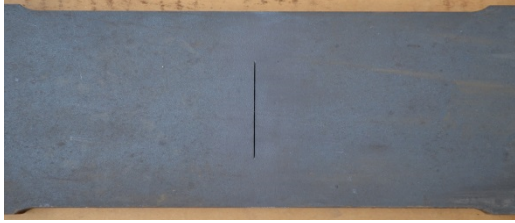
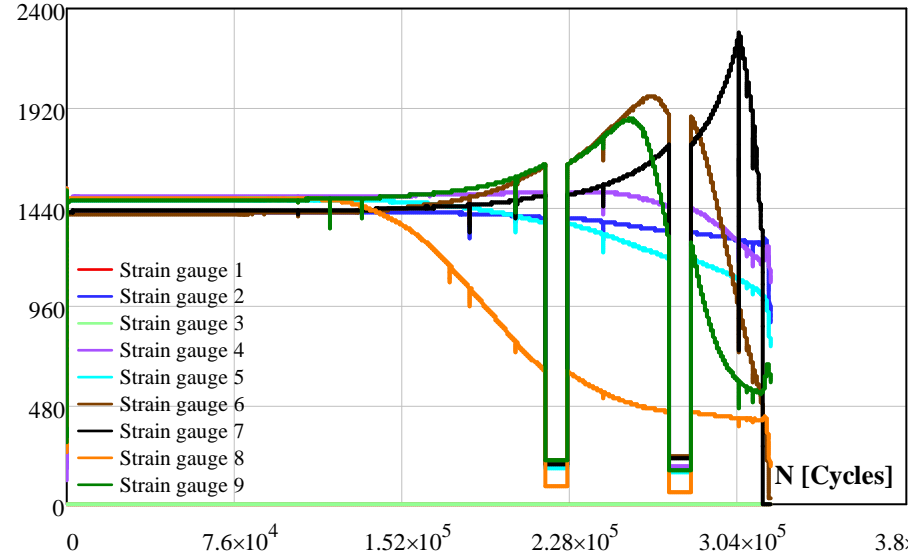
Specimen: BR695	Thickness [mm]	Rolled	25.2
<i>Artificial crack</i>			
			
<p><i>Repair of the crack:</i> The artificial crack is removed by the grinding process and the prepared groove is filled by welding.</p>			
			
<i>Test results of repaired specimen</i>			
N_i : 189479		N_f : 369480	
<p><i>Crack initiation location:</i> At the end of the weld, start-stop points. Strain measurements;</p>			
<p>$\Delta\epsilon$ [μstrain]</p>  <p>N [Cycles]</p>			

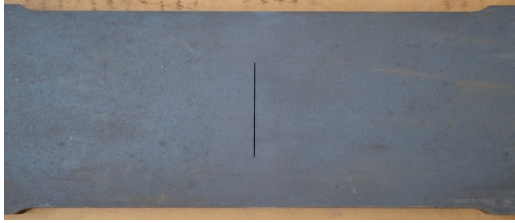
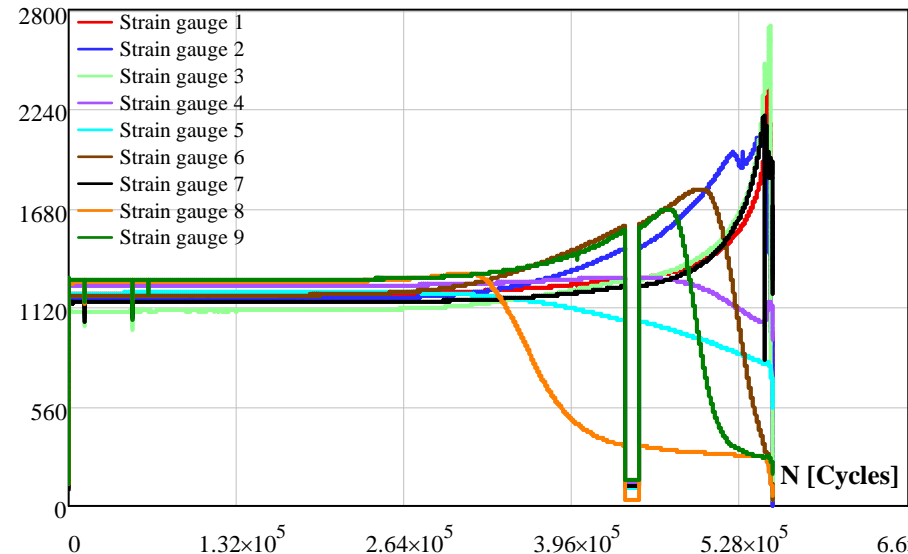
Specimen: BR696	Thickness [mm]	Rolled	24.7
<i>Artificial crack</i>			
			
<i>Repair of the crack:</i> The artificial crack is removed by the grinding process and the prepared groove is filled by welding.			
			
<i>Test results of repaired specimen</i>			
N_i : 208737		N_f : 426718	
<i>Crack initiation location:</i> At the end of the weld, start-stop points. Strain measurements;			
$\Delta\epsilon$ [μstrain]			
			

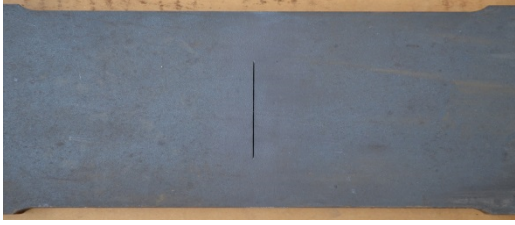
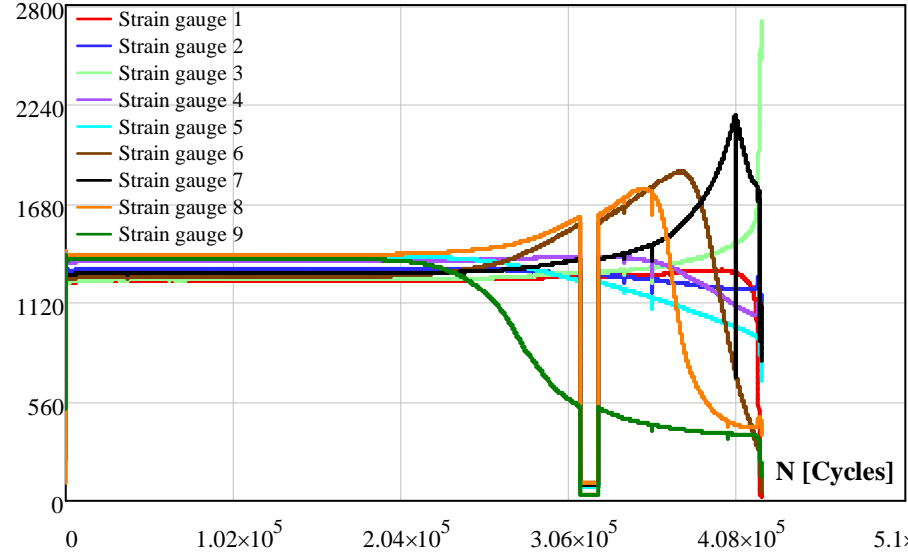
Specimen: BR697	Thickness [mm]	Rolled	25
<i>Artificial crack</i>			
			
<p><i>Repair of the crack:</i> The artificial crack is removed by the grinding process and the prepared groove is filled by welding.</p>			
			
<i>Test results of repaired specimen</i>			
N_i : 278974		N_f : 522477	
<p><i>Crack initiation location:</i> At the end of the weld, start-stop points. Strain measurements;</p>			
<p>$\Delta\epsilon$ [μstrain]</p>  <p>N [Cycles]</p> <ul style="list-style-type: none"> — Strain gauge 1 — Strain gauge 2 — Strain gauge 3 — Strain gauge 4 — Strain gauge 5 — Strain gauge 6 — Strain gauge 7 — Strain gauge 8 — Strain gauge 9 			

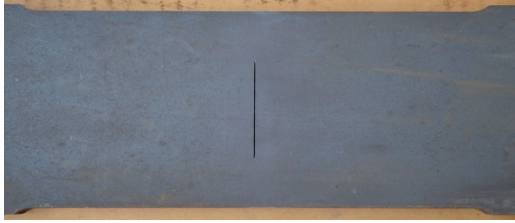
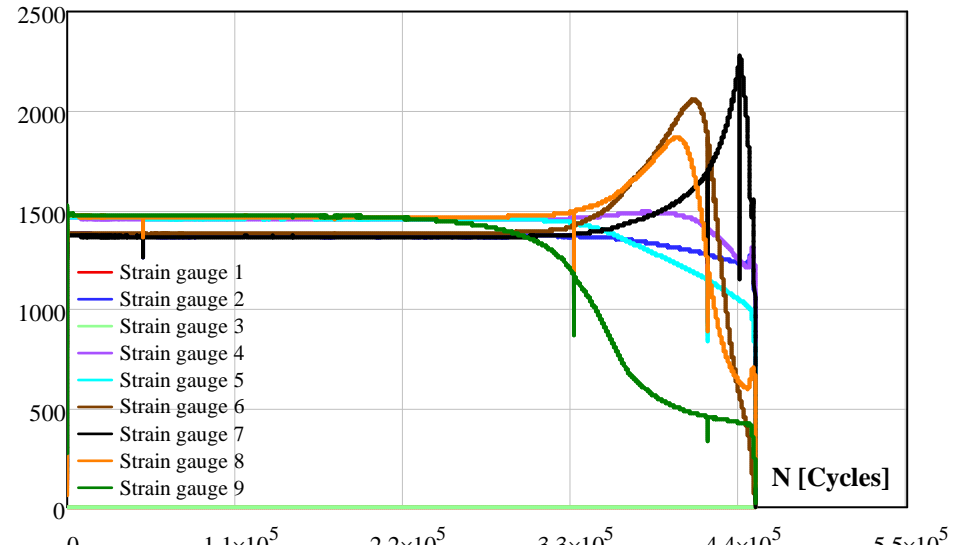
Specimen: BR698	Thickness [mm]	Rolled	24.9
<i>Artificial crack</i>			
			
<i>Repair of the crack:</i> The artificial crack is removed by the grinding process and the prepared groove is filled by welding.			
			
<i>Test results of repaired specimen</i>			
N_i : 861753		N_f : 1956636	
<i>Crack initiation location:</i> At the end of the weld, start-stop points. Strain measurements;			
$\Delta\epsilon$ [μstrain]			
			

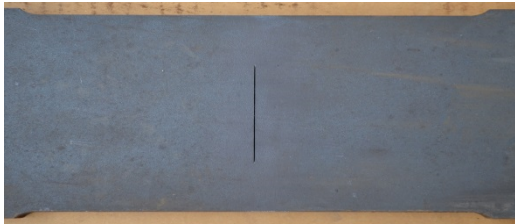
Specimen: BR699	Thickness [mm]	Rolled	24.8
<i>Artificial crack</i>			
			
<p><i>Repair of the crack:</i> The artificial crack is removed by the grinding process and the prepared groove is filled by welding.</p>			
			
<i>Test results of repaired specimen</i>			
N _i : 265024		N _r : 566885	
<p><i>Crack initiation location:</i> At the end of the weld, start-stop points. Strain measurements;</p>			
<p>Δε [μstrain]</p>  <p>N [Cycles]</p> <ul style="list-style-type: none"> — Strain gauge 1 — Strain gauge 2 — Strain gauge 3 — Strain gauge 4 — Strain gauge 5 — Strain gauge 6 — Strain gauge 7 — Strain gauge 8 — Strain gauge 9 			

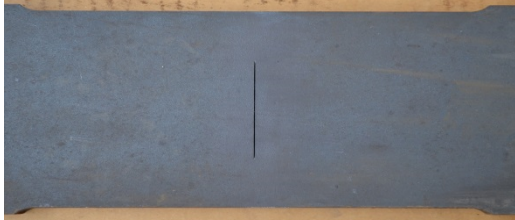
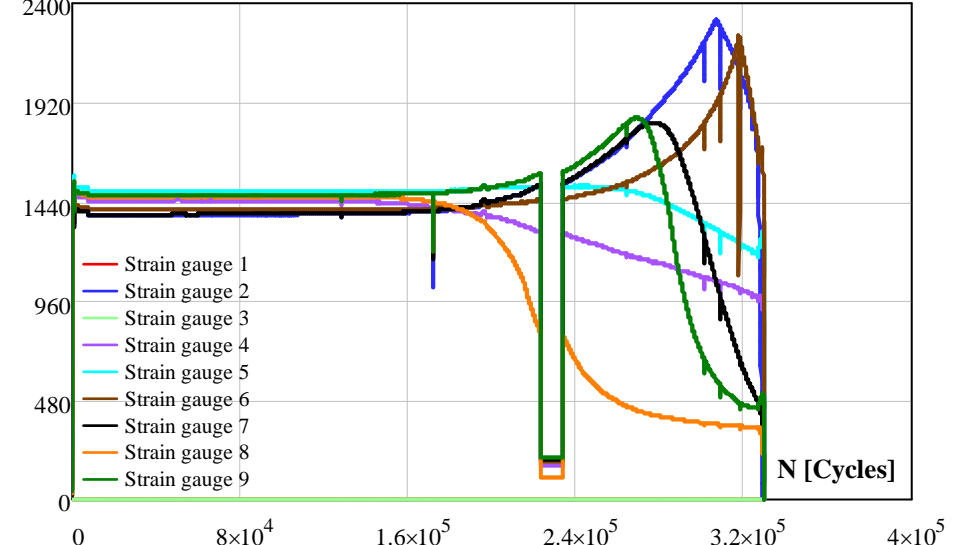
Specimen: BR891	Thickness [mm]	Rolled	25
<i>Artificial crack</i>			
			
<i>Repair of the crack:</i> The artificial crack is removed by the grinding process and the prepared groove is filled by welding.			
			
<i>Test results of repaired specimen</i>			
N_i : 131804		N_f : 298194	
<i>Crack initiation location:</i> At the end of the weld, start-stop points. Strain measurements; $\Delta\epsilon$ [μstrain]			
			

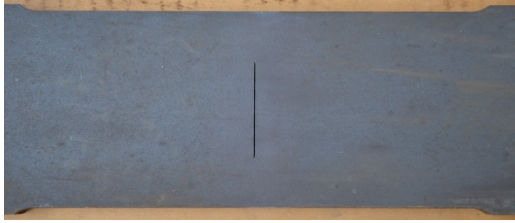
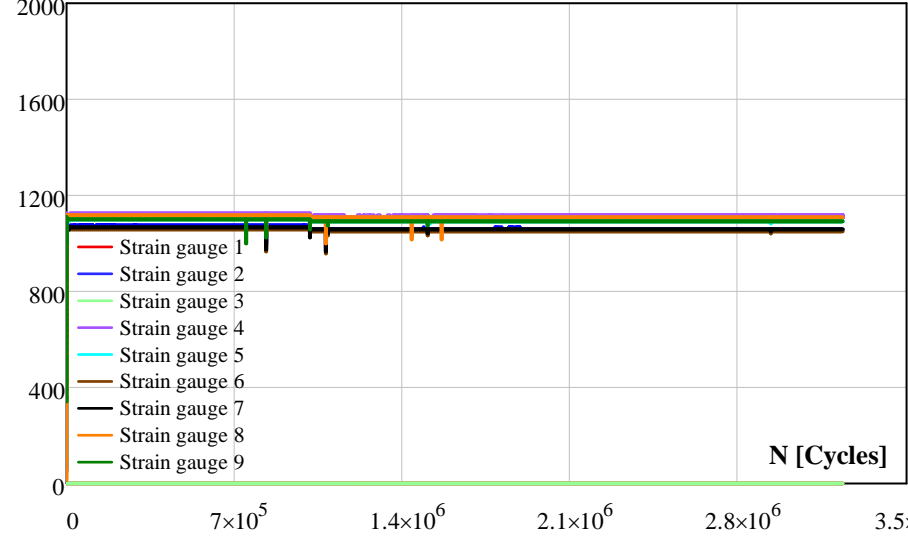
Specimen: BR892	Thickness [mm]	Rolled	24.6
<i>Artificial crack</i>			
			
<p><i>Repair of the crack:</i> The artificial crack is removed by the grinding process and the prepared groove is filled by welding.</p>			
			
<i>Test results of repaired specimen</i>			
N_i : 260297		N_f : 543492	
<p><i>Crack initiation location:</i> At the end of the weld, start-stop points. Strain measurements;</p>			
<p>$\Delta\epsilon$ [μstrain]</p>  <p>N [Cycles]</p>			

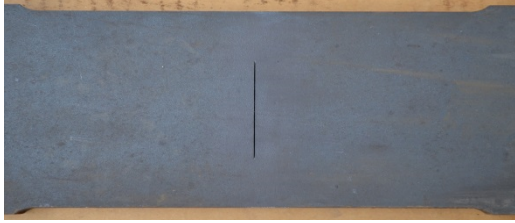
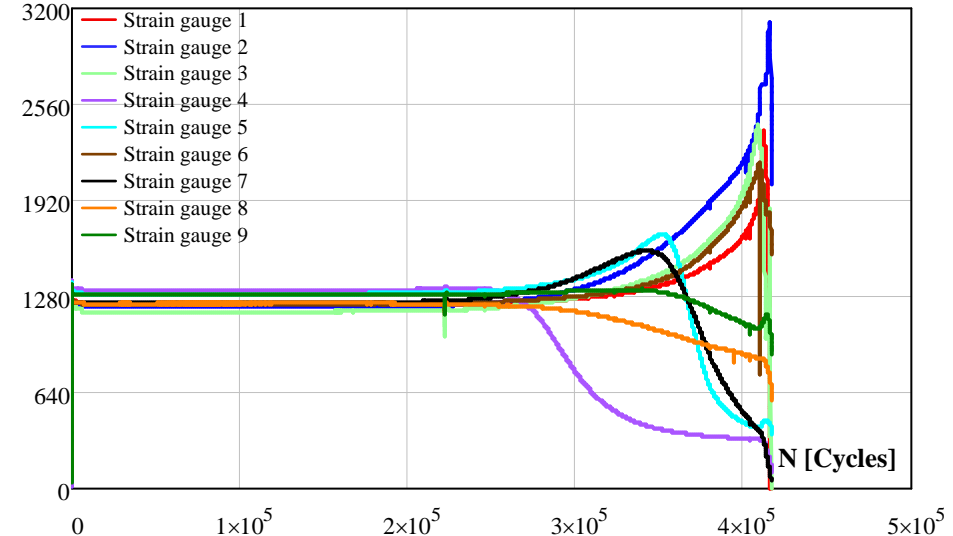
Specimen: BR893	Thickness [mm]	Rolled	24.7
<i>Artificial crack</i>			
			
<i>Repair of the crack:</i> The artificial crack is removed by the grinding process and the prepared groove is filled by welding.			
			
<i>Test results of repaired specimen</i>			
N_i : 193805		N_f : 412565	
<i>Crack initiation location:</i> At the end of the weld, start-stop points. Strain measurements;			
$\Delta\epsilon$ [μstrain]			
			

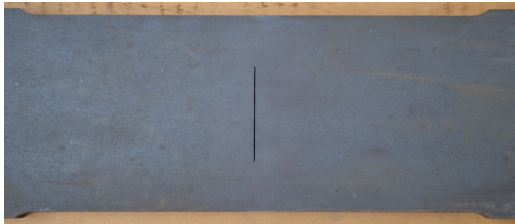
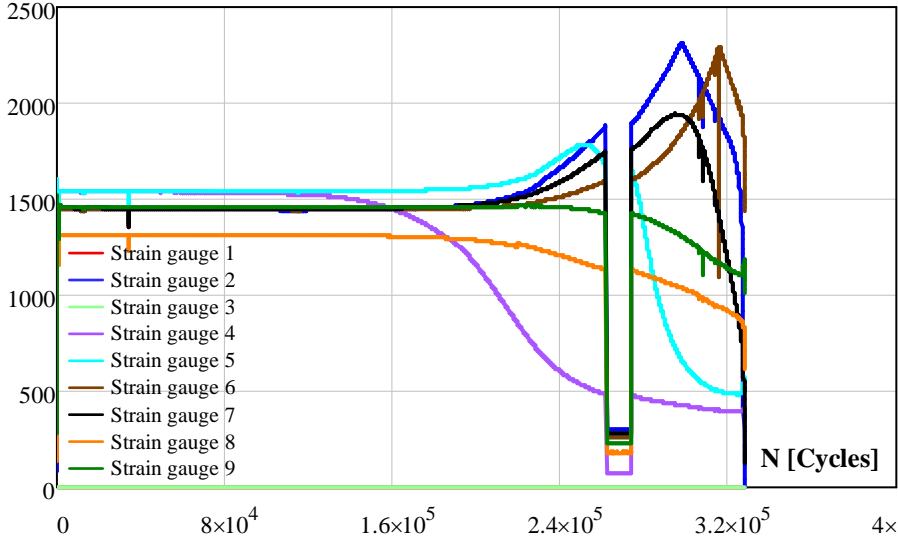
Specimen: BR894	Thickness [mm]	Rolled	24.8
<i>Artificial crack</i>			
			
<p><i>Repair of the crack:</i> The artificial crack is removed by the grinding process and the prepared groove is filled by welding.</p>			
			
<i>Test results of repaired specimen</i>			
N_i : 242539		N_f : 451488	
<p><i>Crack initiation location:</i> At the end of the weld, start-stop points. Strain measurements;</p>			
<p>$\Delta\epsilon$ [μstrain]</p>  <p>N [Cycles]</p> <ul style="list-style-type: none"> — Strain gauge 1 — Strain gauge 2 — Strain gauge 3 — Strain gauge 4 — Strain gauge 5 — Strain gauge 6 — Strain gauge 7 — Strain gauge 8 — Strain gauge 9 			

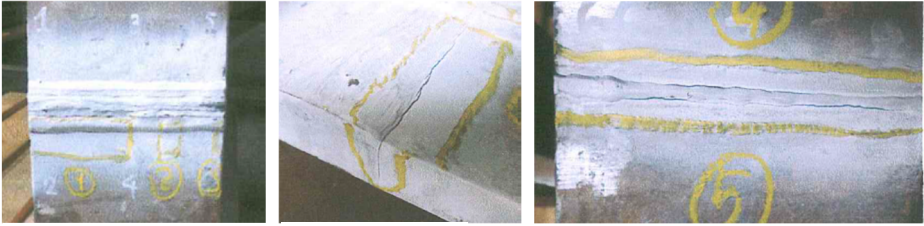
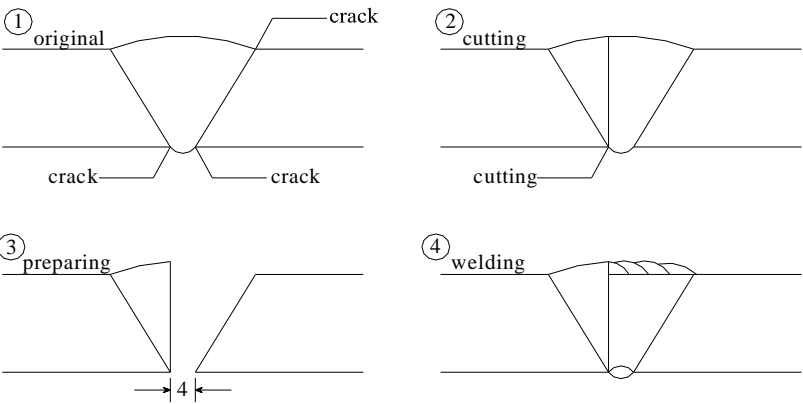
Specimen: BR895	Thickness [mm]	Rolled	24.9
<i>Artificial crack</i>			
			
<i>Repair of the crack:</i> The artificial crack is removed by the grinding process and the prepared groove is filled by welding.			
			
<i>Test results of repaired specimen</i>			
N_i : 188651		N_f : 522955	
<i>Crack initiation location:</i> At the end of the weld, start-stop points. Strain measurements;			
$\Delta\epsilon$ [μstrain]			

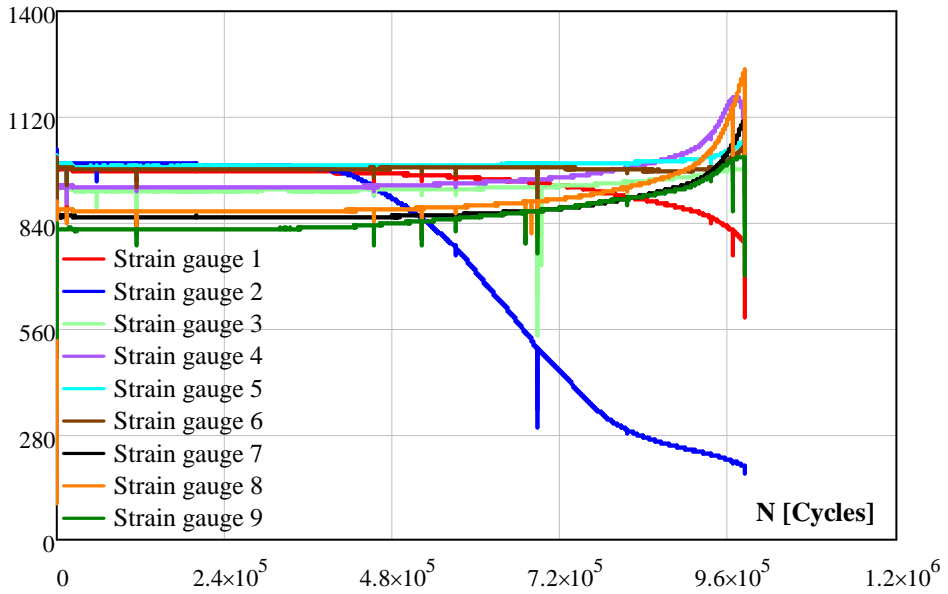
Specimen: BR896	Thickness [mm]	Rolled	24.7
<i>Artificial crack</i>			
			
<p><i>Repair of the crack:</i> The artificial crack is removed by the grinding process and the prepared groove is filled by welding.</p>			
			
<i>Test results of repaired specimen</i>			
N_i : 165550		N_f : 319821	
<p><i>Crack initiation location:</i> At the end of the weld, start-stop points. Strain measurements;</p>			
<p>$\Delta\epsilon$ [μstrain]</p>  <p>N [Cycles]</p> <ul style="list-style-type: none"> — Strain gauge 1 — Strain gauge 2 — Strain gauge 3 — Strain gauge 4 — Strain gauge 5 — Strain gauge 6 — Strain gauge 7 — Strain gauge 8 — Strain gauge 9 			

Specimen: BR897	Thickness [mm]	Rolled	25
<i>Artificial crack</i>			
			
<i>Repair of the crack:</i> The artificial crack is removed by the grinding process and the prepared groove is filled by welding.			
			
<i>Test results of repaired specimen</i>			
N_i : 0	N_f : 3234243		
<i>Crack initiation location:</i> Runout. Strain measurements;			
$\Delta\epsilon$ [μstrain]			
			

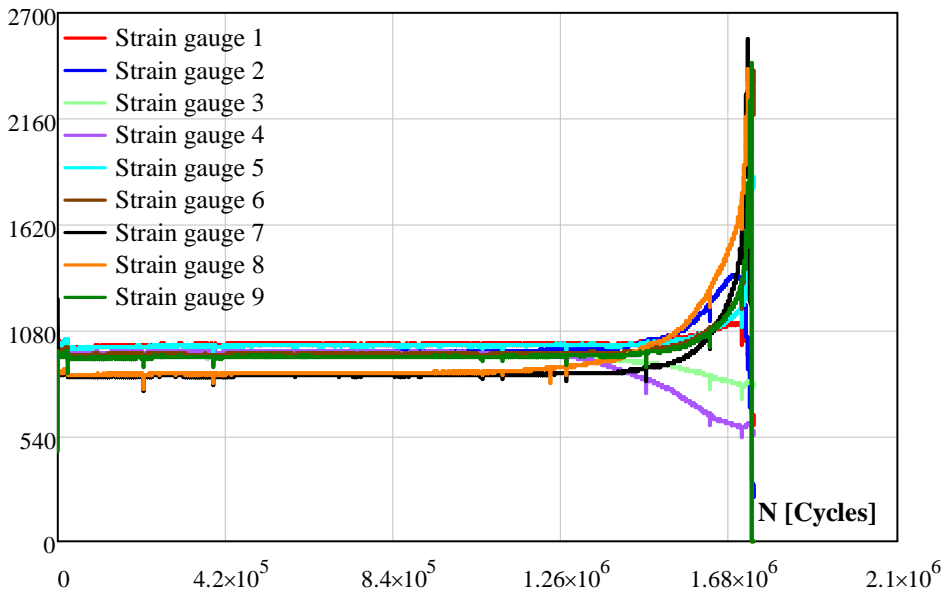
Specimen: BR898	Thickness [mm]	Rolled	24.8
<i>Artificial crack</i>			
			
<p><i>Repair of the crack:</i> The artificial crack is removed by the grinding process and the prepared groove is filled by welding.</p>			
			
<i>Test results of repaired specimen</i>			
N_i : 239380		N_f : 416519	
<p><i>Crack initiation location:</i> At the end of the weld, start-stop points. Strain measurements;</p>			
<p>$\Delta\varepsilon$ [μstrain]</p>  <p>N [Cycles]</p>			

Specimen: BR899	Thickness [mm]	Rolled	24.9
<i>Artificial crack</i>			
			
<i>Repair of the crack:</i> The artificial crack is removed by the grinding process and the prepared groove is filled by welding.			
			
<i>Test results of repaired specimen</i>			
N_i : 152946		N_f : 318024	
<i>Crack initiation location:</i> At the end of the weld, start-stop points. Strain measurements;			
			

Specimen: VR691	Thickness [mm]	Rolled	25.02
		Cast	-
<i>Fatigue crack creation stage</i>			
N_i : 378927	N_s : 983687		
<i>Crack initiation location during testing</i>	Near the edge of the weld toe of the weld cap		
<i>Detected cracks by magnetic particle</i>			
			
Edge of the weld cap and two other locations	Edge crack	Long crack indication at the weld root	
<p><i>Repair of fatigue cracks:</i> The specimen cut from the middle and the weld material is removed such that the root and one side of the cap are suspended. Thus, half a V-shape groove is prepared.</p> 			
<i>Test results of the repaired specimen</i>			
N_i : 1239493	N_f : 1738721		
<i>Crack initiation location:</i> Repaired side of the connection and middle of the weld toe of the weld cap.			

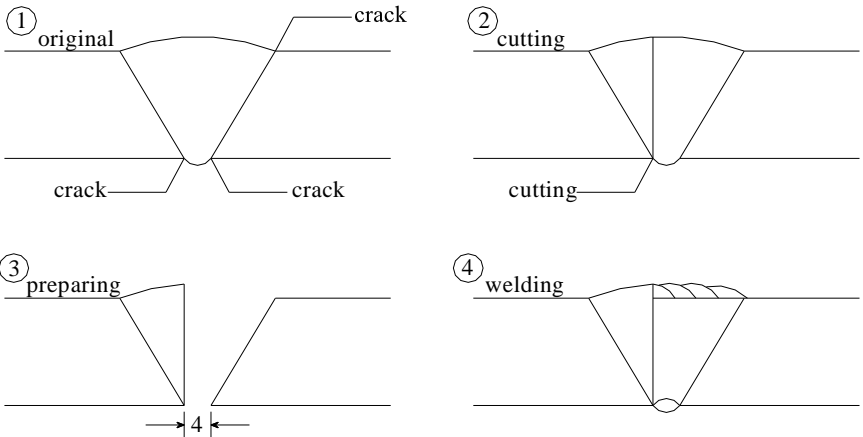
$\Delta\varepsilon$ [μstrain]

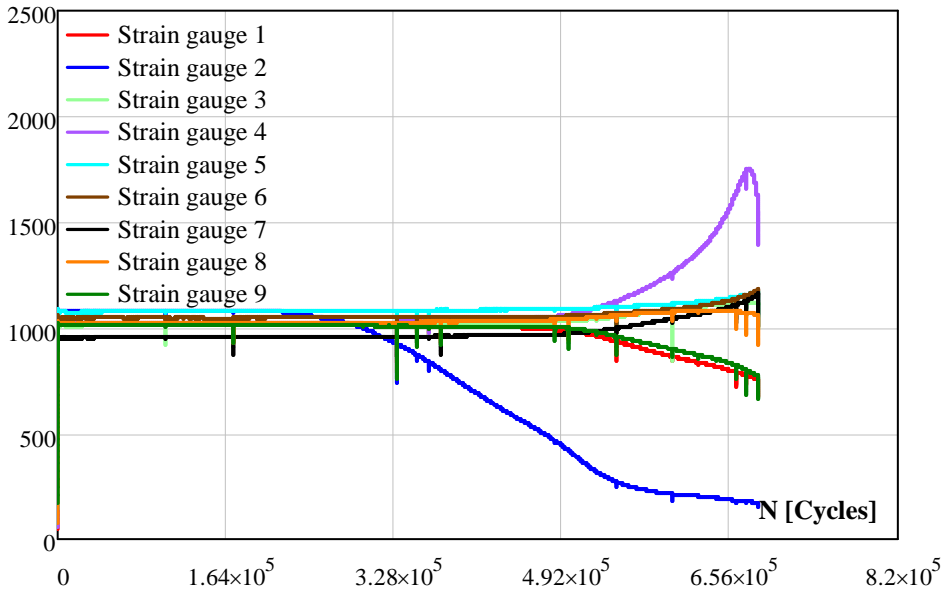
a) Crack creation stage.

 $\Delta\varepsilon$ [μstrain]

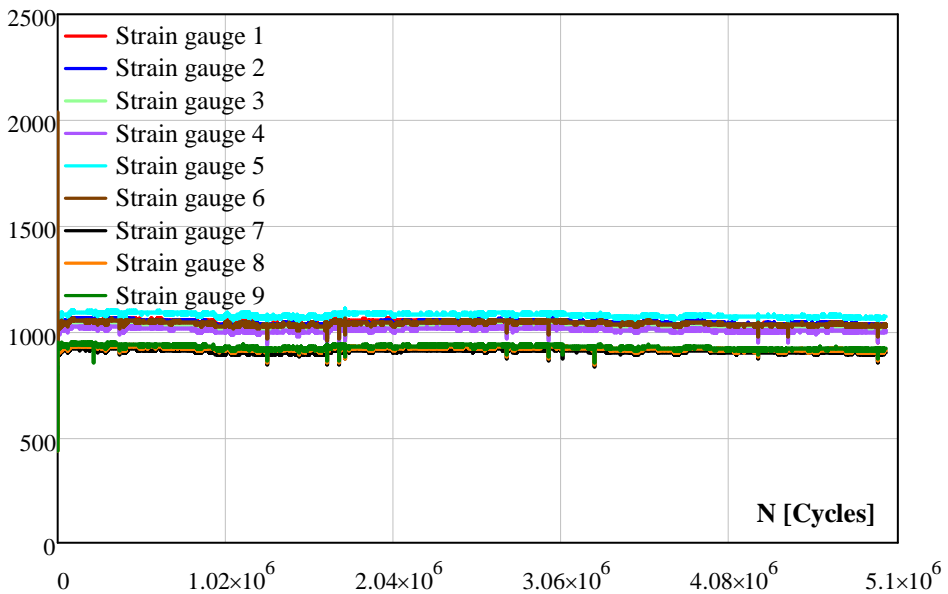
b) Repaired specimen.

Figure D.1 Strain gauge measurements of VR691 specimen.

Specimen: VR692	Thickness [mm]	Rolled	25.07
		Cast	-
<i>Fatigue crack creation stage</i>			
N_i : 208560	N_s : 684565		
<i>Crack initiation location during testing</i>	Near the edge of the weld toe of the weld cap		
<i>Detected cracks by magnetic particle</i>			
			
Edge of the weld cap	Edge crack	Long crack indication at the weld root	
<p><i>Repair of fatigue cracks:</i> The specimen cut from the middle and weld material is removed such that the root and one side of the cap are suspended. Thus, half a V-shape groove is prepared.</p>			
			
<i>Test results of the repaired specimen</i>			
N_i : 0	N_f : 5022891		
<i>Crack initiation location:</i> Runout. No any crack initiation has been observed.			

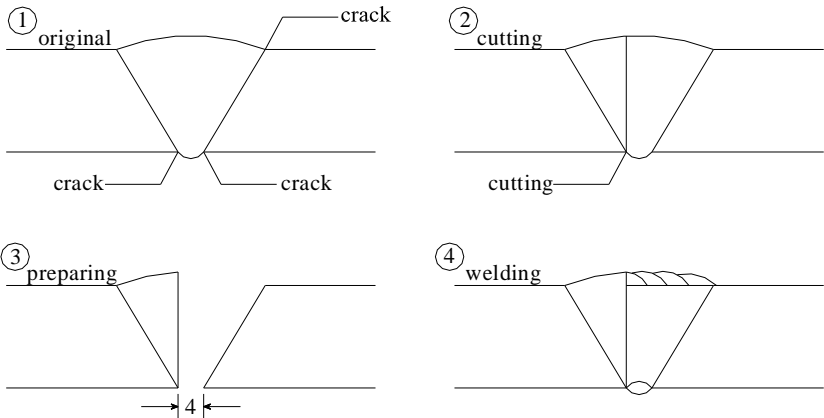
$\Delta\varepsilon$ [μstrain]

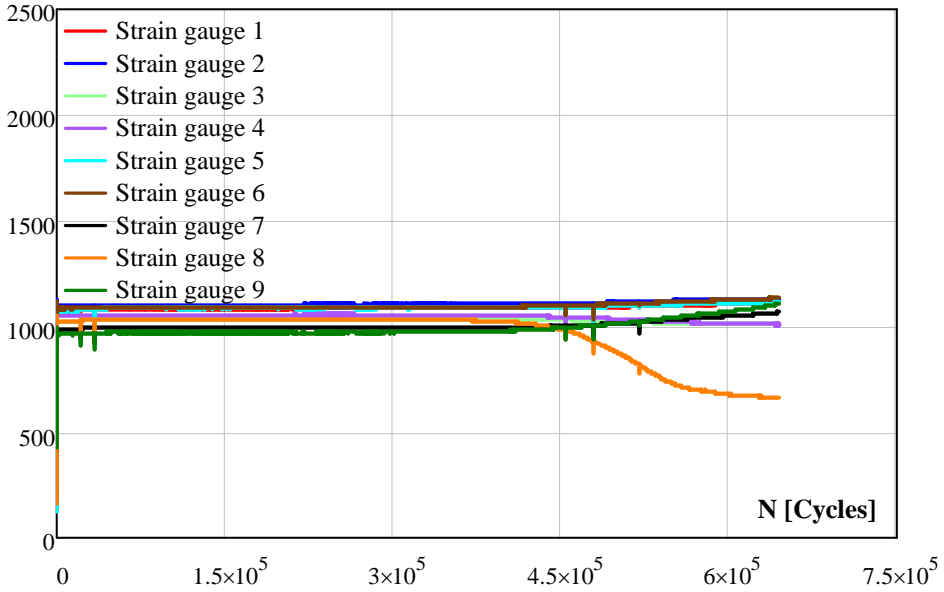
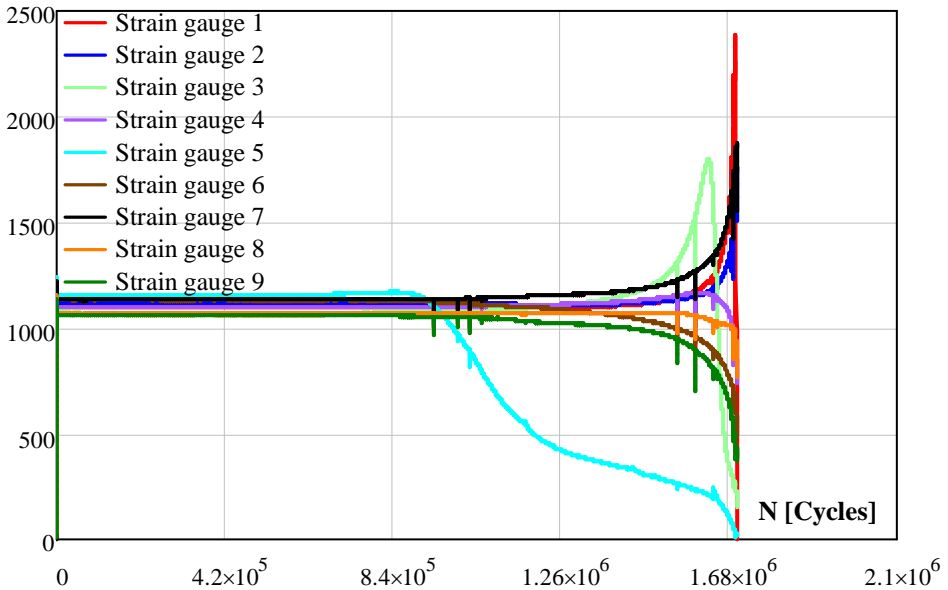
a) Crack creation stage.

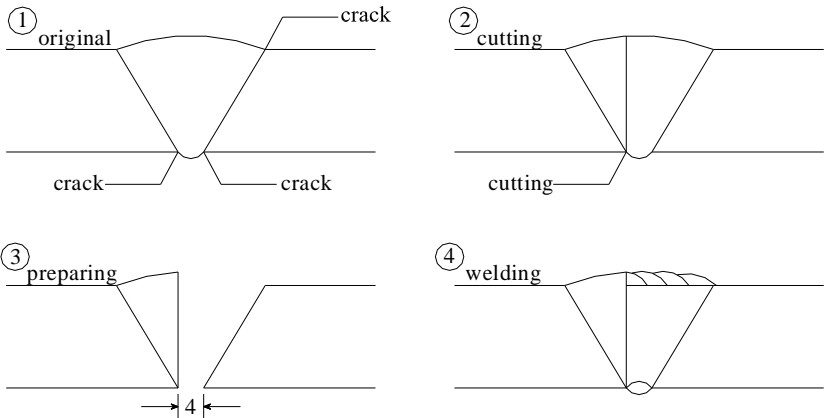
 $\Delta\varepsilon$ [μstrain]

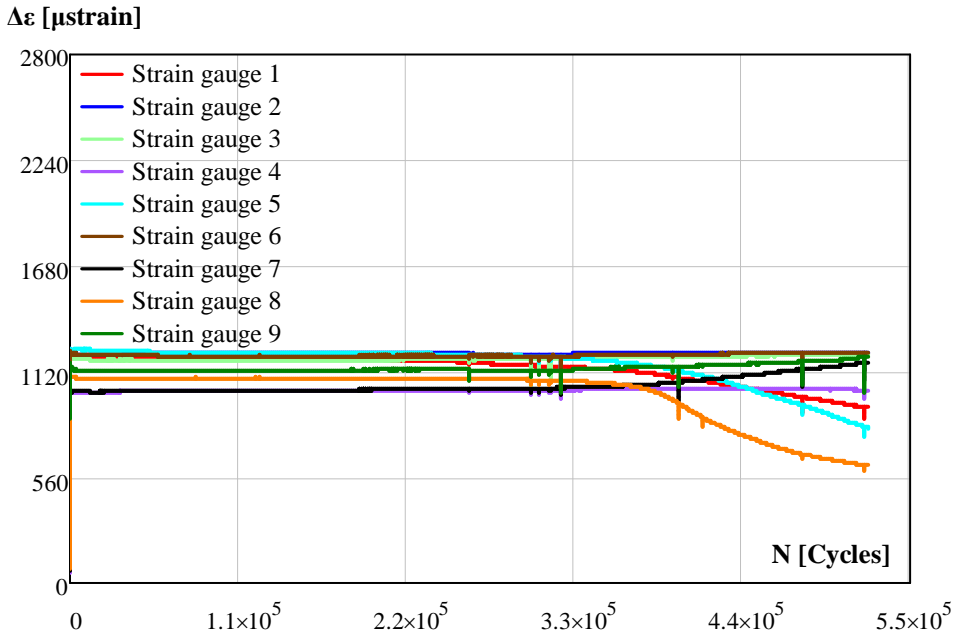
b) Repaired specimen.

Figure D.2 Strain gauge measurements of VR692 specimen.

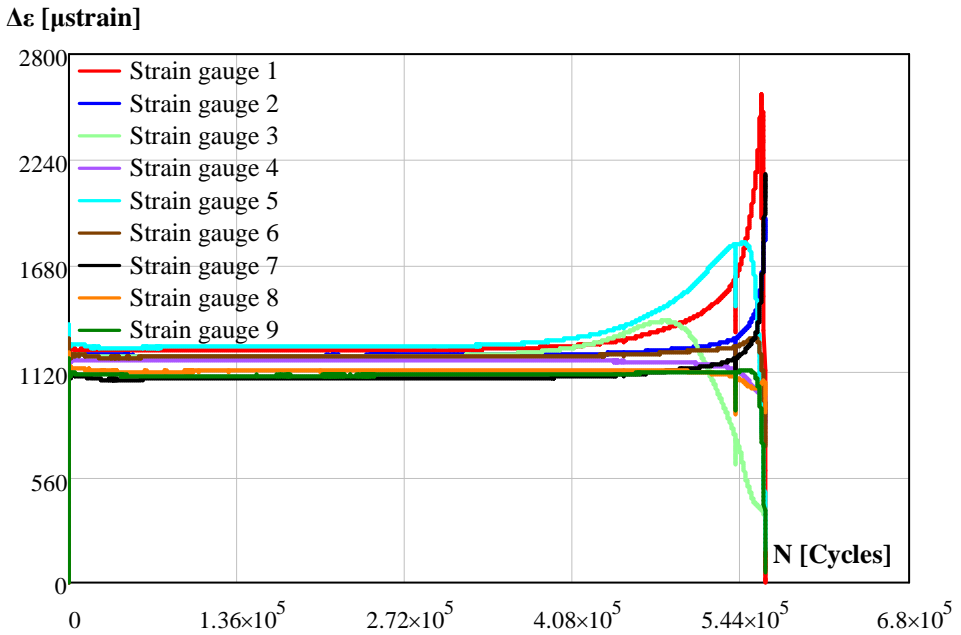
Specimen: VR693	Thickness [mm]	Rolled	25.1
		Cast	-
<i>Fatigue crack creation stage</i>			
N _i : 413035	N _s : 644946		
<i>Crack initiation location during testing</i>	Middle of the weld toe of the weld root		
<i>Detected cracks by magnetic particle</i>			
			
Small crack at middle of the weld cap		Long crack indication at the weld root	
<p><i>Repair of fatigue cracks:</i> The specimen cut from the middle and weld material is removed such that the root and one side of the cap are suspended. Thus, half a V-shape groove is prepared.</p>			
			
<i>Test results of the repaired specimen</i>			
N _i : 894634	N _f : 1699000		
<i>Crack initiation location:</i> At weld toe of the weld cap, near the plate edge.			

$\Delta\varepsilon$ [μstrain]*a) Crack creation stage.* $\Delta\varepsilon$ [μstrain]*b) Repaired specimen.**Figure D.3 Strain gauge measurements of VR693 specimen.*

Specimen: VR694	Thickness [mm]	Rolled	25.04
		Cast	-
<i>Fatigue crack creation stage</i>			
N_i : 166843	N_s : 522021		
<i>Crack initiation location during testing</i>	Edge of the weld toe of the weld cap		
<i>Detected cracks by magnetic particle</i>			
			
At edge of the weld toe and weak indication along the weld toe		Long crack indication at the weld root	
<p><i>Repair of fatigue cracks:</i> The specimen cut from the middle and weld material is removed such that the root and one side of the cap are suspended. Thus, half a V-shape groove is prepared.</p>			
			
<i>Test results of the repaired specimen</i>			
N_i : 313418	N_f : 564136		
<i>Crack initiation location:</i> Near middle of the weld toe of the weld cap.			

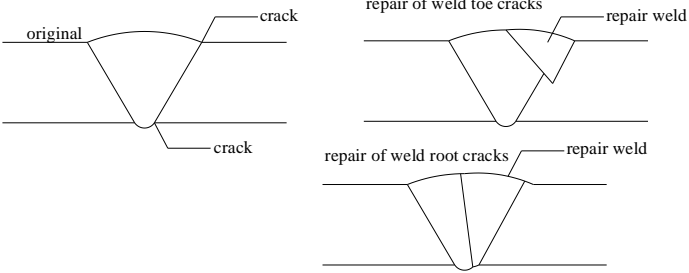


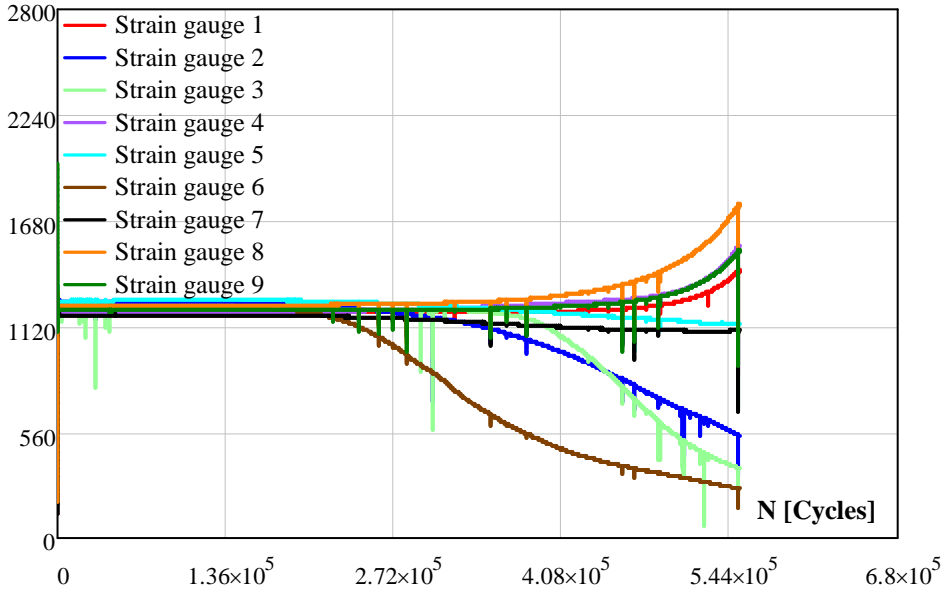
a) Crack creation stage.



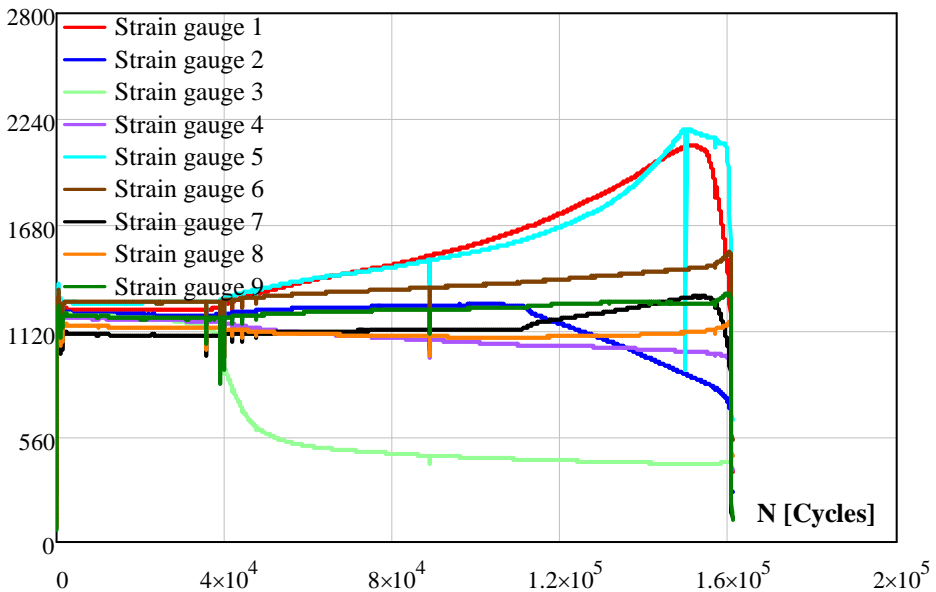
b) Repaired specimen.

Figure D.4 Strain gauge measurements of VR694 specimen.

Specimen: VR695	Thickness [mm]	Rolled	25.02
		Cast	-
<i>Fatigue crack creation stage</i>			
N_i : 198636	N_s : 551732		
<i>Crack initiation location during testing</i>	Edge of the weld toe of the weld cap.		
<i>Detected cracks by magnetic particle</i>			
 <p>Weld toe crack at three locations; middle and both edges</p>  <p>Edge crack at the weld root</p>			
<p><i>Repair of fatigue cracks:</i> All cracks are removed from the weld toe of the cap and the prepared weld groove is filled by weld material.</p> 			
<i>Test results of the repaired specimen</i>			
N_i : 30696	N_f : 160895		
<p><i>Crack initiation location:</i> At middle of the weld toe of the cap. From the fracture surface of the specimen, it is seen that it contained an initial imperfection which caused premature failure.</p>			

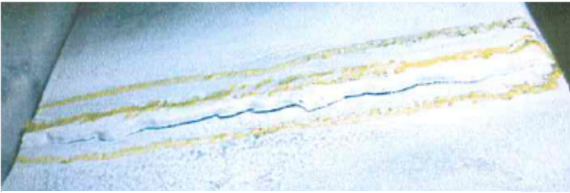
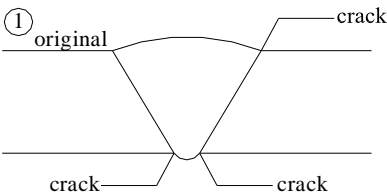
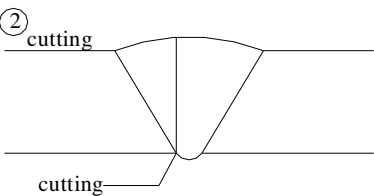
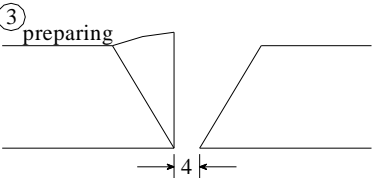
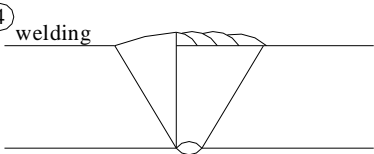
$\Delta\varepsilon$ [μstrain]

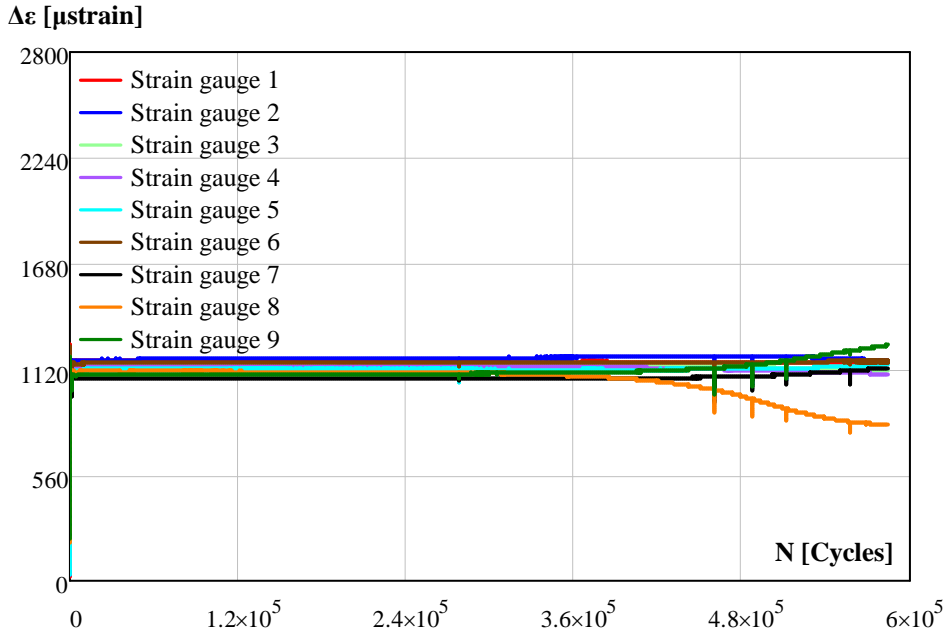
a) Crack creation stage.

 $\Delta\varepsilon$ [μstrain]

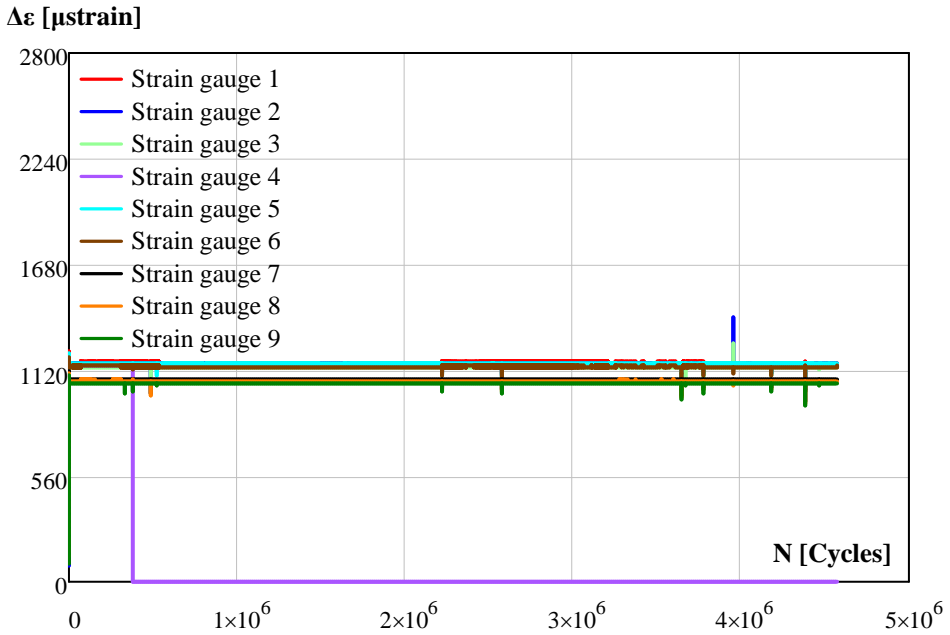
b) Repaired specimen.

Figure D.5 Strain gauge measurements of VR695 specimen.

Specimen: VR696	Thickness [mm]	Rolled	25.12
		Cast	-
<i>Fatigue crack creation stage</i>			
N_i : 337073	N_s : 584540		
<i>Crack initiation location during testing</i>	At weld toe of the root, near the plate edge.		
<i>Detected cracks by magnetic particle</i>			
<div style="display: flex; justify-content: space-around;">   </div> <div style="display: flex; justify-content: space-around; margin-top: 10px;"> <div style="text-align: center;"> <p>Indication at the weld toe of the cap</p> </div> <div style="text-align: center;"> <p>Long crack at the weld root</p> </div> </div>			
<p><i>Repair of fatigue cracks:</i> The specimen cut from the middle and weld material is removed such that the root and one side of the cap are suspended. Thus, half a V-shape groove is prepared.</p> <div style="display: flex; justify-content: space-around;"> <div style="text-align: center;"> <p>① original</p>  </div> <div style="text-align: center;"> <p>② cutting</p>  </div> </div> <div style="display: flex; justify-content: space-around; margin-top: 20px;"> <div style="text-align: center;"> <p>③ preparing</p>  </div> <div style="text-align: center;"> <p>④ welding</p>  </div> </div>			
<i>Test results of the repaired specimen</i>			
N_i : 0	N_f : 4575656		
<i>Crack initiation location:</i> Runout. No any crack initiation has been observed.			

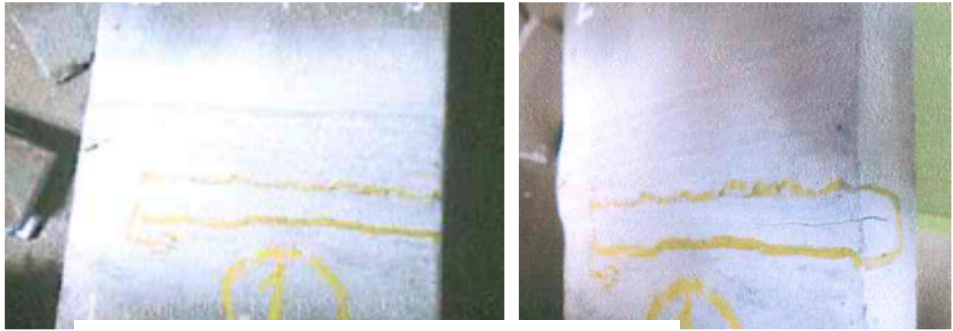
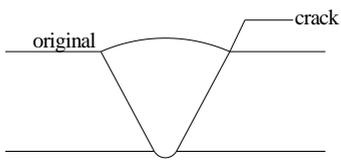
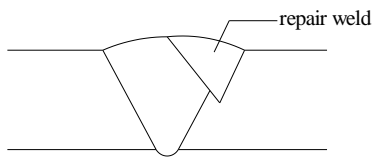
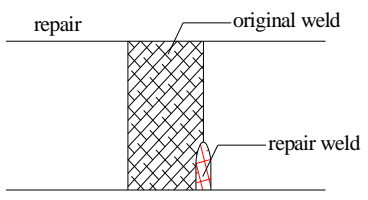
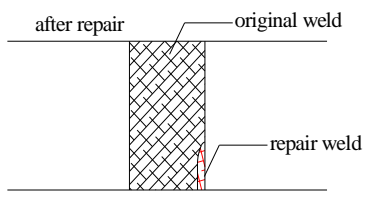


a) Crack creation stage.

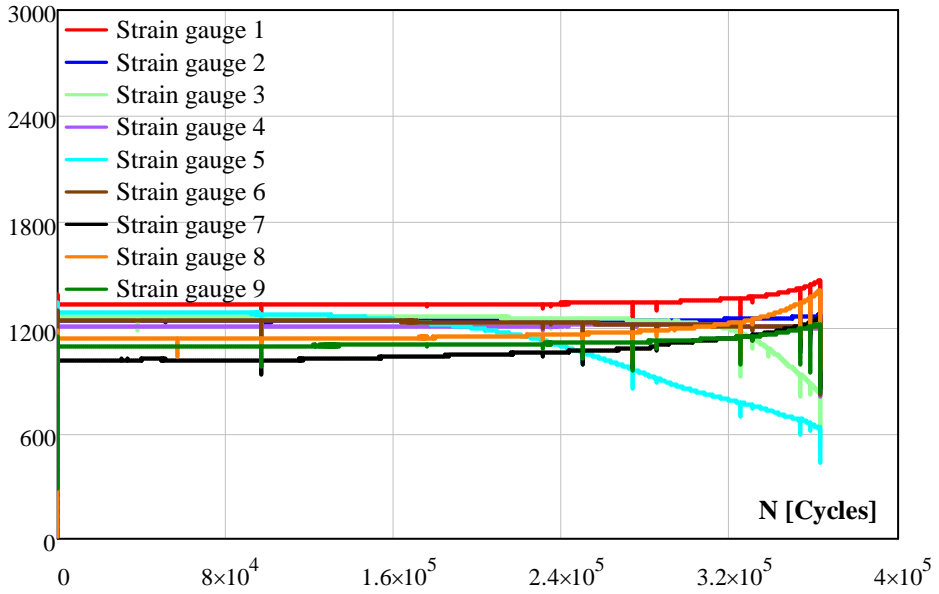


b) Repaired specimen.

Figure D.6 Strain gauge measurements of VR696 specimen.

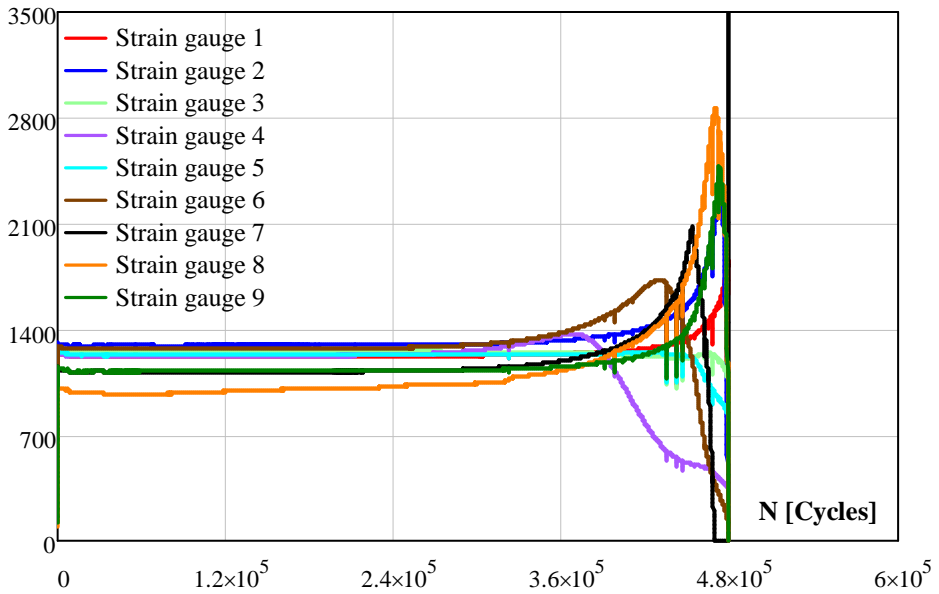
Specimen: VR697	Thickness [mm]	Rolled	25.04
		Cast	-
<i>Fatigue crack creation stage</i>			
N_i : 153723	N_s : 362879		
<i>Crack initiation location during testing</i>	At the weld toe of the cap, near the plate edge.		
<i>Detected cracks by magnetic particle</i>			
 <p style="text-align: center;">Crack at the weld toe, edge of the plate.</p>			
<p><i>Repair of fatigue cracks:</i> The crack is removed by a burr grinder and the prepared groove is filled by weld material. After the repair, discontinuities due to repair weld are ground.</p> <div style="display: flex; justify-content: space-around;"> <div style="text-align: center;">  <p>original</p> <p>crack</p> </div> <div style="text-align: center;">  <p>repair weld</p> </div> </div> <div style="display: flex; justify-content: space-around; margin-top: 10px;"> <div style="text-align: center;">  <p>repair</p> <p>original weld</p> <p>repair weld</p> </div> <div style="text-align: center;">  <p>after repair</p> <p>original weld</p> <p>repair weld</p> </div> </div>			
<i>Test results of the repaired specimen</i>			
N_i : 275968	N_f : 479221		
<i>Crack initiation location:</i> At the middle of the weld toe of the cap.			

$\Delta\epsilon$ [μstrain]



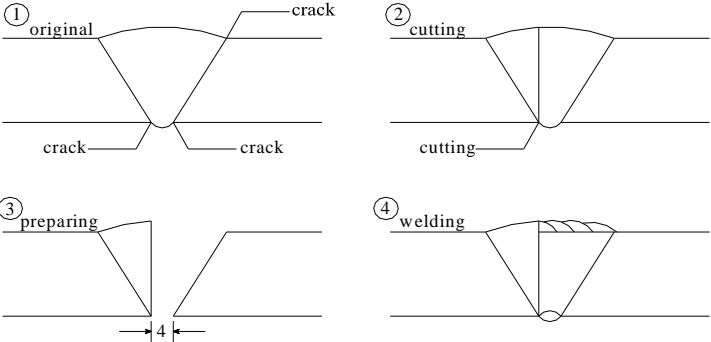
a) Crack creation stage.

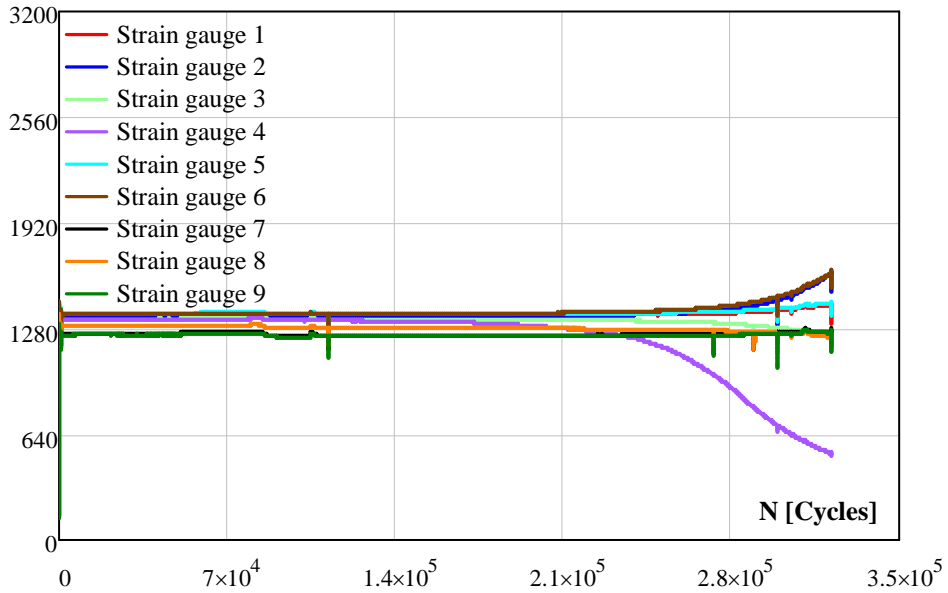
$\Delta\epsilon$ [μstrain]



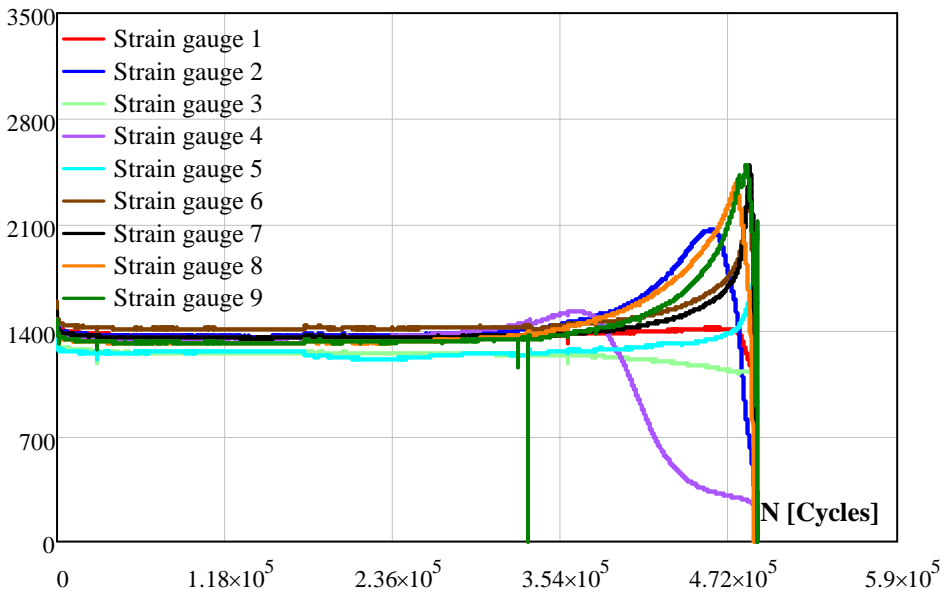
b) Repaired specimen.

Figure D.7 Strain gauge measurements of VR697 specimen.

Specimen: VR698	Thickness [mm]	Rolled	25.07
		Cast	-
<i>Fatigue crack creation stage</i>			
N_i : 186480	N_s : 321962		
<i>Crack initiation location during testing</i>	At the weld toe of the cap, near the middle of the plate.		
<i>Detected cracks by magnetic particle</i>			
 <p>Crack at the weld toe, longer than expected</p>  <p>Crack at the weld root</p>			
<p><i>Repair of fatigue cracks:</i> The specimen cut from the middle and weld material is removed such that the root and one side of the cap are suspended. Thus, half a V-shape groove is prepared.</p> 			
<i>Test results of the repaired specimen</i>			
N_i : 269302	N_f : 491536		
<i>Crack initiation location:</i> At the middle of the weld toe of the cap.			

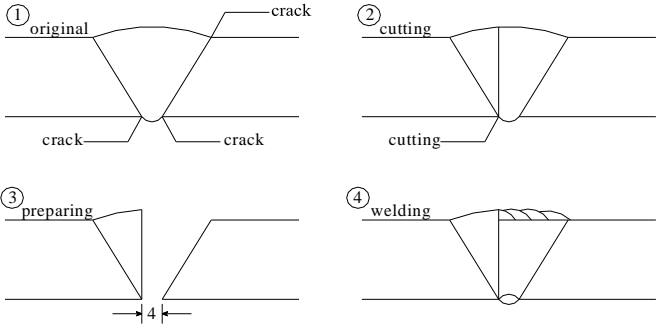
$\Delta\varepsilon$ [μstrain]

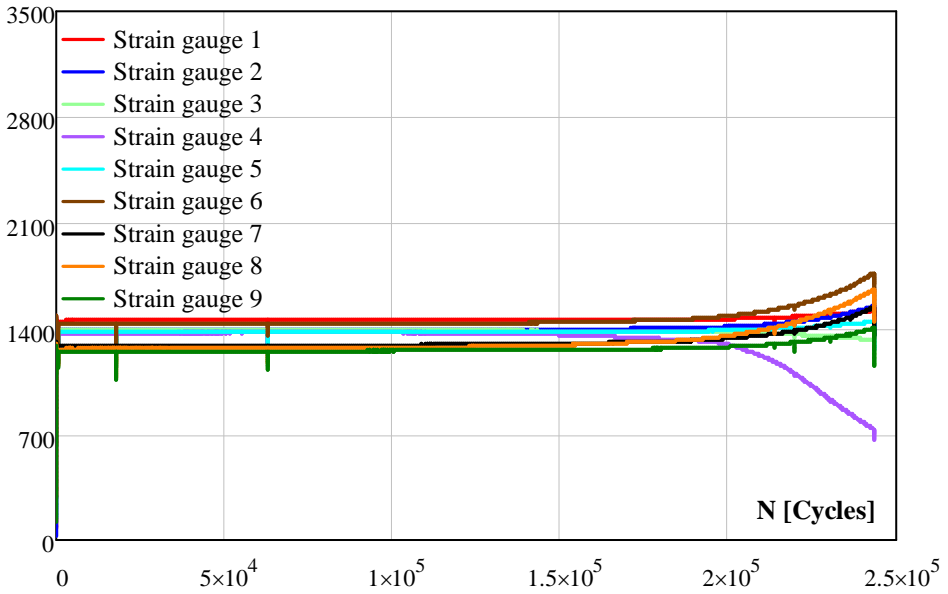
a) Crack creation stage.

 $\Delta\varepsilon$ [μstrain]

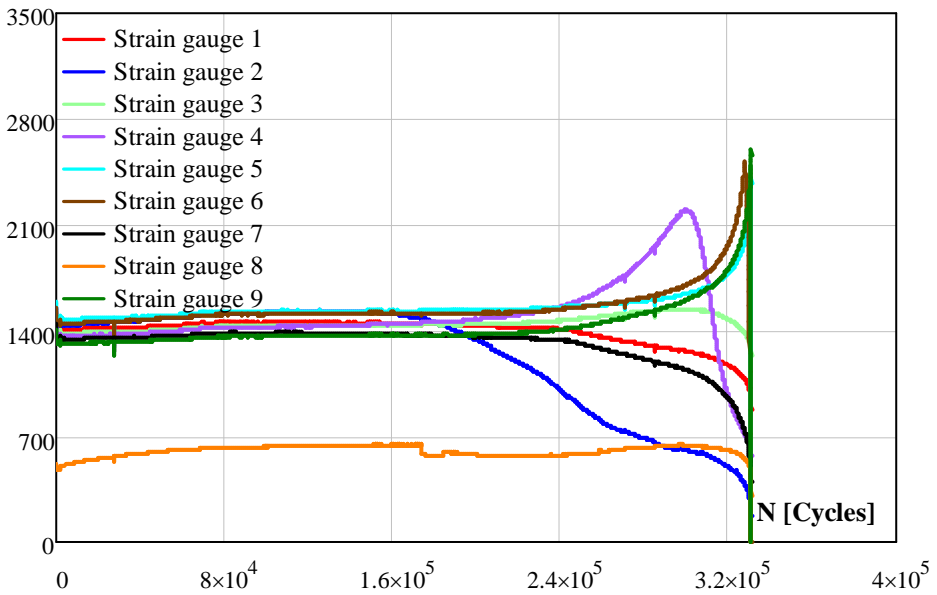
b) Repaired specimen.

Figure D.8 Strain gauge measurements of VR698 specimen.

Specimen: VR699	Thickness [mm]	Rolled	25.09
		Cast	-
<i>Fatigue crack creation stage</i>			
N_i : 161106	N_s : 243422		
<i>Crack initiation location during testing</i>	At the weld toe of the cap, near the middle of the plate.		
<i>Detected cracks by magnetic particle</i>			
 <p>Crack at the weld toe, longer than expected</p>  <p>Crack at the weld root</p>			
<p><i>Repair of fatigue cracks:</i> The specimen cut from the middle and weld material is removed such that the root and one side of the cap are suspended. Thus, half a V-shape groove is prepared.</p> 			
<i>Test results of the repaired specimen</i>			
N_i : 163269	N_f : 331122		
<i>Crack initiation location:</i> At weld toe of the cap, near the plate edge.			

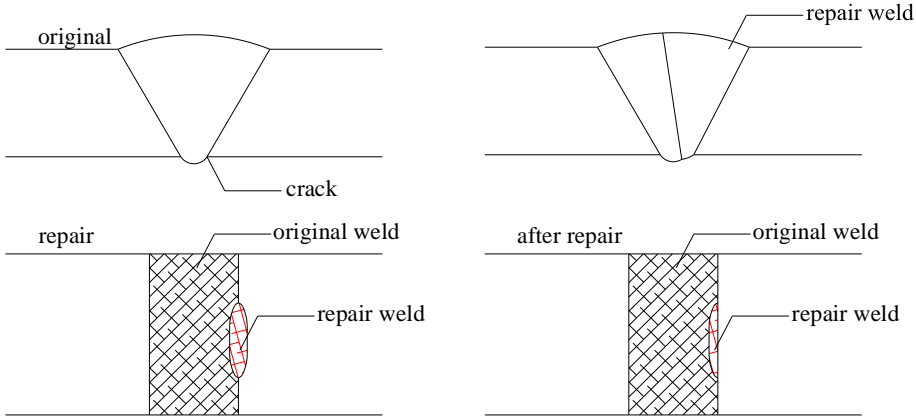
$\Delta\varepsilon$ [μstrain]

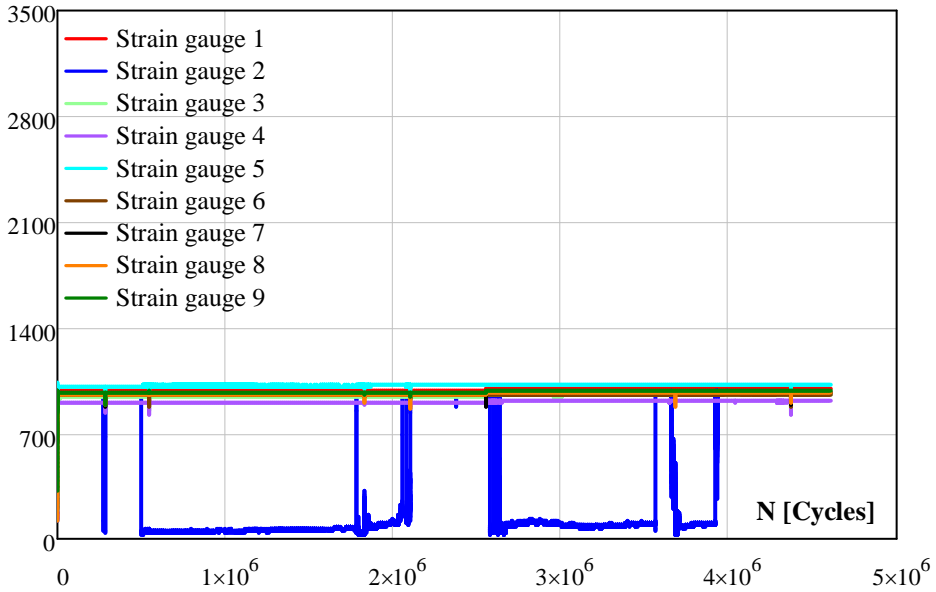
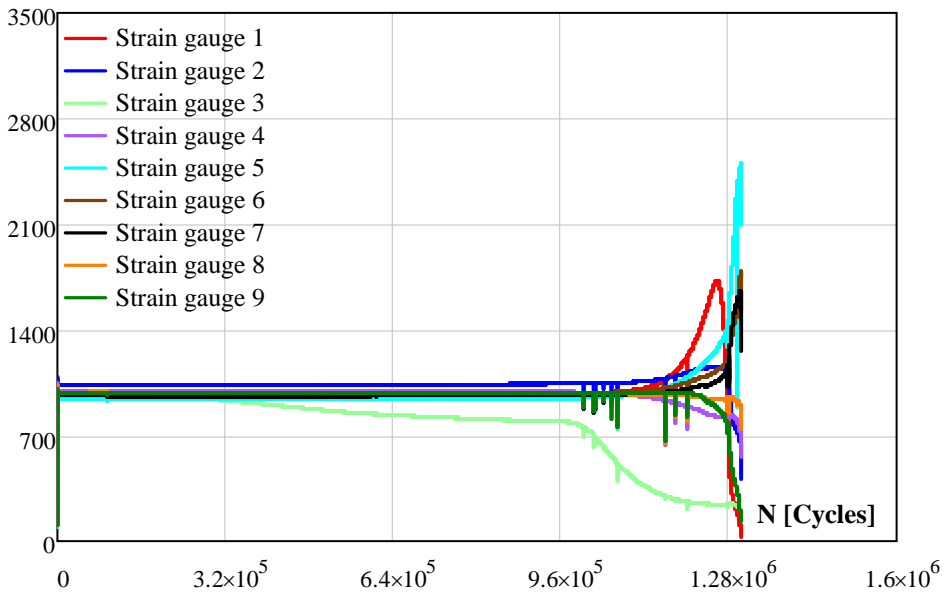
a) Crack creation stage.

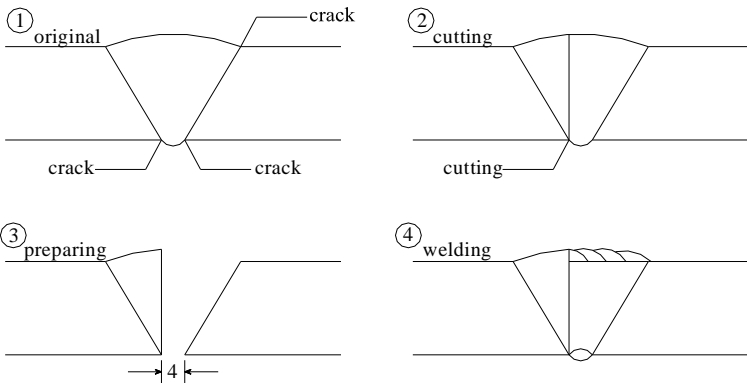
 $\Delta\varepsilon$ [μstrain]

b) Repaired specimen.

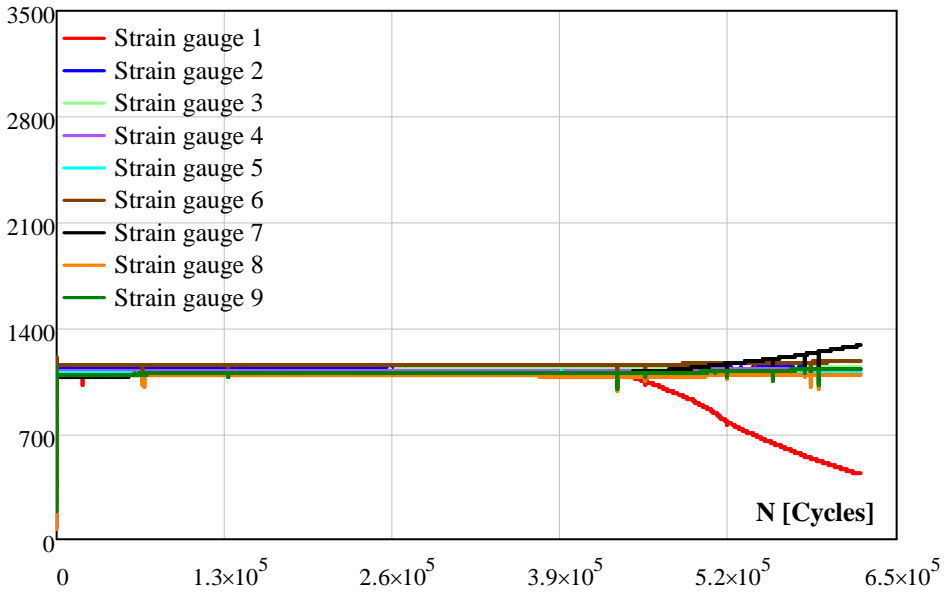
Figure D.9 Strain gauge measurements of VR699 specimen.

Specimen: CR691	Thickness [mm]	Rolled	25.04
		Cast	25.8
<i>Fatigue crack creation stage</i>			
N_i : 0	N_s : 4602408		
<i>Crack initiation location during testing</i>	Runout. No any crack initiation has been observed.		
<i>Detected cracks by magnetic particle</i>			
 <p>Small crack indication at the weld root of cast steel side</p>			
<p><i>Repair of fatigue cracks:</i> The crack is removed from the weld cap. The prepared groove is filled by weld material and the discontinuity after the repair is ground.</p> 			
<i>Test results of the repaired specimen</i>			
N_i : 224510	N_f : 1302160		
<i>Crack initiation location:</i> At middle of the weld toe of the cap, cast steel side.			

$\Delta\varepsilon$ [μstrain]*a) Crack creation stage.* $\Delta\varepsilon$ [μstrain]*b) Repaired specimen.**Figure D.10 Strain gauge measurements of CR691 specimen.*

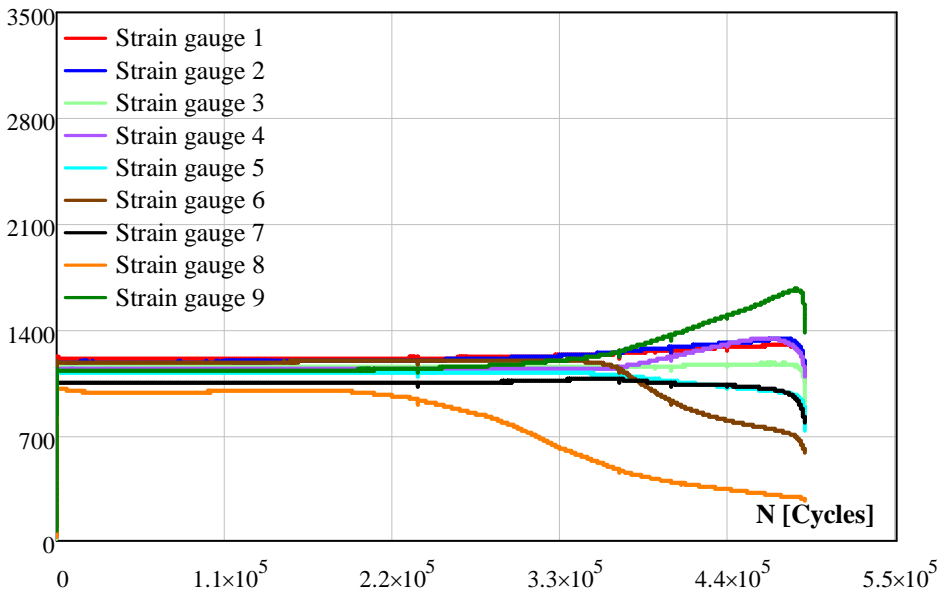
Specimen: CR-1 692	Thickness [mm]	Rolled	25.1
		Cast	25.5
<i>Fatigue crack creation stage</i>			
N_i : 393318	N_s : 621920		
<i>Crack initiation location during testing</i>	At the edge of the base material of the cast steel and at the middle of the weld of the weld root.		
<i>Detected cracks by magnetic particle</i>			
			
Small crack in the base material of cast steel		Long crack at the weld root.	
<p><i>Repair of fatigue cracks:</i> The specimen cut from the middle and weld material is removed such that the root and one side of the cap are suspended. Thus, half a V-shape groove is prepared. The crack in the base material is removed and the groove is filled by the weld material and subsequently the repair weld is ground, a smooth surface is created.</p>			
			
<i>Test results of the repaired specimen</i>			
N_i : 370566	N_f : 489277		
<p><i>Crack initiation location:</i> Failure in the base material of cast steel and crack is observed at the middle of the plate. On the fracture surface, a small internal imperfection is detected at the crack initiation point.</p>			

$\Delta\epsilon$ [μstrain]



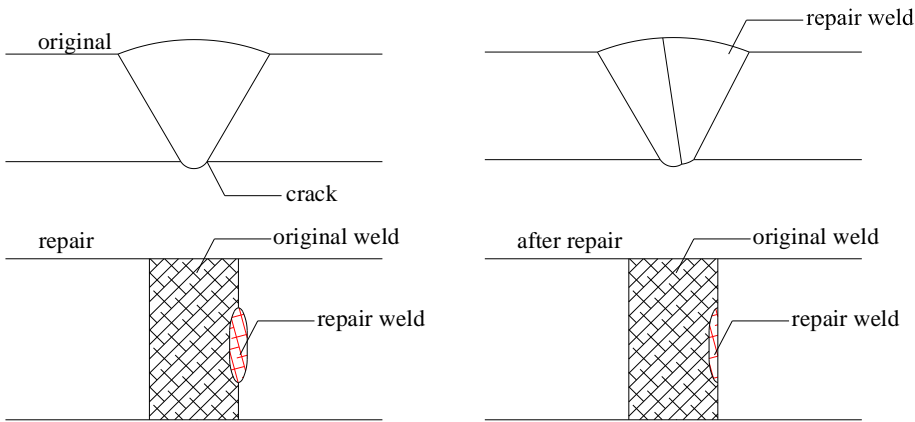
a) Crack creation stage.

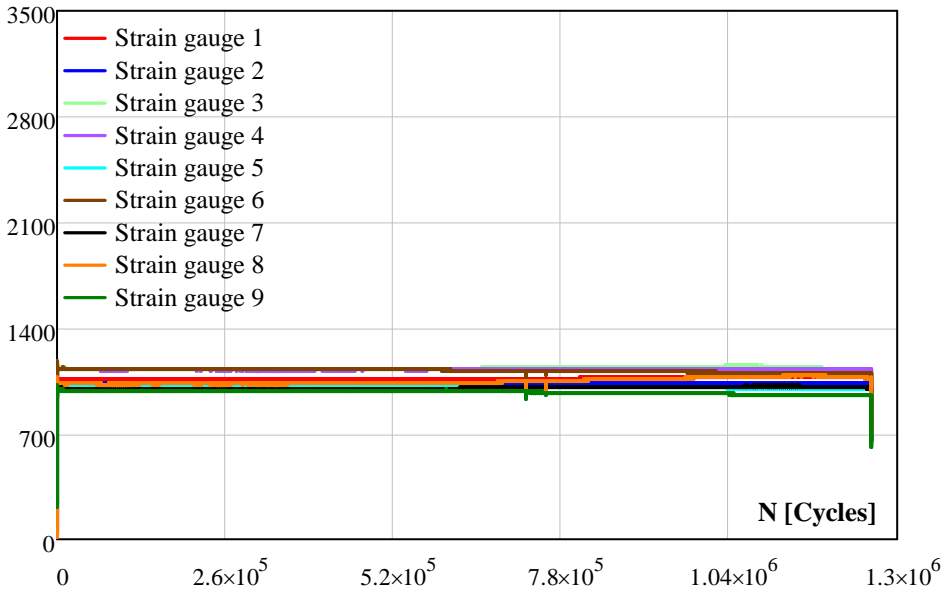
$\Delta\epsilon$ [μstrain]



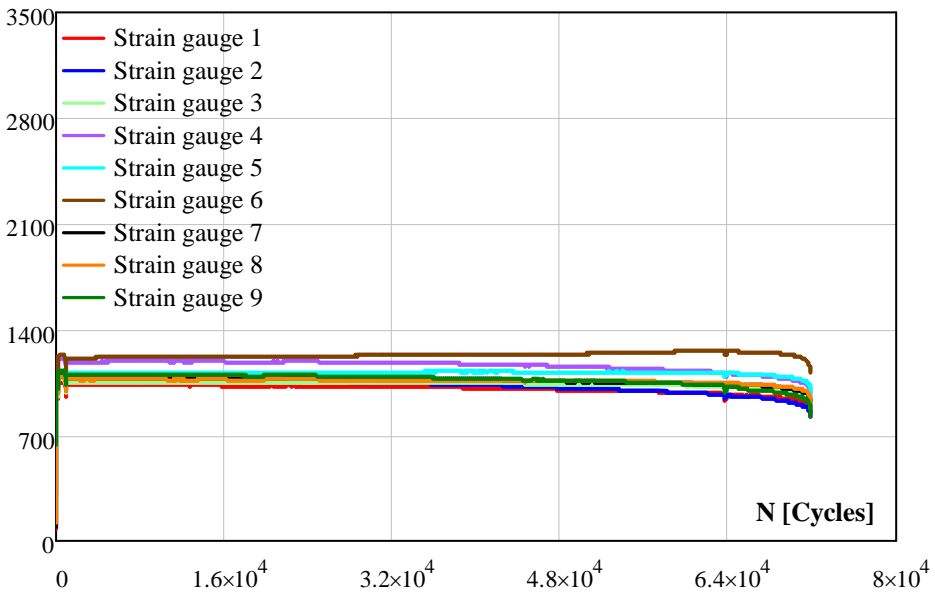
b) Repaired specimen.

Figure D.11 Strain gauge measurements of CR692 specimen.

Specimen: CR693	Thickness [mm]	Rolled	25.15
		Cast	24.8
<i>Fatigue crack creation stage</i>			
N _i : 660161	N _s : 1260937		
<i>Crack initiation location during testing</i>	At the edge of the weld toe of the root, cast side.		
<i>Detected cracks by magnetic particle</i>			
 <p>Crack at weld root</p>			
<p><i>Repair of fatigue cracks:</i> The crack is removed by a burr grinder and the prepared groove is filled by weld material. After the repair, the discontinuity due to the repair weld is ground.</p>			
			
<i>Test results of the repaired specimen</i>			
N _i : 71789	N _f : 1332726		
<p><i>Crack initiation location:</i> Failure in the base material of cast steel and crack is observed at the edge of the plate. The fracture surface of the specimen shows that the crack was already initiated during the crack creation stage. This is concluded from the colour at the crack initiation location, which was already highly corroded.</p>			

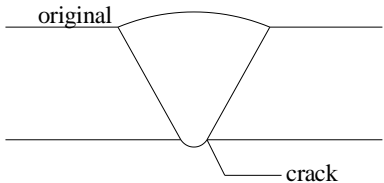
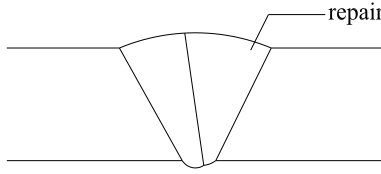
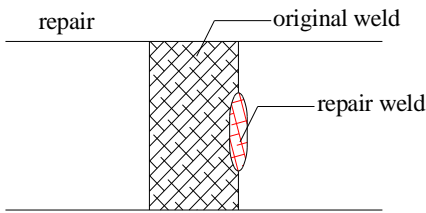
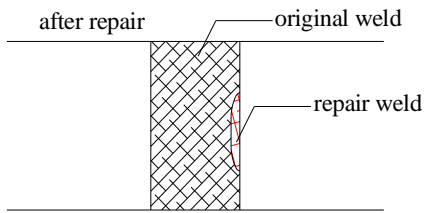
$\Delta\varepsilon$ [μstrain]

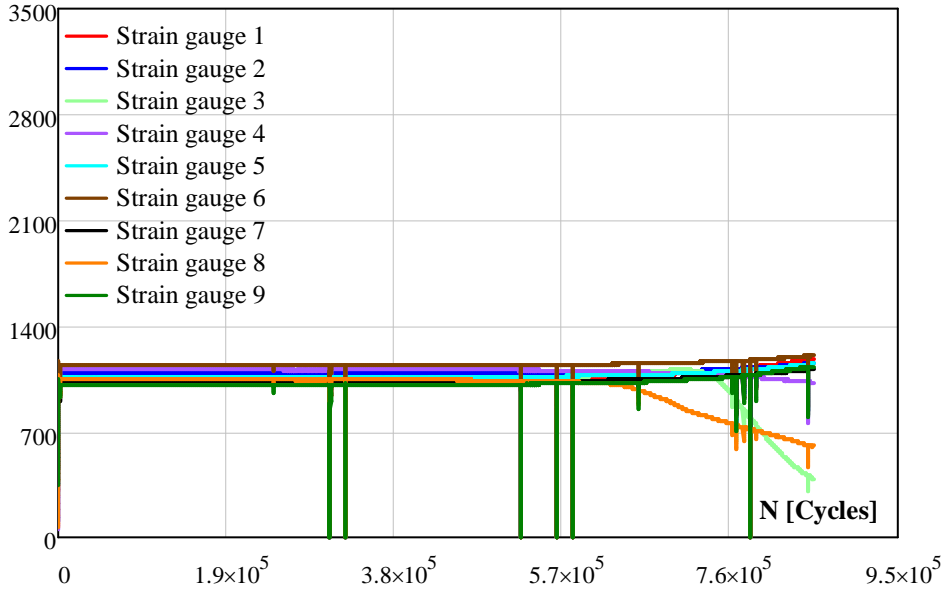
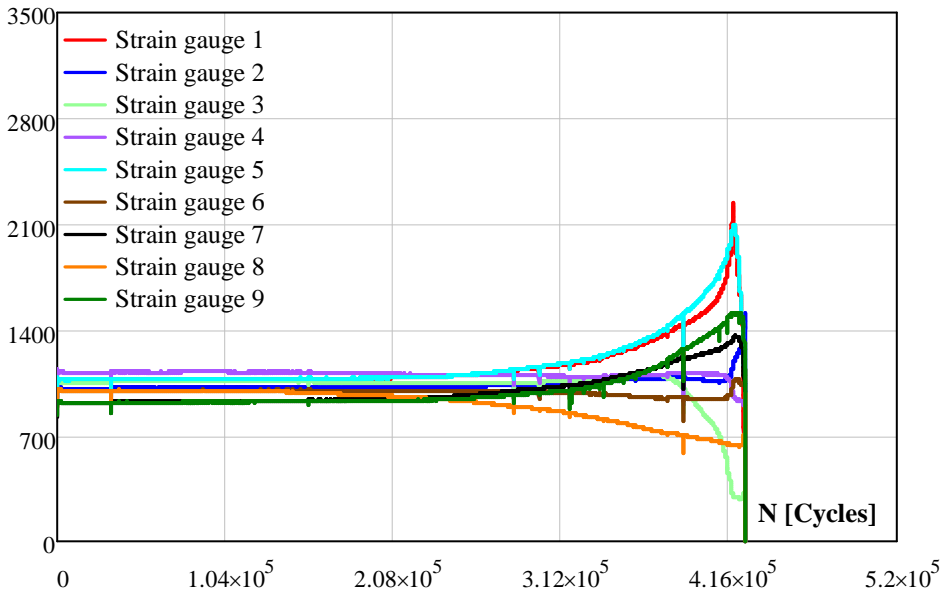
a) Crack creation stage.

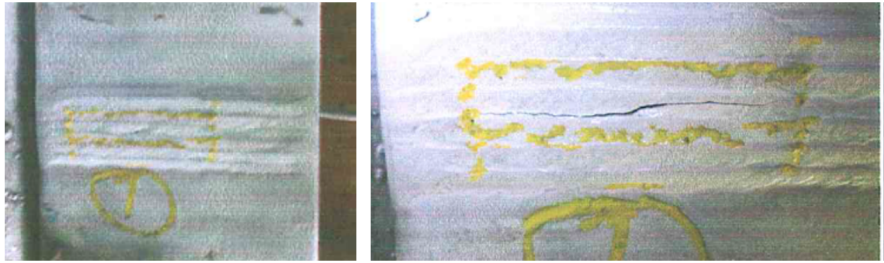
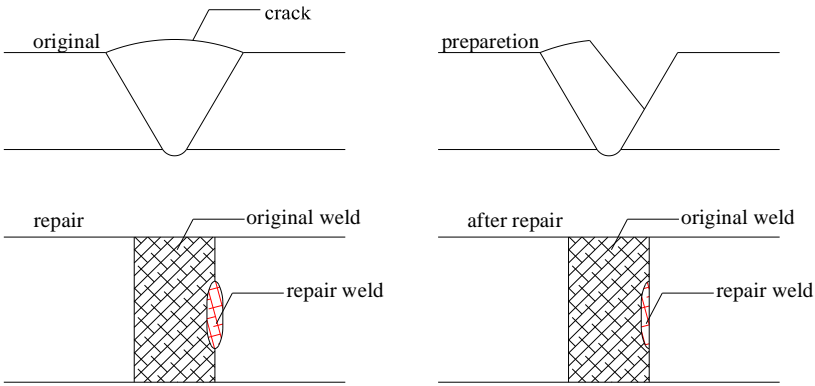
 $\Delta\varepsilon$ [μstrain]

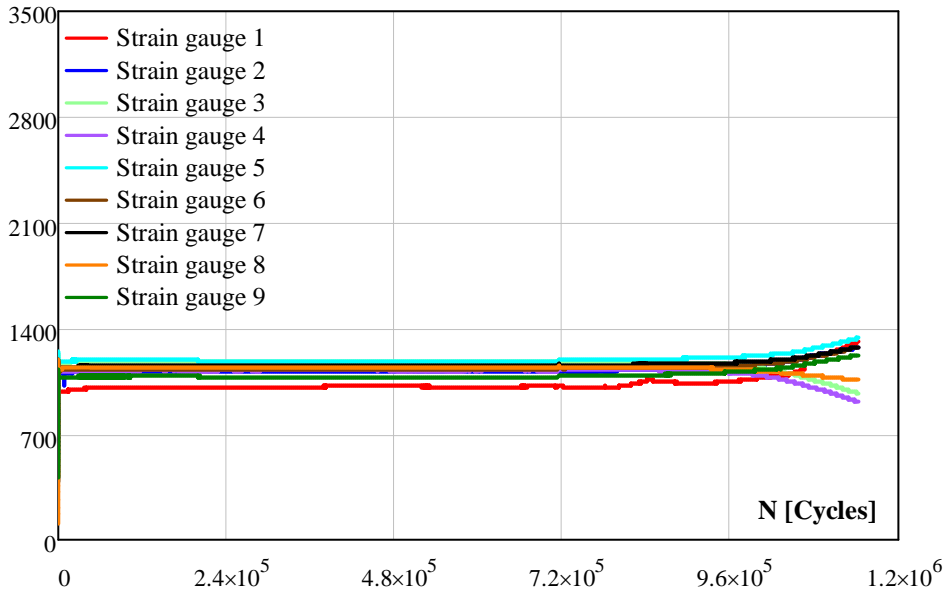
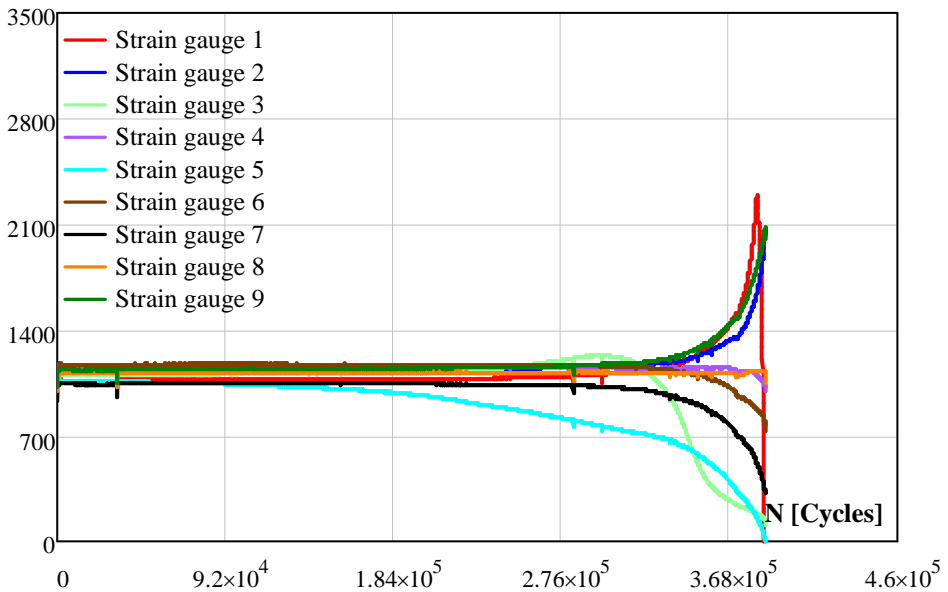
b) Repaired specimen.

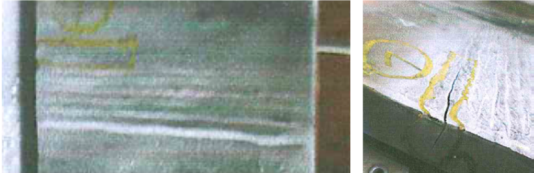
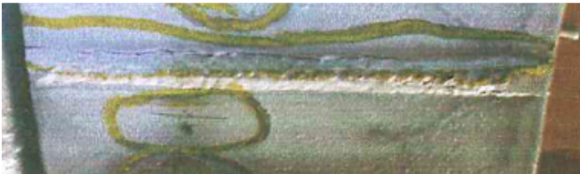
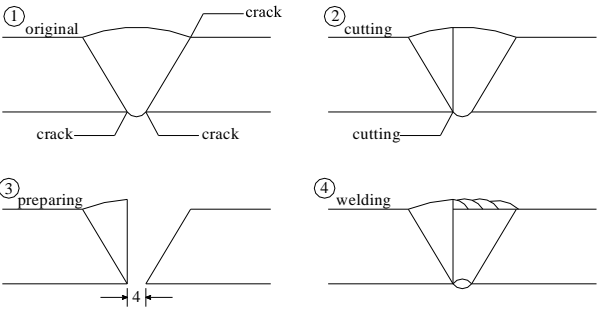
Figure D.12 Strain gauge measurements of CR693 specimen.

Specimen: CR694	Thickness [mm]	Rolled	25.18
		Cast	25.45
<i>Fatigue crack creation stage</i>			
N_i : 626931	N_s : 854386		
<i>Crack initiation location during testing</i>	At the middle of the weld toe of the cap and at the middle of the weld toe of the root.		
<i>Detected cracks by magnetic particle</i>			
			
Crack at weld toe of the cap of cast steel side		Cracks on both sides of the weld toe of the root	
<i>Repair of fatigue cracks:</i> The crack is removed from the weld cap. The prepared groove is filled by weld material and discontinuity the after repair is ground.			
			
			
<i>Test results of the repaired specimen</i>			
N_i : 165382	N_f : 425808		
<i>Crack initiation location:</i> Weld toe at rolled steel parts near to middle of the weld.			

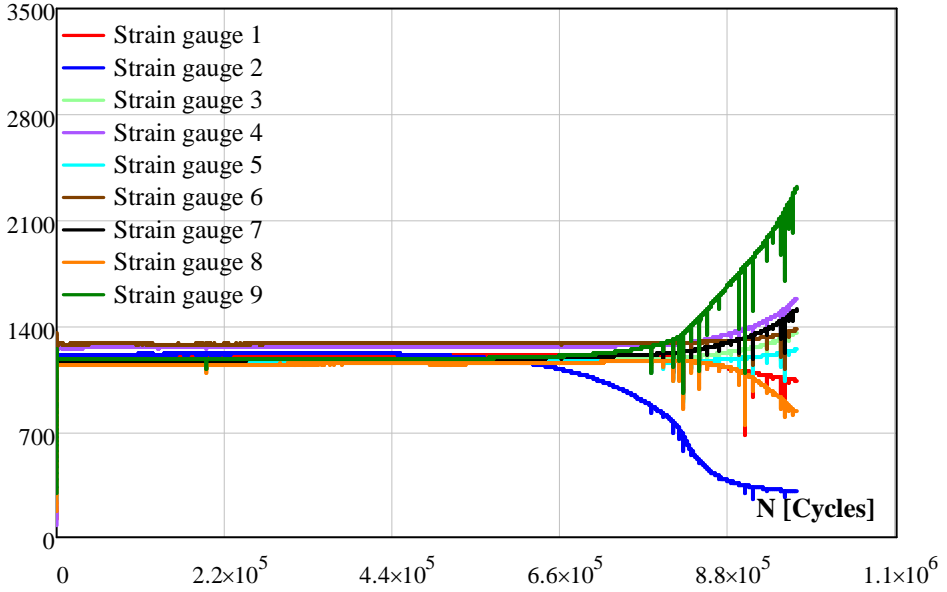
$\Delta\varepsilon$ [μstrain]*a) Crack creation stage.* $\Delta\varepsilon$ [μstrain]*b) Repaired specimen.**Figure D.13 Strain gauge measurements of CR694 specimen.*

Specimen: CR695	Thickness [mm]	Rolled	25.22
		Cast	25.93
<i>Fatigue crack creation stage</i>			
N_i : 890585	N_s : 1141717		
<i>Crack initiation location during testing</i>	At the middle of the weld material of the cap.		
<i>Detected cracks by magnetic particle</i>			
			
Middle of the weld material, weld cap		Crack in the weld material of the cap	
<i>Repair of fatigue cracks:</i> The crack is removed from the weld cap. The prepared groove is filled by weld material and discontinuity the after repair is ground.			
			
<i>Test results of the repaired specimen</i>			
N_i : 723839	N_f : 387686		
<i>Crack initiation location:</i> Cracks are initiated at the weld toe of the cast steel side. Cracks are observed at the middle and edge of the weld toe.			

$\Delta\varepsilon$ [μstrain]*a) Crack creation stage.* $\Delta\varepsilon$ [μstrain]*b) Repaired specimen.**Figure D.14 Strain gauge measurements of CR695 specimen.*

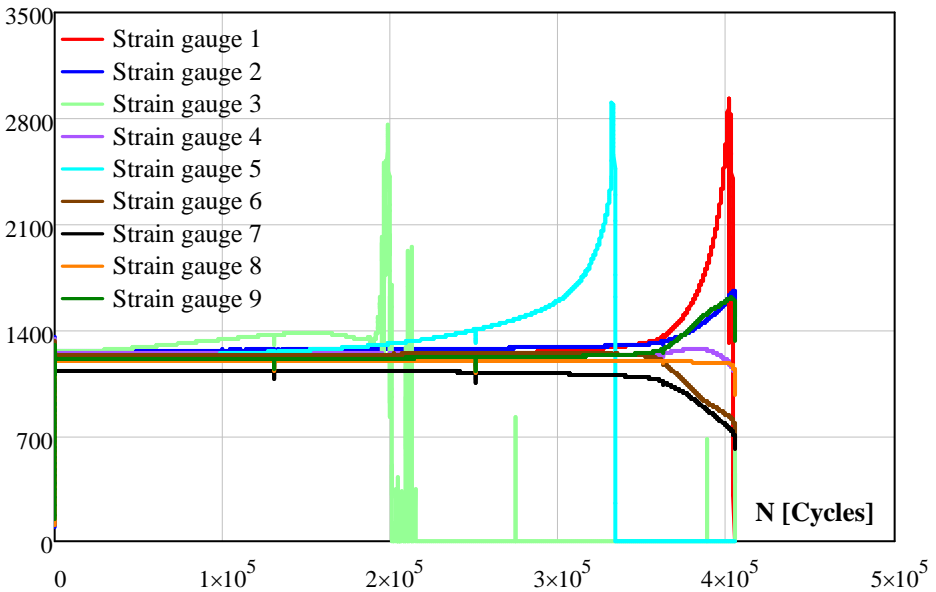
Specimen: CR696	Thickness [mm]	Rolled	25.16
		Cast	25.7
<i>Fatigue crack creation stage</i>			
N _i : 534523	N _s : 969052		
<i>Crack initiation location during testing</i>	At weld toe of the cap edge rolled steel side		
<i>Detected cracks by magnetic particle</i>			
 <p>Crack at weld toe of the cap, edge of rolled steel side</p>  <p>Long crack indication at the weld root</p>			
<p><i>Repair of fatigue cracks:</i> The specimen cut from the middle and weld material is removed such that the root and one side of the cap are suspended. Thus, half a V-shape groove is prepared.</p> 			
<i>Test results of repaired specimen</i>			
N _i : 104233	N _f : 1374056		
<i>Crack initiation location:</i> Failure in the base material of the cast steel and crack is observed at the middle of the plate.			

$\Delta\varepsilon$ [μstrain]



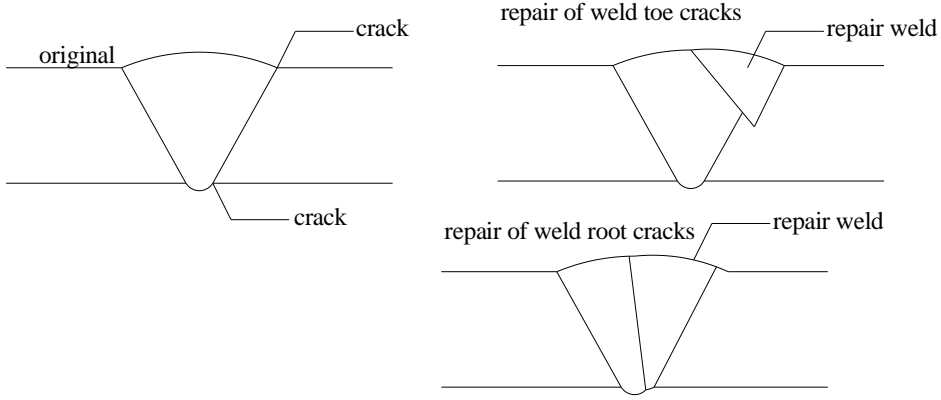
a) Crack creation stage.

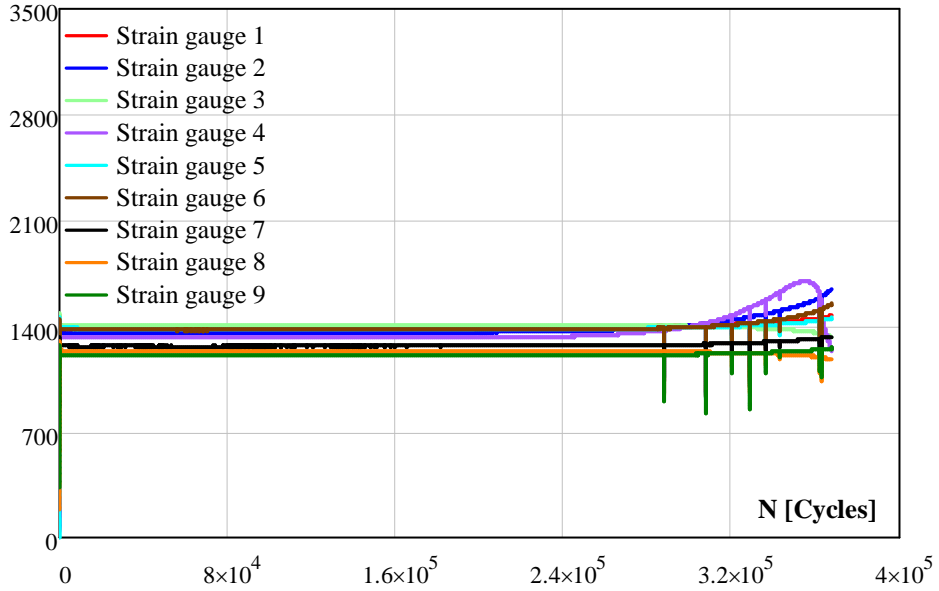
$\Delta\varepsilon$ [μstrain]



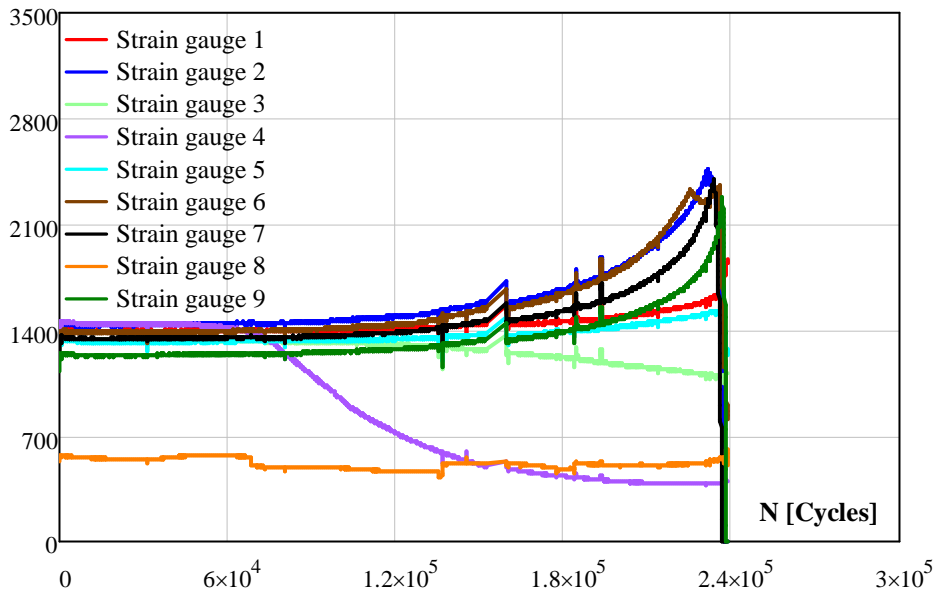
b) Repaired specimen.

Figure D.15 Strain gauge measurements of CR696 specimen.

Specimen: CR697	Thickness [mm]	Rolled	25.02
		Cast	25.25
<i>Fatigue crack creation stage</i>			
N_i : 216127	N_s : 367946		
<i>Crack initiation location during testing</i>	At the middle of the weld toe of the cap, cast steel side.		
<i>Detected cracks by magnetic particle</i>			
			
Crack at weld toe of the cap, the cast steel side		Crack at weld toe of the root, rolled steel side	
<i>Repair of fatigue cracks: All cracks are removed from the weld toe and the prepared weld groove is filled by weld material.</i>			
			
<i>Test results of the repaired specimen</i>			
N_i : 52813	N_f : 238523		
<i>Crack initiation location: The crack initiation and the propagation are observed at the weld toe of the hot rolled steel side. Crack is initiated at start-stop point of the repair weld.</i>			

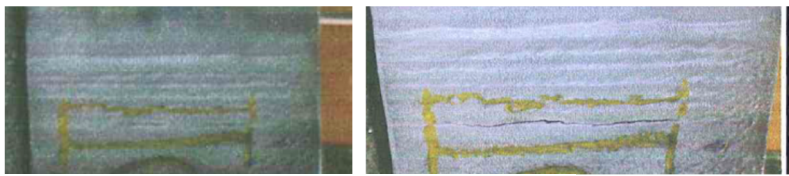
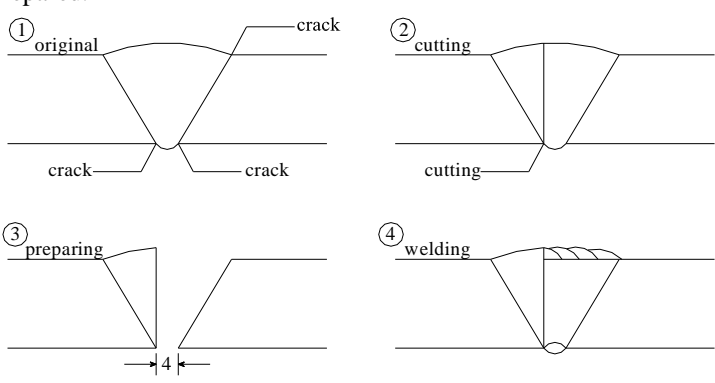
$\Delta\varepsilon$ [μstrain]

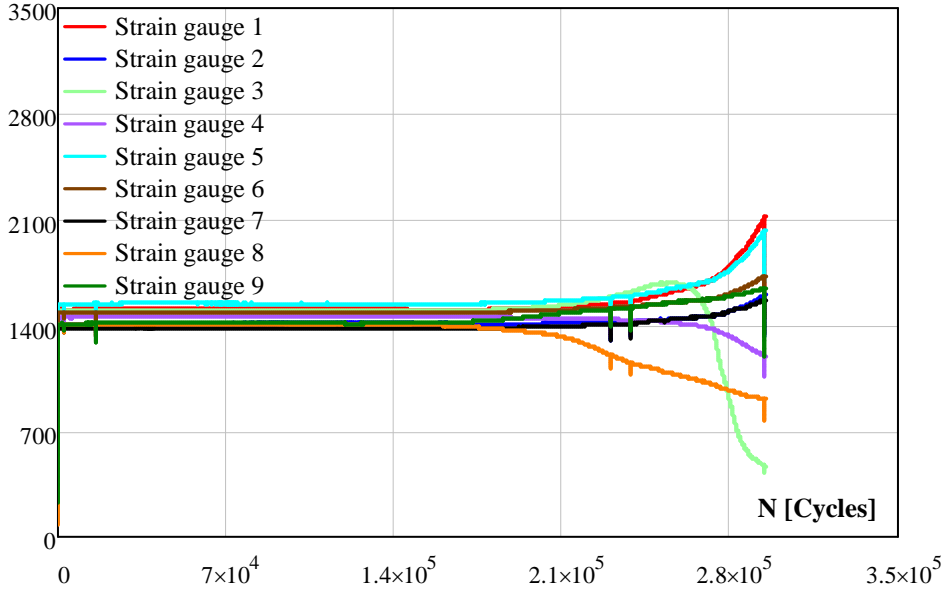
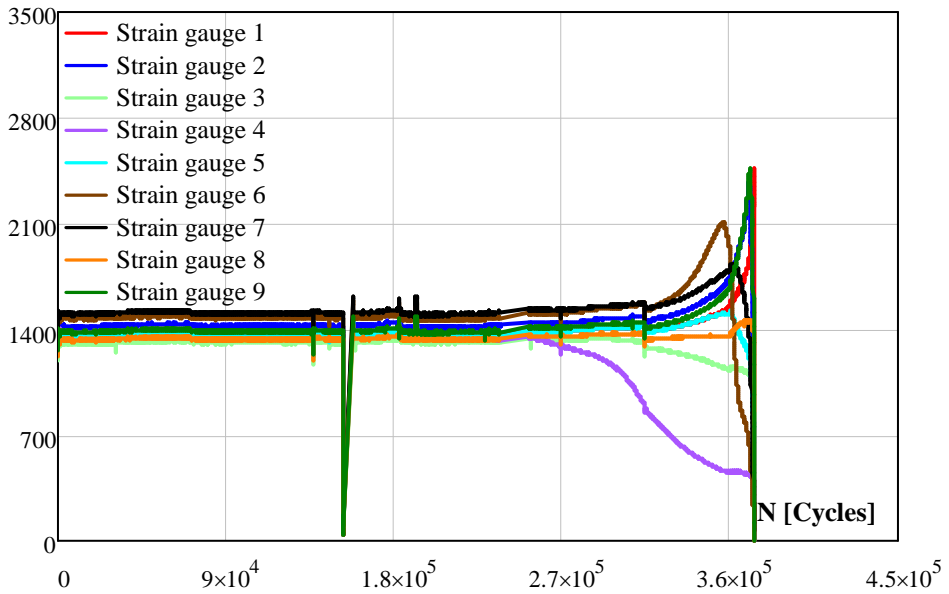
a) Crack creation stage.

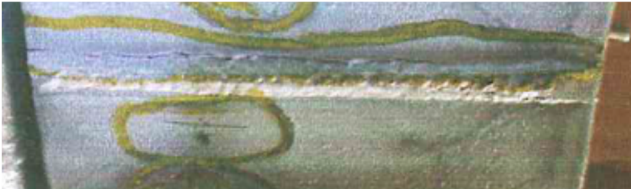
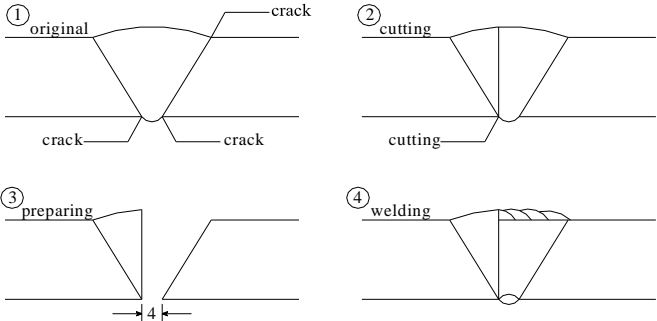
 $\Delta\varepsilon$ [μstrain]

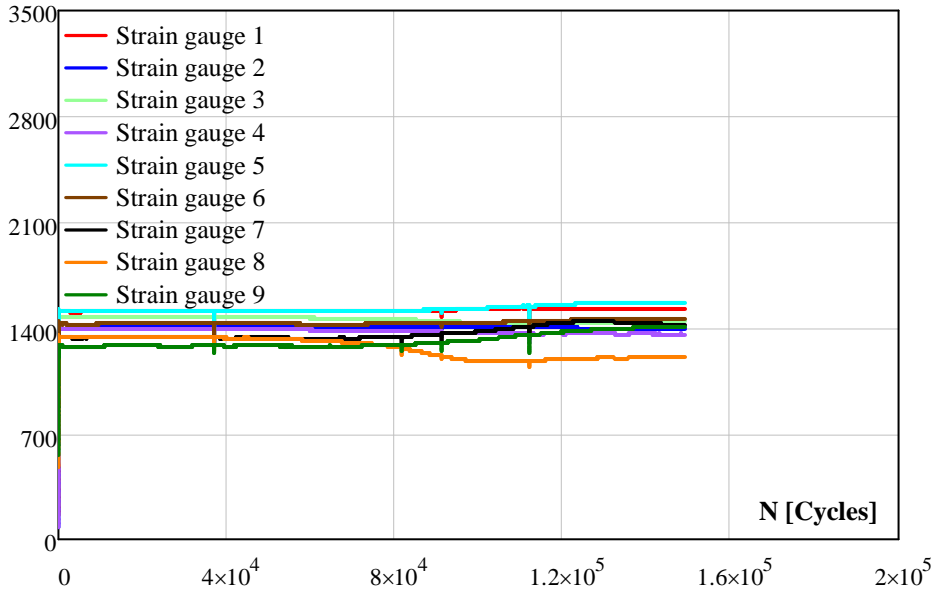
b) Repaired specimen.

Figure D.16 Strain gauge measurements of CR697 specimen.

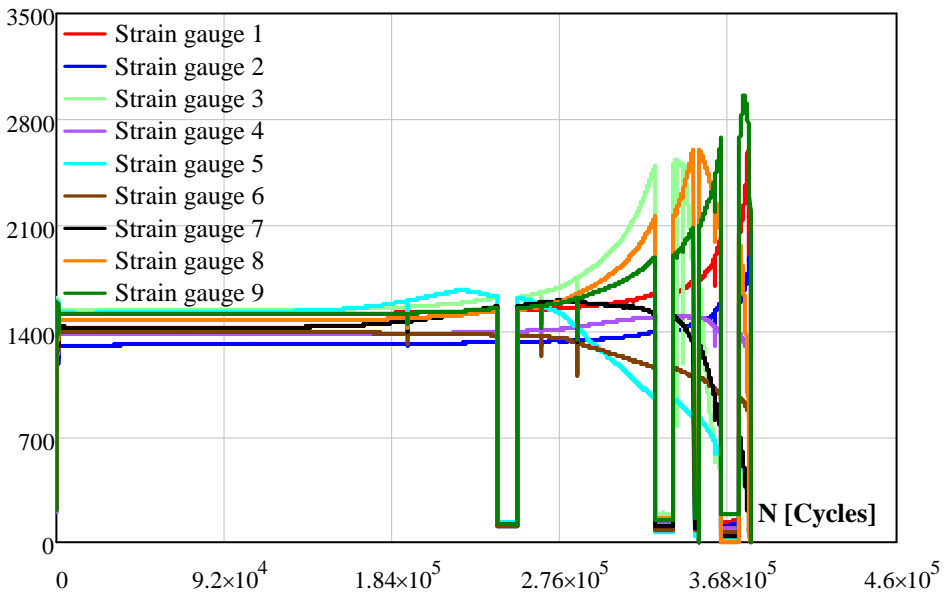
Specimen: CR698	Thickness [mm]	Rolled	25.03
		Cast	25.09
<i>Fatigue crack creation stage</i>			
N_i : 166295	N_s : 294947		
<i>Crack initiation location during testing</i>	At the middle of the weld toe of the cap, and at the middle of the weld toe of the root cast steel side		
<i>Detected cracks by magnetic particle</i>			
 <p>Crack at weld toe the hot rolled steel</p>  <p>Long crack at the weld root of the cast steel.</p>			
<p><i>Repair of fatigue cracks:</i> The specimen cut from the middle and weld material is removed such that the root and one side of the cap are suspended. Thus half a V-shape groove is prepared.</p> 			
<i>Test results of the repaired specimen</i>			
N_i : 253770	N_f : 373052		
<i>Crack initiation location:</i> At the middle weld toe of the cap the cast steel side.			

$\Delta\varepsilon$ [μstrain]*a) Crack creation stage.* $\Delta\varepsilon$ [μstrain]*b) Repaired specimen.**Figure D.17 Strain gauge measurements of CR698 specimen.*

Specimen: CR699	Thickness [mm]	Rolled	25.01
		Cast	24.6
<i>Fatigue crack creation stage</i>			
N_i : 73537	N_s : 149284		
<i>Crack initiation location during testing</i>	At middle of the weld toe of the root, the cast steel side		
<i>Detected cracks by magnetic particle</i>			
 <p>Small crack at weld toe the cast steel</p>  <p>Long crack at the weld root of the cast steel.</p>			
<p><i>Repair of fatigue cracks:</i> The specimen cut from the middle and weld material is removed such that the root and one side of the cap are suspended. Thus half a V-shape groove is prepared.</p> 			
<i>Test results of the repaired specimen</i>			
N_i : 150430	N_f : 347728		
<i>Crack initiation location:</i> At the near edge of the weld toe of the cap, the cast steel side.			

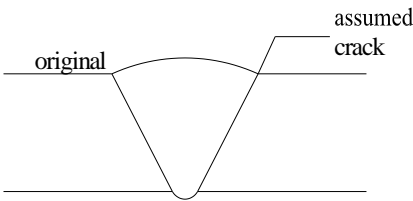
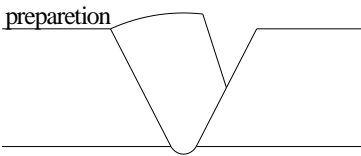
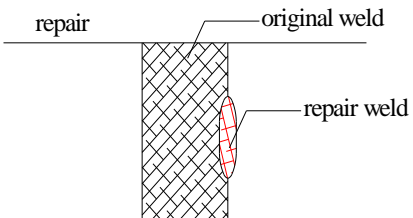
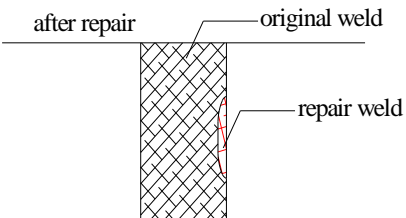
$\Delta\varepsilon$ [μstrain]

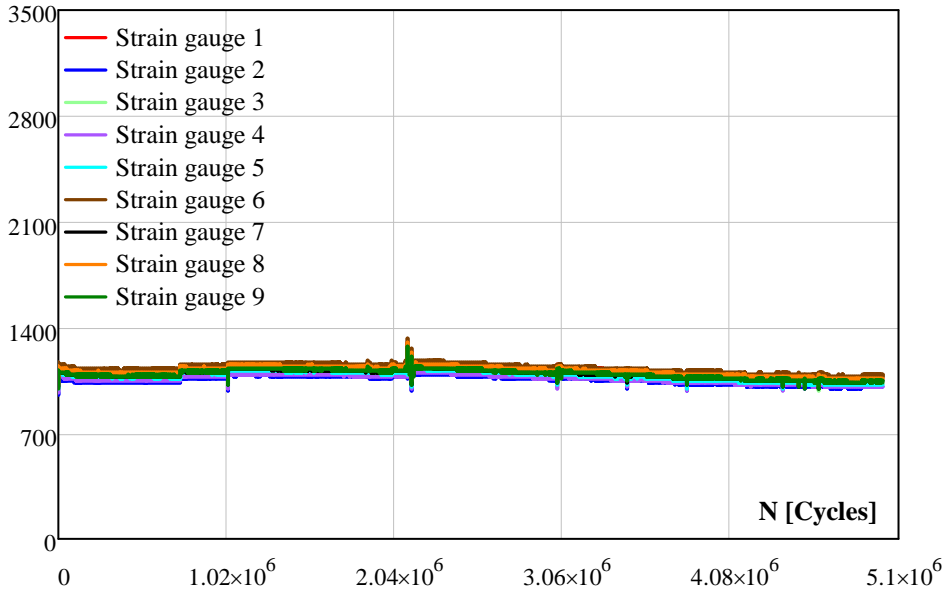
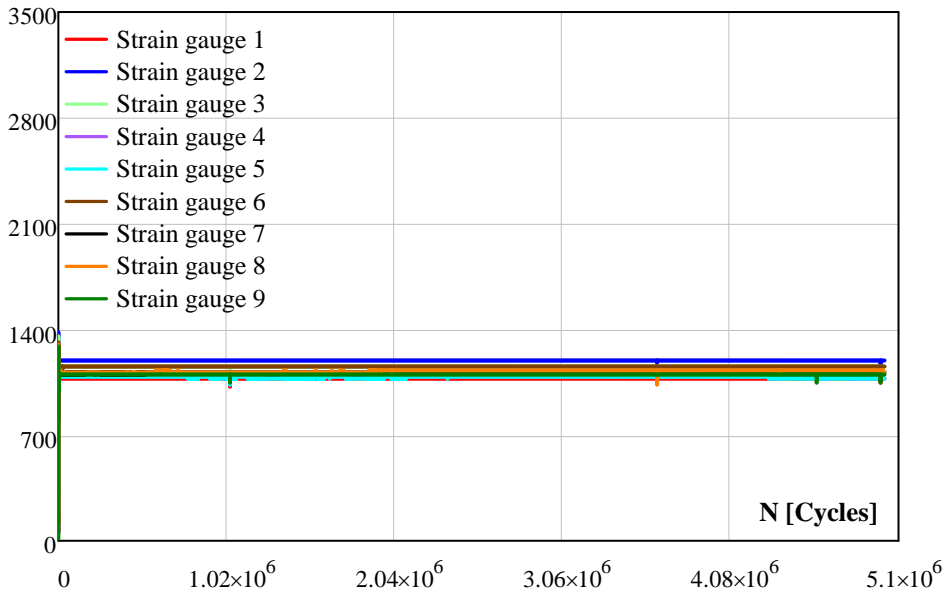
a) Crack creation stage.

 $\Delta\varepsilon$ [μstrain]

b) Repaired specimen.

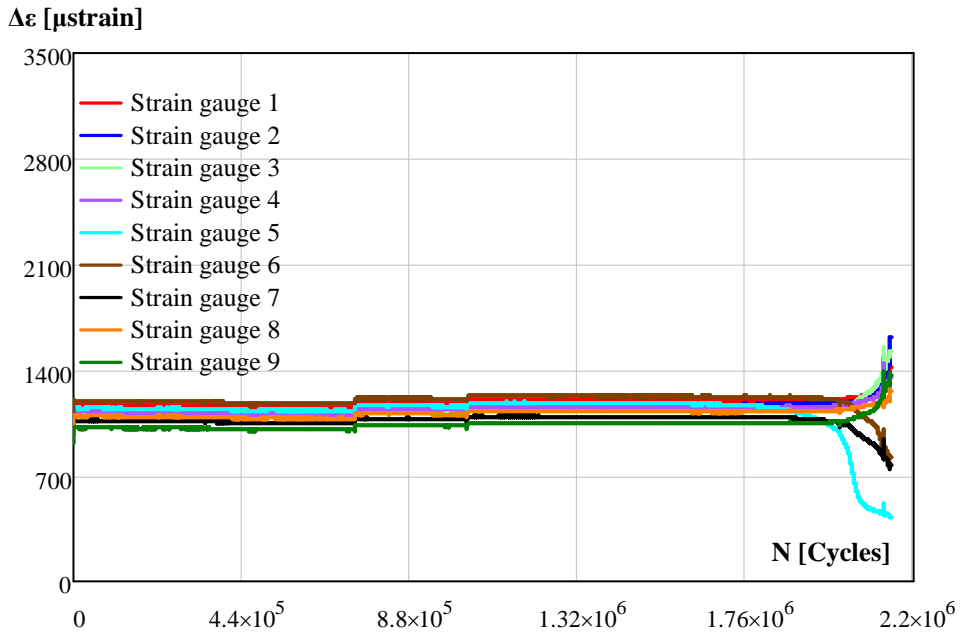
Figure D.18 Strain gauge measurements of CR699 specimen.

Specimen: VR891	Thickness [mm]	Rolled	25.04
		Cast	-
<i>Fatigue crack creation stage</i>			
N_i : 0	N_s : 4999697		
<i>Crack initiation location during testing</i>	Runout. No any crack initiation has been observed.		
<i>Detected cracks by magnetic particle</i>			
 <p>There are no any cracks at the cap and the roof of the weld</p>			
<p><i>Repair of fatigue cracks:</i> It is assumed that there is a crack in the middle of the weld toe of the cap and it is repaired.</p> <div style="display: flex; justify-content: space-around;"> <div style="text-align: center;">  </div> <div style="text-align: center;">  </div> </div> <div style="display: flex; justify-content: space-around; margin-top: 20px;"> <div style="text-align: center;">  </div> <div style="text-align: center;">  </div> </div>			
<i>Test results of the repaired specimen</i>			
N_i : 0	N_f : 5010863		
<i>Crack initiation location:</i> Runout. No any crack initiation has been observed.			

$\Delta\varepsilon$ [μstrain]*a) Crack creation stage.* $\Delta\varepsilon$ [μstrain]*b) Repaired specimen.**Figure D.19 Strain gauge measurements of VR891 specimen.*

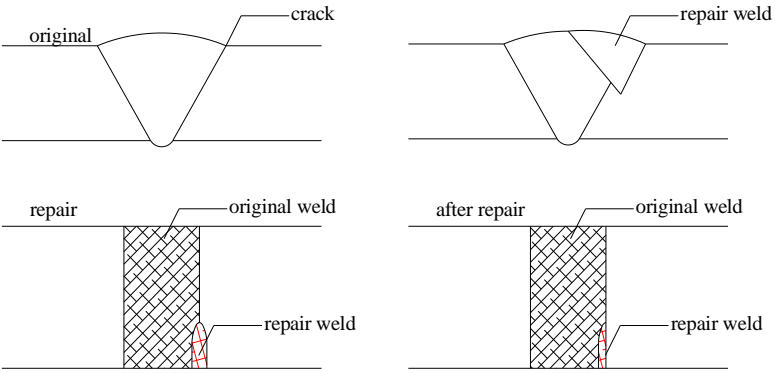
Appendices

Specimen: VR892	Thickness [mm]	Rolled	
		Cast	-
<i>Fatigue crack creation stage</i>			
N_i : 1751873	N_s : 2139962		
<i>Crack initiation location during testing</i>	Base material failure		
Detected cracks by magnetic particle			
<p>Specimen was broken into two pieces. Crack initiated and propagated in the base material.</p>			
<i>Repair of fatigue cracks:</i> No repair has taken place for this specimen.			
<i>Test results of repaired specimen</i>			
N_i : -	N_f : -		
<i>Crack initiation location:</i>			

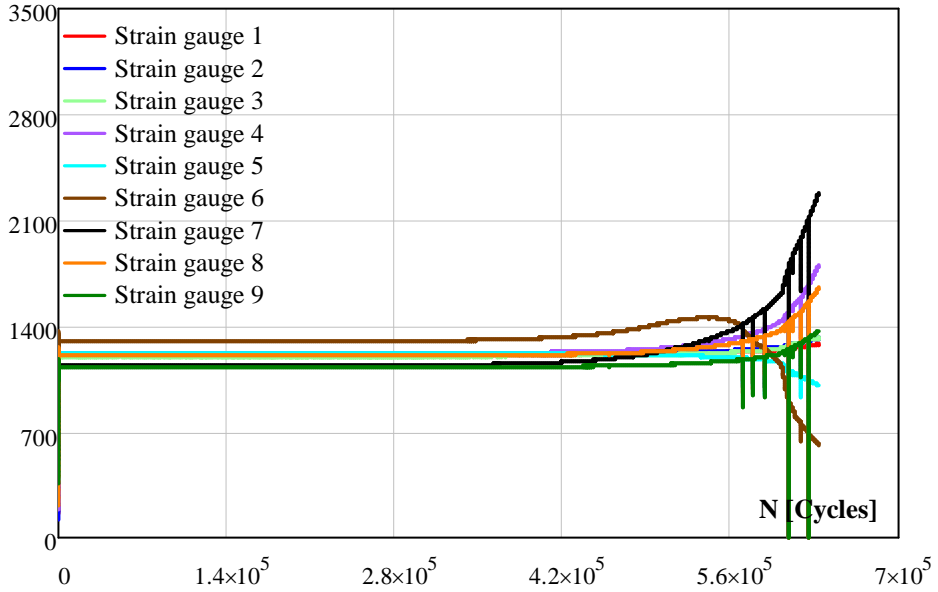


a) Crack creation stage.

Figure D.20 Strain gauge measurements of VR892 specimen.

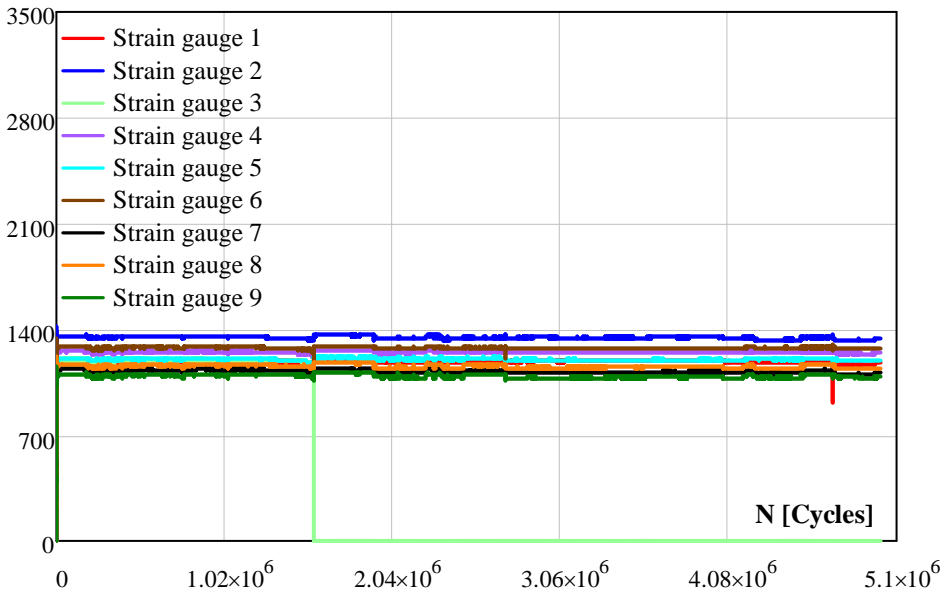
Specimen: VR893	Thickness [mm]	Rolled	25.17
		Cast	-
<i>Fatigue crack creation stage</i>			
N_i : 363294	N_s : 633670		
<i>Crack initiation location during testing</i>	At the edge of the weld toe of the cap.		
<i>Detected cracks by magnetic particle</i>			
 <p>Crack at the edge of the weld toe of the cap</p>			
<p><i>Repair of fatigue cracks:</i> The crack is removed by a burr grinder and the prepared groove is filled by weld material. After the repair, discontinuity due to the repair weld is ground.</p> 			
<i>Test results of the repaired specimen</i>			
N_i : 0	N_f : 5000001		
<i>Crack initiation location:</i> Runout. No crack initiation has been observed.			

$\Delta\varepsilon$ [μstrain]



a) Crack creation stage.

$\Delta\varepsilon$ [μstrain]

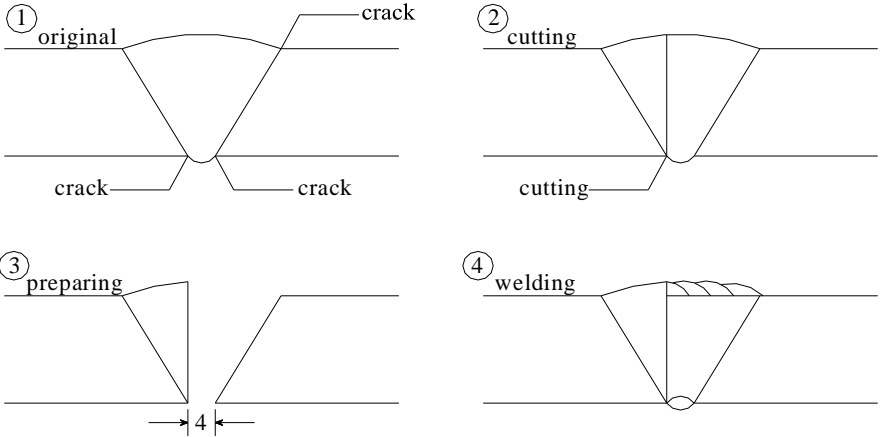


b) Repaired specimen.

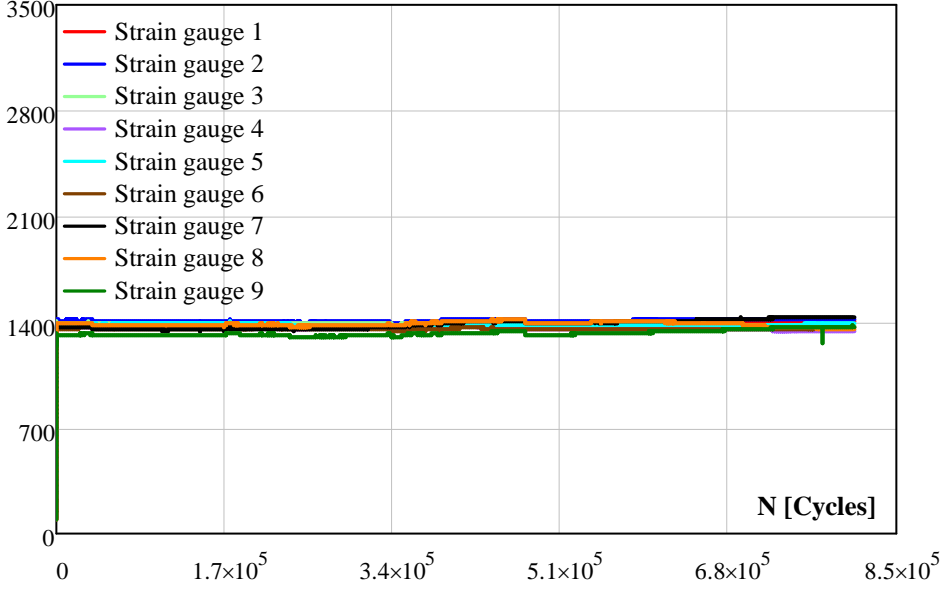
Figure D.21 Strain gauge measurements of VR893 specimen.

Specimen: VR894	Thickness [mm]	Rolled	
		Cast	-
<i>Fatigue crack creation stage</i>			
N_i : 799191	N_s : 1070343		
<i>Crack initiation location during testing</i>	Base material failure		
<i>Detected cracks by magnetic particle</i>			
Specimen was brokend into two pieces. Crack inititated and propagated in the base material.			
<p>$\Delta\epsilon$ [μstrain] <i>a) Crack creation stage.</i></p>			
<i>Repair of fatigue cracks:</i> No repair has taken place for this specimen.			
<i>Test results of repaired specimen</i>			
N_i : -	N_f : -		
<i>Crack initiation location:</i>			

Specimen: VR895	Thickness [mm]	Rolled	
		Cast	-
<i>Fatigue crack creation stage</i>			
N_i : 516272	N_s : 807332		
<i>Crack initiation location during testing</i>	Base material failure		
<i>Detected cracks by magnetic particle</i>			
Specimen was brokend into two pieces. Crack inititated and propagated in the base material.			
<p>$\Delta\epsilon$ [μstrain] a) Crack creation stage.</p> <p style="text-align: right;">N [Cycles]</p>			
<i>Repair of fatigue cracks:</i> No repair has taken place for this specimen.			
<i>Test results of repaired specimen</i>			
N_i : -	N_f : -		
<i>Crack initiation location:</i>			

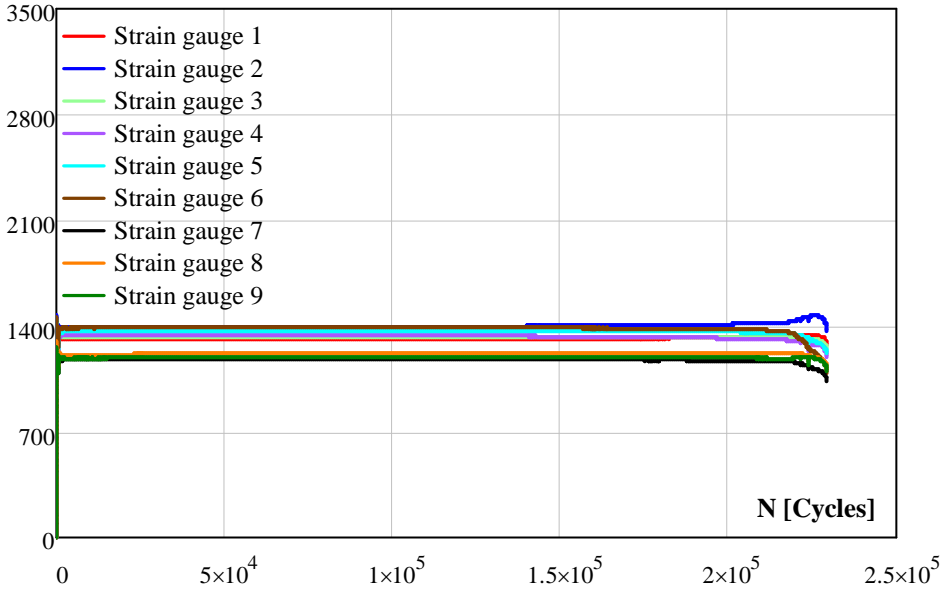
Specimen: VR896	Thickness [mm]	Rolled	25.04
		Cast	-
<i>Fatigue crack creation stage</i>			
N_i : 338877	N_s : 806596		
<i>Crack initiation location during testing</i>	At the middle of the weld toe of the root		
<i>Detected cracks by magnetic particle</i>			
			
Long crack at the weld root			
<p><i>Repair of fatigue cracks:</i> The specimen cut from the middle and the weld material is removed such that the root and one side of the cap are suspended. Thus, half a V-shape groove is prepared.</p>			
			
<i>Test results of the repaired specimen</i>			
N_i : 101392	N_f : 229142		
<i>Crack initiation location:</i> Crack initiation and propagation in the base material, middle of the plate.			

$\Delta\epsilon$ [μstrain]



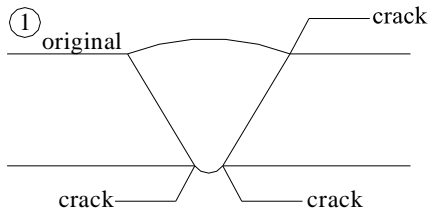
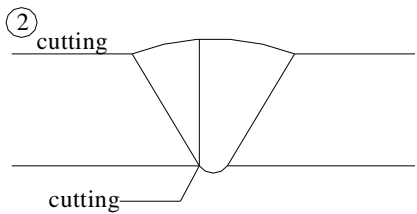
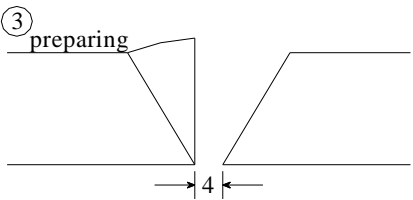
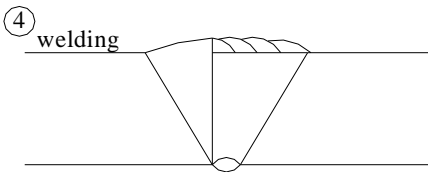
a) Crack creation stage.

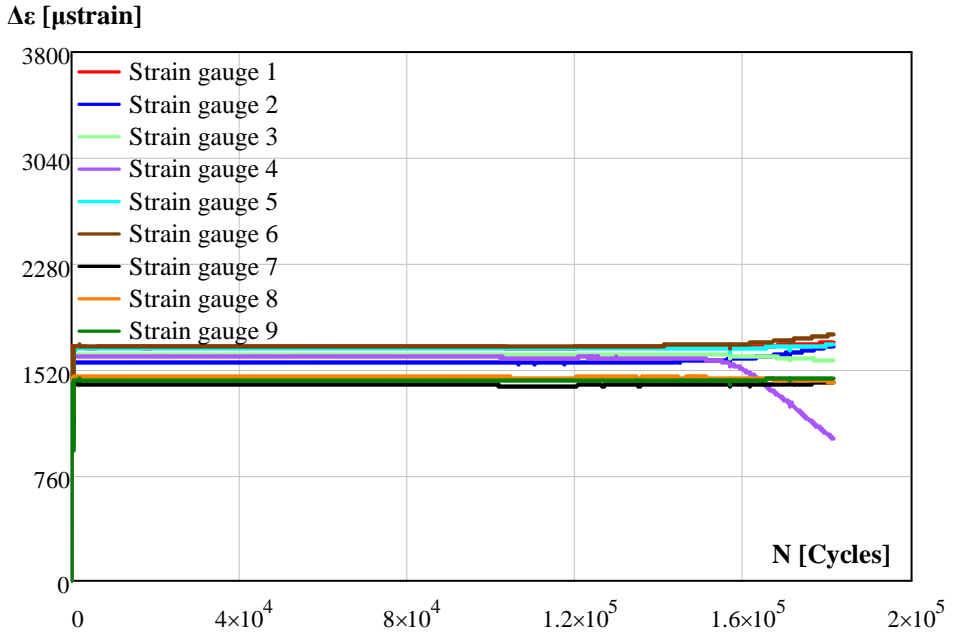
$\Delta\epsilon$ [μstrain]



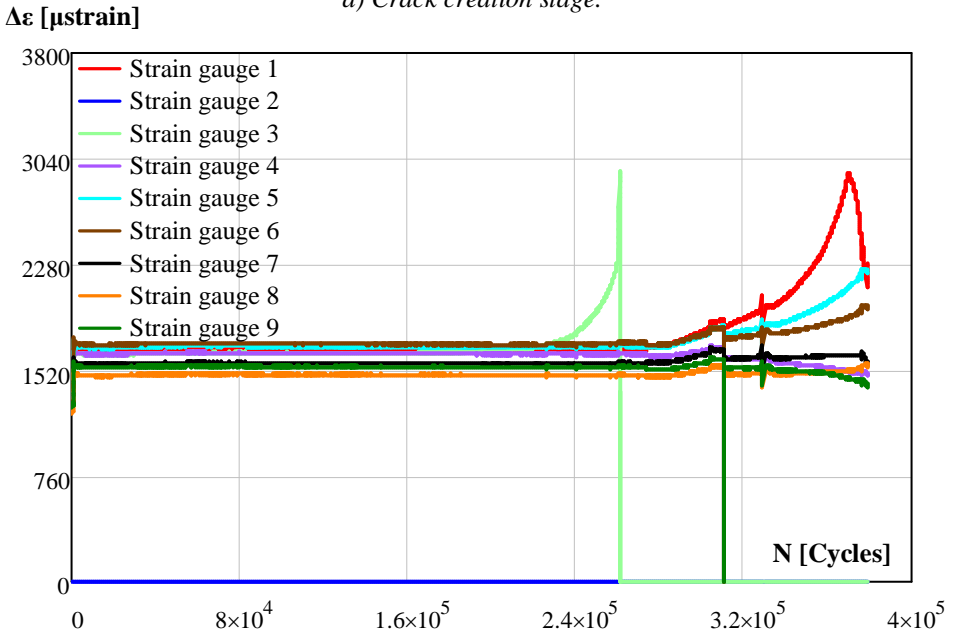
b) Repaired specimen.

Figure D.22 Strain gauge measurements of VR896 specimen.

Specimen: VR897	Thickness [mm]	Rolled	25.02
		Cast	-
<i>Fatigue crack creation stage</i>			
N_i : 143425	N_s : 181706		
<i>Crack initiation location during testing</i>	At the middle of the weld toe of the cap.		
<i>Detected cracks by magnetic particle</i>			
			
Crack at the middle of the weld toe of the cap		Long crack indication at weld toe of the root	
<p><i>Repair of fatigue cracks:</i> The specimen cut from the middle and the weld material is removed such that the root and one side of the cap are suspended. Thus, half a V-shape groove is prepared.</p>			
			
			
<i>Test results of the repaired specimen</i>			
N_i : 226237	N_f : 379331		
<i>Crack initiation location:</i> Crack initiation and propagation in the base material, middle and edge of the plate.			

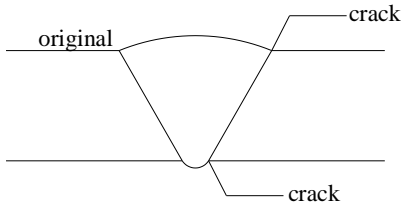
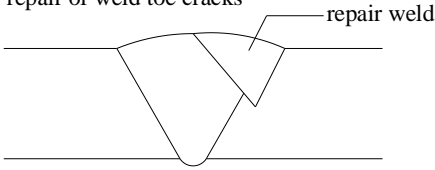
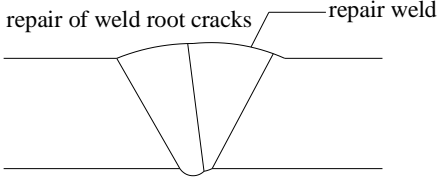


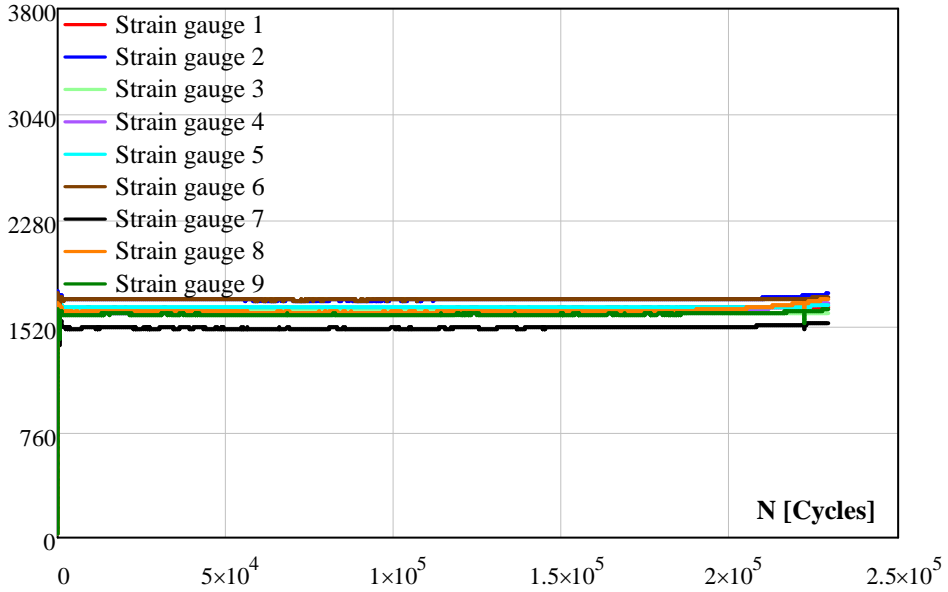
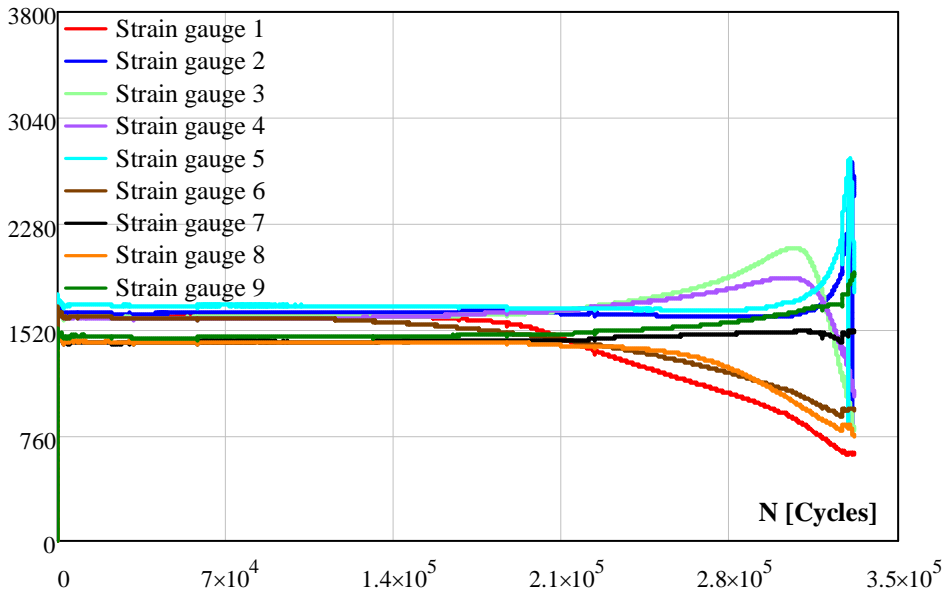
a) Crack creation stage.

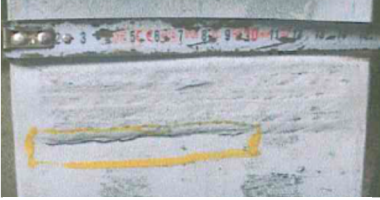
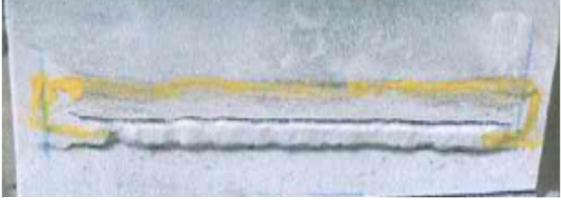
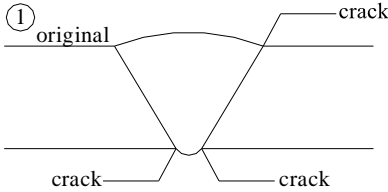
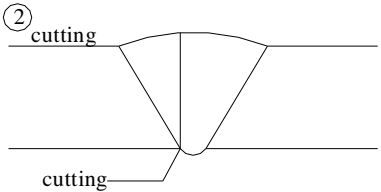
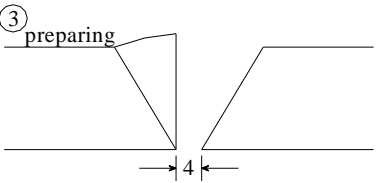
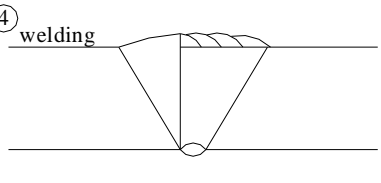


b) Repaired specimen.

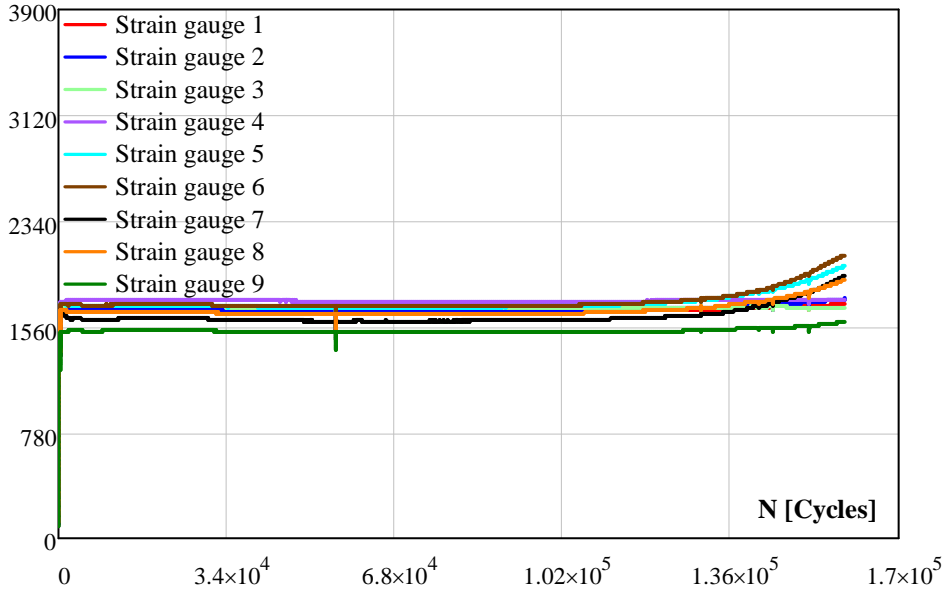
Figure D.23 Strain gauge measurements of VR897 specimen.

Specimen: VR898	Thickness [mm]	Rolled	25.04
		Cast	-
<i>Fatigue crack creation stage</i>			
N_i : 187028	N_s : 229239		
<i>Crack initiation location during testing</i>	At the middle of the weld toe of the cap		
<i>Detected cracks by magnetic particle</i>			
			
Several cracks at the weld toe of the cap		Small crack at the weld root	
<i>Repair of fatigue cracks: All cracks are removed from the weld toe and the prepared weld groove is filled by weld material.</i>			
			
			
<i>Test results of the repaired specimen</i>			
N_i : 106595	N_f : 331625		
<i>Crack initiation location:</i> Crack initiation and propagation in the base material, the edge of the plate.			

$\Delta\varepsilon$ [μstrain]*a) Crack creation stage.* $\Delta\varepsilon$ [μstrain]*b) Repaired specimen.**Figure D.24 Strain gauge measurements of VR898 specimen.*

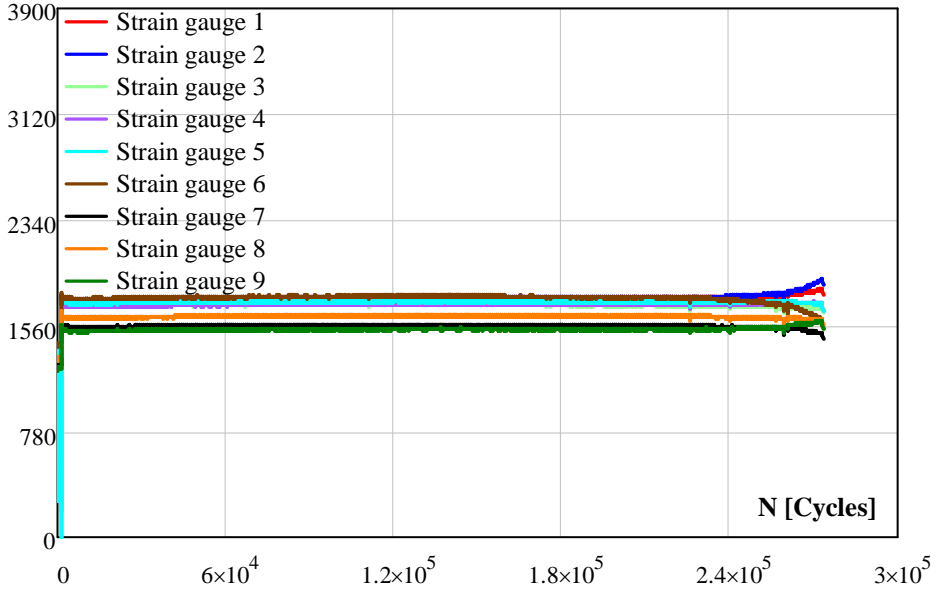
Specimen: VR899	Thickness [mm]	Rolled	25.05
		Cast	-
<i>Fatigue crack creation stage</i>			
N_i : 106951	N_s : 159115		
<i>Crack initiation location during testing</i>	Near the edge at the weld toe of the cap and at the weld toe of the root		
<i>Detected cracks by magnetic particle</i>			
			
Crack at the weld toe		Long crack at the weld root	
<p><i>Repair of fatigue cracks:</i> The specimen cut from the middle and the weld material is removed such that the root and one side of the cap are suspended. Thus, half a V-shape groove is prepared.</p>			
<p>① original</p> 		<p>② cutting</p> 	
<p>③ preparing</p> 		<p>④ welding</p> 	
<i>Test results of the repaired specimen</i>			
N_i : 228910	N_f : 273282		
<i>Crack initiation location:</i> Crack initiation and propagation in the base material, middle and edge of the plate.			

$\Delta\varepsilon$ [μstrain]



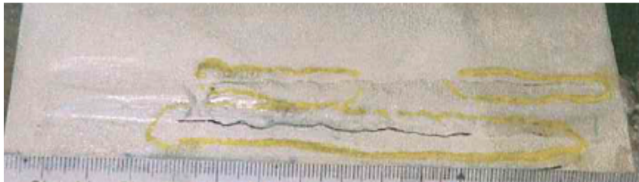
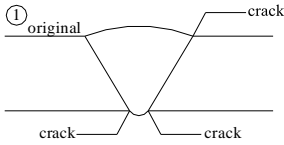
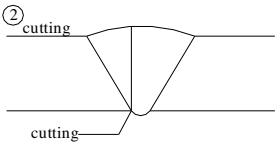
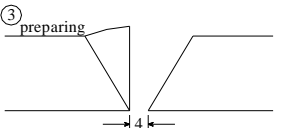
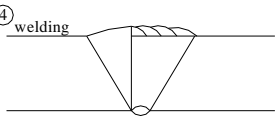
a) Crack creation stage.

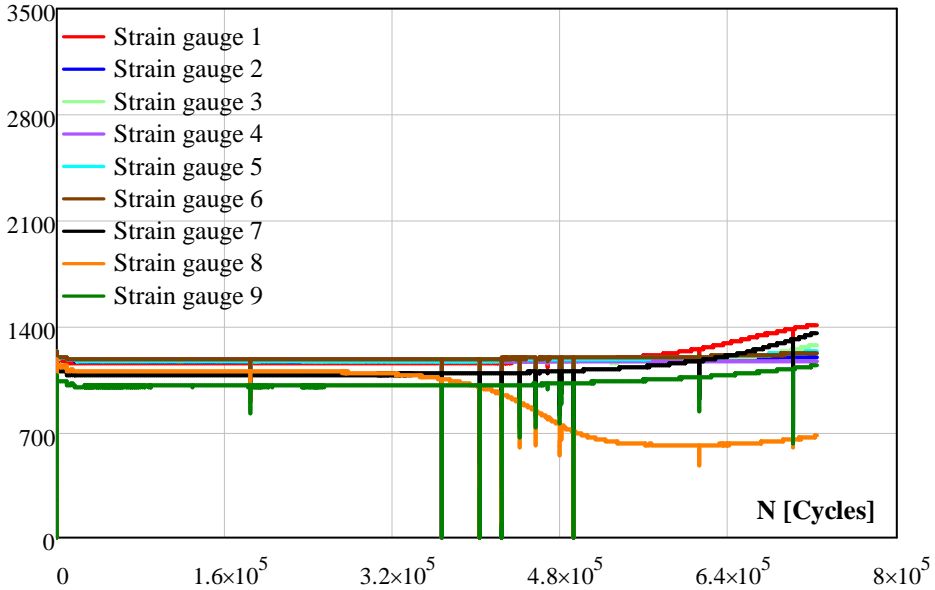
$\Delta\varepsilon$ [μstrain]



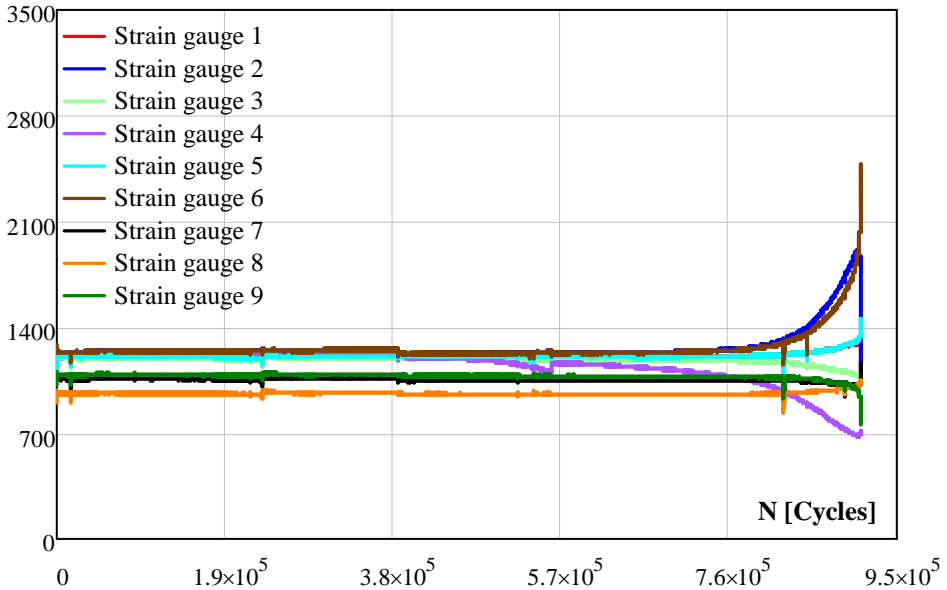
b) Repaired specimen.

Figure D.25 Strain gauge measurements of VR899 specimen.

Specimen: CR891	Thickness [mm]	Rolled	25.2
		Cast	25.0
<i>Fatigue crack creation stage</i>			
N_i : 282866	N_s : 723354		
<i>Crack initiation location during testing</i>	Near the middle of the weld toe of the cap and at the middle of the weld toe of the root rolled steel side		
<i>Detected cracks by magnetic particle</i>			
 <p>Crack at the weld toe</p>  <p>Three cracks at the weld root</p>			
<p><i>Repair of fatigue cracks:</i> The specimen cut from the middle and the weld material is removed such that the root and one side of the cap are suspended. Thus, half a V-shape groove is prepared.</p> <div style="display: flex; justify-content: space-around;"> <div style="text-align: center;"> <p>① original</p>  </div> <div style="text-align: center;"> <p>② cutting</p>  </div> </div> <div style="display: flex; justify-content: space-around;"> <div style="text-align: center;"> <p>③ preparing</p>  </div> <div style="text-align: center;"> <p>④ welding</p>  </div> </div>			
<i>Test results of the repaired specimen</i>			
N_i : 218923	N_f : 910192		
<i>Crack initiation location:</i> Crack initiation and propagation in the base material of the cast steel, middle of the plate.			

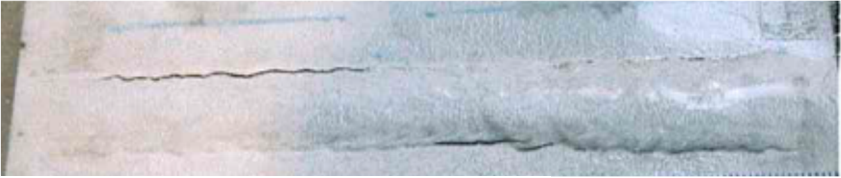
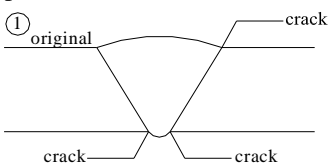
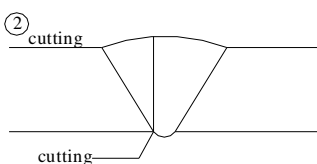
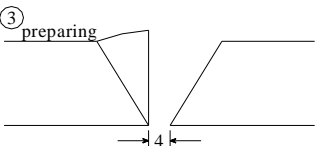
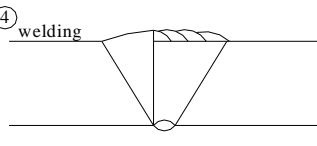
$\Delta\epsilon$ [μstrain]

a) Crack creation stage.

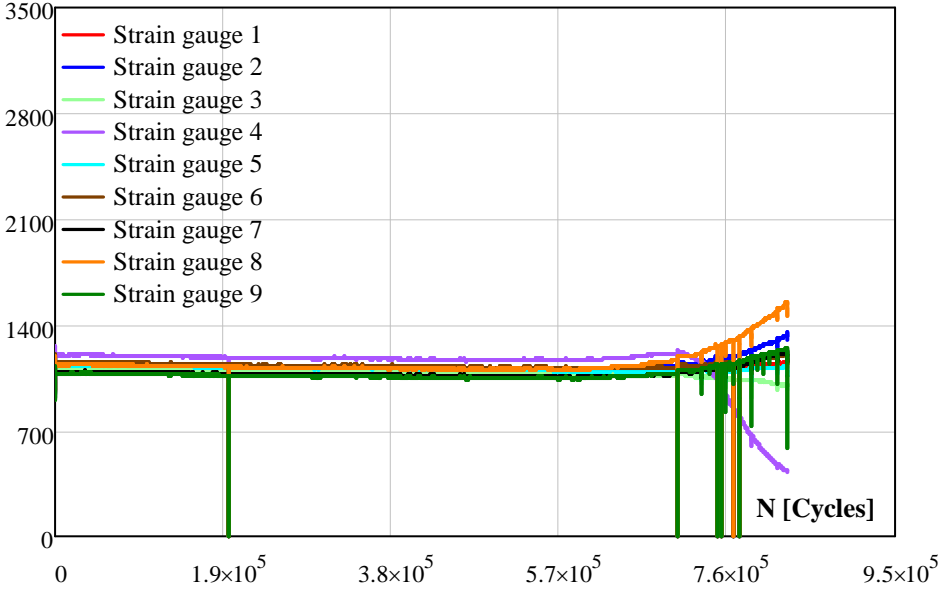
 $\Delta\epsilon$ [μstrain]

b) Repaired specimen.

Figure D.26 Strain gauge measurements of CR891 specimen.

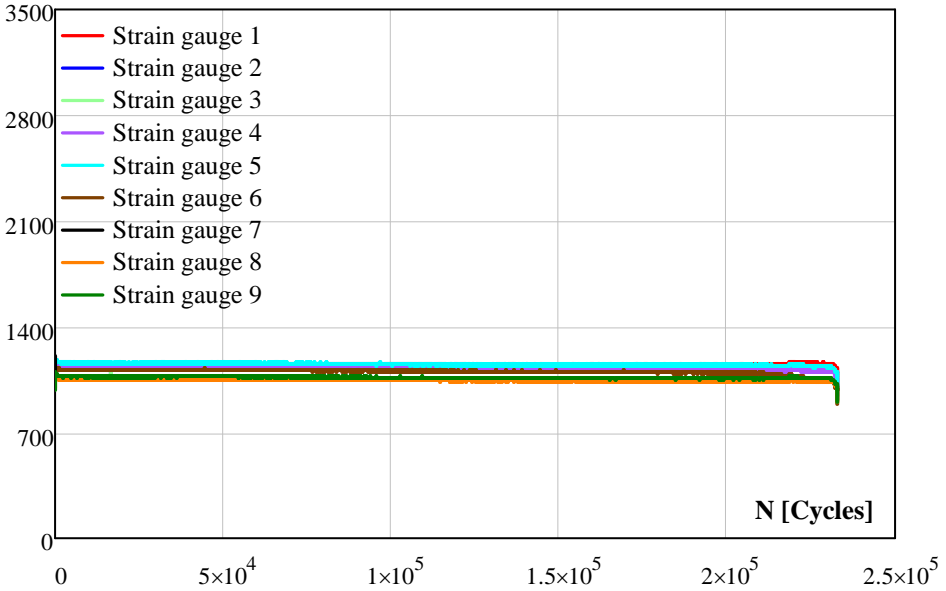
Specimen: CR892	Thickness [mm]	Rolled	25.2
		Cast	25.50
<i>Fatigue crack creation stage</i>			
N_i : 608598	N_s : 827965		
<i>Crack initiation location during testing</i>	At the middle of the weld toe of the cap rolled steel side		
<i>Detected cracks by magnetic particle</i>			
 <p>Crack at the weld toe</p>  <p>Crack on the sides of the weld root</p>			
<p><i>Repair of fatigue cracks:</i> The specimen cut from the middle and the weld material is removed such that the root and one side of the cap are suspended. Thus, half a V-shape groove is prepared.</p> <div style="display: flex; justify-content: space-around;"> <div style="text-align: center;"> <p>① original</p>  </div> <div style="text-align: center;"> <p>② cutting</p>  </div> </div> <div style="display: flex; justify-content: space-around; margin-top: 10px;"> <div style="text-align: center;"> <p>③ preparing</p>  </div> <div style="text-align: center;"> <p>④ welding</p>  </div> </div>			
<i>Test results of repaired specimen</i>			
N_i : 218923	N_f : 232814		
<i>Crack initiation location:</i> Crack initiation and propagation in the base material of the cast steel, middle of the plate.			

$\Delta\varepsilon$ [μstrain]



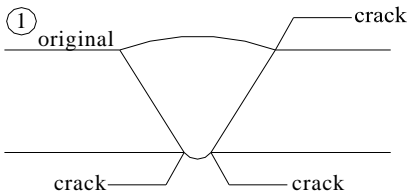
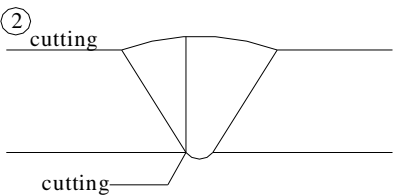
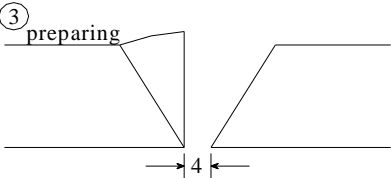
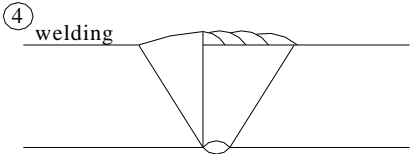
a) Crack creation stage.

$\Delta\varepsilon$ [μstrain]

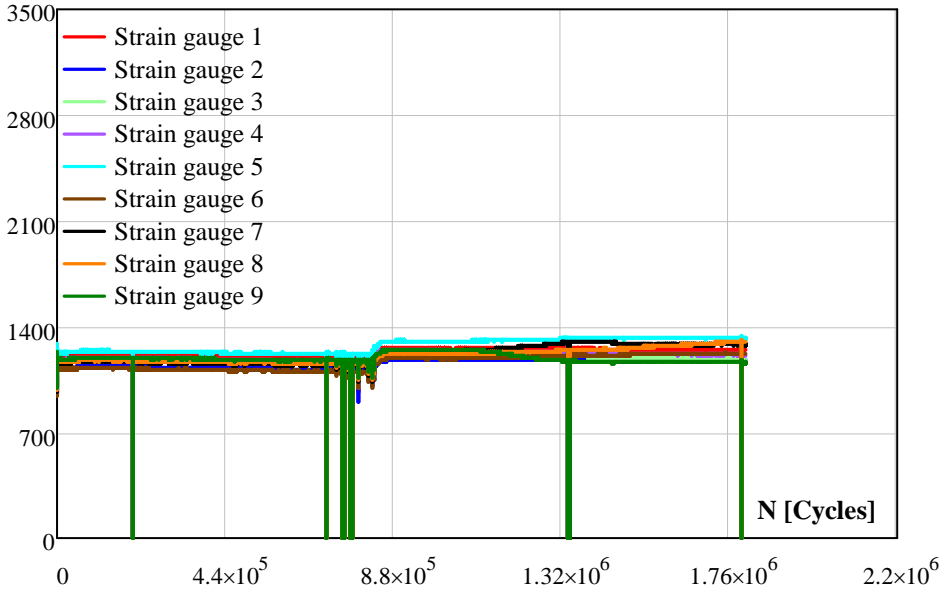


b) Repaired specimen.

Figure D.27 Strain gauge measurements of CR892 specimen.

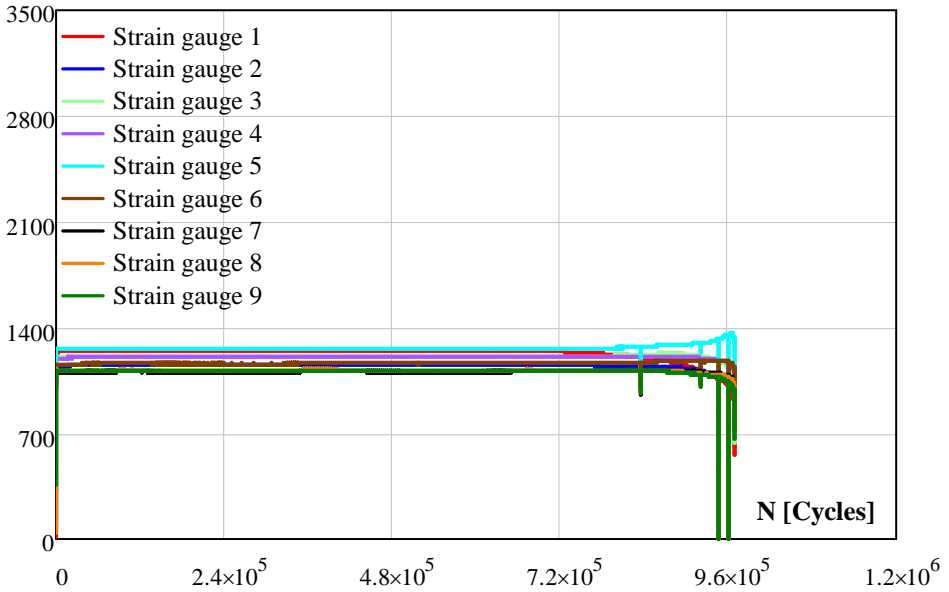
Specimen: CR893	Thickness [mm]	Rolled	25.19
		Cast	26
<i>Fatigue crack creation stage</i>			
N_i : 1041977	N_s : 1802861		
<i>Crack initiation location during testing</i>	Middle of the weld toe of root, rolled steel side		
<i>Detected cracks by magnetic particle</i>			
 <p>Long crack at weld root side</p>			
<p><i>Repair of fatigue cracks:</i> The specimen cut from the middle and weld material is removed such that the root and one side of the cap are suspended. Thus, half a V-shape groove is prepared.</p>			
<div style="display: flex; justify-content: space-around;"> <div style="text-align: center;"> <p>① original</p>  </div> <div style="text-align: center;"> <p>② cutting</p>  </div> </div> <div style="display: flex; justify-content: space-around; margin-top: 20px;"> <div style="text-align: center;"> <p>③ preparing</p>  </div> <div style="text-align: center;"> <p>④ welding</p>  </div> </div>			
<i>Test results of repaired specimen</i>			
N_i : 703437	N_f : 968194		
<i>Crack initiation location:</i> Crack initiation and propagation in the base material of the rolled steel, near edge of the plate.			

$\Delta\varepsilon$ [μstrain]



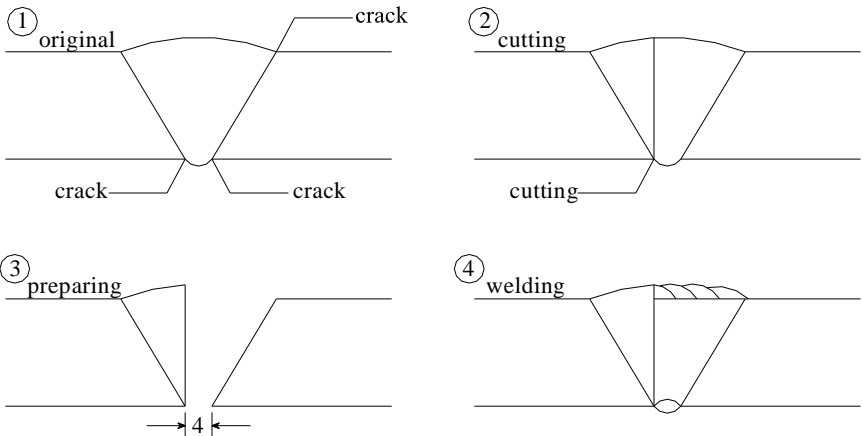
a) Crack creation stage.

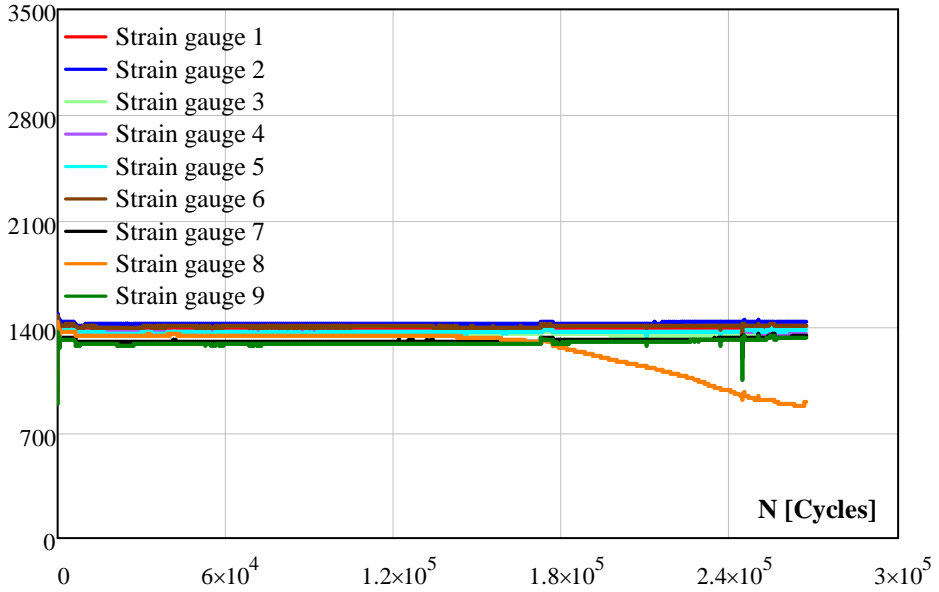
$\Delta\varepsilon$ [μstrain]



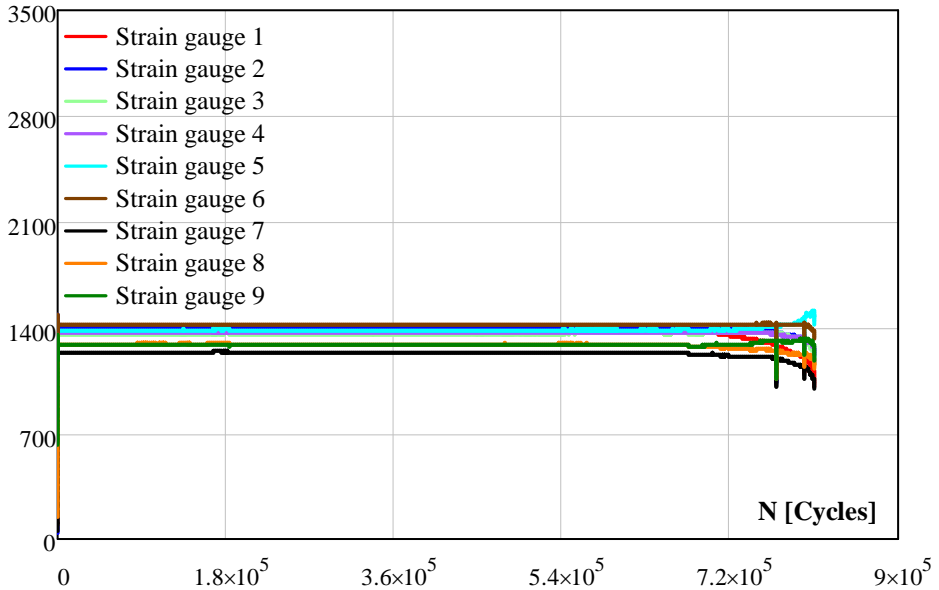
b) Repaired specimen.

Figure D.28 Strain gauge measurements of CR893 specimen.

Specimen: CR894	Thickness [mm]	Rolled	25.131
		Cast	25.32
<i>Fatigue crack creation stage</i>			
N_i : 137528	N_s : 266940		
<i>Crack initiation location during testing</i>	Middle of the weld toe of the root, rolled steel side		
<i>Detected cracks by magnetic particle</i>			
			
Long crack at the weld root			
<p><i>Repair of fatigue cracks:</i> The specimen cut from the middle and the weld material is removed such that the root and one side of the cap are suspended. Thus, half a V-shape groove is prepared.</p>			
			
<i>Test results of repaired specimen</i>			
N_i : 627418	N_f : 810848		
<i>Crack initiation location:</i> Crack initiation and propagation in the base material of the rolled steel, edge of the plate.			

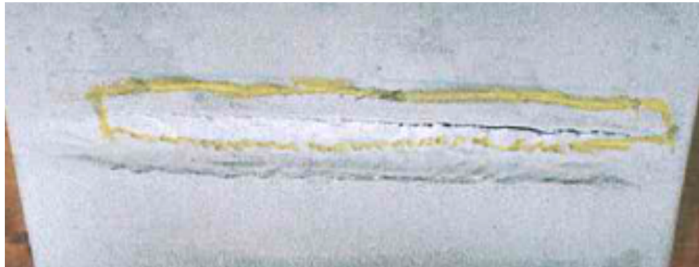
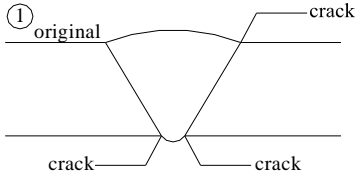
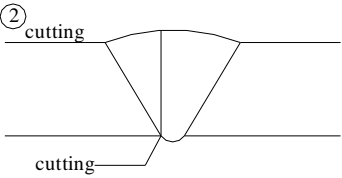
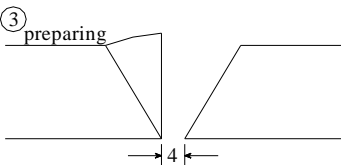
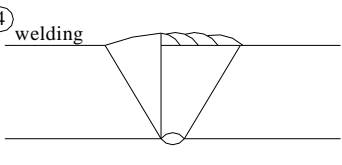
$\Delta\varepsilon$ [μstrain]

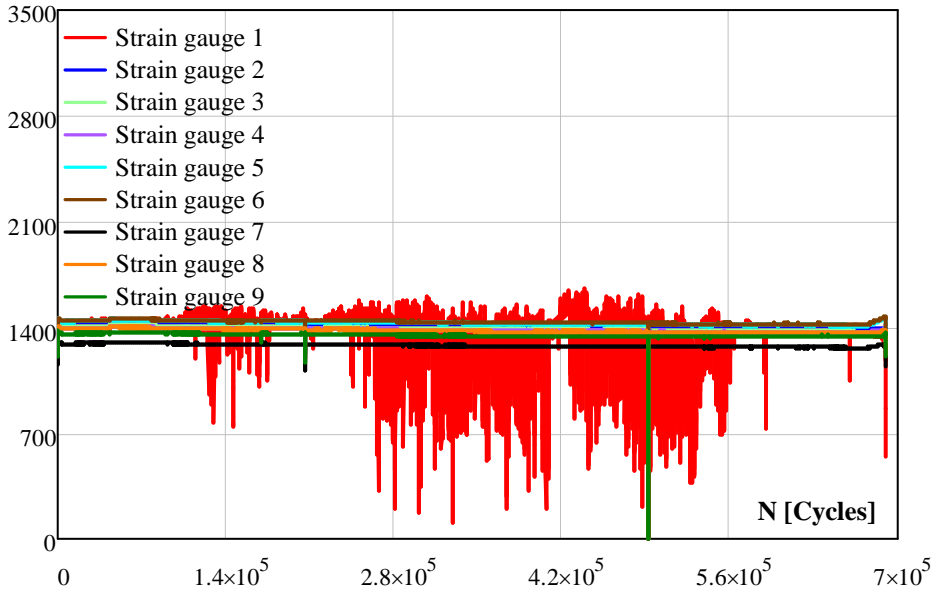
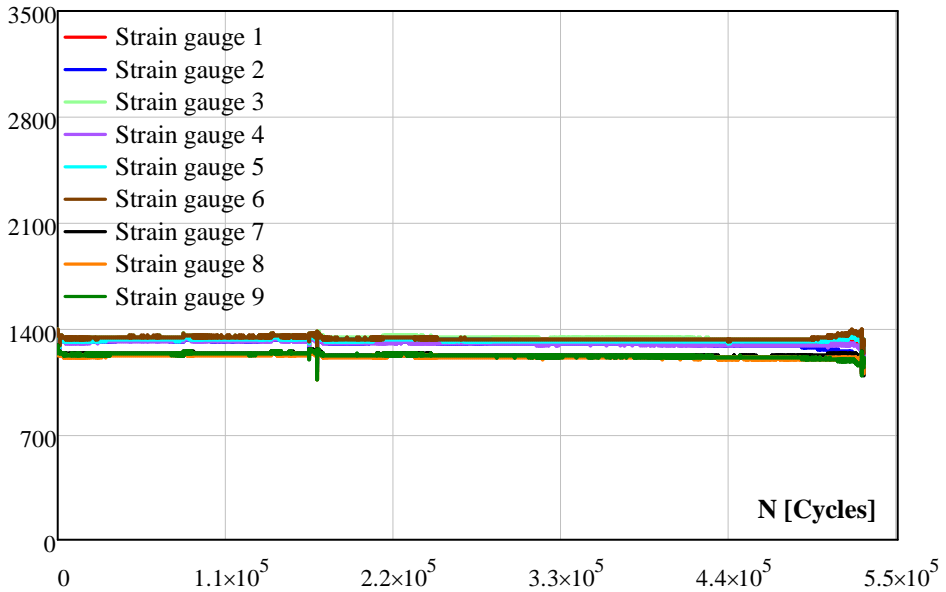
a) Crack creation stage.

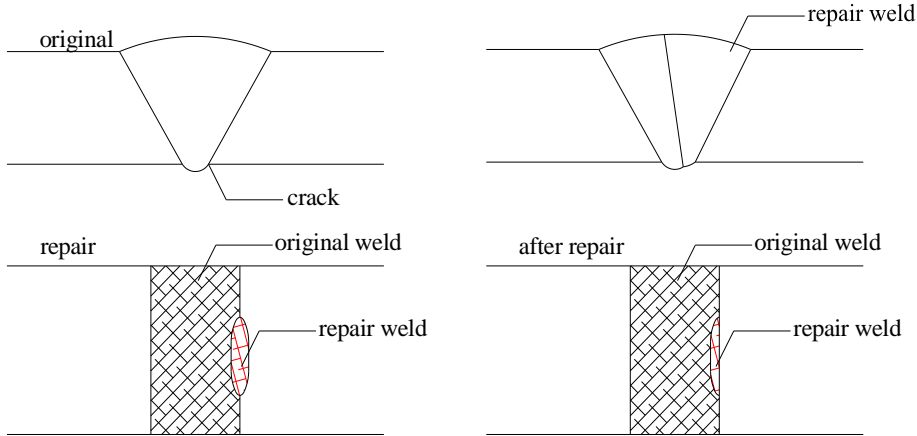
 $\Delta\varepsilon$ [μstrain]

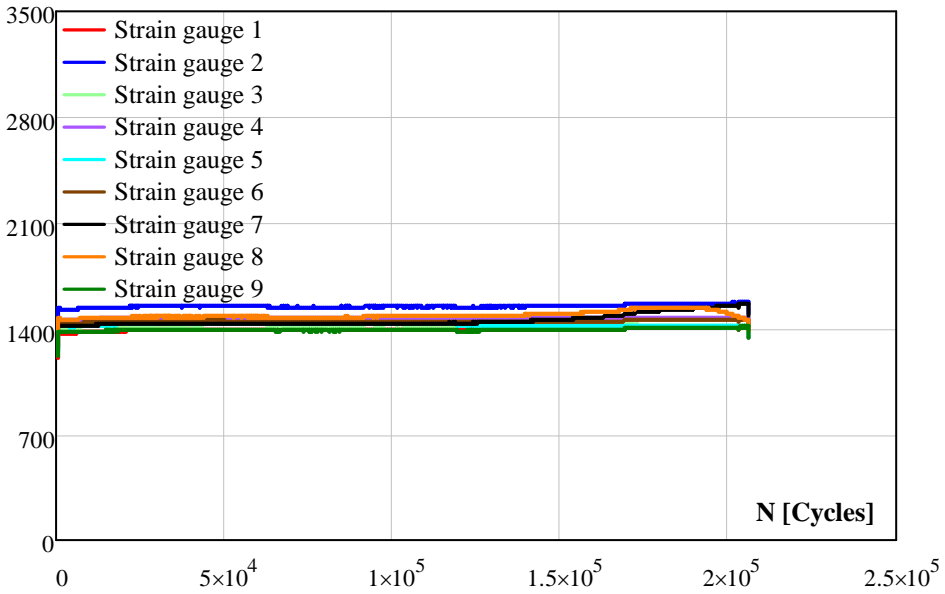
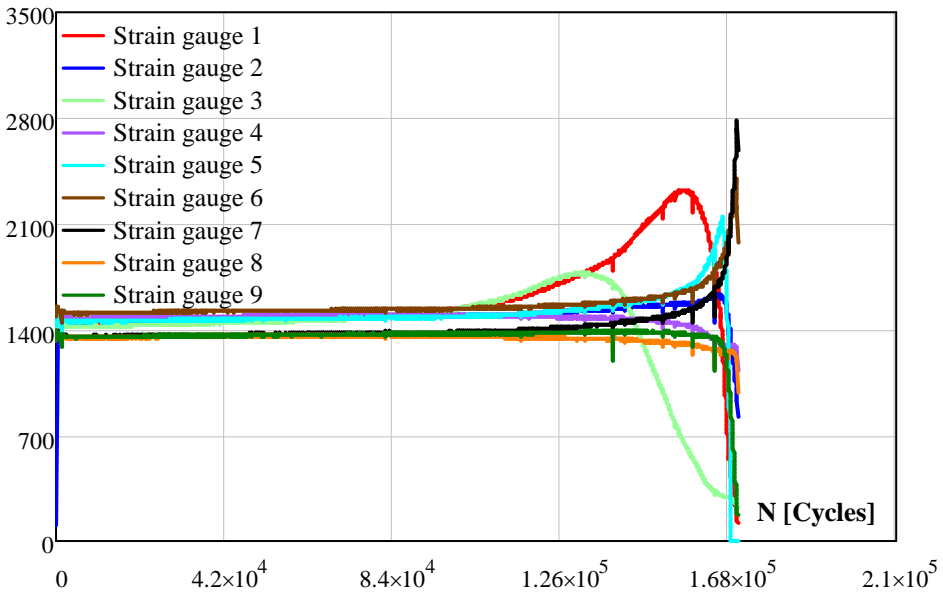
b) Repaired specimen.

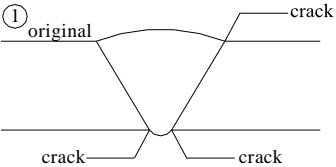
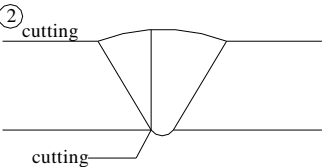
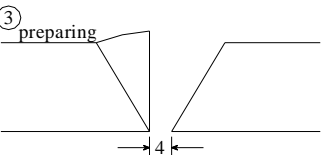
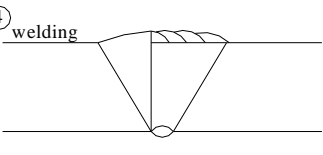
Figure D.29 Strain gauge measurements of CR894 specimen.

Specimen: CR895	Thickness [mm]	Rolled	25.3
		Cast	25
<i>Fatigue crack creation stage</i>			
N_i : 0	N_s : 690108		
<i>Crack initiation location during testing</i>	Base material of the cast steel		
<i>Detected cracks by magnetic particle</i>			
			
Long crack at the weld root		Base material crack in cast steel	
<p><i>Repair of fatigue cracks:</i> The specimen cut from the middle and weld material is removed such that the root and one side of the cap are suspended. Thus, half a V-shape groove is prepared. Crack in the base material is repaired by X-shape welding. After the repair the weld caps on both sides of X-shape weld are ground to obtain a smooth surface.</p>			
			
			
<i>Test results of the repaired specimen</i>			
N_i : 305269	N_f : 527817		
<i>Crack initiation location:</i> Crack initiation and propagation in the base material of the rolled steel, middle of the plate.			

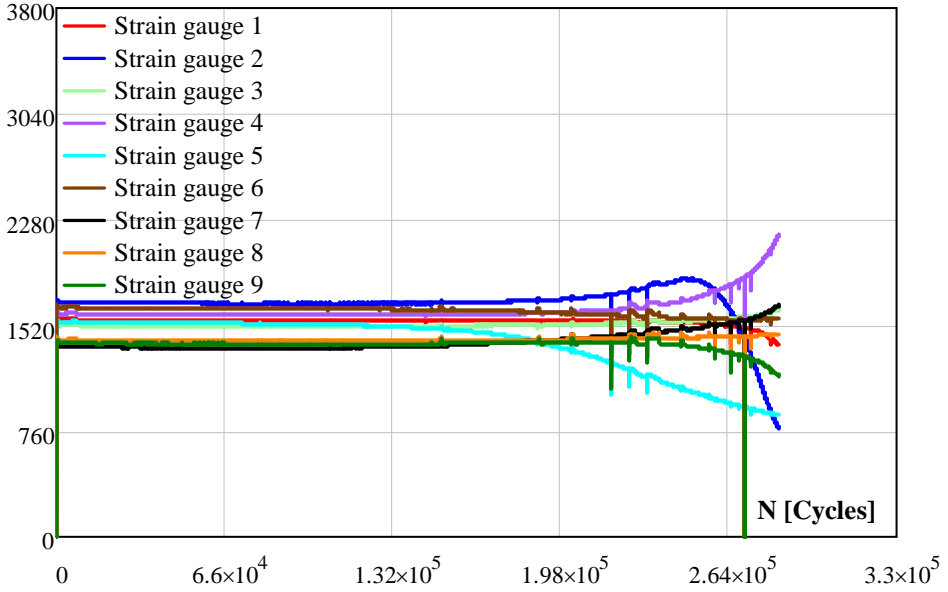
$\Delta\epsilon$ [μstrain]*a) Crack creation stage.* $\Delta\epsilon$ [μstrain]*b) Repaired specimen.**Figure D.30 Strain gauge measurements of CR895 specimen.*

Specimen: CR896	Thickness [mm]	Rolled	25.2
		Cast	25.64
<i>Fatigue crack creation stage</i>			
N_i : 125050	N_s : 205904		
<i>Crack initiation location during testing</i>	At the weld toe of the root, rolled steel side		
<i>Detected cracks by magnetic particle</i>			
			
Crack at the weld root			
<p><i>Repair of fatigue cracks:</i> The crack is removed from the weld cap. The prepared groove is filled by weld material and discontinuity the after repair is ground.</p>			
			
<i>Test results of the repaired specimen</i>			
N_i : 69460	N_f : 170371		
<i>Crack initiation location:</i> At the middle of the weld toe of the cap, the cast steel side.			

$\Delta\epsilon$ [μstrain]*a) Crack creation stage.* $\Delta\epsilon$ [μstrain]*b) Repaired specimen.**Figure D.31 Strain gauge measurements of CR896 specimen.*

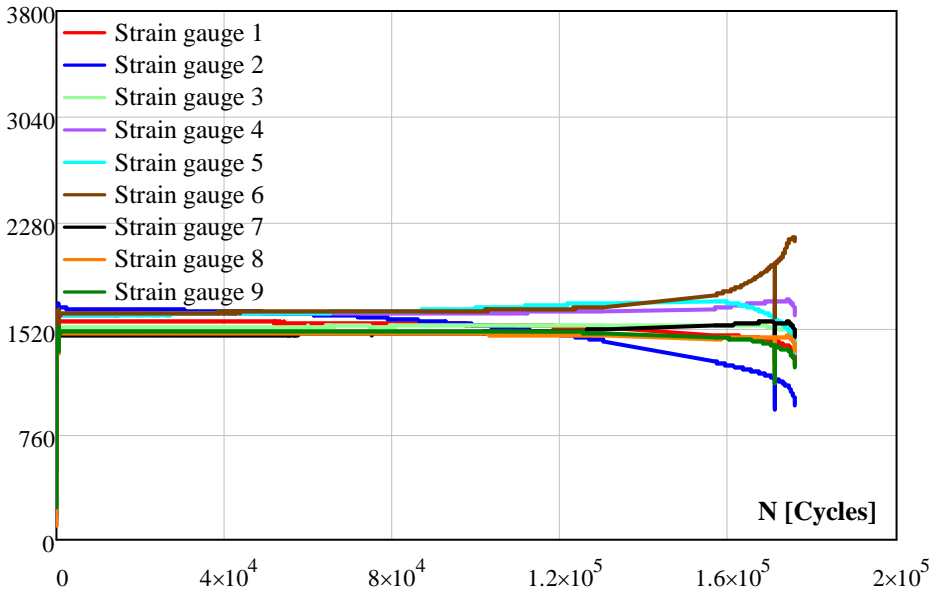
Specimen: CR897	Thickness [mm]	Rolled	25.16
		Cast	25.75
<i>Fatigue crack creation stage</i>			
N_i : 138727	N_s : 284028		
<i>Crack initiation location during testing</i>	At the edge of both sides of the weld toe of the cap.		
<i>Detected cracks by magnetic particle</i>			
 <p>Crack at both side of the weld toe</p>  <p>Long crack at weld root</p>			
<p><i>Repair of fatigue cracks:</i> The specimen cut from the middle and the weld material is removed such that the root and one side of the cap are suspended. Thus, half a V-shape groove is prepared.</p> <div style="display: flex; justify-content: space-around;"> <div style="text-align: center;"> <p>① original</p>  </div> <div style="text-align: center;"> <p>② cutting</p>  </div> </div> <div style="display: flex; justify-content: space-around; margin-top: 20px;"> <div style="text-align: center;"> <p>③ preparing</p>  </div> <div style="text-align: center;"> <p>④ welding</p>  </div> </div>			
<i>Test results of the repaired specimen</i>			
N_i : 52386	N_f : 175929		
<i>Crack initiation location:</i> Crack initiation and propagation in the base material of the rolled steel, edge of the plate.			

$\Delta\varepsilon$ [μstrain]



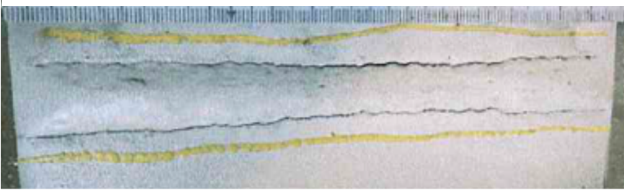
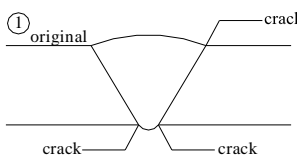
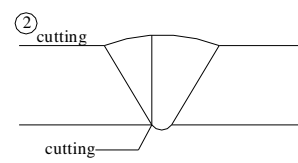
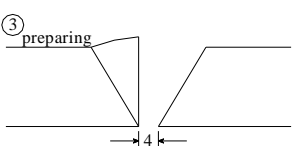
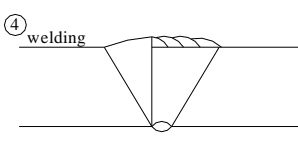
a) Crack creation stage.

$\Delta\varepsilon$ [μstrain]

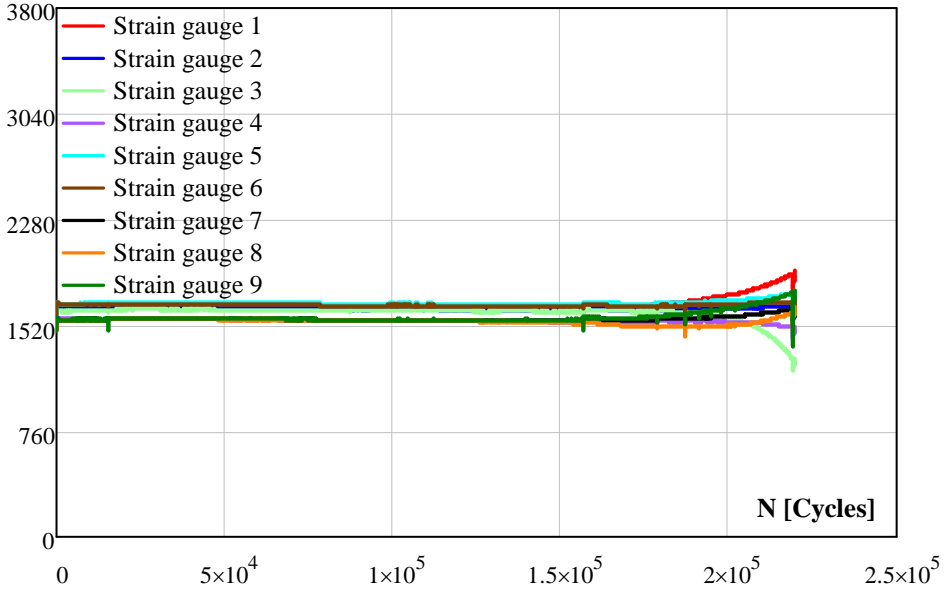


b) Repaired specimen.

Figure D.32 Strain gauge measurements of CR897 specimen.

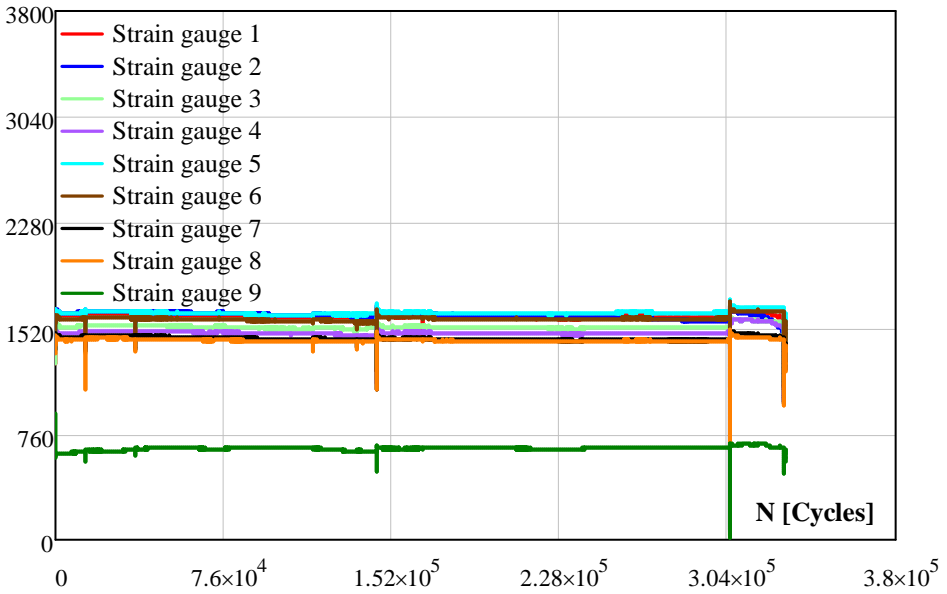
Specimen: CR898	Thickness [mm]	Rolled	25.25
		Cast	25.31
<i>Fatigue crack creation stage</i>			
N_i : 175374	N_s : 219639		
<i>Crack initiation location during testing</i>	At the middle of the weld toe of cap, rolled steel side		
<i>Detected cracks by magnetic particle</i>			
 <p>Crack at middle of the weld toe</p>  <p>Long crack at weld root</p>			
<p><i>Repair of fatigue cracks:</i> The specimen cut from the middle and the weld material is removed such that the root and one side of the cap are suspended. Thus, half a V-shape groove is prepared.</p> <div style="display: flex; justify-content: space-around;"> <div style="text-align: center;"> <p>① original</p>  </div> <div style="text-align: center;"> <p>② cutting</p>  </div> </div> <div style="display: flex; justify-content: space-around; margin-top: 20px;"> <div style="text-align: center;"> <p>③ preparing</p>  </div> <div style="text-align: center;"> <p>④ welding</p>  </div> </div>			
<i>Test results of the repaired specimen</i>			
N_i : 237299	N_f : 329984		
<i>Crack initiation location:</i> Crack initiation and propagation in the base material of the rolled steel, middle and edge of the plate.			

$\Delta\varepsilon$ [μstrain]



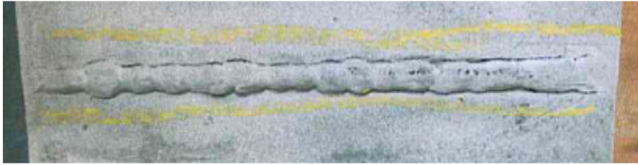
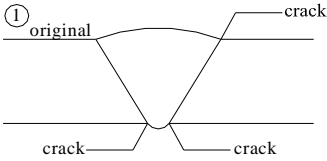
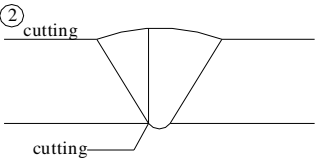
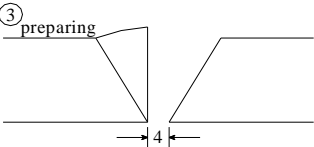
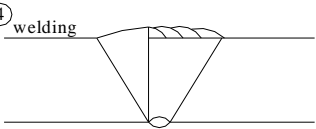
a) Crack creation stage.

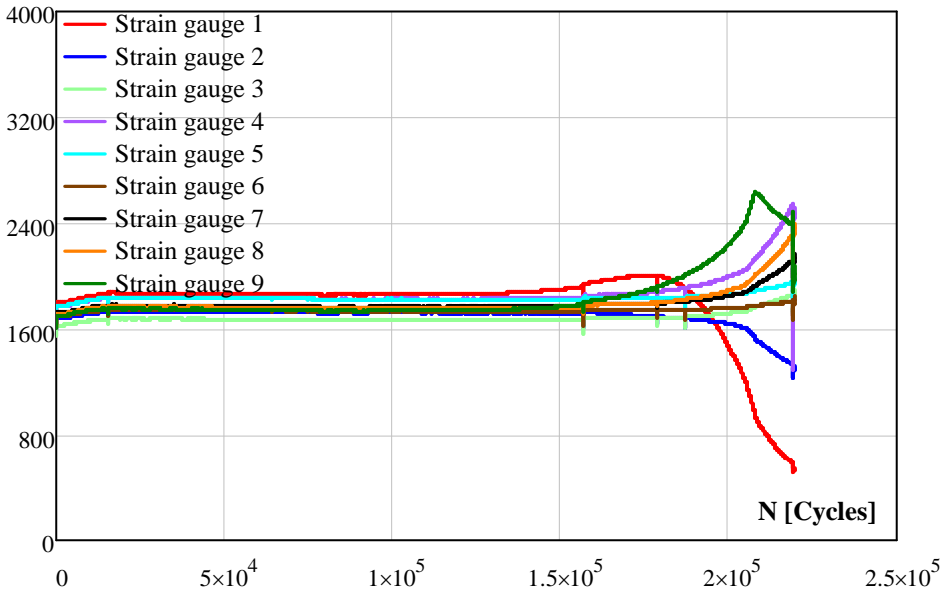
$\Delta\varepsilon$ [μstrain]



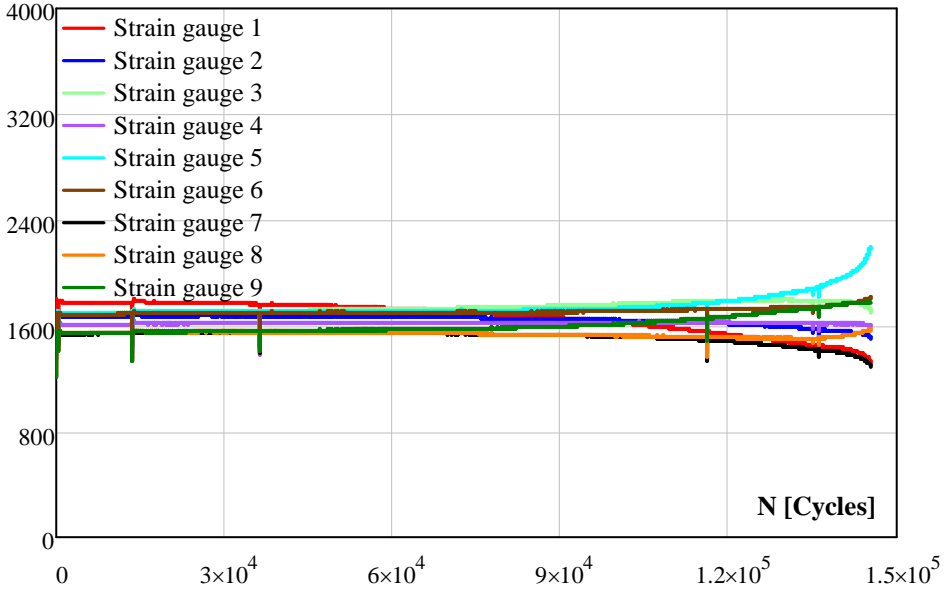
b) Repaired specimen.

Figure D.33 Strain gauge measurements of CR898 specimen.

Specimen: CR899	Thickness [mm]	Rolled	25.15
		Cast	25.6
<i>Fatigue crack creation stage</i>			
N_i : 135186	N_s : 219639		
<i>Crack initiation location during testing</i>	Near the middle of the weld toe of the cap, rolled steel side		
<i>Detected cracks by magnetic particle</i>			
 <p>Crack at middle of the weld toe of the cap</p>  <p>Long crack at weld root</p>			
<p><i>Repair of fatigue cracks:</i> The specimen cut from the middle and the weld material is removed such that the root and one side of the cap are suspended. Thus, half a V-shape groove is prepared.</p> <div style="display: flex; justify-content: space-around;"> <div style="text-align: center;"> <p>① original</p>  </div> <div style="text-align: center;"> <p>② cutting</p>  </div> </div> <div style="display: flex; justify-content: space-around; margin-top: 20px;"> <div style="text-align: center;"> <p>③ preparing</p>  </div> <div style="text-align: center;"> <p>④ welding</p>  </div> </div>			
<i>Test results of repaired specimen</i>			
N_i : 50268	N_f : 145292		
<i>Crack initiation location:</i> Crack initiation and propagation in the base material of the rolled steel, edge of the plate.			

$\Delta\varepsilon$ [μstrain]

a) Crack creation stage.

 $\Delta\varepsilon$ [μstrain]

b) Repaired specimen.

Figure D.34 Strain gauge measurements of CR899 specimen.

Appendix E. Fatigue test results

This appendix presents the results of the fatigue tests on the repaired artificial crack in the base material and the repaired V-shape welded connections. The fatigue crack initiation life N_i , fatigue crack propagation life N_p and total fatigue life N_f are indicated in the tables. In addition, the influence factors for fatigue crack initiation life and propagation life are presented for each prediction models. For each specimen, the fatigue crack initiation location is specified for the testing stage after the repair.

Specimen	Crack initiation location	Raw test results						Adjustment according to Hück et al. (1981) ¹					
		$\Delta\sigma_n$	Ni	Np	Nr	Ni/Nr	f _m Nr	f _m Ni	f _m Np	f _m	$\Delta\sigma_{n,Nr}$	$\Delta\sigma_{n,Ni}$	$\Delta\sigma_{n,Np}$
BR691	WT, cap, start-stop	253	169423	276599	446022	0.38	1.30	1.20	1.35	0.82	161	173	154
BR692	WT, cap, start-stop	287	248143	252253	500396	0.50	1.28	1.20	1.35	0.83	186	198	176
BR693	WT, cap, start-stop	257	400383	354425	754808	0.53	1.27	1.20	1.35	0.82	166	176	156
BR694	WT, cap, start-stop	224	578058	381769	959827	0.60	1.26	1.20	1.35	0.82	145	153	136
BR695	WT, cap, start-stop	307	189479	180001	369480	0.51	1.28	1.20	1.35	0.83	201	213	189
BR696	WT, cap, start-stop	273	208737	217981	426718	0.49	1.28	1.20	1.35	0.83	176	188	167
BR697	WT, cap, start-stop	298	278974	243503	522477	0.53	1.27	1.20	1.35	0.83	195	206	183
BR698	WT, cap, start-stop	192	861753	1094883	1956636	0.44	1.29	1.20	1.35	0.81	121	130	115
BR699	WT, cap, start-stop	290	265024	301861	566885	0.47	1.28	1.20	1.35	0.83	188	200	178
Specimen	Crack initiation location	Raw test results						Adjustment according to the nominal approach of the FKM guideline ¹					
		$\Delta\sigma_n$	Ni	Np	Nr	Ni/Nr	f _m Nr	f _m Ni	f _m Np	f _m	$\Delta\sigma_{n,Nr}$	$\Delta\sigma_{n,Ni}$	$\Delta\sigma_{n,Np}$
BR691	WT, cap, start-stop	253	169423	276599	446022	0.38	1.27	1.14	1.35	1.00	199	222	187
BR692	WT, cap, start-stop	287	248143	252253	500396	0.50	1.25	1.14	1.35	1.00	230	251	212
BR693	WT, cap, start-stop	257	400383	354425	754808	0.53	1.24	1.14	1.35	1.00	207	225	190
BR694	WT, cap, start-stop	224	578058	381769	959827	0.60	1.23	1.14	1.35	1.00	183	196	166
BR695	WT, cap, start-stop	307	189479	180001	369480	0.51	1.24	1.14	1.35	1.00	247	269	227
BR696	WT, cap, start-stop	273	208737	217981	426718	0.49	1.25	1.14	1.35	1.00	218	239	201
BR697	WT, cap, start-stop	298	278974	243503	522477	0.53	1.24	1.14	1.35	1.00	241	261	220
BR698	WT, cap, start-stop	192	861753	1094883	1956636	0.44	1.26	1.14	1.35	1.00	152	168	142
BR699	WT, cap, start-stop	290	265024	301861	566885	0.47	1.25	1.14	1.35	1.00	231	254	214
Specimen	Crack initiation location	Raw test results						Adjustment according to the local approach of the FKM guideline ¹					
		$\Delta\sigma_n$	Ni	Np	Nr	Ni/Nr	f _m Nr	f _m Ni	f _m Np	f _m	$\Delta\sigma_{n,Nr}$	$\Delta\sigma_{n,Ni}$	$\Delta\sigma_{n,Np}$
BR691	WT, cap, start-stop	253	169423	276599	446022	0.38	1.22	1.00	1.35	1.00	208	253	187
BR692	WT, cap, start-stop	287	248143	252253	500396	0.50	1.18	1.00	1.35	1.00	243	287	212
BR693	WT, cap, start-stop	257	400383	354425	754808	0.53	1.17	1.00	1.35	1.00	220	257	190
BR694	WT, cap, start-stop	224	578058	381769	959827	0.60	1.14	1.00	1.35	1.00	196	224	166
BR695	WT, cap, start-stop	307	189479	180001	369480	0.51	1.17	1.00	1.35	1.00	262	307	227
BR696	WT, cap, start-stop	273	208737	217981	426718	0.49	1.18	1.00	1.35	1.00	231	273	201
BR697	WT, cap, start-stop	298	278974	243503	522477	0.53	1.16	1.00	1.35	1.00	256	298	220
BR698	WT, cap, start-stop	192	861753	1094883	1956636	0.44	1.20	1.00	1.35	1.00	160	192	142
BR699	WT, cap, start-stop	290	265024	301861	566885	0.47	1.19	1.00	1.35	1.00	244	290	214

¹ Adjustment for the crack initiation life, the crack propagation life adjusted by the fracture mechanics approach.

Specimen	Crack initiation location	Raw test results						Adjustment according to Hüeck et al. (1981) ¹					
		$\Delta\sigma_n$	N_i	N_p	N_f	N_i/N_f	$f_{im}N_f$	$f_{im}N_i$	$f_{im}N_p$	f_{im}	$\Delta\sigma_{n,Nf}$	$\Delta\sigma_{n,Ni}$	$\Delta\sigma_{n,Np}$
BR891	WT, cap, start-stop	312	131804	166390	298194	0.44	1.29	1.20	1.35	0.78	189	202	180
BR892	WT, cap, start-stop	257	260297	283195	543492	0.48	1.28	1.20	1.35	0.77	155	165	147
BR893	WT, cap, start-stop	292	193805	218760	412565	0.47	1.28	1.20	1.35	0.78	177	189	168
BR894	WT, cap, start-stop	309	242539	208949	451488	0.54	1.27	1.20	1.35	0.78	190	200	178
BR895	WT, cap, start-stop	308	188651	334304	522955	0.36	1.30	1.20	1.35	0.78	185	199	177
BR896	WT, cap, start-stop	307	165550	154271	319821	0.52	1.28	1.20	1.35	0.78	188	199	177
BR897	run out	236	3234243	0	3234243	1.00	1.20	1.20	1.35	0.77	151	151	134
BR898	WT, cap, start-stop	268	239380	177139	416519	0.57	1.27	1.20	1.35	0.77	164	172	153
BR899	WT, cap, start-stop	324	152946	165078	318024	0.48	1.28	1.20	1.35	0.78	198	210	187
Specimen	Crack initiation location	Raw test results						Adjustment according to the nominal approach of the FKM guideline ¹					
		$\Delta\sigma_n$	N_i	N_p	N_f	N_i/N_f	$f_{im}N_f$	$f_{im}N_i$	$f_{im}N_p$	f_{im}	$\Delta\sigma_{n,Nf}$	$\Delta\sigma_{n,Ni}$	$\Delta\sigma_{n,Np}$
BR891	WT, cap, start-stop	312	131804	166390	298194	0.44	1.26	1.14	1.35	1.00	248	274	230
BR892	WT, cap, start-stop	257	260297	283195	543492	0.48	1.25	1.14	1.35	1.00	206	226	190
BR893	WT, cap, start-stop	292	193805	218760	412565	0.47	1.25	1.14	1.35	1.00	233	257	216
BR894	WT, cap, start-stop	309	242539	208949	451488	0.54	1.24	1.14	1.35	1.00	250	272	228
BR895	WT, cap, start-stop	308	188651	334304	522955	0.36	1.28	1.14	1.35	1.00	241	271	227
BR896	WT, cap, start-stop	307	165550	154271	319821	0.52	1.24	1.14	1.35	1.00	247	270	227
BR897	run out	236	3234243	0	3234243	1.00	1.14	1.14	1.35	1.00	208	208	174
BR898	WT, cap, start-stop	268	239380	177139	416519	0.57	1.23	1.14	1.35	1.00	218	236	198
BR899	WT, cap, start-stop	324	152946	165078	318024	0.48	1.25	1.14	1.35	1.00	259	285	239
Specimen	Crack initiation location	Raw test results						Adjustment according to the local approach of the FKM guideline ¹					
		$\Delta\sigma_n$	N_i	N_p	N_f	N_i/N_f	$f_{im}N_f$	$f_{im}N_i$	$f_{im}N_p$	f_{im}	$\Delta\sigma_{n,Nf}$	$\Delta\sigma_{n,Ni}$	$\Delta\sigma_{n,Np}$
BR891	WT, cap, start-stop	312	131804	166390	298194	0.44	1.20	1.00	1.35	1.00	260	312	230
BR892	WT, cap, start-stop	257	260297	283195	543492	0.48	1.18	1.00	1.35	1.00	217	257	190
BR893	WT, cap, start-stop	292	193805	218760	412565	0.47	1.19	1.00	1.35	1.00	246	292	216
BR894	WT, cap, start-stop	309	242539	208949	451488	0.54	1.16	1.00	1.35	1.00	266	309	228
BR895	WT, cap, start-stop	308	188651	334304	522955	0.36	1.23	1.00	1.35	1.00	251	308	227
BR896	WT, cap, start-stop	307	165550	154271	319821	0.52	1.17	1.00	1.35	1.00	262	307	227
BR897	run out	236	3234243	0	3234243	1.00	1.00	1.00	1.35	1.00	236	236	174
BR898	WT, cap, start-stop	268	239380	177139	416519	0.57	1.15	1.00	1.35	1.00	233	268	198
BR899	WT, cap, start-stop	324	152946	165078	318024	0.48	1.18	1.00	1.35	1.00	273	324	239

¹ Adjustment for the crack initiation life, the crack propagation life adjusted by the fracture mechanics approach.

Specimen	Crack initiation location	Raw test results					Adjustment according to Hück et al. (1981) ¹						
		$\Delta\sigma_n$	N _i	N _p	N _f	N _i /N _f	f _{imNf}	f _{imNi}	f _{imNp}	f _m	$\Delta\sigma_{n,Nf}$	$\Delta\sigma_{n,Ni}$	$\Delta\sigma_{n,Np}$
VR691	WT.cap,middle	203	1239493	499228	1738721	0.71	1.25	1.20	1.35	0.83	135	140	124
VR692	run out	228	5022891	0	5022891	1.00	1.20	1.20	1.35	0.83	158	158	140
VR693	WT.cap,middle	221	894634	804366	1699000	0.53	1.27	1.20	1.35	0.83	144	153	136
VR694	WT.cap,middle	256	313418	250718	564136	0.56	1.27	1.20	1.35	0.84	169	178	158
VR695	WT.cap,middle	253	30696	130289	160985	0.19	1.32	1.20	1.35	0.84	160	176	156
VR696	run out	244	4575656	0	4575656	1.00	1.20	1.20	1.35	0.83	169	169	150
VR697	WT.cap,middle	257	275968	203253	479221	0.58	1.27	1.20	1.35	0.84	169	178	158
VR698	WT.cap,middle	285	269302	222234	491536	0.55	1.27	1.20	1.35	0.84	188	199	177
VR699	WT.cap,middle	310	163269	167853	331122	0.49	1.28	1.20	1.35	0.85	205	218	193
Specimen	Crack initiation location	Raw test results					Adjustment according to the nominal approach of the FKM guideline ¹						
$\Delta\sigma_n$	N _i	N _p	N _f	N _i /N _f	f _{imNf}	f _{imNi}	f _{imNp}	f _m	$\Delta\sigma_{n,Nf}$	$\Delta\sigma_{n,Ni}$	$\Delta\sigma_{n,Np}$		
VR691	WT.cap,middle	203	1239493	499228	1738721	0.71	1.20	1.14	1.35	1.00	169	178	150
VR692	run out	228	5022891	0	5022891	1.00	1.14	1.14	1.35	1.00	200	200	169
VR693	WT.cap,middle	221	894634	804366	1699000	0.53	1.24	1.14	1.35	1.00	178	194	164
VR694	WT.cap,middle	256	313418	250718	564136	0.56	1.24	1.14	1.35	1.00	207	224	189
VR695	WT.cap,middle	253	30696	130289	160985	0.19	1.31	1.14	1.35	1.00	192	221	187
VR696	run out	244	4575656	0	4575656	1.00	1.14	1.14	1.35	1.00	213	213	180
VR697	WT.cap,middle	257	275968	203253	479221	0.58	1.23	1.14	1.35	1.00	208	225	190
VR698	WT.cap,middle	285	269302	222234	491536	0.55	1.24	1.14	1.35	1.00	230	249	210
VR699	WT.cap,middle	310	163269	167853	331122	0.49	1.25	1.14	1.35	1.00	248	271	229
Specimen	Crack initiation location	Raw test results					Adjustment according to the local approach of the FKM guideline ¹						
$\Delta\sigma_n$	N _i	N _p	N _f	N _i /N _f	f _{imNf}	f _{imNi}	f _{imNp}	f _m	$\Delta\sigma_{n,Nf}$	$\Delta\sigma_{n,Ni}$	$\Delta\sigma_{n,Np}$		
VR691	WT.cap,middle	203	1239493	499228	1738721	0.71	1.10	1.00	1.35	1.00	185	203	150
VR692	run out	228	5022891	0	5022891	1.00	1.00	1.00	1.35	1.00	228	228	169
VR693	WT.cap,middle	221	894634	804366	1699000	0.53	1.17	1.00	1.35	1.00	190	221	164
VR694	WT.cap,middle	256	313418	250718	564136	0.56	1.16	1.00	1.35	1.00	221	256	189
VR695	WT.cap,middle	253	30696	130289	160985	0.19	1.29	1.00	1.35	1.00	197	253	187
VR696	run out	244	4575656	0	4575656	1.00	1.00	1.00	1.35	1.00	244	244	180
VR697	WT.cap,middle	257	275968	203253	479221	0.58	1.15	1.00	1.35	1.00	223	257	190
VR698	WT.cap,middle	285	269302	222234	491536	0.55	1.16	1.00	1.35	1.00	245	285	210
VR699	WT.cap,middle	310	163269	167853	331122	0.49	1.18	1.00	1.35	1.00	263	310	229

¹ Adjustment for the crack initiation life, the crack propagation life adjusted by the fracture mechanics approach.

Specimen	Crack initiation location	Raw test results						Adjustment according to Hiick et al. (1981) ¹					
		$\Delta\sigma_n$	Ni	Np	Nf	Ni/Nf	f _m Nf	f _m Ni	f _m Np	f _m	$\Delta\sigma_{n,Nf}$	$\Delta\sigma_{n,Ni}$	$\Delta\sigma_{n,Np}$
CR691	WT, cap, middle, cast	203	224510	1077650	1302160	0.17	1.33	1.20	1.35	0.83	127	141	125
CR692	BM, middle, cast	254	370566	740631	1111197	0.33	1.03	1.00	1.05	0.85	208	215	205
CR693	BM, edge, cast	255	71789	1260937	1332726	0.05	1.04	1.00	1.05	0.85	206	215	206
CR694	WT, cap, middle, rolled	222	165382	260426	425808	0.39	1.29	1.20	1.35	0.83	142	153	136
CR695	WT, cap, middle, cast	227	72839	314847	387686	0.19	1.32	1.20	1.35	0.84	144	158	141
CR696	BM, middle, cast	265	104233	1269823	1374056	0.08	1.04	1.00	1.05	0.85	215	225	215
CR697	WT, cap, middle, rolled	303	52813	185710	238523	0.22	1.32	1.20	1.35	0.84	193	212	189
CR698	WT, cap, middle, cast	290	253770	119282	373052	0.68	1.25	1.20	1.35	0.86	199	207	184
CR699	WT, cap, middle, cast	321	150430	197298	347728	0.43	1.29	1.20	1.35	0.86	213	229	203
Specimen	Crack initiation location	Raw test results						Adjustment according to the nominal approach of the FKM guideline ¹					
		$\Delta\sigma_n$	Ni	Np	Nf	Ni/Nf	f _m Nf	f _m Ni	f _m Np	f _m	$\Delta\sigma_{n,Nf}$	$\Delta\sigma_{n,Ni}$	$\Delta\sigma_{n,Np}$
CR691	WT, cap, middle, cast	203	224510	1077650	1302160	0.17	1.32	1.14	1.35	1.00	154	178	150
CR692	BM, middle, cast	254	370566	740631	1111197	0.33	1.03	1.00	1.05	0.80	197	203	194
CR693	BM, edge, cast	255	71789	1260937	1332726	0.05	1.04	1.00	1.05	0.80	195	204	195
CR694	WT, cap, middle, rolled	222	165382	260426	425808	0.39	1.27	1.14	1.35	1.00	175	194	164
CR695	WT, cap, middle, cast	227	72839	314847	387686	0.19	1.31	1.14	1.35	1.00	173	199	168
CR696	BM, middle, cast	265	104233	1269823	1374056	0.08	1.04	1.00	1.05	0.80	203	212	203
CR697	WT, cap, middle, rolled	303	52813	185710	238523	0.22	1.31	1.14	1.35	1.00	232	265	224
CR698	WT, cap, middle, cast	290	253770	119282	373052	0.68	1.21	1.14	1.35	1.00	240	254	214
CR699	WT, cap, middle, cast	321	150430	197298	347728	0.43	1.26	1.14	1.35	1.00	254	281	237
Specimen	Crack initiation location	Raw test results						Adjustment according to the local approach of the FKM guideline ¹					
		$\Delta\sigma_n$	Ni	Np	Nf	Ni/Nf	f _m Nf	f _m Ni	f _m Np	f _m	$\Delta\sigma_{n,Nf}$	$\Delta\sigma_{n,Ni}$	$\Delta\sigma_{n,Np}$
CR691	WT, cap, middle, cast	203	224510	1077650	1302160	0.17	1.29	1.00	1.35	1.00	157	203	150
CR692	BM, middle, cast	254	370566	740631	1111197	0.33	1.03	1.00	1.05	0.83	203	210	200
CR693	BM, edge, cast	255	71789	1260937	1332726	0.05	1.04	1.00	1.05	0.83	201	210	201
CR694	WT, cap, middle, rolled	222	165382	260426	425808	0.39	1.22	1.00	1.35	1.00	182	222	164
CR695	WT, cap, middle, cast	227	72839	314847	387686	0.19	1.29	1.00	1.35	1.00	177	227	168
CR696	BM, middle, cast	265	104233	1269823	1374056	0.08	1.04	1.00	1.05	0.82	209	218	208
CR697	WT, cap, middle, rolled	303	52813	185710	238523	0.22	1.28	1.00	1.35	1.00	237	303	224
CR698	WT, cap, middle, cast	290	253770	119282	373052	0.68	1.11	1.00	1.35	1.00	261	290	214
CR699	WT, cap, middle, cast	321	150430	197298	347728	0.43	1.20	1.00	1.35	1.00	267	321	237

¹ Adjustment for the crack initiation life, the crack propagation life adjusted by the fracture mechanics approach.

Specimen	Crack initiation location	Raw test results					Adjustment according to Hüeck et al. (1981) ¹						
		$\Delta\sigma_n$	N_i	N_p	N_f	N_i/N_f	$f_{im}N_f$	$f_{im}N_i$	$f_{im}N_p$	f_m	$\Delta\sigma_{n,Nf}$	$\Delta\sigma_{n,Ni}$	$\Delta\sigma_{n,Np}$
VR891	run out	250	5010863	0	5010863	1.00	1.20	1.20	1.35	0.77	160	160	142
VR892	Base material failure at the crack creation stage												
VR893	run out	285	5000001	0	5000001	1.00	1.20	1.20	1.35	0.78	184	184	164
VR894	Base material failure at the crack creation stage												
VR895	Base material failure at the crack creation stage												
VR896	BM, middle, rolled	292	101392	934346	1035738	0.10	1.04	1.00	1.05	0.78	218	218	217
VR897	BM, middle, rolled	358	226237	334800	561037	0.40	1.03	1.00	1.05	0.79	275	275	270
VR898	BM, edge, rolled	356	106595	454269	560864	0.19	1.04	1.00	1.05	0.79	270	270	268
VR899	BM, middle, rolled	370	228910	203487	432397	0.53	1.02	1.00	1.05	0.79	286	286	280
Specimen	Crack initiation location	Raw test results					Adjustment according to the nominal approach of the FKM guideline ¹						
		$\Delta\sigma_n$	N_i	N_p	N_f	N_i/N_f	$f_{im}N_f$	$f_{im}N_i$	$f_{im}N_p$	f_m	$\Delta\sigma_{n,Nf}$	$\Delta\sigma_{n,Ni}$	$\Delta\sigma_{n,Np}$
VR891	run out	250	5010863	0	5010863	1.00	1.14	1.14	1.35	1.00	220	220	184
VR892													
VR893	run out	285	5000001	0	5000001	1.00	1.14	1.14	1.35	1.00	251	251	211
VR894													
VR895													
VR896	BM, middle, rolled	292	101392	934346	1035738	0.10	1.04	1.00	1.05	0.70	196	196	195
VR897	BM, middle, rolled	358	226237	334800	561037	0.40	1.03	1.00	1.05	0.70	243	250	239
VR898	BM, edge, rolled	356	106595	454269	560864	0.19	1.04	1.00	1.05	0.70	240	249	238
VR899	BM, middle, rolled	370	228910	203487	432397	0.53	1.02	1.00	1.05	0.70	253	258	247
Specimen	Crack initiation location	Raw test results					Adjustment according to the local approach of the FKM guideline ¹						
		$\Delta\sigma_n$	N_i	N_p	N_f	N_i/N_f	$f_{im}N_f$	$f_{im}N_i$	$f_{im}N_p$	f_m	$\Delta\sigma_{n,Nf}$	$\Delta\sigma_{n,Ni}$	$\Delta\sigma_{n,Np}$
VR891	run out	250	5010863	0	5010863	1.00	1.00	1.00	1.35	1.00	250	250	184
VR892													
VR893	run out	285	5000001	0	5000001	1.00	1.00	1.00	1.35	1.00	285	285	211
VR894													
VR895													
VR896	BM, middle, rolled	292	101392	934346	1035738	0.10	1.04	1.00	1.05	0.76	212	221	211
VR897	BM, middle, rolled	358	226237	334800	561037	0.40	1.03	1.00	1.05	0.73	254	261	250
VR898	BM, edge, rolled	356	106595	454269	560864	0.19	1.04	1.00	1.05	0.73	251	260	248
VR899	BM, middle, rolled	370	228910	203487	432397	0.53	1.02	1.00	1.05	0.73	262	268	256

¹ Adjustment for the crack initiation life, the crack propagation life adjusted by the fracture mechanics approach.

Specimen	Crack initiation location	Raw test results						Adjustment according to Hück et al. (1981) ¹					
		$\Delta\sigma_n$	Ni	Np	Nf	Ni/Nf	f _m Nf	f _m Ni	f _m Np	f _m	$\Delta\sigma_n$ Nf	$\Delta\sigma_n$ Ni	$\Delta\sigma_n$ Np
CR891	BM, middle, cast	260	218923	1414623	1633546	0.13	1.04	1.00	1.05	0.76	189	197	188
CR892	BM, middle, cast	244	218923	841856	1060779	0.21	1.04	1.00	1.05	0.75	177	184	175
CR893	BM, edge, rolled	265	703437	2067618	2771055	0.25	1.04	1.00	1.05	0.77	198	205	196
CR894	BM, edge, rolled	298	627418	450370	1077788	0.58	1.02	1.00	1.05	0.78	228	232	222
CR895	BM, middle, rolled	281	305269	912656	1217925	0.25	1.04	1.00	1.05	0.78	211	218	209
CR896	WT, cap, middle, cast	302	69460	100911	170371	0.41	1.29	1.20	1.35	0.77	181	194	173
CR897	BM, edge, rolled	349	52386	407571	459957	0.11	1.04	1.00	1.05	0.79	264	275	262
CR898	BM, edge, rolled	343	237299	312324	549623	0.43	1.03	1.00	1.05	0.79	263	270	258
CR899	BM, edge, rolled	372	50268	314663	364931	0.14	1.04	1.00	1.05	0.79	283	295	282
Specimen	Crack initiation location	Raw test results						Adjustment according to the nominal approach of the FKM guideline ¹					
		$\Delta\sigma_n$	Ni	Np	Nf	Ni/Nf	f _m Nf	f _m Ni	f _m Np	f _m	$\Delta\sigma_n$ Nf	$\Delta\sigma_n$ Ni	$\Delta\sigma_n$ Np
CR891	BM, middle, cast	260	218923	1414623	1633546	0.13	1.04	1.00	1.05	0.69	172	179	171
CR892	BM, middle, cast	244	218923	841856	1060779	0.21	1.04	1.00	1.05	0.69	163	169	161
CR893	BM, edge, rolled	265	703437	2067618	2771055	0.25	1.04	1.00	1.05	0.70	179	185	177
CR894	BM, edge, rolled	298	627418	450370	1077788	0.58	1.02	1.00	1.05	0.70	204	208	199
CR895	BM, middle, rolled	281	305269	912656	1217925	0.25	1.04	1.00	1.05	0.99	269	279	266
CR896	WT, cap, middle, cast	302	69460	100911	170371	0.41	1.26	1.14	1.35	1.00	239	266	223
CR897	BM, edge, rolled	349	52386	407571	459957	0.11	1.04	1.00	1.05	0.70	234	244	233
CR898	BM, edge, rolled	343	237299	312324	549623	0.43	1.03	1.00	1.05	0.70	233	240	229
CR899	BM, edge, rolled	372	50268	314663	364931	0.14	1.04	1.00	1.05	0.70	250	260	248
Specimen	Crack initiation location	Raw test results						Adjustment according to the local approach of the FKM guideline ¹					
		$\Delta\sigma_n$	Ni	Np	Nf	Ni/Nf	f _m Nf	f _m Ni	f _m Np	f _m	$\Delta\sigma_n$ Nf	$\Delta\sigma_n$ Ni	$\Delta\sigma_n$ Np
CR891	BM, middle, cast	260	218923	1414623	1633546	0.13	1.04	1.00	1.05	0.73	182	189	181
CR892	BM, middle, cast	244	218923	841856	1060779	0.21	1.04	1.00	1.05	0.74	173	180	172
CR893	BM, edge, rolled	265	703437	2067618	2771055	0.25	1.04	1.00	1.05	0.69	177	183	175
CR894	BM, edge, rolled	298	627418	450370	1077788	0.58	1.02	1.00	1.05	0.75	220	225	214
CR895	BM, middle, rolled	281	305269	912656	1217925	0.25	1.04	1.00	1.05	0.76	207	214	204
CR896	WT, cap, middle, cast	302	69460	100911	170371	0.41	1.21	1.00	1.35	1.00	249	302	223
CR897	BM, edge, rolled	349	52386	407571	459957	0.11	1.04	1.00	1.05	0.73	246	256	244
CR898	BM, edge, rolled	343	237299	312324	549623	0.43	1.03	1.00	1.05	0.74	246	252	241
CR899	BM, edge, rolled	372	50268	314663	364931	0.14	1.04	1.00	1.05	0.72	259	269	257

¹ Adjustment for the crack initiation life, the crack propagation life adjusted by the fracture mechanics approach.

Appendix F. Hardness measurements

Appendix F presents the hardness measurements on the welded specimens in as welded condition. The welding procedure and the weld cross sections are presented in Chapter 5. The measurements were performed on the weld cross section on the cap side, at the middle of the weld and at the root of the weld with 1 mm distance. In addition, the hardness of the heat affected zones was determined with 0.2 mm distance. Hence, the hardness profile of the weld cross section was created. Figure F.1 shows the locations of the hardness measurement on the cross section of welded specimens.

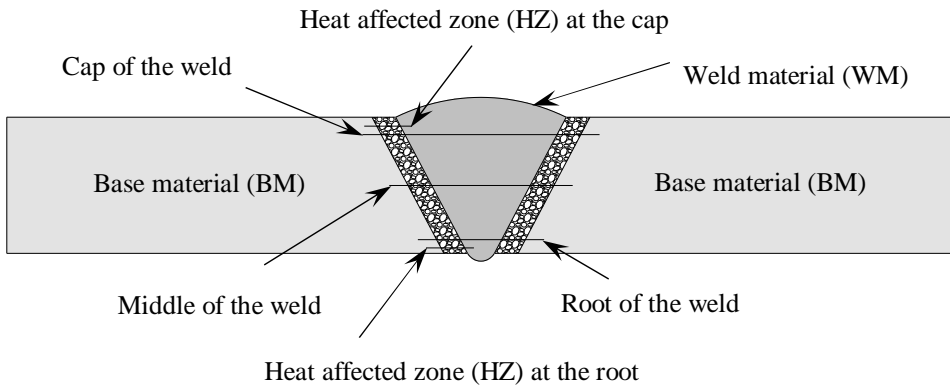
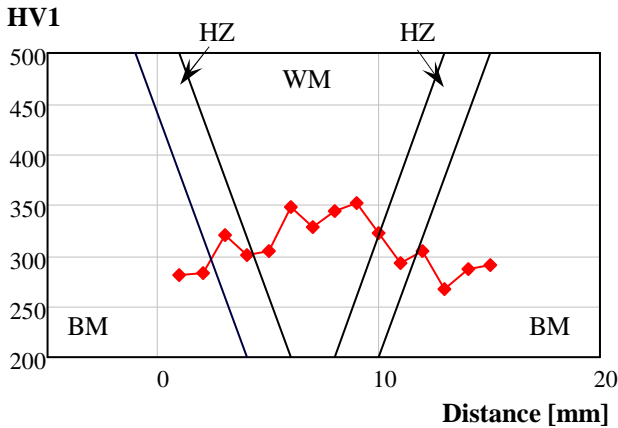
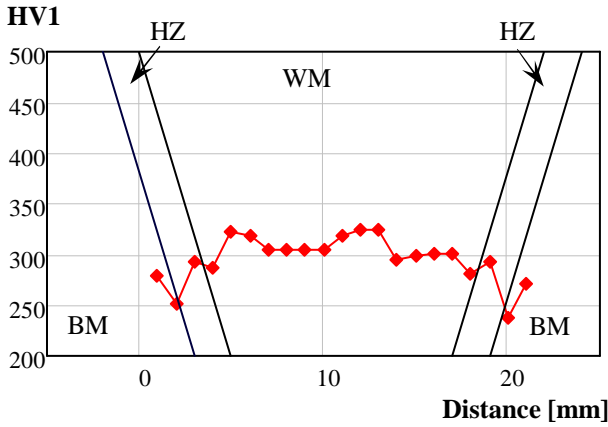
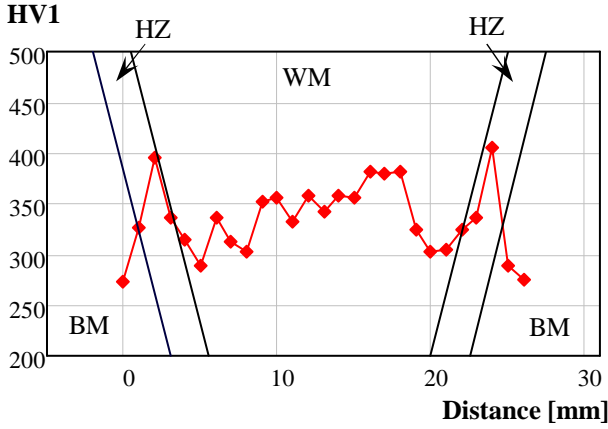


Figure F.1 Hardness measurements locations on a weld cross section.

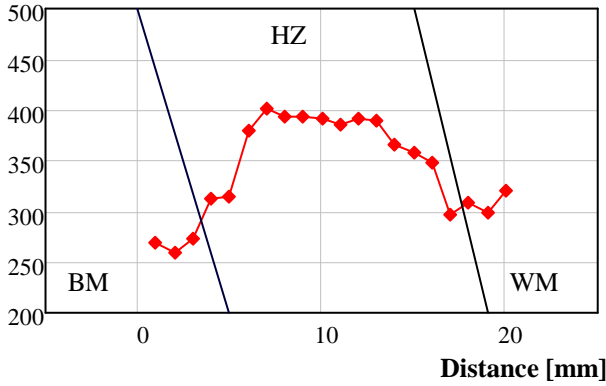
HV1 applied load 9.807 N

HV0.5 applied load 4.903 N

BR 69x series



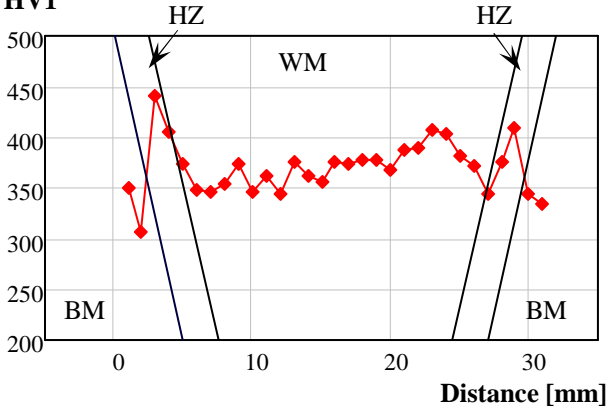
HV0.5



HZ at the cap

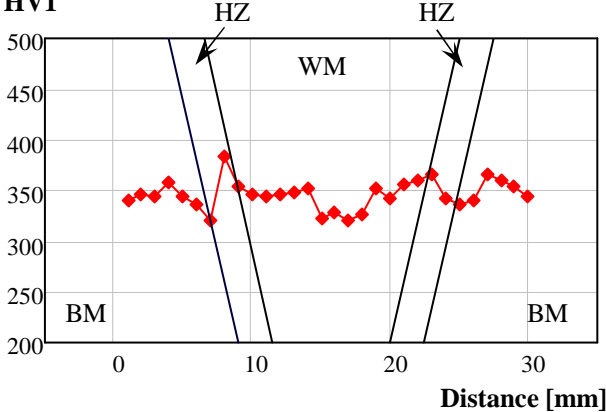
BR 89x series

HV1



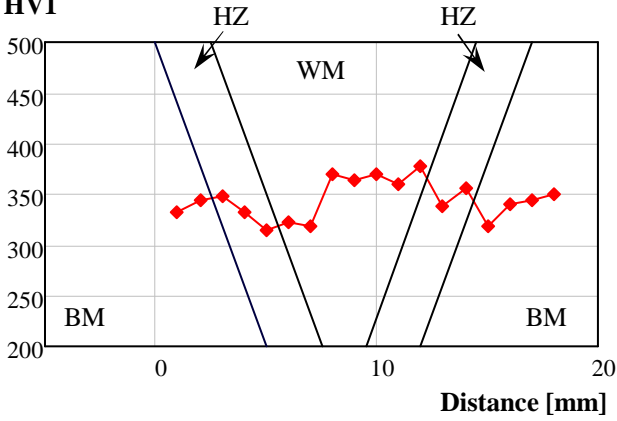
Cap of the weld

HV1

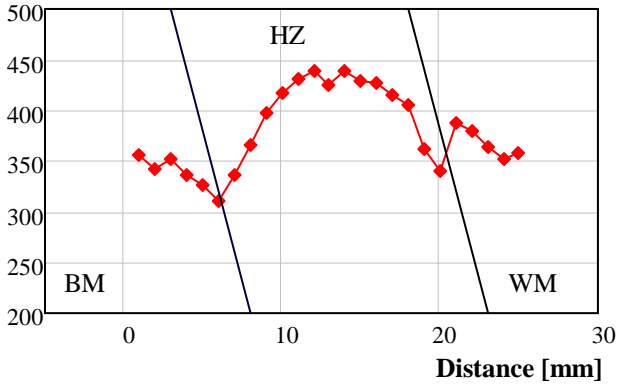


Middle of the weld

HV1

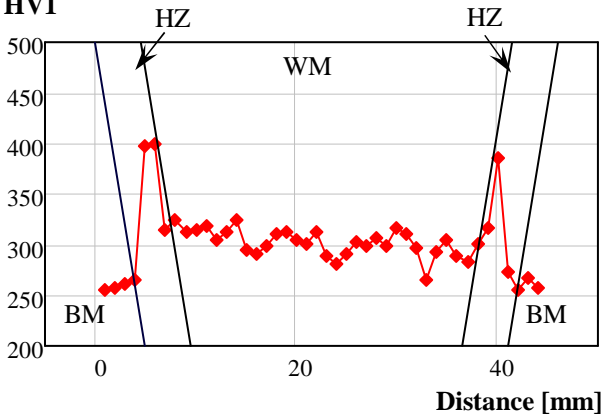


HV0.5

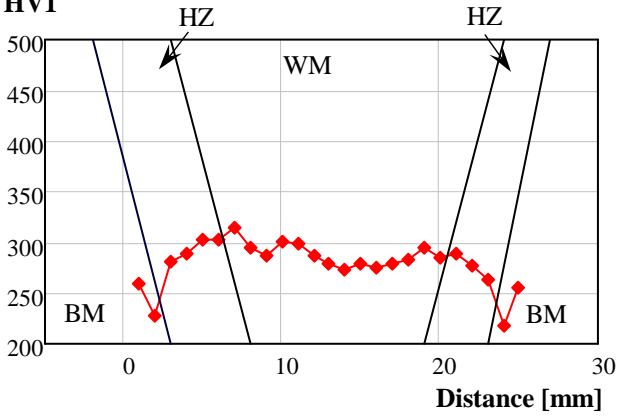


V 69x series

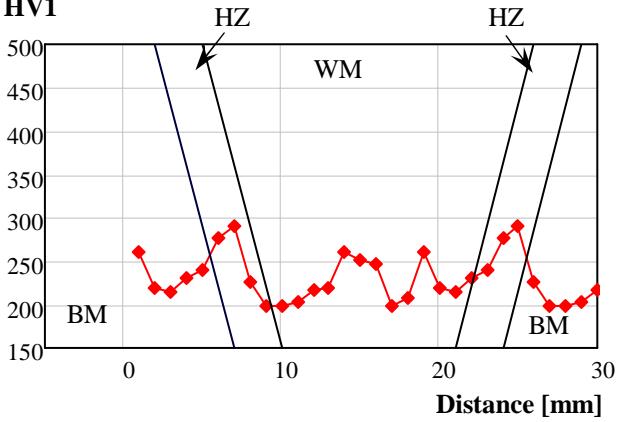
HV1



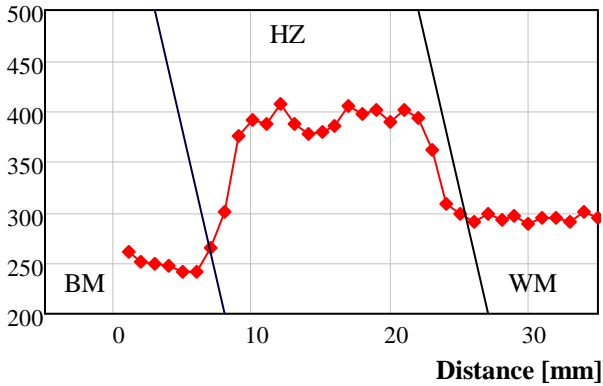
HV1



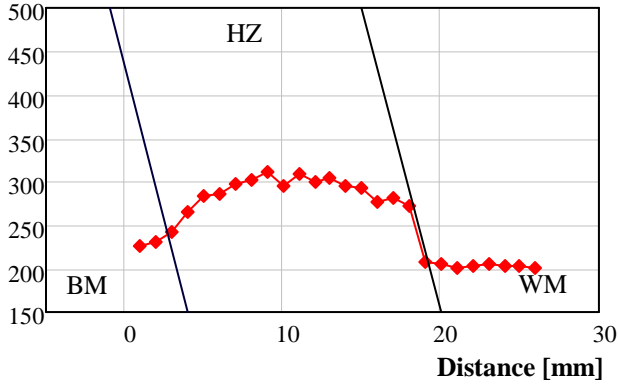
HV1



HV0.5



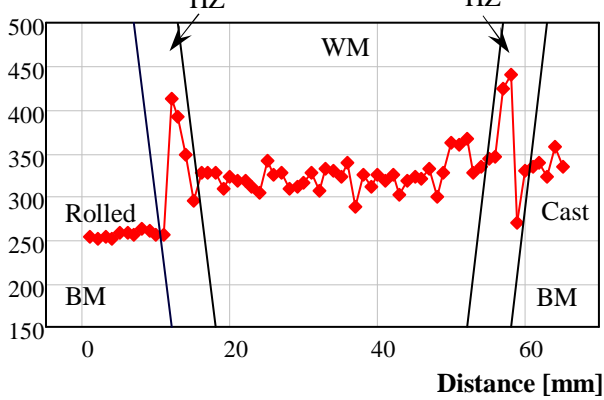
HV0.5



HZ at the root

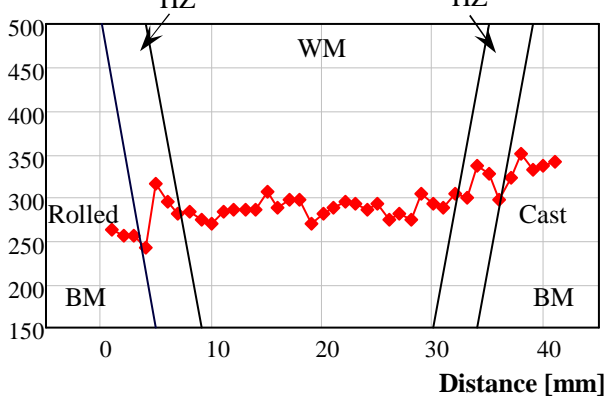
C 69x series

HV1

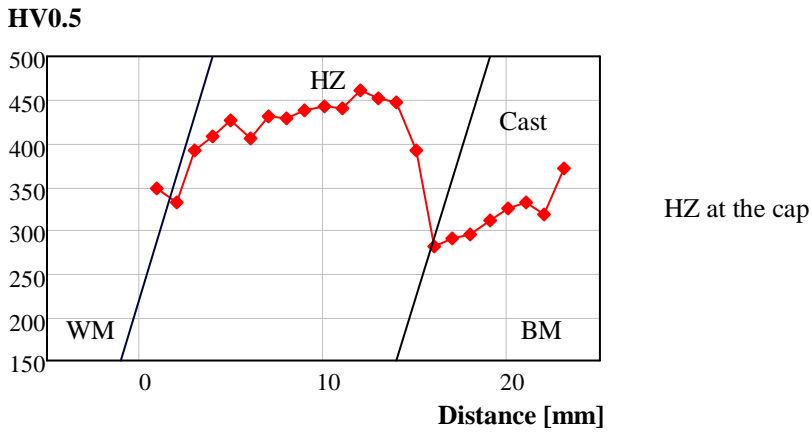
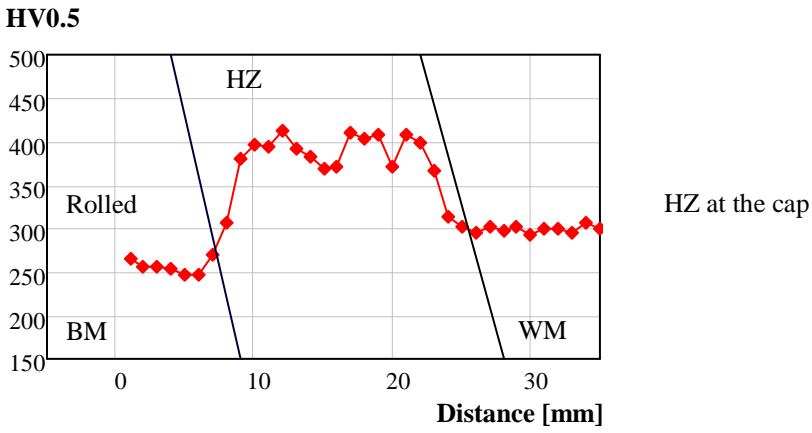
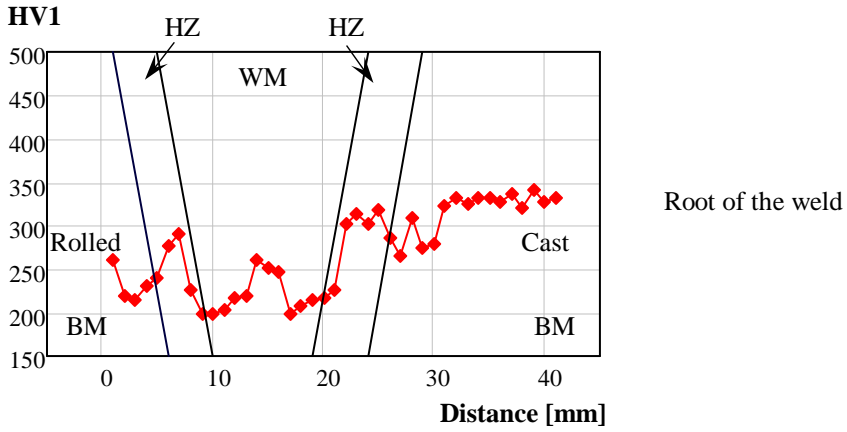


Cap of the weld

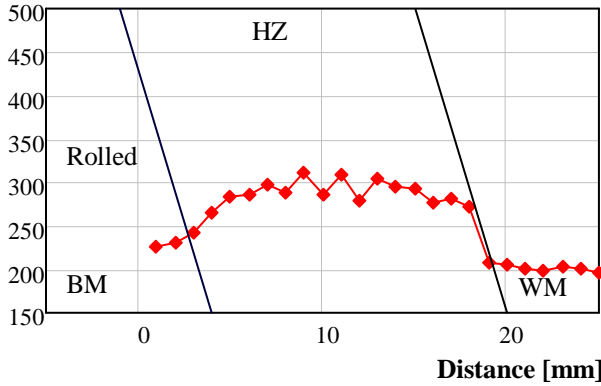
HV1



Middle of the weld

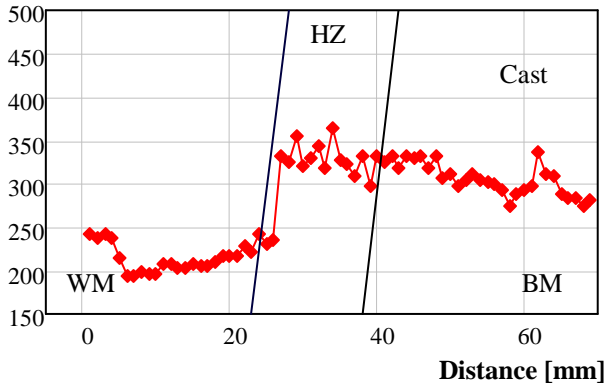


HV0.5



HZ at the root

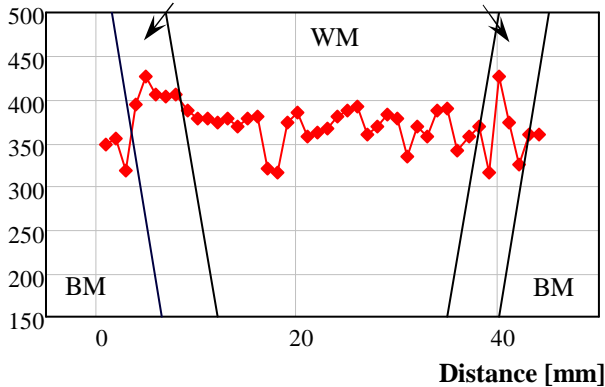
HV0.5



HZ at the root

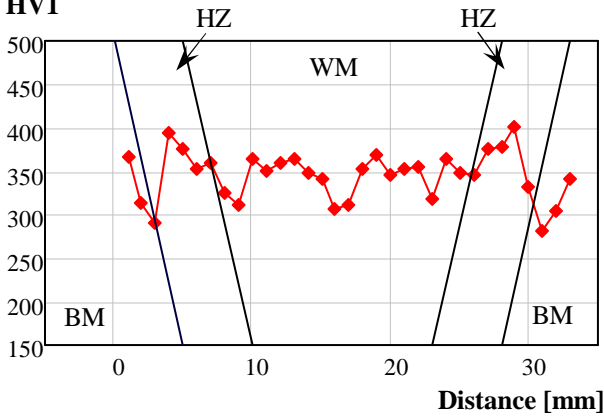
V 89x series

HV1

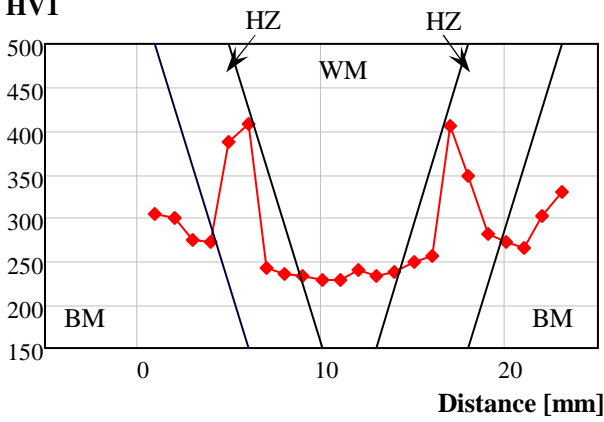


Cap of the weld

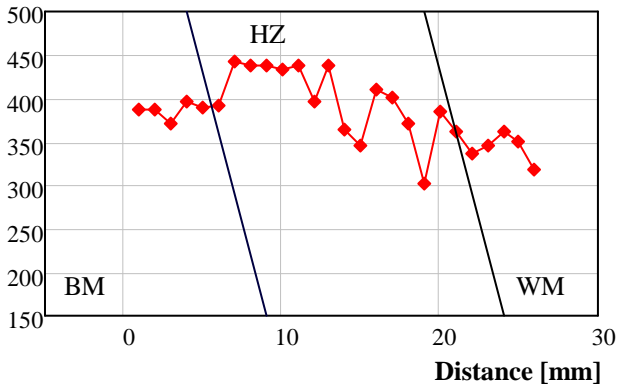
HV1



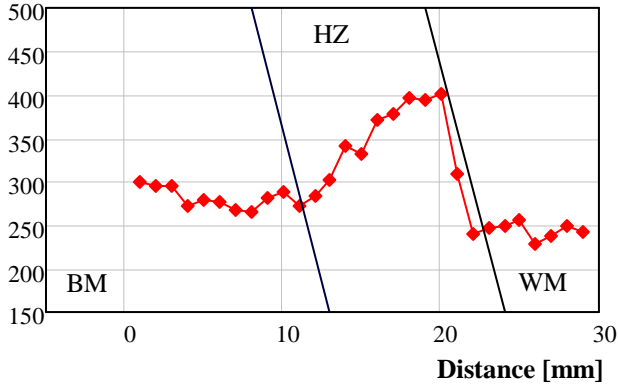
HV1



HV0.5

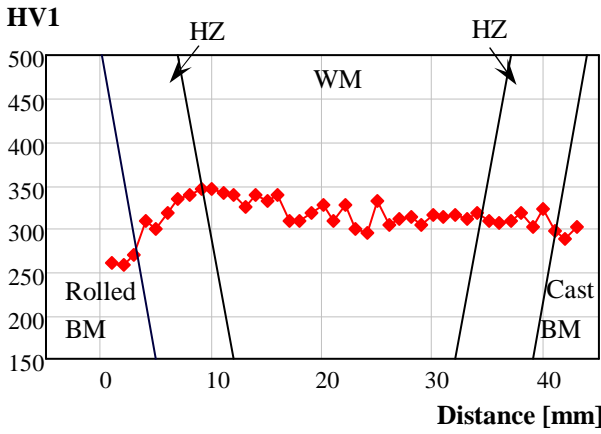


HV0.5

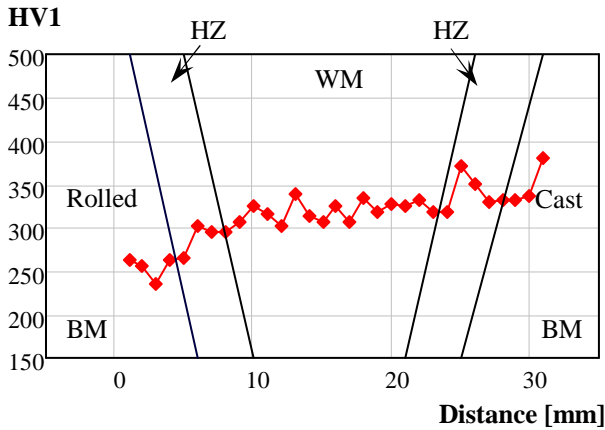


HZ at the root

C 89x series

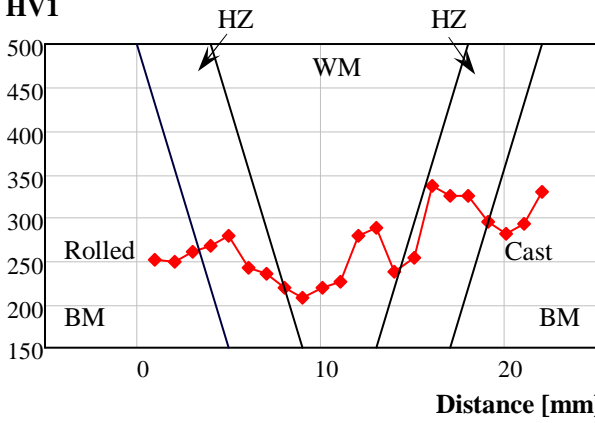


Cap of the weld



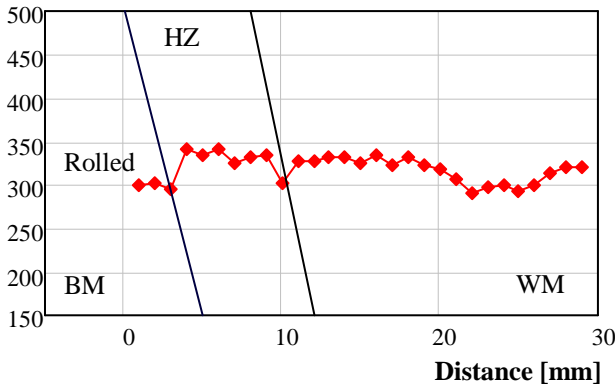
Middle of the weld

HV1



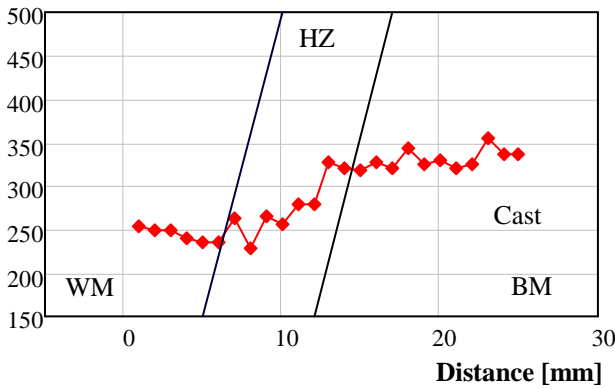
Root of the weld

HV0.5



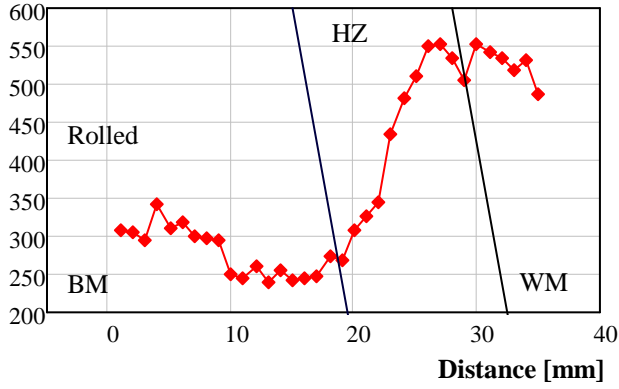
HZ at the cap

HV0.5



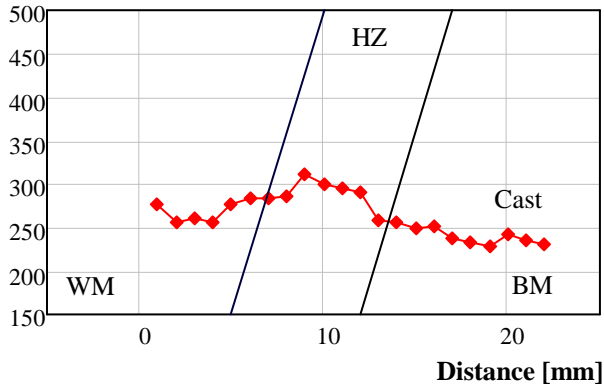
HZ at the cap

HV0.5



HZ at the root

HV0.5



HZ at the root